

2019:00247- Unrestricted

Report

EERA DeepWind'2019 Conference 16 – 18 January 2019

Radisson Blu Royal Garden Hotel, Trondheim

John Olav Tande (editor)

Report

EERA DeepWind'2019 Conference 16 – 18 January 2019

Radisson Blu Royal Garden Hotel, Trondheim

KEYWORDS:

VERSION

1.0

DATE

2019-02-22

AUTHOR(S)

John Olav Tande (editor)

CLIENT(S)

CLIENT'S REF.

PROJECT NO.

502000965-5

NUMBER OF PAGES/APPENDICES:

277

ABSTRACT

This report includes the presentations from the 16th Deep Sea Offshore Wind R&D Conference, EERA DeepWind'2018, 16 – 18 January 2019 in Trondheim, Norway.

Presentations include plenary sessions with broad appeal and parallel sessions on specific technical themes:

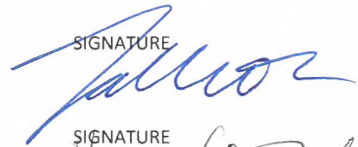
- a) New turbine and generator technology
- b) Grid connection and power system integration
- c) Met-ocean conditions
- d) Operations & maintenance
- e) Installation & sub-structures
- f) Wind farm optimization
- g) Experimental Testing and Validation
- h) Wind farm control systems

Plenary presentations include frontiers of science and technologies and strategic outlook. The presentations and further conference details are also available at the conference web page: <https://www.sintef.no/projectweb/eera-deepwind/previous-conferences/>

PREPARED BY

John Olav Tande

SIGNATURE



CHECKED BY

Hans Christian Bolstad

SIGNATURE



APPROVED BY

Knut Samdal

SIGNATURE



REPORT NO.
2019:00247

ISBN
978-82-14-06817-7

CLASSIFICATION
Unrestricted

CLASSIFICATION THIS PAGE
Unrestricted

Document history

VERSION	DATE	VERSION DESCRIPTION
1.0	2019-02-21	

Table of contents

Detailed programme	6
List of participants	10
Scientific Committee and Conference Chairs	15
Opening Session – Frontiers of Science and Technology	
Opening:	
Welcome to EERA DeepWind, John Olav Tande, SINTEF Energi	17
EERA Deepwind 2019, Trond Kvamsdal, NTNU.....	18
Cooperation on offshore wind: DTU president Anders Overgaard Bjarklev, NTNU rector Gunnar Bovim and SINTEF CEO Alexandra Bech Gjørsv	
Collaboration on Offshore Wind Energy R&I, Peter Hauge Madsen, DTU.....	20
Horizon 2020 Work Programme for Research & Innovation 2018 – 2020, Nuno Quental, EU	21
Experiences from Hywind Scotland and The Way Forward for Floating Offshore Wind Jon Barrat Nysæter, Hywind at Equinor.....	26
Floating offshore wind, Tor-Eivind Moen, ABB, Einar Wilhelmsen, Zero.....	29
North Sea Energy Infrastructure: Status and outlook, Patrick Peapers, TenneT	31
A1 New turbine and generator technology	
The X-Rotor Offshore Wind Turbine Concept, W.Leithead, Strathclyde University	37
Comparison of the capacity factor of stationary wind turbines and weather-routed energy ships in the far-offshore, J.Roshamida, LHEEA, Ecole Centrale de Nantes	40
Development of coupling module between BHawC aeroelastic software and OrcaFlex for coupled dynamic analysis of floating wind turbines, V.Arramounet, INNNOSEA	43
A new approach for comparability of two- and three-bladed 20 MW offshore wind turbines, F.Anstock, Hamburg University of Applied Science	46
A2 New turbine and generator technology	
Damping analysis of a floating hybrid wind and ocean-current turbine, S.V.Kollappillai Murugan, Halmstad University.....	49
On Design and Modelling of 10 MW Medium Speed Drivetrain for Bottom-Fixed Offshore Wind Turbines, S.Wang, NTNU	51
Modelling the dynamic inflow effects of floating vertical axis wind turbines, D.Tavernier, Delft University of Technology	55
B1 Grid connection and power system integrating	
Power quality in offshore grids, E.Tedeschi, NTNU.....	61
Reducing Rapid Wind Farm Power Fluctuations Using Energy Storage of the Modular Multilevel Converter, S.Sanchez, NTNU	66
An Improved and Expanded Fault Detection and Clearing Strategy Application to a Hybrid Wind Farm integrated to a Hybrid HVDC Main Transmission Level Converter, J.K.Amoo-Otoo, Univ Idaho .	72
Prolonged Response of Offshore Wind Power Plants to DC Faults, Ö.Göksu, DTU.....	82

B2 Grid connection and power system integrating

Control challenges for grid integration, N.Cutululis, DTU.....	85
Heuristics-based design and optimization of offshore wind farms collection systems, J.A.Pérez-Rúa, DTU	89
Resonance Characteristics in Offshore Wind Power Plants with 66 kV Collection Grids, A. Holdyk, SINTEF Energi	94

C1 Met-ocean conditions

The Influence of Unstable Atmospheric Conditions on the Motions and Loads on a Floating Wind Turbine, R.M.Putri, University of Stavanger	98
Using Machine Learning Methods to find a Representative and Conservative Set of Conditions for Fatigue Analysis of Offshore Wind Turbines, S.Kanner, Principle Power Inc.....	101
Processing of sonic measurements for offshore wind turbine relevance, A.Nybø, Univ Bergen	107
Uncertainties in offshore wind turbulence intensity, S.Caires, Deltares	112

C2 Met-ocean conditions

COTUR - estimating the Coherence of TURbulence with wind lidar technology M. Flügge, NORCE.....	115
Towards a high-resolution offshore wind Atlas - The Portuguese Case, T.Simões, LNEG	119
The DeRisk design database: extreme waves for Offshore Wind Turbines, F.Pierella, DTU	124

D1 Operations & maintenance

Evaluation and Mitigation of Offshore HVDC Valve Hall Magnetic and Electric Field Impact on Inspection Quadcopter, M.Heggo, Univerity of Manchester.....	131
Piezoelectric Patch Transducers: Can alternative sensors enhance bearing failure prediction? L.Schilling, Hamburg University	136
Excluding context by means of fingerprint for wind turbine condition monitoring, K.López de Calle, IK4-TEKNIKER	139
Condition monitoring by use of time domain monitoring and pattern recognition, A.Barikmo, VibSim.....	144

D2 Operatons & maintenance

Drivetrain technology trend in multi megawatt offshore wind turbines considering design, fabrication, installation and operation, F.K.Moghadam, NTNU.....	148
Recommended Key Performance Indicators for Operational Management of Wind Turbines, S.Pfaffel, Fraunhofer IEE	151


E1 Installation and sub-structures

Fatigue sensitivity to foundation modelling in different operational states for the DTU 10MW monopile-based offshore wind turbine, G.Katsikogiannis, NTNU.....	155
Integrated Project Logistics and Costs Calculation for Gravity Based Structure, N.Saraswati, TNO	160

E2 Installation and sub-structures

Upscaling and levelised cost of energy for offshore wind turbines supported by semi-submersible floating platforms, Y.Kikuchi, University of Tokyo	166
Wave Cancelling Semi-Submersible Design for Floating Offshore Wind Turbines, Wei Yu, University of Stuttgart	169

Summary of LIFES50+ project results: from the Design Basis to the floating concepts	
Industrialization, G.Pérez, TECNALIA	173
F Wind farm optimization	
Analysis of wake effects on global responses for a floating two-turbine case, A.Wise, NTNU	180
Effect of Wake Meandering on Aeroelastic Response of a Wind Turbine Placed in a Park, B.Panjwani, SINTEF	183
Effect of wind flow direction on the loads at wind farm, R.Kzacoks, Strathclyde Univ.	187
How Risk Aversion Shapes Overplanting in Offshore Wind Farms, E.B.Mora, EDF Energy R&D	189
G1 Experiment testing and validation	
Experimental modal analysis of aeroelastic tailored rotor blades in different boundary conditions, J.Gundlach, German Aerospace Center	193
Low-frequency second-order drift-forces experimental validation for a Twin Hull Shape Offshore Wind Platform – SATH, A.M.Rubio, Saitec Offshore Technologies	202
Numerical prediction of hydrodynamic coefficients for a semi-sub platform by using large eddy simulation with volume of fluid method and Richardson extrapolation method, J.Pan, University of Tokyo	206
Assessment of Experimental Uncertainty in the Hydrodynamic Response of a Floating Semi- submersible, Including Numerical Propagation of Systematic Uncertainty, A.Robertson, NREL	209
G2 Experimental testing and validation	
A review of heave plate hydrodynamics for use in floating offshore wind sub-structures, K.Thiagarajan, University of Massachusetts	214
Variable-speed Variable-pitch control for a wind turbine scale model, F.Taruffi, Politecnico di Milan	219
Experimental Investigation of a Downwind Coned Wind Turbine Rotor under Yawed Conditions, C.W.Schulz, Hamburg University	222
H Wind farm control systems	
A survey on wind farm control and the OPWIND way forward, L.E.Andersson, NTNU	227
Hierarchy and complexity in Control of large Offshore Wind Power Plant Clusters A.Kavimandan, DTU.....	231
Verification of Floating Offshore Wind Linearization Functionality in OpenFAST, J. Jonkman, NREL	234
Closing session - Strategic Outlook	
The way forward for offshore wind, A. Cronin, Chair ETIPWind.....	238
Real time structural analyses of wind turbines enabled by sensor measurements and Digital Twin models, M.Graczyk, SAP Norway, Engineering Center of Excellence	243
EERA DeepWind'2019 – Closing, J.O.Tande, SINTEF Energi.....	249
Posters	250



EERA DeepWind'2019

16th Deep Sea Offshore Wind R&D Conference,

Trondheim, 16 - 18 January 2019


Wednesday 16 January		
09.00	Registration & coffee	
	Opening session – Frontiers of Science and Technology Chairs: John Olav Tande, SINTEF and Trond Kvamsdal, NTNU	
09.30	Opening and welcome by chair	
09.40	Cooperation on offshore wind, DTU president Anders Overgaard Bjarklev, NTNU rector Gunnar Bovim, and SINTEF CEO Alexandra Bech Gjørv	
10.00	Nuno Quental, Policy Officer, European Commission, DG Research and Innovation	
10.30	Experiences from Hywind Scotland and the way forward for floating offshore wind, Jon Barratt Nysæther, Technology Manager, Hywind at Equinor	
11.00	A vision for offshore wind in Norway, Tor-Eivind Moen, VP market development new energy, ABB and Einar Wilhelmsen, Zero	
11.30	North Sea Energy Infrastructure: status and outlook; Patrick Piepers, head of Asset Management Offshore, Tennet	
11.55	Closing by chair	
12.00	Lunch	
	Parallel sessions	
	A1) New turbine and generator technology Chairs: Karl Merz, SINTEF Energi Prof Gerard van Bussel, TU Delft	C1) Met-ocean conditions Chairs Joachim Reuder, Univ of Bergen, Erik Berge, Meteorologisk institutt
13.00	Introduction by Chair	Introduction by Chair
13.05	The X-Rotor Offshore Wind Turbine Concept, W.Leithead, University of Strathclyde	The Influence of Unstable Atmospheric Conditions on the Motions and Loads on a Floating Wind Turbine, R.M.Putri, University of Stavanger
13.30	Comparison of the capacity factor of stationary wind turbines and weather-routed energy ships in the far-offshore, J.Roshamida, LHEEA, Ecole Centrale de Nantes	Representative Selection of a Set of Environmental Conditions for Fatigue Analysis of Floating Offshore Wind Platforms, S.Kanner, Principle Power Inc.
13.50	Development of coupling module between BHawC aeroelastic software and OrcaFlex for coupled dynamic analysis of floating wind turbines, V.Arramounet, INNOSEA	Processing of sonic measurements for offshore wind turbine relevance, A. Nybø, Univ in Bergen
14.10	A new approach for comparability of two- and three-bladed 20 MW offshore wind turbines, F.Anstock, Hamburg University of Applied Science	Uncertainties in offshore wind turbulence intensity, S.Caires, Deltares
14.30	Closing by Chair	Closing by Chair
14.35	Refreshments	
	A2) New turbine and generator technology (cont.)	C2) Met-ocean conditions (cont.)
15.05	Introduction by Chair	Introduction by Chair
15.10	Damping analysis of a floating hybrid wind and ocean-current turbine, S.V.Kollappillai Murugan, Halmstad University	COTUR - estimating the Coherence of TURbulence with wind lidar technology, M.Flügge, NORCE Technology
15.30	On Design and Modelling of 10 MW Medium Speed Drivetrain for Bottom-Fixed Offshore Wind Turbines, S.Wang, NTNU	Towards a high-resolution offshore wind Atlas - The Portuguese Case, T.Simões, LNEG
15.50	Modelling the dynamic inflow effects of floating vertical axis wind turbines, D.Tavernier, Delft University of Technology	The DeRisk design database: extreme waves for Offshore Wind Turbines, F.Pierella, DTU
16.10	Closing by Chair	Closing by Chair
18.00	Conference reception 18.10 Nidaros Cathedral Boy's Choir – Nidaros Cathedral 18.45 Reception at restaurant To Tårn	

EERA DeepWind'2019

16th Deep Sea Offshore Wind R&D Conference,

Trondheim, 16 - 18 January 2019

Thursday 17 January		
Parallel sessions		
	D1) Operation & maintenance Chairs: Thomas Welte, SINTEF Energi Sebastian Pfaffel, Fraunhofer IEE	E1) Installation and sub-structures Chairs: Arno van Wingerde, Fraunhofer IWES, Prof. Michael Muskulus, NTNU
09.00	Introduction by Chair	Introduction by Chair
09.05	Evaluation and Mitigation of Offshore HVDC Valve Hall Magnetic and Electric Field Impact on Inspection Quadcopter, M. Heggo, University of Manchester	Fatigue sensitivity to foundation modelling in different operational states for the DTU 10MW monopile-based offshore wind turbine, G. Katsikogiannis, NTNU
09.30	Piezoelectric Patch Transducers: Can alternative sensors enhance bearing failure prediction? L. Schilling, Hamburg University	Ultra-High Performance Concrete Lightweight Jackets, J.Markowski, Leibniz Univ Hannover
09.50	Excluding context by means of fingerprint for wind turbine condition monitoring, K. López de Calle, IK4-TEKNIKER	Integrated Project Logistics and Costs Calculation for Gravity Based Structure, N.Saraswati, TNO
10.10	Condition monitoring by use of time domain monitoring and pattern recognition, Aasmund Barikmo, VibSim	Effects of wind-wave misalignment on a wind turbine blade mating process, A.S.Verma, NTNU
10.30	Refreshments	
	D2) Operation & maintenance (cont.)	E2) Installation and sub-structures (cont.)
11.00	Drivetrain technology trend in multi megawatt offshore wind turbines considering design, fabrication, installation and operation, F. K. Moghadam, NTNU	Upscaling and levelised cost of energy for offshore wind turbines supported by semi-submersible floating platforms, Y.Kikuchi, Univ of Tokyo
11.20	Operation & Maintenance Planning of Floating Offshore Wind Turbines using Stochastic Petri Networks, O.Adedipe, Cranfield University	Wave Cancelling Semi-Submersible Design for Floating Offshore Wind Turbines, Wei Yu, University of Stuttgart
11.40	Recommended Key Performance Indicators for Operational Management of Wind Turbines, S. Pfaffel, Fraunhofer IEE	Summary of LIFES50+ project results: from the Design Basis to the floating concepts industrialization, G.Pérez, TECNALIA
12.00	Closing by Chair	Closing by Chair
12.05	Lunch	
	B1) Grid connection and power system integration Chair: Prof Olimpo Anaya-Lara, Strathclyde University Salvatore D'Arco, SINTEF Energi	G1) Experimental Testing and Validation Chairs: Luca Oggiano, IFE, Marit Kvittem, SINTEF Ocean, Amy Robertson, NREL
13.05	Introduction by Chair	Introduction by Chair
13.10	Power quality in offshore grids; Prof. Elisabetta Tedeschi, NTNU	Experimental modal analysis of aeroelastic tailored rotor blades in different boundary conditions, J.Gundlach, German Aerospace Center
13.35	Reducing Rapid Wind Farm Power Fluctuations Using Energy Storage of the Modular Multilevel Converter, S.Sanchez, NTNU	Low-frequency second-order drift-forces experimental validation for a Twin Hull Shape Offshore Wind Platform – SATH, A.M.Rubio, Saitec Offshore Technologies
13.55	An Improved and Expanded Fault Detection and Clearing Strategy Application to a Hybrid Wind Farm integrated to a Hybrid HVDC Main Transmission Level Converter, J.K. Amoo-Otoo	Numerical prediction of hydrodynamic coefficients for a semi-sub platform by using large eddy simulation with volume of fluid method and Richardson extrapolation method, J.Pan, Univ Tokyo
14.15	Prolonged Response of Offshore Wind Power Plants to DC Faults, Ö. Göksu, DTU	Assessment of Experimental Uncertainty in the Hydrodynamic Response of a Floating Semisubmersible, Including Numerical Propagation of Systematic Uncertainty, A.Robertson, NREL
14.35	Refreshments	
	B2) Grid connection and power system integration (cont.)	G2) Experimental Testing and Validation (cont.)
15.05	Control challenges for grid integration; Nikos Cutululis, DTU	A review of heave plate hydrodynamics for use in floating offshore wind sub-structures, K. Thiagarajan, University of Massachusetts
15.25	Design and Build of a Grid Emulator for Full Scale Testing of the Next Generation of Wind Turbines, Chong Ng, ORE Catapult	Variable-speed Variable-pitch control for a wind turbine scale model, F.Taruffi, Politecnico di Milano
15.45	Heuristics-based design and optimization of offshore wind farms collection systems, J.A. Pérez-Rúa, DTU	Experimental Investigation of a Downwind Coned Wind Turbine Rotor under Yawed Conditions, C.W.Schulz, Hamburg University
16.05	Resonance Characteristics in Offshore Wind Power Plants with 66 kV Collection Grids, A.Holdyk, SINTEF	Enhanced Yaw Stability of Downwind Turbines, H.Hoghooghi, ETH Zürich
16.25	Closing by Chair	Closing by Chair
16.30	Refreshments	
17.00	Poster session	
19.00	Conference dinner	



EERA DeepWind'2019

16th Deep Sea Offshore Wind R&D Conference, Trondheim, 16 - 18 January 2019

Thursday 17 January

17.00 | Poster Session with refreshments

Session A

1. Electrical Collector Topologies for Multi-Rotor Wind Turbine Systems, I.H. Sunde, NTNU

Session B

2. Virtual Synchronous Machine Control for Wind Turbines: A Review, L. Lu, DTU
3. Use of energy storage for power quality enhancement in wind-powered oil and gas applications, E.F.Alves, NTNU-IEL

Session C

4. The OBLO infrastructure project – measurement capabilities for offshore wind energy research in Norway, M. Flügge, NORCE Technology
5. Abnormal Vertical Wind Profiles at a Mid-Norway Coastal Site, M. Møller, NTNU
6. Wind power potential and benefits of interconnected wind farms on the Norwegian Continental Shelf, I.M. Solbrekke, UiB
7. Wind conditions within a Norwegian fjord, Z. Midjiyawa, NTNU

Session D

8. Experimental study of structural resonance in wind turbine's bearing fault detection, M.A. Rasmussen, NTNU
9. New coatings for leading edge erosion of turbine blades, A. von Bonin, NTNU

Session E


10. Mooring System Design for the 10MW Triple Spar Floating Wind Turbine at a 180 m Sea Depth Location, J.Azcona, CENER
11. Consideration of the aerodynamic negative damping in the design of FWT platforms, C.E. Silva de Souza, NTNU
12. Hydrodynamic Loads on a Floating Spar Offshore Wind Turbine Using Relaxation and Impulse Wave Generation Methods, A.Moghtadaei, Queen's University Belfast
13. Code-to-code comparison of hydrodynamic loads on a tension-leg platform wind turbine in regular waves using OpenFOAM and FAST, H.S. Brede, Queen's University Belfast
14. Wind-Wave Directional Effects on Fatigue of Bottom-Fixed Offshore Wind Turbine, S.H.Sørum, NTNU
15. Numerical Study of Load Effects On Floating Wind Turbine Support Structures, S.Okpokparoro, University of Aberdeen
16. Conceptual Design of a 12 MW Floating Offshore Wind Turbine in the Ulsan Offshore Area, Korea, P.T.Dam, University of Ulsan
17. Motion Performances of 5-MW Floating Offshore Wind Turbines under Combined Environmental Conditions in the East Sea, Korea, Y.Yu, University of Ulsan
18. Influence of ballast material on the buoyancy dynamics of cylindrical floaters of FOWT, C.Molins, UPC-BarcelonaTech
19. Hydrodynamic analysis of a novel floating offshore wind turbine, W.Shi, Dalian University of Technology
20. A tool to simulate decommissioning Offshore Wind Farms, C. Desmond, University College Cork
21. Identification of distributed beam properties from shell models for finite element analysis of offshore wind turbine structures, B.Hofmeister, Leibniz University Hannover
22. Code-to-Code Comparison of Numerical Integrated Models of the 10MW Telwind Floating Wind Turbine, J.Azcona, CENER
23. Can cloud computing help bend the cost curve for FOWTs? P.E.Thomassen, Simis AS
24. Performance study for a simplified floating wind turbine model across various load cases, F.J.Madsen, DTU
25. Simulation Methods for Floating Offshore Wind Turbine Farms with Shared Moorings, P.Connolly, University of Prince Edward Island
26. Spatial met-ocean data analysis for the North Sea using copulas: application in lumping of offshore wind turbine fatigue load cases, A. Koochekali, NTNU
27. Numerical design concept for axially loaded grouted connections under submerged ambient conditions, P.Schaumann, Leibniz University Hannover, ForWind

Session F

28. Collection Grid Optimization of a Floating Offshore Wind Farm Using Particle Swarm Theory, M.Lerch, IREC
29. Investigating the influence of tip vortices on deflection phenomena in the near wake of a wind turbine model, L.Kuhn, Technical University Berlin

(The list of posters continues at the next page.)

19.00 | Dinner



EERA DeepWind'2019

16th Deep Sea Offshore Wind R&D Conference, Trondheim, 16 - 18 January 2019

Thursday 17 January

17.00 Poster Session with refreshments (cont.)

Session G

- 30. On the effect of hydrodynamic modelling on the response of a floating offshore wind turbine with flexible platform, S. OH, ClassNK
- 31. Implementation of potential flow hydrodynamics to time-domain analysis of flexible platforms of floating offshore wind turbines, S. OH, ClassNK
- 32. Validation against at-sea data of Bladed numerical model of a 2MW wind turbine on an Ideol floating platform, A.Alexandre, DNV GL
- 33. The physical representation of a catenary mooring system for floating wind energy platforms in a laboratory environment, C.Desmond, University College Cork
- 34. Validating numerical predictions of floating offshore wind turbine structural frequencies in Bladed using measured data from Fukushima Hamakaze, H.Yoshimoto, Japan Marine United Corporation
- 35. Prediction of dynamic response of a semi-submersible floating offshore wind turbine in combined wave and current condition by a new hydrodynamic coefficient model, Y.Liu, University of Tokyo
- 36. Sensitivity of the natural frequency of fixed offshore wind turbines to variations in site conditions, E.Petrovska, University of Edinburgh
- 37. The experimental investigation of the TELWIND second loop platform, T.Battistella, IH Cantabria
- 38. Model validation through scaled tests comparisons of a semi-submersible 10MW floating wind turbine with active ballast, R.F.Guzmán, University of Stuttgart

Session H

- 39. Linear dynamics and modal analysis of a wind turbine array, K.Merz, SINTEF

19.00 Dinner

Friday 18 January

Parallel sessions		
	H) Wind farm control systems Chairs: Karl Merz, SINTEF Energi Prof Olimpo Anaya-Lara, Strathclyde University	F) Wind farm optimization Chairs: Yngve Heggelund, NORCE Henrik Bredmose, DTU Wind Energy
09.00	Introduction by Chair	Introduction by Chair
09.05	Development of the Hywind Concept, Bjørn Skaare, Equinor	Analysis of wake effects on global responses for a floating two-turbine case, A. Wise, NTNU
09.25	A survey on wind farm control and the OPWIND way forward, Leif Erik Andersson, NTNU	Effect of Wake Meandering on Aeroelastic Response of a Wind Turbine Placed in a Park, B. Panjwani, SINTEF
09.45	Hierarchy and complexity in Control of large Offshore Wind Power Plant Clusters, A. Kavimandan, DTU	Effect of wind flow direction on the loads at wind farm, R. Kazacoks, Strathclyde University
10.05	Verification of Floating Offshore Wind Linearization Functionality in OpenFAST, J. Jonkman, NREL	How Risk Aversion Shapes Overplanting in Offshore Wind Farms, E.B. Mora, EDF Energy R&D
10.25	Closing by Chair	Closing by Chair
10.30	Refreshments	
	Closing session – Strategic Outlook Chairs: John Olav Tande, SINTEF and Michael Muskulus, NTNU	
11.00	Introduction by Chair	
11.05	The way forward for offshore wind, Aidan Cronin, chair ETIPwind	
11.35	Next Generation Offshore Wind Turbines; Dr. Fabian Vorpahl, Leading Expert Offshore & Loads, Senvion GmbH	
12.05	Real time structural analyses of wind turbines enabled by sensor measurements and Digital Twin models, M. Graczyk, SAP Norway Engineering Center of Excellence	
12.35	Poster award and closing	
13.00	Lunch	

Side event: IEA Wind Task 30 Offshore Code Comparison Collaboration, Continued with Correlation and unCertainty (OC6) Project.
1st Full Committee Meeting. January 18, 2019. 9:00 – 17:00. Meeting Room is upstairs from where the conference sessions are held.



Last Name	First name	Company
ABD JAMIL	Roshamida	Ecole Centrale de Nantes
Abelsen	Atle	
Adedipe	Oluwatosin	Cranfield University
Alveberg	Hans-Kristian	Seatower AS
Alves	Erick	NTNU-IEL
Amoo-Otoo	John Kweku	Saudi Aramco
Anaya-Lara	Olimpo	Strathclyde University
Andersson	Leif Erik	NTNU
Anstock	Fabian	Hamburg University of Applied Science
Arramounet-Laborbe	Valentin	INNOSEA
Ashok	Anand	Maritime Research Institute Netherlands (MARIN)
Azcona	Jose	CENER
Bachynski	Erin	NTNU
Badger	Jake	DTU Wind Energy
Barikmo	Aasmund	VibSim AS
Battistella	Tommaso	FUNDACION INSTITUTO DE HIDRAULICA AMBIENTAL
Berge	Erik	Meteorologisk institutt
Berthelsen	Petter Andreas	SINTEF Ocean
Borras Mora	Esteve	University of Edinburgh and EDF Energy R&D UK Centre
Bottasso	Carlo L.	Technical University of Munich
Bredmose	Henrik	DTU
Cai	Zhisong	China General Certification
Caires	Sofia	Deltares
Capelli	Flaminia Riccioni	EERA
Castro Casas	Natalia	D-ICE Engineering
Chabaud	Valentin	NTNU
Cheyne	Etienne	University of Stavanger
Connolly	Patrick	University of Prince Edward Island
Cronin	Aidan	ETIPwind
Cutululis	Nicolaos A.	DTU Wind Energy
D'Arco	Salvatore	SINTEF Energi
De Tavernier	Delphine	TU Delft
De Vaal	Jabus	NTNU
De Winter	Corine	Siemens Gamesa
Desmond	Cian	University College Cork, MaREI
Domagalski	Piotr	Lodz Univ
Donnelly	Glen	ECN.TNO
Dragsten	Gunder Audun	LLoyd's Register
Eecen	Peter	ECN part of TNO



Eliassen	Lene	SINTEF Ocean
Espvik	Joachim	Stud NTNU
Faerron	Ricardo	Stuttgart Wind Energy
Flügge	Martin	NORCE Norwegian Research Centre
Gao	Zhen	NTNU
Gilloteaux	Jean-Christophe	Centrale Nantes
Goldberg	Mats	RISE, Research Institutes of Sweden AB
Gonzales	Elena	Oreseide Renewable Energy
Graczyk	Mateusz	SAP Norway Engineering Center of Excellence
Guldbrandsen	Susanne	Stud NTNU
Gundlach	Janto	German Aerospace Center (DLR)
Göksu	Ömer	DTU Wind Energy
Halse	Karl H.	NTNU
Hanssen-Bauer	Øyvind Waage	IFE
Haudin	Florence	Vulcain Ingénierie
Heggelund	Yngve	NORCE
Heggo	Mohammad	University of Manchester
Hjelmstad	Ole Petter	Ægir Harvest AS
Hoghooghi	Hadi	ETH Zurich
Holdyk	Andrzej	SINTEF Energi
Høiland	Knut	Rosenberg WorleyParsons AS
Ishihara	Takeshi	The Univ.of Tokyo
Jakobsen	Jasna Bogunovic	University of Stavanger
Jingzhe	Jin	SINTEF Ocean
Johanning	Lars	University of Exeter
Jonkman	Jason	National Renewable Energy Laboratory (NREL)
Kanner	Samuel	Principle Power Inc
Karl	Christian	Leibniz University Hannover/ForWind
Karlsen	Benjamin	Stud NTNU
Katsikogiannis	George	NTNU
Kavimandan	Anup	Technical University of Denmark, DTU Wind Energy
Kazacoks	Romans	University of Strathclyde_EEE/WECC
Khazaeli Moghaddam	Farid	NTNU
Kikuchi	Yuka	The Univ.of Tokyo
Kollappillai Murugan	Sai Varun	Uppsala University
Koochekali	Alahyar	NTNU
Korsgaard	John	LM Wind Power A/S
Kuchma	Daniel	Tufts University
Kuhn	Ludwig	NTNU
Kullandairaj	George Paul	TechnipFMC
Kvamsdal	Trond	NTNU
Kvittem	Marit	SINTEF Ocean



Kölle	Konstanze	SINTEF Energi
Le Dreff	Jean-Baptiste	EDF R&D
Leithead	William	University of Strathclyde
Lerch	Markus	IREC - FUND. INST. RECERCA ENERGIA CATALUNYA
Liu	Yuliang	The Univ. of Tokyo
Liu	Yongqian	North China Electric Power University
López de Calle	Kerman	IK4-TEKNIKER
Lu	Liang	Technical University of Denmark
Mackay	Edward	University of Exeter
Madsen	Freddy	DTU Wind Energy
Madsen	Peter Hauge	DTU Wind Energy
Maljaars	Nico	Siemens Gamesa Renewable Energy
Markowski	Jan	Institute of Building Materials Science / Leibniz Universität Hannover
Marti	Ignacio	DTU Wind Energy
Martínez Rubio	Araceli	Saitec Offshore Technologies, S.L.
Masuda	Katsumi	Tokyo electric power company holdings
Mathew	Sathyajith	University of Agder
Mawarni Putri	Rieska	Universitetet i Stavanger
McKeever	Paul	ORE Catapult
Merz	Karl	SINTEF Energi
Midtbø	Knut Helge	Meteorologisk Institutt
Mochet	Clement	Vryhof
Moen	Tor-Eivind	ABB
Molins	Climent	Universitat Politècnica de Catalunya
Morin	Nicolas	SAP Norway Engineering Center of Excellence
Murata	Junsuke	Wind Energy Institute of Tokyo
Muskulus	Michael	NTNU
Myklebust	Skjalg	Leirvik AS
Møller	Mathias	NTNU
Nejad	Amir	NTNU
Neshaug	Vegar	Fugro Norway AS, avd. Trondheim
Ng	Chong	ORE Catapult
Nguyen	Minh Quan	Vulcain Ingénierie
Nicholson	Eoin	Mainstream Renewable Power
Nysæther	Jon Barratt	Equinor
Nishikouri	Kazumasa	Japan
Nybø	Astrid	University of Bergen
Obhrai	Charlotte	University of stavanger
Oggiano	Luca	IFE
Oh	Sho	ClassNK
Okpokparoro	Salem	UNIVERSITY OF ABERDEEN



Opseth	Kurt	Kleon AS
Otterå	Geir Olav	Leirvik AS
Page	Ana	Norwegian Geotechnical Institute (NGI)
Paillard	Benoit	Eolfi
Pan	Jia	The Univ.of Tokyo
Panjwani	Balram	SINTEF
Pathirana	Irene	Fugro Norway AS, OCEANOR
Perez Moran	German	TECNALIA
Pérez-Rúa	Juan-Andrés	DTU Department of Wind Energy
Pettinotti	Matthieu	EOLFI
Pfaffel	Sebastian	Fraunhofer IEE
Pham	Thanh Dam	University of Ulsan
Philippe	Gilbert	IFPEN
Piepers	Patrick	Tennet
Pierella	Fabio	DTU Wind Energy
Pillai	Ajit	University of Exeter
Popko	Wojciech	Fraunhofer IWES
Potestio	Sabina	WindEurope
Quental	Nuno	European Commission
Rasmussen	Morten Aleksander	MainTech AS
Reiso	Marit	SAP Norway Engineering Center of Excellence
Reuder	Joachim	Universitet of Bergen
Robertson	Amy	National Renewable Energy Laboratory
Rogier	Etienne	IDEOL
Sanchez	Santiago	NTNU
Saraswati	Novita	TNO
Sato	Koya	TEPCO
Schaumann	Peter	Leibniz University Hannover Inst for Steel Construction
Schilling	Levin	HAW Hamburg
Schmitt	Pal	Queen's University Belfast
Schouten	Jan-Joost	Deltares
Schramm	Rainer	Subhydro AS
Schulz	Christian	Technische Universität Hamburg (TUHH)
Schünemann	Paul	Universität Rostock
Schütt	Marcel	Hamburg University of Applied Science
Shi	Wei	Dalian University of Technology
Shin	Hyunyoung	University of Ulsan
Silva de Souza	Carlos Eduardo	NTNU
Simões Esteves	Teresa	LNEG - Laboratório Nacional de Energia e Geologia, I.P.
Skaare	Bjørn	Equinor
Smilden	Emil	Equinor



Solaas	Frøydis	SINTEF Ocean
Sølbrekke	Ida Marie	University in Bergen
Steen	Knut Erik	Norwegian Energy Partners
Stenbro	Roy	IFE
Sterenborg	Joost	MARIN
Sunde	Ingvar Hinderaker	NTNU
Sørum	Stian Høegh	NTNU
Tande	John Olav	SINTEF Energi
Taruffi	Federico	Politecnico di Milano - Department of Mechanical Engineering
Tedeschi	Eilisabetta	NTNU
Thiagarajan Sharman	Krish	University of Massachusetts Amherst
Thomassen	Paul E.	Simis AS
Thys	Maxime	SINTEF Ocean
Toyama	Kazushi	JGC CORPORATION
Tutkun	Murat	IFE
Tveiten	Bård Wathne	SINTEF Ocean
Uchino	Keita	JGC Cooperation
Van Bussel	Gerard	TU Delft
Van Wingerde	Arno	Fraunhofer IWES
Vandenberghe	Alexander	WindEurope asbl
Vatn Tranulis	Erling	Stud NTNU
Verma	Amrit Shankar	NTNU
Vince	Florent	WEAMEC
Von Bonin	Aidan	NTNU
Vorpahl	Fabian	Senvion GmbH
Wang	Shuaishuai	NTNU
Welte	Thomas	SINTEF Energi
Wickstrom	Anders	RISE
Wigum	Hanne	Equinor
Wilhelmsen	Einar	Zero
Wise	Adam	NTNU
Yoshimoto	Haruki	Japan Marine United Corporation
Yoshinaga	Tsuyoshi	Tokyo Electric Power Company Holdings, Inc.
Yu	YoungJae	University of Ulsan
Yu	Wei	University of Stuttgart
Zakari	Midjiyawa	Meteorologisk institutt

Scientific Committee and Conference Chairs

An international Scientific Committee is established with participants from leading institutes and universities. These include:

Anaya-Lara, Olimpo, Strathclyde University
Berge, Erik, Meteorologisk institutt
Bredmose, Henrik, DTU
Busmann, Hans-Gerd, Fraunhofer IWES
D'Arco, Salvatore,, SINTEF Energi
Eecen, Peter, ECN
Heggelund, Yngve, CMR
Jørgensen, Hans Ejsing, DTU
Kvamsdal, Trond, NTNU
Leithead, William, Strathclyde University
Madsen, Peter Hauge, DTU
Merz, Karl, SINTEF Energi
Muskulus, Michael, NTNU
Nielsen, Finn Gunnar, UiB
Oggiano, Luca, IFE
Pfaffel, Sebastian, Fraunhofer IEE
Reuder, Joachim, UiB
Robertson, Amy, NREL
Rohrig, Kurt, Fraunhofer IWES
Tande, John Olav, SINTEF Energi
Van Wingerde, Arno, Fraunhofer IWES
Van Bussel, Gerard, TU Delft
Welte, Thomas, SINTEF Energi

The Scientific Committee will review submissions and prepare the programme. Selection criteria are relevance, quality and originality.

The conference chairs were:

- John Olav Giæver Tande, Chief scientist, SINTEF Energi AS
- Trond Kvamsdal, Professor NTNU
- Michael Muskulus, Professor NTNU

Opening session – Frontiers of Science and Technology

Opening and welcome by chair, John Olav Tande, SINTEF Energi

EERA DeepWind'2019, Trond Kvamsdal, NTNU

Collaboration on Offshore Wind Energy R&I, Peter Hauge Madsen, Director, DTU

Horizon 2020 Work Programme for Research and Innovation 2018 – 2020,
Nuno Quental, Policy Officer, European Commission, DG Research and Innovation

Experiences from Hywind Scotland and the way forward for floating offshore wind,
Jon Barratt Nysæther, Technology Manager, Hywind at Equinor

Floating offshore wind,
Tor-Eivind Moen, VP market development new energy, ABB, and Einar Wilhelmsen, Zero

North Sea Energy Infrastructure: status and outlook,
Patrick Piepers, head of Asset Management Offshore, TenneT



Welcome to EERA DeepWind

John Olav Giæver Tande
Conference chair, Chief scientist, SINTEF Energy Research

Trond Kvamsdal
Conference co-chair, Professor NTNU







EERA JP WIND - a vehicle for collaboration

- EERA is an organisation under the EU SET-Plan
- EERA JP WIND is one of 18 Joint Programmes
- 50 member organisations
- Building trust & knowledge exchange
- Vision: To be the globally leading R&D community in wind energy
- Mission: Build and maintain a world-class wind energy research and innovation community in Europe




EERA JP WIND OBJECTIVES

1. **Strategic leadership** in prioritizing and promoting research at TRL 1-5 and working with Industry to coordinate research priority setting at higher TRLs towards the European and national policy makers
2. Enhance **knowledge sharing** through joint events and communication platforms
3. Coordinate dedicated **mobility programmes** for researchers to increase collaboration through dedicated mobility programmes
4. **Sharing infrastructures** to improve the efficiency of use and easy of access of state of the art infrastructure
5. **Enable data sharing and management** in accordance with the European Commission's F.A.I.R principles







EERA JP WIND

Lean. Transparent. Independent.

EERA JP WIND is organised in eight sub-programme:

- SP1: Programme planning and outreach – Peter Eecen, ECN part of TNO
- SP2: Research Infrastructure, testing and standards – Paul McKeever, ORE Catapult
- SP3: Wind conditions and climatic effects – Jake Badger, DTU
- SP4: Aerodynamics, loads and control – Xabier Munduate, CENER
- SP5: System integration – Nicolaos Cutululis, DTU
- SP6: Offshore Balance of Plant – John Olav Tande, SINTEF
- SP7: Structures, materials and components – Arno van Wingerde, Fraunhofer IWES
- SP8: Planning & Deployment, social, environmental and economic issues – Lena Kitzing, DTU

Wednesday 16 January		
09.00	Registration & coffee	
	Opening session – Frontiers of Science and Technology Chairs: John Olav Tande, SINTEF and Trond Kvamsdal, NTNU	
09.30	Opening and welcome by chair	
09.40	Cooperation on offshore wind, DTU president Anders Overgaard Bjarklev, NTNU rector Gunnar Bovim, and SINTEF CEO Alexandra Bech Gjør	
10.00	Nuno Quental, Policy Officer, European Commission, DG Research and Innovation	
10.30	Experiences from Hywind Scotland and the way forward for floating offshore wind, Jon Barratt Nysæther, Technology Manager, Hywind at Equinor	
11.00	A vision for offshore wind in Norway, Tor-Eivind Moen, VP market development new energy, ABB and Einar Wilhelmssen, Zero	
11.30	North Sea Energy Infrastructure: status and outlook, Patrick Piepers, head of Asset Management Offshore, Tennet	
11.55	Closing by chair	
12.00	Lunch	
	Parallel sessions	
13.00	A1) New turbine and generator technology	C1) Met-ocean conditions
16.15	Chairs: Karl Merz, SINTEF Energi Prof Gerard van Bussel, TU Delft Conference reception	Chairs Joachim Reuder, Univ of Bergen, Erik Berge, Meteorologisk institutt
18.00	18.10 Nidaros Cathedral Boy's Choir – Nidaros Cathedral 18.45 Reception at restaurant To Tårn	



EERA Deepwind 2019

Mission: Accelerate deployment of large scale offshore wind parks

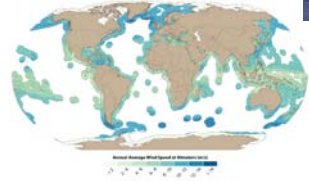
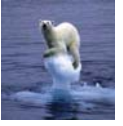
Trond Kvamsdal
Professor NTNU

Page 1

Offshore wind is vital for reaching climate targets

- ✓ Currently small compared to onshore wind, but in strong growth
- ✓ Potential to supply 192 800 TWh/y, i.e. ~8 times the global el generation in 2014
- ✓ Can be deployed in proximity to big urban centres
- ✓ Provide long-term security of supply of clean energy
- ✓ Create new employment and industries
- ✓ Low negative environmental impact (WWF)

Stern Review (2006):
..strong, early action on climate change far outweigh the costs of not acting.



Acem, D. et al (2012) Improved Offshore Wind Resource Assessment in Global Climate Stabilization Scenarios. Technical Report, NREL/TP-6A20-55049

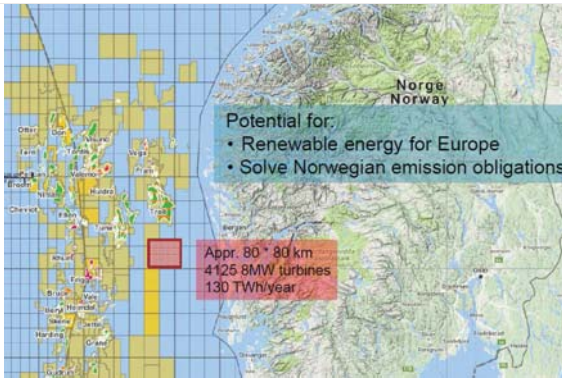
Page 2

Potential put into context

Norwegian hydropower:
130 TWh/year

Courtesy:
Finn G. Nielsen, UiB

Page 3

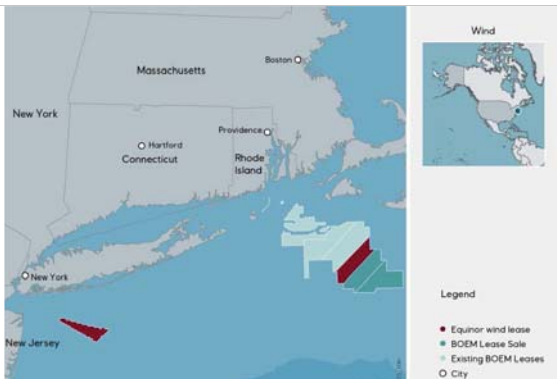


Update since last EERA Deepwind

Page 4

Equinor US OW-Licenses

2017: Empire Wind (\$43 M)
2018: OCS-A (\$135 M)
Power to 2 million homes



Page 5

Offshore wind is in an exciting development

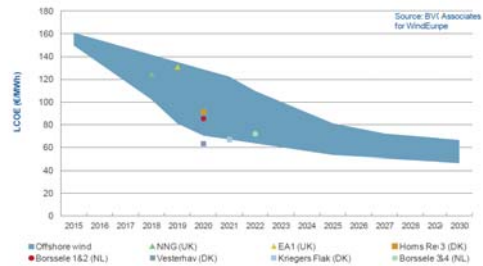


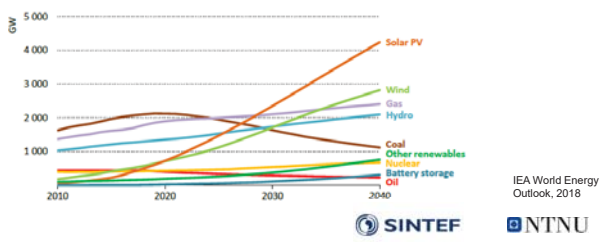
Figure 6. Projected evolution of the LCOE of offshore wind energy in Europe from 2022 to 2030.

Page 6

Wind power largest energy provider in 2040

Wind power (onshore and offshore) becomes the second-largest technology in terms of capacity, with more than 2 800 GW in 2040.

Figure 9.23 Total power generation capacity in the Sustainable Development Scenario



Deployment of large scale offshore wind parks: A great science and engineering challenge!



Collaboration on Offshore Wind Energy R&I

Peter Hauge Madsen
Director, DTU Wind Energy



Complementary competence profiles

DTU

Globally leading in wind energy research including wind turbine loads and control, aerodynamics, and resource assessment

Operating three wind turbine test sites in Denmark and several large test facilities. PhD and MSc education

Total staff of about 5900: incl. approx. 1200 PhD students

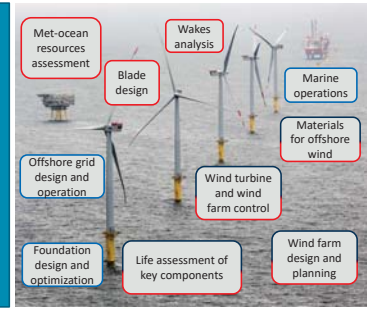
SINTEF & NTNU

Strong competence on offshore wind technology, including substructures, O&M, materials, grid connection and control

Relevant laboratories include ocean basin, smart grids and wind tunnel

PhD and MSc education

Total staff of about 2000: SINTEF, 6900; NTNU incl. approx. 1200 PhD students



Nordic Offshore Wind R&I Centre

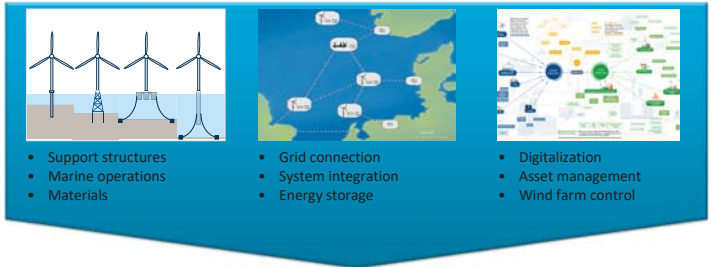
Vision: Accelerating deployment of offshore wind

Mission:

- a strong platform for academic and industrial collaboration
- focused research within prioritized areas



Research priorities



✓ New knowledge and reduced risks ✓ Innovation and value creation ✓ Reliable and affordable energy supply

Internationally outstanding together



#InvestEUresearch

European Commission

Horizon 2020 Work Programme for Research & Innovation 2018-2020

Wind energy

Nuno Quental
DG RTD – Policy Officer

Research and Innovation

Climate neutral Europe by 2050

- Europe can lead the way to **climate neutrality** by investing into **technology**, empowering citizens, and aligning action in key areas such as industrial policy, finance, or research – while ensuring social fairness for a just transition.
- 93% of Europeans believe climate change to be caused by human activity** and 85% agree that fighting climate change and using energy more efficiently can create economic growth and jobs in Europe.

THE RENEWABLE ENERGY REVOLUTION

Year	Renewable Energy %
2005	9%
2017	17%
2020	20%
2030	32%

R&D matters

- Acceleration of technological innovation** (...) can limit the risks from global warming of 1.5°C – ‘high confidence’ (IPCC, 2018, ‘Global Warming of 1.5’)
- Only **4 out of 38 energy technologies/sectors on track** to meet **long-term climate goals**, energy access and air pollution goals; 23 ‘in need of improvement.’ (IEA, 2017)
- In 2007-2014, a 4-fold rise in EU public and private R&D funding EU led to a 5-fold increase in patents filed (EC / JRC)

#H2020Energy

R&D matters

- Relatively **high spending of wind industry on R&D** (3-5% of turnover vs 2% economy-wide) probably explains EU’s leadership and positive trade balance of EUR 6 billion in 2015
- Feed-in tariffs and public R&D spending stimulate patenting activity in renewable energy technologies (OECD, 2017, ‘The empirics of enabling investment and innovation in renewable energy’ – based on more than 70 explanatory variables across multiple countries)

#H2020Energy

- Both ‘learning by doing’ (deployment) and ‘learning by searching’ (R&D) are important to achieve **cost-reductions** – R&D often more. Significant correlations also found between cumulative R&D expenditures and subsequent cost reductions (Rubin et al., 2015)

Table A2
Multi-factor learning-diffusion models for wind power.

Study	Time period	Region	Scope	Learning rates ^a
Jamasb and Kohler (2007)	1980-1998	Global	Wind farm	LBD = 13.1%, LBR = 26.8%
Klaassen et al. (2005)	1986-2000	Denmark, UK, and Germany	Wind farm	LBD = 5.4%, LBR = 12.6%
Miketa and Schratzenholzer (2004)	1979-1997	Global	Turbine	LBD = 9.73%, LBR = 10%
Ek and Söderholm (2010)	1986-2002	Global	Wind farm	LBD = 17%, LBR = 20%
Söderholm and Klaassen (2007)	Varies by country	Global based on data from Denmark (1986-1999), Germany (1990-1999), Spain (1990-1999), Sweden (1991-2002), and UK (1991-2000)	Wind farm	LBD = 3.1%, LBR = 13.2%
Jamasb and Kohler (2007)	1994-2001	OECD	Offshore wind farm	LBD = 1% LBR = 4.9%

From new to established markets

(\$/MWh)

Time

First project, Developer-led projects, Formalizing policies and permitting processes, Growing experience, Established domestic supply chain, Phase change at 3-4GW mark, Clear routes to market, Streamlined projects, Project clustering.

New markets, Experienced markets

Source: BloombergNEF

European Commission

Offshore wind Implementation Plan

SET PLAN



#H2020Energy

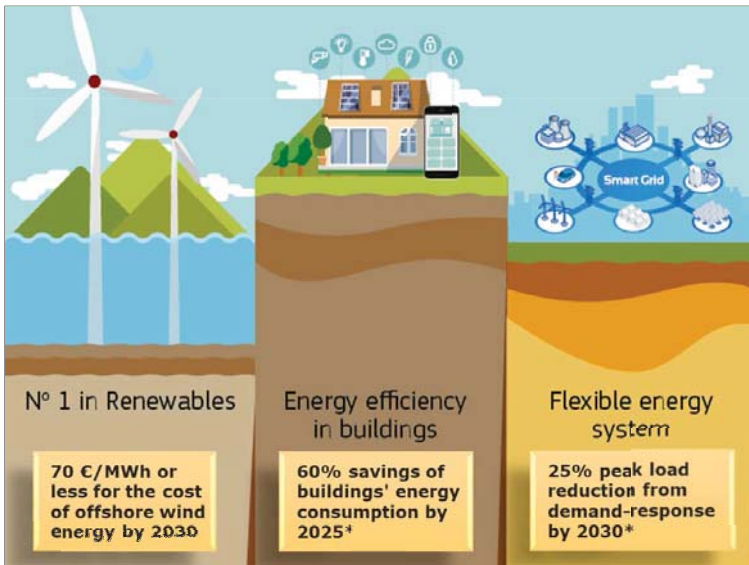
European Commission

SET Plan goals

- Transform the energy system by **accelerating the development and deployment of low-carbon technologies**
- Maximise impact of public investments by **coordinating national & European efforts**
- Promote **cooperation** amongst EU countries, companies, research institutions, and the EU itself




#H2020Energy



European Commission

Offshore wind targets

- **Reduce the levelised cost of energy for fixed offshore wind** by improving performance and efficiency over the entire value chain, leading to a no-subsidy deployment situation
- Develop the **floating offshore wind** subsector to **reduce the LCoE to <12 ct€/kWh by 2025 and <9 ct€/kWh by 2030**



#H2020Energy

European Commission

Implementation Plans

- Take stock of R&I progress so far
- In order to meet the targets, identify:
 - Technological R&I activities
 - Demonstration projects
 - Non-technological barriers/enablers
- Joint R&I activities between SET Plan countries: a key dimension for implementation



The Implementation Plans
Research & Innovation enabling the EU's energy transition

European Commission

Offshore wind Implementation Plan

12 COUNTRIES



STAKEHOLDERS
3 (representing together 88 organisations):
European Technology and Innovation Platform on Wind (Co-Chair, representing 26 organisations), European Energy Research Alliance – Joint Programme on Wind Energy (representing 52 organisations), and European Energy Research Alliance – Joint Programme on Ocean Energy (representing 10 organisations)



268 MILLION €
375 MILLION €
446 MILLION €

■ Private sector ■ National programmes ■ EU Funds





ETIPWind

- Coordinator: WindEurope
- Timeline: Jan. 2019 – Dec. 2021
- Budget: €726 thousand
- Goal
 - Support to R&I policy and SET Plan implementation (stronger industrial focus)
- Main deliverables
 - Technology roadmap
 - Strategic research and Innovation agenda
- Others: workshops, webinars, fact sheets, video



#H2020Energy



SETWind

- Coordinator: DTU
- Timeline: Mar. 2019 – Feb. 2022
- Budget: €1 million
- Goals
 - Organising cross-border research projects
 - Support to R&I policy (stronger research focus)
- Main deliverables
 - Cross-border research projects (10)
 - Criteria to evaluate the impact of wind energy R&I
 - Mapping of R&I policies and priorities for offshore wind
 - Rolling R&I agenda / updated Implementation Plan
 - Proposal for a European Lighthouse project



#H2020Energy



Coming soon...

- Re-establishing the Working Group / Steering Group and make it more inclusive
- Ensure coordination and cooperation between ETIPWind and SETWind, and with the DEMOWIND ERA-Net
- Achieve measurable results



#H2020Energy



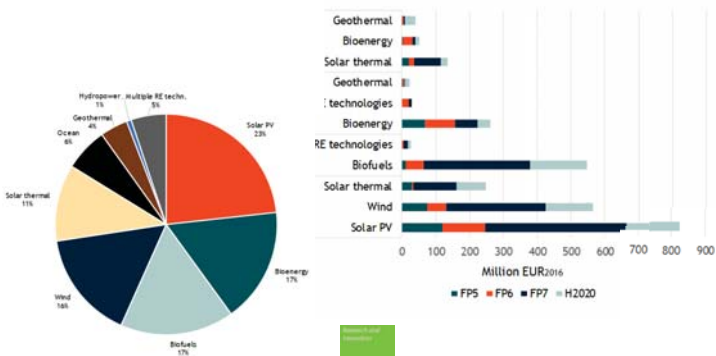
HORIZON 2020



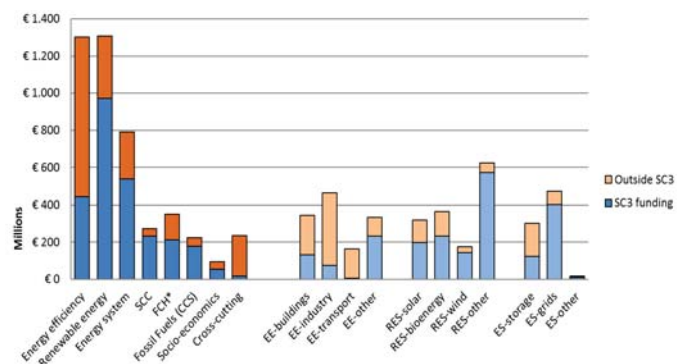
#H2020Energy

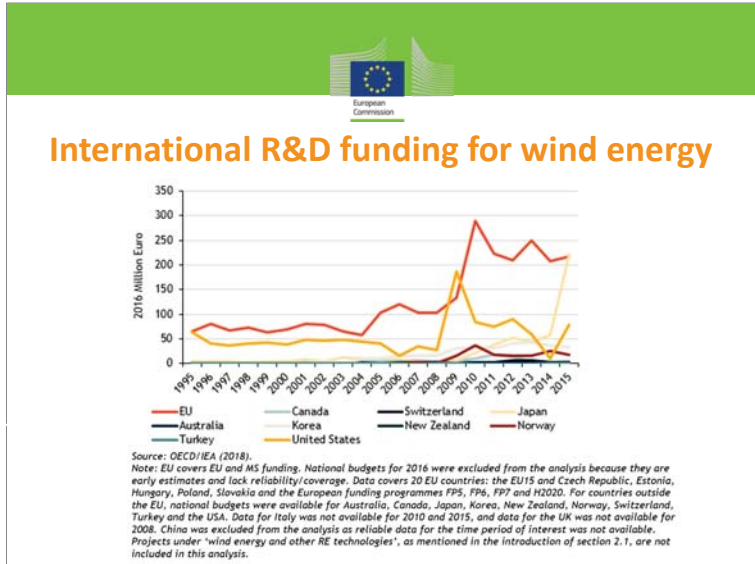
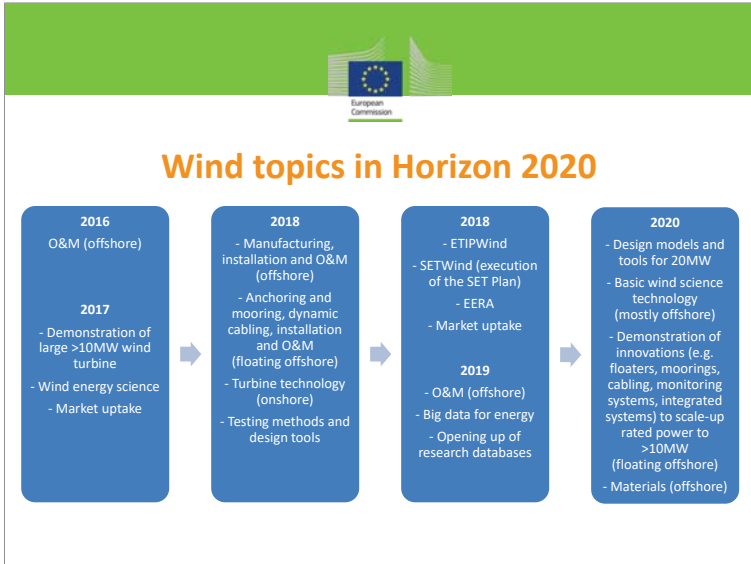
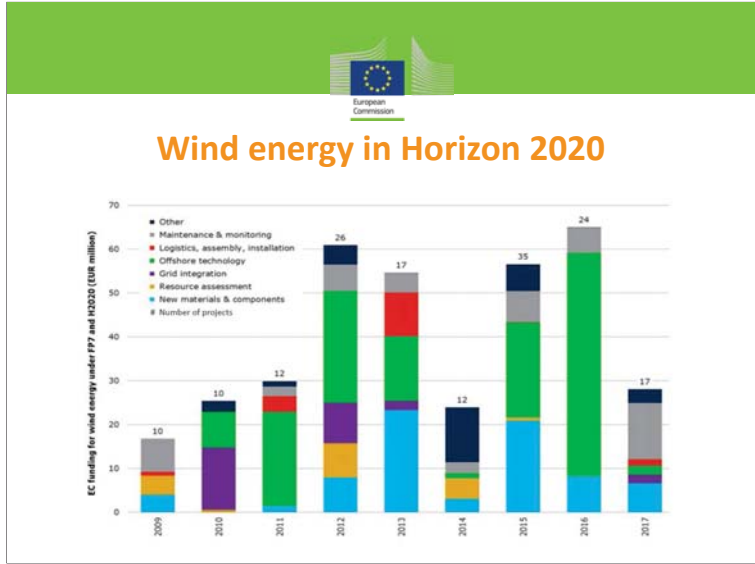
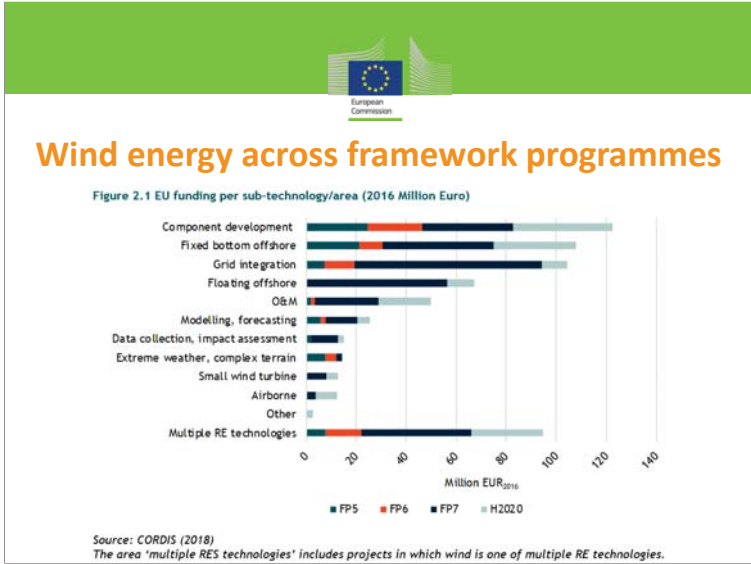


Wind vs others across framework programmes



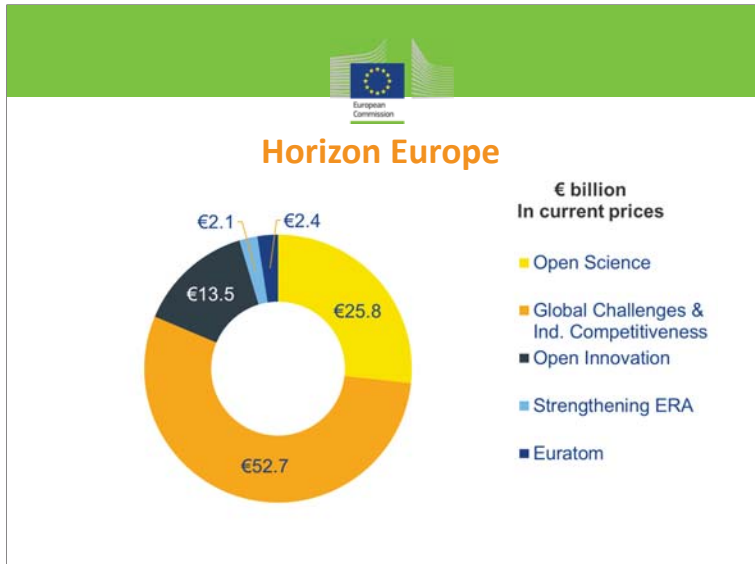
Wind vs others in Horizon 2020





HORIZON EUROPE

#H2020Energy





Horizon Europe

Pillar 2
Global Challenges & Industrial Competitiveness:
 boosting key technologies and solutions underpinning
 EU policies & Sustainable Development Goals

Clusters implemented through usual calls, missions & partnerships	Budget (€ billion)
Health	€ 7.7
Inclusive and Secure Societies	€ 2.8
Digital and Industry	€ 15
Climate, Energy and Mobility	€ 15
Food and Natural Resources	€ 10
Joint Research Centre supports European policies with independent scientific evidence & technical support throughout the policy cycle	€ 2.2



European Innovation Council

The EIC will support innovations with breakthrough and disruptive nature and scale up potential that are too risky for private investors.

European Innovation Council

Helping innovators create markets of the future, leverage private finance, scale up their companies, Innovation centric, risk taking & agile, proactive management and follow up

Two complementary instruments bridging the gap from idea to investable project

Pathfinder: grants
 (from early technology to pre-commercial)

Accelerator:
 grants & blended finance
 (from pre-commercial to market & scale-up)



CHALLENGES



#H2020Energy



Challenges for EU R&I funding on wind power

- Be targeted and mission-oriented without over-prescribing
- Avoid funding research that would take place anyway
- Be more impactful ('more bang for the buck')
- Make more data available for research
- Adapt to Horizon Europe rules, governance and processes
- Seize other FP Challenges / Clusters and profit from research in neighbouring areas
- Create synergies with innovation funding (e.g. innovFin Energy Demonstration Projects, EIC, Innovation Fund)



#H2020Energy



Thank you!

#H2020Energy

EU Participant Portal
www.ec.europa.eu/research/participants



#H2020Energy





Experiences from Hywind Scotland and The Way Forward for Floating Offshore Wind

EERA DeepWind, Trondheim, June 16, 2019

Jon Barratt Nysæther, Technology Manager, Hywind Development, Equinor New Energy Solutions

Expanding a competitive offshore wind portfolio



© New Energy Solutions

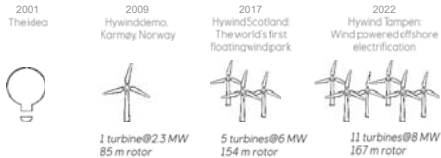
Open

16 January 2019

What is Hywind?

A standard offshore wind turbine placed on a ballasted substructure and anchored to the seabed

- Conventional technology used in a new way
- Simple substructure construction that enables mass production
- Inshore assembly reduces time and risk of offshore operations
- Equinor's floating motion controller uses blade pitch control to dampen out motions



© New Energy Solutions

Open

16 January 2019

Hywind Scotland Project



- Investing around NOK 2 billion
- 60-70% cost reduction from the Hywind Demo project in Norway
- Powering ~20,000 UK homes
- Installed capacity: 30 MW
- Water depth: 95-120 m
- Avg. wind speed: 10.1 m/s
- Area: ~4 km²
- Average wave height: 1.8 m
- Export cable length: Ca. 30 km
- Operational base: Peterhead
- Start power production: Q4 2017



© New Energy Solutions

Open

16 January 2019

Hywind Scotland – Main Objectives

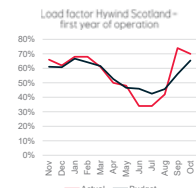
- Demonstrate cost-efficient and low risk solutions for commercial scale floating wind
- Test, verify and further develop the Hywind motion controller (EMC) for a larger turbine
- Verify up-scaled design
- Verify reliability and availability of optimized multi-turbine concept
- Develop, test and verify a developed motion controller using individual pitch to control yaw motions



© New Energy Solutions

Hywind Scotland – first year of operation

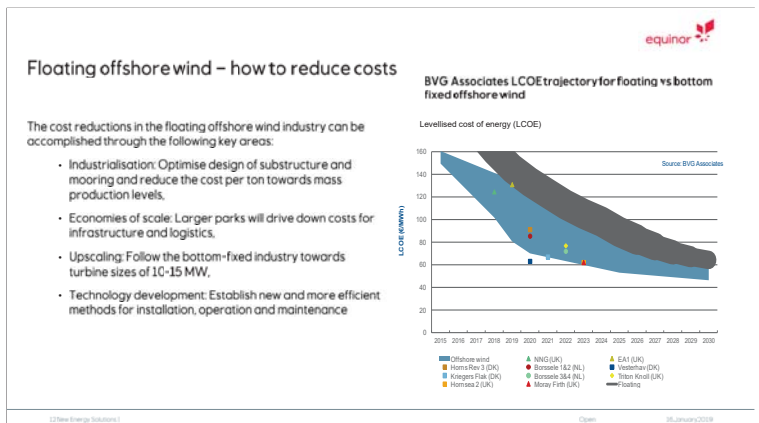
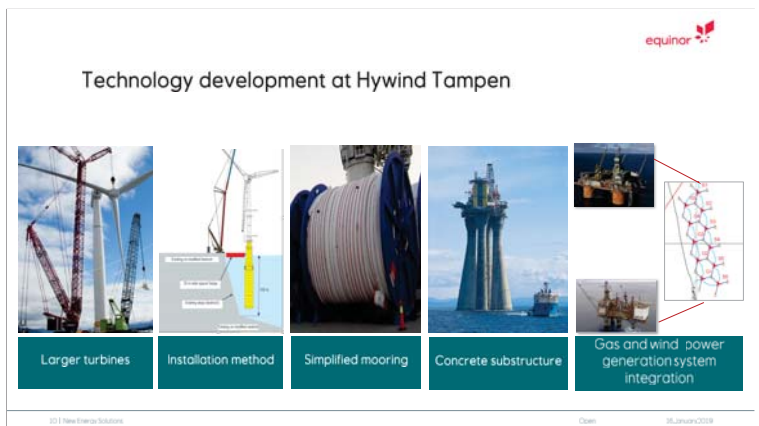
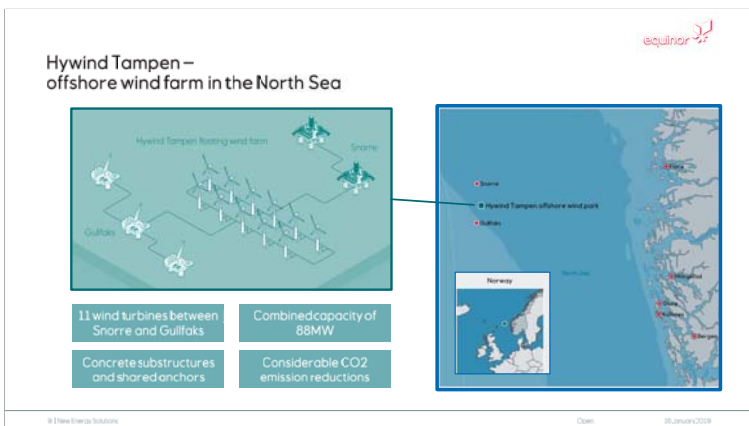
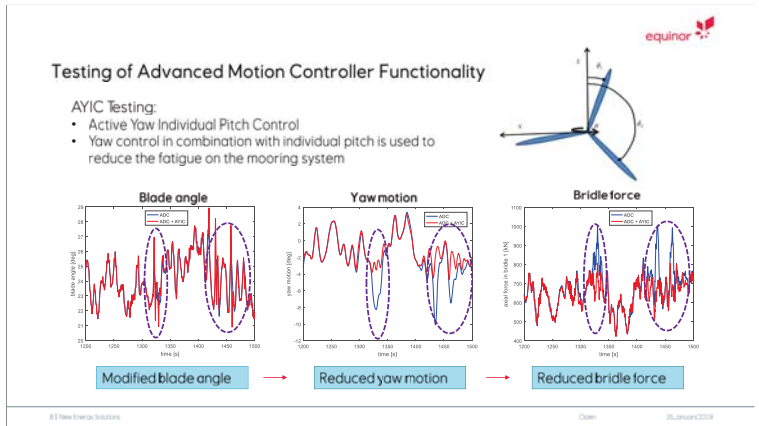
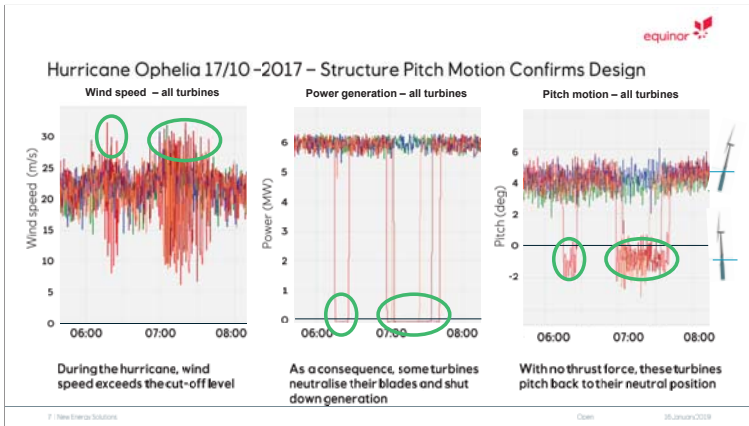
- Successful commissioning and start-up
 - Project delivered on time and without serious incidents
 - Opening in Scotland 18/10 2017
 - Handover to operations 15/11 2017
- First year - performance
 - Production and performance significantly exceeding expectations
 - Average availability: 95%
 - Average capacity factor: 56%
- Next steps
 - Optimize operations, production, costs
 - Test, qualify and develop the technology
 - Input to ongoing and new projects

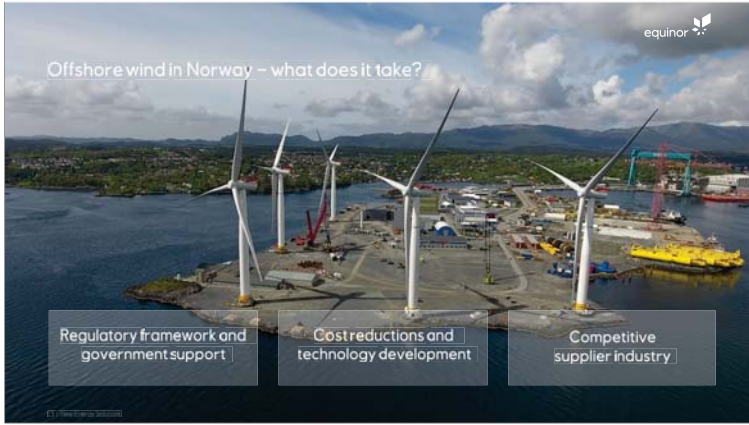


© New Energy Solutions

Open

16 January 2019







TOR-ERVIND MOEN, ABB / EINAR WILHELMSEN, ZERO
Floating offshore wind
 Norway's next offshore boom?



Offshore Wind EU
 Vision 2030



©ABB January 22, 2019 | Slide 2



Floating Offshore Wind in Norway?



©ABB January 22, 2019 | Slide 3



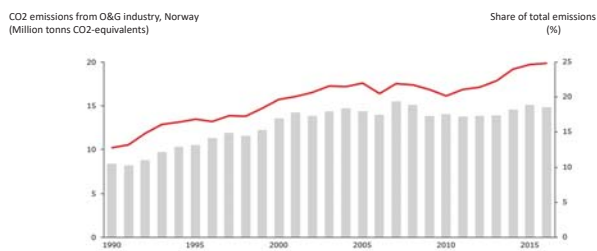
Technology – CO2 Reduction – Employment - Export



©ABB January 22, 2019 | Slide 4



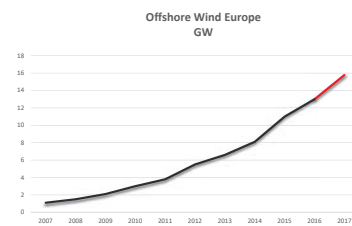
O&G industry must reduce emissions



©ABB January 22, 2019 | Slide 5



Fast growth



©ABB January 22, 2019 | Slide 6



2030 Roadmap
Political engagement



- Political vision
- Efficient subsidies
- Explore and allocate offshore fields
- Clarify rules and regulations
- Transmission & Infrastructure planning
- Social economic business case

2030 Roadmap
Business case for the society



SCOE – Society's Cost of Electricity

- The sum of benefits:
- LCOE –Levelized cost of energy
 - Emission reduction
 - Employment
 - First mover advantage
 - Technology export
 - Energy export

2030 Roadmap
Research community



- Think Big
- Explore the Business Case
- Time is critical
 - Think 2025 - 2030 – What does it take
 - Solve the short-term challenges
- Be even closer to the Industry
- Make it Happen!



North Sea Energy Infrastructure:
Status and outlook

Patrick Piepers
Asset Management TennaT
EERA Deepwind 2019

20 YEARS
POWERING SOCIETY

Deepwind?

X: -6628.00
Y: 600213.00

- ✓ Average depth DEA: -36,0m LAT
- ✓ Deepest point (1): -71,5m LAT

Strategy 2002: "strengthen and build"

- ✓ One strong, independent transmission grid
- ✓ Expansion cross border connections
- ✓ One cross border high voltage grid
- ✓ Strengthen the Dutch electricity grid

A leading TSO in Europe

	2002	2017	
Asset base (€ bn)	1	20.4	X 20
Staff	276	4,068	X 15
Connections (km)	2,686	22,500	X 8
Offshore connections (km)	0	4,700	
Offshore platforms	0	12	

Investments (10Y): € 28 bn

Strong development offshore wind

COP21 : radical change in electricity generation mix

- 230 GW offshore wind capacity, 180 GW to be developed in the North Sea in 2050

WindEurope forecast

- 70 GW offshore wind capacity in the North Sea in 2030

PBL forecast

- 60 GW offshore wind capacity in the Dutch part of the North Sea in 2050

IRISH SEA, ATLANTIC OCEAN, BAL TIC SEA, 180 GW NORTH SEA

NL: Phase I: 2019 – 2023 (+3.5 GW)

- 3,500 MW: 5 x 700 MW
- Standardized concept
- AC connections

Year	Capacity	Area
2019	700 MW	Borssele
2020	700 MW	Borssele
2021	700 MW	Hollandse Kust (zuid)
2022	700 MW	Hollandse Kust (zuid)
2023	700 MW	Hollandse Kust (noord)

Hollandse Kust (noord), Hollandse Kust (zuid), Borssele

700MW AC Substations, focus

• Standardization

- Layout
- Functionality
- Operation
- However some freedom for contractor (EPC contract)



• Lean Design

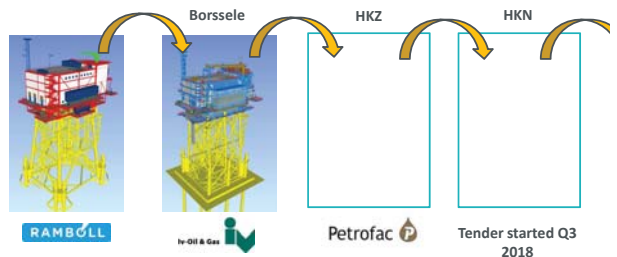
- Unmanned
- No helideck
- No seawater
- No diesel generator
- Simple HVAC



7

700MW AC Substations, focus

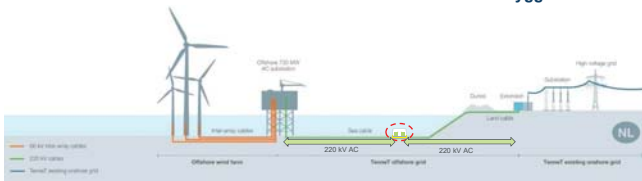
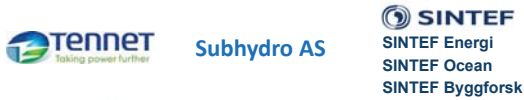
• Lessons learned



Significant cost reduction due to standardization
 (Engineering, Risk profile, Project management, Efficiency, ...).

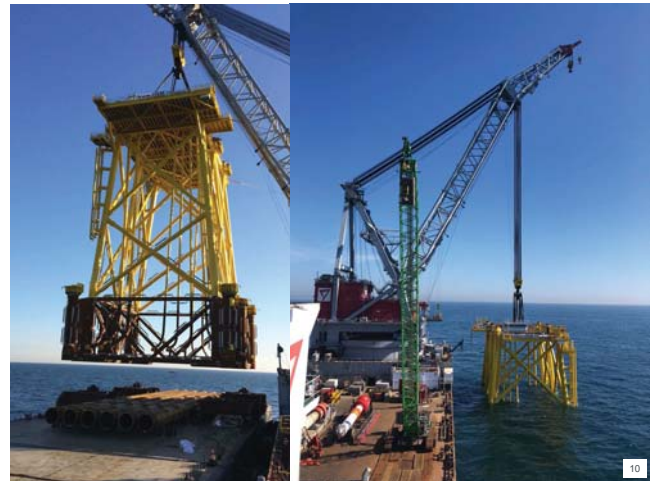
8

700MW AC Substations, innovation



AC technology limited due to increasing reactive power in longer cables.
 Intermediate compensation feasible but costly
Possible cost reduction due to subsea intermediate compensation

9



10



11

GE: Until 2025 yearly 900MW HVDC

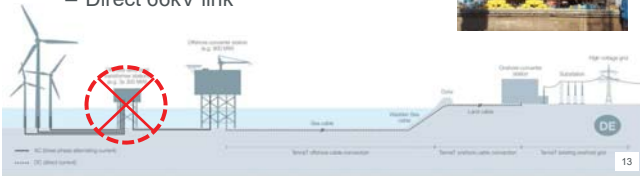
Year	Capacity	Project
Operational		
2009	62	alpha ventus
2010	400	BorWin1
2015	800	BorWin2
2015	800	DoIWin1
2016	916	DoIWin2
2015	576	HelWin1
2015	690	HelWin2
2014	113	Riffgat
2015	864	SylWin1
2017	111	Nordergründe
Under construction		
2019	900	BorWin3
2018	900	DoIWin3
2023	900	DoIWin6
To be built		
2023	900	DoIWin5
2024	900	BorWin5
2025	?	BorWin6



12

900MW HVDC, focus

- Existing Platforms → OPEX reduction
 - Long term unmanned
 - New logistic concepts
- New Platforms → CAPEX reduction
 - Lean design
 - Standardization
 - Direct 66kV link



13

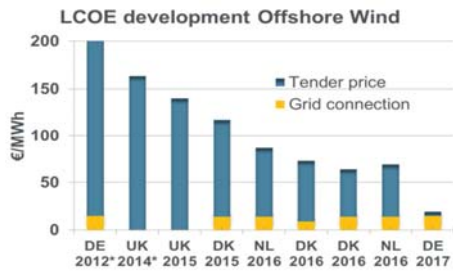
NL: Phase II: 2024 – 2030 (+7 GW)

Year	Wind Area	Power
2024	HKWest Alpha	700 MW HVAC
2025	HKWest Beta	700 MW HVAC
2026	Ten Noorden van de Waddeneilanden	700 MW HVAC
2027-2030	Ulmuiden Ver	4000 MW HVDC
2027-2030	?	900 MW



14

Challenge: Cost



- Limited cost reduction in grid connections.
- Longer offshore connections lead to increase in cost

15



Large HVDC connections (1,2-2GW)

- Grid quality (HVAC cables result in deteriorating grid quality)
- More cost effective than HVAC
- Less cables (Ecology & Stakeholder)

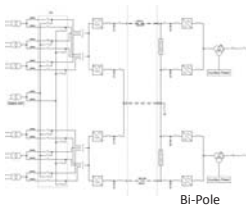
Netherlands aim → 2GW (525kV)

Requires market adaptations to ensure system reserve

Germany → limited by 2K criteria (Cable temperature)

18

Large HVDC connections (1.2-2GW)



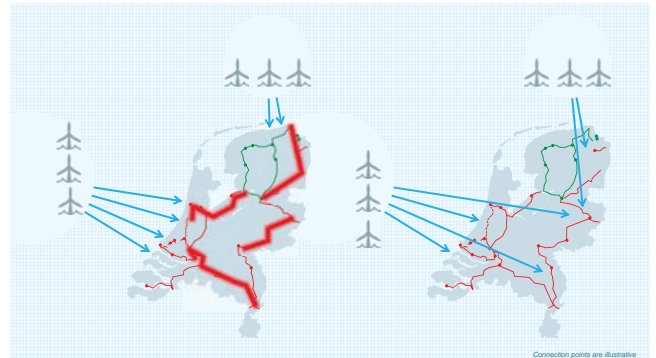
Bi-Pole



- 2GW
- 525kV
- Bi-Pole
- Double converter rooms
- ≥6 transformers

19

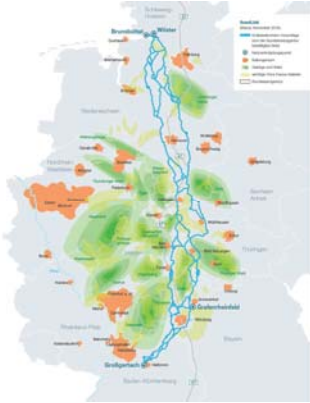
NL challenge: Onshore connections



Connecting >7 GW directly to shore results in significant congestion

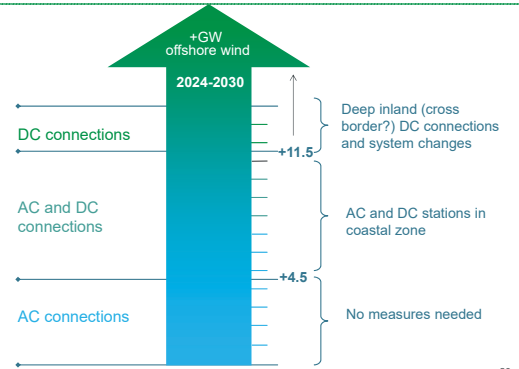
16

GE challenge: Onshore connections



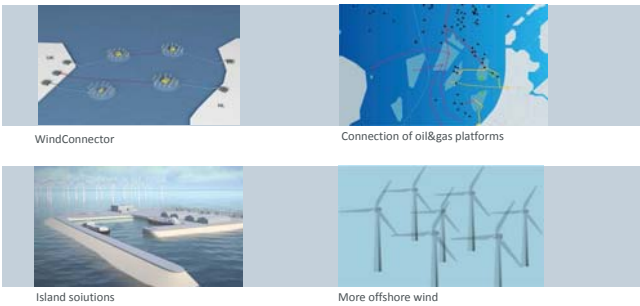
17

Conclusion: grid analysis 2024 - 2030



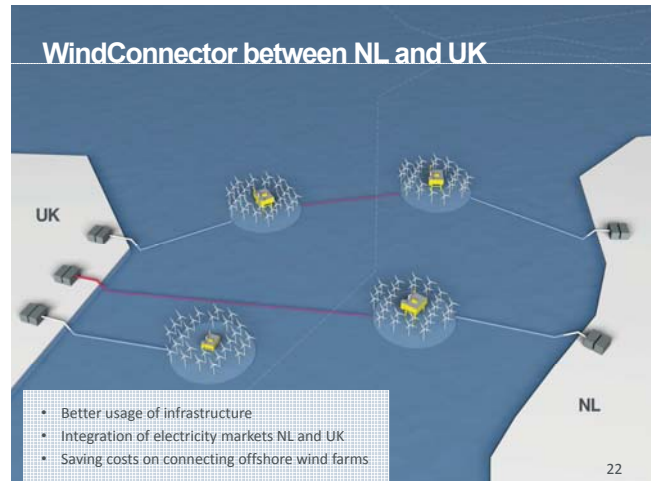
20

Future development will need innovation



21

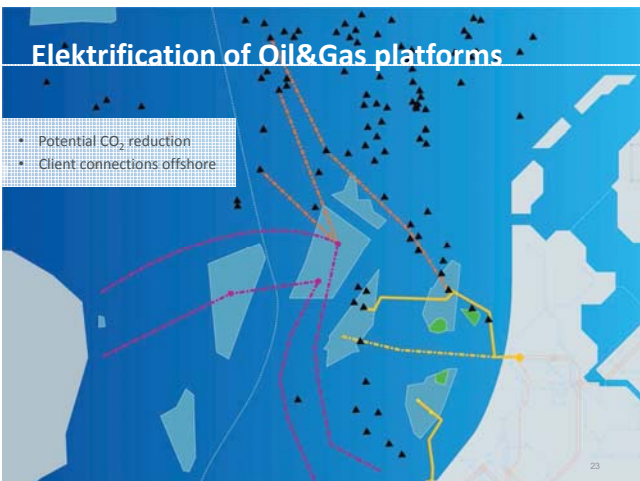
WindConnector between NL and UK



22

Elektrifikation of Oil&Gas platforms

- Potential CO₂ reduction
- Client connections offshore



23

Cost optimization: jacket or island?



22

Phase III: 2030 – 2050

For large scale offshore wind everything is needed

- One international offshore grid
- System integration
- Power to Gas
- Storage
- Electrification of Industry & Transport
- Interconnection
- Most of all: clarity on the way forward!

Think Big!



24

Phase III: 2030 – 2050 (+ 48 GW?)

- Large scale wind farms
- Location: depth & wind
- Power Link Hub
- Wind Connector
- Hub & Spoke




25

Questions



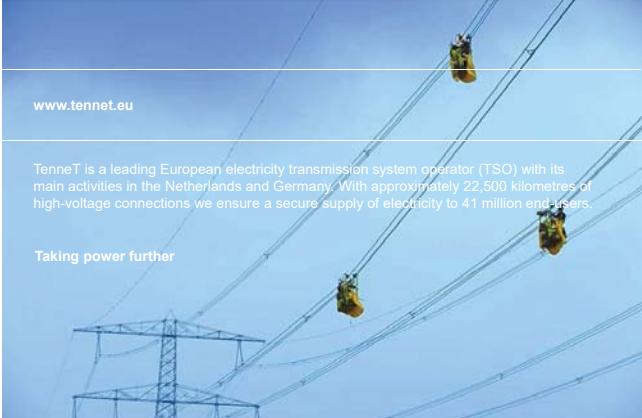
26



www.tennet.eu

TenneT is a leading European electricity transmission system operator (TSO) with its main activities in the Netherlands and Germany. With approximately 22,500 kilometres of high-voltage connections we ensure a secure supply of electricity to 41 million end-users.

Taking power further



Disclaimer

Liability and copyright of TenneT

This PowerPoint presentation is offered to you by TenneT TSO B.V. ("TenneT"). The content of the presentation – including all texts, images and audio fragments – is protected by copyright laws. No part of the content of the PowerPoint presentation may be copied, unless TenneT has expressly offered possibilities to do so, and no changes whatsoever may be made to the content. TenneT endeavours to ensure the provision of correct and up-to-date information, but makes no representations regarding correctness, accuracy or completeness.

TenneT declines any and all liability for any (alleged) damage arising from this PowerPoint presentation and for any consequences of activities undertaken on the strength of data or information contained therein.

A1) New turbine and generator technology

The X-Rotor Offshore Wind Turbine Concept, W.Leithead, University of Strathclyde

Comparison of the capacity factor of stationary wind turbines and weather-routed energy ships in the far-offshore, J.Roshamida, LHEEA, Ecole Centrale de Nantes

Development of coupling module between BHawC aeroelastic software and OrcaFlex for coupled dynamic analysis of floating wind turbines, V.Arramounet, INNOSEA

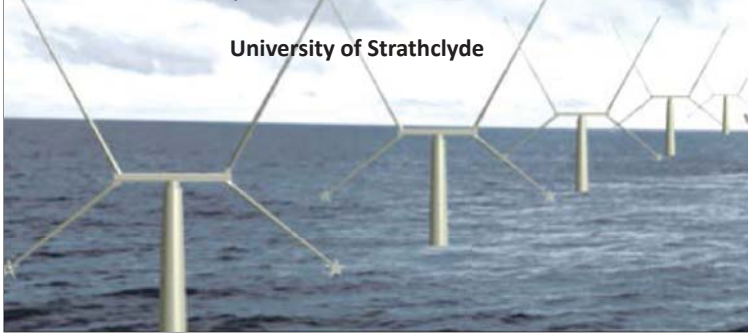
A new approach for comparability of two- and three-bladed 20 MW offshore wind turbines, F.Anstock, Hamburg University of Applied Science

DeepWind 2019



The X-Rotor Offshore Wind Turbine Concept

Bill Leithead
Arthur Camciuc, Abbas Kazemi Amiri and James Carroll
University of Strathclyde

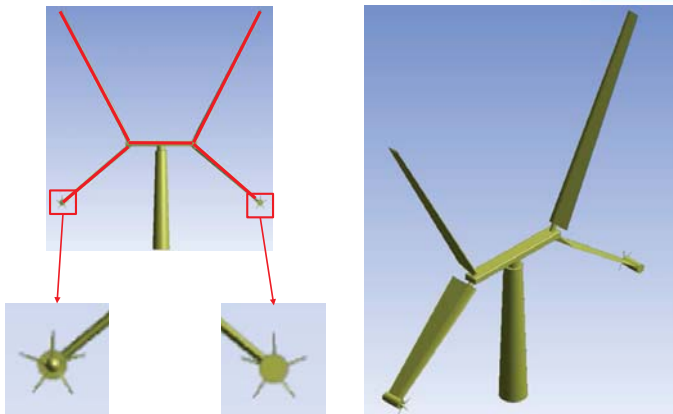


Outline



1. X-Rotor Concept
2. X- Rotor Potential Benefits
3. Exemplary Configuration
4. Structural Analysis
5. CoE Assessment
6. Conclusion

X-Rotor Concept



X-Rotor Potential Concept



- Primary Rotor rotates on the vertical axis
- No Power take off on vertical axis
- High speed horizontal axis secondary rotors



- No Requirement for gearbox or multi-pole generator
- X-Shape reduces overturning moments
- Reduced requirement for Jack up vessel and reduced failure rates

X-Rotor Benefits



1. Cost of energy reduction
2. Floating platform potential
3. Up-scaling potential



Exemplary Configuration



1. Tip speed of the secondary rotors, $\lambda_s \lambda_p V$, is constrained above
 - λ_s is tip speed ratio of secondary rotors
 - λ_p is tip speed ratio of primary rotor
 - V is wind speed
 - $(\lambda_s \lambda_p)$ is net tip speed ratio
2. Rotational speed of the secondary speed is constrained below
3. Efficiency of power conversion by the secondary rotor, $P_s / (\Omega_s T_s)$, must be high
 - P_s is power extracted by secondary rotor
 - Ω_s is rotational speed of secondary rotor
 - T_s is thrust on secondary rotor

Exemplary Configuration



To achieve high efficiency of power conversion

- Primary vertical axis rotor has high efficiency, $\lambda_p \sim 4 - 5$.
- Secondary horizontal axis rotor has low efficiency, $\lambda_s \sim 3 - 4$. maximise power for fixed root bending moment corresponds to induction factor of 0.2.

To keep within tip speed constraint

- $\lambda_p \lambda_s \sim 14 - 16$

Exemplary Configuration



Upper and lower primary rotors have 2 blade with single secondary rotor on each lower blade.

With generators having 4 pole pairs with nominal frequency of 25Hz suitable for turbines up to 5MW

Primary rotor $C_{pmax} = 0.39$ at $\lambda_{pmax} = 4.65$ and area=12,352m²

Secondary rotor $C_{pmax} = 0.27$ at $\lambda_{pmax} = 3.13$, $C_p/C_1=0.8$ and area=139m²

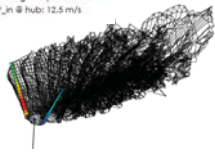
5.02MW of mechanical power is delivered in 12.66m/s wind speed, 5.50MW in 20m/s

Structural Analysis

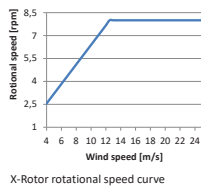


1. Chord lengths of the upper and lower blades 10 and 14 m at the blade roots, respectively
2. Chord lengths linearly reduce to 5 and 7 m at blade tips
3. NACA 0025 (root) and NACA 0008 (tip) for both upper and lower blades
4. Ideal power production of 6.47 MW at rated wind speed (12.5 m/s) and rotational speed of 0.838 rad/sec
5. Aerodynamic analysis for turbine operation simulation in QBlade

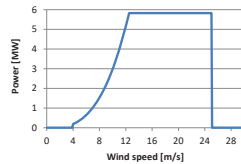
Time: 30.0001 s
Averaged Power: 4199.1 kW
Averaged Cp: 0.40343
V_{in} @ hub: 12.5 m/s



Operational load simulation, upper blades, QBlade



X-Rotor rotational speed curve



X-Rotor power curve with efficiency of 90%

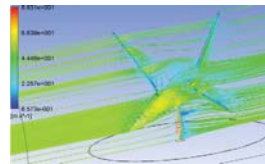


Upper rotor profile layout along blade axis

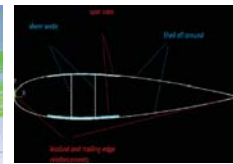
Structural Analysis



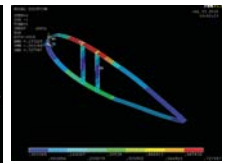
1. Blade profile pre-dimensioning based on ultimate strength criteria and strain constraints for high quality laminate
 - Rotor at parked position under extreme wind parallel to rotor plane with speed of 52.5 m/sec
 - Buckling control passed as blade stability under above conditions fulfilled
2. All designs based on IEC 61400-1:2005 and Certification of Wind Turbines, Germanischer Lloyd, 2010
3. Operational wind speeds between 4.5 - 25 m/sec



Extreme loads simulation, ANSYS CFX



Blade internals layout

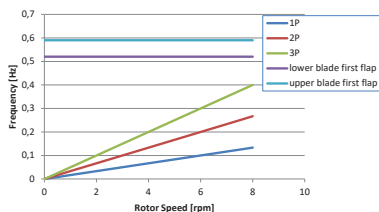


Blade profile stress analysis, NACA 0025, ANSYS mechanical

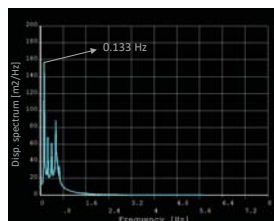
Structural Analysis



1. Mass of upper and lower blades 40500 and 23384 kg, respectively
 - Total mass of 2-blade rotor design 127768 kg
2. Modal analysis and dynamic response simulation of isolated blades
 - Blade resonance control through Campbell plot
3. HAWT blade tip deflection check irrelevant for X-Rotor, due to its special design
 - Excessive tip deflection prevented



Rotor blades Campbell plot



Power spectrum of upper blade at rated wind speed (12.5 m/sec), rotor speed 8 rpm (0.133 Hz)

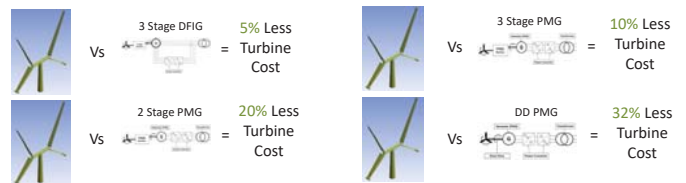
Cost of Energy



Capital costs differences between X-Rotor and existing HAWTs:

Savings on no Gearbox and no multi-pole Generator

Comparison to different drive-train configurations

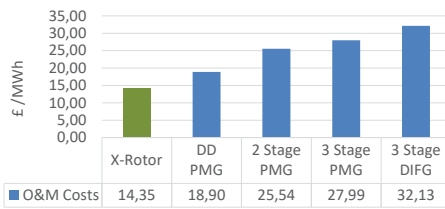


X-Rotor capital cost on average **17% lower** than existing HAWT turbine costs

Rotor mass and consequently cost similar to existing HAWTs

Cost of Energy

- X-Rotor O&M costs compared to 4 different turbine types
- Strathclyde O&M cost model used
- Model inputs adjusted to represent the X-Rotor
- O&M costs from existing turbines come from a published paper
- Same methodology and hypothetical site used for like for like comparison with results



- **X-Rotor O&M costs 43% lower than the average O&M cost for four existing turbine types**
- No gearbox or multipole generator failures.
- Greatly reduced requirement for Jack-up vessel.

Cost of Energy

X-Rotor CoE comparison with existing turbines:

- X-Rotor average **capital costs savings** compared existing turbines is **17%**
- X-Rotor average **O&M cost savings** compared to existing turbines is **43%**

Assumptions

- O&M costs make up 30% of the overall CoE
- Capital costs make up 30% each of overall CoE

The X-Rotor CoE saving compared to existing wind turbines ranges from 22%-26% depending on existing turbine type used in the comparison.

X-Rotor CoE on average 24% lower than existing HAWT turbine costs

Conclusion

- X-Rotor structure/rotor is similar cost to existing wind turbine rotors based on mass
- Turbine costs compared to existing wind turbines is on average 17% less
- O&M costs compared to existing turbines is on average 43% less
- CoE compared to existing turbines is on average 24% less
- Other investigations
 - Further exemplary designs suitable for 4MW to 7.5MW
 - Loading and design of jackets for both designs.



University of
Strathclyde
Glasgow

Comparison of the capacity factor of stationary wind turbines & weather-routed energy ships in the far-offshore

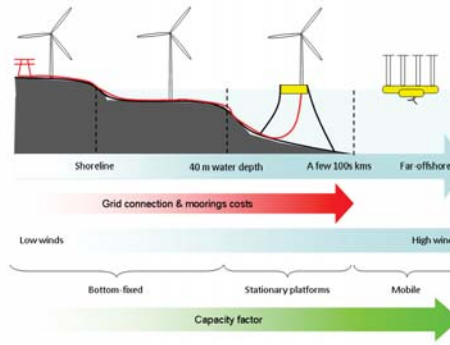
A research in progress

Roshamida ABD JAMIL^{1,2}
PHD Student

Alis e CHAIGNEAU¹, Jean-Christophe GILLOTEAUX¹, Philippe LELONG³ & Aur lien BABARIT¹

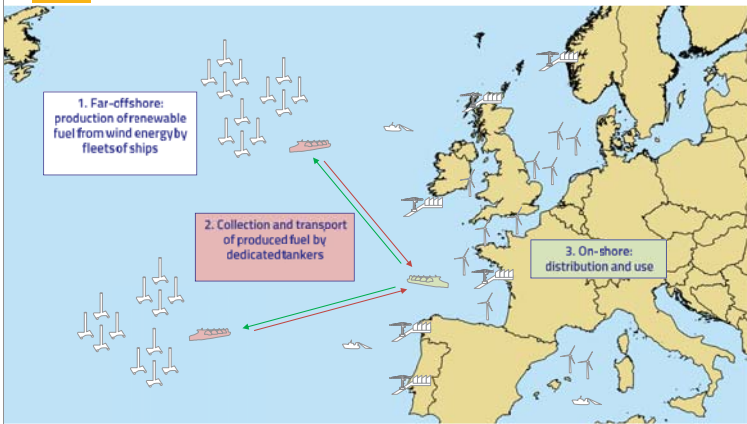
¹ LHEEA, Ecole Centrale de Nantes - CNRS, Nantes, FRANCE
² Faculty of Science and Defense Technology, NDU, Kuala Lumpur, MALAYSIA
³ MELTEMUS, 7 all e du Jardin, 44240 La Chapelle sur Erdre, FRANCE

Significance & Motivation

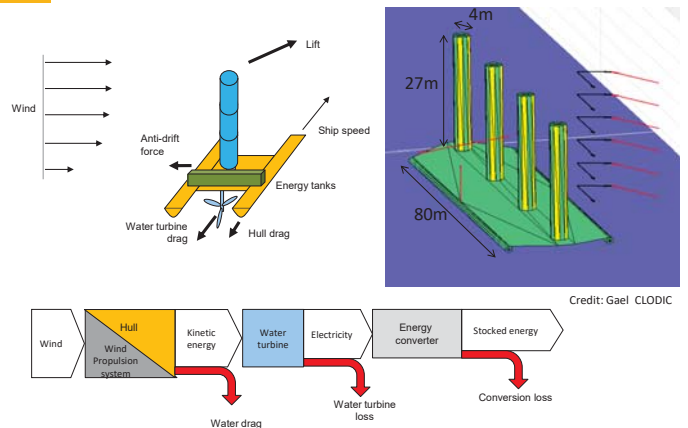


FARWIND energy ship	Offshore wind turbines
Far-offshore	Land-based or nearshore
On-board energy storage	Grid-connected
Mobile	Bottom-fixed or stationary
Target: 80% capacity factor thanks to mobility and weather-routing	Range 40% - 50%
Repair at docks → low maintenance costs	Maintenance at site → high maintenance costs
No grid connection No moorings / foundations No installation operations → Low CAPEX	Grid-connection Moorings/foundations Installation operations → High CAPEX
Target: 0 conflicts of uses: far-offshore ocean is a desert	Multiple conflicts of uses

FARWIND project's vision



FARWIND project's vision: Boat Design



Study objectives

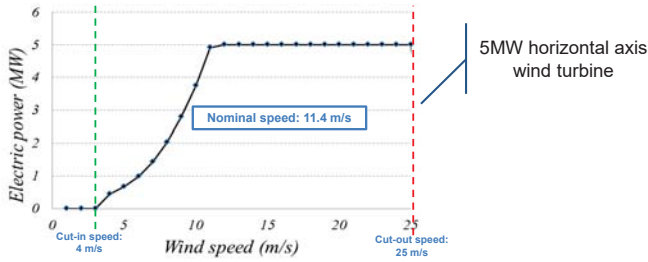
- Investigate how high the capacity factor can be, with optimized routings, depending on the energy ship sailing capabilities and deployment area.
- Compare this CF to that of hypothetical stationary floating wind turbines

Data

- WIND SPEED DATA
 - 10m wind speed data for years 2015, 2016 and 2017
 - ERA-Interim dataset by European Centre for Medium-Range Weather Forecasts (ECMWF) reanalysis.
- OFFSHORE WIND TURBINE POWER CURVE
- BOAT SPEED & POWER POLAR

Data

1. WIND SPEED DATA
2. OFFSHORE STATIONARY WIND TURBINE POWER CURVE

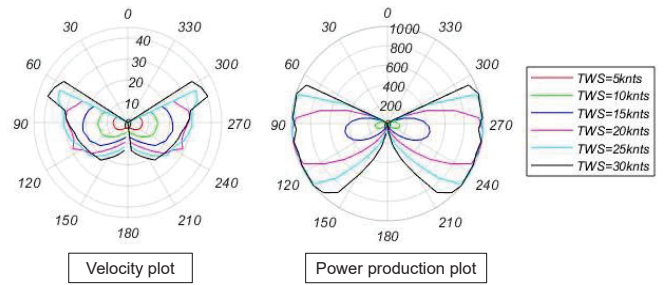


3. BOAT SPEED & POWER POLAR



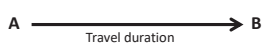
Data

1. WIND SPEED DATA
2. OFFSHORE WIND TURBINE POWER CURVE
3. 1MW BOAT SPEED & POWER PRODUCTION POLAR



Optimization using qtVlm software

Standard qtVlm



- Uses isochrones method to find an optimal route.
- Then further improve the travel duration by optimizing the location of the nodes of the optimal route using the simplex method

Dedicated & modified qtVlm version
New optimization criterion:

Capacity factor;

$$C_F = \frac{\int_0^T \bar{P}(t) dt}{(T + 6)P_{rated}}$$

With:
 C_F is the capacity factor
 T is the route duration (in hours)
 \bar{P} is the power produced by the energy ship
 P_{rated} is the rated power of the ship

Filling ratio;

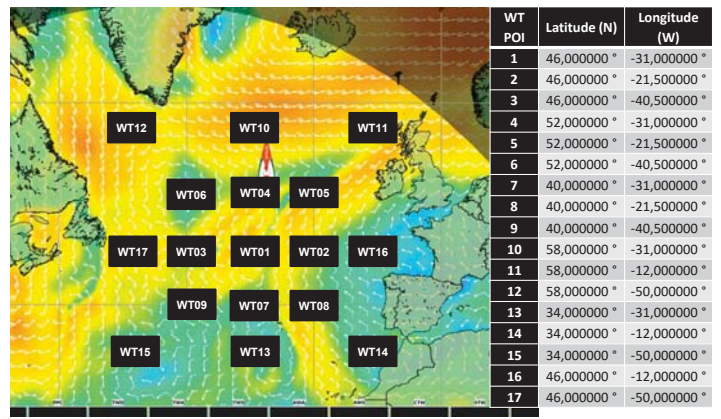
$$F = \frac{\int_0^T \bar{P}(t) dt}{174P_{rated}}$$

With: Energy stored: $E = \int_0^T \bar{P}(t) dt$
 Reservoir capacity: $E_{max} = 174P_{rated}$

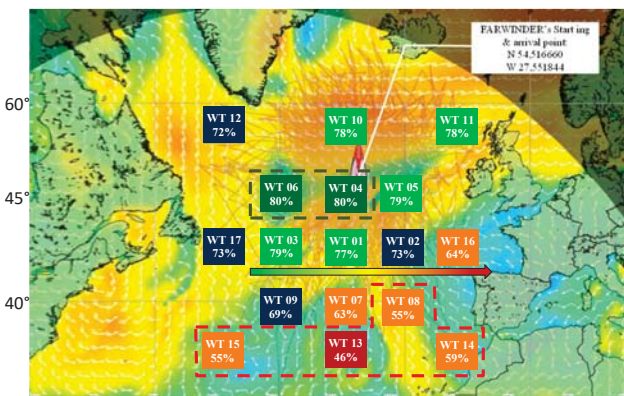
$$\bar{P}(t) = \begin{cases} 0 & \text{if } F \geq 1 \\ 0.25P(TWS, TWA) & \text{during maneuver} \\ P(TWS, TWA) & \text{otherwise} \end{cases}$$



Floating wind turbines CF using QtVlm



Average CF for stationary WT (2015, 2016 & 2017)

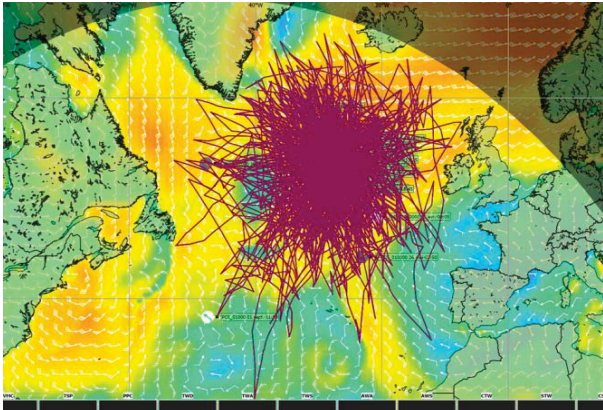


Optimization of 1MW FARWINDER capacity factor

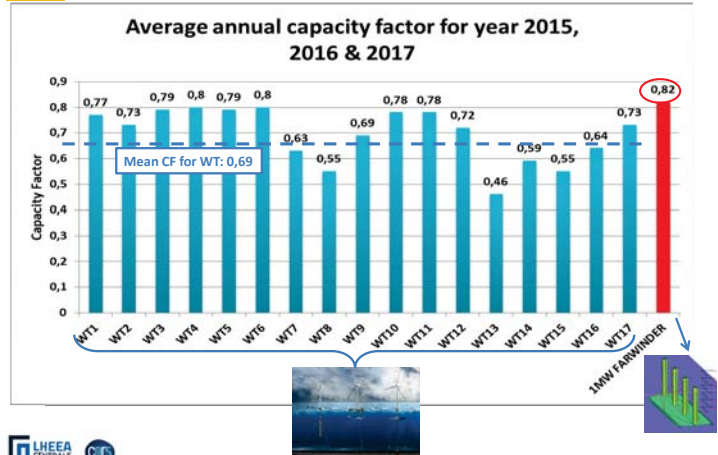
Year	-	2015	2016	2017
Annual average CF	%	81	83	81
Best CF over one route	%	95	95	94
Worst CF over one route	%	46	55	60
Average route duration	Day (s)	6	6	6
Longest route duration	Day (s)	15	11	11
Shortest route duration	Day (s)	1	2	2
Longest route distance	NM	7480	6073	5730
Shortest route distance	NM	907	1140	1576
Average filling ratio at the end of the routes	%	68	71	69



Optimized route traces for 1MW energy ship (2015, 2016 & 2107)



Capacity factor at far offshore



Conclusion

Average CF of year 2015, 2016 & 2017	
Energy Ship	Stationary wind turbines
82%	69%

- Moving further offshore increase significantly the CF of stationary WT
- With the same resource and over the same geographical area, a mobile device, such as a wind energy ship, may increase even more the CF.
- Capacity factor of energy ships needs to be refined includes **sensitivity studies as function of the storage capacity** aboard the energy ships and the **rated power**
- taking into account the effect of **sea conditions on energy ships' performance**.



References

1. C Mone, M Hand, M Bolinger, J Rand, D Heimiller and J Ho 2015 Cost of wind energy review. *Technical report* NREL/TP-6A20-66861 May 2017
2. A Possner and K Caldeira 2017 Geophysical potential for wind energy over the open oceans. *Proceedings of the National Academy of Sciences of the United States of America* 114(43) pp 11338-43
3. A Babarit, JC Gilloteaux, G Clodic, M Duchet, A Simoneau and M F Platzer 2018 Techno-economic feasibility of fleets of far offshore hydrogen-producing wind energy converters. *International Journal of Hydrogen Energy* 43(15) pp 7266-89
4. H Hagiwara 1989 Weather routing of (sail-assisted) motor vessels *PhD Thesis of Delft University of Technology*
5. Kim J and Park C 2010 *Wind power generation with a parawing on ships, a proposal Energy, Elsevier* 35(3) 1425-32
6. JC Gilloteaux and A Babarit 2017 Preliminary design of a wind driven vessel dedicated to hydrogen production. *6th International Conference on Ocean, Offshore and Arctic Engineering (OMAE2017)* June 2017 Trondheim, Norway
7. Manual of qtVlm version 5.8.3 downloaded at http://download.melltemus.com/qtVlm/qtVlm_documentation_en.pdf
8. L Walther, A Rizvanoli, M Wendebourg and C Jahn 2016 Modeling and optimization algorithms in ship weather routing *International Journal of e-Navigation and Maritime Economy* 4 pp 31-45
9. M F Platzer, Sarigul-Klijn, J Young, M A Ashraf and J C S Lai 2014 Renewable hydrogen production using sailing ships *ASME Journal of Energy Resources Technology* 136 / 021203-1
10. S B Capps and C S Zender 2009 Global ocean wind power sensitivity to surface layer stability *Geophysical Research Letters* 36
11. S B Capps and C S Zender 2010 estimated global ocean wind power potential from QUIKSCAT observations, accounting for turbine characteristics and siting *Journal of Geophysical Research* 115
12. Enercon 2013 Enercon e-ship 1: A wind-hybrid commercial cargo ship *Presentation at 4th Conference on Ship efficiency* Hamburg, Germany
13. Det Norske Veritas (DNV) 2010 Recommended practice DNV-RP-C205: Environmental conditions and environmental loads downloaded at <http://www.dnv.com>



SHAKE THE FUTURE.



Thank you
for your attention

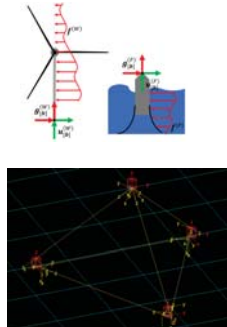
Development of coupling module between BHawC aeroelastic software and OrcaFlex for coupled dynamic analysis of floating wind turbines

Table of content

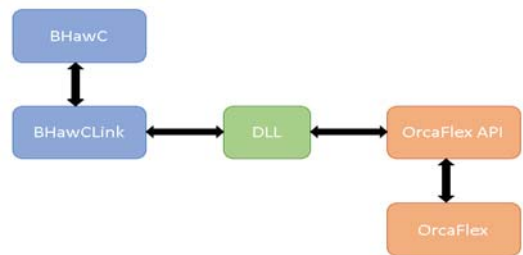
- Introduction
- Coupling methodology
- Mathematical background
- Data exchange during Newton Raphson iterations
- Verification
- Conclusion

Introduction

- Modelization of floating wind turbines
 - Wind turbine and floater structural dynamics
 - Control
 - Aerodynamics
 - Hydrodynamics
 - Moorings
- Coupled software
 - BHawC: non-linear aeroelastic tool for dynamic analysis of wind turbines
 - OrcaFlex: dynamic analysis tool for offshore marine systems



Coupling methodology



Mathematical background

'Decoupled' equation of motion for substructure (S):

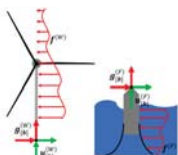
$$M^{(S)}(\dot{u}^{(S)} + p^{(S)}(u^{(S)}, \dot{u}^{(S)})) = f^{(S)}(u^{(S)}, \dot{u}^{(S)}) + g^{(S)}$$

Introduce compatibility, and Lagrange multipliers for interface load:

$$u_b^{(W)} - u_b^{(F)} = B^{(W)}u^{(W)} + B^{(F)}u^{(F)} = 0; \quad g^{(S)} = B^{(S)T}\lambda$$

Generalized alpha time integration of the wind turbine DOF is performed according to:

$$\Delta u_n^{(W)} = -\tilde{S}^{(W)-1} \left(r_n^{(W)} + B^{(W)T} \left((1 - \alpha_f) S_{int}^{(F)-1} B^{(F)} \Delta \tilde{u}^{(F)} \right) \right)$$



$$S^{(W)} = S^{(W)} + B^{(W)T} (S_{int}^{(F)})^{-1} B^{(W)}$$

$$S_{int}^{(F)} = B^{(F)} S^{(F)-1} B^{(F)T}$$

Mathematical background

Condensing Foundation DOF onto 6 equivalent interface DOF

$$M_{eqv}^{(F)}(\dot{u}^{(F)}) + p_{eqv}^{(F)}(u^{(F)}, \dot{u}^{(F)}) + B^T \lambda = f_{eqv}^{(F)}(u^{(F)}, \dot{u}^{(F)})$$

$$S_{int}^{(F)} = B^{(F)} S^{(F)-1} B^{(F)T} \approx S_{eqv}^{(F)}$$

Advantages of this approach:

- Allows for limited data exchange
- Linearised per timestep: accurate for slow floater dynamics

Challenges:

- Linearization of trussframe structures

Data Exchanged during Newton Raphson iterations



Matrix / Vector	Part modelled	Contribution
Mass ($M_{eqv}^{(F)}$)	Floater	Mass
	Mooring lines	Hydrodynamic added mass
Stiffness ($K_{L,eqv}^{(F)}$)	Floater	Hydrostatic stiffness
	Mooring lines	Mooring stiffness
Damping ($C_{L,eqv}^{(F)}$)	Floater	Linear & Quadratic damping
	Mooring lines	Hydrodynamic drag Structural damping Radiation damping
Load ($g_i^{(W)}$)	Floater	Excitation loads Weight Hydrostatic stiffness Radiation damping Hydrodynamic drag Structural stiffness Structural damping
	Mooring lines	Linear & Quadratic damping Weight Hydrodynamic drag Mooring stiffness

Development of coupling module between BHawC aeroelastic software and OrcaFlex for coupled dynamic analysis of floating wind turbines

7

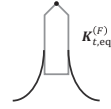
Data Exchanged during Newton Raphson iterations



- Load vector $g_i^{(W)}$
 - FASTExtractAddedMassAndLoad OrcaFlex-API function;
 - Contains the frequency dependent added mass contribution.
- Mass matrix $M_{eqv}^{(F)}$
 - FASTExtractAddedMassAndLoad OrcaFlex-API function;
 - Only contains the frequency independent added mass.
- Stiffness matrix $K_{L,eqv}^{(F)}$
 - $K_{L,eqv}^{(F)} = K_{mooring} + K_{vessel}$;
 - $K_{mooring}$ evaluated in shadow stiffness model;
 - K_{vessel} directly read in OrcaFlex model.
- Damping matrix $C_{L,eqv}^{(F)}$
 - $C_{ij}(t) = \frac{f_i(t) - f_j(t - \Delta t)}{t_i(t) - t_j(t - \Delta t)}$;
 - $f_i(t)$ evaluated in a shadow damping model.

$$g_i^{(W)} = \begin{pmatrix} p^{(F)} + f^{(F)}(\omega) \end{pmatrix}$$

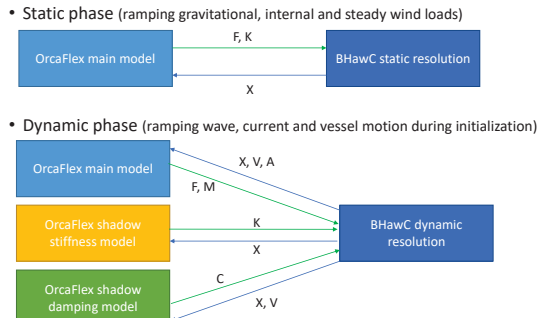
$$M_{eqv}^{(F)} = \begin{pmatrix} M^{(F)} + M^{(F)}(\omega_{inf}) \end{pmatrix}$$



Development of coupling module between BHawC aeroelastic software and OrcaFlex for coupled dynamic analysis of floating wind turbines

8

Data Exchanged during Newton Raphson iterations



Development of coupling module between BHawC aeroelastic software and OrcaFlex for coupled dynamic analysis of floating wind turbines

9

Data Exchanged during Newton Raphson iterations



- Shadow models
 - Shadow damping model
 - Environment:
 - Wave, current and wind are deactivated;
 - Excitation loads neglected;
 - OrcaFlex elements:
 - Mass, added mass and buoyancy neglected.
 - Damping contributions are kept.
 - Shadow stiffness model
 - Interface position imposed
 - System static equilibrium solved by OrcaFlex
 - The stiffness matrix at that position is then calculated by OrcaFlex.

Development of coupling module between BHawC aeroelastic software and OrcaFlex for coupled dynamic analysis of floating wind turbines

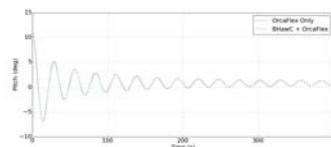
10

Verification



- Static equilibrium test with and without wind;
- Decay tests with and without wind;
- Regular and irregular waves with and without wind simulations.

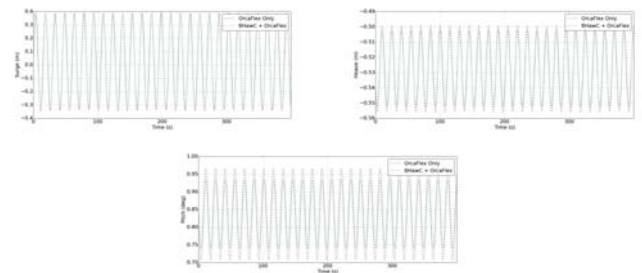
DOF	Eigen Period (s)		Difference (%)
	BHawC + OrcaFlex	OrcaFlex only	
Surge	112.5 s	113.4 s	1.0%
Sway	112.9 s	112.6 s	0.3%
Heave	17.6 s	17.5 s	0.6%
Roll	27.8 s	27.6 s	0.7%
Pitch	27.5 s	27.6 s	-0.4%
Yaw	80.1 s	80.8 s	-0.9%



Development of coupling module between BHawC aeroelastic software and OrcaFlex for coupled dynamic analysis of floating wind turbines

11

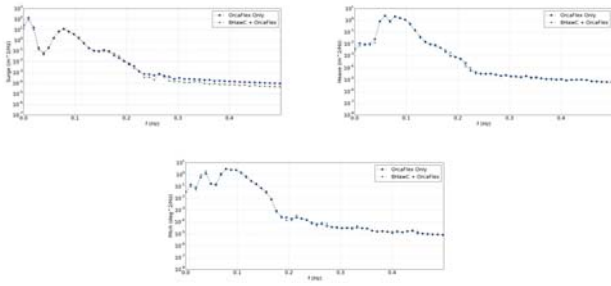
Verification



Development of coupling module between BHawC aeroelastic software and OrcaFlex for coupled dynamic analysis of floating wind turbines

12

Verification



Conclusion



- Large range of floaters and mooring system
- Flexibility offered by OrcaFlex and coupling methodology
- Verifications on rigid floater showed a very good agreement
- Verifications on flexible floater still on going but showed a very good agreement

- Further developments:
 - Simulation CPU time for complex model
 - Different timestep for each domain
 - Improve convergence of flexible floaters models
 - Modal analysis

Difference between Fast-OrcaFlex and BHawC-OrcaFlex



Fast-OrcaFlex	BHawC-OrcaFlex
Rigid floater only	Rigid and Flexible floater
Total floater mass defined in FAST	Floater can be defined into separated elements in OrcaFlex
Wind turbine modelization and interface motion calculation done in FAST	Wind turbine modelization and interface motion calculation done in BHawC
Load vector and Mass matrix exchanged at each time step	Load vector, Mass, Damping and Stiffness matrix exchanged at each time step
	Iterations are done in BhawC using stiffness and damping matrices
Position, Velocity and Acceleration imposed in OrcaFlex at each time step	Position, Velocity and Acceleration imposed in OrcaFlex at each time step

HAW HAMBURG | CC4E

New approach on the comparability of two- and three-bladed 20 MW offshore wind turbines

F. Anstock, M. Schütt and V. Schorbach 16.01.2019

Who are we?

Cooperation project:
“X-Rotor – two-bladed wind turbines”
 20 MW turbines of the next generation

HAW HAMBURG | CC4E

- University of Applied Sciences Hamburg
- Competence Center for Renewable Energy and Energy Efficiency
 - 70 associates working in 30 renewable energy projects

SIEMENS Gamesa
 RENEWABLE ENERGY

- One of the biggest companies for wind turbines

2 **HAW HAMBURG | CC4E**

Why two-bladed turbines?

Onshore:

Pro	Contra
<ul style="list-style-type: none"> Cheaper rotor and drivetrain 	<ul style="list-style-type: none"> More noise More unpleasant looks Lower power coefficient (Cp) More harmful dynamics

3 **HAW HAMBURG | CC4E**

Why two-bladed turbines?

Offshore:

Pro	Contra
<ul style="list-style-type: none"> Cheaper rotor and drivetrain Faster and easier erection <ul style="list-style-type: none"> Small weather windows Less components <ul style="list-style-type: none"> Less maintenance Better access by helicopter <ul style="list-style-type: none"> Faster maintenance Lower turbine head mass <ul style="list-style-type: none"> Less inertia if floating 	<ul style="list-style-type: none"> More noise More unpleasant looks Lower power coefficient (Cp) <ul style="list-style-type: none"> Extend rotor size by 2% Today better controllable (active or passive) More harmful dynamics

Why are there only few two-bladed turbines?
 > Investors demand proven technology and long-time track record of turbines
 > Benefits not yet completely quantified

4 **HAW HAMBURG | CC4E**

Comparability and the lower Cp-value

“Clear-cut comparisons between two- and three-bladed machines are notoriously difficult because of the impossibility of establishing equivalent designs.”
 - Tony Burton, Wind Energy Handbook

5 **HAW HAMBURG | CC4E**

Comparability and the lower Cp-value

Usual constrain: Rotor diameter remains unchanged
 > Result: Higher tip losses, thus lower Cp, thus lower power

VS.

Our approach: Absolute power-curve remains unchanged
 > Result: Rotor diameter is around 2% higher
 Mass increases by around 8%

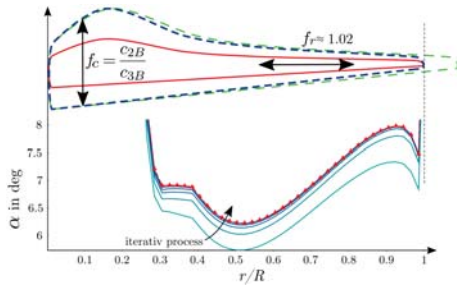
6 **HAW HAMBURG | CC4E**

Comparability and the lower Cp-value

Our approach in detail:

- Similar aerodynamics due to same airfoils, same relative chord length c , same angle of attack α , thus same optimal glide angle
- Scale blade by

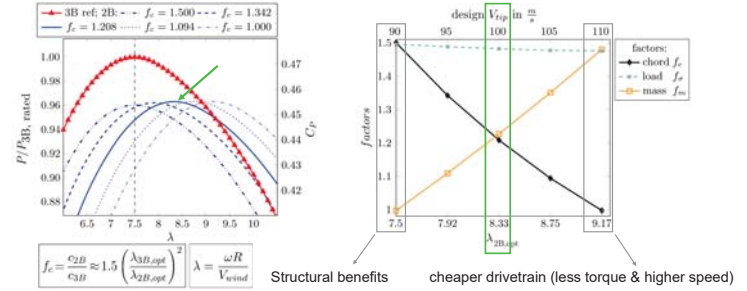
$$f_r = \frac{R_{2B}}{R_{3B}} = \sqrt{\frac{P_{3B, rated}}{P_{2B, rated}}}$$



7

Chord variation (f_c) of the INNWIND 20 MW RWT

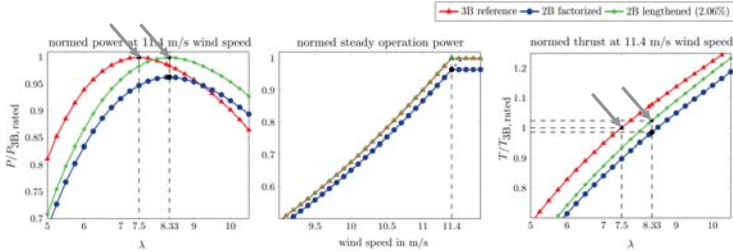
Comparison with equal diameter:



8

Power vs. Thrust

Loads, e.g. thrust, can be compared directly:



9

Summary and Conclusions

- Equal absolute power is only possible with increased rotor radius of ~2% (for Cp-max designs) ➔ Design point at rated remains together with all its implications on the turbine
- Before: 2- and 3-bladed turbines were compared by leveled cost of energy at the end of the design ➔ Now: Compare loads (e.g. thrust), masses or costs, during the whole design process and derive clues about diverging values
- Clear method to redesign a 2-bladed turbine out of a 3-bladed one ➔ High reproducibility and similar aerodynamics, thus clear assessments of symptoms and causes

10

Funded by

Thank you for your attention!

Fabian Anstock, M.Sc.
Research Associate

T +49 40 428 75 8768
fabian.anstock@haw-hamburg.de

HAW HAMBURG UNIVERSITY OF APPLIED SCIENCES
Competence Center for Renewable Energy and Energy Efficiency
Berliner Tor 21 / 20099 Hamburg
haw-hamburg.de

CC4E

Source: Leoni Schäfer

11

A2) New turbine and generator technology

Damping analysis of a floating hybrid wind and ocean-current turbine,
S.V.Kollappillai Murugan, Halmstad University

On Design and Modelling of 10 MW Medium Speed Drivetrain for Bottom-Fixed Offshore Wind
Turbines, S.Wang, NTNU

Modelling the dynamic inflow effects of floating vertical axis wind turbines,
D.Tavernier, Delft University of Technology

DAMPING ANALYSIS OF A FLOATING HYBRID WIND AND OCEAN-CURRENT TURBINE

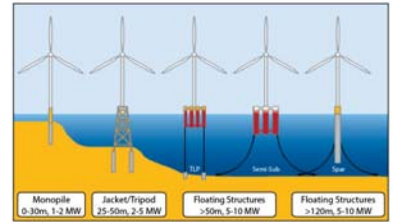
SAI VARUN KOLLAPPILLAI MURUGAN^{1,2} AND FREDRIC OTTERMO¹

¹THE RYDBERG LABORATORY FOR APPLIED SCIENCES, HALMSTAD UNIVERSITY, SWEDEN.

²WIND ENERGY CAMPUS GOTLAND, UPPSALA UNIVERSITY, SWEDEN.

CONCEPT

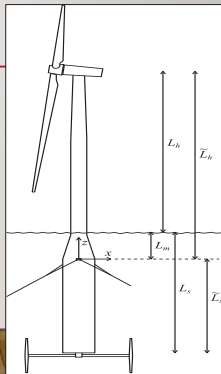
- Monopile
- Tripod
- TLP is fixed rigid to the surface
- Spar buoy is considered in this paper



Source: Principal Power. CC BY 4.0

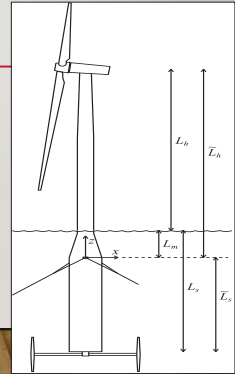
HYWIND SCOTLAND

Quantity	Variable	Value
Nacelle and rotor mass	m_n	370 tons
Tower mass	m_t	670 tons
Submerged tube mass	m_s	2300 tons
Ballast mass	m_b	7700 tons
Rotor diameter	d	156 m
Hub height	L_h	100 m
Submerged tube depth	L_s	78 m
Mooring depth	L_m	15 m
Ballast center of mass depth	L_b	70 m



HYBRID CASE

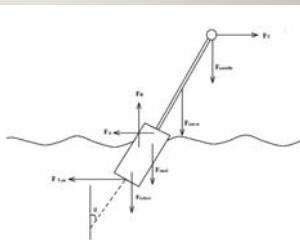
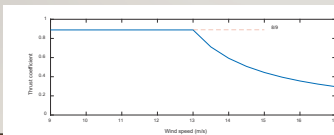
- Vertical axis ocean-current turbine attached at 78 m depth
- Swept area = 1000 m²
- Spar buoy floating structure



HYBRID CASE

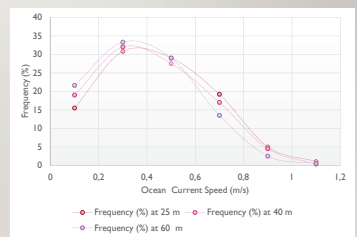
- Wind speed is taken in x direction and ocean current is allowed in 0°, 90°/180°
- Thrust force:

$$F_t = \frac{1}{2} C_t A \rho v^2$$



OCEAN DATA

- Ocean current data are taken from 25 m, 40 m, and 60 m
- 60-m distribution assumed at 78 m depth
- Swept area 1000 m², $C_p = 0.35$
- Average production: ~20 kW (0.18 GWh/yr)
- Ocean current turbine is simulated at 0.4 m/s.

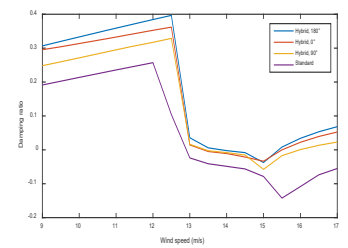


DYNAMIC CASE

- Damping Ratio
- The tower is allowed to oscillate from 3°
- Ocean current turbine is receiving ocean-current speeds up to roughly 1 m/s.

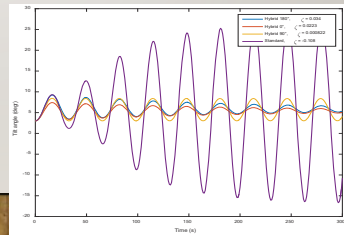
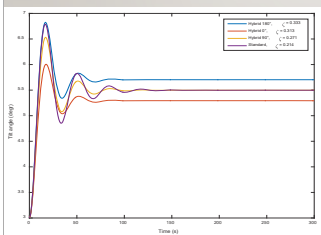
RESULT

- Std case- Negative damping after rated speed
- Hybrid case improves damping mostly in parallel and antiparallel direction
- Increasing the swept area of ocean current turbine positive damping can be achieved.



RESULT

- Hybrid case is well damped at less than 90 sec below rated wind speed
- Negative damping is introduced in standard case after rated wind speed



8. CONCLUSION & FUTURE REFERENCE

- The damping is improved to a greater amount using with the submerged turbine.
- Increasing the swept area of ocean current turbine positive damping can be achieved.
- Further dynamic analysis and 3d simulations to be conducted.

THANK YOU

On design and modelling of a 10 MW medium speed drivetrain for bottom fixed offshore wind turbines

Shuaishuai Wang,
 Amir R. Nejad, Torgeir Moan

Department of Marine Technology
 Norwegian University of Science and Technology
 January 16, 2019



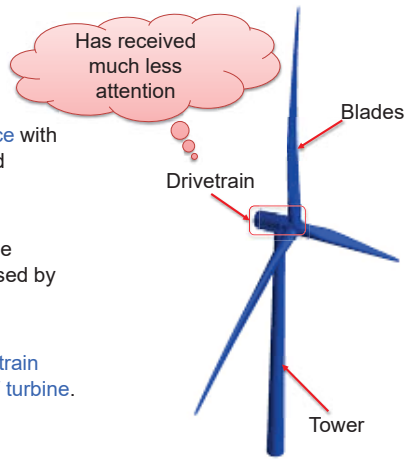
Outline

- Introduction
- Methodology
- Drivetrain design
- Drivetrain modelling
- Model comparison
- Concluding remarks



Background

- There is **no industrial experience** with 10 MW wind turbine design and manufacturing.
- The **earliest 10 MW wind turbine concept description** was proposed by DTU in 2013.
- **No attention** was paid on **drivetrain design** and study of the 10 MW turbine.



DTU 10 MW wind turbine

Background

The most common drivetrain concepts



High Speed

Medium Speed

Direct Drive

- One **medium speed drivetrain configuration** was proposed by DTU.
- **Advantageous** of medium speed drivetrain?
- Applications: AREVA 5 MW, Winergy 8 MW and Vestas 9.5 MW, etc.
- **No reference medium speed drivetrain** for public study and analysis today.

Motivation

- To provide a **baseline medium speed drivetrain** for DTU 10 MW RWT.
- The baseline model **could be used as a reference model** for multi-megawatt scale offshore wind turbines.

Objective

- To establish a **detailed drivetrain numerical model** for dynamic and reliability analysis.
- To provide all modelling parameters to **support public research studies**.

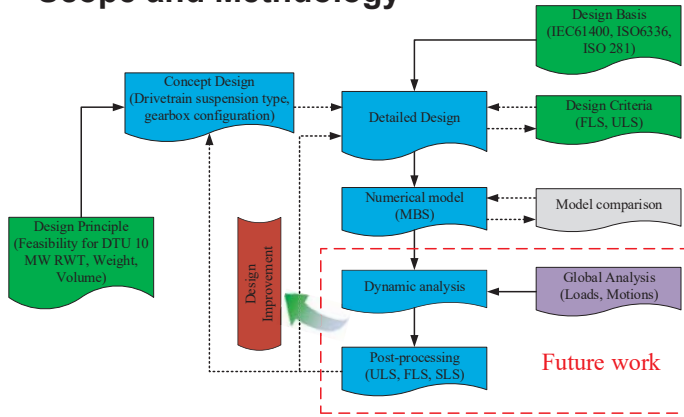


Outline

- Introduction
- **Methodology**
- Drivetrain design
- Drivetrain modelling
- Model comparison
- Concluding remarks



Scope and Methodology



Outline

- Introduction
- Methodology
- **Drivetrain design**
- Drivetrain modelling
- Model comparison
- Concluding remarks



Drivetrain design

Design basis: IEC 61400-4



- ✓ Gear design: ISO 6336-2, 3, 6
- ✓ Bearing design: ISO 76, 281
- ✓ Shaft design: DIN 743

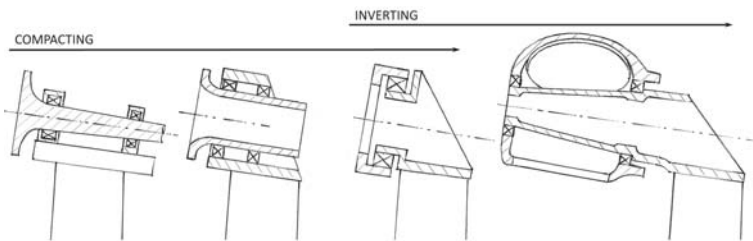


Design loads: IEC 61400-1, DNVGL-ST-0361

Design criteria:

- ✓ All components-gears, bearings and shafts-are designed to **withstand fatigue loads and ultimate loads** during normal operating conditions.
- ✓ All components are designed to **satisfy the relevant safety requirements** of wind turbine drivetrain design codes.

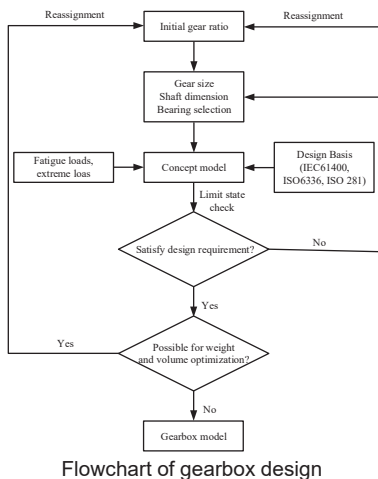
Drivetrain design - Drivetrain configuration



Main bearing arrangements (Torsvik et al. (2018))

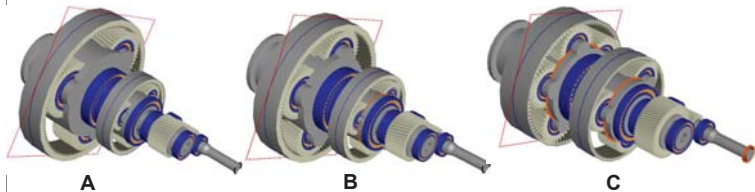
A **four-point supports**, two main bearings and two torque arms, **drivetrain configuration** is selected in this study.

Drivetrain design – Gearbox design flow



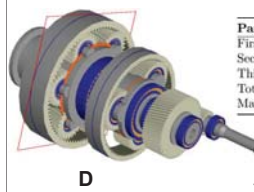
Flowchart of gearbox design

Drivetrain design – Gearbox layout options



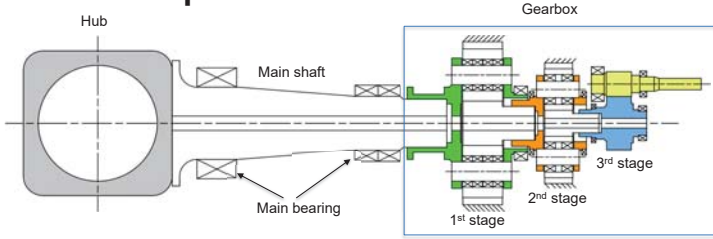
Comparison of 4 gearbox layout options

Parameter	A	B	C	D
First stage	1:6000 (3p)	1:5.280 (4p)	1:4.423 (5p)	1:3.316 (6p)
Second stage	1:5.348 (3p)	1:5.160 (3p)	1:5.192 (3p)	1:5.625 (3p)
Third stage	1:1.556	1:1.826	1:2.179	1:2.680
Total dry weight (×1000kg)	65.66	60.59	60.43	57.16
Maximum outer diameter (m)	3.878	3.396	3.098	3.068



- Principle: minimize drivetrain weight and volume
- Priority consideration: maximum outer diameter

Drivetrain specifications



10 MW wind turbine drivetrain schematic layout

10 MW wind turbine drivetrain specifications

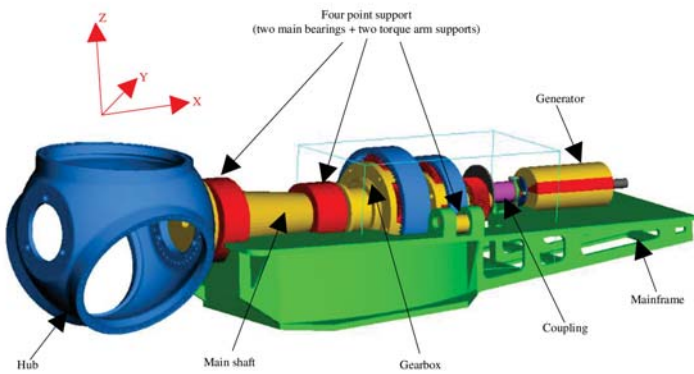
Parameter	Value
Drivetrain type	4-point supports
Gearbox type	Two planetary + one parallel
First stage gear ratio	1:4.423
Second stage gear ratio	1:5.192
Third stage gear ratio	1:2.179
Total gear ratio	1:50.039
Designed power (kw)	10000
Rated input shaft speed (rpm)	9.6
Rated generator shaft speed (rpm)	480.374
Total gearbox dry weight (x1000kg)	60.43
Maximum gearbox outer diameter (m)	3.098
Service life (year)	20

Outline

- Introduction
- Methodology
- Drivetrain design
- **Drivetrain modelling**
- Model comparison
- Concluding remarks

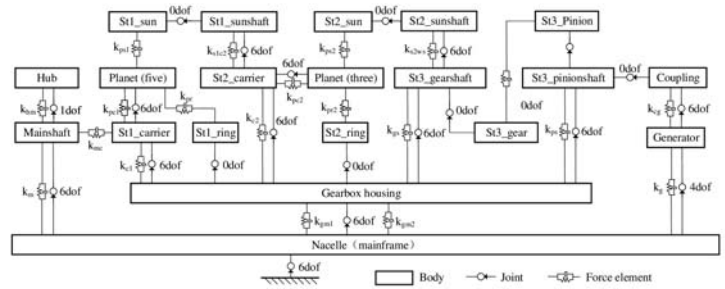


Drivetrain modelling – MBS model



10 MW wind turbine drivetrain MBS model

Drivetrain modelling – Topography diagram



Topography diagram of the 10 MW wind turbine drivetrain MBS model

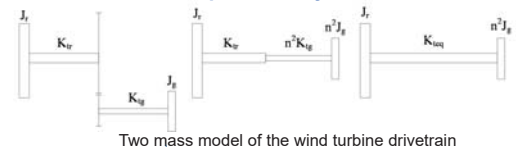
Outline

- Introduction
- Methodology
- Drivetrain design
- Drivetrain modelling
- **Model comparison**
- Concluding remarks



Model comparison

Simplified drivetrain model provided by DTU:



Two mass model of the wind turbine drivetrain

First eigenfrequency

$$f_n = \frac{1}{2\pi} \sqrt{\frac{k_{teq}(J_r + n^2 J_g)}{J_r n^2 J_g}} \quad f_n = \frac{1}{2\pi} \sqrt{\frac{k_{teq}}{J_r}} \quad k_{teq} = \frac{k_{tr} n^2 k_{tg}}{k_{tr} + n^2 k_{tg}}$$

Natural frequency for the shaft torsion mode.

Shaft torsion mode	Simulation frequency [Hz]	Reference frequency [Hz]
F free-free	4.003	3.889
F free-fixed	0.612	0.6116

The first eigenfrequency obtained from detailed drivetrain model match well with the corresponding value derived from simplified model.

Outline

- Introduction
- Methodology
- Drivetrain design
- Drivetrain modelling
- Model comparison
- **Concluding remarks**



19

Concluding remarks

- A four-point supports **drivetrain configuration** and a two planetary stages + one parallel stage **gearbox structure is designed** for DTU 10 MW wind turbine.
- Four **gearbox layout options** are provided and **compared** and one **optimized option** is finally selected with compromised consideration of volume, weight and load sharing performance principles.
- A high fidelity **numerical drivetrain model is developed** using MBS method.
- **Model comparison** is conducted, and the **rationality** of the developed drivetrain model is **initially verified**.

20



Thanks

21

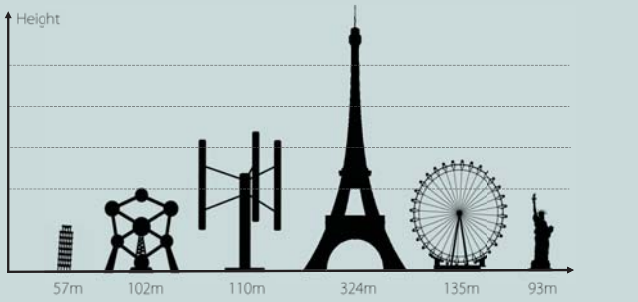


THE NEED FOR DYNAMIC
INFLOW MODELS
FOR VERTICAL AXIS WIND TURBINES

D. DE TAVERNIER, C. FERREIRA



VERTICAL-AXIS WIND TURBINES



LARGEST VAWT:



EOLE4, 4MW, QUEBEC

DYNAMIC INFLOW MODELLING TECHNIQUES:

- > Computational fluid dynamics or vortex methods
 - > Wake modelled in time and space
 - > Time-consuming
- > Engineering modes
 - > Wake not modelled in time and space
 - > Fast calculation



FLOATING VAWTS

RESEARCH QUESTION

Do we need **NEW DYNAMIC INFLOW MODELS** to enhance the modelling of floating vertical axis wind turbines?



CONTENT



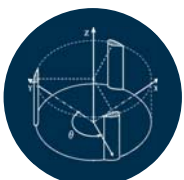
- Part 1 Theoretical approach
- Part 2 Practical approach
- Part 3 Conclusion

1

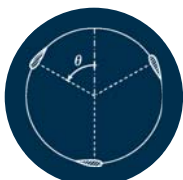
THEORETICAL APPROACH

The flow around a uniformly loaded unsteady actuator disk: methodology, results and discussion

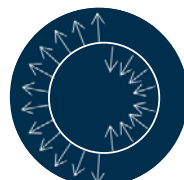
SIMPLIFY ROTOR




3D ROTOR



2D ROTOR



2D ACTUATOR



$$C_T(t) = C_{T0} + \Delta C_T \cdot \cos\left(\frac{2kV_{\infty}}{D}t\right)$$

↑ Baseline thrust ↑ Amplitude ↑ Reduced frequency

DYNAMIC INFLOW > DYNAMIC THRUST

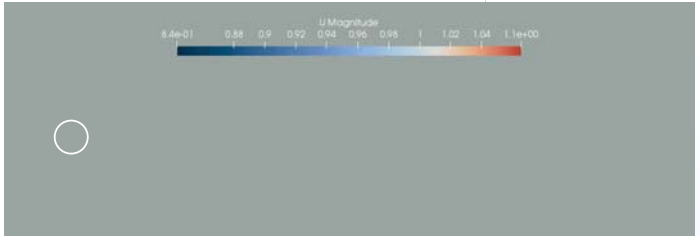
- ✓ Cyclic thrust coefficient
- ✓ Uniformly loaded
- ✓ velocity field computed using CFD

MODELLING VELOCITY FIELD

CFD MODEL

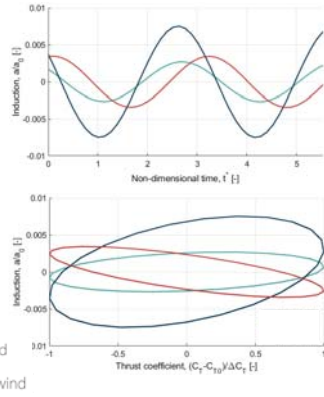
- ✓ 2D transient solver for incompressible flows (pisoFOAM)
- ✓ Uniformly distributed volume forces
- ✓ Grid dense around actuator, gradually coarser further away
- ✓ Initial conditions = steady case

MODELLING VELOCITY FIELD

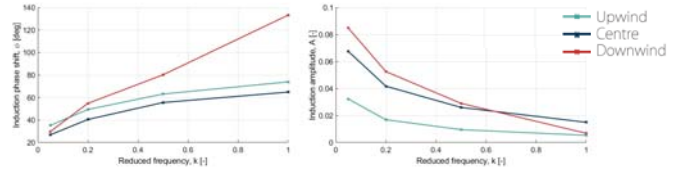


$C_{T0} = 0.11, \Delta C_T = 0.11, k=0.5$

INDUCTION AT 3 LOCATIONS



— Upwind
— Centre
— Downwind



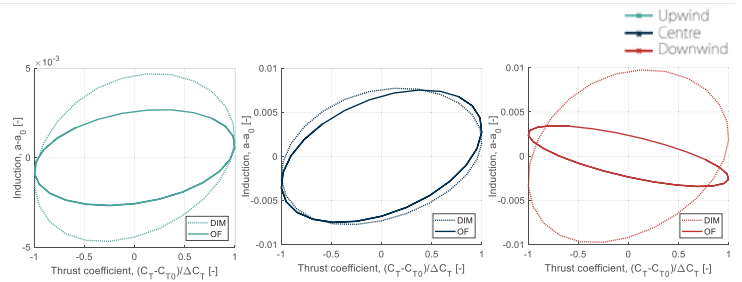
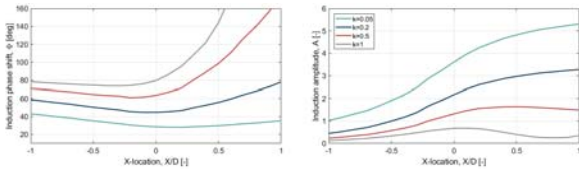
PHASE SHIFT & AMPLITUDE

- Phase shift increases with reduced frequency
- Phase shift different for various locations
- Induction amplitude decreases with reduced frequency
- Induction amplitude different at various locations

- Around the centre location, lowest phase shift
- Increasing rate highest downwind

- Induction amplitude decreases with increasing reduced frequency
- Induction amplitude increases with increasing x-location

PHASE SHIFT & AMPLITUDE



$C_{T0} = 0.77, \Delta C_T = 0.11, k = 1.0$

LARSEN AND MADSEN DYNAMIC INFLOW MODEL

OVERVIEW

Behaviour of induction depends on

- Reduced frequency
- Baseline and amplitude thrust
- Location of interest

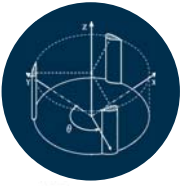
>> Larsen and Madsen model doesn't capture behaviour upwind and downwind



PRACTICAL APPROACH

The performance of a cyclic surging YAWF: methodology, results and discussion

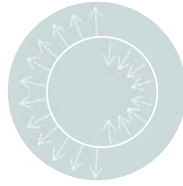
SIMPLIFY ROTOR



3D ROTOR



2D ROTOR



2D ACTUATOR

$$s(t) = s_0 + \Delta s \cdot \cos\left(\frac{2kV_{\infty}}{D} t\right)$$

↑ Baseline surge
 ↑ Amplitude
 ↓ Reduced frequency

DYNAMIC INFLOW > SURGING MOTION
 ✓ Cyclic surging motion
 ✓ Loading computed for reference turbine

MODELLING ROTOR LOADING

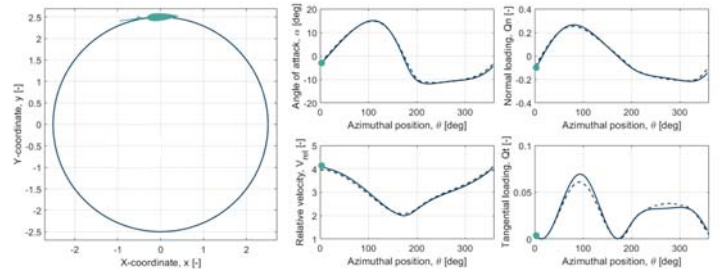
ACTUATOR LINE OPENFOAM MODEL

- ✓ 3D model
- ✓ TurbineFOAM library in OpenFOAM
- ✓ Blade element theory: 2D lift and drag
- ✓ Velocity field is modelled directly in space and time

ACTUATOR CYLINDER MODEL

- ✓ 2D engineering model
- ✓ Blade element theory: 2D lift and drag
- ✓ Velocity field from 2D incompressible Euler equations and equation of continuity
- ✓ With and without Larsen and Madsen dynamic inflow model

MODELLING ROTOR LOADING



LOADING FROM 3 MODELS

- ✓ Actuator line OpenFOAM model
- ✓ Actuator cylinder – no dynamic inflow model
- ✓ Actuator cylinder – with dynamic inflow model

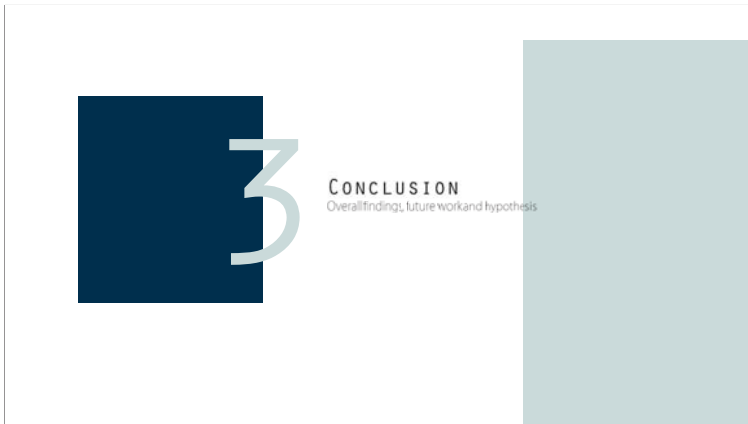
— OF
 — AC – no DIM
 — AC – with DIM

OVERVIEW

Engineering dynamic inflow model

- ✓ Capture overall behaviour better
- ✓ No improvement on average power coefficient

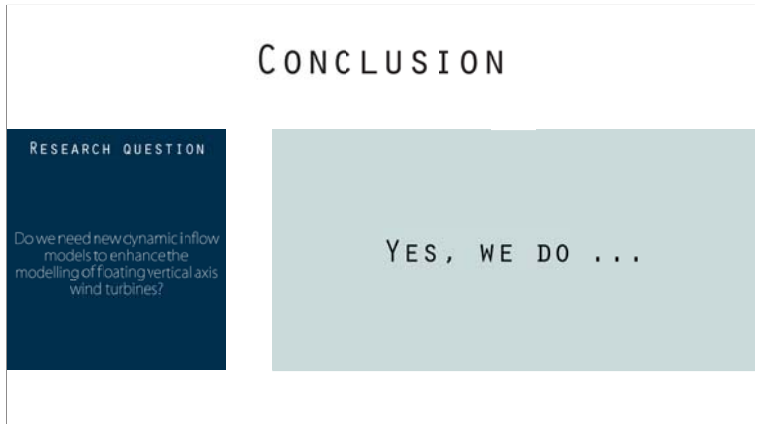
>> Current dynamic inflow model is not enough



3

CONCLUSION
Overall findings, future work and hypothesis

A slide with a dark blue square on the left containing a large white number '3'. To the right of the square, the word 'CONCLUSION' is written in bold, uppercase letters. Below it, the text 'Overall findings, future work and hypothesis' is written in a smaller font. A light blue vertical bar is on the right side of the slide.



CONCLUSION

RESEARCH QUESTION

Do we need new dynamic inflow models to enhance the modelling of floating vertical axis wind turbines?

YES, WE DO ...

A slide with the word 'CONCLUSION' at the top right. Below it, a dark blue box contains the text 'RESEARCH QUESTION' and a question: 'Do we need new dynamic inflow models to enhance the modelling of floating vertical axis wind turbines?'. To the right of this box, a light blue box contains the text 'YES, WE DO ...'.



B1) Grid connection and power system integration

Power quality in offshore grids; Prof. Elisabetta Tedeschi, NTNU

Reducing Rapid Wind Farm Power Fluctuations Using Energy Storage of the Modular Multilevel Converter, S.Sanchez, NTNU

An Improved and Expanded Fault Detection and Clearing Strategy Application to a Hybrid Wind Farm integrated to a Hybrid HVDC Main Transmission Level Converter, J.K. Amoo-Otoo, University of Idaho

Prolonged Response of Offshore Wind Power Plants to DC Faults, Ö. Göksu, DTU

Power quality in offshore grids

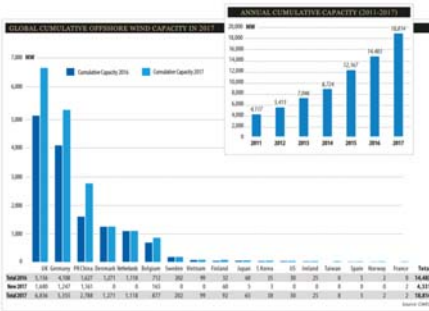
Prof. Elisabetta Tedeschi
Dept. of Electric Power Engineering, NTNU

EERA DeepWind Conference,
Trondheim, 17 January 2019

Presentation lay-out

- Trends in offshore generation
- Overview of **power quality** issues in offshore grids:
 - in **distribution** systems
 - Offshore wind farms
 - Other marine energy farms
 - Oil and gas platforms
 - in **transmission** systems
- Conclusions

Offshore wind - Trends



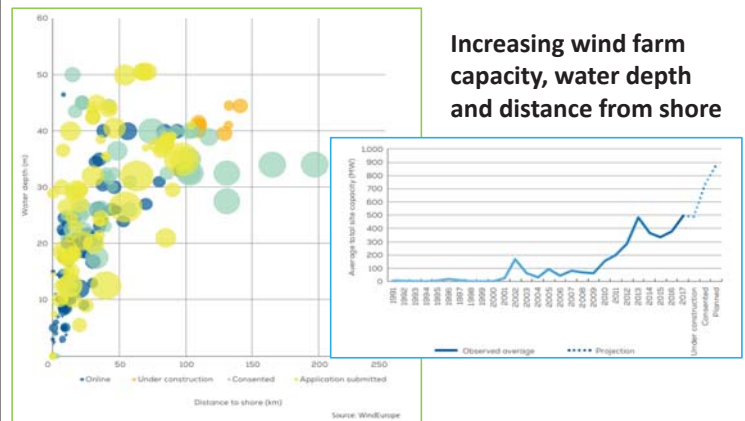
Offshore wind represents 3.5% of the global installed wind capacity

In Europe, offshore wind is expected to increase from 15.8 GW in 2017 to 66 GW in 2030

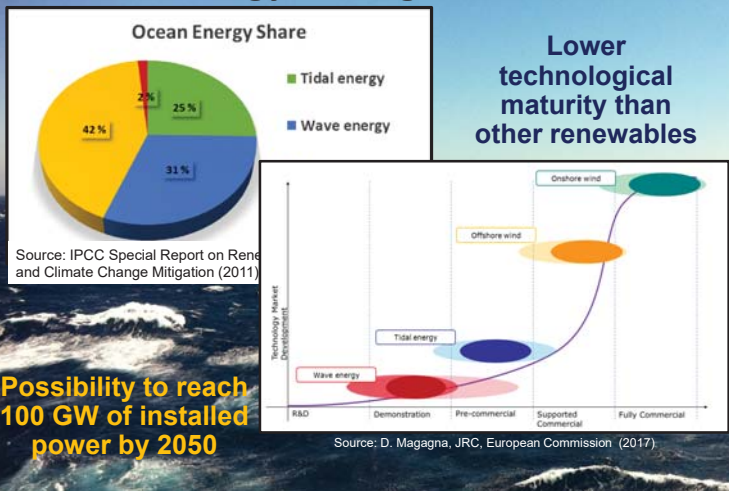


Source: DONG energy

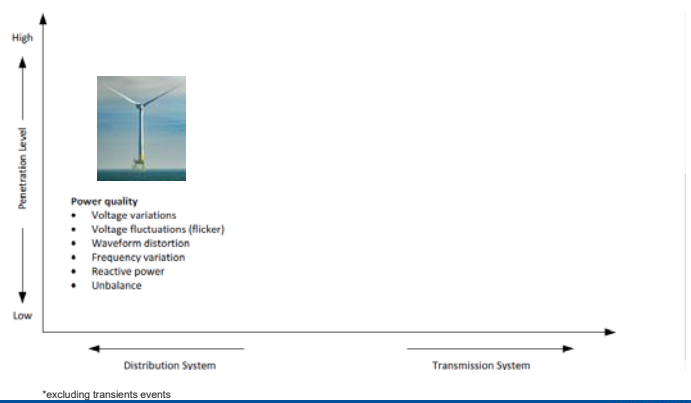
Offshore wind development



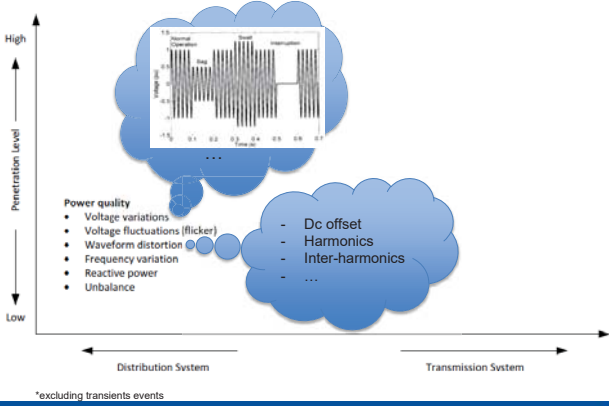
Marine Energy - Background



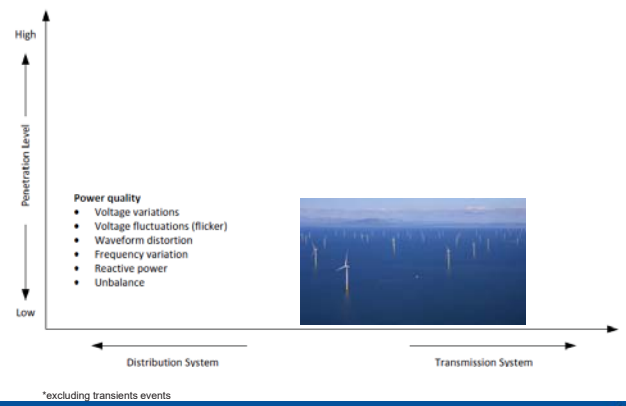
Power quality (PQ) in offshore grids



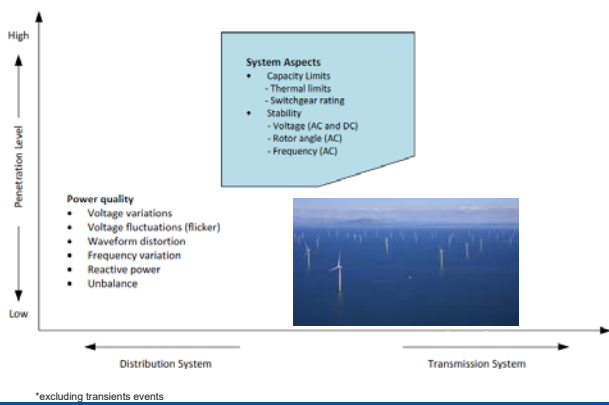
Power quality (PQ) in offshore grids



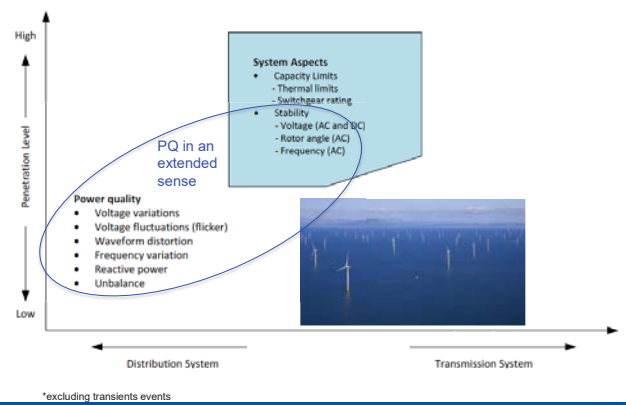
Power quality (PQ) in offshore grids



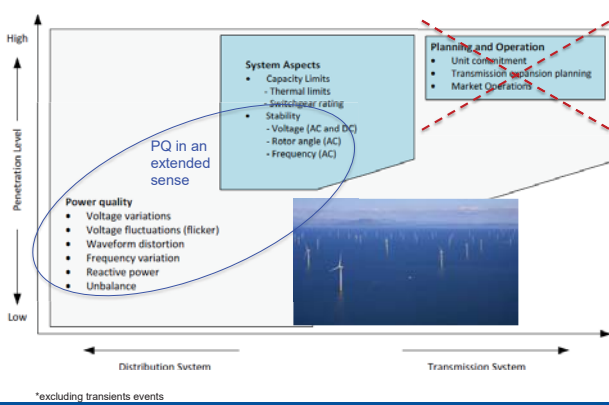
Power quality (PQ) in offshore grids



Power quality (PQ) in offshore grids



Power quality (PQ) in offshore grids

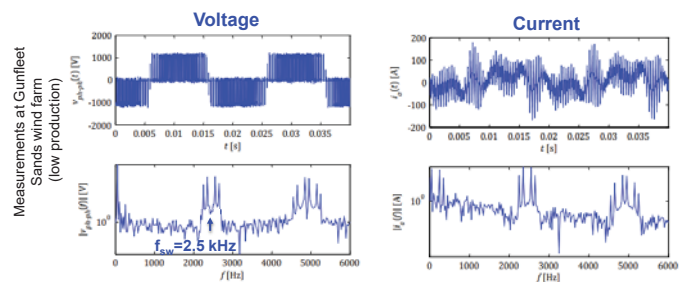
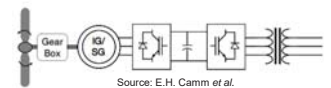


PQ in AC offshore grids: wind farms

Waveform distortion

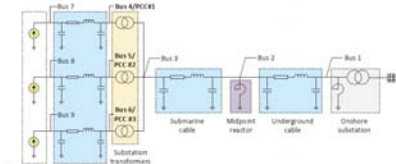
The type of (generators,) power electronic interfaces and their control impact the harmonic generation...

Type 4 Wind turbine



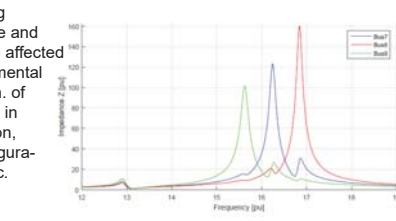
PQ in AC offshore grids: wind farms

Waveform distortion



Risk of resonance

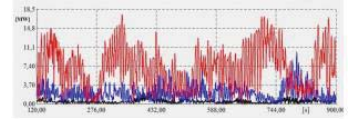
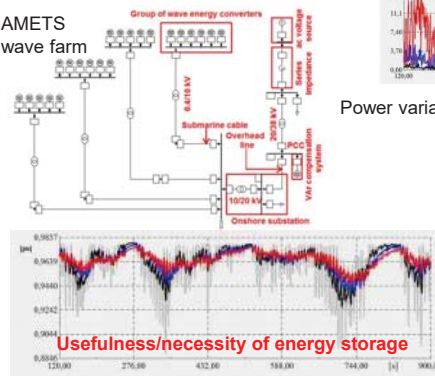
Driving impedance and resonance are affected by environmental factors, n. of turbines in operation, farm configuration etc.



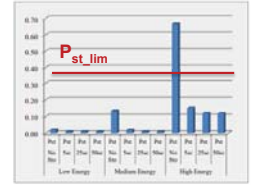
PQ in AC offshore grids: wave farms

Flicker and voltage variations

AMETS wave farm



Power variability due to resource intermittency



Criticality of voltage fluctuations

Usefulness/necessity of energy storage

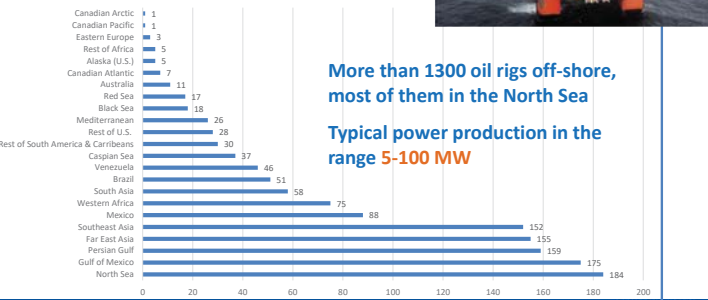
Offshore Oil and Gas - Status

Offshore production accounts for 30% of global oil production and 27% of global gas production



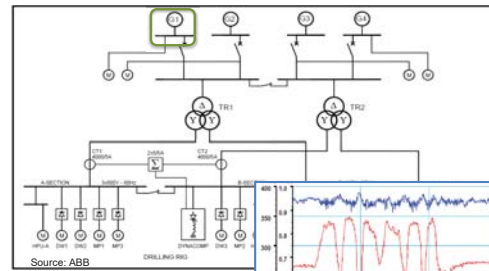
Source: Equinor

Number of offshore rigs (January 2018)



More than 1300 oil rigs off-shore, most of them in the North Sea
Typical power production in the range 5-100 MW

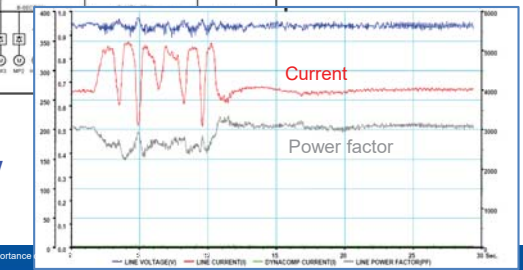
Electrical power system on O&G rigs



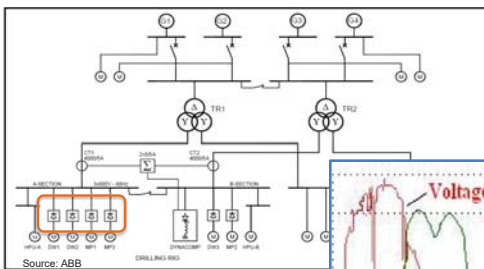
O&G platforms can be classified as electrically «weak grids»

Power quality is low

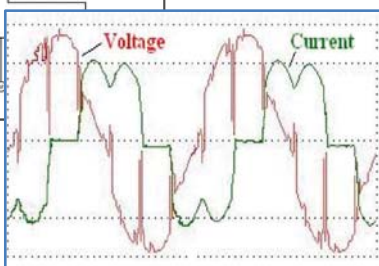
- High reactive power demand/low power factor



Electrical power system on O&G rigs



O&G platforms can be classified as electrically «weak grids»

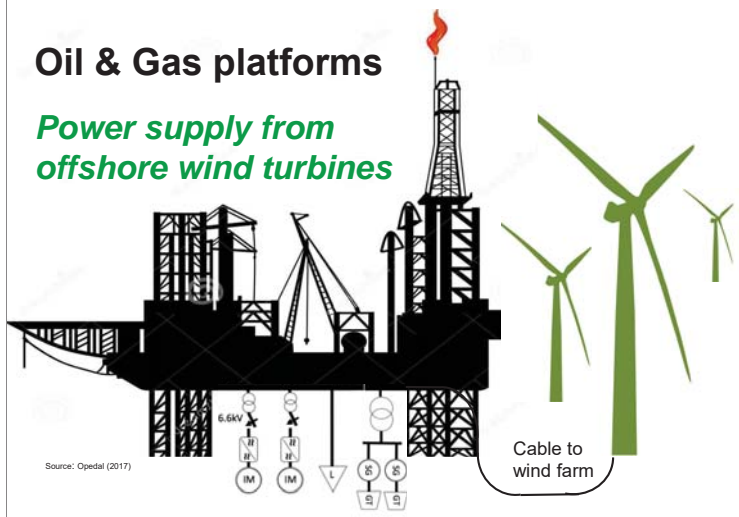


- Voltage notching

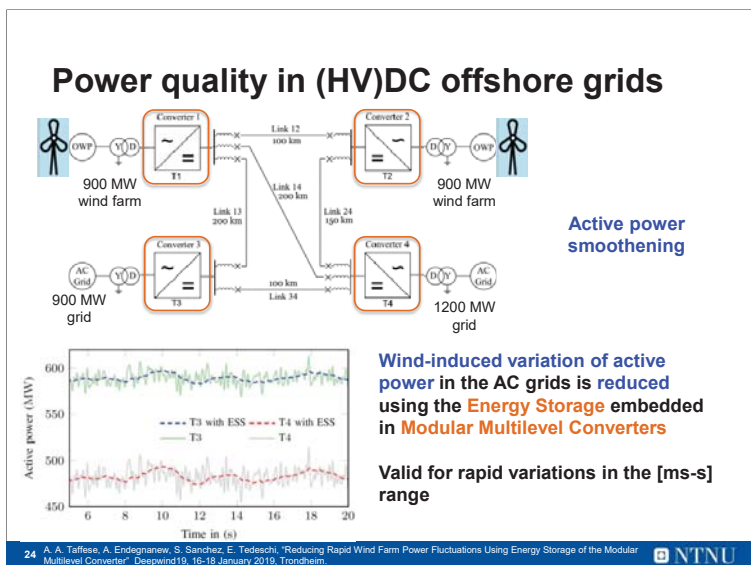
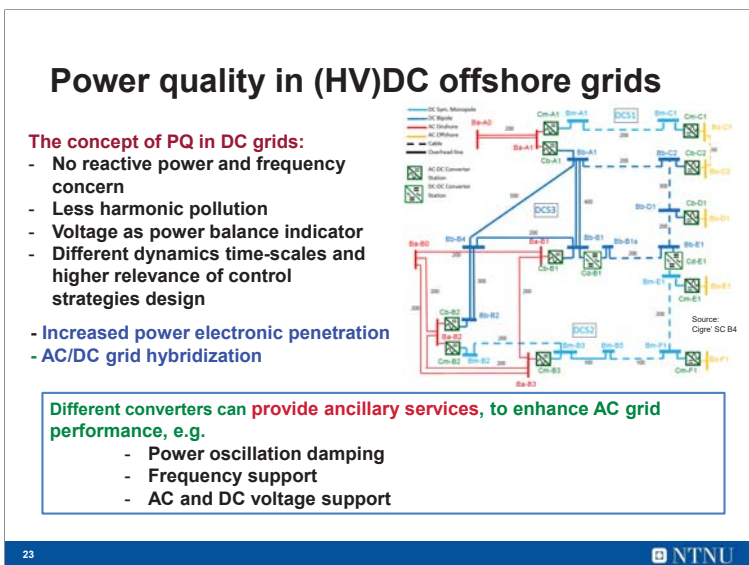
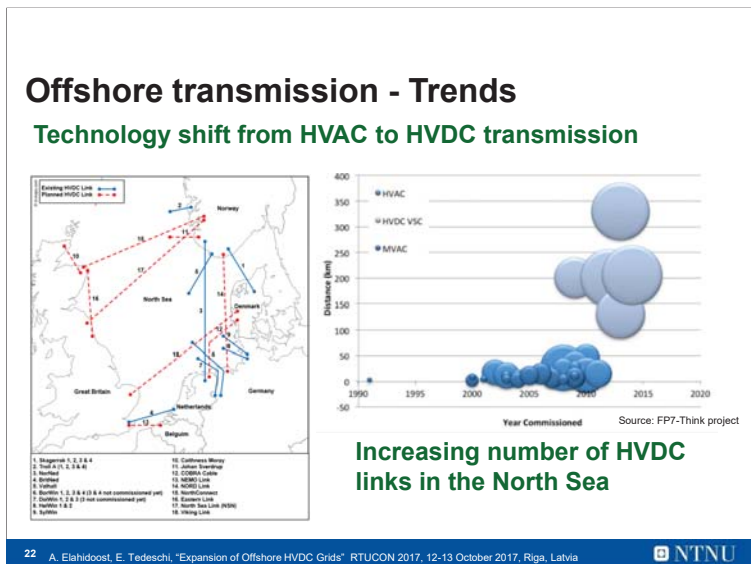
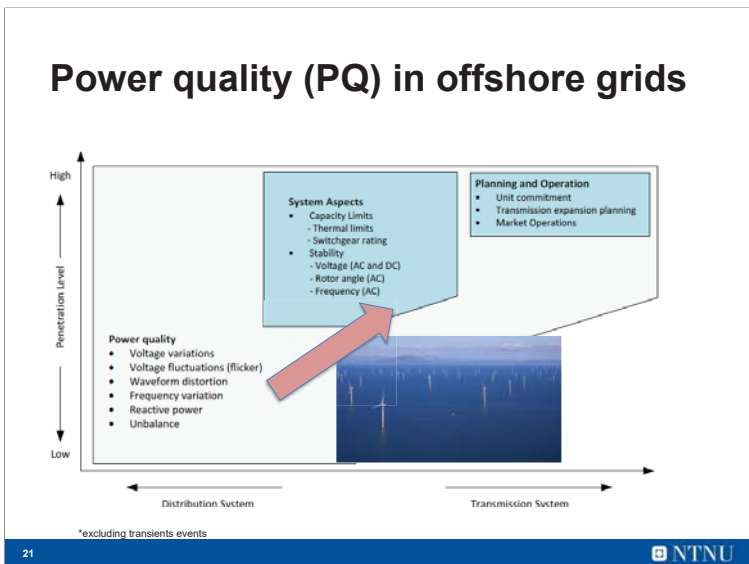
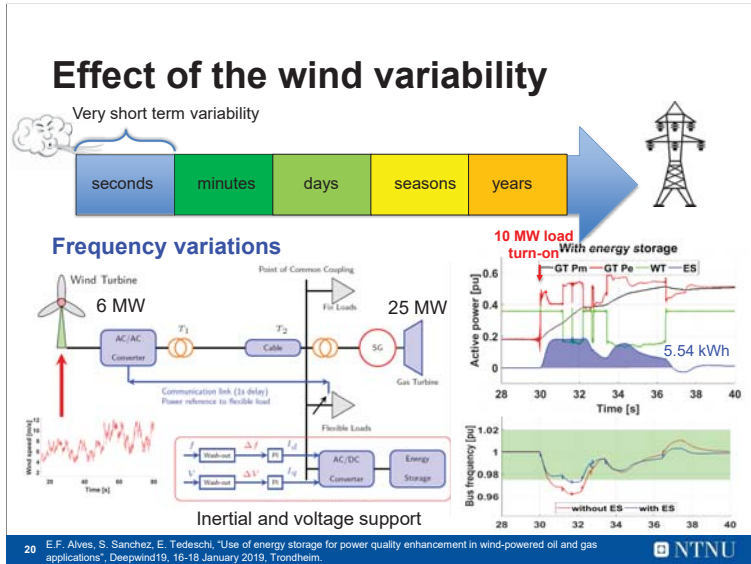
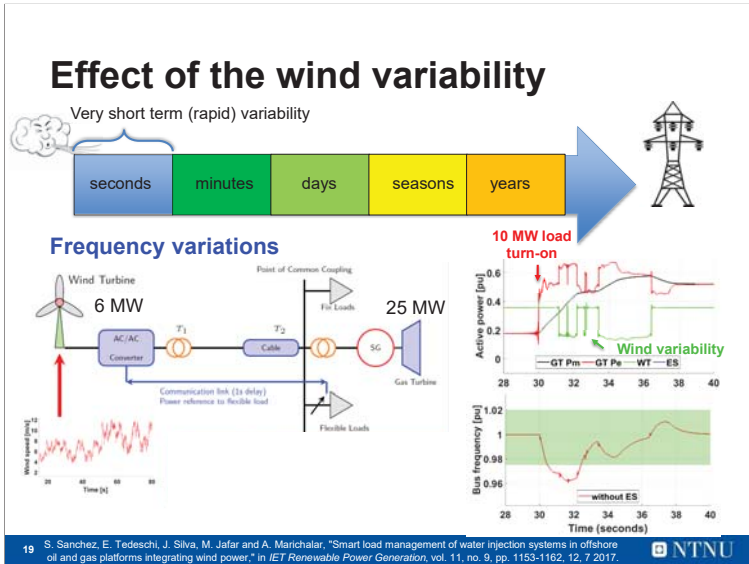
Estimated financial loss (2010) for incidents due to poor power quality in O&G is 250-750 KEUR/day

Oil & Gas platforms

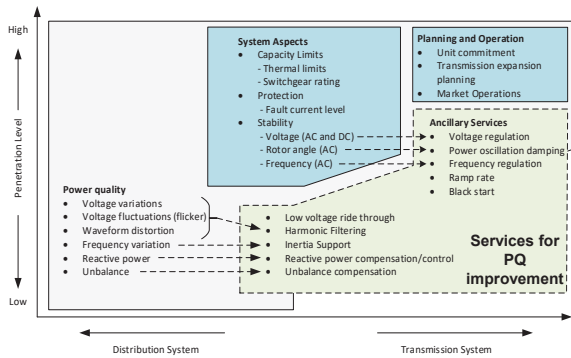
Power supply from offshore wind turbines



Source: Opedal (2017)



Power quality in offshore grids



*excluding transients events

25 A. A. Taffese, E. Tedeschi, "Electrical Power Transmission and Grid Integration", Chapter 8 of the book "Renewable Energy from the Oceans: From wave, tidal and gradient systems to marine-based wind and solar" Institution of Engineering and Technology (IET) (2019 - *in press*)



Conclusions

- **Intermittency** of wind and marine sources significantly affects the power quality of the electric grid
- **Power electronics** can contribute to the problem, but also help providing **countermeasures**
- Use of **energy storage** may be pivotal with the increase of offshore energy penetration
- Need for **harmonization** in the grid codes

26 E. Robles, M. Haro-Larrode, M. Santos-Mugica, A. Etxegarai, E. Tedeschi, "Comparative analysis of European grid codes relevant to offshore renewable energy installations", Renewable and Sustainable Energy Reviews, Volume 102 pp 171-185, 2019.



References

- GWEC, "Global Wind Report" 2017.
- WindEurope, "Wind in Power 2017", February 2018.
- IPCC Special Report on Renewable Energy Sources and Climate Change Mitigation (2011)
- D. Magagna, JRC, European Commission (2017)
- A. A. Taffese, E. Tedeschi, "Electrical Power Transmission and Grid Integration", Chapter 8 of the book "Renewable Energy from the Oceans: From wave, tidal and gradient systems to marine-based wind and solar" Institution of Engineering and Technology (IET) (2019 - *in press*)
- L. H. Kocewjak, "Harmonics in large offshore wind farms". PhD Thesis, Department of Energy Technology, Aalborg University, 2012
- H. Brantsæther, "Harmonic Resonance Mode Analysis and Application for Offshore Wind Power Plants". MSc Thesis, Department of Electric Power Engineering, NTNU, 2015.
- M. Santos, A. Blavette, E. Tedeschi, D. O'Sullivan, F. Salcedo, "Case studies on the benefits of energy storage for power quality enhancement: point absorber arrays" 4th International Conference on Ocean Energy 2012 (ICOE12), Dublin, 17-19 October 2012.
- Schipman, K., & Delincé, F. "The importance of good power quality". ABB Power Qual. Prod., Charleroi, Belgium, ABB Review 2010.
- Evans, I. C., & Richards, M. J. (2011, April). The price of poor power quality. In 2011 AAE National Technical Conference (pp. 1-17).
- S. Sanchez, E. Tedeschi, J. Silva, M. Jafar and A. Marichalar, "Smart load management of water injection systems in offshore oil and gas platforms integrating wind power", in *IET Renewable Power Generation*, vol. 11, no. 9, pp. 1153-1162, 12, 7 2017.
- E. F. Alves, S. Sanchez, E. Tedeschi, "Use of energy storage for power quality enhancement in wind-powered oil and gas applications", Deepwind19, 16-18 January 2019, Trondheim.
- A. Elahidoost, E. Tedeschi, "Expansion of Offshore HVDC Grids" RTUCON 2017, 12-13 October 2017, Riga, Latvia
- A. A. Taffese, A. Endegnanew, S. Sanchez, E. Tedeschi, "Reducing Rapid Wind Farm Power Fluctuations Using Energy Storage of the Modular Multilevel Converter" Deepwind19, 16-18 January 2019, Trondheim
- E. Robles, M. Haro-Larrode, M. Santos-Mugica, A. Etxegarai, E. Tedeschi, "Comparative analysis of European grid codes relevant to offshore renewable energy installations", Renewable and Sustainable Energy Reviews, Volume 102 pp 171-185, 2019.

27



Thanks for your attention!



elisabetta.tedeschi@ntnu.no



Reducing Rapid Wind Farm Power Fluctuations Using the Modular Multilevel Converter

Abel A. Taffese, Atsede G. Endegnanew,
Santiago Sanchez, and Elisabetta Tedeschi
Department of Electric Power Engineering, NTNU
Sintef Energy Research
January, 2019

Table of Contents

- Introduction
 - Outcomes
- Modular multilevel converter
- Method
- Results
 - Simulation
 - Laboratory
- Conclusions

Outcomes of the paper

Objective

- To *Develop* a tool to smooth the rapid power fluctuations of wind farms with MMC.

Problem description

Offshore wind farms integration



Problem description

There are **three power fluctuations** types that are linked with the wind variability:

1. Long-term → seasonal variations.
2. Short-term → time scale of minutes to few hours.
3. **Rapid changes** → fast variations (wind gusts, tower shadow, ...).

Problem description

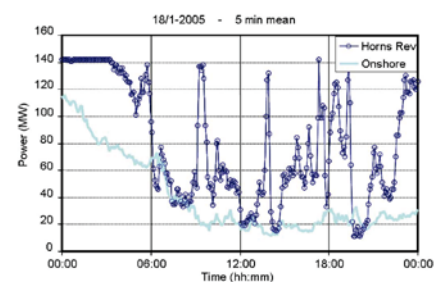


Fig. 1. Power generation of Horns Rev offshore wind farm and onshore wind turbines on January 18, 2005.

HVDC grid
 Introduction
 Outcomes

Problem description

Since **short-term and rapid changes** are **difficult to predict**, **energy storage solutions** are being proposed to smooth the variations out.

Santiago S. NTNU HVDC grid January, 2019 3 / 10

HVDC grid
 Introduction
 Outcomes

Problem description

Multiterminal HVDC grid for wind farms integration.

Network Topologies North Sea MTDC

- Radial
- Mesh or Ring

Santiago S. NTNU HVDC grid January, 2019 3 / 10

Table of Contents

- Introduction
 - Outcomes
- Modular multilevel converter
- Method
- Results
 - Simulation
 - Laboratory
- Conclusions

Santiago S. NTNU HVDC grid January, 2019 4 / 10

HVDC grid
 Modular multilevel converter

Capability of an MMC to store energy (W)

The aim is to control W in order to smooth the **fast power fluctuation**.

Santiago S. NTNU HVDC grid January, 2019 4 / 10

HVDC grid
 Modular multilevel converter

Capability of an MMC to store energy (W)

The aim is to control W in order to smooth the **fast power fluctuation**.

Santiago S. NTNU HVDC grid January, 2019 4 / 10

HVDC grid
 Modular multilevel converter

Capability of an MMC to store energy (W)

The aim is to control W in order to smooth the **fast power fluctuation**.

Santiago S. NTNU HVDC grid January, 2019 4 / 10

HVDC grid
Modular multilevel converter

Capability of an MMC to store energy (W)

source \leftrightarrow DC power MMC

Level

sink

P flow

The aim is to control W in order to smooth the fast power fluctuation.

Santiago S. NTNU HVDC grid January, 2019 4 / 10

HVDC grid
Modular multilevel converter

Capability of an MMC to store energy (W)

source \leftrightarrow energy storage capability MMC

Level

sink

P flow

The aim is to control W in order to smooth the fast power fluctuation.

Santiago S. NTNU HVDC grid January, 2019 4 / 10

HVDC grid
Modular multilevel converter

Capability of an MMC to store energy (W)

Arm energy dynamics:

$$\frac{dW}{dt} = \frac{1}{3C} (P_{dc} - P_{ac}) \quad (1)$$

W: Arm energy
C: equivalent arm capacitor
 P_{dc} : DC power
 P_{ac} : AC power

The aim is to control W in order to smooth the fast power fluctuation.

Santiago S. NTNU HVDC grid January, 2019 4 / 10

Table of Contents

- Introduction
 - Outcomes
- Modular multilevel converter
- Method
- Results
 - Simulation
 - Laboratory
- Conclusions

HVDC grid
Method

Energy control scheme

$P_{ac,ref} + \frac{V_{dc,ref} - V_{dc}}{\rho}$

$P_{ac,ref}$

PI $V_{d,ref}$

Current control

V_d

P_{ac}

HVDC grid
Method

Energy control scheme

$P_{ac} + \frac{V_{dc,ref} - V_{dc}}{\rho}$

$P_{ac,ref}$

PI $V_{d,ref}$

Current control

V_d

P_{ac}

$W_{ref} + \Delta W$

W control

Circulating current

I_c

$3V_{dc}$

P_{dc}

$\frac{1}{3Cs}$

W

HVDC grid
Method

Energy control

We use a Non-linear control for W.

$$I_{c,ref} = \frac{1}{u_c} \left(\frac{d(W_{ref} + \Delta W)}{dt} + P_{ac} - K(W_{ref} + \Delta W - W) \right) \quad (2)$$

K: virtual gain.

Santiago S. NTNU HVDC grid January, 2019 6 / 10

HVDC grid
Method

Energy control

We use a Non-linear control for W.

$$I_{c,ref} = \frac{1}{u_c} \left(\frac{d(W_{ref} + \Delta W)}{dt} + P_{ac} - K(W_{ref} + \Delta W - W) \right) \quad (2)$$

K: virtual gain.

Remove DC component Low pass filter

Santiago S. NTNU HVDC grid January, 2019 6 / 10

Table of Contents

- Introduction
 - Outcomes
- Modular multilevel converter
- Method
- Results
 - Simulation
 - Laboratory
- Conclusions

Santiago S. NTNU HVDC grid January, 2019 7 / 10

HVDC grid
Results
Simulation

Simulation

Test system

Power fluctuation

Constant P

Droop mode

W. Leterme, et al., A new HVDC grid test system for HVDC grid dynamics and protection studies in EMTF-type software, in 11th IET International Conference on AC and DC Power Transmission, 2015.

Santiago S. NTNU HVDC grid January, 2019 7 / 10

HVDC grid
Results
Simulation

Simulation

Active power (MW)

DC voltage (pu)

Time in (s)

Start $\Delta P_1 = \pm 10MW$ → Fluctuation of Power 3 and 4

Santiago S. NTNU HVDC grid January, 2019 7 / 10

HVDC grid
Results
Simulation

Simulation

Active power (MW)

DC voltage (pu)

Time in (s)

Start $\Delta P_1 = \pm 10MW$ → Fluctuation of DC voltage

Santiago S. NTNU HVDC grid January, 2019 7 / 10

HVDC grid
Results
Simulation

Simulation

When smoothening function is enabled the active powers and dc voltage show improvements

Santiago S. NTNU HVDC grid January, 2019 7 / 10

HVDC grid
Results
Simulation

Simulation

- The arm energy \rightarrow larger variation (ΔW enabled).
- The method is distributed.

Onshore converters (3 and 4) \leftrightarrow arm energy variation.

Santiago S. NTNU HVDC grid January, 2019 7 / 10

HVDC grid
Results
Laboratory

National Smart Grid Laboratory (Norway)

Rated power: 60 KVA
Number of sub-modules: 18 sm
AC voltage: 400 V
DC voltage: 700 V

Santiago S. NTNU HVDC grid January, 2019 8 / 10

HVDC grid
Results
Laboratory

National Smart Grid Laboratory (Norway)

Step W_{ref}

Santiago S. NTNU HVDC grid January, 2019 8 / 10

HVDC grid
Results
Laboratory

National Smart Grid Laboratory (Norway)

Santiago S. NTNU HVDC grid January, 2019 8 / 10

HVDC grid
Results
Laboratory

National Smart Grid Laboratory (Norway)

Step W_{ref}

Santiago S. NTNU HVDC grid January, 2019 8 / 10

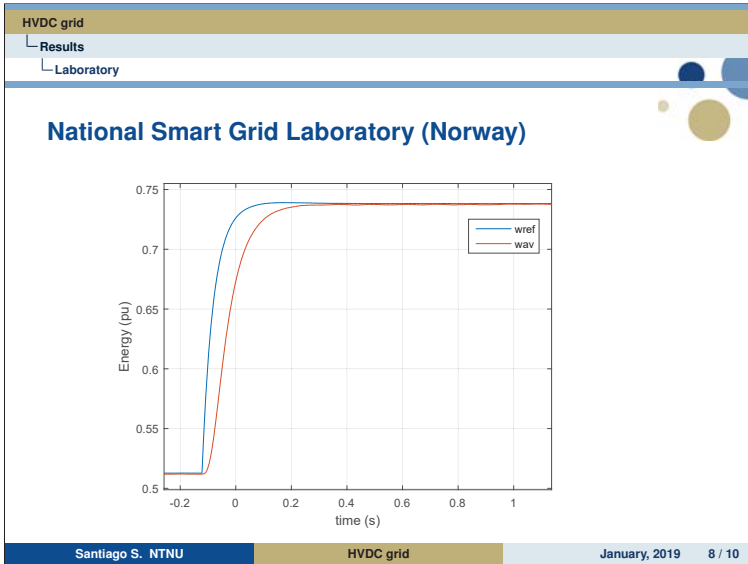


Table of Contents

- Introduction
 - Outcomes
- Modular multilevel converter
- Method
- Results
 - Simulation
 - Laboratory
- Conclusions

- HVDC grid
- Conclusions
- ### Conclusions
- We developed an energy controller that helps to exploit the energy storage capability of the MMC.
 - We validated the energy control technique in the laboratory.
 - Fast power fluctuations from wind farms can be compensated applying such controller to the MMCs of the HVDC grid.
- Santiago S. NTNU HVDC grid January, 2019 9 / 10

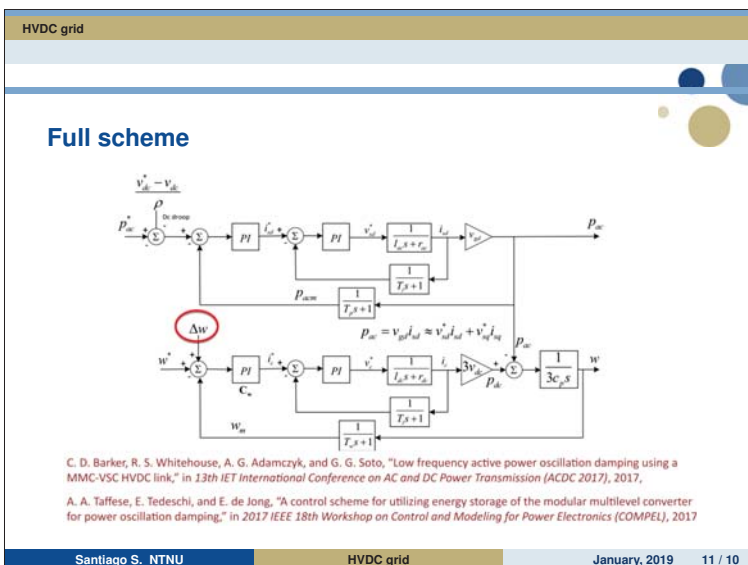
HVDC grid

Conclusions

Thank you!

Questions

Santiago S. NTNU HVDC grid January, 2019 10 / 10



An Expanded Fault Detection and Clearing Strategy
Application to a Hybrid Wind Farm integrated to an AC grid

JOHN KWEKU AMOO-OTOO, P.E
UNIVERSITY OF IDAHO
Electrical and Computer Engineering Department
Dissertation Committee

Prof Brian K. Johnson, University of Idaho, Moscow, Idaho(Major Prof)
Prof Herbert Hess, University of Idaho, Moscow, Idaho
Prof Oriol Gomis-Bellmunt, UPDC, Barcelona, Spain

*EERA Deep Wind Energy 2019 Conference, Trondheim, Norway
16th January-18th January, 2019*

Non-Business Use

1

My Contribution to Research

- My contribution to this dissertation research
 - Hybrid Wind Farm (DFIG plus PMSG Wind Turbines) integrated to Main DC Grid and Main Transmission Level HVDC Hybrid Converter and AC grid
 - Topology consists of 3 nodes or groups of aggregate models of total wind turbine generation source totaling 1800MW, 60Hz.
 - The first node or group generation source consists of a 600MW of DFIG, each DFIG with an output of 5MW which have been grouped in 3 subgroups of Qty (40) DFIG.
 - Rating of DFIG is 5MW, 60Hz with stator rating of 0.69kV and Rotor rating of 4.16kV
 - The output of the stringed DFIG AC windfarm is integrated to an internal 33kV AC collector bus which is stringed together to form the main offshore AC collector bus with an output of 34.5kVac.
 - The main 34.5kVAC collector bus is then integrated with a step-up power transformer which steps the output voltage from 34.5kVac to 150kV ac.
 - The 150kV side of the step-up transformer is integrated with a one terminal full scale Main HVDC MMC-VSC₁ which act as a rectifier which converts the AC voltage to DC voltage before it is integrated to an HVDC main +/-150kV DC collection grid bus all located offshore.

Non-Business Use

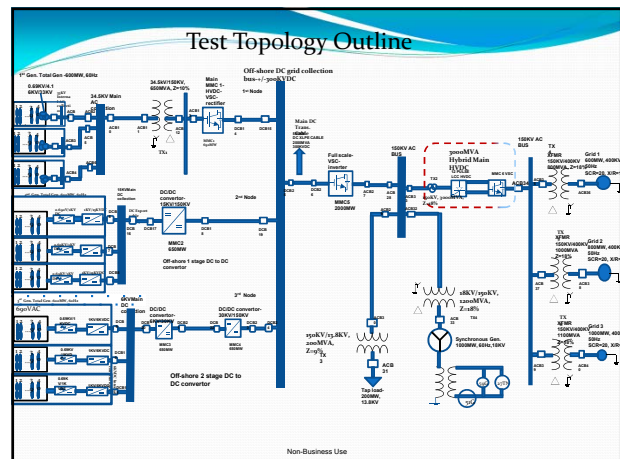
4

AGENDA

- Abstract
- My contribution to the dissertation
- Problem Statement
- Research Methodology(**Remaining Task**)
- Test Topology or Outline
- Why DC Fault Interruption in VSC₂ based technology is a challenge?
- Identification of Different Zones of Protection
- DC Fault Clearing Strategies
- Fault Ride Through Schemes for DFIG and PMSG
- MMC Converters Used in Research
- Modeling of Cable and Transmission Line
- Control schemes Implemented for the Topology
- DC Fault Detection, Localization and Classification
- Main Reference and Contributory Literature

Non-Business Use

2



5

Abstract and Introduction

- **Abstract**
 - LCC_HVDC
 - VSC_HVDC
 - Hybrid HVDC
 - Doubly Fed Induction Generator(DFIG)
 - Permanent Magnet Synchronous Generator(PMSG)
 - MMC_VSC Topology
 - DC Grids

Non-Business Use

3

My Contribution to Research

- **My contribution to this dissertation research**
 - The second aggregate of generation consists of 600MW of 3 sets of Qty (40) of Permanent Magnet Synchronous Generator
 - The rating of each PMSG is 5MW, 60Hz, 0.69kV
 - PMSG AC output of 0.69kV is converted to 1kV dc through 3-level NPC VSC
 - PMSG internal Booster DC-DC Converter steps the voltage from 1kV to 15kVDC
 - The overall PMSG output is integrated with only one stage of step-up voltage 15kV/150kV DC to DC converter located offshore,
 - The entire outline is integrated to a +/-150kV DC grid collector bus.

Non-Business Use

6

My Contribution to Research

My contribution to this dissertation research

- The third aggregate of generation consists of a 600MW of 3 sets of Qty (40)PMSG each
- The rating of each PMSG is 5MW,0.69kv
- The PMSG is integrated to an internal 3-level NPC VSC acting as a rectifier to convert 0.69KV to 1KV dc
- PMSG internal Booster DC-DC Converter steps the voltage from 1kv to 6kvDC
- The overall PMSG output is integrated with two stage DAB_MMC_VSC of step-up voltage 6KV/30KV DC and 30KV/150KV all located offshore
- The entire outline is integrated to a +/-150KV DC grid collector bus.

Non-Business Use

7

My Contribution to Research

My Contribution to Research

- **My Contribution to Research**
- ❑ **Fault Detection and Location using Travelling Wave Algorithm in compliment with Discrete Wavelet Transform(DWT)**
- A novel fault detection and location technique utilizing Travelling Wave theory and Discrete Wavelet Transform after extraction, analysis and classification of the type of fault from the data of transient voltages and currents will be implemented

Non-Business Use

10

My Contribution to Research

My Contribution to Research

- **My Contribution to Research**
- ❑ **Expanded AC and DC Fault with Fault Resistance Application**
- ❑ A focus on an expanded and improved AC and DC fault application
- ❑ For AC side Faults,SLG,DLG,DLL,3-Phase, 3-Phase to ground at 10%, 20%, 40%,60%,80% of the cable and line length with different fault resistances ranging from (0 to 40ohms)
- ❑ DC Faults Pole to ground and Pole to Pole with fault resistance will be considered. The expanded faults on the windfarm side will be faults that will be internal to the wind farm, internal and external AC and DC collection grid.
- ❑ Expanded faults will also be extended to the Main AC and DC collection grid, internal and external components of DC to DC converter, Main MMC-VSC HVDC converters, Main Hybrid HVDC Converters, internal and terminal faults of the infeed synchronous generator

Non-Business Use

8

My Contribution to Research

My Contribution

- ❑ **Protection of Hybrid Wind Farm (Doubly Fed Induction Generator and Permanent Synchronous Generator) and Fault Ride Through and Low Voltage Ride through Techniques**
- Fault Clearing Strategy will be complimented with the traditional DFIG Protection scheme of utilizing Active Crowbar Protection to protect overvoltage condition on the rotor and the generator side converter and a DC Chopper to limit overvoltage conditions on the DC link due to active power in-balance.
- For the PMSG, the traditional protection scheme will consist of an AC side Power Electronics Controlled Dynamic Resistor and AC Load Damper to limit overcurrent, prevent rotor acceleration during faults, maintain balance of active power and stability. On the DC side DC breaker will be used to interrupt the DC overcurrent during Capacitor discharge and a DC Link Chopper Resistor will be used to limit any overvoltage that might occur.
- In addition, there will be a DC series Dynamic resistor that will be implemented to limit overcurrent in the DC cable and DC Link.

Non-Business Use

11

My Contribution to Research

My Contribution to Research

- **My Contribution to Research**
- ❑ **Fault Clearing Strategies**
- Fault clearing strategy which consist of Fully Selective Fault Clearing strategy with back-up protection plan will be implemented in various zones of protection utilizing various or combination of Fault Blocking and fault current control capability of Full Bridge Sub Module MMC-VSC topology Fault Blocking Schemes or
- Hybrid MMC-VSC which is a combination of Full Bridge and Half Bridge Sub Module MMC-VSC and High-Speed DC disconnect Switches
- DC-DC Converters with Full Bridge Sub Module MMC-VSC(DAB-FBSM) Fault blocking and isolation or galvanization capability
- Solid State DC breakers(DCCB) and High Speed Mechanical DC Disconnect Switches and DC-DC Converters with Full Bridge Sub Module and using AC circuit breaker on the AC side.

Non-Business Use

9

My Contribution to Research

My Contribution

- ❑ **Validation of the proposed protection scheme detection and location algorithm will be validated in PSCAD-EMTDC software platform and Matlab Simulink Tool Box**
- The testing and validation of the developed hybrid algorithm will be performed in PSCAD software and the Discrete Wavelet Transform fault extraction and analysis will be performed in Matlab/Simulink Power System Tool box in a closed loop environment of a microprocessor protective relay or Intelligent Electronic Device(IED) identified for each zone of protection.

Non-Business Use

12

Problem Statement

- Current protection methods that are employed and implemented in LCC_HVDC cannot be implemented in VSC_HVDC
- MMC is one of the main topologies of the VSC and has been an excellent choice for long-bulk power transmission and HVDC network grid. However, due to the use of long distance transmission lines and cables, the HVDC is prone to faults.
- VSC-HVDC integrated to Wind Energy Conversion system are vulnerable to DC faults
- Wind Energy Conversion system are vulnerable to DC faults because DC Faults have significant difference in fault characteristic in terms of absence of zero crossing and having very low impedance of DC fault which makes it to achieve very fast rise with steep slope when compared to the traditional AC fault current.
- Several fault detection, classification and localization techniques have been proposed such as overcurrent, under-voltage and rate of change of voltage and current but lacks the required sensitivity for detecting high resistance fault.
- Other fault detection schemes like impedance-based fault detection and location have also been proposed and implemented but the drawback associated with this type of fault detection includes influence from transmission line parameters, fault resistance, mutual zero sequence just to mention a few.

Non-Business Use

13

Remaining Work to be done

- **Methodology**
 - Design Parameters and Control Schemes
 - PSCAD Modeling of the Components of the Topology
 - Matlab/Simulink Code programming of Travelling wave Interface with PSCAD
- **Simulation-COMTRADE**

Non-Business Use

16

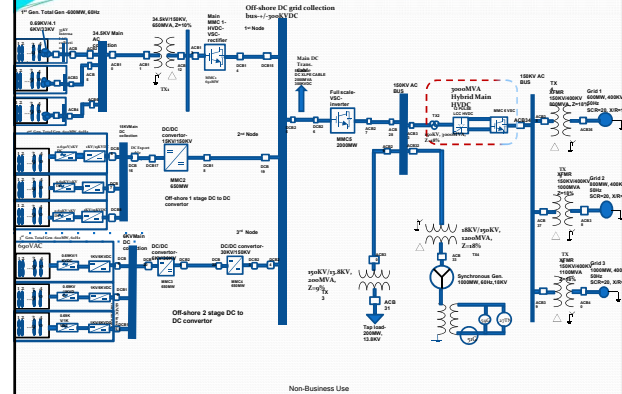
Problem Statement

- The capacity of offshore wind power increases in addition to continuously increasing rating of the individual wind turbine power rating which will require a large geographical area and footprint and large offshore substation for interconnection and because of the larger power rating of the wind turbines it will require larger separation distance.
- The wind power when generated need to be integrated to the grid through the most less costly technology.

Non-Business Use

14

Test Topology Outline



Non-Business Use

17

Research Methodology

- **Main Remaining Items Methodology**
 - Identify the type of fault detection technique that will be used for this test model, most likely it will be a hybrid algorithm which consist of a combination of Travelling Wave and Discrete Wavelet transformation technique
 - Identify the zones of protection for the proposed test topology and the IED or protective relays that will be used in compliment with the fault detection algorithms
 - Identify the best mother wavelet technique which will characterize the fault classification for the Discrete Wavelet Transformation decomposition.
 - Design and validate the proposed hybrid fault detection algorithm, discrete wavelet transformation using wavelet energy spectrum entropy in Matlab/Simulink power system tools and travelling wave in PSCAD

Non-Business Use

15

Why DC faults associated with MMC HVDC are Difficult to Interrupt?

- **Difficult interruption of DC fault**
 - DC Faults have a significant fault characteristics when compared with the traditional AC
 - DC faults Rise Up quickly with a steep slope when compared with the traditional AC fault
 - The impedance of the DC fault is very small when compared with AC faults
 - DC Faults do not have a zero crossing when compared with the traditional AC faults
 - VSC does not have the capability to control the DC fault

Non-Business Use

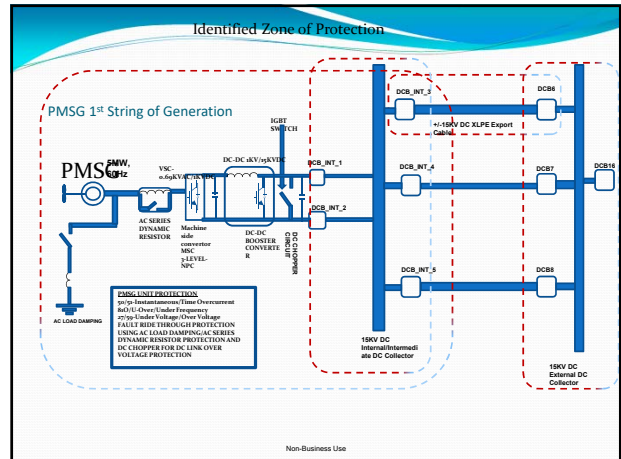
18

Selection of Protection scheme and Fault Coordination Strategy

- DFIG and PMSG
- AC Bus
- DC Bus
- Power Transformer and Converter Transformer
- MMC
- DC-DC Converter
- 150KV DC Main Transmission Line
- 400KV Main AC Transmission Line
- 1000MW Synchronous Generator

Non-Business Use

19



22

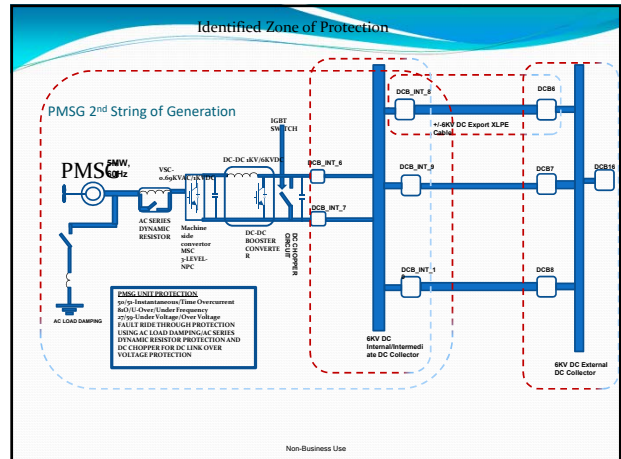
Fault Control and Clearing Strategies

- Fault Clearing strategy of MMC and DC-DC Converter

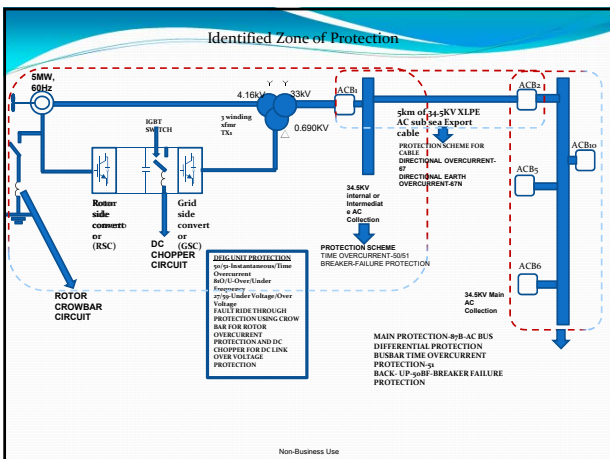
- Full Selective Fault Clearing Strategy-Using DC solid state breakers and High Speed Mechanical Switches
- Non-Selective Fault Clearing Strategy-Using Fault Blocking capability of MMC-Full Bridge Sub Module and DC-DC Converter-DAB
- Back-Up Protection using AC Breakers

Non-Business Use

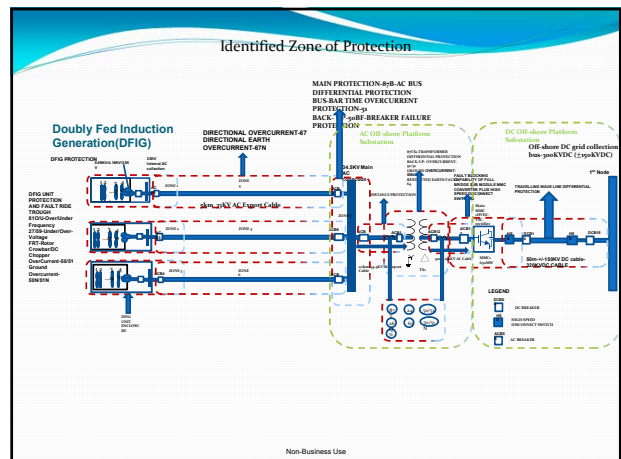
20



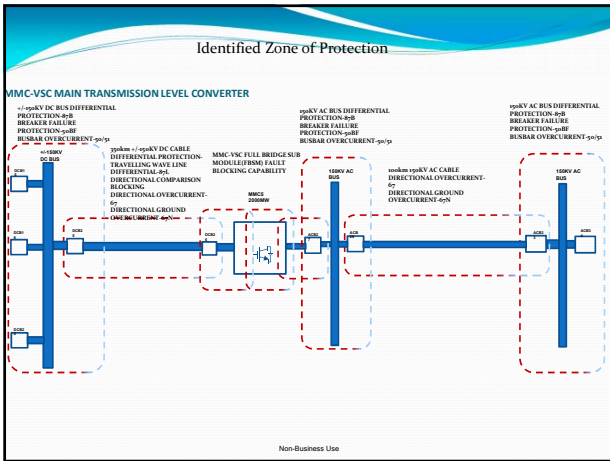
23



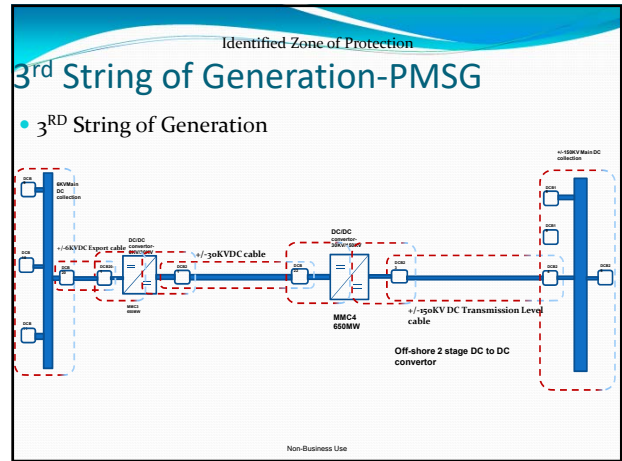
21



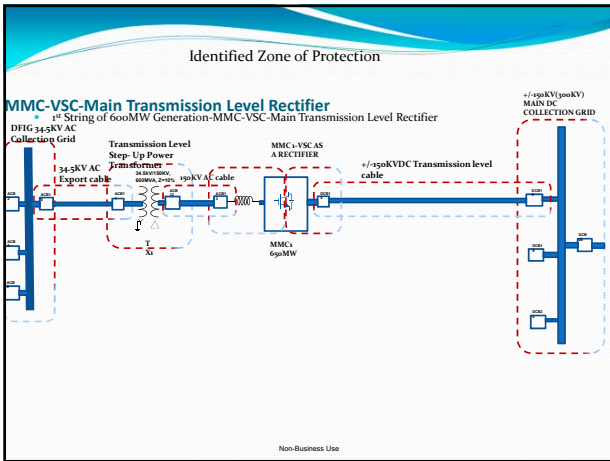
24



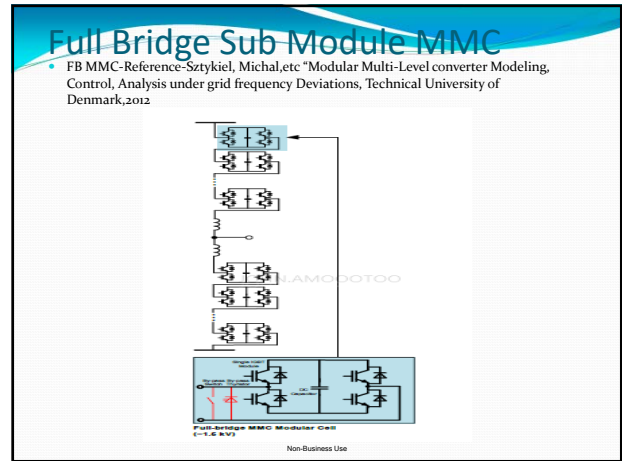
31



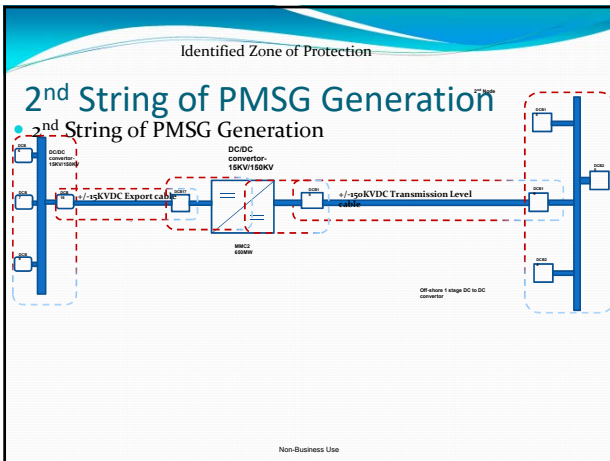
34



32



35



33



36

Asymmetric Model-Hybrid MMC

- Asymmetric Model-Reference- DAB-MMC-Reference-Satykiet, Michalec: "Modular Multi-Level converter Modeling, Control, Analysis under grid frequency Deviations, Technical University of Denmark, 2012

(b)

Non-Business Use

37

DFIG ANG PMSG DYNAMIC EQUATION

- DFIG Dynamic Modeled Equations

$$v_{abc} = i_{abc} R_{abc} + \frac{d}{dt} \lambda_{abc}$$

Non-Business Use

40

Modelling of MMC

- Modelling of MMC-Detailed Equivalent Model
 - Performs a circuit reduction of the simplified circuit
 - Thevenin's equivalent for each converter arm which used the nest fasted simulation to improve upon the time for simulation
 - The topology can be reduced to subnetworks with admittance matrix of each network reducing computation time
 - Easy calculation of multivale voltage based on the measurement of resistance and current values of the valve
 - In conducting state the resistance is low and in blocked state the resistance is high

Non-Business Use

38

DFIG AND PMSG DYNAMIC MODEL EQUATION

- DFIG Model Equations

$$\lambda_{ds} = \lambda_{ds} = L_{ds} i_{ds} + L_{m} i_{ds}$$

$$\lambda_{qs} = \lambda_{qs} = L_{qs} i_{qs} + L_{m} i_{qs}$$

$$\lambda_{dr} = \lambda_{dr} = L_{dr} i_{dr} + L_{m} i_{dr}$$

$$\lambda_{qr} = \lambda_{qr} = L_{qr} i_{qr} + L_{m} i_{qr}$$

$$\lambda_{ds} = L_{ds} i_{ds} + L_{m} i_{ds}$$

$$\lambda_{qs} = L_{qs} i_{qs} + L_{m} i_{qs}$$

$$\lambda_{dr} = L_{dr} i_{dr} + L_{m} i_{dr}$$

$$\lambda_{qr} = L_{qr} i_{qr} + L_{m} i_{qr}$$

$$T_{em} = \frac{3P}{2} (i_{dr} \lambda_{ds} - i_{ds} \lambda_{dr})$$

$$P_r = \frac{3}{2} (v_{dr} i_{dr} + v_{qr} i_{qr})$$

$$Q_r = \frac{3}{2} (v_{qr} i_{dr} - v_{dr} i_{qr})$$

Non-Business Use

41

Modeling of Transmission Line

- Modelling of AC Transmission Line and DC Cable
 - Resistance in ohms/km
 - Inductance in henries/Km
 - Capacitance in Microfarad/Km
 - Conductance in S/km
 - Length of the AC Transmission Line
- Frequency Dependent Phase(Cable Model) and Mode(Transmission Line) Model
 - Based on the travelling wave theory
 - Frequency dependent of the parameters and termed to be the best
 - Accurate representation of the current and voltages both in steady state and transient
 - PSCAD-simulation in time domain and converted to frequency domain using wavelet transformation or Fourier transform

Non-Business Use

39

Vector Control Schemes

- Field Oriented Vector Control Schemes
- DFIG Vector Control
 - Stator Flux Oriented Vector Control
 - Grid Voltage Oriented Vector Control
 - Pitch Angle Control
 - Maximum Power Point Tracking(MPPT)
- PMSG Vector Control
 - Stator Voltage Oriented Control
 - Grid Vector Oriented Vector Control

Non-Business Use

42

Control Schemes

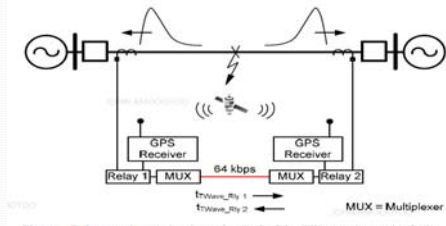
- **Control of PMSG and DFIG**
- **Inner Control Loop with PI**
 - Current Control Loop
- **Outer Control Loop with PI**
 - DC Link Voltage Control Loop
 - Stator Voltage Control Loop
 - Active Power/MPPT Control Loop

Non-Business Use

43

Travelling Wave

- Travelling Wave-Reference-B. K. Johnson, Stephen Marx, et al" Travelling Wave Fault Location in Protective Relays, Design Testing and Results, 16th Annual Georgia Tech Relay Conference, May 6-7, 2013



Non-Business Use

46

Travelling Wave

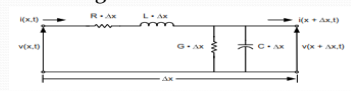
- **Travelling Wave**
 - When faults occur it develops into transients(voltages and currents) that move back and forth
 - The transients move close to the speed of light
 - Concept is based on the time it takes to travel from the point of discontinuity to the measuring point
 - The velocity of the travelling wave is much based on the inductance and capacitance of the line
 - Knowing the speed of the travelling wave and the time, the distance of the fault location can be calculated
 - Success of the travelling wave is much based on the accurate detection or capturing the wavefront

Non-Business Use

44

Travelling Wave Equations

- **Travelling Wave**



- Developing Kirchoff's voltage and current equation based on the current and voltage at x and x+Delta x

$$v(x,t) = R\Delta x i(x,t) + L\Delta x \frac{\partial i(x,t)}{\partial t} + v(x+\Delta x,t) + i(x,t) = G\Delta x v(x+\Delta x,t) + C\Delta x \frac{\partial v(x+\Delta x,t)}{\partial t} + i(x+\Delta x,t)$$

Equations of voltage and current as a function of time

$$\frac{\partial v(x,t)}{\partial t} = -R i(x,t) - L \frac{\partial i(x,t)}{\partial t}$$

$$\frac{\partial i(x,t)}{\partial t} = -G v(x,t) - C \frac{\partial v(x,t)}{\partial t}$$

Differentiating with respect to t

$$\frac{\partial^2 v(x,t)}{\partial x^2} = -R \frac{\partial i(x,t)}{\partial x} - L \frac{\partial^2 i(x,t)}{\partial x \partial t}$$

$$\frac{\partial^2 i(x,t)}{\partial x^2} = -G \frac{\partial v(x,t)}{\partial x} - C \frac{\partial^2 v(x,t)}{\partial x \partial t}$$

Non-Business Use

47

Travelling Wave

- **Travelling Wave**
 - Because the speed of a travelling wave is little quite less than the speed of light, it requires a high sampling rate
 - Wave-front close to the end of the line are difficult to detect because of the high speed of the wave
 - Components of travelling wave are high frequency and vulnerable to interference
 - Faults that occur for zero voltage inception are difficult to detect

Non-Business Use

45

Travelling Wave Equations

- **Travelling Wave Equations**
- **Substituting the values of into equations**

$$\frac{\partial v(x,t)}{\partial t} = -R i(x,t) - L \frac{\partial i(x,t)}{\partial t}$$

$$\frac{\partial^2 v(x,t)}{\partial x^2} = LC \frac{\partial^2 v(x,t)}{\partial t^2} + (RC + GL) \frac{\partial v(x,t)}{\partial t} + GR v(x,t)$$

$$\frac{\partial^2 v(x,t)}{\partial x^2} = -R \frac{\partial i(x,t)}{\partial x} - L \frac{\partial^2 i(x,t)}{\partial x \partial t}$$

$$\frac{\partial^2 i(x,t)}{\partial x^2} = -G \frac{\partial v(x,t)}{\partial x} - C \frac{\partial^2 v(x,t)}{\partial x \partial t}$$

- **Substituting to derive the current equation**

$$\frac{\partial v(x,t)}{\partial t} = -G \left(-R i(x,t) - L \frac{\partial i(x,t)}{\partial t} \right) - L \left(-R \frac{\partial i(x,t)}{\partial x} - L \frac{\partial^2 i(x,t)}{\partial x \partial t} \right)$$

$$\frac{\partial^2 i(x,t)}{\partial x^2} = LC \frac{\partial^2 v(x,t)}{\partial x^2} + (RC + GL) \frac{\partial v(x,t)}{\partial x} + GR i(x,t)$$

Non-Business Use

48

Main Travelling Wave Equations

$$\frac{\partial^2 v(x,t)}{\partial x^2} = -R \frac{\partial i(x,t)}{\partial x} - L \frac{\partial^2 i(x,t)}{\partial t^2}$$

$$\frac{\partial^2 i(x,t)}{\partial x^2} = LC \frac{\partial^2 v(x,t)}{\partial t^2} + (RC + GL) \frac{\partial v(x,t)}{\partial x} + GR i(x,t)$$

$$TWFL = \frac{LL + (TWA - TWB) c_{Prop_Vel}}{2}$$

Non-Business Use

49

Discrete Wavelet Transform

- **Discrete Wavelet Transform**

w is the scaling function of the mother wavelet and are the wavelet coefficient

- The coefficient will consist of dominant patterns of high and low filter

Process of DWT

- Clark Modal Transformation to the voltage and current samples
- DWT is applied to the modal voltage and the squares of the wavelet transform coefficient to determine the peak of the energy
- Faulty Classification-Grounded, Phase
- Fault Location is based on the use of the lattice diagram of the aerial mode voltages using two ended synchronized measurements and GPS

Non-Business Use

52

Fault Detection Types

- **Other Forms of Fault Detection Techniques**
 - Fourier Transformer
 - Short Time Fourier Transform
 - Artificial Neural Network
 - Fuzzy Logic
 - Hybrid Fault Detection
 - Impedance Fault Detection
 - Change in voltage-dv/dt and Change in Current-di/dt
 - Wavelet Transform
- **Examples of Wavelet Families**
 - Daubechies
 - Coiflet
 - Haar
 - Symlet
 - Mexican Hat
 - Morlet

Non-Business Use

50

Clark's Transformation

- **Phase to Modal Transformation**

- This is much based on the electromagnetic coupling of the transmission line and cable
- Modal Transformation Matrix allows the decomposition of the matrix into several independent modes
- Three phase model can be decomposed into three single phase having its own characteristic impedance Z_c and time delay τ
- Each mode will have a distinct time delay and velocity

Non-Business Use

53

DC Fault Detection, Location, classification

- **My focus will be on Discrete Wavelet Transform**

- It analyzes small wavelets in terms of dilation and translation
- Capability to analyze in time and frequency
- At high frequencies used narrow window and at low frequencies uses wider window
- Very good in the capturing and analysis of Power System Transients that have sharp discontinuities and abrupt signals
- Analysis starts with a mother wavelet
- They are computationally fast and have the capability to provide effective analysis during fault analysis
- The general form of the Discrete wavelet Transform is where j,k are integers id the dilation factor and is the translation factor

$$DWT = W_{j,k}(t) = \frac{1}{\sqrt{d_0^j}} W\left(\frac{t - k\tau d_0^j}{d_0^j}\right) \quad w(t) = \sum_{k=-\infty}^{\infty} -1^k C_{j+1} W(2t + k)$$

Non-Business Use

51

Travelling Wave Lattice Diagram

- TW-Reference-Megger "New Possibilities of Testing Travelling Wave Fault location functions in the field"

Bewely lattice diagram

Non-Business Use

54

Questions

- Questions

Non-Business Use

55

Prolonged Fault Response of Offshore Wind Power Plants

Omer Gökcu, Jayachandra Sakamuri, Amir Arasteh, Nicolaos Cutululis
DTU Wind Energy

EERA DeepWind'2019,
16th Deep Sea Offshore Wind R&D Conference,
17 January 2019, Trondheim, Norway

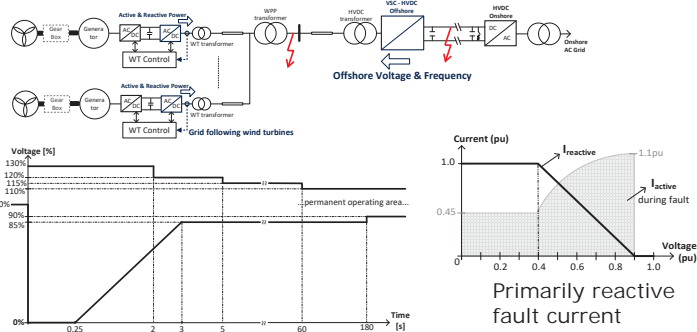


This work has been supported by the PROMOTiON project through the European Union's Horizon 2020 research and innovation programme under grant agreement No 691714.
<https://www.promotion-offshore.net/>

Outline

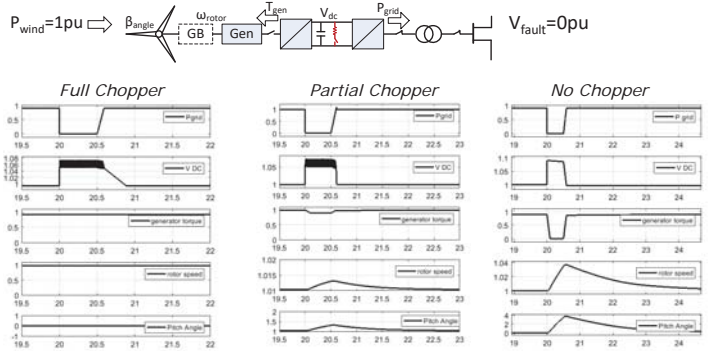
- Today's FRT requirements
- Today's FRT solutions
- Disconnection-reconnection requirements
- DC fault in meshed HVDC offshore grids
- Next-generation WTs
 - Black-startable / Self-sustaining WTs
- Prolonged FRT case

Today's FRT requirement



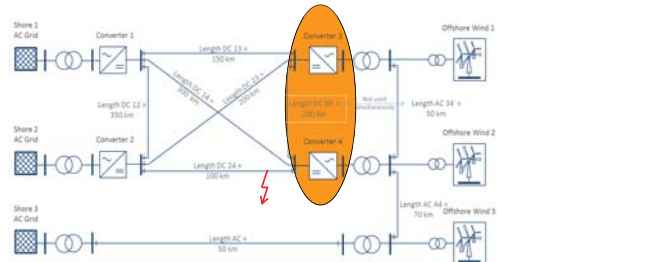
Same as onshore WTs: allowed to disconnect outside the band

FRT solutions



Different design choices by WT OEMs – all proven

DC fault in meshed offshore HVDC grids



Fully-selective DC fault clearing:
DC Circuit Breakers
5-10ms

Non-selective DC fault clearing:
High-Speed DC Switch & AC Circuit Breakers
HVDC Converter Blocking & De-blocking

→ WPP(s) might disconnect due to long outage

Reconnection requirements

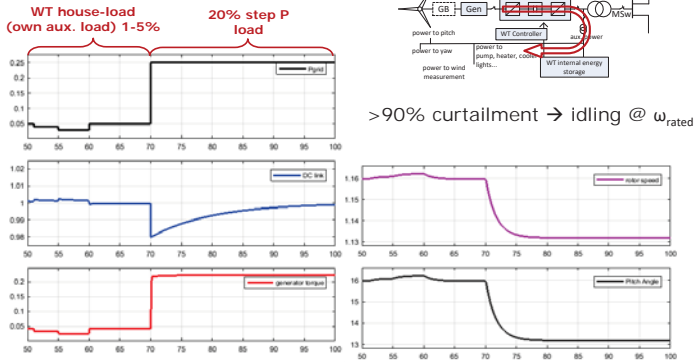
"HVDC systems, including DC overhead lines, shall be capable of fast recovery from transient faults within the HVDC system" in article 27 (Fast recovery from DC faults) of ENTSO-E HVDC code

"after a short-time-interruption resynchronization of the plant must take place within 2 seconds at the latest. The active power infeed must be increased to the original value with a gradient between 0.1 and 0.2 pu/s" in TenneT TSO GmbH HV and EHV grid code

- (i) "in case of disconnection of the power-generating module from the network, the power-generating module shall be capable of quick re-synchronization"
 - (ii) "power-generating module with a minimum re-synchronisation time greater than 15 minutes after its disconnection from any external power supply must be designed to trip to houseload"
 - (iii) "power-generating modules shall be capable of continuing operation following tripping to houseload"
- in article 15.5.(c) of ENTSO-E RFG code

Next Generation: Self-sustaining (black-startable) wind turbines

Stand alone (HouseLoad) operation

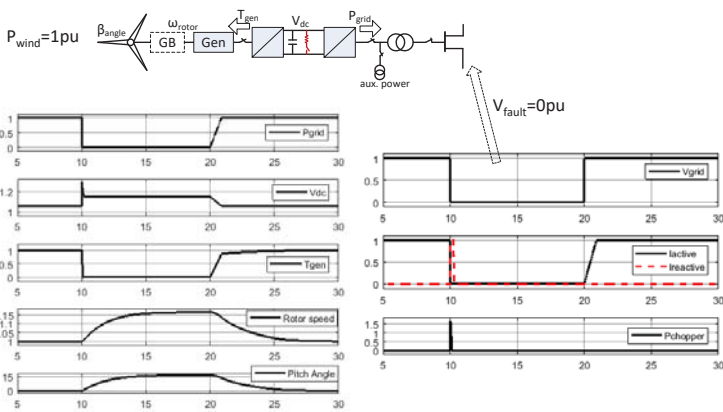


In summary



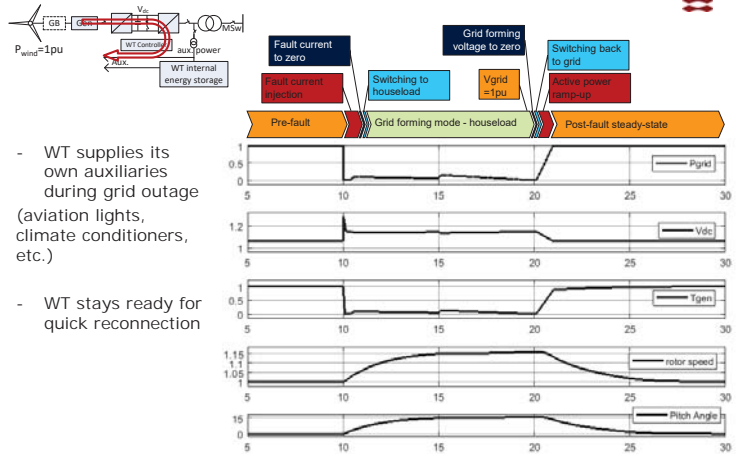
1. Ride-through faults!
2. Ride-through longer, if possible!
3. Otherwise trip to houseload! (possible)
4. Reconnect quickly!

Prolonged FRT case



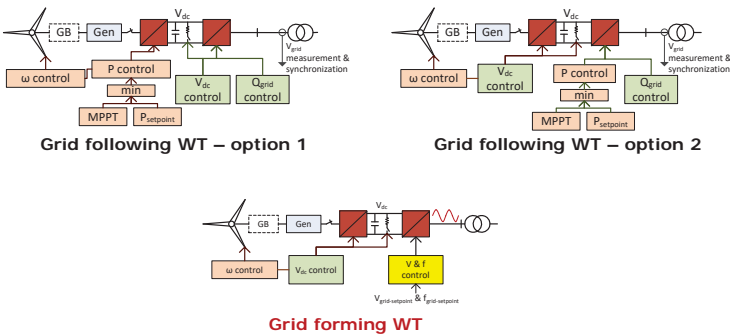
$V_{grid}=0, P_{grid}=0$
 \rightarrow WT aux. power?

Prolonged FRT case – grid forming



- WT supplies its own auxiliaries during grid outage (aviation lights, climate conditioners, etc.)
- WT stays ready for quick reconnection

Grid forming WT – stand alone



- Grid side converter behaves as stiff voltage source

Conclusion



- Future WTs are expected to be **stand-alone** active units
 - Grid forming
- **New FRT concepts** for WTs to be developed
- **Quick reconnection** for the sake of power system
- Self-sustaining **houseload** mode for the sake of WT
- Mechanical loads during torque transients – to be investigated
- Aerodynamic during excessive curtailment – to be investigated
- Electrical transients during energization – to be investigated

This work has been supported by the PROMOTiON project through the European Union's Horizon 2020 research and innovation programme under grant agreement No 691714. <https://www.promotion-offshore.net/>



B2) Grid connection and power system integration

Control challenges for grid integration; Nikos Cutululis, DTU

Heuristics-based design and optimization of offshore wind farms collection systems,
J.A. Pérez-Rúa, DTU

Resonance Characteristics in Offshore Wind Power Plants with 66 kV Collection Grids,
A.Holdyk, SINTEF

PROMOTiON
PROGRESS ON MESHED HVDC OFFSHORE TRANSMISSION NETWORKS





Control challenges for grid integration

Nicolaos A. Cutilulis, DTU Wind Energy
17 January 2019, DeepWind Conference, Trondheim

© PROMOTiON - Progress on Meshed HVDC Offshore Transmission Networks
This project has received funding from the European Union's Horizon 2020 research and innovation programme under grant agreement No 801714.

© Irena / ITC GmbH



- Background
- Diode Rectifier as offshore HVDC
- Grid Forming Wind Turbines
- Offshore AC Grid Start-up
- Black Start by Offshore Wind Turbines

Acknowledgements:
Ramón Blasco Jiménez & team, UPV
Lie Xu & team, UoS
Ömer Göksu & Oscar Saborío-Romano, DTU

© PROMOTiON - Progress on Meshed HVDC Offshore Transmission Networks
This project has received funding from the European Union's Horizon 2020 research and innovation programme under grant agreement No 801714.

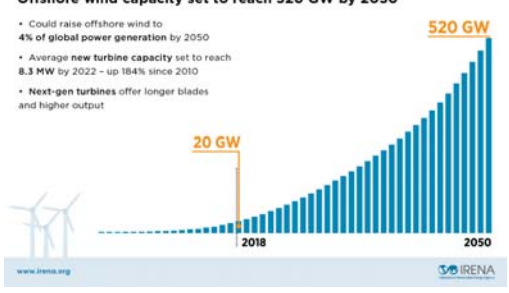
Trondheim 17.01.2019 2

Control challenges for grid integration

Offshore wind development

Offshore wind capacity set to reach 520 GW by 2050

- Could raise offshore wind to 4% of global power generation by 2050
- Average new turbine capacity set to reach 8.3 MW by 2022 - up 184% since 2010
- Next-gen turbines offer longer blades and higher output



Source: IRENA, Offshore innovation widens renewable energy options, September 2018

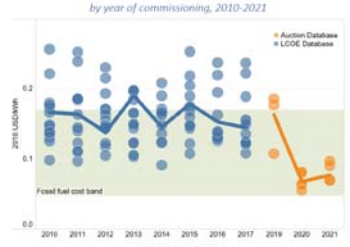
© PROMOTiON - Progress on Meshed HVDC Offshore Transmission Networks
This project has received funding from the European Union's Horizon 2020 research and innovation programme under grant agreement No 801714.

Trondheim 17.01.2019 3

Control challenges for grid integration

Offshore wind development

Figure 1: Global levelised cost of electricity from offshore wind farms by year of commissioning, 2010-2021



Source: IRENA, Offshore innovation widens renewable energy options, September 2018

© PROMOTiON - Progress on Meshed HVDC Offshore Transmission Networks
This project has received funding from the European Union's Horizon 2020 research and innovation programme under grant agreement No 801714.

Trondheim 17.01.2019 4

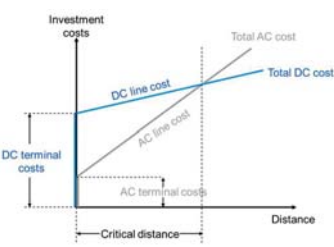
Control challenges for grid integration

Offshore wind development

Main cost components of offshore wind farms:

- turbines (including towers)
- the foundations
- the grid connection to shore
 - AC or DC?

Power flow is in one direction only
Why not use a diode rectifier offshore?



Source: IRENA, Offshore innovation widens renewable energy options, September 2018

Source figure: ABB, www.abb.com

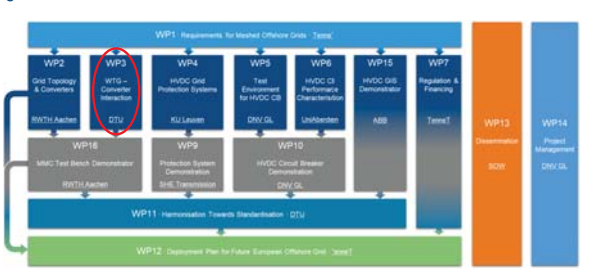
© PROMOTiON - Progress on Meshed HVDC Offshore Transmission Networks
This project has received funding from the European Union's Horizon 2020 research and innovation programme under grant agreement No 801714.

Trondheim 17.01.2019 5

Control challenges for grid integration

PROMOTiON project

Progress on Meshed HVDC Offshore Transmission Networks



© PROMOTiON - Progress on Meshed HVDC Offshore Transmission Networks
This project has received funding from the European Union's Horizon 2020 research and innovation programme under grant agreement No 801714.

Trondheim 17.01.2019 6

Control challenges for grid integration

Objectives

Objective 1
Define functional requirements to OWFs

Objective 2
Develop test cases & control algorithms

Objective 3
Define & apply compliance evaluation

Objective 4
Recommend grid code requirements

© PROMOTION - Progress on Meshed HVDC Offshore Transmission Networks
This project has received funding from the European Union's Horizon 2020 research and innovation programme under grant agreement No 691714.

Tuebingen 17.01.2019 7

Control challenges for grid integration

Diode Rectifier Units as offshore HVDC

current VSC solution

new DRU solution

Advantages of the Diode Rectifier Unit

- Reduced weight
- Reduced volume
- Reduced maintenance
- High efficiency
- High power density
- High reliability
- Low cost
- Simple control
- Simple installation

30% weight reduction

© PROMOTION - Progress on Meshed HVDC Offshore Transmission Networks
This project has received funding from the European Union's Horizon 2020 research and innovation programme under grant agreement No 691714.

Tuebingen 17.01.2019 8

Control challenges for grid integration

Grid Forming Wind Turbines

Grid forming wind turbines control

- dq current control based
- voltage/angle control based
- VSM control
- GPS synchronization based
- master/slave based

© PROMOTION - Progress on Meshed HVDC Offshore Transmission Networks
This project has received funding from the European Union's Horizon 2020 research and innovation programme under grant agreement No 691714.

Tuebingen 17.01.2019 9

Control challenges for grid integration

Offshore AC Grid Start-up Options

Umbilical AC Cable

Nearby VSC-HVDC (or AC)

Local Energy Storage (e.g. battery, diesel)

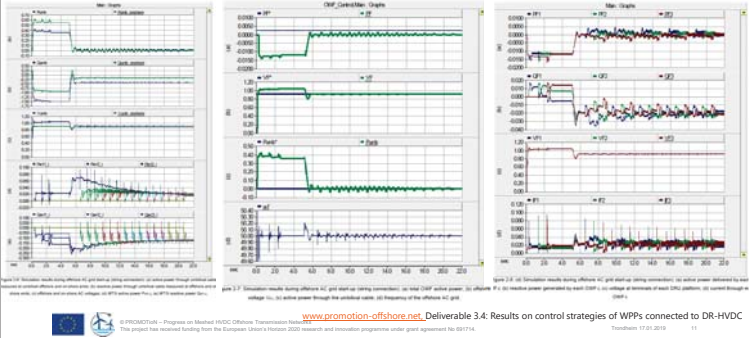
Black-startable wind turbines

© PROMOTION - Progress on Meshed HVDC Offshore Transmission Networks
This project has received funding from the European Union's Horizon 2020 research and innovation programme under grant agreement No 691714.

Tuebingen 17.01.2019 10

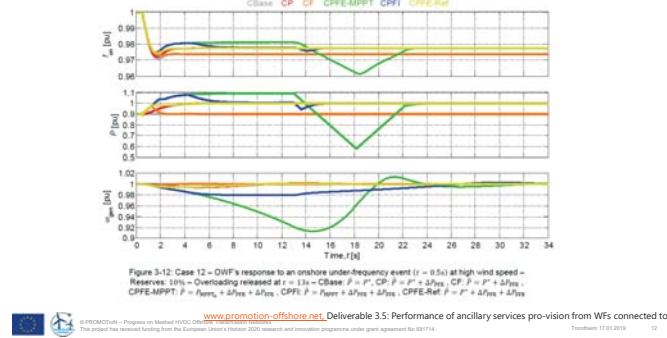
Control challenges for grid integration

Some results - AC grid start-up (string connection)



Control challenges for grid integration

Some results - Frequency control



Black-start - Progress Towards Demonstration

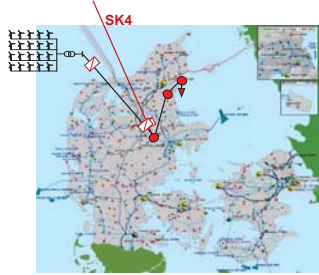
Outside PROMOTiON
Energinet performs Black Start field test with Skagerrak 4 (SK4) HVDC interconnector

WP3 Performs Black Start Simulation Test with Offshore WPP

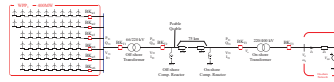
To energize:

- 3 buses
- Overheadline & underground cable
- Shunt reactor & transformer
- Step MW++ load
 - Load changes
 - Frequency & voltage setpoint changes
 - Load disconnection

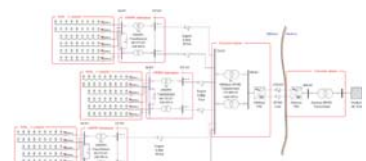
Results to be compared against HVDC field tests by Energinet



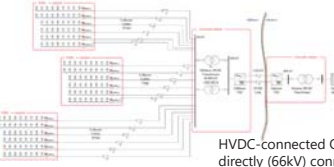
Scenarios – Self-Energization & Black Start



HVAC-connected OWPP

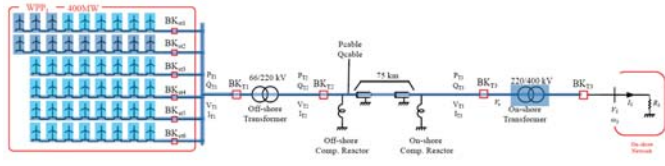


HVDC-connected OWPP(s) with AC collector substation(s)

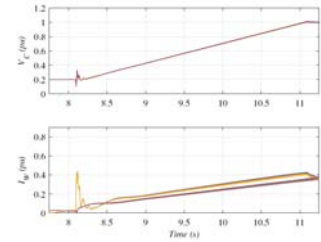
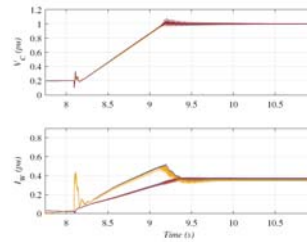


HVDC-connected OWPP(s) directly (66kV) connected to the HVDC

Some results – black-start



Some results – black-start

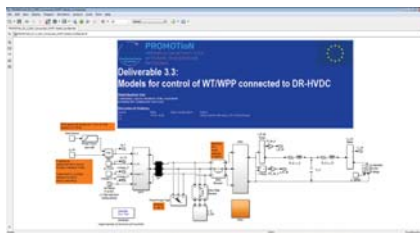


Models for Control of WT/WPP Connected to DR- HVDC

~~Confidential – only for members of the consortium~~

- Aggregated single WT
- Ideal onshore DC voltage
- Ideal WT DC voltage

- ✓ Offshore AC start-up
- ✓ Voltage & frequency control
- ✓ Active power setpoint control
- ✓ Offshore AC fault ride-through
- ✓ Intentional islanded operation



Achievements

- ✓ Control and Modelling
 - ✓ Novel grid forming wind turbine controls
 - ✓ Confidential grid forming WPP simulation models
 - ✓ Academic (white-box) & Industrial (black-box)
- ✓ Operation of DRU HVDC Systems
 - ✓ Functional requirements for Diode-Rectifier (DRU) connection of Wind Power Plants
 - ✓ Control algorithms and simulation test cases & results
 - ✓ Proof of DRU concept via simulations

Control challenges for grid integration

Main Findings and Challenges

Operation of DRUs

- Wind turbines can operate with DRU-connection without any degradation compared to VSC
- Wind turbines can operate as islanded (idling, self-sustaining)

Fault Handling in DRU-connected OWPP

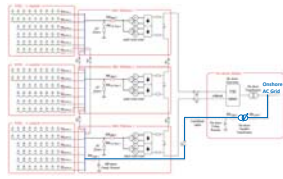
- DRU inherent response to DC link voltage eases onshore AC fault ride-through

Ancillary Services by DRU-connected OWPP

- DRU connected OWPP can contribute to frequency support and oscillation damping

OWPP Self-energization and Black Start

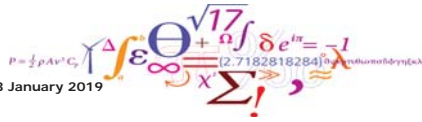
- OWPP can energize its AC network and might be able to contribute to black start



Heuristics-based design and optimization of offshore wind farms collection systems

Juan-Andrés Pérez-Rúa
Daniel Hermsilla Minguijón
Kaushik Das
Nicolao A. Cutululis

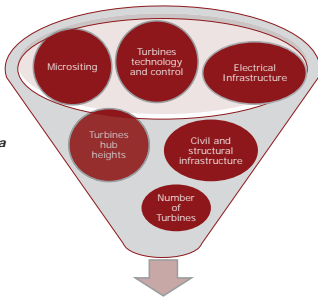
EERA DeepWind'19, Trondheim, 16 – 18 January 2019



INDEX

- 01 INTRODUCTION
- 02 PROBLEM DEFINITION
- 03 METHODOLOGY
- 04 COMPUTATIONAL EXPERIMENTS
- 05 SUMMARY

1 INTRODUCTION



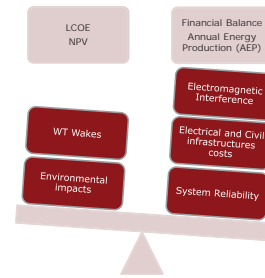
Numerical optimization plays a major role by considering all variables involved:

Enormous amount.

Offshore Wind Farm Design and Optimization Problem (OWIFDO)

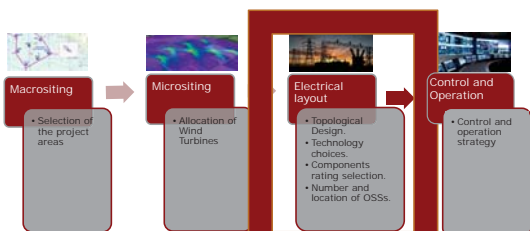
1 INTRODUCTION

Balance between adverse factors to extremize performance metrics



Offshore Wind Farm Design and Optimization Problem (OWIFDO)

1 INTRODUCTION



Multi-step optimization approach

1 INTRODUCTION



Figure 14. Capital expenditures for the 2015 floating offshore wind reference project (Source: NREL).

Figure 15. Capital expenditures for the 2015 floating offshore wind reference project (Source: NREL).

- Overall electrical infrastructure costs can range from 8.6% to 10.5% of the total costs.
- The collection systems of OWFs represent an important share of the electrical infrastructure capex.
- The collection systems of OWFs have a critical impact on the operation: losses and overall reliability.

DTU

INDEX

- 01 INTRODUCTION
- 02 PROBLEM DEFINITION**
- 03 METHODOLOGY
- 04 COMPUTATIONAL EXPERIMENTS
- 05 SUMMARY

7 DTU Wind Energy, Technical University of Denmark 17 January 2019

DTU

2 PROBLEM DEFINITION

NP-Hard Problem

$$t \times \left[N_{t-1} + 0.5 \sum_{i=1}^{t-2} \frac{(t-1)!}{i!(t-1-i)!} N_i N_{t-1-i} \right] \times \frac{(t\sigma)!}{(t!)^\sigma \times \sigma!}$$

Jenkins, A. M., M. Scutaru, and K. S. Smith. "Offshore wind farm inter-array cable layout." PowerTech (POWERTECH), 2013.IEEE Grenoble. IEEE, 2013.

Where *t* is the number of turbines per string (TPS) and *σ* is the number of strings.

Consider an instance with **75 WTs** and **5 TPS**, this result in **1.19 × 10¹⁰⁷ potentials**, taking around **9.45 × 10⁸⁹ years** using a high-speed 4.0 GHz computer to check all possible solutions!

The age of the Earth is 4.54 ± 0.05 billion years (4.54 × 10⁹ years)

8 DTU Wind Energy, Technical University of Denmark 17 January 2019

DTU

2 PROBLEM DEFINITION

Applicability in OWFs

9 DTU Wind Energy, Technical University of Denmark 17 January 2019

DTU

2 PROBLEM DEFINITION

Applicability in OWFs

Efficient implementations would require combinations with heuristics and/or decomposition strategies. Needs external solver.

10 DTU Wind Energy, Technical University of Denmark 17 January 2019

DTU

INDEX

- 01 INTRODUCTION
- 02 PROBLEM DEFINITION
- 03 METHODOLOGY**
- 04 COMPUTATIONAL EXPERIMENTS
- 05 SUMMARY

11 DTU Wind Energy, Technical University of Denmark 17 January 2019

DTU

3 METHODOLOGY

Full methodology flow chart

12 DTU Wind Energy, Technical University of Denmark 17 January 2019

3 METHODOLOGY



The heuristics

- Define for each branch e_{ij} the trade-offs values: $t_{ij} = w_{ij} - p_i$ and $t_{ji} = w_{ij} - p_j$. Get the triple set $T(i, j, t_{ij})$.
- Where $p = a \cdot (b \cdot w_{i1} + (1 - b) \cdot w_{im}) \forall v \in P$. See table below for each heuristic.

Table 1. Nodal weight parameter definition.

Heuristic	Initialization	Update when $\{i, j\}$ is chosen
Prim	$p_i = 0 \forall i, p = -\infty \forall v \in V \setminus \{i\}$	$p_j = 0$
Kruskal	$p = 0 \forall v \in V$	No update
Esau-Williams	$p = w_{i2} \forall v \in V$	$w_i = w_{i2} \forall v \in C_{max}(i)$
Nagel's Approximation Method	$p = h_i \forall v \in V$	$w_i = h_i \forall v \in C_{max}(i)$

3 METHODOLOGY



The heuristics

```

Input:  $C, V, E, W, L, Coordinates(V), L, J, A, B, S, m$ 
Output:  $(T, V, E, W, L)$ 
1. Initialize  $p = 0, p_i = 0 \forall i \in V$ 
2. Initialize  $P$  as function of the input (Heuristic)
3. Initialize  $E$  as set of all edges in  $E$ 
4. Initialize  $C, W, C_{max}, H_{max}$ 
5.  $g = 0$ 
6. While  $E \neq \emptyset$ 
7.    $(i, j, t_{ij}) = \text{select}(E, t_{ij})$ 
8.    $E = E - \{i, j, t_{ij}\}$ 
9.   If  $\{i, j, t_{ij}\} \in C_{max}(i)$  or  $\{i, j, t_{ij}\} \in C_{max}(j)$ 
10.     $E = E - \{i, j, t_{ij}\}$ 
11.   If  $\{i, j, t_{ij}\} \in C_{max}(i)$  and  $\{i, j, t_{ij}\} \in C_{max}(j)$ 
12.     $E = E - \{i, j, t_{ij}\}$ 
13.   If  $\{i, j, t_{ij}\} \in C_{max}(i)$  and  $\{i, j, t_{ij}\} \in C_{max}(j)$ 
14.     $E = E - \{i, j, t_{ij}\}$ 
15.   If  $\{i, j, t_{ij}\} \in C_{max}(i)$  and  $\{i, j, t_{ij}\} \in C_{max}(j)$ 
16.     $E = E - \{i, j, t_{ij}\}$ 
17.   If  $\{i, j, t_{ij}\} \in C_{max}(i)$  and  $\{i, j, t_{ij}\} \in C_{max}(j)$ 
18.     $E = E - \{i, j, t_{ij}\}$ 
19.   If  $\{i, j, t_{ij}\} \in C_{max}(i)$  and  $\{i, j, t_{ij}\} \in C_{max}(j)$ 
20.     $E = E - \{i, j, t_{ij}\}$ 
21.   If  $\{i, j, t_{ij}\} \in C_{max}(i)$  and  $\{i, j, t_{ij}\} \in C_{max}(j)$ 
22.     $E = E - \{i, j, t_{ij}\}$ 
23.   If  $\{i, j, t_{ij}\} \in C_{max}(i)$  and  $\{i, j, t_{ij}\} \in C_{max}(j)$ 
24.     $E = E - \{i, j, t_{ij}\}$ 
25.   Update  $p_j$ 
26.   Update  $P$  as function of the input (Heuristic)
27.   Update  $T, V, E, W, L$  as function of updated  $P$ 
28.   Update  $C, W, C_{max}, H_{max}$ 
29.    $g = g + 1$ 
30.    $E = E - \{i, j, t_{ij}\}$ 
31.    $E = E - \{i, j, t_{ij}\}$ 
32.    $E = E - \{i, j, t_{ij}\}$ 
33.    $E = E - \{i, j, t_{ij}\}$ 
34.    $E = E - \{i, j, t_{ij}\}$ 
35.    $E = E - \{i, j, t_{ij}\}$ 
36.    $E = E - \{i, j, t_{ij}\}$ 
37.    $E = E - \{i, j, t_{ij}\}$ 
38.    $E = E - \{i, j, t_{ij}\}$ 
39.    $E = E - \{i, j, t_{ij}\}$ 
40.    $E = E - \{i, j, t_{ij}\}$ 
41.    $E = E - \{i, j, t_{ij}\}$ 
42.    $E = E - \{i, j, t_{ij}\}$ 
43.    $E = E - \{i, j, t_{ij}\}$ 
44.    $E = E - \{i, j, t_{ij}\}$ 
45.    $E = E - \{i, j, t_{ij}\}$ 
46.    $E = E - \{i, j, t_{ij}\}$ 
47.    $E = E - \{i, j, t_{ij}\}$ 
48.    $E = E - \{i, j, t_{ij}\}$ 
49.    $E = E - \{i, j, t_{ij}\}$ 
50.    $E = E - \{i, j, t_{ij}\}$ 
51.    $E = E - \{i, j, t_{ij}\}$ 
52.    $E = E - \{i, j, t_{ij}\}$ 
53.    $E = E - \{i, j, t_{ij}\}$ 
54.    $E = E - \{i, j, t_{ij}\}$ 
55.    $E = E - \{i, j, t_{ij}\}$ 
56.    $E = E - \{i, j, t_{ij}\}$ 
57.    $E = E - \{i, j, t_{ij}\}$ 
58.    $E = E - \{i, j, t_{ij}\}$ 
59.    $E = E - \{i, j, t_{ij}\}$ 
60.    $E = E - \{i, j, t_{ij}\}$ 
61.    $E = E - \{i, j, t_{ij}\}$ 
62.    $E = E - \{i, j, t_{ij}\}$ 
63.    $E = E - \{i, j, t_{ij}\}$ 
64.    $E = E - \{i, j, t_{ij}\}$ 
65.    $E = E - \{i, j, t_{ij}\}$ 
66.    $E = E - \{i, j, t_{ij}\}$ 
67.    $E = E - \{i, j, t_{ij}\}$ 
68.    $E = E - \{i, j, t_{ij}\}$ 
69.    $E = E - \{i, j, t_{ij}\}$ 
70.    $E = E - \{i, j, t_{ij}\}$ 
71.    $E = E - \{i, j, t_{ij}\}$ 
72.    $E = E - \{i, j, t_{ij}\}$ 
73.    $E = E - \{i, j, t_{ij}\}$ 
74.    $E = E - \{i, j, t_{ij}\}$ 
75.    $E = E - \{i, j, t_{ij}\}$ 
76.    $E = E - \{i, j, t_{ij}\}$ 
77.    $E = E - \{i, j, t_{ij}\}$ 
78.    $E = E - \{i, j, t_{ij}\}$ 
79.    $E = E - \{i, j, t_{ij}\}$ 
80.    $E = E - \{i, j, t_{ij}\}$ 
81.    $E = E - \{i, j, t_{ij}\}$ 
82.    $E = E - \{i, j, t_{ij}\}$ 
83.    $E = E - \{i, j, t_{ij}\}$ 
84.    $E = E - \{i, j, t_{ij}\}$ 
85.    $E = E - \{i, j, t_{ij}\}$ 
86.    $E = E - \{i, j, t_{ij}\}$ 
87.    $E = E - \{i, j, t_{ij}\}$ 
88.    $E = E - \{i, j, t_{ij}\}$ 
89.    $E = E - \{i, j, t_{ij}\}$ 
90.    $E = E - \{i, j, t_{ij}\}$ 
91.    $E = E - \{i, j, t_{ij}\}$ 
92.    $E = E - \{i, j, t_{ij}\}$ 
93.    $E = E - \{i, j, t_{ij}\}$ 
94.    $E = E - \{i, j, t_{ij}\}$ 
95.    $E = E - \{i, j, t_{ij}\}$ 
96.    $E = E - \{i, j, t_{ij}\}$ 
97.    $E = E - \{i, j, t_{ij}\}$ 
98.    $E = E - \{i, j, t_{ij}\}$ 
99.    $E = E - \{i, j, t_{ij}\}$ 
100.   $E = E - \{i, j, t_{ij}\}$ 
    
```

Algorithm 1: The method heuristic algorithm

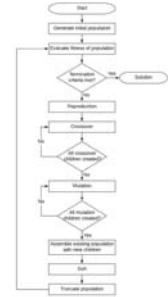
3 METHODOLOGY



The Metaheuristic

Genetic Algorithm

- Uses an implementation of genetic algorithms
- cMST -> NP-hard
- Formulation of graph problems adapts well
- Offer great flexibility for adding constraints
- Implementations present in literature



Hernandez-Munoz, D., Perez-Rosa, J. A., Diaz, K. and Corral, R. A. 2019. Metaheuristic-based Design and Optimization of Offshore Wind Farm Collection Systems. IEEE PowerTech at Milan (submitted) pp 1-6

INDEX

- 01 INTRODUCTION
- 02 PROBLEM DEFINITION
- 03 METHODOLOGY
- 04 COMPUTATIONAL EXPERIMENTS
- 05 SUMMARY

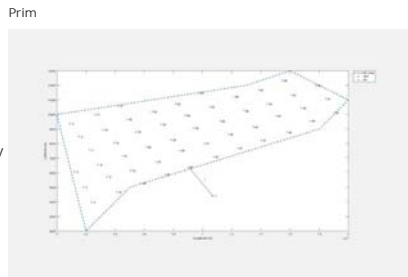
4 COMPUTATIONAL EXPERIMENTS



Single cable

The OWF:

- WTs number: 51
- WT nominal power: 4 MW
- Collection system nominal voltage: 33 kV
- Set of cables available: {500 mm²}
- Capacity constraint: 9



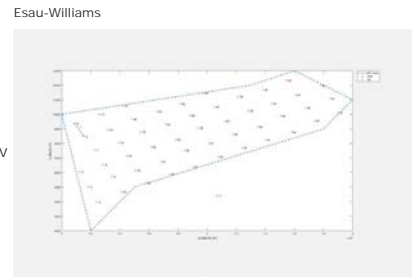
4 COMPUTATIONAL EXPERIMENTS



Single cable

The OWF:

- WTs number: 51
- WT nominal power: 4 MW
- Collection system nominal voltage: 33 kV
- Set of cables available: {500 mm²}
- Capacity constraint: 9



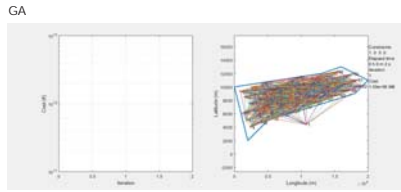
4 COMPUTATIONAL EXPERIMENTS



Single cable

The OWF:

WTs number: 51
 WT nominal power: 4 MW
 Collection system nominal voltage: 33 kV
 Set of cables available: {500 mm²}
 Capacity constraint: 9



4 COMPUTATIONAL EXPERIMENTS



Single cable

Table 2. Single cable results.

	Prim		Kruskal		Esau-Williams		Vogel's Appx. Method		Genetic Algorithm	
	Yes	Yes	Yes	Yes	Yes	Yes	Yes	Yes	Yes	Yes
AEP [GWh]	4.82	3.73	4.17	855.30	3.75	4.41				
Losses [GWh]										
Initial Investment CS [M€]	41.22	39	38.13	39	39.30	39.08				
Diff. with best [%]	8.12	2.30	0	2.30	2.82	2.92				
LCOE _{CS} [€/MWh]	2.96	2.80	2.74	2.80	2.82	2.82				
Diff. with best [%]	8	2.19	0	2.19	2.92	2.92				
NPV _{CS} ²⁰¹⁸ [M€]	356.64	358.36	360	359.36	358.75					
NPV _{CS} ²⁰¹⁸ [M€]	621.89	624.94	625.40	624.94	624.14					
Δdiff. with best w.r.t BC [%]	6	-19	-	-19	6					
NPV _{CS} ²⁰¹⁸ [M€]	887.13	890.52	890.94	890.52	889.56					
Δdiff. with best w.r.t BC [%]	12	-38	-	-38	12					

4 COMPUTATIONAL EXPERIMENTS



Multiple cables

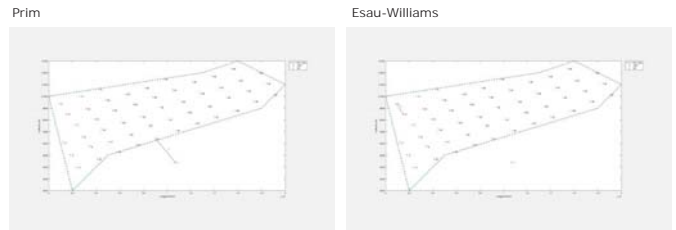
The OWF:

WTs number: 51
 WT nominal power: 4 MW
 Collection system nominal voltage: 33 kV
 Set of cables available: {138, 300 mm²}
 Capacity constraint: 7
 (Single case was 9)

4 COMPUTATIONAL EXPERIMENTS



Multiple cables



4 COMPUTATIONAL EXPERIMENTS



Multiple cables

Table 3. Multiple cables results.

	Prim		Kruskal		Esau-Williams		Vogel's Appx. Method		Genetic Algorithm	
	No	Yes	Yes	Yes	Yes	Yes	Yes	Yes	Yes	Yes
AEP [GWh]				7.3	855.36	7.99				
Losses [GWh]		7								
Initial Investment CS [M€]	-28.42	27.93	28.42	27.93	27.90	27.90				
Diff. with best [%]	1.80	0.05	1.80	0	0	0				
LCOE _{CS} [€/MWh]	2.05	2.01	2.05	2.01	2.01	2.01				
Diff. with best [%]	1.99	0	1.99	0	0	0				
NPV _{CS} ²⁰¹⁸ [M€]	368.42	368.77	368.42	368.42	368.47					
NPV _{CS} ²⁰¹⁸ [M€]	632.88	633.24	632.88	632.88	632.73					
Δdiff. with best w.r.t BC [%]	-25	-	-25	-	70					
NPV _{CS} ²⁰¹⁸ [M€]	897.54	897.71	897.54	896.99	896.99					
Δdiff. with best w.r.t BC [%]	-51	-	-51	139	139					

INDEX

- 01 INTRODUCTION
- 02 PROBLEM DEFINITION
- 03 METHODOLOGY
- 04 COMPUTATIONAL EXPERIMENTS
- 05 SUMMARY

5 SUMMARY



- Heuristic represents a good tool for designing collection systems in OWFs. They have mathematical expressions for worst case running time, and can come up with very good solutions very fast.
- Exhaustive computational experiments indicate that, Esau-Williams is the most likely heuristic to provide feasible solutions. This is due to its trade-off function. For single cable, provides the best solution, and in the case of multiple cables, provide the solution with the best investment-losses balance.
- Exhaustive computational experiments indicate that, Kruskal and VAM, are the most likely heuristics to come up with the lowest losses. This is due to their trade-off function.
- Exhaustive computational experiments indicate that, Prim, is the most likely heuristic to provide infeasible solutions. This is due to its trade-off function.
- Evolutionary algorithms, such as the Genetic Algorithm, are a very valuable tool for solving the unfeasibility problem from heuristics. They can be designed to optimize the initial investment, in contrast to the heuristics.
- The Genetic Algorithm tends to form smaller WT clusters into feeders than Esau-Williams, therefore, being able to provide cheaper initial investment solutions, albeit with greater power losses.
- Future work consists on implementing a MILP-heuristic-based solver to tackle this problem: combining mathematical formulations and high-level heuristics (as the ones designed in this work).



THANKS!

Questions?

SINTEF EERA DeepWind'2019
16th Deep Sea Offshore Wind R&D Conference,
Trondheim, 16 – 18 January 2019

RESONANCE CHARACTERISTICS IN OFFSHORE WIND POWER PLANTS WITH 66 KV COLLECTION GRIDS

Andrzej Holdyk Łukasz Kocewiak
SINTEF Energy Research, Norway Ørsted Wind Power, Denmark

NOWITECH Norwegian Research Centre for Offshore Wind Technology

Introduction

- Doubling the collection grid voltage might provide technical or economic benefits
 - We will be seeing many 66 kV col. grids soon
- This change might influence harmonic and transient behaviour of OWPPs
- How the increase of the collection grid voltage level changes the electrical environment characteristic of an OWPP in a wide frequency range
 - What happens to resonances?

2 Andrzej.Holdyk@sintef.no

- EERA DeepWind'2019 -

January 2019, Trondheim, Norway

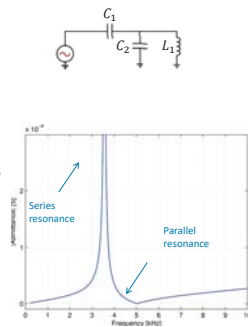


Electrical resonance

- Excitation of an electric system containing inductances and capacitances results in oscillations
- Natural frequency:

$$f = \frac{1}{2 \cdot \pi \cdot \sqrt{L \cdot C}}$$

- Impedance/admittance frequency sweep often used to find resonances



3 Andrzej.Holdyk@sintef.no

- EERA DeepWind'2019 -

January 2019, Trondheim, Norway



Electrical resonances (in OWPP)

- Resonance when (periodic) source has frequency similar to the circuit's natural frequency
 - Harmonics: $f < 2500$ Hz
 - Transients: $\text{Hz} < f < \text{MHz}$
- High amplification of voltage/current due to energy exchange between electric and magnetic field
- Harmonic/transient resonances can result in anything from a lack of compliance with a grid code to a component overheating or damage

4 Andrzej.Holdyk@sintef.no

- EERA DeepWind'2019 -

January 2019, Trondheim, Norway



About the study

- Design and model (a simple) offshore wind power plant
 - Frequency dependent admittance matrix in Matlab, 30 Hz – 1 MHz
 - Positive sequence only
- Use of state-of-the-art wide-band component models
- Create corresponding models of 33 kV and 66 kV collection grids
- Compare differences and explain where they came from

5 Andrzej.Holdyk@sintef.no

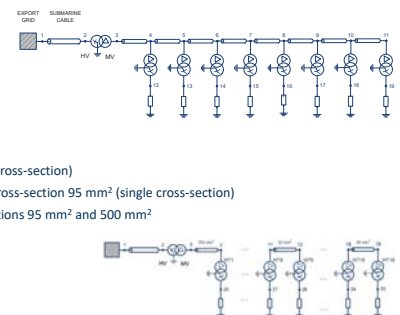
- EERA DeepWind'2019 -

January 2019, Trondheim, Norway



Assumptions

- 3 models:
 - 33 kV: 8 turbines /radial, 500 mm² (single cross-section)
 - 66 kV: 8 turbines /radial → smaller cable cross-section 95 mm² (single cross-section)
 - 66 kV: 16 turbines /radial → two cross-sections 95 mm² and 500 mm²
- Wind turbine: 6 MW
- Wind farm transformer: 90 MW



6 Andrzej.Holdyk@sintef.no

- EERA DeepWind'2019 -

January 2019, Trondheim, Norway



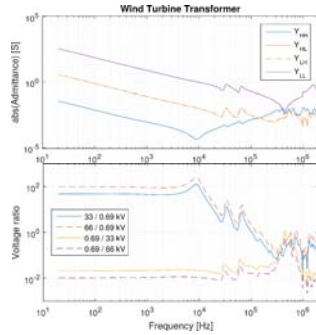
Transformer models

- Admittance matrix measurements
- Wind turbine and wind farm transformers
- 20 Hz – 2 MHz

$$\begin{bmatrix} I_p(\omega) \\ I_s(\omega) \end{bmatrix} = \begin{bmatrix} Y_{pp}(\omega) & Y_{ps}(\omega) \\ Y_{sp}(\omega) & Y_{ss}(\omega) \end{bmatrix} \begin{bmatrix} V_p(\omega) \\ V_s(\omega) \end{bmatrix}$$

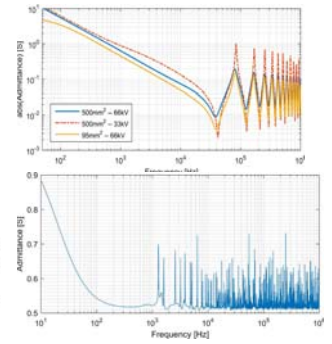
- Admittance scaling to change voltage ratio

$$\begin{bmatrix} I_p(\omega) \\ I_s(\omega) \end{bmatrix} = \begin{bmatrix} a^2 Y_{pp}(\omega) & a Y_{ps}(\omega) \\ a Y_{sp}(\omega) & Y_{ss}(\omega) \end{bmatrix} \begin{bmatrix} V_p(\omega) \\ V_s(\omega) \end{bmatrix}$$



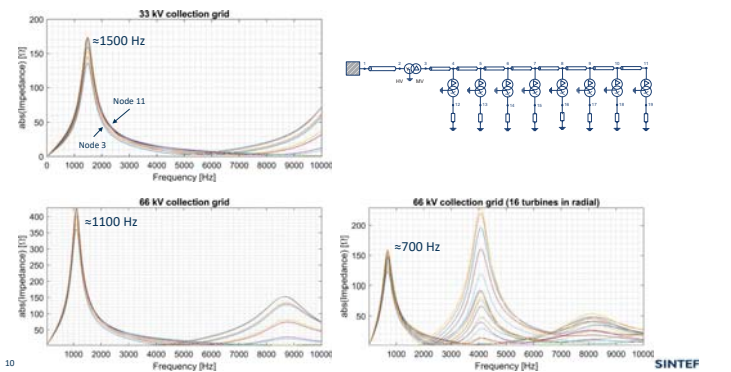
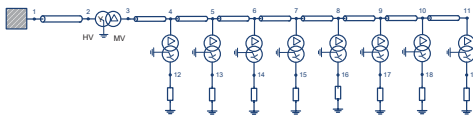
Component models

- Cables
 - Cable parameters based on material properties and dimensions
 - Freq. dependent traveling wave model. Similar to EMTPs
- Export grid
 - IEEE 118 bus reference system
 - Impedance sweep at 138 kV node



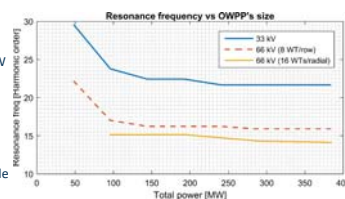
Results

- Look at nodes 3-11
- Check driving point impedance/admittance



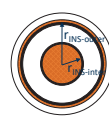
Resonance freq. vs OWPP's size

- Increased number of strings (1:8)
- Each string approx. 50 MW
- Park transformer scaled to total power above 90 MW
- OWPPs with 66 kV have resonances in lower order harmonic levels
- Main resonance frequency
 - Depends mostly on transformer inductance and cable capacitance



Cable capacitance...

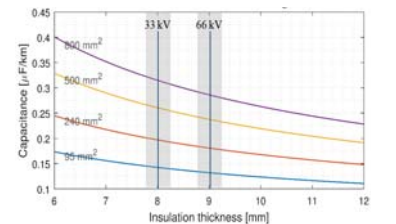
...depends on insulation material



$$C = \frac{2\pi\epsilon}{\ln \frac{r_{INS-outer}}{r_{INS-inner}}}$$

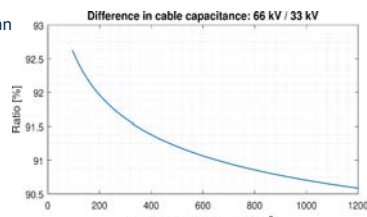
$$r_{INS-inner} = \sqrt{\frac{A_c}{\pi}}$$

$$r_{INS-outer} = r_{INS-inner} + d_{INS}$$



Difference in capacitance

- 66 kV cables capacitance is lower than capacitance of 33 kV cables for corresponding cross-sections
- The larger the conductor cross-section, the larger the difference in capacitance

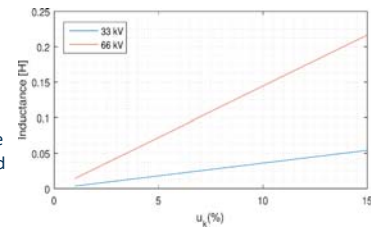


Transformer inductance

- Leakage inductance proportional to short circuit impedance

$$L_{sc} = \frac{V_p^2}{S} \frac{u_k(\%)}{2\pi f} = \frac{V_p^2}{S} \frac{u_k(\%)}{100} \cdot \frac{1}{2\pi f}$$

- Doubling the voltage quadruples the inductance, assuming the power and percent of short circuit voltage constant



Conclusions

- Change of voltage of the collection grid influences its resonance frequencies
 - Cable capacitance decreases with increase of voltage
 - Transformer inductance increases with increase of voltage
- Main resonance frequency will be shifted towards lower frequencies
 - Possible harmonic issues
 - Should be investigated by developers

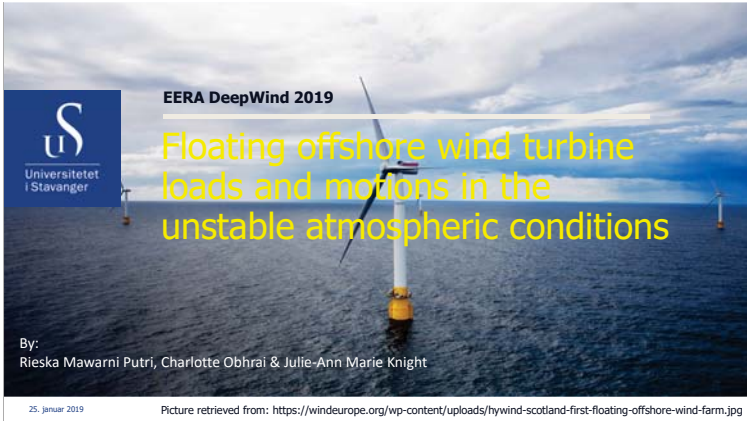
C1) Met-ocean conditions

The Influence of Unstable Atmospheric Conditions on the Motions and Loads on a Floating Wind Turbine, R.M.Putri, University of Stavanger

Using Machine Learning Methods to find a Representative and Conservative Set of Conditions for Fatigue Analysis of Offshore Wind Turbines, S.Kanner, Principle Power Inc

Processing of sonic measurements for offshore wind turbine relevance,
A. Nybø, Univ in Bergen

Uncertainties in offshore wind turbulence intensity, S.Caires, Deltares

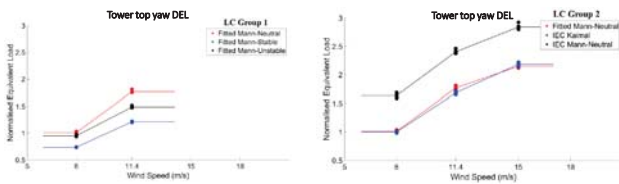


Outline

- Motivation
- Background
- Højstrup spectral model parametric study
- Results – coupled SIMO-RIFLEX on OC3-Hywind
- Conclusion
- Future work

Motivation

- Initial study from the master thesis project 'A study of the coherences of turbulent wind on a floating offshore wind turbine'



Background

- Højstrup spectral model: derived based on Kaimal spectral model, especially developed for unstable diabatic conditions:

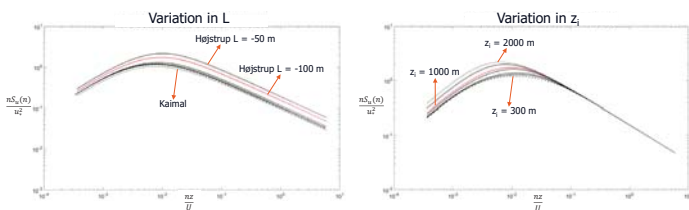
$$S(n) = S_L(n) + S_M(n)$$

↓ Low-frequency part ↓ High-frequency part

- Parameters: boundary layer height z_i , Obukhov-length L , height z
- In combination with Davenport coherence:

$$Coh_i(n) = \exp \left[-\frac{n}{u} \sqrt{(C_i^y d_y)^2 + (C_i^z d_z)^2} \right]$$

Højstrup spectral model – parametric study



Benchmark: $z_i=1000$ m, $L=-100$ m

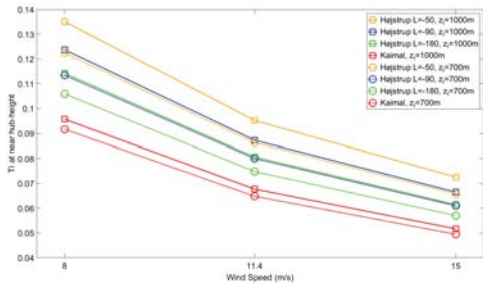
Simulations

- Turbulence box generation using MATLAB®

Spectral model	Load case		Decay coefficient (Davenport Coherence)						
	z_i (m)	L (m)	Value	C_H^y	C_V^y	C_W^y	C_H^z	C_V^z	C_W^z
Højstrup	700	-50	8, 11.4, 15 ms ⁻¹	7	7	6.5	10	10	3
		-90							
	-180								
	Wind speed								
1000	-50	#seed	6						
	-90	Wave	JONSWAP						
Kaimal	700	∞	$H_S = 6$ m						
	1000	∞	$T_p = 12$ s						
			$\gamma = 3.3$						

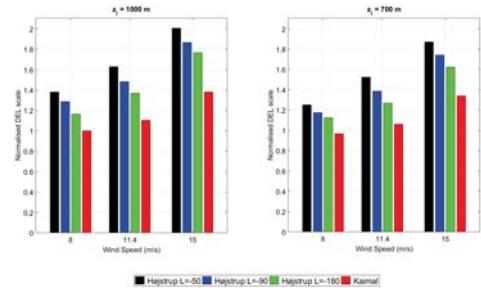
- Coupled SIMO-RIFLEX® simulations on the OC3-Hywind

Results – Turbulence Intensity



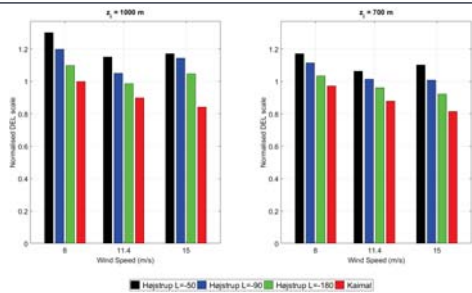
- 40% TI difference between neutral (Kaimal) and very unstable (Højstrup L=50 m), considering the same z_1
- 14% TI difference between $z_1 = 700\text{m}$ and $z_1 = 1000\text{m}$, considering the same L

Results – DEL tower top yaw torsion



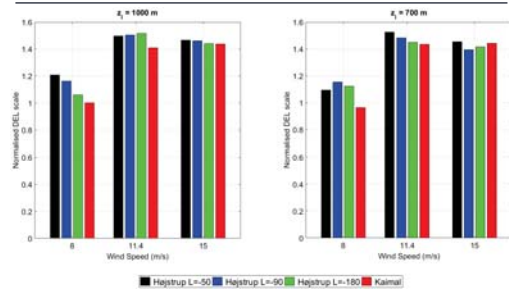
65% difference between neutral (Kaimal) and very unstable (Højstrup L=50m)

Results – DEL tower base side-side bending



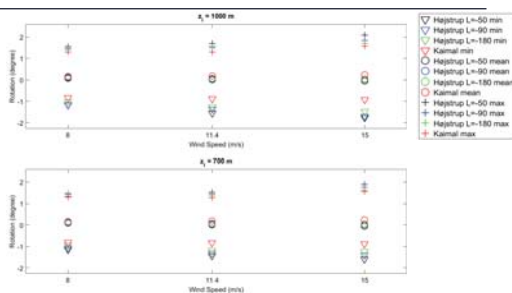
37% difference between neutral (Kaimal) and very unstable (Højstrup L=50m)

Results – DEL blade root flap-wise bending



24% difference between neutral (Kaimal) and very unstable (Højstrup L=50m)

Results – platform yaw motions



Results – other DEL and motions

- Tower base fore-aft bending DEL: 7% difference between neutral (Kaimal) and very unstable (Højstrup L=50) conditions
- Blade root edge-wise bending DEL: 3% difference between neutral (Kaimal) and very unstable (Højstrup L=50) conditions
- Other platform motions mode variations were not noticeable (except for roll, despite its small magnitude of -0.3° to 0.6°)

Limitations – Davenport decay coefficients

- A modified Davenport coherence by Cheynet et. al (2018) for vertical coherence:

$$Coh_i(d_z, n) = \exp \left[- \sqrt{\left(\frac{c_1^i f d_z}{\bar{u}} \right)^2 + \left(\frac{d_z}{l_z} \right)^2} \right]$$

- $l_z = \bar{u}/c_2^i$, proportional to a typical length scale of turbulence
- Decay coefficient depending on stability conditions ($-2 < z/L < -0.2$) derived from FINO1 data:

Decay coefficient			
c_1^u	c_1^v	c_1^w	c_2^w
$11+1.8\exp(4.5z/L)$	$7.1+3.4\exp(6.8z/L)$	$3.5+0.7\exp(2.5z/L)$	$0.05+0.13\exp(5z/L)$



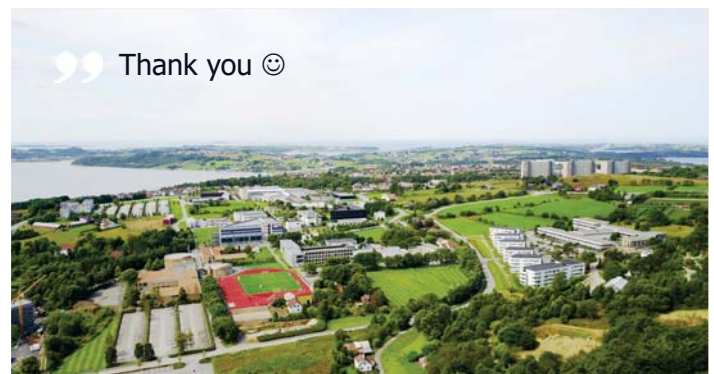
Conclusions

- The addition of low-frequency component in Højstrup model increases the spectral energy and TI
 - L and z_t are the parameters driving the TI
 - OC3-Hywind DELs for tower top yaw torsion showed a variation up to 65% for the different load cases. Also up to 37% for tower base side-side bending
- Højstrup spectral model was developed based on onshore measurement
- The importance of selecting a proper wind model representative for offshore environment in the OWT simulations, particularly for unstable conditions



Future work

- Simulations using spectral & coherence model as derived in the study of (Cheynet et al., 2018) using data from FINO1 measurement platform. This is only verified for vertical separations
- New measurements from the COTUR project will hopefully provide new information on coherence for horizontal separations
- Simulations using modified Mann spectral tensor model (Chougule et al., 2018) – with the possibility of deriving parameters from offshore data into the models
- Comparing various floater models and rotor sizes (Bachynski & Eliassen, 2018)



” Thank you ☺



Using Machine Learning Methods to find a Representative and Conservative Set of Conditions for Fatigue Analysis of Offshore Wind Turbines



Sam Kanner PhD, R&D Lead
Bingbin Yu PhD, Global Performance Lead

EERA Deepwind '19 Conference
Trondheim, Norway
16 Jan 2019

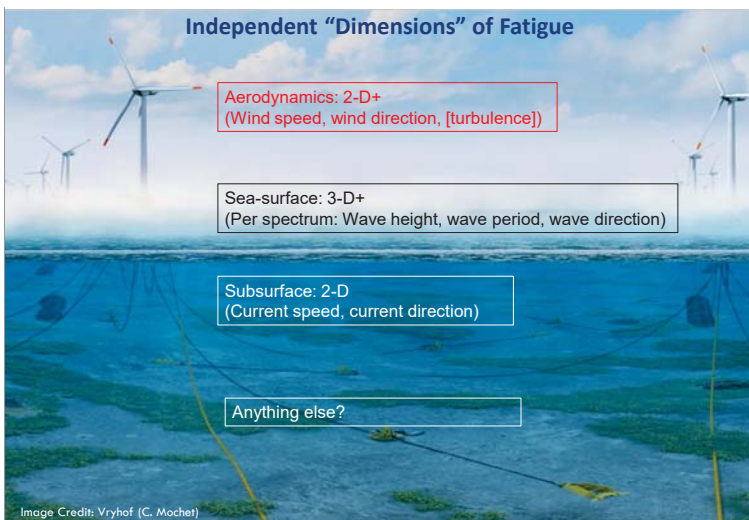
skanner@principlepowerinc.com



Outline

- Motivation
- Algorithm
 - LASSO
 - Gradient Descent
 - Clustering
- Metocean Data
- Results
- Conclusion

Independent "Dimensions" of Fatigue



Aerodynamics: 2-D+
(Wind speed, wind direction, [turbulence])

Sea-surface: 3-D+
(Per spectrum: Wave height, wave period, wave direction)

Subsurface: 2-D
(Current speed, current direction)

Anything else?

Image Credit: Vryhof (C. Mochet)

Estimation of Fatigue Life of an Offshore Structure & Mooring

DNV-OS-J103, DNV-OS-E301

(most accurate and computationally intensive procedure)

1. Numerous specific environmental conditions (load cases)

1. Wave direction: 8-12 bins
2. Wave height/period: 10-50 bins
3. Wind speed/direction: ? Bins
4. Current speed/direction: ? bins

2. Time-domain modelling tool

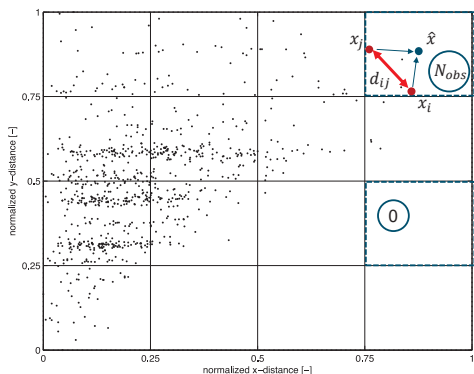
3. Rainflow counting method to assess range of "sensor" (e.g., tension in mooring line, principal stress at specific location)

4. Estimate damage from each load case using properties of material (e.g., S-N, T-N curve)

5. Estimate fatigue life from sum of damage, taking into account the probability of occurrence of each load case during design life of structure

Dowling SD, Socie DF. Simple rainflow counting algorithms. Int J Fatigue 1982;4:31-40.
B. Yeter, Y. Garbatov, C. Guedes Soares, Evaluation of fatigue damage model predictions for fixed offshore wind turbine support structures, Intl J. Fatigue, 2016; 87:71-80

Traditional clustering method (visualized in 2D)



$$P_{bin} = \frac{N_{obs}}{N_{tot}}$$

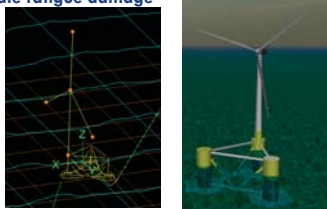
Conservative?

Representative?

**BEGIN:
ALGORITHM**

Proposed (Machine Learning-based) Algorithm

1. Load p -dimensional set of multi-decadal environmental conditions
 - i. Normalize data to all lie in $[0,1]$.
2. Initialize with a "representative" set of M clusters (or bins)
 - i. Modified Maximum Dissimilarity Algorithm (MDA-based) clustering method to associate all observations with closest cluster
3. Run time-domain simulations to estimate fatigue damage
 - i. OrcaFAST coupled aero-hydro-mooring simulations
 - ii. OrcaFlex: Time domain solver including first and second-order hydrodynamics (from WAMIT) and instantaneous mooring force
 - iii. FAST: Open-source BEM tool with linearized structural dynamics
 - iv. In-house rainfall counting algorithm



Representative

Kanner, S., Yu, B., Aubault, A., Pfeiffer, A., 2018. Maximum Dissimilarity-Based Algorithm for Discretization of Metocean Data into Clusters of Arbitrary Size and Dimension OMAE2018-77977

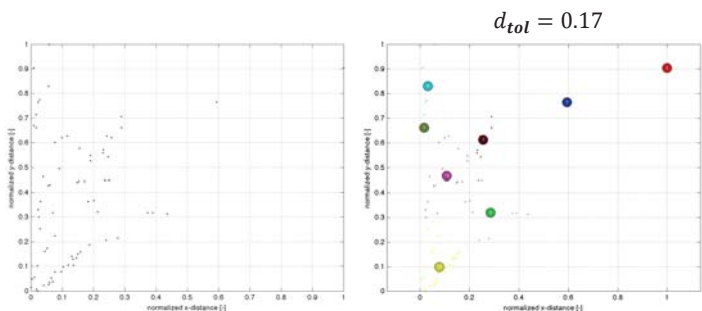
PRINCIPLE POWER

Proposed (Machine Learning-based) Algorithm (cont.)

4. Choose a set of predictors to estimate how environmental conditions effect fatigue damage
 - i. Damage = $H_s + H_s^2 + H_s^3 + T_p + T_p^2 + T_p^3, \dots, + H_s T_p$?
5. Run regularized linear regression analysis: Least Absolute Shrinkage and Selection Operator (LASSO)
 - i. Come up with a 'constrained' model on how fatigue damage depends on predictors
6. Use gradient ascent algorithm to determine direction of maximum damage
 - i. Pick step-size to determine speed of approach to maxima Conservative
 - ii. Select clusters that are in 'high-damage' areas and spawn N new clusters that may be more damaging Conservative
 - iii. Keep number of clusters M constant by creating $(M-N)$ new "representative" clusters using MDA-based method. Representative
7. Re-cluster all observational data using M new clusters.
8. Iterate (steps 3-7) to try and find a conservative value of fatigue damage

PRINCIPLE POWER

Step 1-2: Modified Maximum Dissimilarity Based Algorithm



$M = 8$

Representative

PRINCIPLE POWER

Step 4-5: Least Absolute Shrinkage and Selection Operator (LASSO)

1. Try to find the best fit: $\hat{y}_i = \sum_{j=1}^M \sum_{l=1}^{N_x} x_{i,j,l} \beta_j = \sum_{j=1}^{N_x} x_i^T \beta$ $x_i = H_{s,i}, H_{s,i}^2, H_{s,i}^3, \theta_{w,i}, \theta_{w,i}^2, \theta_{w,i}^3, \dots$
2. For a given λ ($\lambda > 0$), LASSO algorithm attempts to solve the problem

$$\min_{\beta, \beta_0} \left(\frac{1}{2N} \sum_{i=1}^M (y_i - \beta_0 - x_i^T \beta)^2 + \lambda \sum_{j=1}^p |\beta_j| \right)$$

Calculated (weighted) damage at i^{th} observation \uparrow Regression coefficients \uparrow
 i^{th} observation, with N_x parameters (using some linear combination of the p parameters) \uparrow Regularization parameter to penalize 'overfitting'

3. Use coordinate descent algorithm to determine "relevant" predictors

PRINCIPLE POWER

Steps 6: Gradient Ascent & Selection Criteria

1. Move in the direction of a local maximum:

Proposed next location of cluster $\hat{x}^{n+1} = \hat{x}^n + \gamma \nabla \hat{y}(\hat{x}^n)$

Previous location of cluster \hat{x}^n \uparrow Learning rate γ \uparrow Gradient of best fit $\nabla \hat{y}(\hat{x}^n)$

2. Selection criteria

- i. If weighted damage from cluster is in top quintile and calculated damage is greater than estimated, then set $\gamma = 0$ and keep it as a good candidate. Conservative
- ii. For all other observations, find the distance between the closest observation and the proposed (more-damaging) location
- iii. If the distance is less than a tolerance AND is in the "right" direction, then it is a good candidate. Conservative
- iv. Count how many observations are good candidates.
- v. Randomly select bins from lower (1st-4th) quintiles to remove from candidacy so that at least 20% of bins are removed from each iteration.

3. Re-run MDA algorithm to 'top-up' set (keeping number of bins constant) Representative

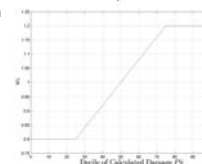
PRINCIPLE POWER

Step 7. Use weights to associate observations with damaging clusters

1. Euclidian distance of k^{th} observation to j^{th} cluster:

$$d_k = w_j \sqrt{\sum_{i=1}^p (\hat{x}_{j,i} - x_{k,i})^2}$$

2. Add in weight function, based upon calculated damage:



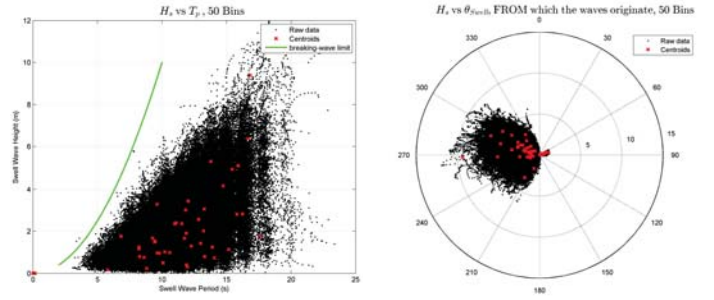
Conservative

3. Re-cluster observations to associate observations with "nearest" cluster

PRINCIPLE POWER

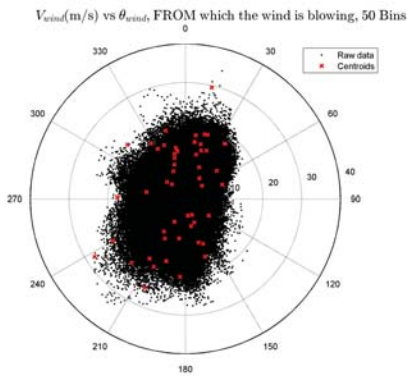
END:
ALGORITHM

Metocean Data: Swell Waves



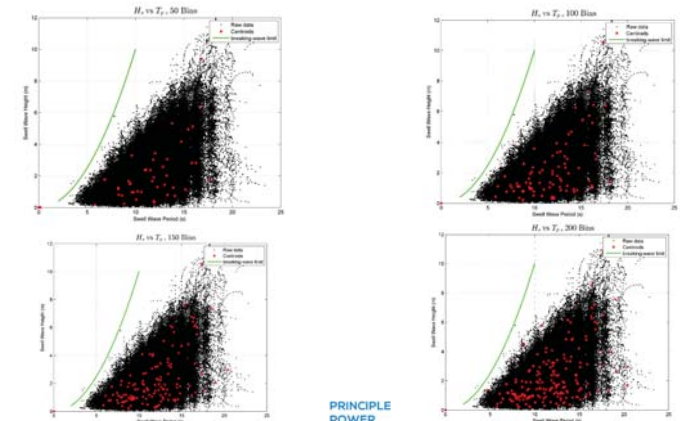
PRINCIPLE
POWER

Metocean Data: Wind



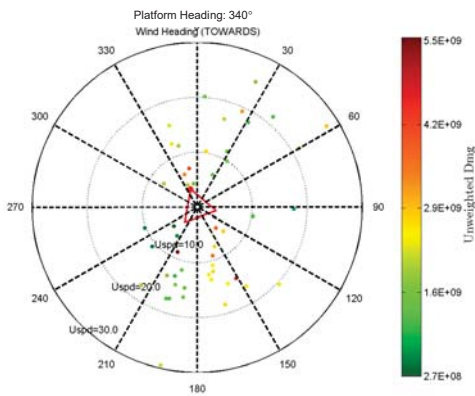
PRINCIPLE
POWER

Metocean Data: Swell Waves, Bin Dependence



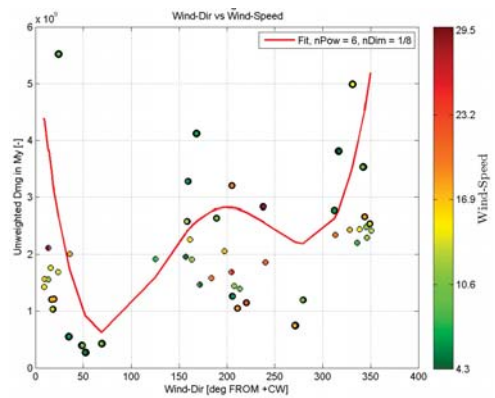
PRINCIPLE
POWER

Results F/A Tower-Base: Damage Dependence on Wind (50 bins)



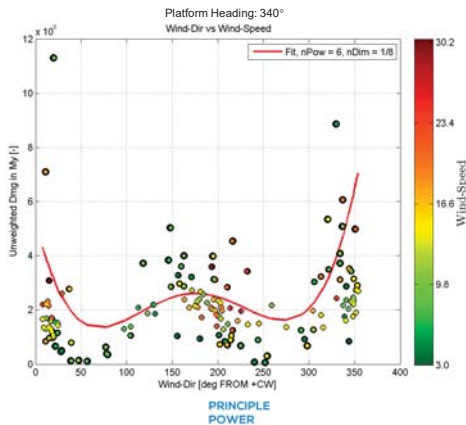
PRINCIPLE
POWER

1-D Regression (Wind-Direction, 50 bins)



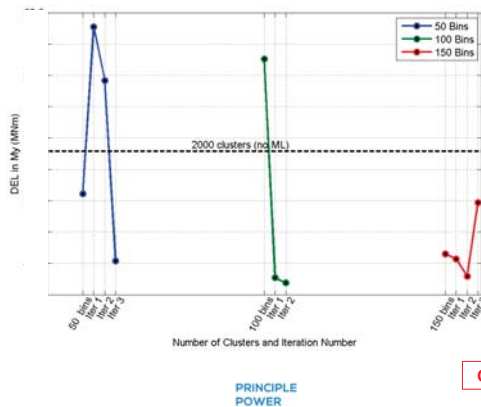
PRINCIPLE
POWER

1-D Regression (Wind-Direction, 150 bins)



19

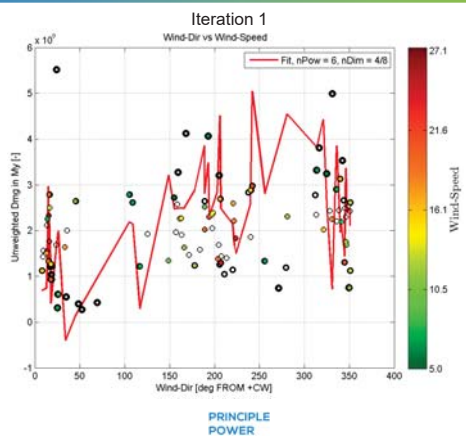
1-D Regression (Wind-Direction) DEL Results



Conservative?

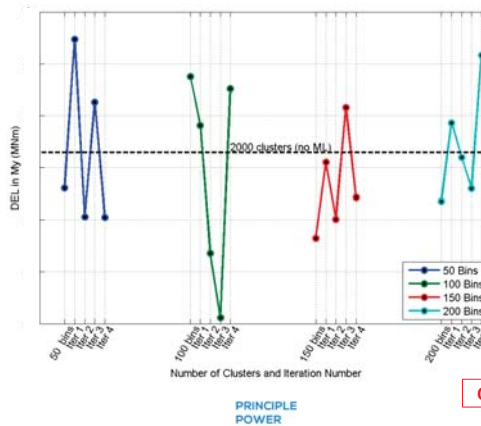
20

4-D Regression (Wind Speed+Direction, Wind-Sea Tp+Direction)



21

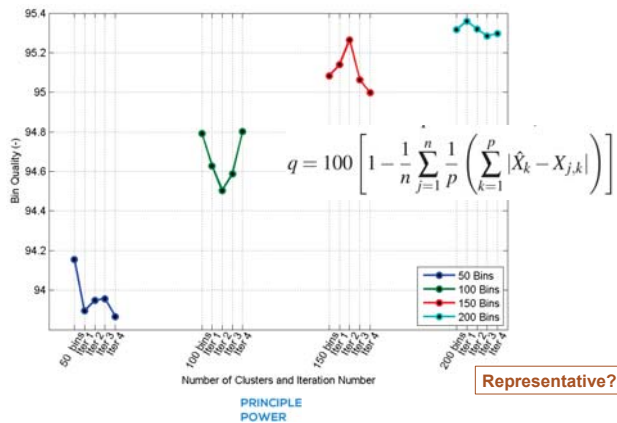
Results, 4-D Regression (Wind Direction, Wind Speed, Wave Direction, Wave Tp)



Conservative?

22

“Quality” Measure as a Proxy for Representativeness



Representative?

23

Wrap-Up

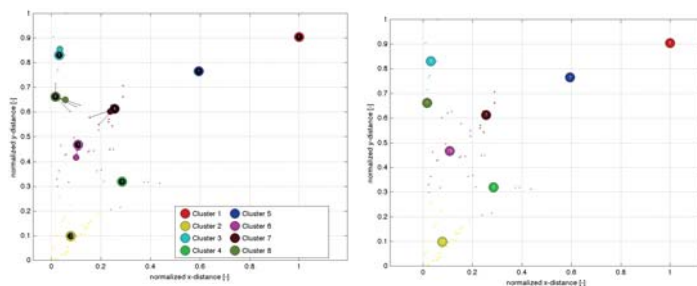
- A machine learning-based algorithm is proposed to try and find the most *representative* and *conservative* set of environmental conditions to estimate fatigue damage on a floating offshore wind turbine.
- While a 1-D linear regression (based on wind-direction) is easily identified, it does not lead to conservative damage estimations.
- A 4-D linear regression (based upon wind and wind-seas) leads to a more wildly behaving fit, but finds better conservativeness.
- The values of *representativeness* and *conservativeness* may be opposed to each other.
- In the future, we hope to improve algorithm to find conservativeness with smaller number of conditions
 - More regularization?
 - Learning rate?

PRINCIPLE POWER

24

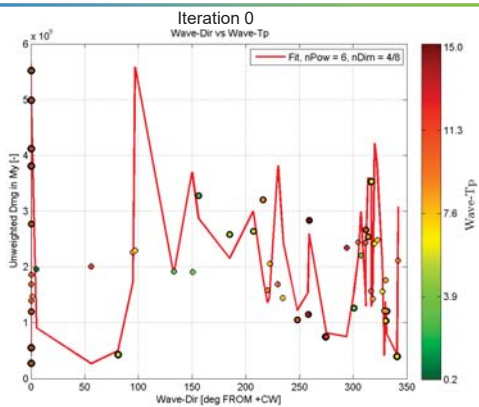


Step 7: Re-cluster observations based on new locations



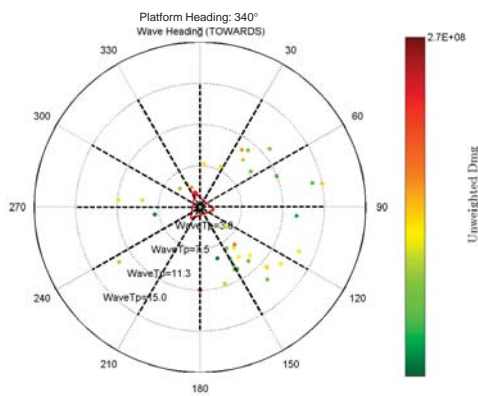
PRINCIPLE POWER

4-D Regression, Wind-Sea Dependence



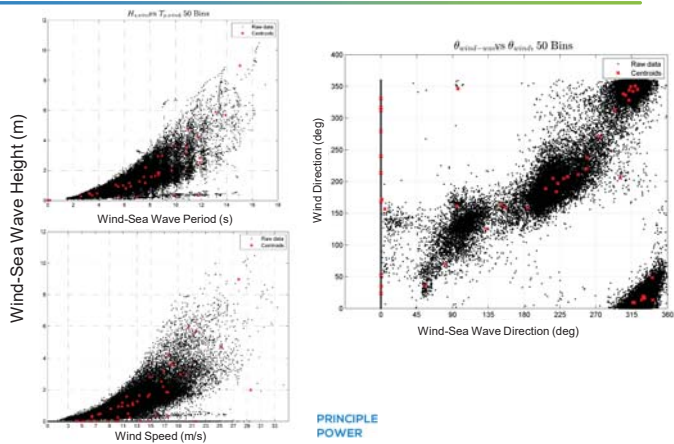
PRINCIPLE POWER

Results F/A: Damage Dependence on Wind-Sea (50 bins)



PRINCIPLE POWER

Metocean Data: Wind-Sea Waves



PRINCIPLE POWER

Step 5 (cont.) Coordinate descent determines relevant parameters

1. Again, trying to find β such that:

$$\min_{(\beta_0, \beta) \in \mathbb{R}^{p+1}} R_\lambda(\beta_0, \beta) = \min_{(\beta_0, \beta) \in \mathbb{R}^{p+1}} \left[\frac{1}{2N} \sum_{i=1}^N (y_i - \beta_0 - x_i^\top \beta)^2 + \lambda P_\alpha(\beta) \right]$$

2. The minimum of the residual:

$$\frac{\partial R_\lambda}{\partial \beta_j} \Big|_{\beta=\tilde{\beta}} = -\frac{1}{N} \sum_{i=1}^N x_{ij} (y_i - \tilde{\beta}_0 - x_i^\top \tilde{\beta}) + \lambda(1 - \alpha)\beta_j$$

3. Update the guess of β :

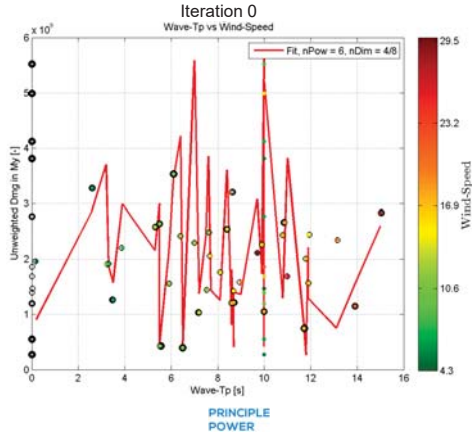
$$\tilde{\beta}_j \leftarrow \frac{S\left(\frac{1}{N} \sum_{i=1}^N x_{ij} (y_i - \tilde{y}_i^{(j)}), \lambda\alpha\right)}{1 + \lambda(1 - \alpha)} \quad \tilde{y}_i^{(j)} = \tilde{\beta}_0 + \sum_{l \neq j} x_{il} \tilde{\beta}_l$$

$$S(z, \gamma) \quad \text{sign}(z)(|z| - \gamma)_+ = \begin{cases} z - \gamma & \text{if } z > 0 \text{ and } \gamma < |z| \\ z + \gamma & \text{if } z < 0 \text{ and } \gamma < |z| \\ 0 & \text{if } \gamma \geq |z|. \end{cases}$$

Friedman, J., R. Tibshirani, and T. Hastie. Regularization paths for generalized linear models via coordinate descent. Journal of Statistical Software, Vol 33, No. 1, 2010. <http://www.jstatsoft.org/v33/i0>

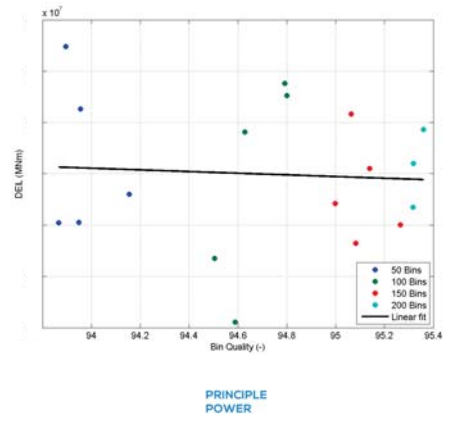
PRINCIPLE POWER

4-D Regression, Wind-Sea Dependence



31

Competing Interests: Representativeness vs Conservativeness



32

EERA DEEPWIND'2019 - 16TH OF JANUARY 2019 - ASTRID NYBØ

Processing of sonic anemometer measurements for offshore wind turbine applications

Astrid Nybø
Finn Gunnar Nielsen & Joachim Reuder
Geophysical Institute & Bergen Offshore Wind Centre

UNIVERSITY OF BERGEN

EERA DEEPWIND'2019 - 16TH OF JANUARY 2019 - ASTRID NYBØ


Motivation

How should the processing of sonic anemometer measurements be tailored to offshore wind turbine applications?

- This work defines such a processing procedure for offshore measurements at FINO1

EERA DEEPWIND'2019 - 16TH OF JANUARY 2019 - ASTRID NYBØ

The measurements



- FINO1
- Sonic anemometers at 40, 60 and 80 m
 - Wind speed (m/s)
 - Sonic temperature (K)
- June 2015 – September 2016
- Other measurements
 - Direction from wind vanes
 - Precipitation

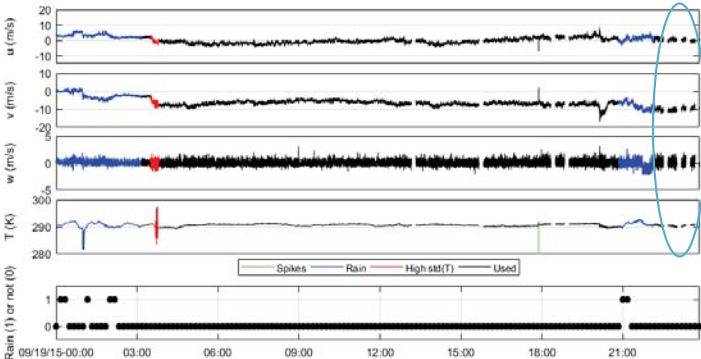
EERA DEEPWIND'2019 - 16TH OF JANUARY 2019 - ASTRID NYBØ

The processing procedure

Assessing data gaps and removing corrupted raw data files

EERA DEEPWIND'2019 - 16TH OF JANUARY 2019 - ASTRID NYBØ

The processing procedure



EERA DEEPWIND'2019 - 16TH OF JANUARY 2019 - ASTRID NYBØ

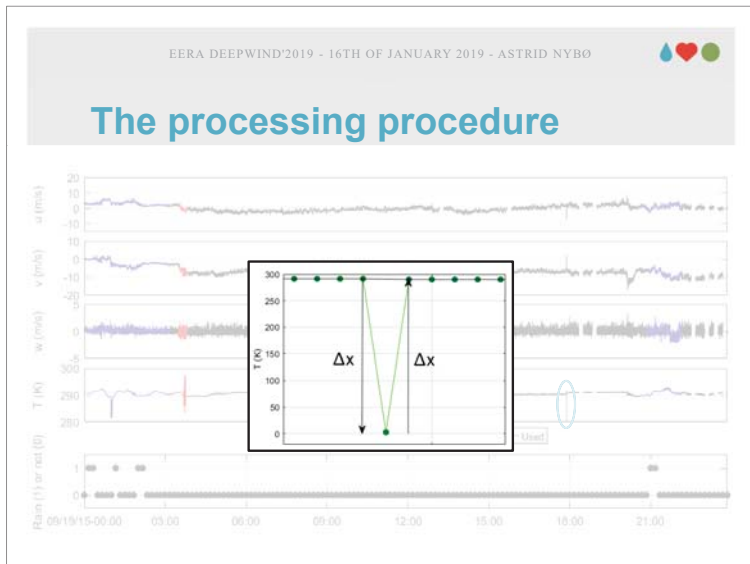
The processing procedure

Assessing data gaps and removing corrupted raw data files

Spike detection and removal

$|\Delta x_{ext}| > a(\sigma_{\Delta x, b} + c)$

- Spike: Δx_{ext} in the first/last N_{spike} → Replace spike by constant
- Spike: $+\Delta x_{ext}$ & $-\Delta x_{ext}$ within N_{spike} → Replace spike by interpolation

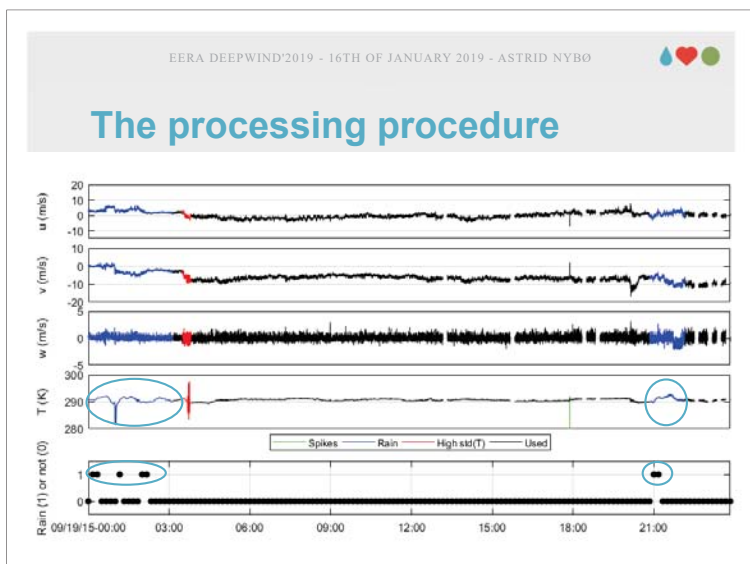


EERA DEEPWIND'2019 - 16TH OF JANUARY 2019 - ASTRID NYBØ

The processing procedure

- Assessing data gaps and removing corrupted raw data files
- Spike detection and removal
- Disregarding measurements close to precipitation events**

- Rain / no rain
- Removing 10 minutes before and 50 minutes after precipitation event

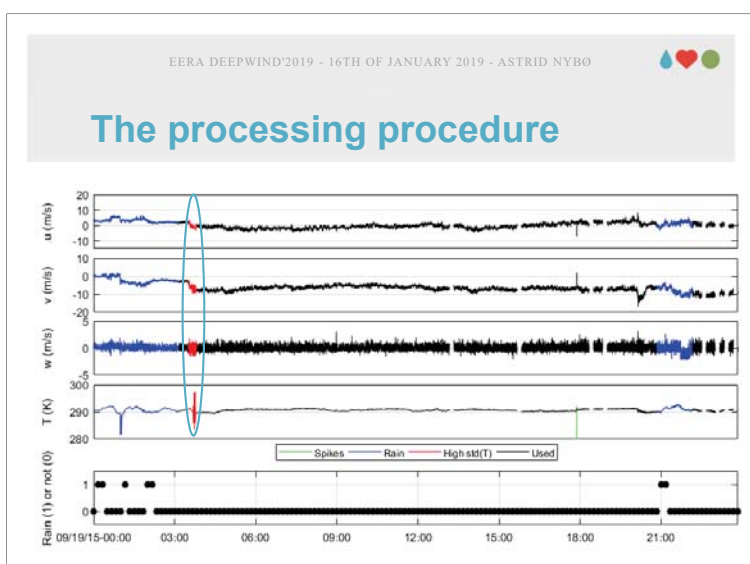


EERA DEEPWIND'2019 - 16TH OF JANUARY 2019 - ASTRID NYBØ

The processing procedure

- Assessing data gaps and removing corrupted raw data files
- Spike detection and removal
- Disregarding measurements close to precipitation events
- Disregarding measurements influenced by other disturbances**

- Fog, frost, sea spray or larger aerosol particles



EERA DEEPWIND'2019 - 16TH OF JANUARY 2019 - ASTRID NYBØ

The processing procedure

- Assessing data gaps and removing corrupted raw data files
- Spike detection and removal
- Disregarding measurements close to precipitation events
- Disregarding measurements influenced by other disturbances
- Disregarding measurements from the geographical exclusion zone**

EERA DEEPWIND'2019 - 16TH OF JANUARY 2019 - ASTRID NYBØ

The processing procedure

EERA DEEPWIND'2019 - 16TH OF JANUARY 2019 - ASTRID NYBØ

The processing procedure

<https://www.4coffshore.com/offshorewind/>

EERA DEEPWIND'2019 - 16TH OF JANUARY 2019 - ASTRID NYBØ

The processing procedure

- Assessing data gaps and removing corrupted raw data files
- Spike detection and removal
- Disregarding measurements close to precipitation events
- Disregarding measurements influenced by other disturbances
- Disregarding measurements from the geographical exclusion zone
- Rotation to mean flow direction

- Double rotation

EERA DEEPWIND'2019 - 16TH OF JANUARY 2019 - ASTRID NYBØ

The processing procedure

- Assessing data gaps and removing corrupted raw data files
- Spike detection and removal
- Disregarding measurements close to precipitation events
- Disregarding measurements influenced by other disturbances
- Disregarding measurements from the geographical exclusion zone
- Rotation to mean flow direction
- Organizing in 30-minute periods

EERA DEEPWIND'2019 - 16TH OF JANUARY 2019 - ASTRID NYBØ

Stationarity assessment

- Step: Linear trend test

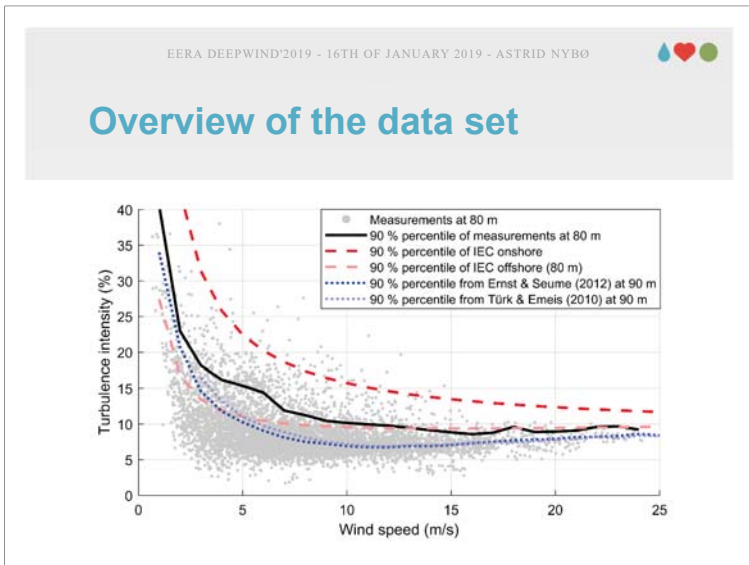
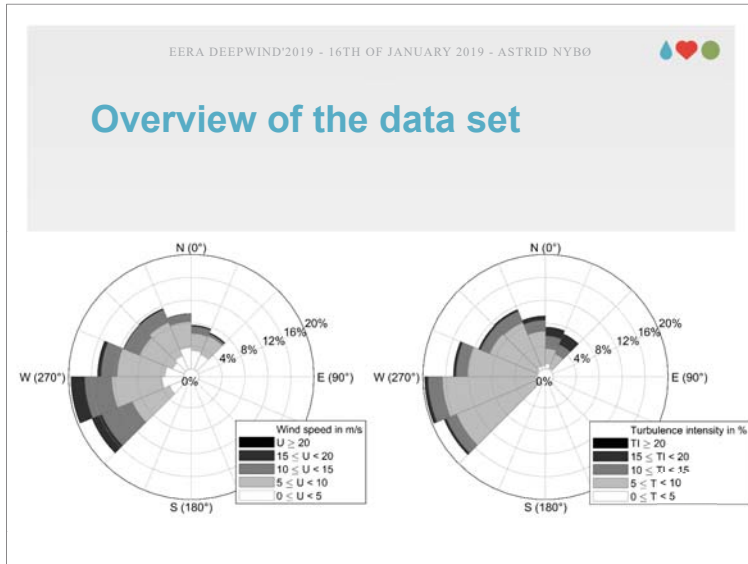
$$\frac{\Delta U}{\bar{U}} \leq \frac{0.2 * \Delta t(\text{min})}{60 \text{ min}}$$
- Step: Moving mean and moving standard deviation test

$$\max\left(\frac{|U_{60\text{min}} - U_{10\text{min}}|}{U_{60\text{min}}}\right) \leq 0.4 \quad \& \quad \max\left(\frac{|\sigma_{U,10\text{min}} - \sigma_{U,60\text{min}}|}{\sigma_{U,10\text{min}}}\right) \leq 0.4$$

EERA DEEPWIND'2019 - 16TH OF JANUARY 2019 - ASTRID NYBØ

Complete data set

Step	Percentage	Data Points
Available	100%	23424x30min
Missing	-11.8%	
Corrupted	-0.6%	
Rainy	-16.2%	
High n_T	-13.2%	
Shadow	-27.7%	
30min	-3.8%	
Processed	26.7%	622x30min



EERA DEEPWIND'2019 - 16TH OF JANUARY 2019 - ASTRID NYBØ

Limitations of the data set

- Reduced data availability
- Biased towards situations without precipitation

Season	Availability after the processing procedure (%)
Summer 15	12
Autumn 15	24
Winter 15/16	23
Spring 16	28
Summer+Sept. 16	42

- Not able to retrieve proper wind or temperature profiles

EERA DEEPWIND'2019 - 16TH OF JANUARY 2019 - ASTRID NYBØ

Other reflections

Conservative approach

Further use:

- Relation between parameters
- Frequency domain
- Validation of standards
- Simulations of dynamic response

EERA DEEPWIND'2019 - 16TH OF JANUARY 2019 - ASTRID NYBØ

Conclusions

A thorough processing procedure of sonic anemometer measurements for offshore wind turbine applications is presented



Conclusions

A thorough processing procedure of sonic anemometer measurements for offshore wind turbine applications is presented

The processing procedure concludes in a data set with a great variety in offshore conditions



Conclusions

A thorough processing procedure of sonic anemometer measurements for offshore wind turbine applications is presented

The processing procedure concludes in a data set with a great variety in offshore conditions

Together with a stationarity assessment, the data set is prepared for numerous applications



UNIVERSITY OF BERGEN
Bergen Offshore Wind Centre



Uncertainties in offshore wind turbulence intensity

$$Turbulence\ Intensity = TI = \frac{wind\ speed\ standard\ deviation}{wind\ speed\ mean} = \frac{\sigma_U}{U}$$

Sofia Caires and Jan-Joost Schouten - Deltares, Netherlands
 Lasse Lønseth, Vegar Neshaug, Irene Pathirana and Ola Storås - Fugro Norway AS, Norway

Acknowledgments:
 The Dutch Ministry of Economic Affairs (rvo)

Motivation


One of the input parameters for the development, design and operation of wind farms is the wind speed and turbulence intensity at hub height.

Given that measurements at hub height are rare, hub height wind speeds and turbulence intensities are often determined using simplified formulations.

$$U_z = U_{z_{ref}} \left(\frac{z}{z_{ref}} \right)^\alpha \quad TI = \beta$$

These formulations are based on assuming a dependence only on wind speed at a reference level and neutral or fixed atmospheric stability.

Such assumptions involve large uncertainties given that the vertical wind profile – i.e. translation of wind speed and TI in height – depend both on the sea surface roughness and atmospheric stability.




Deltares

Aim & Approach

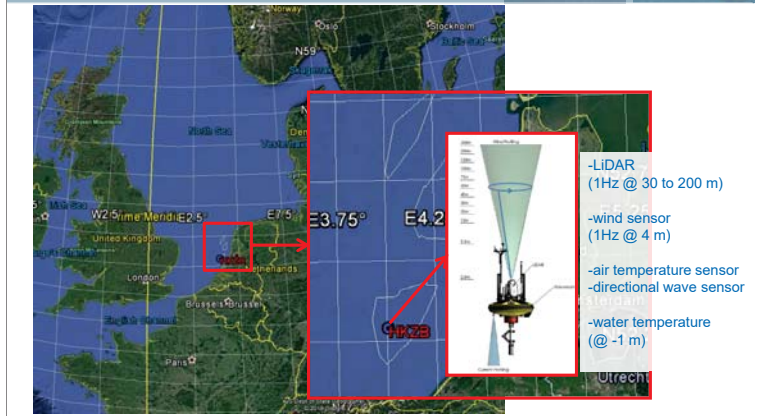
Aim:
 Study the dependence of turbulent intensity (and wind speed) on atmospheric stability and surface roughness.

Approach:
 Use a comprehensive dataset of North Sea meteocean observations to determine the variability of the turbulence intensity and wind speed with vertical temperature gradients, wind severity and surface roughness.




Deltares

Data



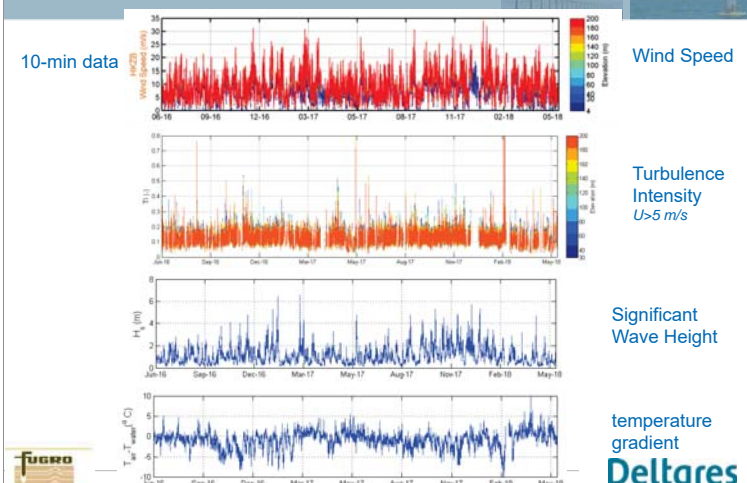
SEAWATCH Wind LIDAR buoy observations from June 2016 until June 2018



Deltares

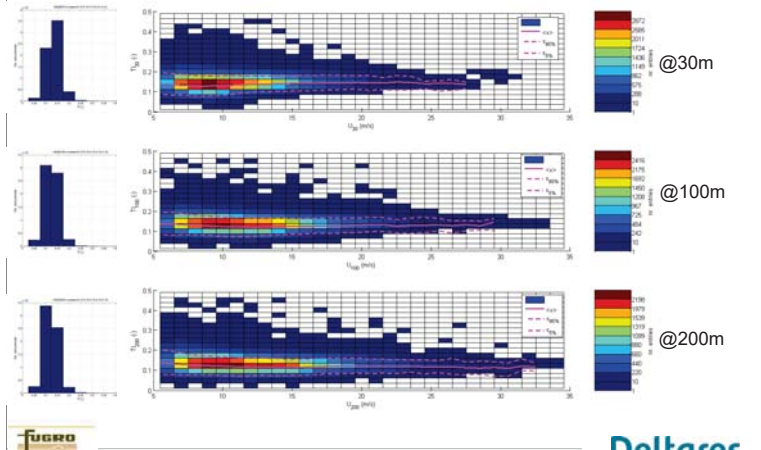
HKZB Field Measurement Campaign Data

10-min data

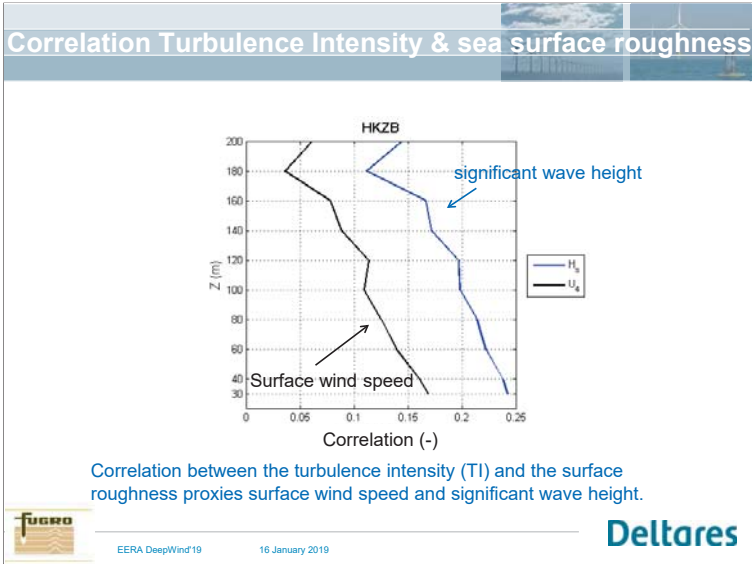
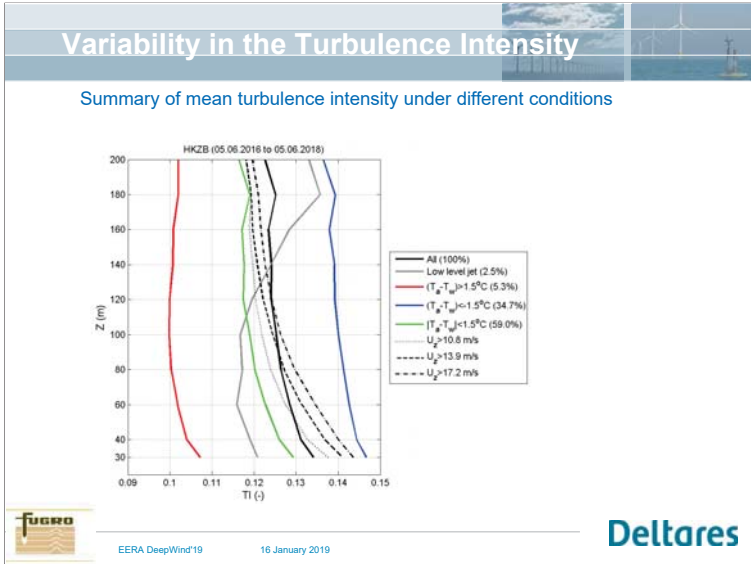
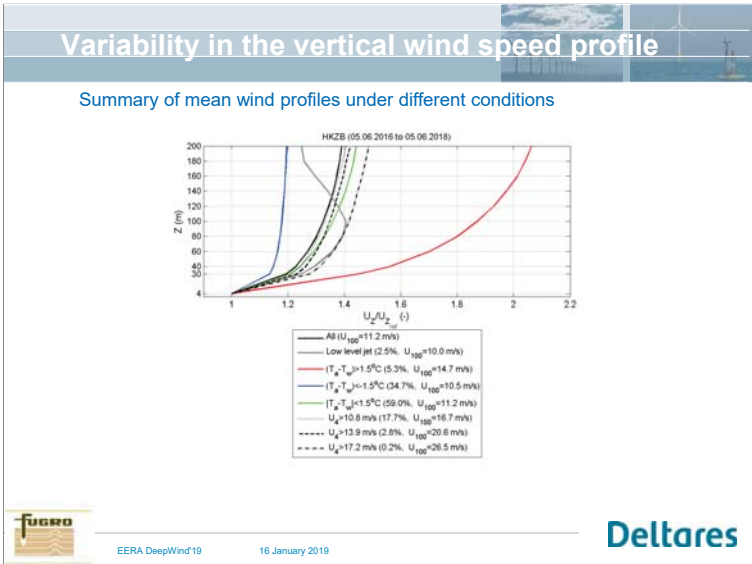
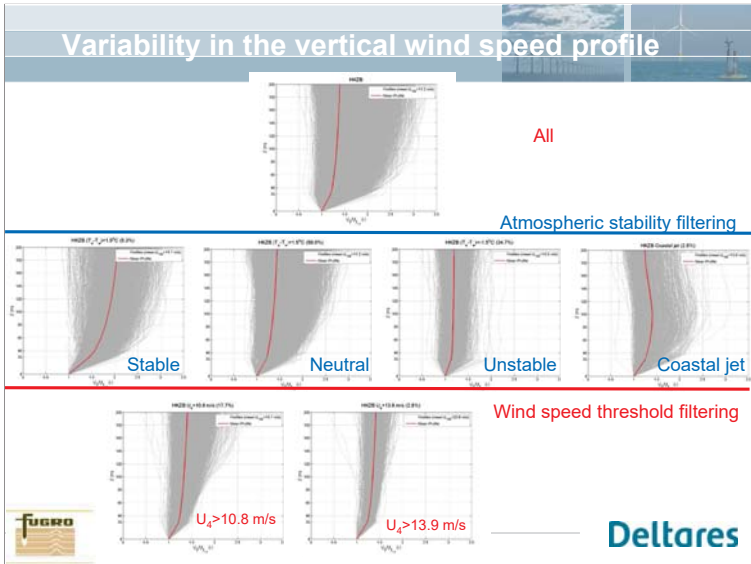


Deltares

Variation of turbulence intensity with wind speed



Deltares



Final remarks

- The turbulence intensity is shown to depend strongly on the atmospheric stability and less strongly on the sea surface roughness.
- The lower turbulence intensity values are observed under stable atmospheric conditions.
- The dependence of the turbulence intensity on the surface roughness is higher at the lower levels.
- The significant wave height is the proxy of the sea surface roughness with the stronger correlation with the turbulence intensity.

↓

- Atmospheric stability should be considered when determining turbulence intensities.**
- If not possible due to lack of data, the uncertainties that result from not accounting for these should be considered when determining turbulence intensities using the standard formulations.**

Deltares

EERA DeepWind'19 16 January 2019

C2) Met-ocean conditions

COTUR - estimating the Coherence of TURbulence with wind lidar technology, M.Flügge, NORCE Technology

Towards a high-resolution offshore wind Atlas - The Portuguese Case, T.Simões, LNEG

The DeRisk design database: extreme waves for Offshore Wind Turbines, F.Pierella, DTU

Main objectives



1. Improve our knowledge regarding offshore wind turbulence and horizontal coherence, with respect to offshore wind energy
2. Create a new, unique and highly relevant dataset which is available for future offshore wind energy research
3. Store the collected data and corresponding meta-data in a database for later analysis

The collected data and the performed analysis is highly relevant with respect to load estimations on multi-megawatt offshore wind turbines.



Relevant key research questions



- What is the appropriate averaging time for turbulence analysis under different meteorological conditions when focusing on large offshore wind turbines?
- What are the characteristics of the horizontal coherence offshore?
- How does horizontal coherence relate to different atmospheric conditions offshore?
- How does the observed horizontal coherence compare to the industry standard?
- Is there a feedback from waves on horizontal coherence structures?



Why was Obrestad selected?



- In a pre-study in 2017 we identified and analyzed several sites based on the following criteria:
 - Access to suitable power supply and infrastructure
 - Accessibility
 - Free wind inflow conditions (over the ocean)
 - Proximity to meteorological reference measurements, e.g. met-masts, radio soundings, meteorological observation stations
 - Site influence on the wind field (as little as possible)
- Obrestad scored high on all criteria
 - Runner up: Marstein Fyr (more difficult access)



Obrestad



Marsteinen

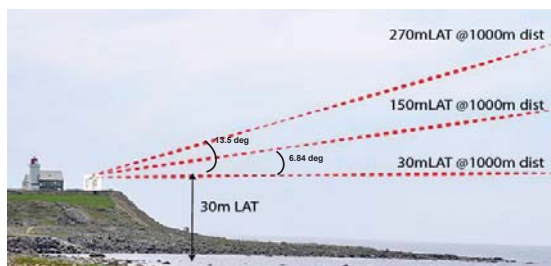
Obrestad site



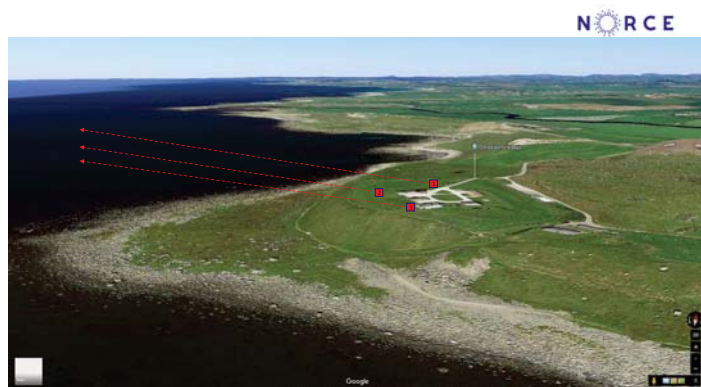
- The overview shows the locations of the LIDAR platforms
- The passive microwave radiometer and the WindCube V1 are located together with the WindCube100S at location 1



Scanning at different heights



Example illustration with vertical trajectory angles for stepwise measurements at different target altitudes.



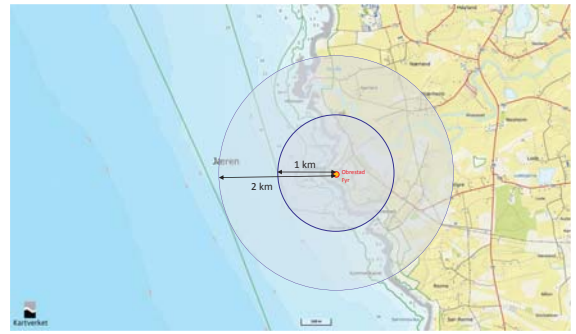
Measuring wind turbulence and coherence with LIDARS



- Horizontal distance between LIDARS: 60-120m
- Parallel scanning beams
 - Enables measurement of horizontal coherence at relevant distances for offshore wind energy
 - We aim to keep the same separation distance at all ranges
 - Enables comparison with results from existing literature



Scanning range



Platforms / frames



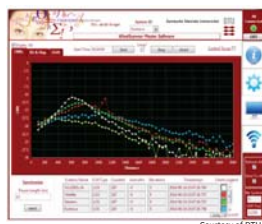
- Original plan: place LIDARS on top of containers
 - Had to be changed due to the visual disturbance (popular place for tourists)
- New plan: Build frames in aluminum beams
 - Deformation/strength study performed by third party
 - LIDARS will be installed by lifting them inside the frame by using pulleys and winches



Windscanner software



- Developed by DTU
- Enables synchronization of the LIDARS and more advanced scan patterns



Courtesy of DTU

Permissions



- Coastal administration – operators of the lighthouse
- Fylkesmannen i Rogaland – natural conservation laws
- Hå kommune – owners of the property
- Rogaland Fylkeskommune – cultural heritage laws

Publication of results



- Results of data analysis will be openly published and will be used for educational purposes
- The data itself is owned by the parties in the project



Thank you for your attention!



Towards a high-resolution offshore wind Atlas - The Portuguese Case

A. Couto, J. Silva, P. Costa, D. Santos, T. Simões and A. Estanqueiro



Presentation outline :

- Introduction
- Mesoscale modelling features to improve the wind resource characterization
- Development of the new offshore wind Atlas: Model calibration - *Step I*
- New offshore wind Atlas: Atlas Validation - *Step II*
- Final Remarks



Introduction



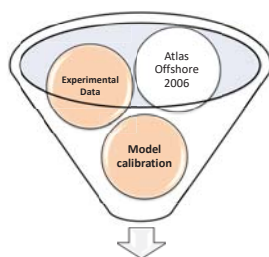
Introduction

- **Offshore wind energy** is a key contributor towards the **decarbonisation** of several electrical power systems.
- A **reliable offshore wind resource assessment** is a **crucial step to establish a strategic plan for the exploitation of marine renewable energies**. Although:
 - experimental measurement campaigns may not be cost effective, especially for deep offshore regions, and these data are, typically, collected inside a limited spatial and time window,
 - while wind observations inferred through satellites still present large amounts of missing/poor quality data and low spatial/temporal resolution .
- **To achieve this goal**, without resort to an extensive and costly network of anemometric stations or buoys, **it becomes necessary to use the so-called mesoscale numerical models**.
- These models have the **ability to describe important atmospheric phenomena for wind power** purposes such as the atmospheric turbulence, stratification, and sea-land-breeze processes.



Introduction

- The first offshore wind Atlas for Portugal was produced in 2006.
- The **improvements** observed in the numerical simulation field, the **lack of measurements to validate** the previous Atlas, **required a new offshore wind Atlas** to support the spatial planning of marine energy sources for the maritime area of Continental Portugal.
- In **this work presents**:
 1. a high spatial resolution (1x1 km) **offshore wind resource Atlas for Portugal**
 2. the mesoscale model calibration steps.



New offshore Atlas

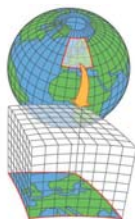


Mesoscale modelling features to improve the wind resource characterization

- *Meteorological boundary and initial conditions*
- *Atmospheric parameterizations*
- *Data assimilation*



• **Meteorological boundary and initial conditions (IBC)**



Source: www.csc.fi

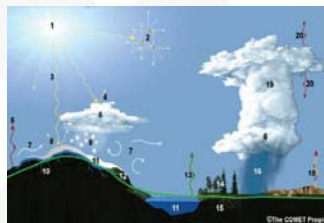
- **Data from global model present low spatial and temporal resolutions for local effects characterization:**
 - Spatial Res.: > 25 km;
 - Temporal Res.: > = 1 h (typically 6 h).
- Data from global models essential for feeding mesoscale models:
 - **Initial and border conditions**

Main characteristics of the most common applied IBC products.

Dataset	Time res. (hours)	Assimilation system	Horizontal res. (Lat. X Lon.)	Vertical levels
NCEP-R2	6	3D-Var	2.50° x 2.50°	28
CFSR	6	3D-Var	0.50° x 0.50°	64
ERA-Interim	6	4D-Var	0.75° x 0.75°	60
GFS	6	3D-Var	0.25° x 0.25°	64
FNL	6	3D-Var	1.00° x 1.00°	52
ERA-5	1	4D-Var	0.28° x 0.28°	72



• **Atmospheric parameterizations**

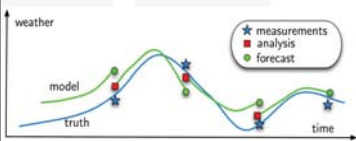


Source: The COMET program (adapted).

- Mesoscale models solve the Navier-Stokes equations.
- **Numerical parameterizations** enable to close the equations using approximations in the simulation to describe the physical processes:
 - *Planetary boundary layer*
 - *Cloud microphysics*
 - *Cumulus*
 - *Radiation processes*
 - Etc. ...



• **Data assimilation schemes**



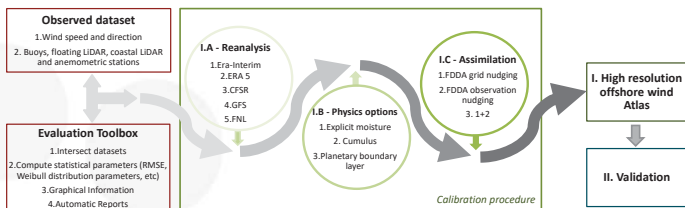
Source: pedagogtech.inp-toulouse.fr

- **Assimilation:** numerical technique that combine observed meteorological data with a "first guest" product derived from the numerical prediction model.
 - Equations and parametrizations of the model assure the atmospheric dynamic consistency;
 - Observations keep the model close to the real conditions compensating the deviations associated with the model physics.
- Most relevant parameters in the assimilation schemes:
 - Influence radius - R;
 - Time window - T;
 - Nudging coefficient - G.



Development of the new offshore wind Atlas: Model calibration - Step I

- *Methodology*
- *Data*
- *MMS model configuration*
- *Results*

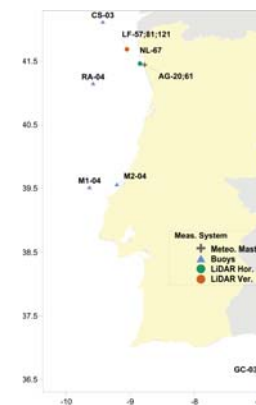


- **Numerical Mesoscale Model** → Fifth-generation Mesoscale Model - MMS5.
- **Evaluation Toolbox** → developed to compute the common statistics metrics (e.g., RMSE, bias, Pearson correlation, Weibull distribution parameters, etc.).
- The model calibration is performed through sensitivity tests using the common statistics metrics and hourly simulated/observational data.

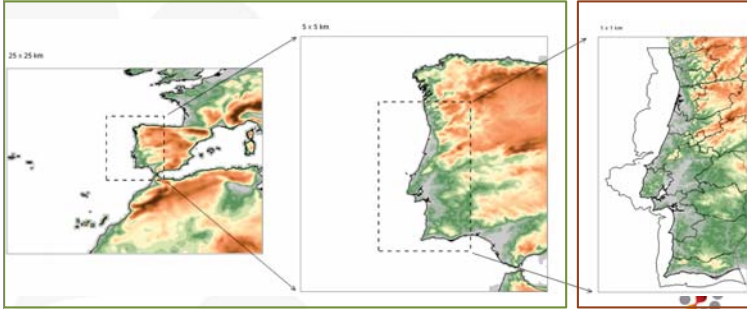


Data – Calibration step

- Observed data used during the calibration step:
 - LNEG database (e.g., FP7 NORSEWind and DEMOWFloat);
 - Buoys publicly available (Instituto Hidrográfico, Puertos del Estado).
- Assimilation data:
 - Satellite → *Global blended ocean wind – scatterometer and radiometer* combined with *ECMWF forecasts*.
- Calibration period:
 - **Summer:** 01-08-2014 a 01-09-2014
 - **Winter:** 29-12-2014 a 29-01-2015

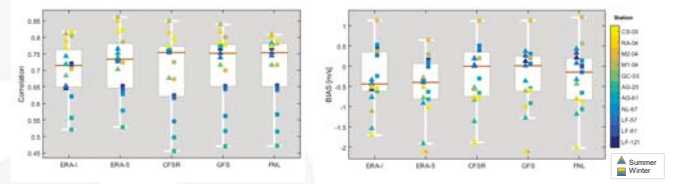


- 3 domains using a one-way nesting technique.
- Spatial resolution : 25x25km, 5x5km e 1x1km (until 300 m bathymetric).
- Simulations were configured i) to restart every day, i.e., runs continuously only 24 hours, and ii) for recording data every hour.

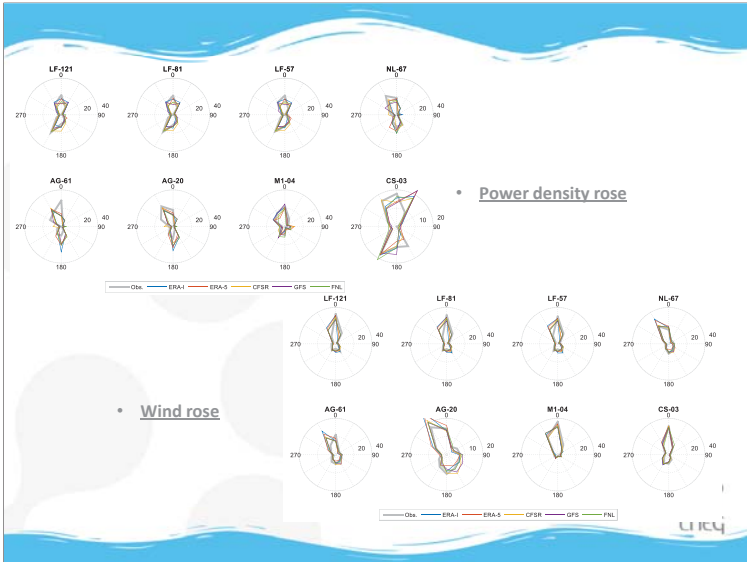


- I.A - Identification of the most adequate meteorological initial and boundary conditions

> 5 products were tested: FNL, ERA-Interim, CFSR, GFS e ERA-5.

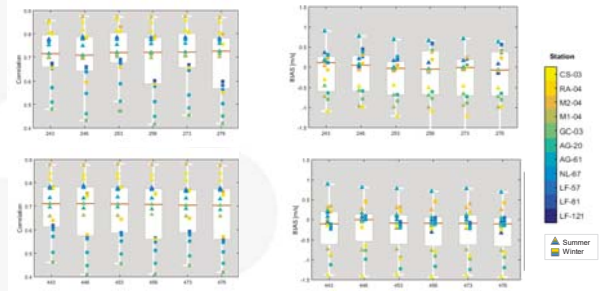


- Overall, the recent ERA-5 (ECMWF) product presents the best performance in the statistical parameters analysed.



- I.B - Identification of the most adequate physical parameterizations:

> 27 different set of parameterizations were tested: Microphysics - IMPHYS (3), PBL - IBLTYP (3), and cumulus- IUCUPA (3).

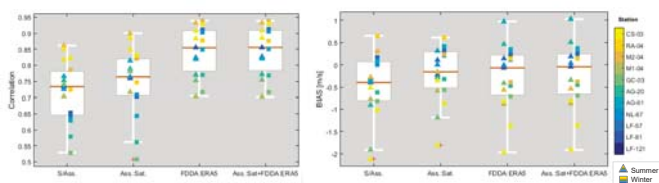


- The sensitivity tests for the atmospheric parameterization showed small differences among the different options tested.

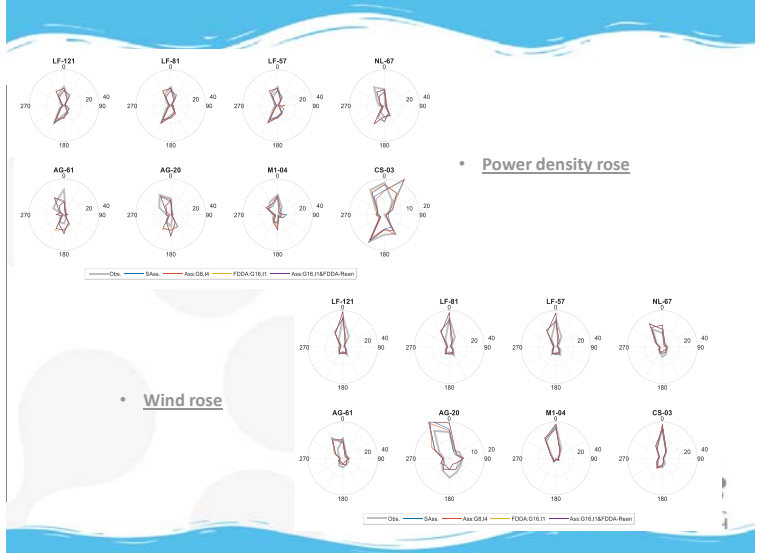


- I.C - Identification of the most adequate assimilation scheme and data:

> Several sensitivity tests (e.g., nudging, obs-FDDA) were implemented to identify the most adequate assimilation scheme, parameters (G, T and R) and dataset.

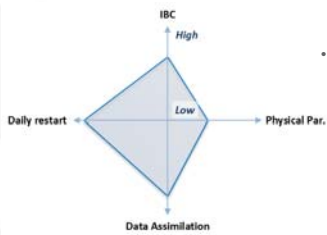


- Using the four-dimensional data assimilation (FDDA) scheme significant improvements were found.
- Best performance was achieved with the data assimilation based on information inferred by satellite in the ocean coupled with data from ECMWF reanalysis ERA-5 project.



• Wind rose

- More than 100 sensitivity tests were performed using the MMS model.



- The highest improvements in the calibration results were associate to:

- > Daily restart of the model → prevents the errors propagations during the simulations;
- > Data assimilation schemes.

- Based on the previous findings → long term simulations were performed to obtain the new offshore wind Atlas for Portugal with a spatial resolution of 1km:
 - > Simulated period : 01.01.2015 – 31.06.2018



New offshore wind Atlas: Atlas Validation - Step II

- Data
- Results: validation performance and the new offshore wind Atlas



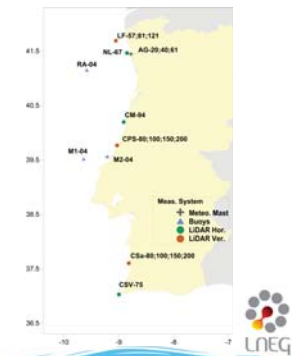
Data – Validation step

- Short-term experimental measurement campaigns took place to validate the new offshore wind Atlas.
- These campaigns were based on Light Detection and Ranging (LiDAR) systems:

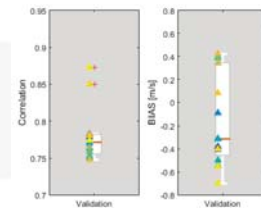
> Horizontal LiDAR system:



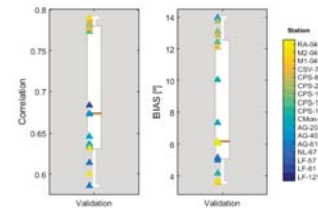
> Vertical Lidar system:



> Wind speed results



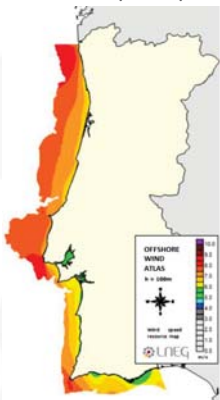
> Wind direction results



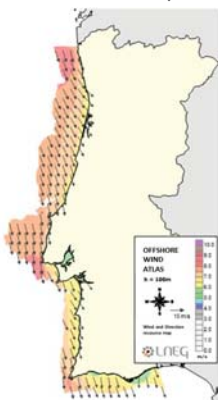
- The average bias error is only -0.14 m/s, while the median value is -0.29 m/s.
 - > Errors showed non-dependency from the measurement height → stratification of the atmosphere was correctly simulated;
- Average wind speed correlation is 0.79, although some measurement points show a correlation of nearly 0.90.
- Average wind direction bias error is always above 15°. For some stations, the correlation is only 0.6.



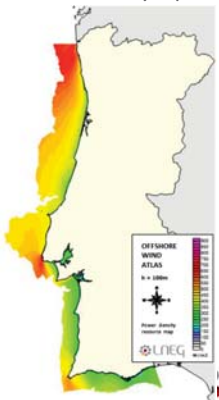
> Wind speed map



> Wind direction map



> Power density map



Final remarks



- This paper presents the calibration procedures and the new offshore wind Atlas for Portugal with a spatial resolution of 1x1km to adequately describe the wind phenomena over the sea and in the cross-border sea/land areas.
- Given the impracticability of studying, in detail, the Portuguese offshore wind potential using experimental data, the only viable way is through numerical mesoscale simulations.
- To overcome uncertainty associated with the use of numerical mesoscale, several sensitivity tests were performed.
- Results show that the calibration procedure is a crucial step to improve the wind speed and direction characterization. The most meaningful improvement was associated with the data assimilation procedure with the observational four-dimensional data assimilation – FDDA, followed by the IBC dataset used.
- On average, the new Atlas shows a bias error equal to -0.14 m/s, and a correlation of 0.79.



- This validated Atlas will support the identification of adequate areas for offshore wind park deployment and allowing to improve the spatial planning of marine energy sources for the maritime area of Continental Portugal.
- Although further research is required to enable its full validation, the adoption of assimilation procedures coupled with the state of art of meteorological IBC presents a promising improvement in the accuracy of the wind resource assessment, especially, at regions where observed wind data are not available.



LNEG
Laboratório Nacional de Energia e Geologia, I. P.

www.lneg.pt

Acknowledgements

This work was co-financed by the Operational Program for Sustainability and Efficiency in the Use of Resources (POSEUR) through Portugal 2020 and the Cohesion Fund (OffshorePlan Project - POEUR - 01-1001-FC-000007) and supported by the FP7 Norsewind (Grant number: 219048) and DEMOWFloat (Grant number: 296050) projects.

Contacts:

antonio.couto@lneg.pt
teresa.simoas@lneg.pt
ana.estanqueiro@lneg.pt





The DeRisk design database: extreme waves for Offshore Wind Turbines

Fabio Pierella, Ole Lindberg, Henrik Bredmose, Harry Bingham, Robert Read



DTU Wind Energy
Department of Wind Energy



About me

Glaciar Perito Moreno (Argentina 2019)

- Mechanical Engineer Uni. Ancona (IT, 2007)
- PhD in wind turbine aerodynamics from NTNU (NO, 2014)
- Working with waves ever since
 - IFE (NO, 2014 – 2017)
 - DTU (DK, 2018 –)



2 DTU Wind Energy, Technical University of Denmark

The DeRisk design database 1/25/2019

Extreme loads from large waves: a possible design driver



- Turbines and monopiles size increases
- Waves and loads are "Extreme" in probabilistic terms
- Stochasticity needs to be handled together with nonlinearity of the waves

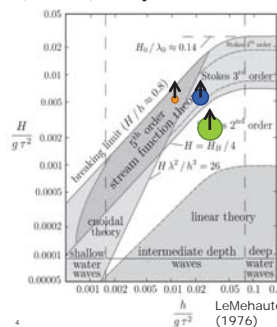


www.derisk.dk

3 DTU Wind Energy, Technical University of Denmark

The DeRisk design database 1/25/2019

Sea states: what does an Offshore Wind Turbine (OWT) experience?



At $h = 22$ [m] depth

- Operational
 - $H_S = 1$ [m]; $T_p = 6$ [s]
- - $H_S = 6$ [m]; $T_p = 9.5$ [s]
- ULS
 - $H_S = 9.5$ [m]; $T_p = 12$ [s]
- - $1.86 \times H_S$

4 DTU Wind Energy, Technical University of Denmark

The DeRisk design database 1/25/2019

Standard IEC61400-3 annex D: extreme waves for design



- D.7.1: Explicit approach
 - Many realizations of fully nonlinear waves
- D.7.2 Wave non-linearity factor approach
- D.7.3 Regular wave approach

Our Approach

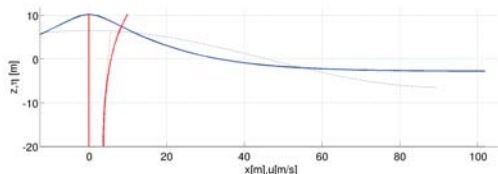
- D.7.4 Constrained wave approach
 - Embed a regular nonlinear wave in irregular, linear waves
 - "Stream Function Embedment"

Common Industry Practice

5 DTU Wind Energy, Technical University of Denmark

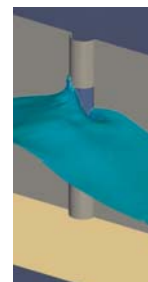
The DeRisk design database 1/25/2019

Embedment of Stream Function waves: limitations



- Fully nonlinear
- Easily computed (e.g. Fenton 1988)
- Can be embedded into background state

- 2D Flat bed theory
- Periodic
- Wave transformation, transient group nature, current, 3D effects?

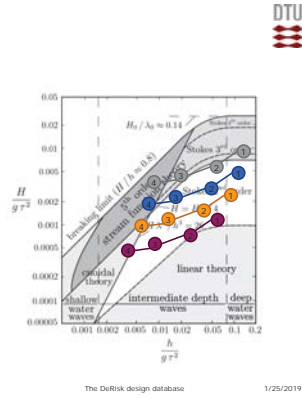


6 DTU Wind Energy, Technical University of Denmark

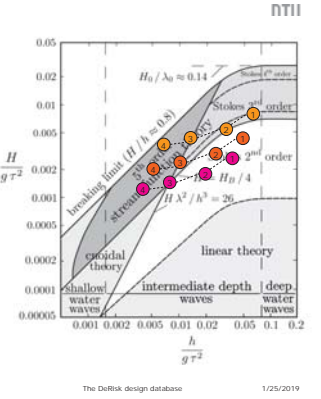
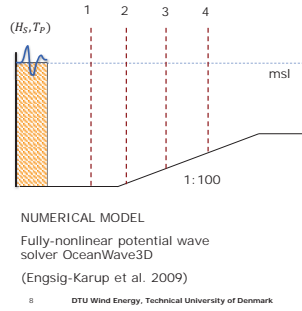
The DeRisk design database 1/25/2019

Nonlinearity + Stochasticity: the DeRisk database

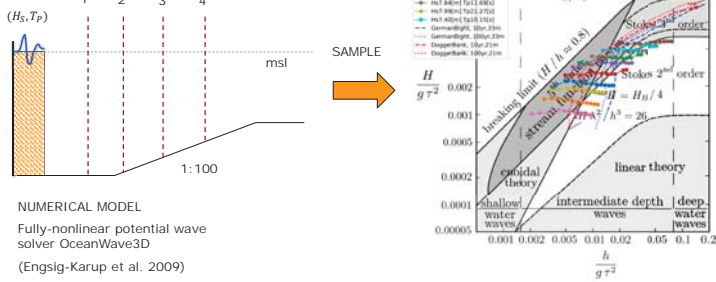
- Fundamental idea:
 - Make a pre-computed database of fully-nonlinear extreme waves
 - Span the nondimensional space (H, T_p, h)
- Make it publicly available
- Users pick suitable nonlinear kinematics
- Perform aeroelastic computations (e.g. HAWC2) by using the nonlinear input waves



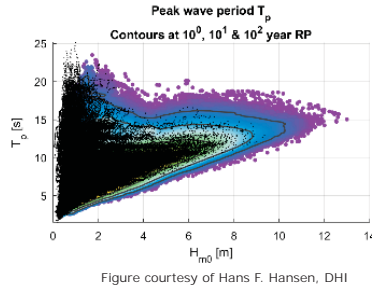
The DeRisk database



The DeRisk database

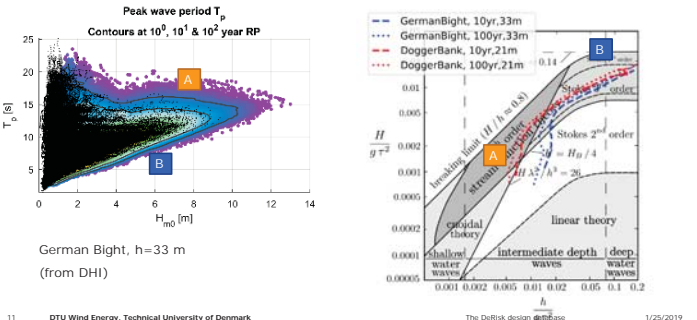


How to use the database: Distribution of H_S and T_p



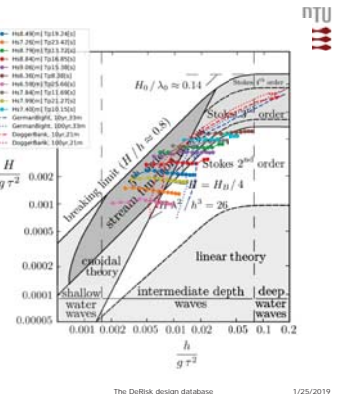
German Bight
h=33 m

How to use the database : Contour plots vs LeMehaute plot



How to use the database Contour plots

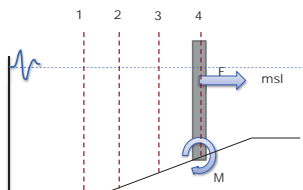
- Pick a realization from the database
- Stochasticity
 - many 1-hr and 3-hr runs ("random seeds") for each combination of (H_S, T_p)
 - Kinematics sampled at many depths $[h = 20m \div 60m]$



How to use the database : Calculating the loads



- Use the kinematics to calculate loads on a foundation
- Choose a suitable slender body force model
 - Morison (1950)
 - Rainey (1995)
 - Kristiansen and Faltinsen (2017)

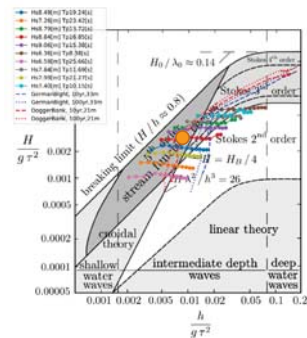


How to use the database : Load on a monopile

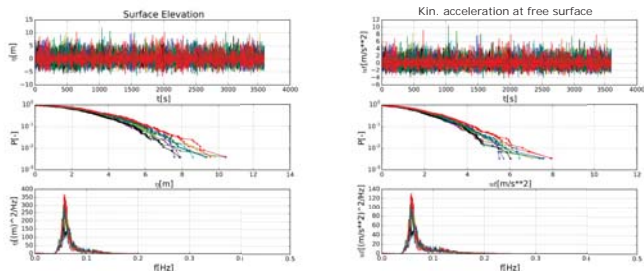


- We use a hypothetical monopile at German Bight
 - $D = 7 [m]$
 - $C_M = 2 C_D = 0.7$ (DNV-RP-205, 2007)
 - Stiff monopile
 - Rainey force model (Rainey 1995)

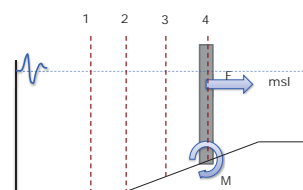
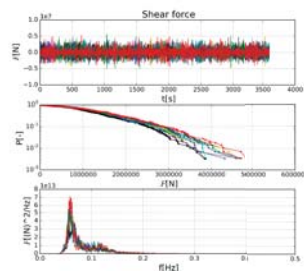
- We got lucky!
We have a simulation which has kinematics sampled at $h=30 [m]$ and which corresponds to a 100-yr storm
 - $H_s = 8.84 [m]$
 - $T_p = 16.85 [s]$



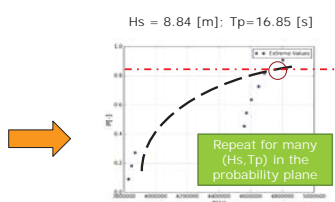
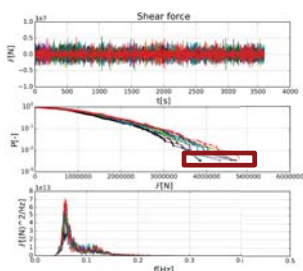
How to use the database : wave elevation and acceleration at free surface



How to use the database : Example of extreme value computation



How to use the database : Example of extreme value computation



Fit an extreme distribution (Gumbel, GEV...) to the non-exceedance probability and estimate confidence level for extreme value

How to extend the database : Froude scaling

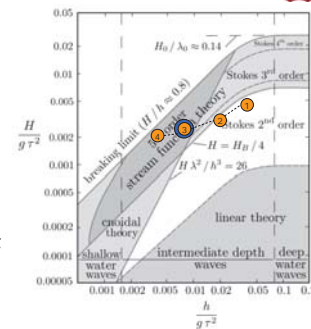


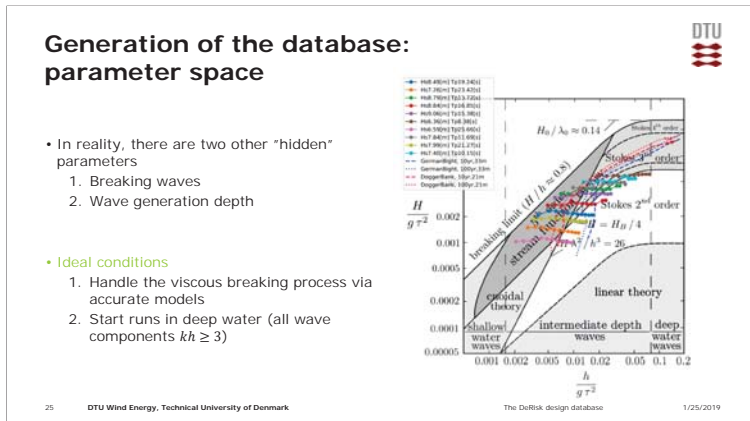
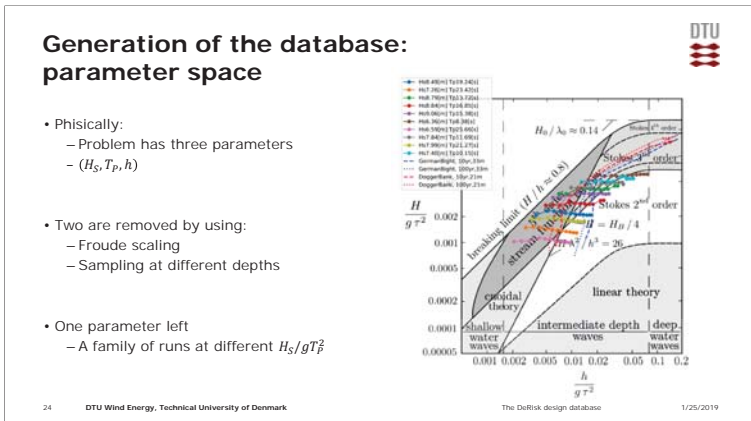
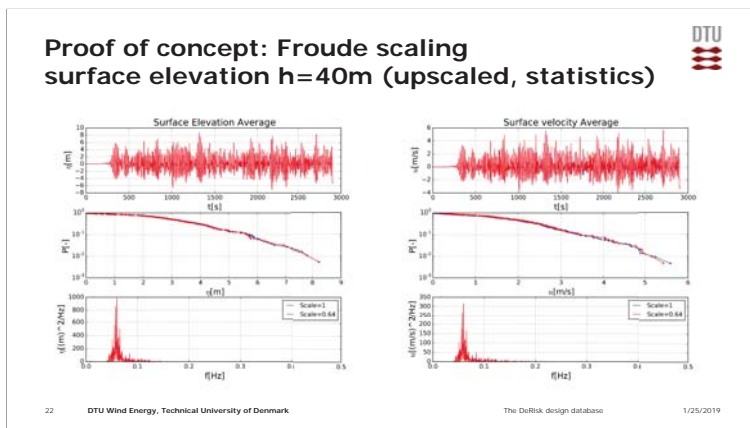
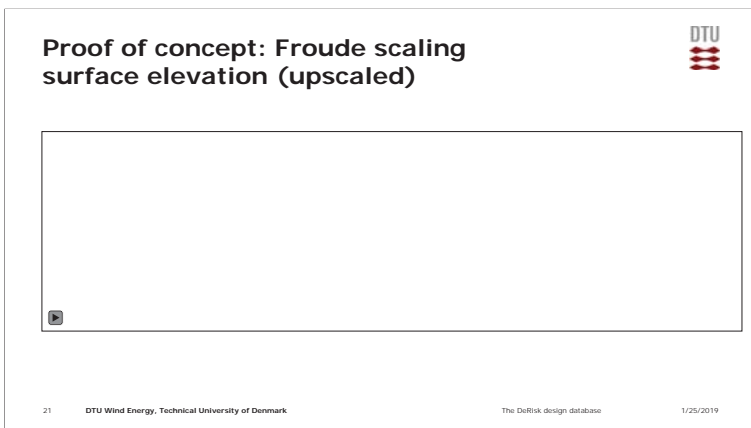
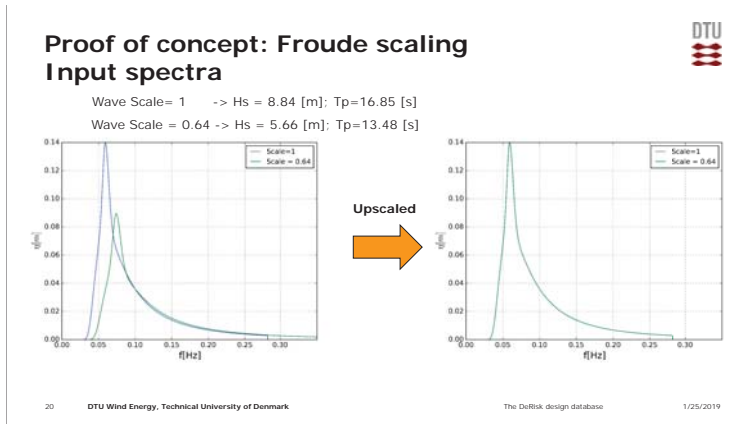
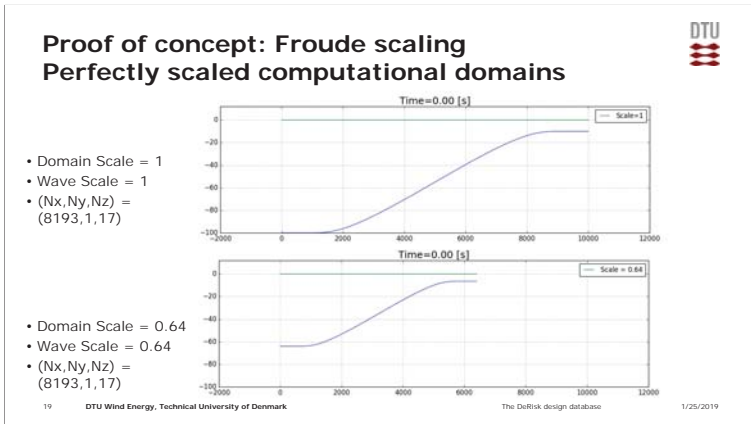
- Waves are kinematically similar if they have the same Froude Number

$$Fr = \frac{L}{gT^2}$$

- "Real life" wind farm
 - $(H_s, T_p, h) = (6[m], 10[s], 25[m])$
 - Point 3 in database
 - $(H_s^{DB}, T_p^{DB}, h^{DB}) = (9.37[m], 12.5[s], 39.1[m])$

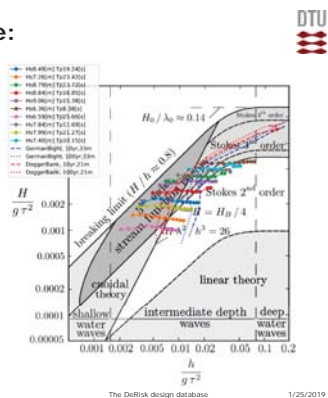
$$Fr = \frac{L}{gT^2} = Fr^{DB} \Rightarrow \lambda = \frac{h}{h^{DB}} = 0.64 \Rightarrow \begin{cases} u = u^{DB} \sqrt{0.64} \\ a = a^{DB} \end{cases}$$





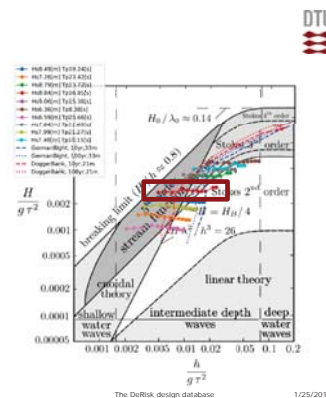
Generation of the database: parameter space

- In reality, there are two other "hidden" parameters
 - Breaking waves
 - Wave generation depth
- Current study
 - Simplified breaking model: energy subtracted when the surface particle acceleration overcomes threshold value (Engsig-Karup et al. 2009)
 - Choose the starting points carefully



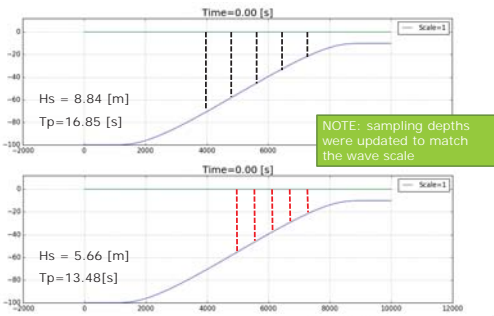
Wave generation depth: "law of the short blanket"

- Generation depth: 100 [m]
 - $kh = 3 \rightarrow k = 0.03$
 - $\lambda = 210 [m] \rightarrow T = 11 [s] \rightarrow 0.091 [Hz]$
- Part of the spectrum is not in deepwater
- To generate all waves in deep water:
 - Very short waves -> high grid resolution
 - Very long waves -> make the domain deeper (longer slope)
- What consequences does it have?
 - Statistically speaking

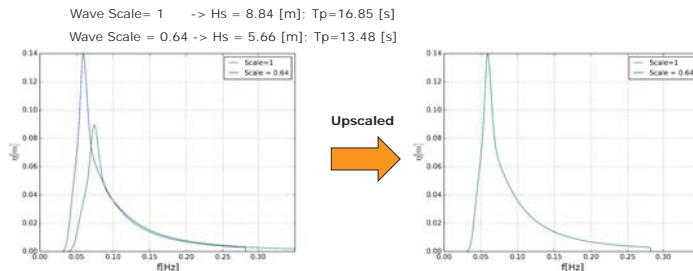


Generation of the database: wave generation depth

- Domain Scale = 1
 - Wave Scale = 1
-
- Domain Scale = 1
 - Wave Scale = 0.64

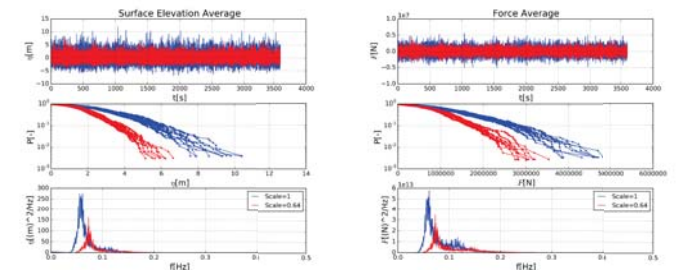


Generation of the database: wave generation depth



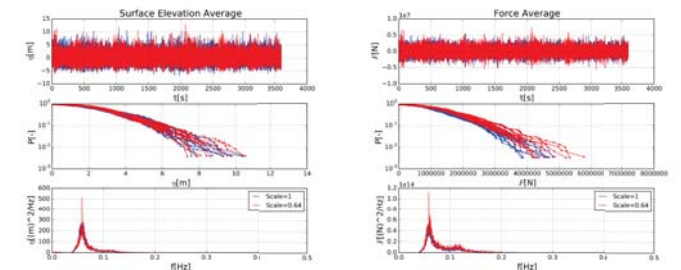
Froude Scaling of database: unscaled results

Hs = 8.84 [m]
Tp = 16.85 [s]
h = 30[m]



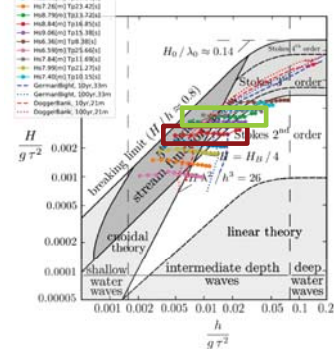
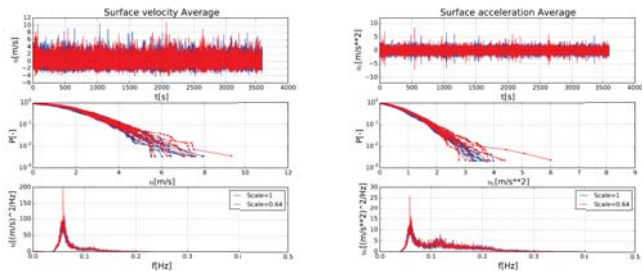
Froude Scaling of database: scaled results

Hs = 8.84 [m]
Tp = 16.85 [s]
h = 30[m]



Froude Scaling of database: scaled results

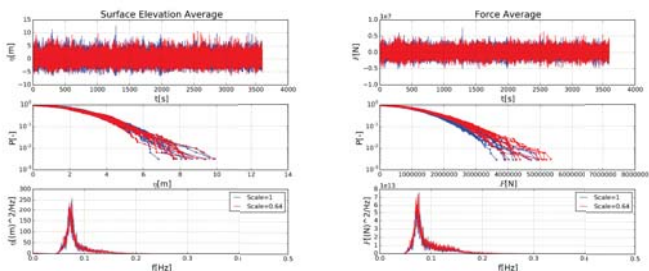
DTU
 Hs = 8.84 [m]
 Tp = 16.85 [s]
 h = 30[m]



Hs = 8.79 [m]
 Tp = 13.72 [s]
 h = 30[m]
 Hs = 8.84 [m]
 Tp = 16.85 [s]
 h = 30[m]

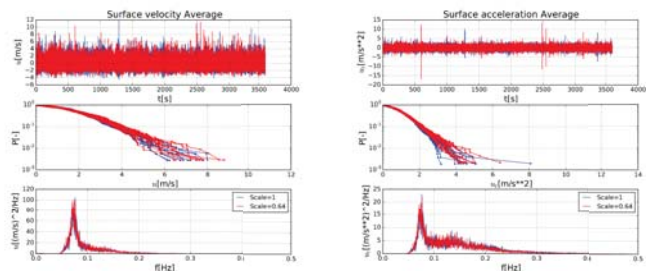
Froude Scaling of database: scaled results

DTU
 Hs = 8.79 [m]
 Tp = 13.72 [s]
 h = 30[m]



Froude Scaling of database: scaled results

DTU
 Hs = 8.79 [m]
 Tp = 13.72 [s]
 h = 30[m]



Conclusions

- The DeRisk database gives a practical way of calculating extreme loads on offshore wind turbines
 - Handles stochasticity and nonlinearity
- The validity of the database can be extended via Froude scaling
 - We verified Froude scaling is respected
- Identified limitations relative to the simplified parameter space
 - Offshore boundary condition must respect sufficiently high kh



DeRisk
 De-risked extreme wave loads for offshore wind energy
www.derisk.dk

D1) Operations & maintenance

Evaluation and Mitigation of Offshore HVDC Valve Hall Magnetic and Electric Field Impact on Inspection Quadcopter, M. Heggo, University of Manchester

Piezoelectric Patch Transducers: Can alternative sensors enhance bearing failure prediction?
L. Schilling, Hamburg University

Excluding context by means of fingerprint for wind turbine condition monitoring,
K. López de Calle, IK4-TEKNIKER

Condition monitoring by use of time domain monitoring and pattern recognition, Aasmund Barikmo, VibSim

HOME Offshore | EPSRC | MANCHESTER 1824

Evaluation and Mitigation of Offshore HVDC Valve Hall Magnetic and Electric Field Impact on Inspection Quadcopter

Dr Simon Watson - WP2.2 lead
Dr Mohammad Heggo - PDRA
Miss Elisabeth Welburn - Ph.D. student

1

1

HOME Offshore | EPSRC | MANCHESTER 1824

Agenda

- Valve Halls in HVDC System.
- Development in Thyristor Technology.
- An Inspection UAV for Valve Hall Monitoring.
- High Electromagnetic Field Risks Inside Valve Hall.
- High Electrostatic Field inside Valve Hall .
- Drone Electrostatic Field Testing.
- High Magnetic Field inside Valve Hall.
- Drone Magnetic Field Testing.

2

2

HOME Offshore | EPSRC | MANCHESTER 1824

Valve Halls in HVDC System

Valve hall length = 16.5 m
Valve tower height = 6.6 m
Distance between valve towers = 4.5 m
An HVDC valve tower 16.8 m tall in a hall at Baltic Cable AB in Sweden
Thyristor Module

3

3

HOME Offshore | EPSRC | MANCHESTER 1824

An Inspection UAV for Valve Hall Monitoring

- We propose an off-shelf drone in which we have integrated number of sensors for indoor monitoring inside the valve hall.

Dual Camera
FLIR DUO R
Allows visible light and thermal images at the same time

Proposed Drone

LiDAR
2D mapping and navigation in GPS denied environment

4

4

HOME Offshore | EPSRC | MANCHESTER 1824

An Inspection UAV for Valve Hall Monitoring (Architecture)

Sensors
Motor
Flight Control
Communications
Storage

Throttle (up/down)
Pitch (Forward/backward)
Roll (Left/Right)
YAW

Is there a problem in navigating a drone inside a valve hall?
How can we guarantee normal operation of the drone in a valve hall?

5

5

HOME Offshore | EPSRC | MANCHESTER 1824

High Electromagnetic Field Risks Inside Valve Hall

Electromagnetic Field Risks

- Electrostatic Field Risks
 - Corona Discharge
 - Air Breakdown
- Magnetic Field Risks
 - Eddy Current Induction
 - Motor Demagnetization
 - Sensor Readings

6

6

HOME Offshore | EPSRC | MANCHESTER 1824

High Electrostatic Field inside Valve Hall (Risks)

- High voltages inside the valve hall creates high electrostatic field which implies two main risks:
 - Corona Discharge current from a stack to the drone.
 - ~ 2000V/mm
 - Air Breakdown or Flashover between 2 stacks.
 - ~ 3000V/mm

Electrostatic risks inside a valve hall

7

7

HOME Offshore | EPSRC | MANCHESTER 1824

High Electrostatic Field inside Valve Hall (Evaluation)

Model of typical double valve used in the high voltage valve hall of 250kV HVDC converter station?

Calculation results of double valve (a) potential distribution (b) the whole E-field distribution (c) E-field distribution on shielding screens (d) E-field distribution on shielding rings?

8

8

HOME Offshore | EPSRC | MANCHESTER 1824

High Electrostatic Field inside Valve Hall (Evaluation)

- As shown in previous figure, the electric field in the normal conditions can reach to 1027 V/mm.
- Q1:** What happens if the electric field exceeds these values in case of faulty conditions? Could our drone help investigating these critical cases?
- Q2:** Can the drone sustain normal operation in high electric field values in the range from 1000 V/mm to 2000 V/mm?

9

9

HOME Offshore | EPSRC | MANCHESTER 1824

Drone Electrostatic Field Testing (Exp. (1) Corona Discharge Risk)

Exp. (1) setup for testing corona discharge current effect

- Aim:** Finding the effect of the corona discharge current on the drone.
- The drone is inserted, and 100 kV voltage is applied with increasing step of 20 kV.
- Obs.:** The motors of the drone stopped working after 200 kV and do not return back to normal operation until the drone is manually restarted.

10

10

HOME Offshore | EPSRC | MANCHESTER 1824

Fig 10: Flight Control Error Signal

This exceeds the normal current of unarmed motor

11

11

HOME Offshore | EPSRC | MANCHESTER 1824

Drone Electrostatic Field Simulations (Corona Discharge Risk)

Electrostatic field distribution on the drone for (a) Autopilot Section, and (b) Actuation Section


12

12

HOME Offshore **EP SRC** **MANCHESTER 1824**
Pioneering research and skills. The University of Manchester

Drone Electrostatic Field Testing (Exp. (1) Conc.)

- The corona discharge current can affect different drone modules like communication module and motor controller module.
- For a drone to avoid interference from corona discharge current, it should be shielded.
- However, this raises another question: **Could this shielding cause any flashover?**

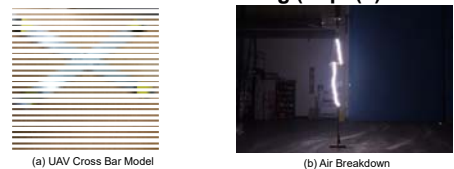


Drone Model (a) Unshielded (b) Shielded

13

HOME Offshore **EP SRC** **MANCHESTER 1824**
Pioneering research and skills. The University of Manchester

Drone Electrostatic Field Testing (Exp. (2) Flashover Risk)



(a) UAV Cross Bar Model (b) Air Breakdown

Tethered UAV model between HV end and the ground

- Aim:** Find the effect of navigating a shielded drone inside a valve hall on changing air breakdown characteristics regarding clearance distances.
- A complete metal cross bar (UAV model) was tethered between HV end (i.e. ~ 1.1 MV) and the ground.
- Obs.:** The breakdown voltage is decreased by 5 % only in the case of negative impulse test and no change at all in the case of positive impulse test.

14

HOME Offshore **EP SRC** **MANCHESTER 1824**
Pioneering research and skills. The University of Manchester

Drone Electrostatic Field Testing (Conclusions)

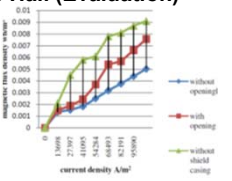
- Navigation of an inspection drone inside the high electrostatic field of HVDC valve halls can cause corona discharge current interference to different drone parts.
- A complete shielding solution is recommended to avoid corona discharge current interference.
- The shielding solution has a limited effect on changing air breakdown clearances inside the valve hall.

15

HOME Offshore **EP SRC** **MANCHESTER 1824**
Pioneering research and skills. The University of Manchester

High Magnetic Field inside Valve Hall (Evaluation)

- The thyristor inside valve hall is rated for high currents (> 4000 A), which induce high magnetic field.
- In [9], the magnetic field is reported for a valve equipped with 182.5 cm² thyristor for a current range between 0 A and 4000 A.
- Shielding of valves can decrease the magnetic field from 9 mT to 5 mT, which still can affect the drone navigation.

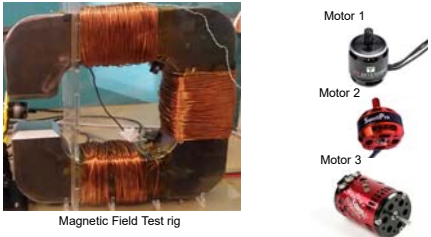


Flux densities at different current densities and different shielding mechanisms^[9]

16

HOME Offshore **EP SRC** **MANCHESTER 1824**
Pioneering research and skills. The University of Manchester

Drone Magnetic Field Testing (Setup)



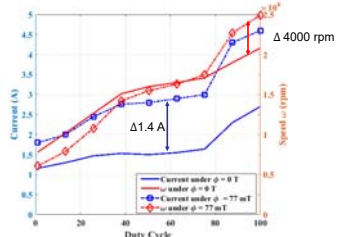
Magnetic Field Test rig

Motor 1
Motor 2
Motor 3

17

HOME Offshore **EP SRC** **MANCHESTER 1824**
Pioneering research and skills. The University of Manchester

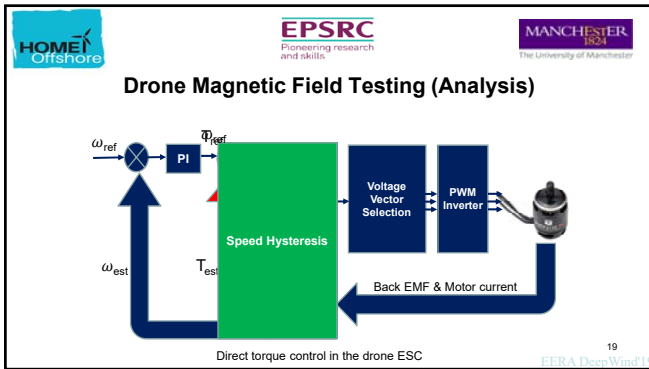
Drone Magnetic Field Testing (Results)



Motor Current and speed in presence/absence of magnetic field

Δ 1.4 A
Δ 4000 rpm

18



19

-
- Drone Magnetic Field Testing (Conclusion)**
- Valve hall magnetic field can influence nominal operation of the drone motors, which are controlled using off-shelf speed controllers.
 - Current speed controllers use torque control algorithm to operate drone motors, which is proved to be inefficient in the presence of high magnetic field.
 - Special design for speed controllers is recommended, which uses the velocity control algorithm to operate the drone motors.

20

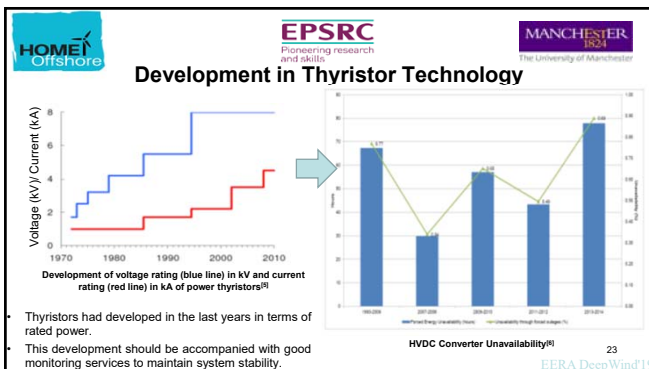
References

1. P. Doobey, "High Voltage Direct Current Transmission" <https://www.slideshare.net/PoojaDubey10/hvdc-transmission-its-applications>, November 2014.
2. <https://www.siemens.com/press/en/pressrelease/?press=en/pressrelease/2016/energymanagement/pr2016020137emen.htm>
3. ABB, "Baltic Cable AB", http://new.abb.com/docs/librariesprovider/114/events/presentations/hvdc-users-conference/baltic-cable-presentation-marjetamn-%C3%A5iland_20170509.pdf?sfvrsn=5d82b512_2_May2017.
4. Siemens Press, "HVDC Classic" <https://www.energy.siemens.com/us/en/power-transmission/hvdc/hvdc-classic.htm#content-Components>.
5. H. Huang, M. Uder, R. Barthelemess, J. Dom, "Application of high power thyristors in HVDC and FACTS systems", in Proc. 17th Conference of the Electric Power Supply Industry, October 2008, Macau, China.
6. M.S.Knight, "Calculating Target Availability Figures for HVDC Interconnectors." ofgem, York, UK (2016).
7. J. Wang, H. Wu, Z. Deng, Z. Peng and J. Liao, "E-field distribution analysis on three types of converter double valve in 800 kV valve hall", in Proc. IEEE 11th Int'l. Conf. Properties and Applications of Dielectric Materials (ICPADM), Sydney, NSW, Australia, pp. 692-695, July 2015.
8. C.L.Hart, K.J.Nixon, and I.R.Jandrell, "The effect of a floating conductor on the breakdown strength of a DC gap at both polarities", in Proc. IEEE Power Engineering Society Conference and Exposition in Africa (PowerAfrica), pp. 1-5, July 2012, Johannesburg, South Africa.
9. M. S. Kher, S. Bindu, "Electromagnetic modelling of three phase UHVDC valve casing", in Proc. IEEE Annual India Cogfeyence (INDICON), pp. 1-4, December 2013, Mumbai, India.

21



22



23




24

HOME Offshore **EPSRC** **MANCHESTER 1824**
Pioneering research and skills The University of Manchester

Drone Magnetic Field Testing (Future Work)

- Implementation & testing of velocity control algorithm to mitigate high magnetic field impact, using evaluation boards of programmable speed controllers.



Texas Instruments evaluation board DRV8303EVM

25 EPRA DeepWater

25

HOME Offshore **EPSRC** **MANCHESTER 1824**
Pioneering research and skills The University of Manchester

Drone Navigation in HVDC substations

- Development of autonomous navigation techniques that are viable in a dark, GPS-denied and confined environment.
- Development of computationally efficient fault identification algorithms using on-board sensors.
- Cooperation with industrial partners for field tests in real-world operational substation

26 EPRA DeepWater

26

HAW HAMBURG | CC4E

Piezoelectric Patch Transducers: Can alternative sensors enhance bearing failure prediction?

L. Schilling and P. Dalhoff 17.01.2019

Who are we?

HAW HAMBURG | CC4E

- University of Applied Sciences Hamburg
- Competence Center for Renewable Energy and Energy Efficiency
 - 70 associates working in 30 different renewable energy projects
 - Topics:
 - Wind energy, energy storage, digitalization, sector coupling, acceptance and sustainability, and systems integration

cms@wind

- Condition monitoring company based in Hamburg
- Development of condition monitoring hardware

Motivation for the project

A GROWTH IN CAPACITY

Correlation between turbine and gear growth

- ⇒ Increase of stiffness and damping
- ⇒ Incipient faults get more intricate to retrieve

Transfer of larger torque

Adaption of gear design and concept

Growth of height and capacity

HAW HAMBURG | CC4E

Fundamental idea – changing the measurement position for planetary bearings

planet wheel, planetary bearing, sun wheel, ring gear, planet carrier, state-of-the-art accelerometer, damage and signal transmission, piezoelectric patch transducer with radio module, receiver module

HAW HAMBURG | CC4E

Test object, competitor and matters of interest

Piezoelectric patch transducer

Questions concerning the applicability of patch transducers as condition monitoring sensors for the drive train:

- Temperature stability?
- Sensitivity toward electromagnetic interference?
- Ability to detect bearing faults?

Accelerometer

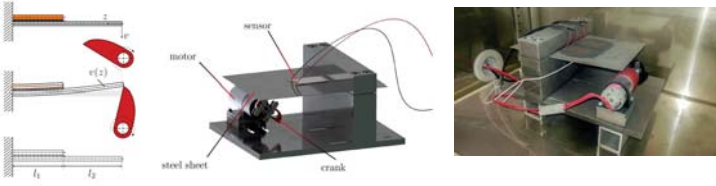
HAW HAMBURG | CC4E

Experimental setup – frame conditions

- Temperature range: -40 °C...+80 °C
- Frequencies: < 12 kHz
- Magnetic field strengths: 0.1 $\frac{kA}{m}$...6.0 $\frac{kA}{m}$
- Rotational speeds: 0 rpm...1500 rpm
- Bearing damages: Inner ring, outer ring, rolling body, wear and combinations

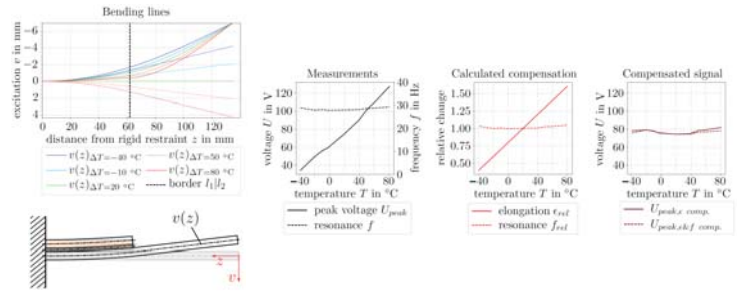
HAW HAMBURG | CC4E

Temperature tests – experimental setup



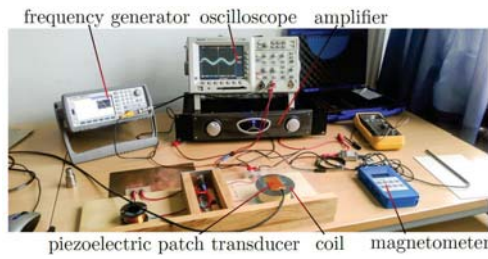
7

Temperature tests - results



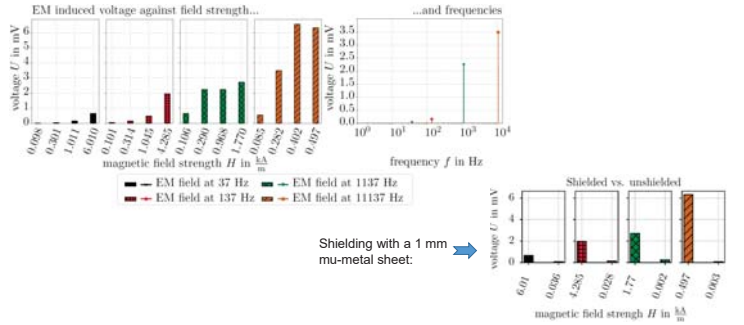
8

Electromagnetic interference test – experimental setup



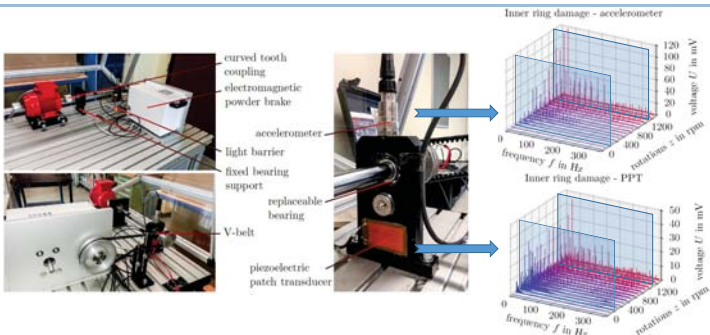
9

Electromagnetic interference test – results



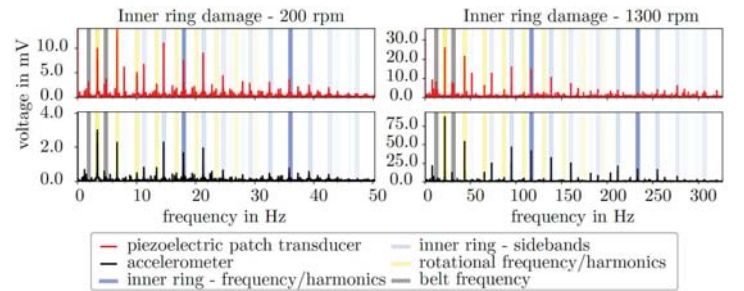
10

Damage detection – experimental setup and run-up plot




11


Damage detection – inner ring damage




12

Summary


- 


Temperature stability is given in the tested range of -40 °C to +80 °C → Sensor produces similar signals at all tested temperatures
- 

Sensitivity toward electromagnetic interference is present, though the induced signal voltage is small compared to the damage frequency peaks → Shielding is yet recommended to fully eliminate any unwanted interference
- 

Damages can be identified in the piezoelectric patch transducer's signal → The sensor shows strong signals at low rotational speed, but is exceeded by the accelerometer's signal voltage and depth at high rotational speed

Conclusion and outlook

- 

Application of the piezoelectric patch transducer for a wind turbine's drive train is possible and might be a welcome alternative to accelerometers in the future
- 

→ Further optimization of the sensor is necessary to make it competitive
 → Integration into the gear may improve its competitiveness, due to the reduced signal path from damage to sensor

This research was funded by  

Thank you for your attention!

Levin Schilling, M.Sc.
 Research Associate
 T +49 40 428 75 8743
levin.schilling@haw-hamburg.de

HAMBURG UNIVERSITY OF APPLIED SCIENCES (HAW HAMBURG)
 Faculty of Engineering & Computer Science
 Department Mechanical Engineering & Production
 Berliner Tor 21 / 20099 Hamburg
haw-hamburg.de



 | CC4E

15


IK4 TEKNIKER © IK4 TEKNIKER 2018

Excluding context by means of fingerprint for wind turbine monitoring

K López de Calle^{1,2}, S Ferreiro¹, C Roldán¹, E Konde¹ and B Sierra²

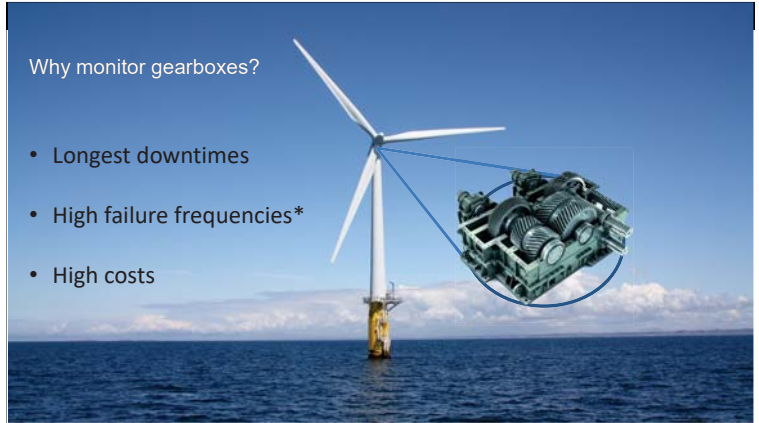
Kerman López de Calle Etxabe| Trondheim, 17th January 2019

IK4 TEKNIKER Research Alliance




Why monitor gearboxes?

- Longest downtimes
- High failure frequencies*
- High costs



Typical sensors for gearboxes



Our research


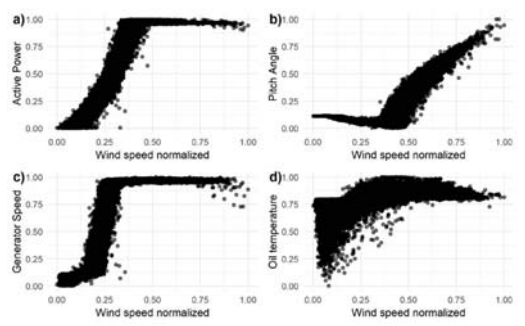


Table 1. Variables available in the dataset by data source.

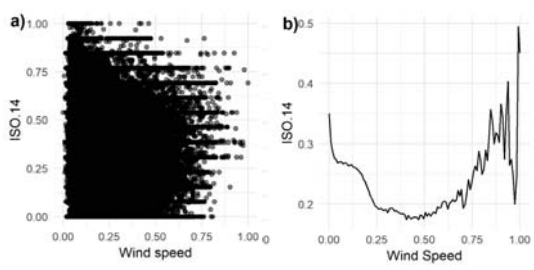
Source	Variable
SCADA	Pitch angle
	Gearbox Temperature
	Wind speed
	Generator speed
Oil-debris sensor	ISO 4
	ISO 6
	ISO 14
	BUBBLES

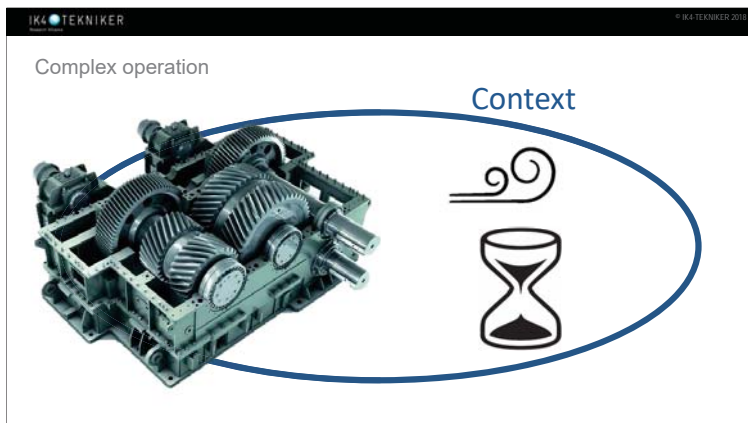
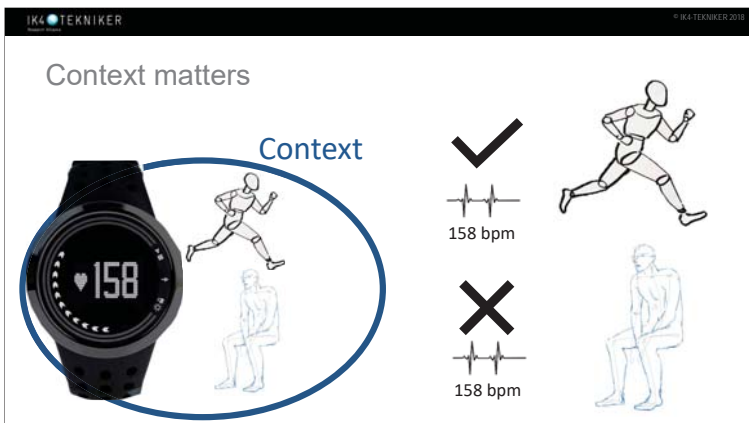
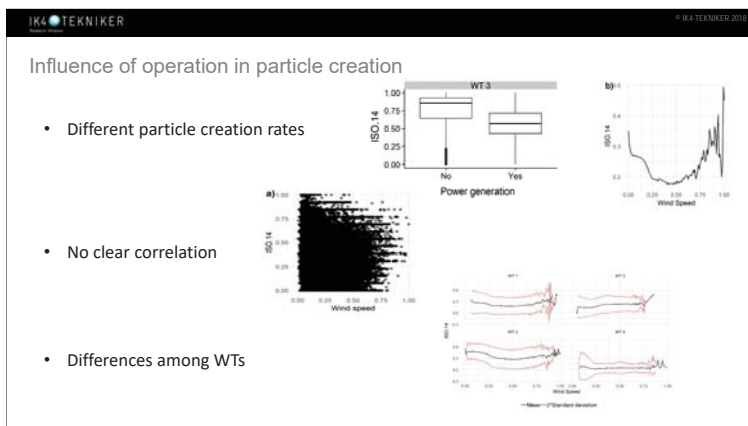
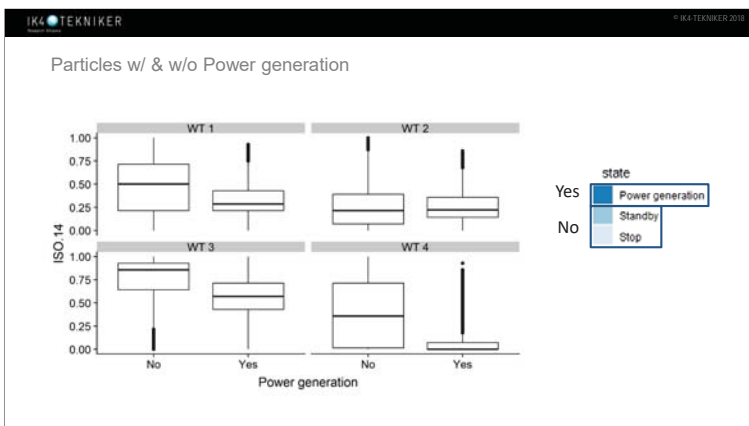
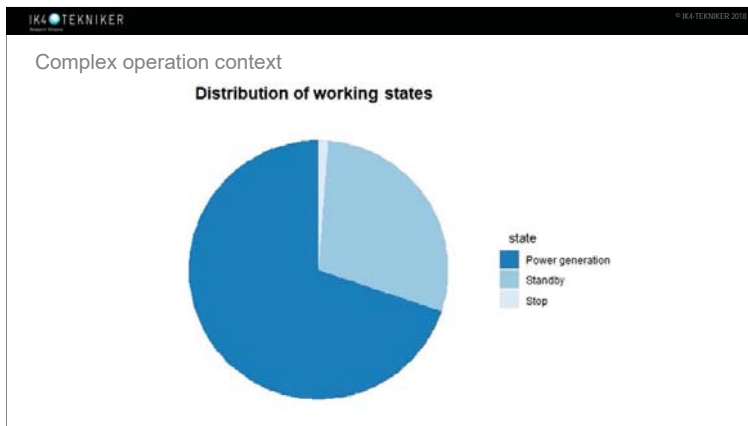
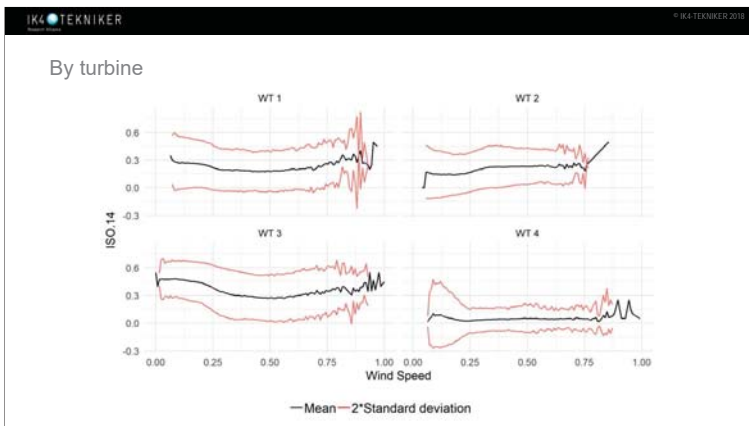
June – January ~ 6 months
T = 1 minute

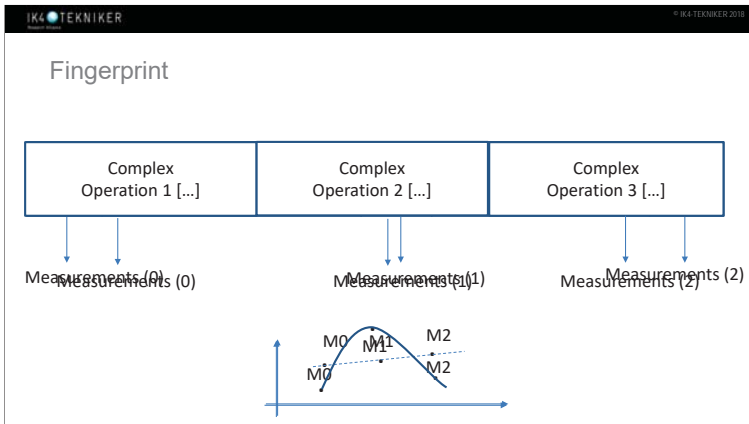
Complex operation context



Particles/wind speed relation during power production







Fingerprint: Not applicable

- Impossible to force operation.

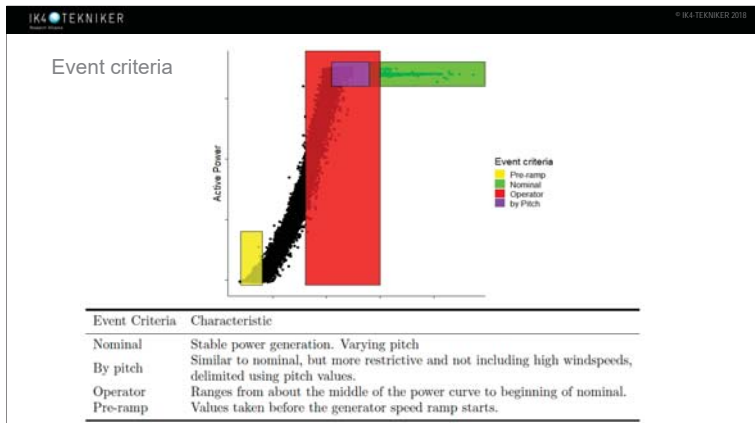
Instead:

- Find equally comparable contexts
 - Analyse frequency of occurrence
 - Analyse steadiness
 - Validate the results

Events

Groups of subsequent data points fulfilling specific criteria.

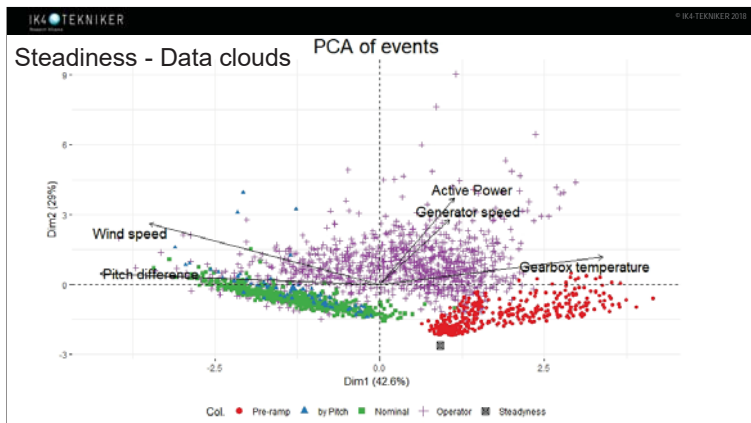
- Follow a chronological order
- Enclosed under some operation conditions



Frequency of occurrence

Table 3. Number of events and week rate by turbine and event criteria with different minimum length time filters.

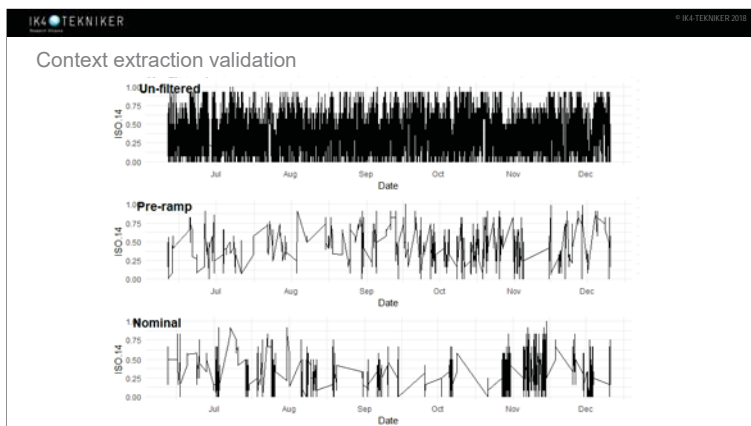
Turbine	Event_kind	>10	>10 week rate	>15	>15 week rate	>30	>30 week rate
WT 1	by Pitch	64	2	30	1	8	0
	Nominal	532	18	357	12	189	6
	Operator	1159	39	794	26	417	14
WT 1	Pre-ramp	367	12	155	5	25	1
	by Pitch	15	1	6	0	2	0
WT 2	Nominal	507	17	339	11	183	6
	Operator	1057	35	758	25	427	14
WT 2	Pre-ramp	325	11	140	5	29	1
	by Pitch	103	3	50	2	21	1
WT 3	Nominal	600	20	410	14	206	7
	Operator	1159	39	820	27	453	15
WT 3	Pre-ramp	403	13	174	6	19	1
	by Pitch	63	2	35	1	11	0
WT 4	Nominal	330	11	216	7	108	4
	Operator	830	28	577	19	315	11
WT 4	Pre-ramp	173	6	76	3	11	0



Distance to steadiness

Table 5. Euclidean distances from centroids to steadiness by turbine

WT	by Pitch	Nominal	Operator	Pre-ramp
WT 1	0.0549	0.0474	0.1191	0.0117
WT 2	0.0404	0.0352	0.1198	0.0136
WT 3	0.0563	0.0483	0.1107	0.0138
WT 4	0.0513	0.0535	0.1267	0.0116



- ### Conclusions
- Measurements influenced by operation. Fuzzy relation.
 - Differences among WT behaviors. Missing information?
 - Higher particle rates at low wind speeds. Generator speed? Inertias?
 - Frequent event criteria. Wide & Short t filter (Nominal/Operator)
 - Steady event criteria*. Not in power-ramp (Pre-ramp<Nom.<byPit.)
 - Coincidences with oil debris sensor. Context is important

- ### Future works
- Inside out
 - Include past in events
 - Try to model behaviour
 - Suggestions?

Suggestions?

Kerman López de Calle Etxabe

kerman.lopezdecalle@tekniker.es

+ 34 943 206 744 9641





VibSim vibration analyzer for wind turbines

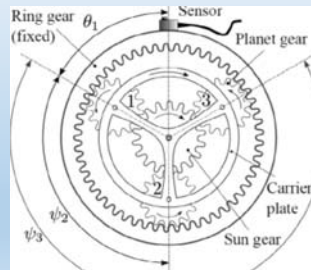
Unique combination of :
Vibrations - Telecommunication techniques - Artificial Intelligence

- 100 times earlier detection of damage
- Calculates remaining lifetime
- Robotization and Fully Automatic

Recently patented in India, USA and EU



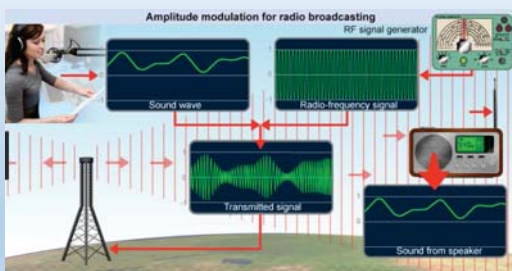
Gearbox vibrations are the sensor data



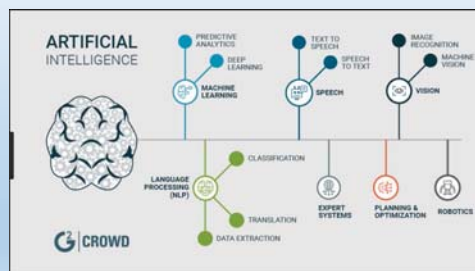
Accelerometer
or
Acoustic microphone



Analysed by Telecommunication technics



Remaining lifetime calculated by use of Artificial Intelligence



Cost saving by new technology

VibSim vibration analyzer is a software package that saves operation cost.

It is a unique combination of:

- Vibration measurements - Telecommunication methods- Artificial Intelligence

- It detects early symptoms of failures 100 times earlier.
- It is fully automatic by robotization.
- Remaining lifetime is calculated.
- Integration in a control system with presentation in a control-room.
- VibSim Analyser also suitable for running on a stand alone PC.
- Or it can run as a part of a server based system.



Cost saving by no more need for Visual borescope inspections



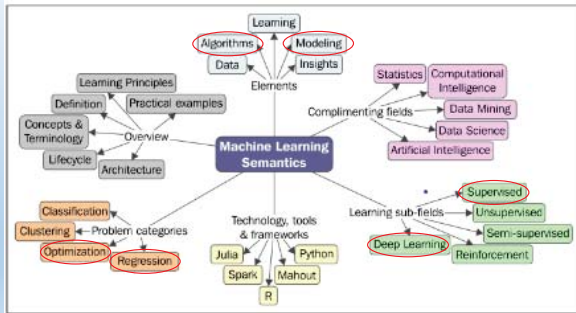
Cost saving by no more fatal damage to windturbines



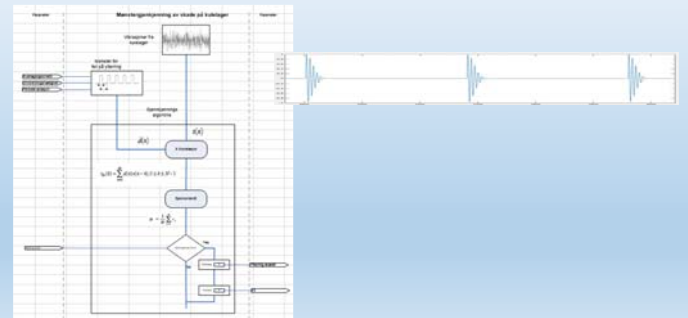
Cost saving by overhaul only when absolutely required, at the best possible point of time



Machine Learning is our toolbox



Pattern Recognition discover symptoms

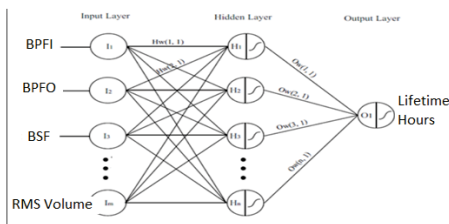


Neural Networks, Deep Learning calculates remaining lifetime.

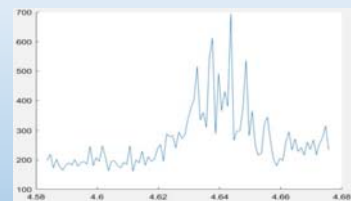


Full control with Weights and Bias, by use of nntool from MATLAB.

- Remaining Lifetime is calculated by Neural Networks



Crack on bearing inner-ring, LSS generator side found with Pattern Recognition in time domain.



BPF1, LSS GS. Indication from pattern recognition is 4,63

Borescope inspection confirm vibration analyse



Low speed shaft bearing generatorside
 normal signs of wear , surface crack on ring
 visible without further impact. Crack must be
 observed regularly.

Cost saving by new technology



VibSim vibration analyzer is a software package that saves operation cost.

It is a unique combination of:

- Vibration measurements - Telecommunication methods- Artificial Intelligence
- It detects early symptoms of failures 100 times earlier than traditional.
- It is fully automatic by robotization.
- Remaining lifetime is calculated.
- Integration in a control system with presentation in a control-room.
- VibSim Analyser also suitable for running on a stand alone PC.
- Or it can run in a server based system.

D2) Operations & maintenance

Drivetrain technology trend in multi megawatt offshore wind turbines considering design, fabrication, installation and operation, F. K. Moghadam, NTNU

Recommended Key Performance Indicators for Operational Management of Wind Turbines, S. Pfaffel, Fraunhofer IEE

Drivetrain Optimization in Multi-megawatt Offshore Wind Turbines

Farid K. Moghadam
Amir R. Nejad

Address: Otto Nielsen veg 10, 7052 Trondheim, Norway
Cell: +47-46 52 84 88- Email: farid.k.moghadam@ntnu.no

EERA DeepWind'19
January 2019



Outline of the Presentation

- 1 Introduction
- 2 Proposed drivetrain optimization approach
- 3 Generator optimization
- 4 Gearbox optimization
- 5 Numerical results
- 5 Conclusion

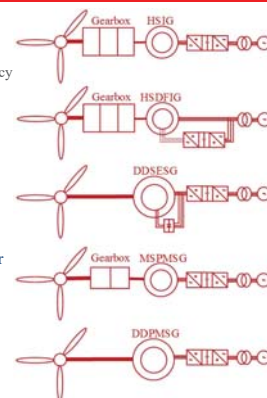


3



Drivetrain Most Conventional Technologies

- High-speed induction generator**
 - Advantages: cheap
 - Disadvantages: sensitive to transients & dynamics, low efficiency
- High speed doubly fed induction generator**
 - Advantages: cheap, fractional converter
 - Disadvantages: brushes, sensitive to transients, low efficiency
- Direct drive self-excited synchronous generator**
 - Advantages: cheap
 - Disadvantages: brushes, low efficiency, higher weight
- Medium speed permanent magnet synchronous generator**
 - Advantages: high efficiency, less weight
 - Disadvantages: expensive
- Direct drive permanent magnet synchronous generator**
 - Advantages: high efficiency
 - Disadvantages: expensive



4



A Glance at Wind Turbine Industry

Most popular in offshore

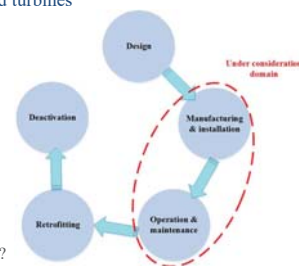
IG	DFIG	DDSESG	DDPMSG	MSPMSG
SWT-4.0-130	GE 5.3-158	EN136-4.2	SG 8.0-167 DD	V164-10.0MW
Siemens	General Electric	Envision	Siemens	Vestas
4MW	5.3MW	4.2MW	8MW	10MW
Off-/onshore	onshore	Off-/onshore	offshore	offshore
1 : 119	geared	direct drive	direct drive	>41
V136-4.2 MW	SG 4.5-145	E-126 7.580	YZ150/10.0	SCD 8.0/168
Vestas	Siemens	Enercon	Swiss Electric	Aerodyn
4MW	4.5MW	7.6MW	10MW	8MW
onshore	onshore	onshore	offshore	offshore
geared (3 stages)	geared (3 stages)	direct drive	direct drive	1:27

5



Permanent Magnet Synchronous Generator

- Most popular technology for offshore wind turbines**
 - High efficiency
 - Low maintenance
- Direct drive**
 - Gearbox removal
- Medium speed**
 - Smaller generator
 - Less manufacturing efforts
 - Easier installation and maintenance
- Research problem:**
 - Which topology gives the highest benefits?
- To answer, we need to see the performance over the life cycle**
- We will focus more on**
 - Production cost
 - Efficiency
 - Operation



6

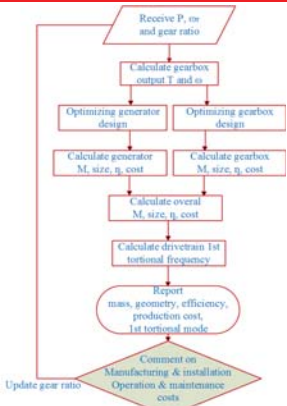




Proposed Drivetrain Optimization


7 

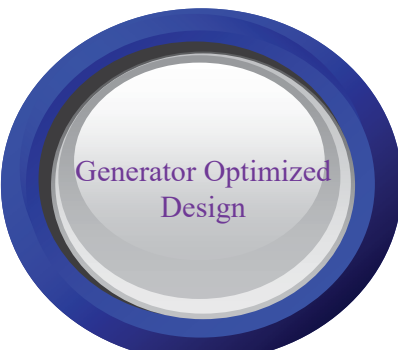
Proposed Drivetrain Optimization Approach




```

    graph TD
      Start([Receive P, ns and gear ratio]) --> CalcGearbox[Calculate gearbox output T and no]
      CalcGearbox --> OptGen[Optimizing generator design]
      CalcGearbox --> OptGear[Optimizing gearbox design]
      OptGen --> CalcGen[Calculate generator M, size, η, cost]
      OptGear --> CalcGear[Calculate gearbox M, size, η, cost]
      CalcGen --> CalcOverall[Calculate overall M, size, η, cost]
      CalcGear --> CalcOverall
      CalcOverall --> CalcTorsion[Calculate drivetrain 1st torsional frequency]
      CalcTorsion --> Report([Report mass, geometry, efficiency, production cost, 1st torsional mode])
      Report --> Comment{Comment on Manufacturing & installation Operation & maintenance costs}
      Comment --> Update([Update gear ratio])
      Update --> CalcGearbox
  
```

8 




Generator Optimized Design

9 

Generator Optimized Design

- Cost function


$$C_{Gen}^{Act} = c_{Fe}m_{Fe} + c_{Cu}m_{Cu} + c_{PM}m_{PM},$$
 where c_{Fe}, c_{Cu} and c_{PM} are the unit costs, and m_{Fe}, m_{Cu} and m_{PM} are the weight of active materials.
- Optimization variables
 - Air gap diameter (Ds), Stack length (Ls), Slot width (bs), Slot height (hs), Magnet height (hm)
 - The other design variables are either a function of optimization variables or constant
- Constant design variables
 - The values will change using an external loop, but will take a constant value in each optimization: Slot per pole per phase, Magnet width to pole pitch ratio, Air gap
- Dependent design variables
 - Air gap/teeth/stator yoke/ rotor yoke flux densities, stator/rotor yoke lengths, teeth width/height
- Subject to
 - A wide range of electrical loading, magnetic loading, insulation requirements, and mechanical forces mitigation, and efficiency based constraints to ensure a secure operation.
- Outputs:
 - Geometry, Weight, Cost, Efficiency
- Constrained nonlinear multi-variable nonconvex problem.
- Using Matlab Fmincon solver to find local optimizers.

10 

Generator Optimization Results

- DTU 10MW PMSG realisation
 - Direct drive
 - Medium speed (G/R= 50)
 - High speed (G/R= 156)
- The following has been modelled
 - Carter impact
 - Iron fill factor
 - Insulation
 - 2-layers, full pitch
- Structure weight
 - Cooling
 - Beams
 - Cylinder
 - Shaft
 - Modeled as a function of design variables

Generator parameters	DDPMSG	MSPMSG	HSPMSG
Results will be reported in the paper.			

11 



Gearbox Optimized Design

12 

Gearbox Optimized Design

- Cost function for a three-stages gearbox

$$C_{Gearbox}^{Gears} = c_{Fe}(m_{Gear}^1 + m_{Gear}^2 + m_{Gear}^3),$$

where c_{Fe} is the unit cost of gears, and m_{Gear}^1, m_{Gear}^2 and m_{Gear}^3 are the weight of 1st, 2nd and 3rd stages.

- Parallel stage: $m_{Gear}^{Parallel} = K_{AG} \frac{2Q_b}{K} (1 + \frac{1}{U_s} + U_s + U_s^2)$
- Planetary stage: $m_{Gear}^{Planetary} = K_{AG} \frac{2Q_b}{K} (\frac{1}{B} + \frac{1}{BU_{SN}} + U_{SN} + U_{SN}^2 + K_r \frac{(U_s-1)^2}{B} + K_r \frac{(U_s-1)^2}{BU_{SN}})$
- The overall cost function for a sample three-stages gearbox with two planetary and one parallel will be:

$$V = \frac{2Q_b}{K} \frac{1}{U_1} \left[\frac{1}{B_1} + \frac{1}{B_1(U_1^2-1)} + (U_1-1) + (U_1-1)^2 + K_{r1} \frac{(U_1-1)^2}{B_1} + K_{r1} \frac{(U_1-1)^2}{B_1(U_1^2-1)} \right] + \frac{2Q_b}{K} \frac{1}{U_1 U_2} \left[\frac{1}{B_2} + \frac{1}{B_2(U_2^2-1)} + (U_2-1) + (U_2-1)^2 + K_{r2} \frac{(U_2-1)^2}{B_2} + K_{r2} \frac{(U_2-1)^2}{B_2(U_2^2-1)} \right] + \frac{2Q_b}{K} \frac{1}{U_1 U_2 U_3} \left[1 + \frac{1}{U_3} + U_3 + U_3^2 \right]$$

where U is gear ratio, B is number of planets, K_r is ring scaling factor, Q is input torque.

- Subject to
 - Constraints related to gear ratio of each stage, and the overall gear ratio, concerning with the mechanical design limitations.
- Outputs: Optimized gear ratios, Weight, Cost, Efficiency
- Constrained nonlinear multi-variable nonconvex problem. Matlab Fmincon solver is used.

Gearbox Optimization Results

- DTU 10MW gearbox realisation
 - Direct drive
 - Medium speed (G/R= 50)
 - High speed (G/R= 156)

Gearbox parameters	MSPMSG	HSPMSG
Results will be reported in the paper.		

- Structure weight
 - Bearings
 - Housing
 - Carriers
 - Moded as a fraction of gears weight




Concluding Remarks

- Results show that medium speed drivetrain seems to be a better option for offshore wind turbines.
- It would help to have a safe distance from the external excitations frequencies, and is recommended for offshore floating applications.
- Reduction of drivetrain weight, and consequently reduction of nacelle weight potentially reduces the required nacelle, tower and platform costs.
- Impacts on reliability, operation and maintenance costs will be investigated in future works.

RECOMMENDED KEY PERFORMANCE INDICATORS FOR OPERATIONAL MANAGEMENT OF WIND TURBINES

17.01.2019 EERA DeepWind'2019, Trondheim
Sebastian Pfaffel, Stefan Faulstich and Shawn Sheng



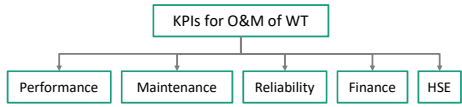
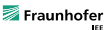
Sebastian Pfaffel, M.Sc. - Sebastian.Pfaffel@iee.fraunhofer.de - +49 561 7294 441

1

KPIs: What are we talking about?

Key Performance Indicator(s)

- Objectively describe the performance of an observed unit
- Provide information as a decision support
- Are repeatedly evaluated (monthly, quarterly, yearly ...)
- Should be SMART
 - Specific
 - Measurable
 - Achievable
 - Relevant
 - Time-bound

2

Motivation and Scope

Situation in the wind industry (O&M)


- Various standards are available (e.g. IEC 61400-25)
- KPIs are commonly used
- Used KPI systematics and definitions vary heavily

Drawbacks

- Additional effort (design, implementation, ...)
- Cross-company benchmarks aren't possible
- Hinders communication and knowledge building
- Makes contracts more complicated

Scope of this work

- Identify and prioritize commonly used KPIs
- Collect and review various definitions
- Propose a set of recommended KPIs including unified definitions



3

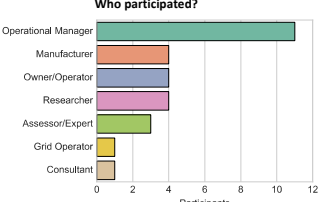

Survey on KPIs

- Survey is part of a standardization task within the FGW e.V.
- 34 different KPIs were considered in the survey
- Survey was open 4th October 2017 till 1st November 2017

What did we ask?

- Is the KPI used in your company?
- Which definition is used?
- Which data serves as a basis?
- How important is the KPI?

Who participated?

4

HSE- and Finance KPIs

HSE-KPIs

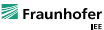
KPI	Answers	Use	Importance (1-5)	Abs. Importance
Total accident rate	5/5	4/5	3.7	14.8
Total lost time occupational illness frequency	5/5	3/5	2.7	8.1
Fatal accident rate	5/5	2/5	4	8
Recoverable injury rate	5/5	2/5	3.5	7
Energy obtained per employee and year	3/5	0/5	3	9
Dollars lost per employee and year	5/5	0/5	0	0

Finance-KPIs

KPI	Answers	Use	Importance (1-5)	Abs. Importance
EBITDA	9/9	5/9	4	20
Maintenance costs	9/9	5/9	3.6	18
Operational expenditures (OPEX)	9/9	4/9	4.4	17.6
Levelized cost of energy (LCOE)	9/9	3/9	3.7	11.1
Debt-service coverage ratio (DSCR)	9/9	2/9	5	10
Free cash flow to equity (FCFE)	9/9	2/9	4.5	9
Break-even point of energy (BEPE)	9/9	1/9	4	4
Levelized energy cost (LEC)	9/9	0/9	0	0

Low importance in the survey

- HSE- and Finance-KPIs are not discussed in detail in this work
- But: Most participants in the survey had a technical background
- Further work on HSE- and Finance-KPIs is required

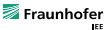


5

Performance KPIs

KPI	Answers	Use	Importance (1-5)	Abs. Importance
Power curve	20/20	19/20	4.5	85.5
Wind conditions	20/20	16/20	4.5	72
Average wind speed				
Wind speed distribution				
Wind direction distribution				
Average wind speed/site assessment				
Full-load hours	20/20	18/20	3.5	63
Energy consumption	20/20	16/20	3.1	49.6
Capacity factor	20/20	13/20	3.7	48.1
Data availability	20/20	11/20	4.1	45.1
Remote-ports	20/20	5/20	3.2	16
Site quality				
No. of telecommunication interruptions				
Forecast fulfillment				
Operating hours				
Specific yield				
Market value factor				

- Power Curves are the most important tool for performance assessment
- Operators use various metrics to describe the wind conditions
- Many more performance KPIs were suggested



6

Maintenance KPIs

KPI	Answers	Use	Importance (1-5)	Abs. Importance
Time-based availability	16/16	16/16	4.7	75.2
Production-based availability	16/16	12/16	4.1	49.2
Yield losses by cause				
Monetary-based availability				
Maintenance tasks	16/16	7/16	4	28
Preventive maintenance tasks	16/16	7/16	3.3	23.1
Number of routine maintenance tasks				
Number of inspections/visual inspections				
Number of repairs				
Reactive maintenance tasks	16/16	7/16	3.3	33.1
Risk priority number (RPN)	16/16	1/16	5	5

- KPIs are defined in IEC 61400-25/26
- A new availability definition will be introduced
- Further categorization for maintenance tasks required

7

Maintenance KPIs – Maintenance Tasks

Structure to categorize maintenance tasks by the maintenance type and activity according to BS EN 13306 and BS EN ISO 14224

8

Reliability KPIs

KPI	Answers	Use	Importance (1-5)	Abs. Importance
Failure rate	10/10	5/10	3.6	28.8
Mean time between failures (MTBF)	10/10	7/10	3.6	25.2
Mean time to repair / restoration (MTTR)	10/10	7/10	3.3	23.1
Mean down time (MDT)	10/10	6/10	3	18
Mean operating time between failures (MOTBF)	10/10	5/10	3.2	16
Mean operating time to failures (MOTF)	10/10	5/10	2.8	14
Repair rate	10/10	3/10	2.3	6.9

- Reliability Mean Time Measures are sometimes tricky to differentiate
- Different standards use different naming rules
- MTTR or MTRRes? MTBF or MOTBF?

Unified definitions and naming rules are essential to avoid misunderstandings and mistakes

9

Reliability KPIs – Reliability Mean Time Measures

Reliability mean time measures for (partially) repairable and non-repairable systems according to ISO and IEC standards.

10

Reliability KPIs – Reliability Mean Time Measures

Taxonomies of MTTR subcategories from ISO/TR 12489

11

Conclusion and Outlook


Conclusion

- Many KPIs and many varying KPI definitions are in use
- Performance KPIs are most important for operational managers
- Current situation can lead to confusion
- A unified set of KPIs makes life easier for everyone
- An international technical guideline would be beneficial
- Make use of unified KPI definitions!

Outlook


- Starting point for committee work on a technical guideline (FGW e.V.)
- The current list is not complete, further KPIs will be developed
- Further topics like aggregation or uncertainties of KPIs have to be addressed.
- A detailed review of HSE- and Finance-KPIs is still required

12



DISCUSSION

Fraunhofer
IEE



Sebastian Pfaffel, M. Sc.
Wind turbine operations analyst
Planning and Operation of Generating Assets
Königsplatz 59 | 34119 Kassel / Germany
+49 561 7294-441
sebastian.pfaffel@iwes.fraunhofer.de
www.iwes.fraunhofer.de

© Fraunhofer IEE

Fraunhofer IEE

13

RECOMMENDED KEY PERFORMANCE INDICATORS FOR OPERATIONAL MANAGEMENT OF WIND TURBINES

1. Motivation and Scope
2. Survey on KPIs
3. HSE- and Finance KPIs
4. Performance KPIs
5. Maintenance KPIs
6. Reliability KPIs
7. Conclusion and Outlook

© Fraunhofer

Fraunhofer IEE

14

E1) Installation and sub-structures

Fatigue sensitivity to foundation modelling in different operational states for the DTU 10MW monopile-based offshore wind turbine, G. Katsikogiannis, NTNU


Integrated Project Logistics and Costs Calculation for Gravity Based Structure, N.Saraswati, TNO

NTNU – Trondheim Norwegian University of Science and Technology

Fatigue sensitivity to foundation modelling in different operational states for the DTU 10MW monopile-based offshore wind turbine

George Katsikogiannis¹, Erin E. Bachynski², Ana M. Page²

EERA DeepWind'19, Trondheim, 17 January 2018



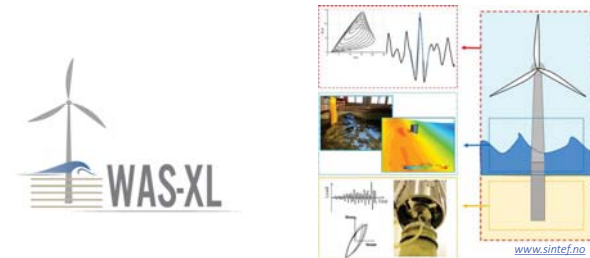
Source: University of Cambridge

¹Department of Marine Technology, Norwegian University of Science and Technology (NTNU)
²Norwegian Geotechnical Institute (NGI)
 *Email: george.katsikogiannis@ntnu.no

Statoil Multiconsult innogy eof GRES ENTRANS NGI NTNU SINTEF Forskningsrådet

Motivation ECs & Structural Model Foundation Models Results Conclusions

Part of [WAS-XL project](#) (Wave Loads and Soil Support for Extra Large Monopiles)



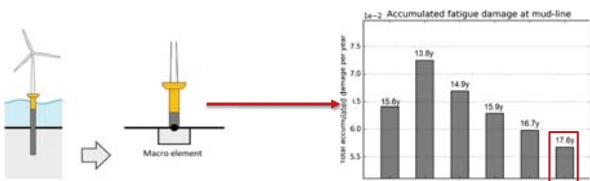
Primary objective: Reduction of uncertainties related to large-diameter monopile foundations.

Foundation modelling: Common methods (API p-y) not accurate -> more realistic representation of soil structure interaction is required.

Statoil Multiconsult innogy eof GRES ENTRANS NGI NTNU SINTEF Forskningsrådet

Motivation ECs & Structural Model Foundation Models Results Conclusions

Macro – element formulation [1] results in fatigue damage reduction [2].



REDWIN - Reducing cost of offshore wind by integrated structural and geotechnical design [1]
 Aasen et al. "Effect of foundation modelling on the fatigue lifetime of a monopile-based offshore wind turbine" [2]

Aim of the present study

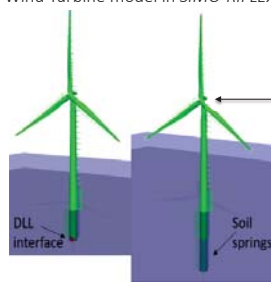
Importance of foundation modelling in fatigue damage when aerodynamic damping is not effective.

Parked States & Wind - Wave Misalignment Conditions

NTNU Norwegian University of Science and Technology 3

Motivation ECs & Structural Model Foundation Models Results Conclusions

Wind Turbine model in SIMO-RIFLEX



Hub-height: 119m
 Cut-in speed : 4m/s
 Cut-out speed : 25 m/s


Monopile structural characteristics

Diameter [m]	Thickness [m]	Penetration Length [m]	Young's modulus [GPa]	Shear Modulus [GPa]
9.0	0.11	36	210	81

NTNU Norwegian University of Science and Technology 4

Motivation ECs & Structural Model Foundation Models Results Conclusions

Depth:30m Example (Wind Bin 14 – 16 m/s)



Hs [m]	2-3	3-4	4-5	5-6	6-7	7-8	8-9	9-10	10-11	11-12	12-13	13-14	14-15	15-16	16-17	17-18
0.25																
0.75																
1.25																
1.75																
2.25																
2.75																
3.25																
3.75																
4.25																
4.75																
5.25																

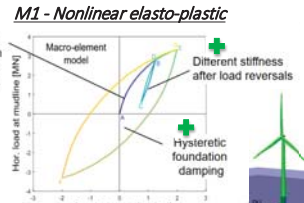
Selection of most contributing sea-states to the long-term fatigue damage for 5 wind bins.

Simulation & Environmental Parameters						
EC number	Time Simulation [s]	U _w [m/s]	H _s [m]	T _p [s]	Wind-Wave Misalignment [degrees]	Wave Spectrum
1	3600	5.06	0.75	5.50		Pierson-Moskowitz
2	3600	9.06	1.25	5.50		Pierson-Moskowitz
3	3600	14.94	2.25	6.50	0°, 15°, 30°	Torsethaugen
4	3600	20.90	3.75	7.50	45°, 90°	JONSWAP
5	3600	26.74	5.25	8.50		JONSWAP

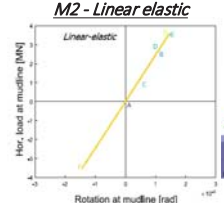
NTNU Norwegian University of Science and Technology 5

Motivation ECs & Structural Model Foundation Models Results Conclusions

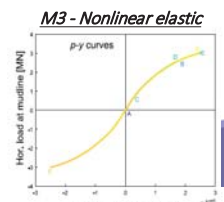
M1 - Nonlinear elasto-plastic



M2 - Linear elastic



M3 - Nonlinear elastic



Page et al. A macro-element pile foundation model for integrated analyses of monopile based offshore wind turbines [3]

NTNU Norwegian University of Science and Technology 6

Motivation ECs & Structural Model Foundation Models Results Conclusions

Decay test for M1: Contribution of foundation damping to global damping

M2 & M3: Soil Damping 0.64% applied as Rayleigh structural damping based on M1.

$$\delta = \ln \left(\frac{A_i}{A_{i+1}} \right) = 2\pi \frac{\xi}{\sqrt{1-\xi^2}} \approx 2\pi\xi$$

Global Damping Ratio [-]

FA Moment Amplitude [kNm]

Nonlinear damping in M1. Increases with respect to the response amplitude

NTNU Norwegian University of Science and Technology 7

Motivation ECs & Structural Model Foundation Models Results Conclusions

Natural frequency dependency on load levels

M1, M3 : For higher load levels → lower foundation stiffness → lower natural frequencies

M2 linear elastic model → Constant natural frequency for all load levels

NTNU Norwegian University of Science and Technology 8

Motivation ECs & Structural Model Foundation Models Results Conclusions

Operational state: Different processes dominate per EC

- EC1 3P component
- EC2 Slowly varying wind component
- EC3 Wide range – Mainly waves
- EC4 Waves – Aerodynamic damping effect at natural frequency range
- EC5 Waves – Large loads at natural frequency range

EC	U _w [m/s]	H _w [m]	T _w [s]
1	5.06	0.75	5.50
2	9.06	1.25	5.50
3	14.94	2.15	6.50
4	20.90	3.75	7.50
5	26.74	5.25	8.50

Combination of stiffness and damping dominance per EC

NTNU Norwegian University of Science and Technology 9

Motivation ECs & Structural Model Foundation Models Results Conclusions

Parked State: Responses close to natural frequency dominate for all ECs

Soil Damping dominance for all ECs

Figure of previous slide (Operation)

NTNU Norwegian University of Science and Technology 10

Motivation ECs & Structural Model Foundation Models Results Conclusions

Comparison of the different soil models (Example - EC4)

Operational

Parked

Stiffness dominance

Aerodynamic damping dominance

Soil Damping dominance

Relative difference to M1

NTNU Norwegian University of Science and Technology 11

Motivation ECs & Structural Model Foundation Models Results Conclusions

Operational State - Various angles of misalignment

M1 - EC4

Soil Damping dominates for misalignment angles over 30 degrees

NTNU Norwegian University of Science and Technology 12

Motivation ECs & Structural Model Foundation Models Results Conclusions

Operational State

EC4 - 90°

EC	U ₁₀ [m/s]	H ₁₀ [m]	T _p [s]
1	5.06	0.75	5.50
2	9.06	1.25	5.50
3	14.94	2.25	6.50
4	20.90	3.75	7.50
5	26.74	5.25	8.50

Soil Damping dominates for misalignment angles over 30 degrees

NTNU Norwegian University of Science and Technology

Motivation ECs & Structural Model Foundation Models Results Conclusions

Conclusions

1. Different processes dominate the dynamic processes depending on the environmental state.
2. Both foundation stiffness and damping formulation affect the behavior in different frequency regimes.
3. Considerably higher fatigue differences in parked state (-60% to 154%) compared to operational state (-10% to 50%).
4. Large differences (up to 183%) for misalignment angles larger than 30 degrees.

Relatively high importance of foundation modelling and hysteretic effects for fatigue damage in cases where aerodynamic damping is negligible.

Statoil Multiconsult innogy edf GREEN ENERGY NGI NTNU SINTEF Forskningsrådet

Motivation ECs & Structural Model Foundation Models Results Conclusions

Acknowledgements

- Erin Bachynski (NTNU)
- Ana Page (NGI)
- Sverre Haver (UiS)

Statoil Multiconsult innogy edf GREEN ENERGY NGI NTNU SINTEF Forskningsrådet

Motivation ECs & Structural Model Foundation Models Results Conclusions

Thank you for your attention!

Questions?

NTNU - Trondheim Norwegian University of Science and Technology

Motivation ECs & Structural Model Foundation Models Results Conclusions

BACK-UP SLIDES

Statoil Multiconsult innogy edf GREEN ENERGY NGI NTNU SINTEF Forskningsrådet

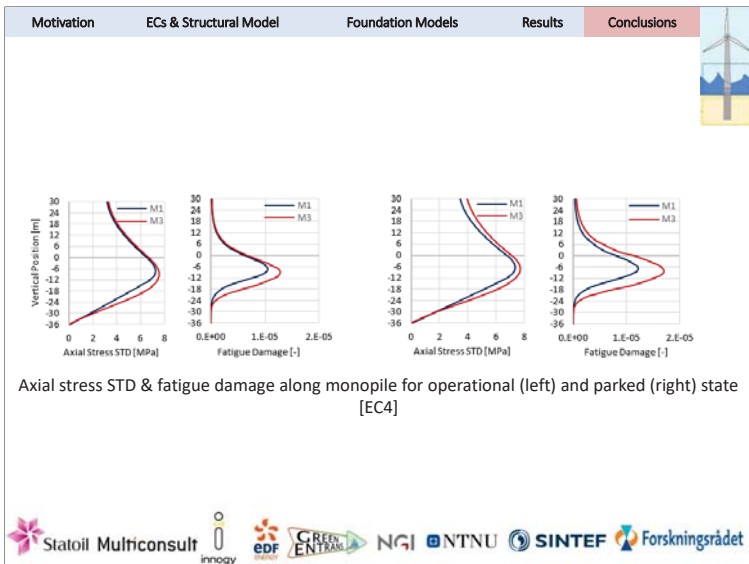
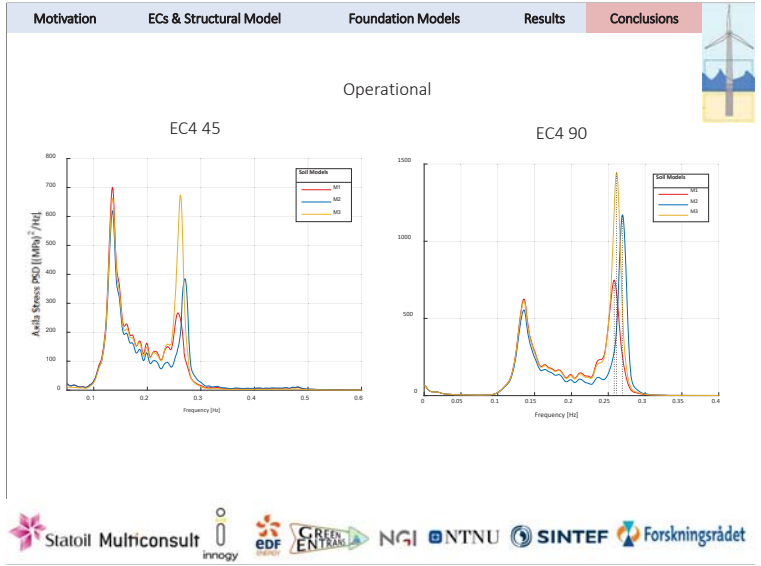
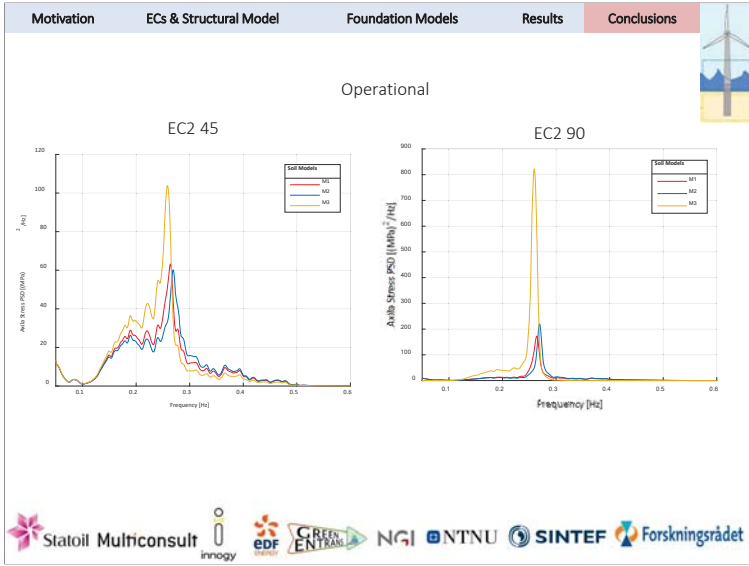
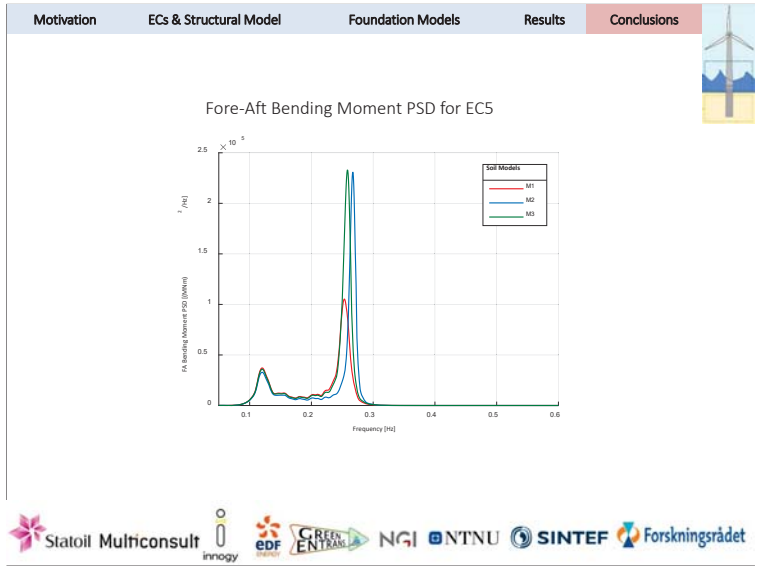
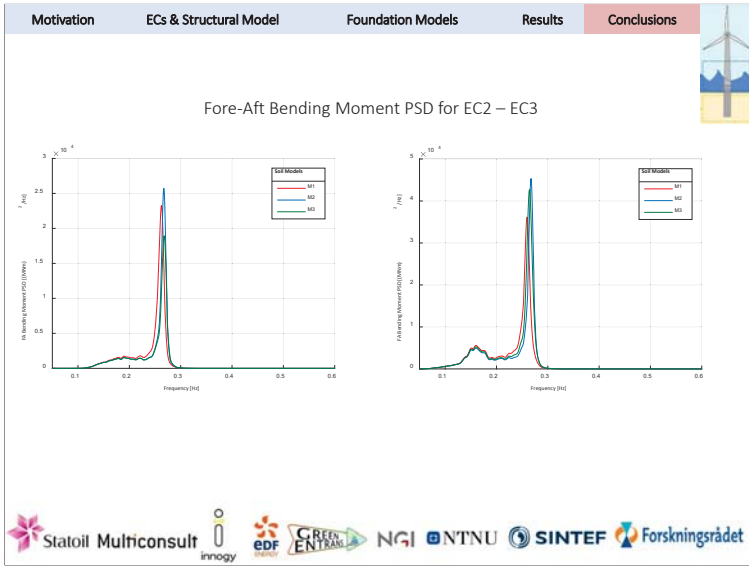
Motivation ECs & Structural Model Foundation Models Results Conclusions

Fore-Aft Bending Moment PSD for M2 with varying of soil damping [%]

Operational

Parked

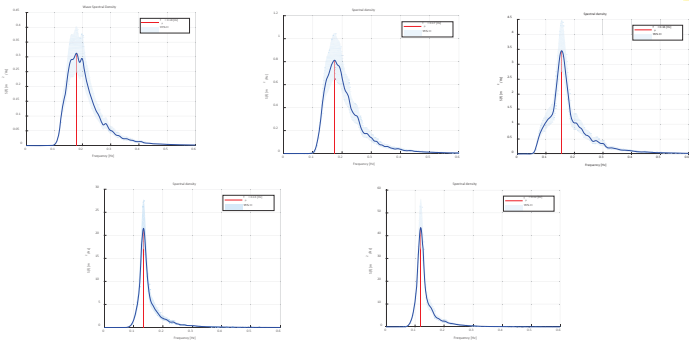
Statoil Multiconsult innogy edf GREEN ENERGY NGI NTNU SINTEF Forskningsrådet



Motivation ECs & Structural Model Foundation Models Results Conclusions

Fatigue Damage [-] EC1		Operational	Parked
0	1.63E-07	180	2.54E-08 180
15	1.58E-07	180	2.30E-08 198
30	1.47E-07	180	1.88E-08 198
45	1.33E-07	180	1.52E-08 216
90	1.06E-07	180	1.02E-08 270
Fatigue Damage [-] EC2		Operational	Parked
0	4.33E-07	0	2.41E-07 180
15	4.18E-07	0	2.18E-07 198
30	3.74E-07	0	1.74E-07 198
45	3.22E-07	18	1.35E-07 216
90	2.48E-07	324	8.97E-08 270
Fatigue Damage [-] EC3		Operational	Parked
0	6.77E-07	180	1.32E-06 180
15	6.27E-07	198	1.13E-06 198
30	6.42E-07	198	9.70E-07 198
45	7.08E-07	216	7.83E-07 216
90	1.22E-06	270	6.18E-07 270
Fatigue Damage [-] EC4		Operational	Parked
0	6.27E-06	180	8.06E-06 180
15	6.05E-06	198	7.20E-06 198
30	5.90E-06	198	6.46E-06 198
45	6.22E-06	216	6.16E-06 216
90	8.16E-06	270	6.56E-06 270
Fatigue Damage [-] EC4		Operational	Parked
0	1.86E-05	180	3.83E-05 180
15	1.87E-05	198	3.27E-05 0
30	1.99E-05	216	2.88E-05 198
45	2.40E-05	234	2.68E-05 216
90	3.95E-05	270	3.36E-05 270

Statoil Multiconsult innogy edf GREEN ENERGY NGI NTNU SINTEF Forskningsrådet



INTEGRATED PROJECT LOGISTICS AND COSTS CALCULATIONS FOR GRAVITY BASED STRUCTURE

Saraswati, N. (Novita)
EERA Deepwind 2019, Trondheim, January 17th 2019

AGENDA

- › Introduction & Motivation
- › Installation modelling and simulation
- › Case studies of different GBS (installation) strategies
- › Optimization opportunity
- › Results and recommendation

2 | Integrated Project Logistics and Costs Calculation for Gravity Based Structure

TOWARDS LARGE-SCALE GENERATION OF WIND ENERGY

3 | Integrated Project Logistics and Costs Calculation for Gravity Based Structure

GBS AS LARGE OFFSHORE WIND TURBINE FOUNDATION

- › Alternative for jacket & monopile in deeper water
- › Experience in oil and gas and civil engineering
- › Provide designs of GBS for offshore wind large WT
- › GBS for wind needs to be transported and installed in rough sea condition
- › **Better understanding** is needed to **reduce costs** and **risk** to make offshore wind with GBS **economically viable**
- › GBS JIP consortium
 - › Marin, Deltares, Witteveen + Bos and Vuyk Engineering
 - › Deme, Besix, Saipem, Jan de Nul, Statoi, Strukton, Bureau Veritas, ALP Maritime and MonobaseWind

Source: Van Oord

4 | Integrated Project Logistics and Costs Calculation for Gravity Based Structure

OUTLINE OF THE WORK

- › Step by step description on constructions, transports and installations operations for GBS
- › Cost of energy analysis
- › Insight into:
 - Cost drivers for LCOE using GBS as foundation (construction, transport, installation)
 - Logistical (time) plan and how to optimize them
 - Resources (material, equipment, technician, harbour) requirements
 - Weather restrictions

5 | Integrated Project Logistics and Costs Calculation for Gravity Based Structure

ECN PART OF TNO IO&M VISION

Strategic Simulation Tools
for
Optimal Decision Making
in
Offshore Wind Farms

6 | Integrated Project Logistics and Costs Calculation for Gravity Based Structure

ECN | TNO Innovation for life

WHY BUILD COMPUTER MODELS?

Simulations (re-)create, as exactly as possible, time series (from history or for future possibilities), considering causes and effects

Computer simulations are safe and low cost, compared with the real world

7 | Integrated Project Logistics and Costs Calculation for Gravity Based Structure

ECN | TNO Innovation for life

ECN INSTALL

Needs of installation modelling tool

- › Design and optimize the installation strategy for an offshore wind farm
- › Determine project planning, delays, costs and risks
- › Monitor progress during installation

Commercial proof / Evaluation

- › Installation methods
- › Support structures & wind turbines
- › Vessels and equipment

4 | Integrated Project Logistics and Costs Calculation for Gravity Based Structure
Source: Gemini

Source: Royal IHC

ECN | TNO Innovation for life

ECN INSTALL: HOW IT WORKS

- › **Input/Simulation**
 - › Deterministic discrete event simulator with historic weather data
 - › Planning using intuitive operations
 - › Multiple actors (vessels, equipment, group of technicians) per operation
 - › Weather window and weather restrictions
 - › Learning curve
- › **Result**
 - › Installation costs, installation planning, resources utilization and installation delays
 - › Excel and graphical

9 | Integrated Project Logistics and Costs Calculation for Gravity Based Structure

ECN | TNO Innovation for life

CASE STUDY

- › Location: Borssele area
- › 60 x 10 MW
- › Construction & installation port: Damen Verolme
- › Wind turbine installation port: Port of Esbjerg
- › 3 GBS concept designs compared
- › ECN Install simulation:
 - › Onshore construction and assembly for GBS
 - › Load out, transport, and installation operation (entire wind farm)

10 | Integrated Project Logistics and Costs Calculation for Gravity Based Structure

ECN | TNO Innovation for life

GBS DESIGN FOR 10 MW TURBINES

Source: MonobaseWind

Parameters	unit	value
Diameter base	[m]	38
Height of base	[m]	12
Height of cone	[m]	13
Diameter of shaft	[m]	10
Total model height	[m]	50
Min draft	[m]	9.7
low draft	[m]	8.6
Dry weight	[t]	11200

11 | Integrated Project Logistics and Costs Calculation for Gravity Based Structure

ECN | TNO Innovation for life

COST COMPONENT CONSIDERED

› **Construction**

```

    graph LR
      MR[Material requirement] --> SW[Steel works]
      SW --> EQ[Equipment]
      EQ --> CR[Craneage]
      CR --> CS[Construction costs and site rent]
      CS --> PC[Profit, contingency, etc.]
    
```

› **Marine Operations**

```

    graph LR
      SP[Seabed Preparation] --> FTI[Foundation Transport and Installation]
      FTI --> P[Parallel *SCOP (OH/S + Export Cable) Installation + Sour Protection]
      P --> ICL[Infield cable laying & burying]
      ICL --> WTI[Wind Turbine Transport & Installation (except case 3)]
      WTI --> COM[Commissioning]
    
```

› **Other LCOE components** (OPEX, power production, other CAPEX costs *components costs and their installation costs)

12 | Integrated Project Logistics and Costs Calculation for Gravity Based Structure

FLOATING GBS

- Constructed in dry dock (batch 20 GBS)
- Advantage:
 - Easy to load out, store
 - Cheap marine logistic (tug boats, ballasting vessels)
- Challenges:
 - Long construction time (~1 year/batch)
 - High costs dry dock
 - Higher risk (delay caused by one GBS)

13 | Integrated Project Logistics and Costs Calculation for Gravity Based Structure

FLOATING GBS

- Constructed in dry dock (batch 20 GBS)
- Advantage:
 - Easy to load out, store
 - Cheap marine logistic (tug boats, ballasting vessels)
- Challenges:
 - Long construction time (~1 year/batch)
 - High costs dry dock
 - Higher risk (delay caused by one GBS)

14 | Integrated Project Logistics and Costs Calculation for Gravity Based Structure

FLOATING GBS

- Constructed in dry dock (batch 20 GBS)
- Advantage:
 - Easy to load out, store
 - Cheap marine logistic (tug boats, ballasting vessels)
- Challenges:
 - Long construction time (~1 year/batch)
 - High costs dry dock
 - Higher risk (delay caused by one GBS)

15 | Integrated Project Logistics and Costs Calculation for Gravity Based Structure Source: Van Oord

NON-FLOATING (LIFTED) GBS

- Constructed in quay side
- Advantage:
 - No batch time
 - Flexible construction site
- Challenges:
 - Still long construction time
 - Expensive heavy lift vessel (>7300 tonnes)

16 | Integrated Project Logistics and Costs Calculation for Gravity Based Structure

NON-FLOATING (LIFTED) GBS

- Constructed in quay side
- Advantage:
 - No batch time
 - Flexible construction site
- Challenges:
 - Still long construction time
 - Expensive heavy lift vessel (>7300 tonnes)

17 | Integrated Project Logistics and Costs Calculation for Gravity Based Structure Source: Jan De Nul

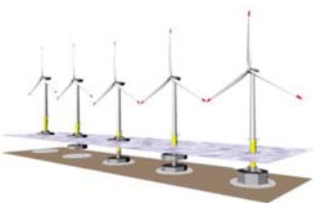
INTEGRATED GBS (PRE-INSTALLED TURBINE)

- Constructed in dry dock
- Advantage:
 - Faster construction time than other designs
 - Less operation offshore and cheap marine logistic
- Challenges:
 - Higher weather restriction (tug boats, turbine)
 - High man-hours required for construction

18 | Integrated Project Logistics and Costs Calculation for Gravity Based Structure Source: MonobaseWind

INTEGRATED GBS (PRE-INSTALLED TURBINE)

- › Constructed in dry dock
- › Advantage:
 - › Faster construction time than other designs
 - › Less operation offshore and cheap marine logistic
- › Challenges:
 - › Higher weather restriction (tug boats, turbine)
 - › High man-hours required for construction

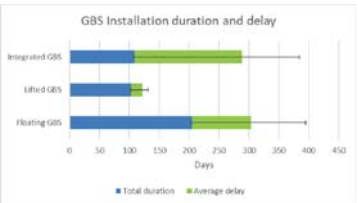


Source: MonobaseWind

13 | Integrated Project Logistics and Costs Calculation for Gravity Based Structure

MARINE OPERATION PLANNING

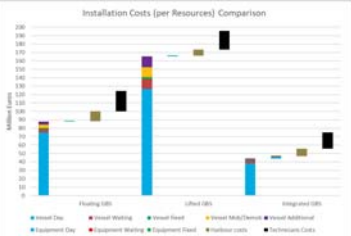
- › One load out at a time
- › Winter is avoided
- › Case 1 & 3 are commissioned within 2 years



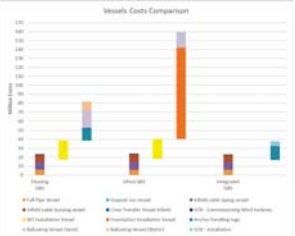
20 | Integrated Project Logistics and Costs Calculation for Gravity Based Structure

COSTS

Installation Costs (per Resources) Comparison



Vessels Costs Comparison




- › Vessels used for all cases → 23 M€
- › Wind turbine installation vessel → 21 M€

21 | GBS JP Case Study

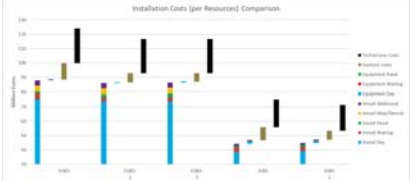
OPTIMIZATION OF INSTALLATION PLANNING

- › Least delay → April – September
- › 2 load out at a time
- › Reduction in installation costs:
 - › Floating GBS: 6% → 7,5M€
 - › Integrated GBS: 5,3% → 4M€
- › 600 MW wind farm can be commissioned within 1 year!

GBS Installation Optimization



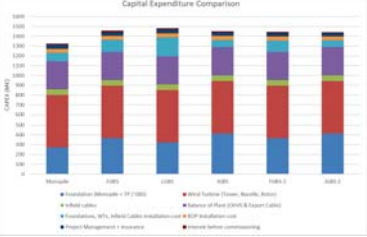
Installation Costs (per Resources) Comparison



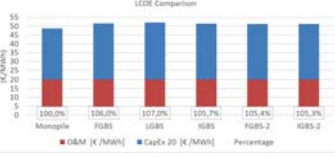
22 | Integrated Project Logistics and Costs Calculation for Gravity Based Structure

CAPEX COMPARISON TOWARDS LCOE

Capital Expenditure Comparison



LCOE Comparison



- › LCOE GBS cases are slightly higher compared to monopile (5-7%)

23 | Integrated Project Logistics and Costs Calculation for Gravity Based Structure

CONCLUSIONS

- › GBS Construction
 - › More GBS per batch has higher risk (drydock). A delay of one of the GBS will impact the whole batch and increase the total construction costs.
- › Offshore Installation
 - › GBS offshore operation is long due to the low speed of towing, extended installation operations with limited weather windows → Optimization needed
 - › Transport and installing GBS with heavy lift vessel is fast but the costs are high
 - › **Lowest installation costs: Integrated GBS – Floating GBS – Lifted GBS**
- › Potential reduction
 - › Higher workability for the longer operations, such as towing, water ballasting and sand ballasting
 - › Installation is only done within favourable seasons (April – September)

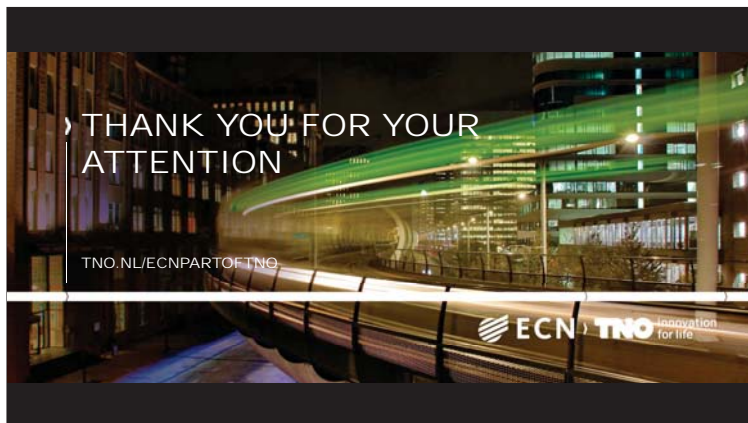
24 | Integrated Project Logistics and Costs Calculation for Gravity Based Structure

RECOMMENDATIONS



- › GBS Construction:
 - › Reducing the costs of GBS construction; the direct material costs and then the costs of the construction site (time required).
 - › Evaluate the effect of constructing GBS in smaller batches (5 or 10 maximum)
- › Offshore installation:
 - › Explore more effective installation scenarios (e.g. fast ballasting)
 - › Investigation of higher workability for towing and installation to reduce delays and eventually installation costs.
- › Investigate the end-of-life options and decommissioning strategy

25 | GBS JP Case Study



E2) Installation and sub-structures

Upscaling and levelised cost of energy for offshore wind turbines supported by semi-submersible floating platforms, Y.Kikuchi, Univ of Tokyo

Wave Cancelling Semi-Submersible Design for Floating Offshore Wind Turbines, Wei Yu, University of Stuttgart

Summary of LIFES50+ project results: from the Design Basis to the floating concepts industrialization, G.Pérez, TECNALIA

Upscaling and levelized cost of energy for offshore wind turbines supported by semi-submersible floating platforms

Department of Civil Engineering, The University of Tokyo
Yuka Kikuchi and Takeshi Ishihara

EERA DeepWind'19
Trondheim, 17 January 2019



Upscaling of floating offshore wind turbine system 2/18

In floating offshore wind farm projects, turbine size is getting larger.



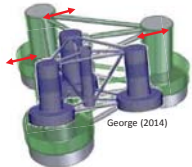
What is upscaling rule of floating offshore windfarm system ?

Previous studies about upscaling 3/18

- ✓ Three previous researches upscaled OC4 floater for 5 MW into that for 10 MW turbine.
- ✓ Satinert et al. (2016) used optimization algorithm. (Not comparable to other researches)

■ Proposed upscaling procedure

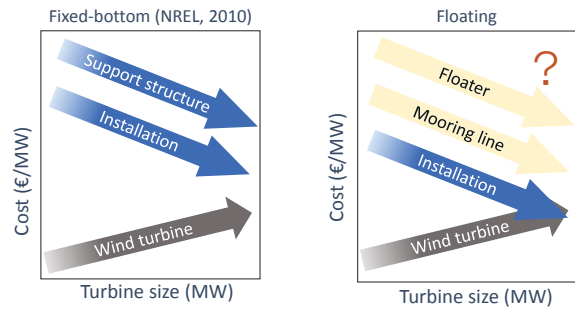
	Main parameter	Leimster et al. (2016) NTNU	George (2014) Lisbon Univ.
Heave	Draft	Scale-up	Dock size
	Freeboard	Scale-up	Scale-up
Pitch	Distance b/w columns	Scale-up	Scale-up
	Diameter of upper column	Static pitch angle $q = F_{S5}/C_{S5}$	Balance b/w gravity and buoyancy
Surge	Mooring line	Mooring line length	Angle at fairlead



What factor has priority for upscaling ?
The relationship between upscaling rule and floater motion or mooring force need to be clearly described.

Requirement for cost-reduction 4/18

Myhr et al. (2016) has investigated the effect of different floater type on cost of energy by using engineering cost model, where the cost is assessed from steel amount of initial design of floater and mooring line.



Upscaling turbine effect of floater and mooring line is quantitatively not clear.

Objectives 5/18

1. Upscaling rule of turbine, floater and mooring line are investigated and upscaling procedure is proposed.
2. The semi-submersible floater for 2 MW used in Fukushima FORWARD project is upscaled that for 5 MW and 10 MW. The relationship between upscaling rule and floater motion or mooring force is investigated by dynamic analysis.
3. The levelized cost of energy is assessed by using upscaled floater and mooring line model.

Upscaling rule of turbine 6/18

	2 MW Bladed Demo	5 MW NREL	10 MW DTU
Rotor diameter	1	1.58	2.23
Turbine mass (RNA mass + Tower mass)	1	2.5	5
Hub height	1	1.22	1.57
Maximum thrust force	1	2.09	4.20
Maximum falling moment	1	2.52	5.26

※The diameter and thickness at tower bottom were enlarged by referring Fukushima 2MW wind turbine.

■ Rational upscaling ratio

$$P \sim s^2 \quad 1^2 : 1.58^2 : 2.23^2 = 1 : 2.5 : 5$$




$$m \sim s^3 \quad 1^3 : 1.58^3 : 2.23^3 = 1 : 3.9 : 11.1$$

The ratio of mass followed s^2 law due to technology progress (Sieros et al. 2012)
The ratio of maximum overturning moment followed s^2 law.

Upscaling rule of floater

7/18

Construction constrains

Draft	Freeboard	Diameter of main column
Dock size and port depth	Designed maximum wave height	The diameter of turbine tower bottom
		

Ref.) Fukushima FORWARD

Design criteria

Surge	Stiffness from mooring line
Heave	Balance between gravity and buoyancy
Pitch	Static pitch angle (The ratio of falling moment to restoring moment)

Construction constrain was prioritized for feasible upscaling.
The design criteria for floater motion was investigated.

Upscaling rule of mooring line

8/18

Design criteria: The allowable stress. (DNV-OS-E301)

Methodology of increasing allowable stress	Cost
Increase diameter of mooring line	↗
Increase number of mooring line	↗
Increase chain quality (strength) of mooring line (R3→R4→R5)	→

The design criteria for mooring force was investigated.

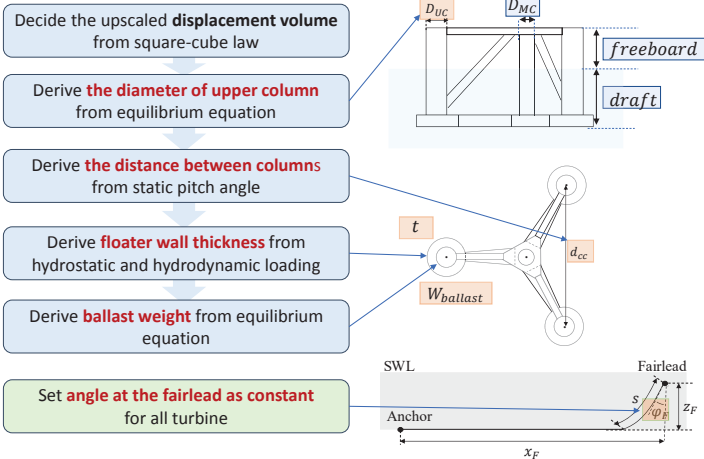
What is the relationship between upscaling and similarity law.

		Floater motion or mooring force	
Turbine	s^2 law ○	Constant	Satisfied
Floater	Kinematic similarity law ?	Decrease	Relaxed
Mooring line	Dynamic similarity law ?	Increase	Change quality

The rule for evaluation of the relationship between upscaling rule and FOWT was decided.

Upscaling procedure of floater

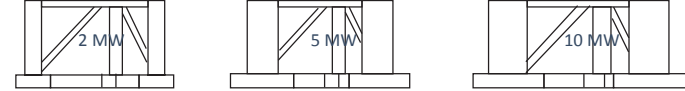
9/18



The upscaling procedure of floater and mooring line was proposed.

Static balance of upscaled floater

10/18



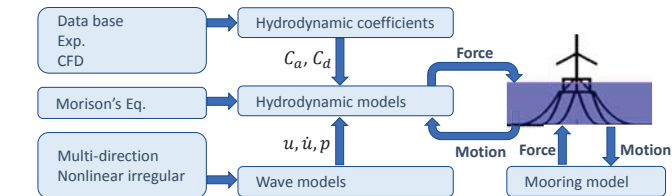
	Unit	2 MW	5 MW	10 MW
Constrains	Draft	[m] 21.3	21.3	21.3
	Freeboard	[m] 10.7	10.7	10.7
	Diameter of main column	[m] 5	6	6
Static balance in heave	Diameter of upper column	[m] 8	12	16
	The ballast weight	[kg] 3,118,971	9,802,573	22,690,528
Static balance in pitch	Moment of inertia of water plane area	[m ⁴] 58542	147526	307932
	Restoring moment in pitch direction	[kg · m ² /s ²] 588,431,626 (1)	1,482,847,699 (2.52)	3,095,150,356 (5.26)
	Distance between columns	[m] 47.3	50.2	54.3
	The angle at fairlead	[deg] 40	40	40
Static balance in surge				

The static balance was satisfied

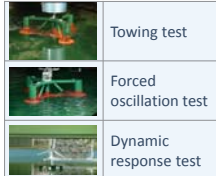
Dynamic analysis of FOWT system

11/18

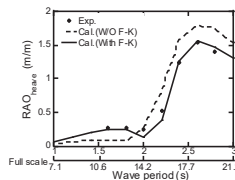
Zhang and Ishihara (2019) Renewable Energy



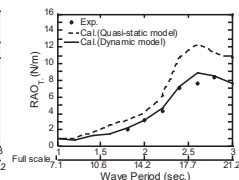
Series of water tank tests



Predicted floater motion



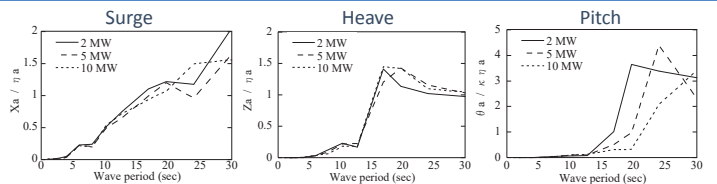
Predicted mooring force



Floater motion and mooring force prediction was validated by water tank test

Floater motion in DLC6.1

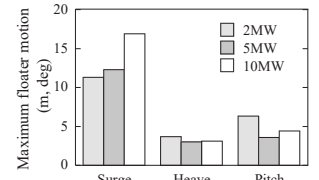
12/18



Kinematic law is relaxed in surge and pitch direction

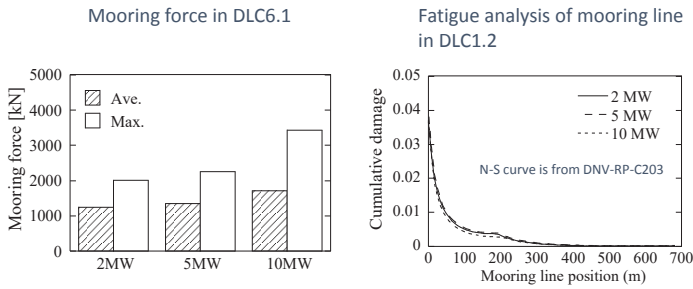
DLC6.1 Environmental condition

Wind	$U_{50} = 50 \text{ m/s}$	$I = 0.11$
Wave	$H_s = 11.7 \text{ m}$	$T_p = 14.76 \text{ sec}$
Current	$U_c = 1.44 \text{ m/s}$	



Mooring force in DLC6.1 and in DLC1.2

13/18



The maximum mooring force increased according to surge motion increase.

The cumulative damage due to fatigue were not affected by the turbine sizes.

Dynamic similarity is satisfied by changing the quality (strength) of mooring line

Assessment of levelized cost of energy

14/18

$$LCOE = \frac{ICC \times FCR + O\&M}{AEP}$$

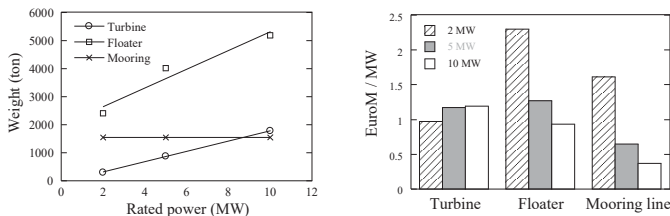
Item		Methodology
Initial Capital Cost	Material	Steel Weight × Cost per ton
	Installation	Vessel cost × Installation day ÷ Weather downtime Installation cost per turbine
Fixed Charge Rate	3 % interest	
Operation & Maintenance cost	Wind and wave time series, Work limit condition, Vessel cost, Turbine failure rate	
Annual	Capacity factor of 40 % and Availability of 90 %	

Assessed from constructed model

Assessed from demonstration project's experience

Estimation of material cost

15/18



The floater and mooring cost per MW decreased with turbine sizes.

	NTNU	Lisbon		Proposed		
		5 MW	10 MW	5 MW	10 MW	5 MW
Draft [m]	20.0	24.9	20.0	20.0	21.3	21.3
Upper column [m]	9.9	14.3	12.0	15.8	12.0	16.0
Distance b/w columns [m]	50	58.62	50.0	63.0	50.2	54.3
Floater steel weight [kg]	3,567,000 (1)	7,598,000 (2.13)	3,850,000 (1)	5,580,000 (1.45)	4,018,045 (1)	5,180,545 (1.29)
Mooring line length [m]	835	1045	835	835	673 × 2	673 × 2

Estimation of installation and O&M cost

16/18

Installation cost

<p>Turbine installation</p>  <p>0.92 €/turbine</p>	<p>Floater towing</p>  <p>0.92 €/turbine</p>	<p>Mooring installation</p>  <p>3.69 €/turbine</p>
---	--	--

Operation and maintenance cost

- ECN O&M Calculator was used
- Simulated wind and wave time series
- The work limit condition was 2 m significant wave height
- Turbine reliability was set from ReliaWind



Summary of estimated LCOE

17/18

	Unit	2 MW × 50	5 MW × 20	10 MW × 10
Design	[€/kW]	0.1	0.1	0.1
Wind turbine	[€/kW]	1.0	1.2	1.2
Floater	[€/kW]	2.3	1.3	1.0
Mooring line	[€/kW]	1.6	0.6	0.4
Installation cost	[€/kW]	2.8	1.1	0.5
Cable	[€/kW]	0.6	0.6	0.6
Initial Capital cost	[€/kW]	8.4	4.9	3.8
Annual O & M cost	[€/kW/year]	0.22	0.14	0.11
LCOE	[c/kWh]	32	19	15

The initial cost was reduced 45 % and 57 % respectively for 5 MW and 10 MW comparing to 2 MW turbine.

※ Here estimated Installation and O&M cost has uncertainty because the assumption was very simple.

Conclusions

18/18

- The upscaling rule of floating offshore wind turbine system was investigated from demonstration project experience and the procedure of upscaling was proposed.
- For floater, static balance was satisfied, but kinematic law was relaxed in surge and pitch direction. For mooring line, dynamic similarity was satisfied.
- By using engineering models and experience of demonstration projects, the initial cost was assessed for 2, 5, 10 MW turbines. The initial cost was reduced 45 % and 57 % respectively for 5 MW and 10 MW comparing to 2 MW turbine.

Acknowledgments

This research is carried out as a part of next-generation floating offshore project supported by National Energy Department Organization. Dr. Namba supported dynamic analysis. Wind Energy Institute of Tokyo provided turbine models. The authors wish to express their deepest gratitude to the concerned parties for their assistance during this study.



Wave Cancelling Semi-Submersible Design for Floating Offshore Wind Turbines

Frank Lemmer, Wei Yu, Kolja Müller, Po Wen Cheng

17.01.2019
EERA Deepwind 2019, Trondheim, Norway



Motivation



Papers of OMAE2016 and TORQUE2016 have shown:

- Wave loads are stronger than wind loads
- Wind turbine controller cannot cancel wave loads
- Wave loads are responsible for large portion of structural fatigue of platform/tower

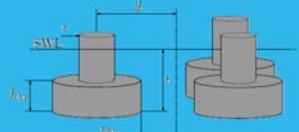
- How to design substructures which are
 - of sustainable lightweight structures
 - „grown into their ocean environment“
 - less excited by environmental loads



What we have done...

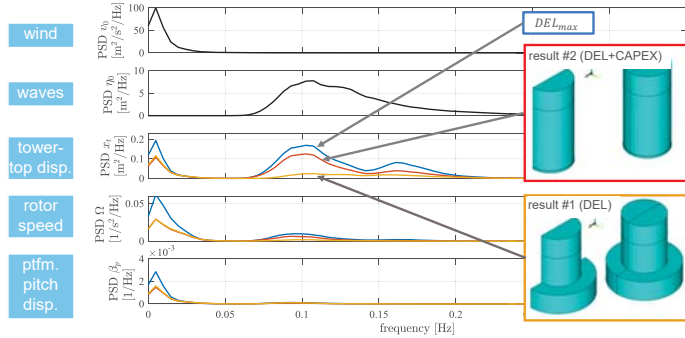
Parametric study of 3-column semi-submersibles in LIFES50+

- variable column spacing
- variable column diameter
- variable heave plate height

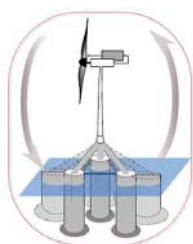


Lemmer, F., Müller, K., Yu, W., Faerron-Guzmán, R., & Kretschmer, M. (2016). LIFES50+ D4.3: Optimization framework and methodology for optimized floater design.

Past study

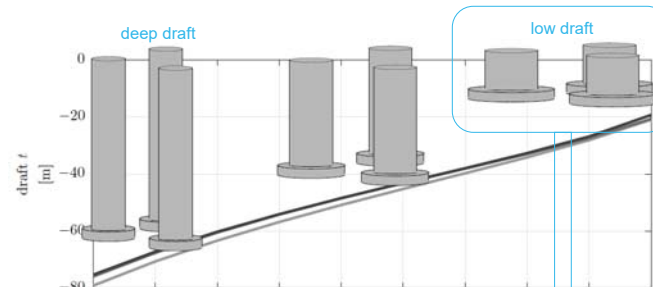


Present study



- Automated preprocessing of panel code coefficients
- Parametric low-order model (SLOW)
- Automatically adjusted controller
- KC-dependent heave-plate drag <http://dx.doi.org/10.3390/jmse6040118>

Present study

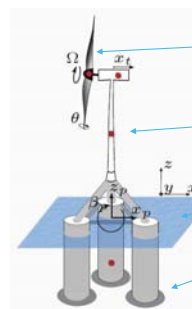


- >30% smaller tower-base bending damage than deep draft
- Electrical power shows no response to 1st order waves

Why do we end up with the low draft configuration?

Linear system analysis

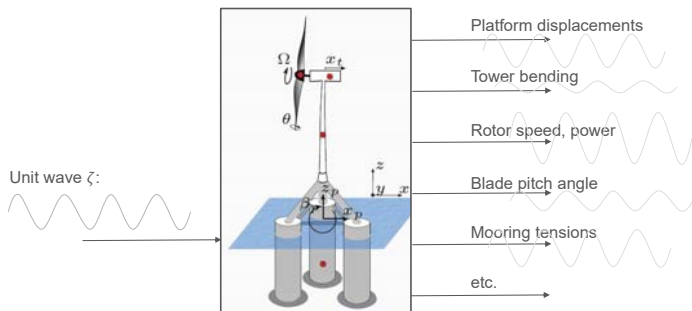
SLOW – Simplified Low-Order Wind turbine model



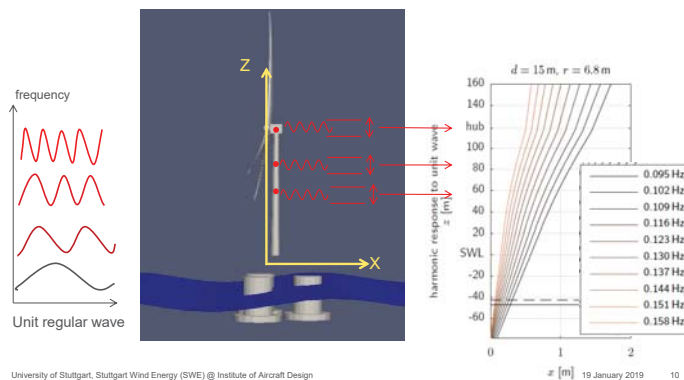
- Linearized aerodynamics, including controller
- Multibody dynamics, including elastic tower
- Linear potential flow hydrodynamics
- Linearized Morison drag (Borgman) with parametric heave plate drag
- 2D motion

Linear system analysis

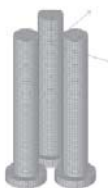
RAO using SLOW



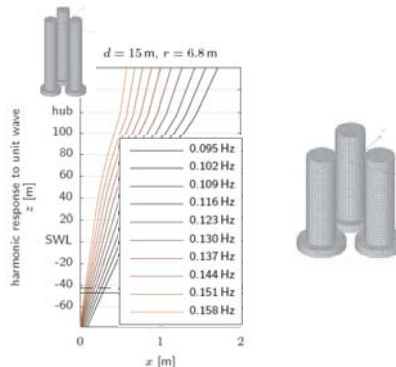
Harmonic Response to Wave



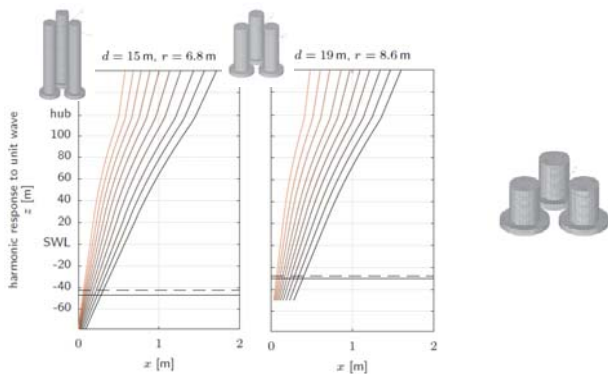
Harmonic Response to Wave



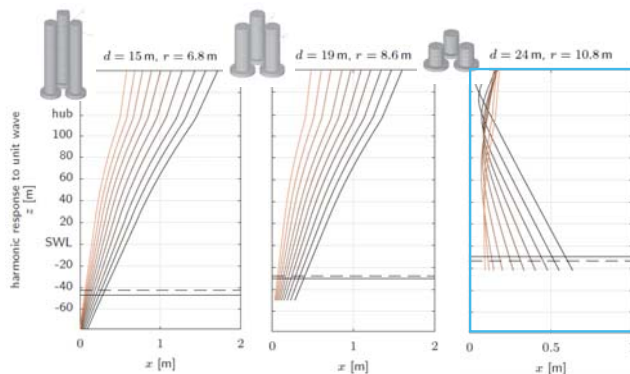
Harmonic Response to Wave



Harmonic Response to Wave

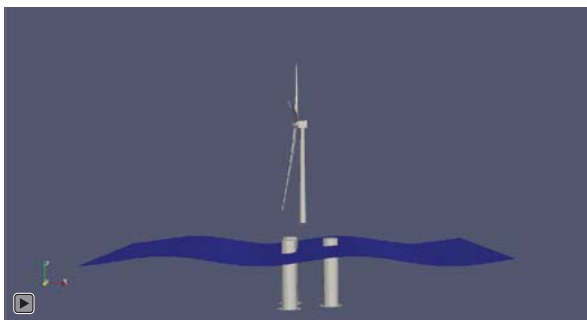


Harmonic Response to Wave



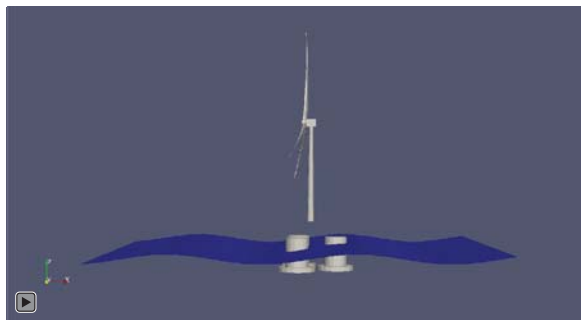
Response to regular waves

Reference design: TripleSpar



Response to regular waves

Optimal design: column spacing 24m, column diameter 21.6m

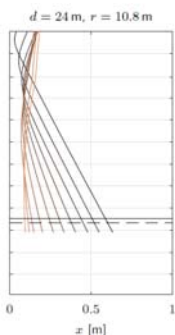


Counter-Phase Pitch Response

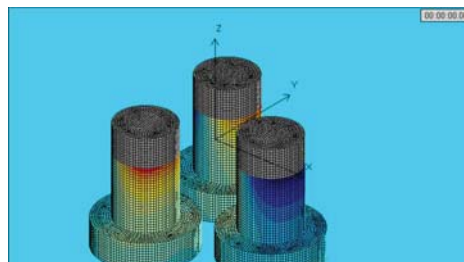
is caused by a favorable design for a given range of peak spectral frequencies

- Platform pitches negatively (into the wind) when surge-velocity is positive
- Turbine pitching about instantaneous center of rotation close to the hub

- Nacelle does not oscillate in fore-aft direction due to wave loads
- Waves have almost no effect on power production
- Tower-base fatigue is reduced by 30%, compared to TripleSpar, slightly larger than for onshore turbines



Counter-Phase Pitch Response



- Spatial magnitude phase distribution of mainly FK-forces yield the desired behavior for given frequencies and system dynamic properties
- Integrated Froude-Krylov+diffraction forces and phases are tailored for the system properties to yield the desired forced-response behavior

Counter-Phase Pitch Response

- Behavior used to be known for TLPs:



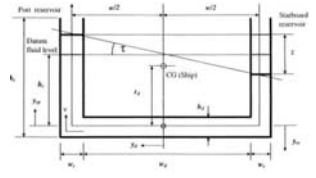
- TLP tendon kinematics impose center of rotation

➤ Here, the same effect is shown for semi-subs with catenary mooring lines



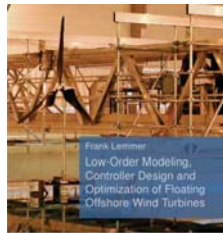
Conclusions


- Although controller cannot mitigate large wave loads, a good design can cancel the wave forces, giving a favorable response behavior
- A good hull shape, combined with a favorable controller, offers the possibility for new, lightweight platforms, which experience little fatigue and extreme loads using less material
- Further measures can improve the global response:
 - Tuned liquid column dampers (see Yu, OMAE2019)
 - Multivariable control (Lemmer, TORQUE2016)
 - Lidar-assisted control (Schlipf, ISOPE2013)




More details...

- Lemmer, F. (2018). *Low-Order Modeling, Controller Design and Optimization of Floating Offshore Wind Turbines*. University of Stuttgart. ISBN: 978-3-8439-3863-1
- Lemmer, F., Müller, K., Yu, W., & Cheng, P. W. (2019). Semi-submersible wind turbine hull shape design for a favorable system response behavior (submitted, revised version under preparation). *Marine Structures*.




University of Stuttgart

Thank you!



Wei Yu, MSc

e-mail yu@ifb.uni-stuttgart.de
 phone +49 (0) 711 685-68258
 fax +49 (0) 711 685-

University of Stuttgart
 Stuttgart Wind Energy (SWE)

Acknowledgements:
 Parts of the research leading to these results has received funding from the European Union's Horizon 2020 research and innovation programme under grant agreement No. 640741 (LIFES50+). The support is highly appreciated

LIFESSO+

Summary of LIFESSO+ project results: from the Design Basis to the floating concepts industrialization

Germán Pérez (TECNALIA)
german.perez@tecnalia.com

EERA DeepWind'19 - Deep Sea Offshore Wind R&D conference
Trondheim, 16 - 18 January 2019

Qualification of innovative floating substructures for 10MW wind turbines and water depths greater than 50m

The research leading to these results has received funding from the European Union Horizon2020 programme under the agreement H2020-LCE-2014-1-640741.



13. januar 2019

LIFESSO+

Outline

LIFESSO+ project overview

Project development and results

- First stage
- Second stage

Summary of results

13. januar 2019

LIFESSO+

LIFESSO+ project overview

Qualification of innovative floating substructures for 10MW wind turbines and water depths greater than 50m

OBJECTIVES:

- Optimize and qualify to a TRL 5, of two innovative substructure designs for 10MW turbines
- Develop a streamlined KPI-based methodology for the evaluation and qualification process of floating substructures

Grant Agreement: H2020-LCE-2014-1-640741


FOCUS:

- Floating wind turbines installed in water depths from 50m to 200m
- Offshore wind farms of large wind turbines (10MW) – identified to be the most effective way of reducing cost of energy in short term

BUDGET: 7.3 M€

DATES: 47 months duration, from 01 June 2015 to 30 April 2019.

Project leader: SINTEF Ocean



13. januar 2019

LIFESSO+

LIFESSO+ project approach

APPROACH

INPUT

5MW
FOUR FLOATING CONCEPTS

CONCEPT DEVELOPMENT

From four to two concepts

EXPERIMENTAL AND NUMERICAL INVESTIGATION

OUTPUT

10MW
TWO FLOATING CONCEPTS FOR

- Large wind turbines (10MW)
- Large water depths (>50m)
- TRL 5

RECOMMENDED PRACTICE AND GUIDELINES

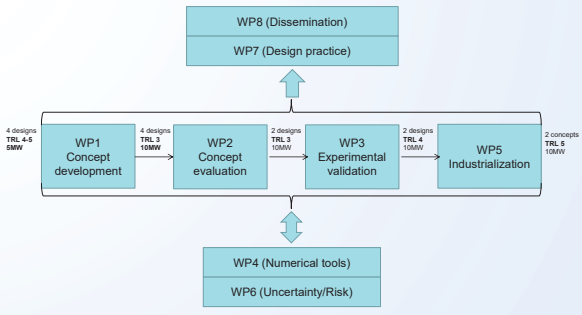
First stage: concepts design and evaluation

Second stage: numerical modelling and experiments; recommended practice and guidelines

13. januar 2019

LIFESSO+

Project work plan



13. januar 2019

LIFESSO+

Project development and results: first stage

First stage of the project focused on concepts design & evaluation...

- Definition of the Design Basis for the concepts design:
 - Identification of three sites and collection of information
 - Definition of the Wind Turbine reference model
 - Design requirements and load cases – DLCs
- Definition of the framework for the concepts assessment:
 - Scope and development of the tools for the LCOE, LCA and risk analysis evaluation
 - Agreement on the evaluation procedure
 - Information for the concepts assessment
- Concepts design
 - Sizing and structural design, mooring design, aero-hydrodynamic simulations
 - Adaptation of the WT controller
 - Analysis of marine operations, including manufacturing strategy

... and preparation of the experiments, and design practices

- Overview of current design procedures, numerical models, tools, methodologies and standards
- Preparation of the experiments:
 - Development of the Real-Time Hybrid Model testing for the wave tank experiments
 - Development of the wind tunnel experiments: hexapod and reduced scale wind turbine
- First steps in the concepts industrialization

13. januar 2019

Information for the concepts design

Sites selection and information



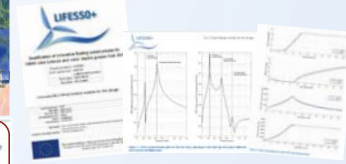
	50-year wind at hub height [m/s]	50-year significant wave height [m]	50-year on state peak period [s]	50-year current [m/s]	Extreme water level range [m]	Design Depth [m]	Soil Type
Site A	37	7.5	8-11	0.9	1.13	70	Sand/Clay
Site B	44	10.9	9-16	1.13	4.3	130	Sand/Clay
Site C	50	15.6	12-18	1.82	4.2	100	Basalt

13. Januar 2019

7

Wind Turbine information

- FAST model of DTU 10MW reference wind turbine
- Generic controller for the wind turbine.
- Tower reference design.



Design basis and DLCs

Main design criteria based on DNV-OS-J103

Public information available on the project's web site

Concepts design process

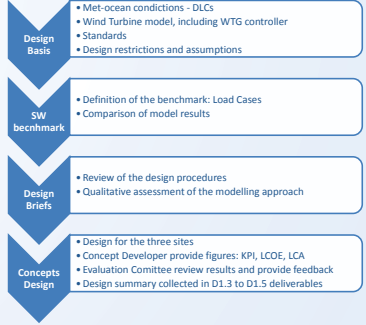
Concept developers used their own design procedures and codes, which were validated at different levels in the consortium, to ensure a common framework for their assessment.

Concepts design, driven by the information required for the evaluation:

- KPIs
- LCOE and LCA figures. Forms for 50 wind turbines wind farms -3 excel sheets-, one wind turbine -1 excel sheet- and 5 wind turbines -1 excel sheet-
- Uncertainty forms for each of the sites
- Information for risk analysis

LIFESSO+ Design Process conditioned for the concepts assessment and evaluation:

1. Onshore benchmark to validate WT models
2. 'Design references' to select and justify the Load Cases for each site and each concept
3. Design Briefs to validate the design process and the assumptions



13. Januar 2019

8

Concepts assessment

Development of **FWAT** assessment tool:

- LCOE (IREC)
- LCA (TECNALIA)
- Risk Assessment (ORE Catapult)
- Technical KPI report
- Comparison module using multi-criteria analysis considering uncertainty and statistical methods (IREC)



13. Januar 2019

9

Concepts assessment

1. **General frame for the calculations:** Description of the methodology and assumptions taken to perform the Evaluation (Common costs data used for the calculations/Onshore substation location/LCA background data)
2. **Several information submissions** were established in order to facilitate the concepts evaluation and improve concepts design.
3. **Concept designs results calculation:** Reporting of the individual results obtained by each design at each site.
4. **Ranking results:** Perform two-way ANOVA statistical test to examine the influence of two different factors (i.e. **concept** and **site**) on one continuous variable (LCOE).
5. **Evaluation workshop** for the final selection of two concepts to be modelled and tested in the second stage. Hosted by IREC in Barcelona, 08-10 March 2017.



13. Januar 2019

10

Risk assessment

Risk assessment as part of the concepts evaluation and for the future design optimization

- It was developed a **public methodology** for risks assessment of floating offshore wind substructures covering four areas: technical; health, safety and environment; manufacturing; commercialization.
- Risk register development, with some 100 risks for floating wind, covering all life cycle phases (Design, fabrication, transportation and storage, installation, commissioning, O&M, decommissioning) and different substructure types and primary materials, which was part of the concepts evaluation.
- Data confidentiality and objectivity** were the main challenges to carry out the risk assessment To solve this 1-2-1 risk identification workshops were organized with each developer at their facilities.
- WP6 engaged the industry interviewing different types of stakeholders (finance, WT OEMs, technology providers, insurance, etc.) on commercial risk identification.



13. Januar 2019

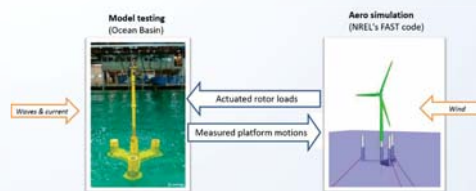
11

Experiments preparation

Wave Tank

Develop Real-Time Hybrid Model testing (Hardware in the Loop) for floating wind turbines:

- Controlled environment
- Flexibility
- Overcome Froude-Reynolds scaling issues



13. Januar 2019

12

Physical model in ocean basin with physical waves coupled in real-time to aerodynamics simulations (FAST).
The aero loads are applied on the model by use of actuators and the position of the model is measured in the basin and used as input to the numerical simulations.

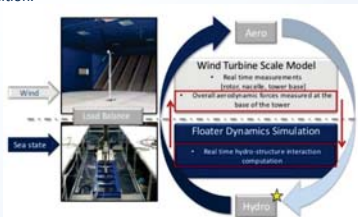
Experiments preparation



Wind Tunnel

Physical wind and wind turbine connected in real time to numerical hydro simulator.

A 6DOF robot at the tower base imposes the simulated platform motions. The loads at base of tower measured in the wind tunnel are used as input to the numerical simulations. The output of the simulations is the floater position.



13. Januar 2019

13

Industrialization



Design Brief describing procedures and methodologies that need to be addressed to develop an industrialized FOWT design process.

Identification of key design elements and challenges which are important for a FOWT design process to be addressed in order to arrive at an industrial reliable and efficient level applicable for industrial scale multiple-unit design.

Analysis of installation restrictions and simulation of different conditions regarding ports, distance to deployment site, types of vessels and weather windows. Identification of challenges and cost estimation.

FABRICATION - STEEL

Advantages	Challenges
<ul style="list-style-type: none"> Established in the offshore wind industry: <ul style="list-style-type: none"> Know-how existing Proven solutions and standards exist to avoid issues related to corrosion due to saltwater and salty air, wind turbine load, etc. Assembly can be executed relatively fast if components are pre-fabricated (consists of welding operations and positioning of the parts only) Lighter structures are possible (compared with concrete) Possibility of serial production in existing facilities for offshore wind monopile or jacket manufacturing 	<ul style="list-style-type: none"> Expensive material, price fluctuating Specialized equipment (e.g. large scale welding machines and cranes with sufficient lift capacity) required, shipyard preferable Large dimension component/parts: <ul style="list-style-type: none"> Need to be built at shipyards/factories, typically not at construction site, which is a challenge for mass production Heavy/large parts need to be transported to construction site, suitable access (road, railway, waterways) required Suitable storage area at port required

FABRICATION CONCRETE

Advantages	Challenges
<ul style="list-style-type: none"> Concrete local supply adaptable to local conditions and project requirements Ready-mix concrete <ul style="list-style-type: none"> Mobile batching plant Installation of a stationary batching plant at the construction site No specialized equipment, but large scale welding machines, required (construction at lower costs) Low costs of concrete is a raw material Ready-mix concrete only, low storage area required (no raw material has to be stored for batching at port) 	<ul style="list-style-type: none"> Limited use in offshore wind industry (Often) larger dimensions of concrete floaters require large construction area for mass production High weight of concrete floaters (restrictions to the bearing capacity and space) Concrete cannot bear tension loads, therefore additional procedures (e.g. pre-tensioning, avoiding of opening actions) necessary Wide range of weather restrictions for construction/drying process (e.g. no construction during frost or heavy rain) Mixing process at the construction site possibly more inaccuracy (additional quality assurance necessary)

13. Januar 2019

14

Design Practice and numerical models

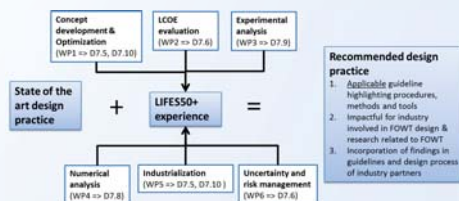


The aim is to develop recommended practices for FOWT design based on the state of the art and the project achievements in the design, modelling and experimental validation of the concepts.

First stage work focused on the analysis of the state of the art on design procedures and numerical models...

- Concept developers design procedures and tools
- Overview of the numerical models used in the consortium and their qualification
- Standards (application the definition of the DLCs for the concepts design)

...to define an optimization framework and methodology for optimized floater design.



13. Januar 2019

15

Summary of results for stage one



- Four concepts designed for the reference wind turbine and the selected sites (Design Basis), including all the information for the evaluation.
- Concepts evaluation and selection of two of them for the second stage.
- Preparation of the tools and methodologies for the experiments: Real-Time Hybrid Model testing for the wave tank experiments; hexapod and reduced scale wind turbine for the wind tunnel experiments.
- Analysis of current design procedures, numerical models, tools, methodologies and standards.
- Industrialization: performance evaluation of available simulation SW and existing design tools. Design Briefs.



13. Januar 2019

Second Stage



Second stage of the project focused on experiments and numerical modelling investigation

- Wave tank and wind tunnel experiments** using the selected concepts to:
 - Characterize the hydrodynamic and aeroelastic behavior of the two concepts
 - Validation of the Real-Time Hybrid Model testing
 - Validate the hardware in the loop methodology
- Numerical modelling** and analysis of the experimental results to calibrate the models.
- Analysis of **advance modelling** to reduce computational time while maintaining the results accuracy.
- Selected **concepts industrialization** analysis and design optimization. Re-calculation of the LCOE and LCA figures for the optimized designs.
- Recommended practices for FOWT design** based on the project achievements in the design, modelling and experimental campaigns.

Work ongoing with some interesting results so far.

13. Januar 2019

17

Wave tank experiments

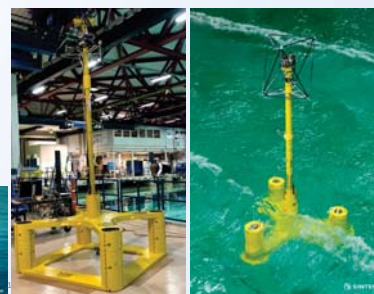
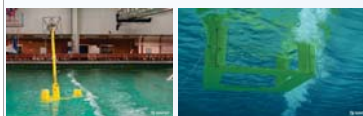


First step: scale models (1:36) preparation for Olav Olsen's OOstar and NAUTILUS semisubmersible concepts.

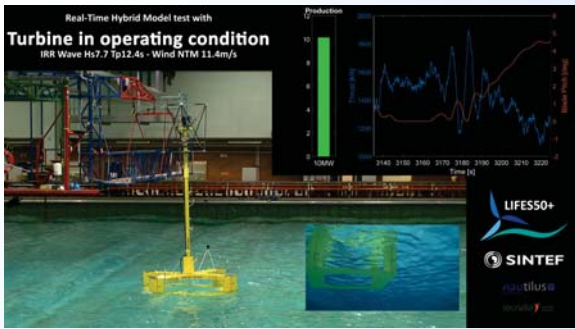
Numerical model adaptation for the Real-Time Hybrid Model testing (ReaTHM® testing) to generate realistic and controlled aerodynamic loads.

Load cases for the experiments.

- inclining tests,
- pullout tests,
- decay tests,
- pink noise (white noise) wave spectrum tests and regular wave,
- wind only tests,
- irregular wave tests



Wave tank experiments results



13. januar 2019

19

Wind tunnel experiments



First wind tunnel campaign carried out in July 2018 with Olav Olsen's OOSTAR concept.
Second wind tunnel campaign carried out in November 2018 with NAUTILUS concept.



13. januar 2019

20

Numerical modelling



Research on advanced numerical modelling.

Different numerical tools are required for different stages in the design of floating wind substructures.

First step: state of the art on numerical modelling

Public definition of selected floater concepts for the 10MW DTU WTG

- Public deliverable with the description of NAUTILUS steel semisubmersible and Olav Olsen concrete semisubmersible models for a 10MW wind turbine.
- FAST numerical models available on the project web site and DTU's repository.



13. januar 2019

21



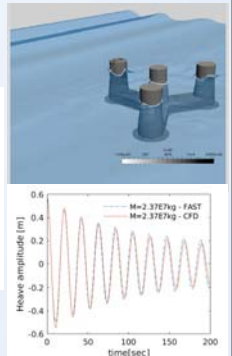
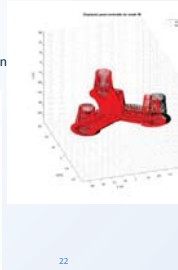
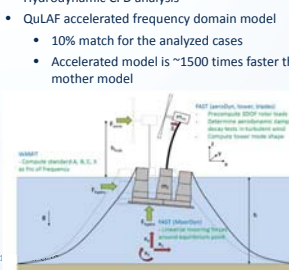
Figure 7: The OO Star floater (left) and the Nautilus floater (right). Figures provided by Ole Jacobs, Ole Olsen and Perter Fjording, Vestas, respectively.

Numerical modelling



...to continue with simplified and advanced modelling applicable to different stages of the design process

- Modelling of floater flexibility and second order forcing
- Hydrodynamic CFD analysis
- QuLAF accelerated frequency domain model
 - 10% match for the analyzed cases
 - Accelerated model is ~1500 times faster than mother model



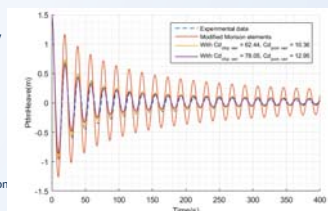
22

Numerical modelling



Numerical models calibration using experimental results

- Benchmark of the numerical tools against physical tests –wave tank-
- Assessment of the state-of-the-art and simplified numerical models for the two public floaters of the LIFESSO+ project: Olav Olsen's OOSTAR and NAUTILUS semisubmersible floating structures.
- Identification of the driving design load cases –DDLCS- and calibration for those cases.
- Public deliverable: D4.6 Model validation against experiments and map of model accuracy across load cases.
 - Calibration of hydrodynamic coefficients in time domain simulation is essential to achieve sufficiently accurate load predictions.
 - Simplified QuLAF and SLOW models provide a big benefit for concept and design studies in the initial stages of the design.



Comparison of heave decay simulation with experimental data for different FAST models - NAUTILUS concept.

13. januar 2019

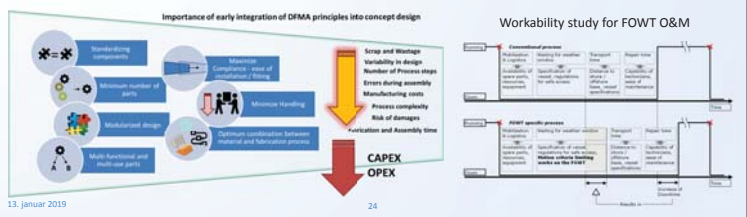
23

Industrialization



Ongoing work with two main objectives:

- Industrialization of the two floating concepts (OO Star and Nautilus) to reduce CAPEX/OPEX, considering floater mass production and identifying industrialization challenges.
- Development of an industry focused and cost-effective lean methodology for floater fabrication and installation, in close collaboration with concept developers, in order to improve manufacturing readiness - MRL at the same level as TRL-



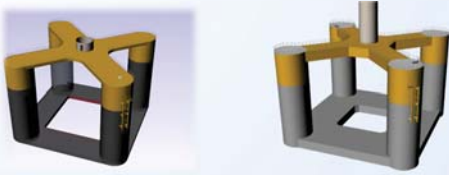
13. januar 2019

24

Concepts Design Optimization

Optimized design of the selected concepts:

- Taking advantage of the project achievements in experiments, numerical modelling and industrialization.
- Re-design for one of the sites and extrapolation to the other two.
- Optimized design in terms of hull, mooring and tower sizing; serial manufacturing; T&I; O&M.
- Updated figures for the LCOE and LCA calculation.



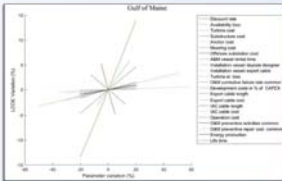
13. Januar 2019 25

Design Practices

Several activities focused on the development of design practices for FOWT

Generalized LCOE assessment and sensitivity analysis across different platform concepts.

- Determination of most influencing parameters on different FOWT platforms
- Identification of design dependent parameters



Guidance on platform and mooring line selection, installation and marine operations

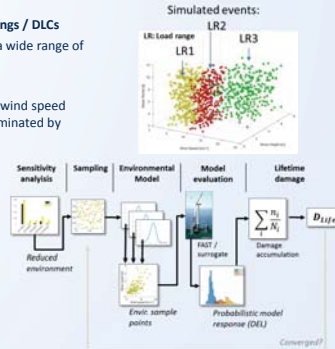
- Mooring design key findings (design, standards, tools, steel chain moorings, hybrid solutions, manufacturing, installation, etc.)
- Analysis on large wind turbines (dynamic cable, number of mooring lines, additional elements)

13. Januar 2019 26

Design Practices

Sensitivity analysis & determination of relevant simulation settings / DLCs

- Goal: determine the critical environmental conditions across a wide range of variables, using FAST simulations & Monte Carlo sampling
- Results:
 - Small wind speeds: increase of fatigue loading dominated by wind speed
 - Larger wind speeds (>= rated): increase of fatigue loading dominated by increasing wave heights.
 - Large wave heights: added impact from wave period



Probabilistic fatigue load assessment

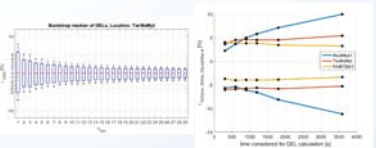
- Goal: consider full uncertainty and reduce safety gap
- Results:
 - FAST simulations & Monte Carlo sampling
 - High accuracy for given site and concept
 - Surrogate model & Monte Carlo sampling
 - Fast results for arbitrary sites and given concept

13. Januar 2019 27

Design Practices

Determination of relevant simulation settings

- Provides recommendations on how to verify the load simulation set up.
- Focus on DLC 1.2, 1.6, 6.1.
- Based on statistical analysis.
- Analysis of the effect of simulation length



- Pre-simulation initial conditions
 - Set up of initial conditions for a simulation
- Run-in time
 - Simulation time to be later disregarded due to initial transients
- Sensitivity to environmental parameters
 - Determination of the important parameters for load calculations
 - Separate: peak shape parameter, marine growth
- Number of seeds needed
 - Variation of seed for fatigue load calculations
- Effect of simulation length
 - Trade-off between shorter simulations on the results of the ultimate and fatigue load


13. Januar 2019 28

Summary of results and dissemination

68 deliverables, 39 of them being public, including numerical models of the two selected floaters and DTU's 10 MW wind turbine. Public deliverables available on the project web site www.lifes50plus.eu

More than 80 dissemination activities carried out so far including:

- Posters and presentations in conferences
- Articles in different types of journals
- Project newsletter on the web site
- Wave tank experiments presentation
- Press releases
- Youtube video
- ... and much more coming soon!!



Design practice

The work package will describe, evaluate and summarize the process and activities of all work packages related to design practice throughout the entire project in a bi-monthly dissemination strategy, design practice (DP) in the design and qualification of large FOWT structures to support the iterative process of the learning by testing a demonstrator in the field through the design to reduce the design, safety or manufacturing design process and activities for testing, offshore and onshore activities will be performed. Additionally, research dissemination, based on the design and manufacturing process will be shared with other work packages of the demonstrator and/or project partners of the other test packages.

- Deliverable 11: Review current guidelines on design practice (2018)
- Deliverable 12: Design rules (2018)
- Deliverable 14: Standardized FOWT design practice and guidelines (2018)
- Deliverable 18: Design practice (2019)

Experimental studies

The work package will focus on the feasibility, safety, and performance of four selected substructures of the first designed and built the test package. The study is focusing techniques for testing offshore wind turbines and the proposed design practice represents the current status of the offshore research. The work package will focus on how and when and how often tests on the substructure of an offshore wind turbine substructure should be performed and on how to control the tests.

- Deliverable 13: Test conditions and test (2018)
- Deliverable 14: Test results and test (2018)
- Deliverable 15: Test results and test (2018)

Qualification of numerical tools

The work package will focus on the qualification of numerical models and their ultimate use in design optimization and design validation. It will identify approaches to obtain confidence based on the use of the numerical models which is a challenge due to design methods. Several different models will be tested and compared to design rules and experimental results. An experimental test will be performed to compare the numerical models with the test results. The test results will be used to validate the numerical models and to identify the most influential parameters for the design practice. The work package will focus on how and when and how often tests on the substructure of an offshore wind turbine substructure should be performed and on how to control the tests.

- Deliverable 16: Test conditions and test (2018)
- Deliverable 17: Test results and test (2018)
- Deliverable 18: Test results and test (2018)
- Deliverable 19: Test results and test (2018)
- Deliverable 20: Test results and test (2018)
- Deliverable 21: Test results and test (2018)
- Deliverable 22: Test results and test (2018)
- Deliverable 23: Test results and test (2018)
- Deliverable 24: Test results and test (2018)
- Deliverable 25: Test results and test (2018)
- Deliverable 26: Test results and test (2018)
- Deliverable 27: Test results and test (2018)
- Deliverable 28: Test results and test (2018)
- Deliverable 29: Test results and test (2018)
- Deliverable 30: Test results and test (2018)
- Deliverable 31: Test results and test (2018)
- Deliverable 32: Test results and test (2018)
- Deliverable 33: Test results and test (2018)
- Deliverable 34: Test results and test (2018)
- Deliverable 35: Test results and test (2018)
- Deliverable 36: Test results and test (2018)
- Deliverable 37: Test results and test (2018)
- Deliverable 38: Test results and test (2018)
- Deliverable 39: Test results and test (2018)
- Deliverable 40: Test results and test (2018)
- Deliverable 41: Test results and test (2018)
- Deliverable 42: Test results and test (2018)
- Deliverable 43: Test results and test (2018)
- Deliverable 44: Test results and test (2018)
- Deliverable 45: Test results and test (2018)
- Deliverable 46: Test results and test (2018)
- Deliverable 47: Test results and test (2018)
- Deliverable 48: Test results and test (2018)
- Deliverable 49: Test results and test (2018)
- Deliverable 50: Test results and test (2018)
- Deliverable 51: Test results and test (2018)
- Deliverable 52: Test results and test (2018)
- Deliverable 53: Test results and test (2018)
- Deliverable 54: Test results and test (2018)
- Deliverable 55: Test results and test (2018)
- Deliverable 56: Test results and test (2018)
- Deliverable 57: Test results and test (2018)
- Deliverable 58: Test results and test (2018)
- Deliverable 59: Test results and test (2018)
- Deliverable 60: Test results and test (2018)

13. Januar 2019 29

Project Management

- LIFESSO+ has been very ambitious with a high level of activity from the project kick-off.
- The competitive nature of the project –stage one- has provided an interesting dynamic driving the work forward and motivated the participants to do their best.
- Partners have delivered very good results and reached agreements on important topics, like the concepts evaluation.
- Good collaboration atmosphere and high quality results, with important public results –i.e. numerical models of two FOWT-
- A project extension has been granted: new end date 30 April 2019.
- Final project event during WindEurope 2019 conference.

13. Januar 2019 30



F) Wind farm optimization

Analysis of wake effects on global responses for a floating two-turbine case, A. Wise, NTNU

Effect of Wake Meandering on Aeroelastic Response of a Wind Turbine Placed in a Park,
B. Panjwani, SINTEF

Effect of wind flow direction on the loads at wind farm, R. Kazacoks, Strathclyde University

How Risk Aversion Shapes Overplanting in Offshore Wind Farms, E.B. Mora, EDF Energy R&D

Analysis of wake effects for a floating two-turbine case

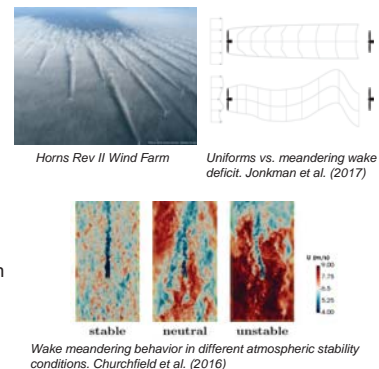
Adam Wise, Erin Bachynski
Department of Marine Technology, NTNU

EERA DeepWind'19, 16-18 January 2019, Trondheim, Norway

Norwegian University of Science and Technology

Motivation

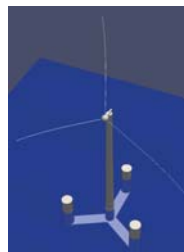
- Wake effects have been observed for many years
- Recent developments in modeling wake meandering
- Little published work on floating wind turbine (FWT) wake interaction
 - How will slow meandering movement affect structures with long natural periods?



Approach

- Two 10 MW semi-submersible FWTs modeled in FAST.Farm
- Moderate environmental conditions with synthetically generated turbulent inflow from TurbSim and the Mann Model
- Compare platform motions and fatigue damage in the tower and mooring lines in the upstream and downstream FWTs

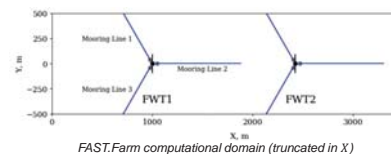
OpenFAST and FAST.Farm Model



Computational model of the CSC 10 MW visualized in OpenFAST

CSC 10 MW natural periods in SIMA and OpenFAST

Degree of Freedom	SIMA	OpenFAST
Surge (s)	88.3	85.1
Pitch (s)	26.3	24.8
Yaw (s)	60.4	58.5
Controlled pitch and tower bending (s)	2.4	2.5, 2.9

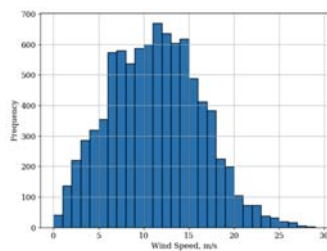


FAST.Farm computational domain (truncated in X)

Environmental Conditions



Location of reference wind site - Site 14. Li et al. (2013)



Frequency of hub height wind speeds at Site 14

Selected environmental conditions

H_s (m)	T_p (s)	U (m/s)	TI (%)	Shear Exponent (-)
2.5	9.5	10	15.72	0.055

Ambient Wind Generation

- Method 1 (Kaimal – Coh u):
 - Turbsim, Kaimal turbulence model, spatial coherence only in u
- Method 2 (Kaimal – Coh u, v, w):
 - Turbsim, Kaimal turbulence model, spatial coherence specified in $u, v,$ and w
- Method 3 (Mann):
 - HAWC2 precursor, Mann turbulence model, spatial coherence in all three dimension inherit to the model

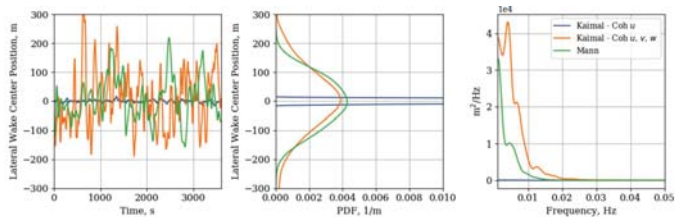
Exponential spatial coherence function in the Kaimal turbulence model:

$$Coh_{i,j,k} = \exp\left(-a_k \sqrt{\left(\frac{fr}{u_{hub}}\right)^2 + (rb_k)^2}\right)$$

Spatial coherence parameters specified in TurbSim

Model name	a_u	b_u	a_v	b_v	a_w	b_w
Kaimal - Coh u	12.0	3.5273E-4	∞	0.0	∞	0.0
Kaimal - Coh u, v, w	10.0	0.0	7.5	0.0	7.5	0.0

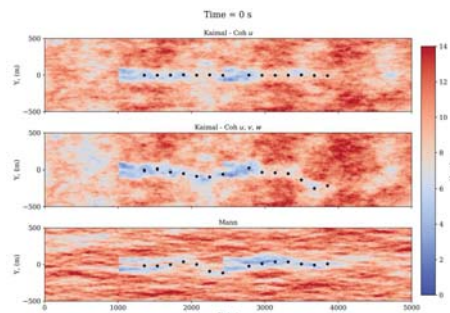
Wake Meandering



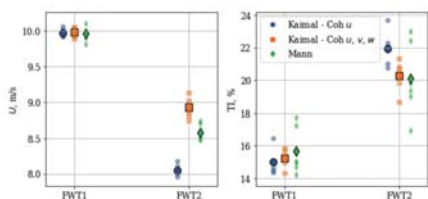
- Method 1 results in a uniform, axial wake deficit
- Methods 2 and 3 result in significant meandering with Method 2 having greater variance and somewhat higher frequency movement

Wake Visualizations – XY Plane

- Lateral meandering is sensitive to spatial coherence in u and v
- Longer coherent shapes in the Mann Model



Velocity Deficit, Turbulence, and 3P



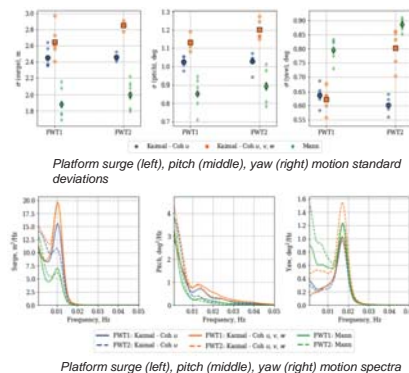
Mean 3P frequencies of each FWT

	FWT1	FWT2
Kaimal - Coh u	0.387 Hz	0.336 Hz
Kaimal - Coh u, v, w	0.387 Hz	0.345 Hz
Mann	0.386 Hz	0.358 Hz

- Velocity deficit is correlated with variance in upstream FWT's lateral wake center
- Mean 3P frequencies are close to the coupled pitch and tower bending frequencies

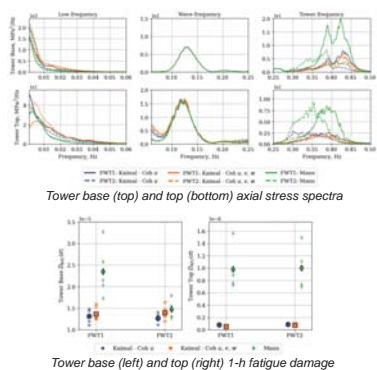
Platform Motions

- Increased surge, pitch, and yaw motions driven by low-frequency response
- Mann Model results in lower surge and pitch and greater yaw motions



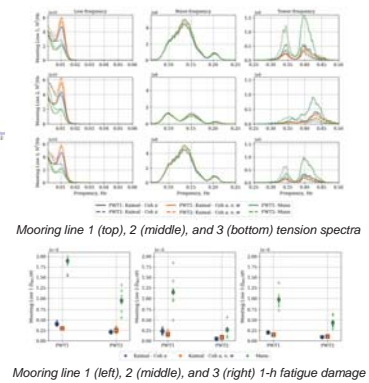
Fatigue - Tower

- Increased low-frequency structural loading does not necessarily translate to increased fatigue damage
- Responses in the 3P range contribute to the fatigue damage due to their large number of cycles



Fatigue - Mooring

- Similarly affected by responses at 3P
- Mean roll offset increases the stiffness in mooring line 1 resulting in greater high-frequency excitation



Conclusions

- Spatial coherence of v - and w -velocity components affect wake meandering behavior
- Low-frequency meandering movement translates to increased low-frequency surge, pitch, and yaw motions
- Increased fatigue damage due to meandering was observed in the top of the tower, but other results were sensitive to 3P

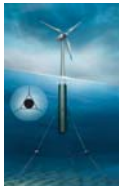
13

Future Work

- Model an FWT with a more representative structural design of the tower, or with modifications made to the controller
- Comparison with other types of FWTs
- Additional load cases and with more rigorous generation of synthetic turbulent inflow



*Lifes50+ OO-Star
Wind Floater*

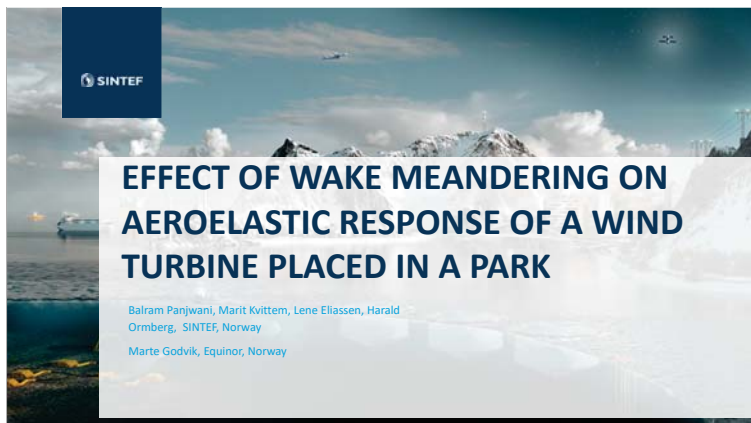


Generic spar FWT

14

Thank you for your attention

Adam Wise
adamsw@stud.ntnu.no



EFFECT OF WAKE MEANDERING ON AEROELASTIC RESPONSE OF A WIND TURBINE PLACED IN A PARK

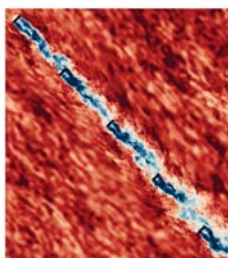
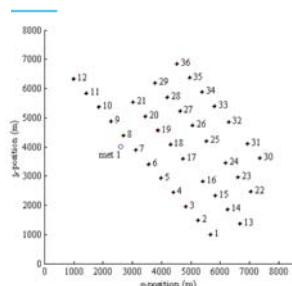
Balram Panjwani, Marit Kvittem, Lene Eliassen, Harald Ormberg, SINTEF, Norway
Marte Godvik, Equinor, Norway

Outline

- Introduction
- Standalone tool (Disturbed Inflow Wind Analyzer: **DIWA**)
- Benchmarking with literature data (HAWC2, SOWFA, FastFarm)
- Power verifications
- Aeroelastic simulations (SIMA-DIWA) and benchmarking with Lillgrund farm data
- Aeroelastic simulation of NREL 5MW turbine
- Conclusions

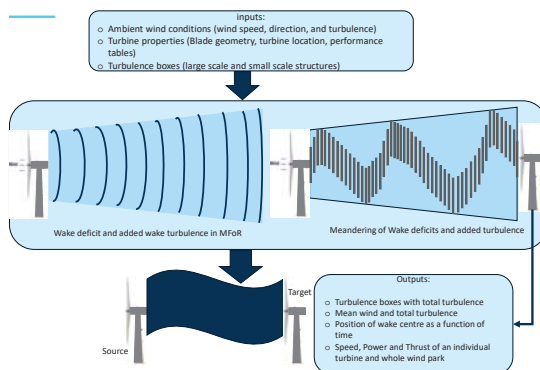
2

Why Meandering is important?



LES SOWFA results*

SIMA-DIWA Concept



4

DIWA Standalone

Start Wake Deficit Models/Near Wake

- Induction profiles based on Blade Element Method (BEM)
- Near wake profiles and Near wake length model

$$r_{w,j+1} = \sqrt{\frac{(1-a_j)}{(1-2a_j)} (r_{w,j}^2 - r_{t,j}^2) + r_{t,j}^2}$$

$$U_{w,j} = \left(\frac{r_{w,j+1} + r_{w,j}}{2} \right) U_0 (1 - 2a_j)$$

Far wake Model (MFOR)

- Discretized thin shear Navier-Stokes (NS) Equations

$$U \frac{\partial U}{\partial x} + V_r \frac{\partial U}{\partial r} = \frac{v_t}{r} \frac{\partial}{\partial r} \left(r \frac{\partial U}{\partial r} \right)$$

- Continuity equation $\frac{\partial U}{\partial x} + \frac{1}{r} \frac{\partial}{\partial r} (rV_r) = 0$

5

Eddy viscosity model

- The eddy viscosity is modelled using the following algebraic equation

$$v_t' = F_2 k_2 \left(\frac{b}{R} \right) (U_0 - U_{def,min}) + F_1 k_1 I_{amb}$$

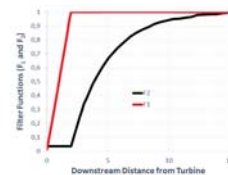
- Filter function plays important role in deficit calculations

- Three filter functions
- FastFarm filter functions : 8 calibration parameters

- Effect of atmospheric stability is introduced

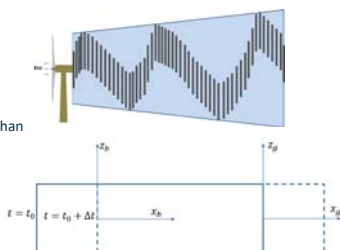
$$v_t = v_t' \frac{dy/dr_{total}}{dy/dr_{dyn}}$$

6



Wake meandering model in DIWA

- Two hypothesis
 - Meandering due to large scale eddies (Plume behaviour)
 - intrinsic instabilities of the wakes (flow behind bluff bodies)
- Current implementation is based on the first hypothesis
- Wake deficits are assumed as a tracer and eddies larger than the rotor diameter are responsible for meandering
- Wake centre position of the deficit



$$x_{c+1} = x_c + U \Delta t$$

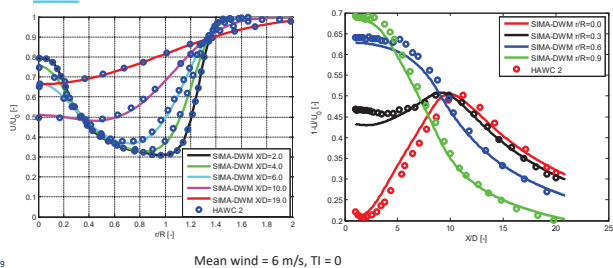
$$y_{c+1} = y_c + v_f(U[T-t_i], y_c, z_c) \Delta t$$

$$z_{c+1} = z_c + w_f(U[T-t_i], y_c, z_c) \Delta t$$

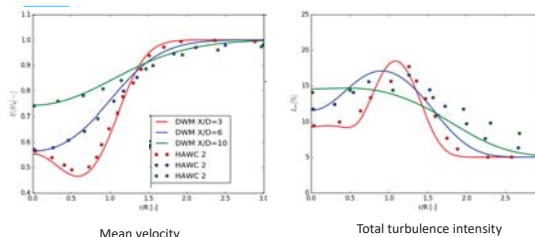
DIWA verification and validation

- Velocity Deficits and turbulence verification of a turbine with HAWC2 data (**Literature data**)
- Benchmarking with Fast Farm and SOWFA
- Power verification of a single (two turbines in row) and double wake scenario (three turbines in a row)
- Lillgrund wind farm

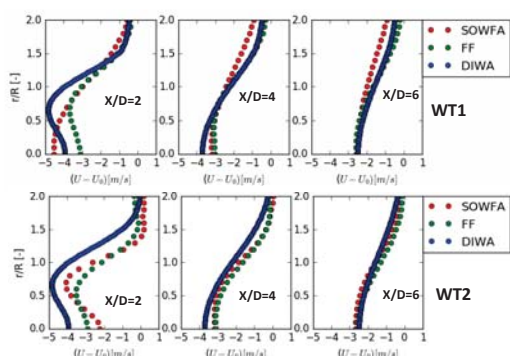
Verification without atmospheric Turbulence (NM 80 wind turbine)



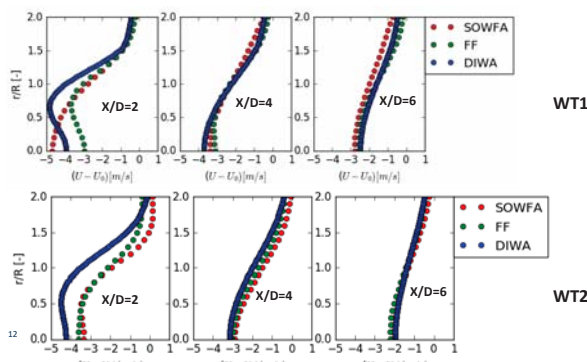
Mean velocity and total turbulence intensity (Wind speed 8 m/s TI 5%, NM80)



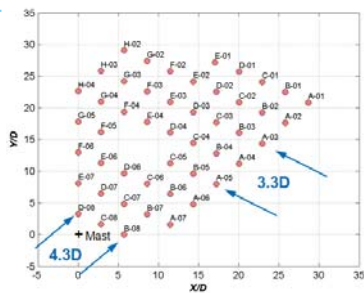
Validation with FastFarm (FF) and SOWFA (8 m/s, Ti = 6%)



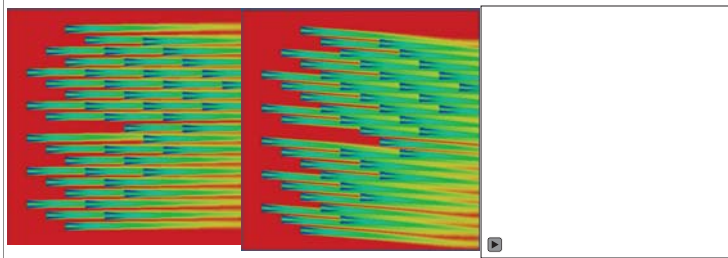
Validation with FF and SOWFA (8 m/s, Ti = 10%)



Flow visualization and power verification (Lillgrund Park)



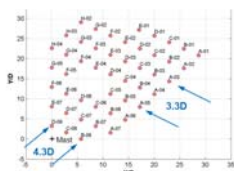
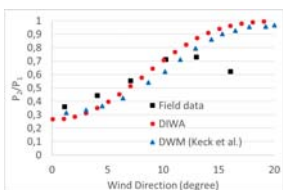
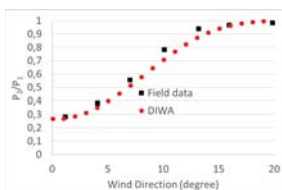
Visualization of flow field (Meandering)



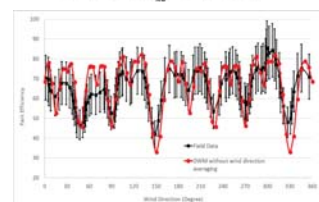
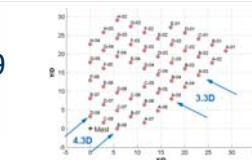
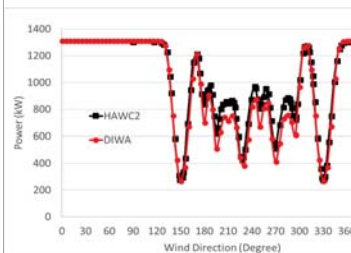
t=10s t=100s

Mean wind 8 m/s, TI=6%

Lillgrund Single wake (two/three turbines in row)



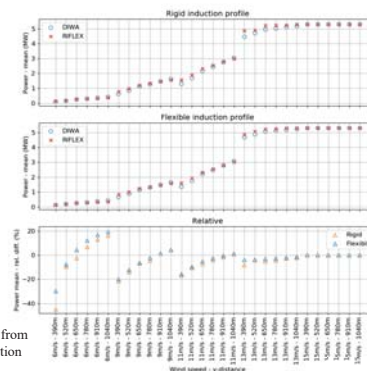
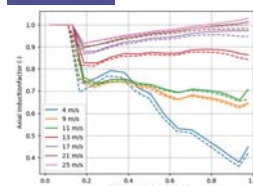
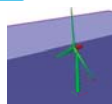
Power Verification: C8 turbine and full park (V=9 m/s; TI = 6)



Aeroelastic simulations

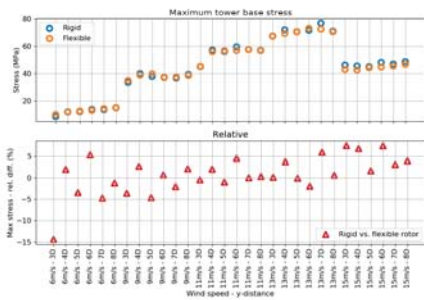
- SIMA Reflex is an advanced tool for static and dynamic analysis of structures.
- Wind boxes were created using DIWA code
- Two NREL 5MW turbines in a row
- Six simulations were performed for each wind direction
- Damage equivalent loads were calculated using SIMA-DIWA

NREL 5MW turbine

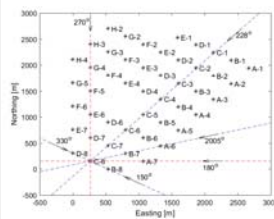
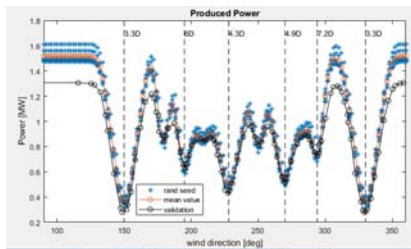


Axial induction profiles for the NREL 5MW derived from aeroelastic analysis. The dashed lines show the induction profiles for rigid blades calculated by DIWA.

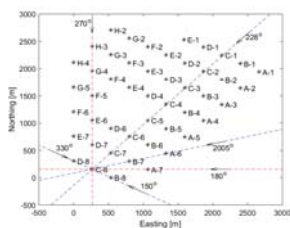
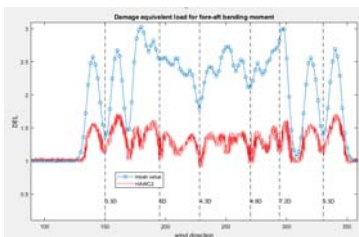
Rigid vs. flexible rotor in aeroelastic simulations



Benchmarking Lillgrund, power



Benchmarking Lillgrund, DEL (ongoing)



Conclusions

- Two hypothesizes for the wake meandering are identified based on the literature study.
- Most of the design codes are based on the first hypothesis.
- "SIMA-DIWA" is benchmarked against the literature data
- The study indicates that the eddy viscosity model parameters play quite an important role in wake deficits.
- The trends of fatigue loads are predicted well, with a few exceptions.
- More work is needed towards improving the eddy viscosity model

Acknowledgement

The work was performed at SINTEF, Norway under a project funded by **Equinor ASA, Norway**. The authors gratefully acknowledge the financial support received from the **Equinor ASA, Norway**.

The authors also want to thank Dr. Jason Jonkman and Nicholas Hamilton from NREL, for providing the SOWFA and FastFarm data.



Effect of wind flow direction on the loads at wind farm

Romans Kazacoks
Lindsey Amos
Prof William Leithead

Objectives:

- Investigate the effect of wind flow direction on the wind turbine loads (fatigue) within a wind farm.
- Two layouts are considered as depicted in Figure 1.
- Wind flow direction ($\epsilon \in [0 : 10 : 90]$) as shown in Figure 2

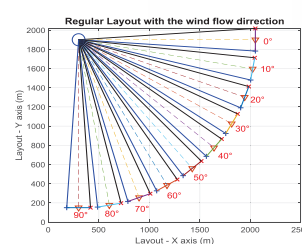
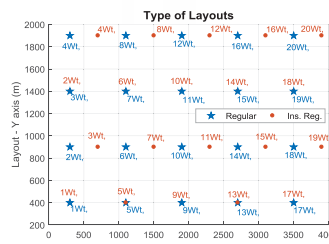


Figure 1: Two layouts of this study (Regular - blue star, Installed regular - red dot).

Figure 2: Wind low direction.



Strathfarm simulation tool:

StrathFarm is the University of Strathclyde's wind farm modelling tool:

- Models wakes and wake interactions.
- Models the turbines in sufficient detail that tower, blade and drive train loads are sufficiently accurate to estimate the impact of turbine and farm controllers on loads.
- Includes commercial standard turbine controllers.
- Includes a wind farm controller.
- Provides very fast simulation of large wind farms; run in real time with 100 turbines.
- Full flexibility of choice of farm layout, choice of turbines & controllers and wind conditions, direction, mean wind speed and turbulence intensity.



Validation of StrathFarm:

Comparison between 5MW Supergen model in StrathFarm (Red line) and 5MW Supergen model in DNV-GL Bladed (Black line).

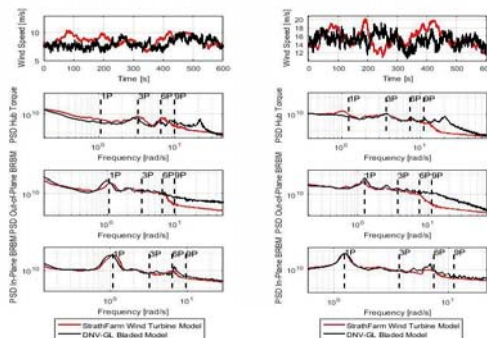


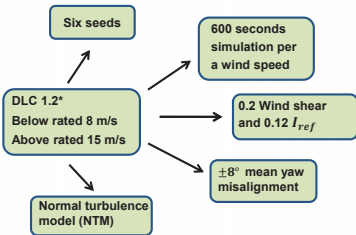
Figure 3: corresponds to a mean wind speed of 8 m/s

Figure 4: corresponds to a mean wind speed of 15 m/s

wind field time series
PSD of output hub torque
PSD of out-of-plane bending moment
PSD of in-plane bending moment
* PSD – Power spectral density



Procedure for estimation of fatigue loads:



- DLC 1.2: design load case – wind turbine is in power production range and connected to the electrical load at normal turbulence model (NTM).
- This study uses 20% power of curtailment for all machines within the wind farm

The damage equivalent loads (DELs) represent the fatigue loads in this study

$$L_{DEL} = \left(\frac{\sum_{ip} (\sum_i n_i L_i^m)}{t_{sim} f} \right)^{\frac{1}{m}}$$

Where, n_i is number of cycles, L_i is load range at bin, m is Wöhler coefficient, t_{sim} is simulation time and f is the reference frequency

- Wöhler coefficient 4 – steel
- Wöhler coefficient 10 – composite



Results for regular layout:

Each figure includes four different conditions as shown below:

- Below rated wind speed (8 m/s) with turbulence (0.12 I_{ref}) and no curtailment.
- Below rated wind speed (8 m/s) with turbulence (0.12 I_{ref}) and 0.2 curtailment.
- Above rated wind speed (15m/s) with turbulence (0.12 I_{ref}) and no curtailment.
- Above rated wind speed (15m/s) with turbulence (0.12 I_{ref}) and 0.2 curtailment.

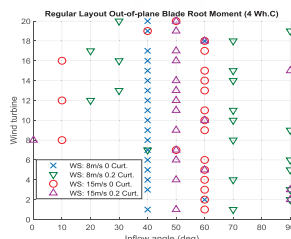


Figure 5: Out-of-plane blade root DELs at Wöhler coefficient 4 for the regular layout.

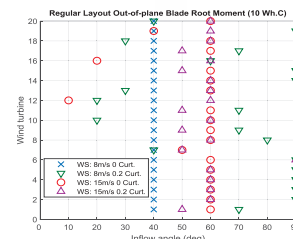


Figure 6: Out-of-plane blade root DELs at Wöhler coefficient 10 for the regular layout.

Results for installed regular layout:



Each figure includes four different conditions as shown below:

- Below rated wind speed (8 m/s) with turbulence (0.12 Iref.) and no curtailment.
- Below rated wind speed (8 m/s) with turbulence (0.12 Iref.) and 0.2 curtailment.
- Above rated wind speed (15m/s) with turbulence (0.12 Iref.) and no curtailment.
- Above rated wind speed (15m/s) with turbulence (0.12 Iref.) and 0.2 curtailment.

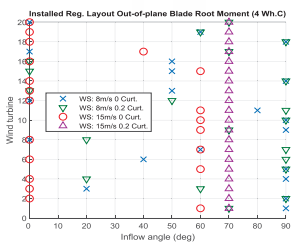


Figure 7: Out-of-plane blade root DELs at Wöhler coefficient 4 for the installed regular layout.

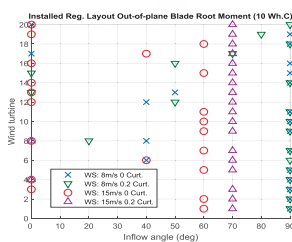


Figure 8: Out-of-plane blade root DELs at Wöhler coefficient 4 the installed regular layout.

Power efficiency:



The effect of wind flow direction on the power efficiency of a wind farm for the regular and installed regular layouts.

$$Eff_{power} = \frac{\text{energy of whole wind farm}}{(\text{energy of one isolated turbine}) * (\text{number of Wts in farm})}$$

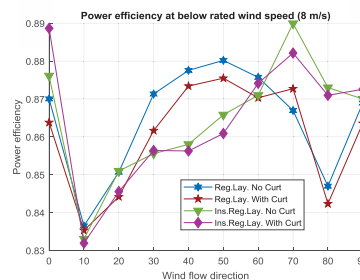


Figure 9: Changes power efficiency as a function different wind flow angle (0:10:90°) for the three layouts

Conclusion:



Key findings:

- Highest power efficiency and fatigue loads occur at same wind flow angles.
- Majority of the highest fatigue loads occur in the range 40 to 70 degrees.
- Power efficiency gets higher with larger spacing among the wind turbines in the layout.
- Uncertainty in results still high with 6 runs of 1250 seconds.

Future work:

- Longer simulation times required to reduce uncertainty
- Validation of results required, particularly by direct comparison to actual performance of a real wind farm.

The University of Strathclyde is a charitable body, registered in Scotland, with registration number SC05263

How does risk aversion shape overplanting in the design of offshore wind farms?





Esteve Borràs Mora^{1,2} James Spelling² Adriaan H. van der Weijde³

¹Industrial Doctoral Centre for Offshore Renewable Energy (IDCORE), University of Edinburgh
Edinburgh, EH9 3JL, UK

²EDF Energy R&D UK Centre
Interchange, 81-85 Station Road, Croydon, CR0 2AJ, UK



³University of Edinburgh School of Engineering and the Alan Turing Institute
Faraday Building, The King's Buildings, Mayfield Road, Edinburgh, EH9 3DW, UK

EERA DeepWind'19 Trondheim, 16-18 January 2019

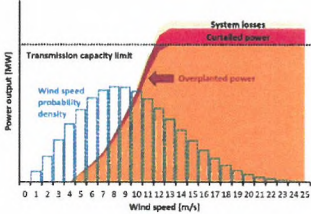
Outline

- 1 Motivation
 - o Overplanting Studies
- 2 Modelling
 - o Offshore Wind Cost Modelling Tool
 - o Factors Affecting Overplanting
 - o Modelling of Overplanting
 - o Modelling Risk Aversion
- 3 Case Study and Results
 - o Case Study
 - o Deterministic Results
 - o Local Sensitivity Analysis
 - o Stochastic Results
- 4 Conclusions and Future Work



Motivation

- Farms subjected to a maximum export capacity agreed with the TSO
- Generators can export up to their contracted maximum export capacity
- Majority of the time offshore wind farms are not generating at full power
- Can overplanting result in better overall economics despite power output being curtailed at generations' peaks?



[Wolter et al. 2016]

Overplanting
Over installing the offshore wind capacity to the fixed electrical infrastructure

Overplanting Studies

Dogger Bank
Forewind UK
[Forewind 2012]



Connection Offer
Policy & Process
CER Ireland
[Brid O'Donovan 2011]

Round 3 Offshore Wind
National Grid UK
[Grid 2008]

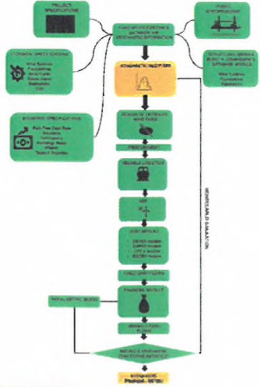
Decision on Installed
Capacity Cap
CER Ireland
[Morris 2014]

Academic Literature
[Mcinerney and Bunn 2017]

Wind Farm
Zone Borssele
TenneT Netherlands
[TenneT 2015]






Offshore Wind Cost Modelling Tool

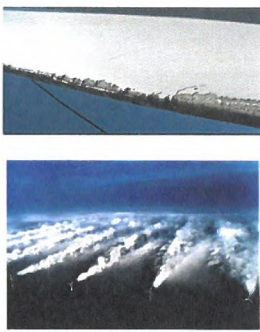


Characteristics

- Aim : rapidly evaluate the financial performance of a farm
- Inputs : project specifications, technology choices and market trends
- Outputs : financial metrics based on LCOE
- Structure : 4 main modules - Design, Cost, Financial and Stochastic
- Stochastic Framework: Quantitative uncertainty management, Double loop Monte Carlo Simulation - inner loop within AEP






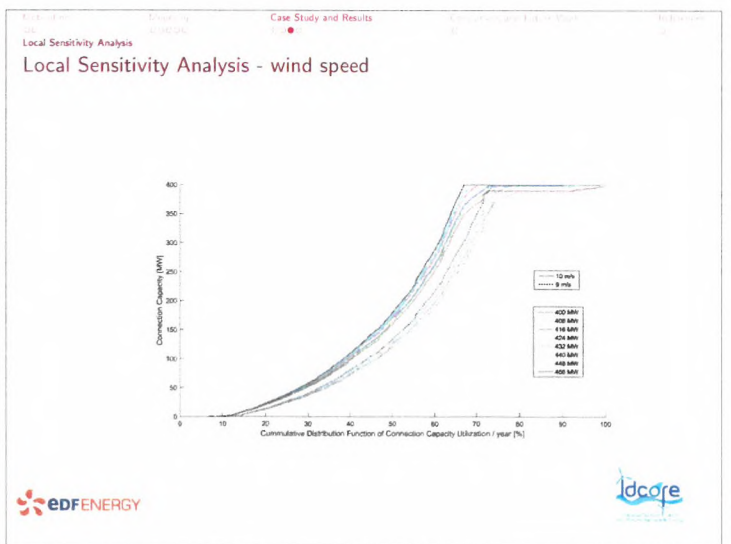
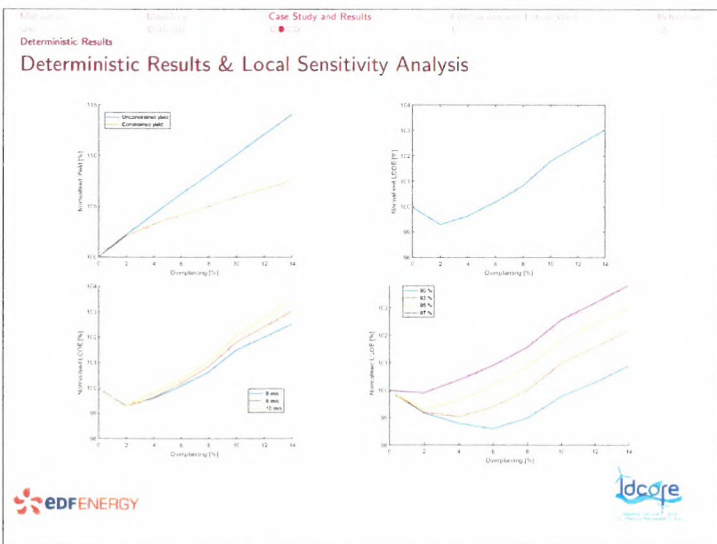
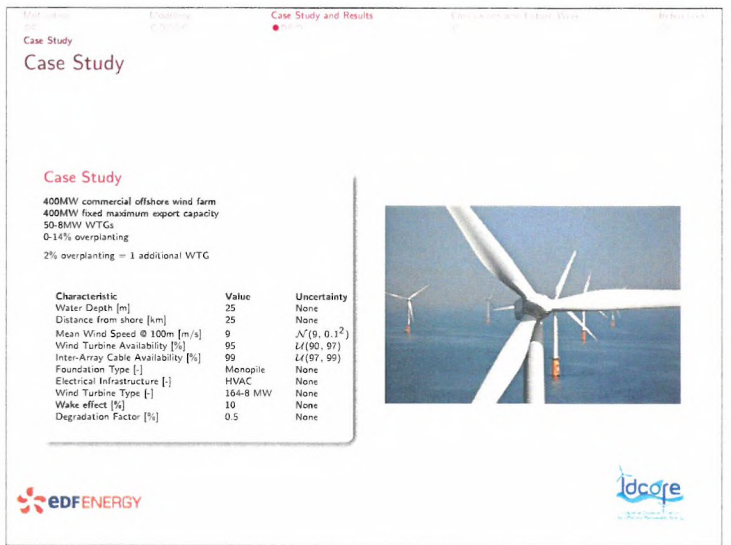
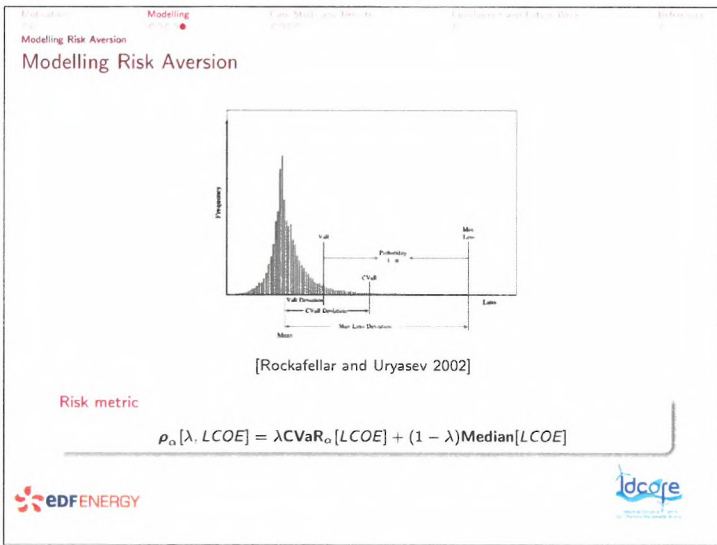
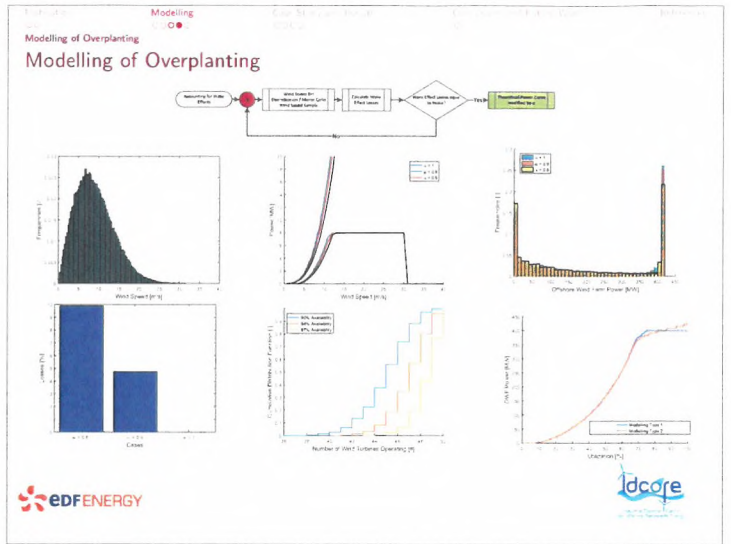
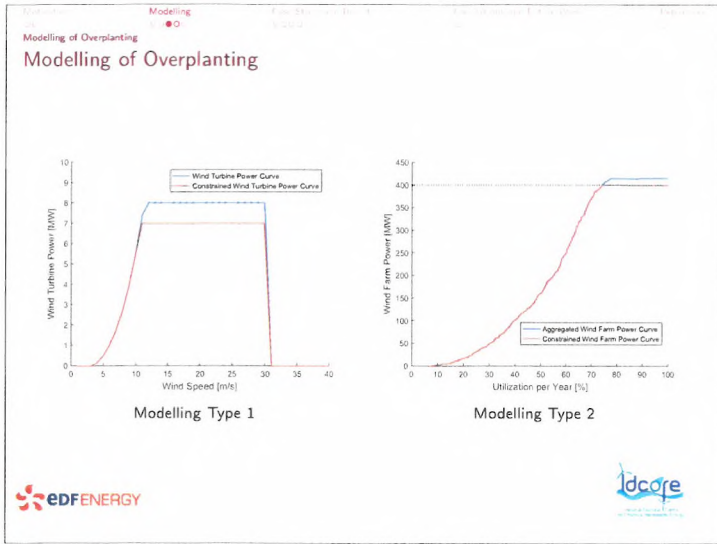
Factors Affecting Overplanting

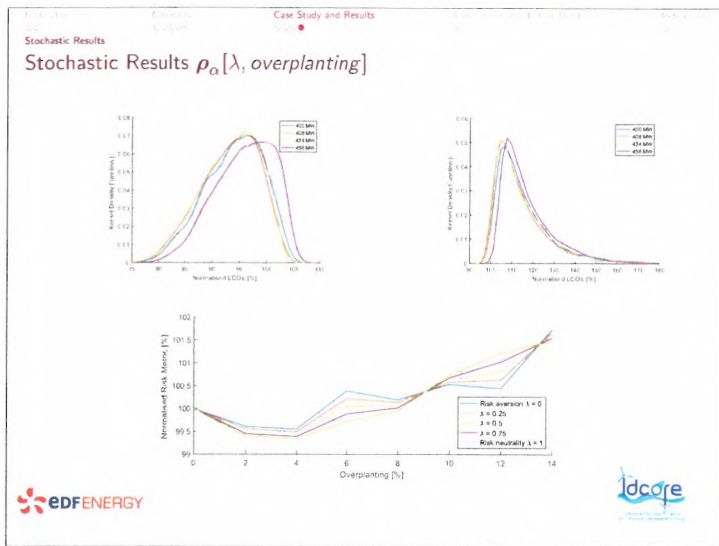


Factors

- Ratio of wind turbine expenditure to electrical infrastructure
- Wind speed distribution
- Wind turbine availability
- Inter-array cable availability
- Wake effects
- Electrical losses
- Degradation factor





Conclusions and Future Work

Conclusions

- Development of a novel framework to evaluate overplanting
- Modelling Type 1 is easier to implement but may lead to an overestimation of the annual energy production
- Modelling Type 2 is more accurate but requires higher computational costs
- Wind turbine availability is the most sensitive parameter to overplanting
- Previous studies based on low wind turbine availabilities rates or on Modelling Type 1, need to be revisited
- Optimal overplanting setup increased when considering the uncertainty quantification framework regardless of risk appetite (from 2% to 4%)
- Overplanting the reference farm from 2% to 8% gives a better result than with no overplanting for a risk neutral setting

Future Work

- How is overplanting influence by larger turbines and sites located further from shore?
- How does risk aversion influence the decision for these new sites?

EDFENERGY IDCORE

References

- Borrás Mora, Esteve (2017). "Transition from Deterministic to Stochastic Cost Models for Offshore Wind Farms". In *Offshore Wind Energy Conference 44* June
- Brid O'Donovan (2011) *Connection Offer Policy & Process (COPP)*. Tech. rep. Commission for Energy Regulation.
- Forewind (2012) *Environmental Statement Chapter 6 Appendix B Offshore Project Boundary Selection Report*. Tech. rep. March
- Grid, National (2008) *Round 3 Offshore Wind Farm Connection Study*. Tech. rep.
- Mcinerney, Celine and Derek W Bunn (2017). "Optimal over installation of wind generation facilities". In *Energy Economics* 61, pp. 87–96. ISSN: 0140-9883. DOI: 10.1016/j.eneco.2016.10.022 URL: <http://dx.doi.org/10.1016/j.eneco.2016.10.022>
- Morris, Nigel (2014) *Decision on Installed Capacity Cap Installed Capacity Cap*. Tech. rep. Commission for Energy Regulation.
- Rockafellar, R Tyrrell and Stanislav Uryasev (2002). "Conditional value-at-risk for general loss distributions". In *Journal of Banking & Finance* 26, pp. 1443–1471
- TenneT (2015) *POSITION PAPER Overplanting*. Tech. rep. TenneT, pp. 1–7
- Wolter, C et al. (2016). "Overplanting in Offshore Wind Power Plants in Different Regulatory Regimes". In *15th Wind Integration Workshop 49.0*, pp. 0–4. URL: 10.1146/annurev-watsci-110614-100303

EDFENERGY IDCORE

Questions

How does risk aversion shape overplanting in the design of offshore wind farms?

Esteve.BorrasMora@edfenergy.com

Acknowledgements

This work is sponsored by EDF Energy R&D UK and the Industrial Doctoral Centre for Offshore Renewable Energy (IDCORE), a consortium of the University of Exeter, University of Edinburgh and University of Strathclyde. IDCORE is funded by both the Energy Technologies Institute and the Research Councils Energy Programme through grant number EP/J500847/1. Additional support came from the UK Engineering and Physical Sciences Research Council through grant number EP/P001173/1 (CESI).

EDFENERGY IDCORE

G1) Experimental Testing and Validation

Experimental modal analysis of aeroelastic tailored rotor blades in different boundary conditions, J.Gundlach, German Aerospace Center

Low-frequency second-order drift-forces experimental validation for a Twin Hull Shape Offshore Wind Platform – SATH, A.M.Rubio, Saitec Offshore Technologies

Numerical prediction of hydrodynamic coefficients for a semi-sub platform by using large eddy simulation with volume of fluid method and Richardson extrapolation method, J.Pan, University of Tokyo

Assessment of Experimental Uncertainty in the Hydrodynamic Response of a Floating Semisubmersible, Including Numerical Propagation of Systematic Uncertainty, A.Robertson, NREL

Experimental modal analysis of aeroelastic tailored rotor blades in different boundary conditions

Dipl.-Ing. Janto Gundlach
 Dr.-Ing. Yves Govers
 Institute of Aeroelasticity
 German Aerospace Center (DLR), Göttingen

Trondheim – EERA DeepWind'19
 January 17, 2019



Experimental modal analysis of aeroelastic tailored rotor blades in different boundary conditions

Content

- 1 Context of modal test campaign
- 2 Test setups and realisation
- 3 Assorted results
- 4 Summary and future work



Context of test campaign

SmartBlades2 T1 rotor blades

Rotor blade properties

- built by DLR
- geometric coupling induced by prebend and sweep
- demo length scale of 20m
- intended to reduce overall loading

Main project goals

- demonstration of technology in operational tests
- validation of numerical tools

pictures: NREL



project partners



Context of test campaign

SmartBlades2 T1 rotor blades

Rotor blade properties

- built by DLR
- geometric coupling induced by prebend and sweep
- demo length scale of 20m
- intended to reduce overall loading

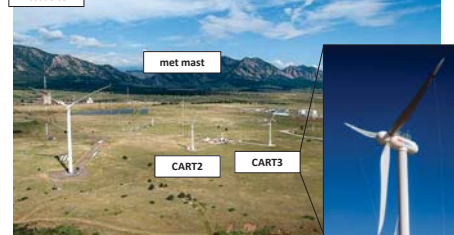
Main project goals

- demonstration of technology in operational tests
- validation of numerical tools

Operational tests on CART3, Boulder, Colorado (blade #2-blade #4)

- varying test conditions (cross wind, start-up, shutdown)
- multitude of measurements
 - met mast
 - aero probes
 - Lidar on nacelle
 - SSB BladeVision
 - strain gauges
 - DIC

NWTC test site



Context of test campaign

Related structural testing

Certification of blade #1 according to IEC61400-23

- static extreme loads
 - flapwise bending, edgewise bending, torsion; before and after fatigue test
- dynamic high-cycle fatigue test

Bend-twist coupled blades

- coupled mode-shapes are predicted with uncertainty
- affects power production, loading, flutter stability



pictures: IWES Bremerhaven

➤ structural dynamic validation of FE shell and beam models

modal tests

- free-free boundary condition (4 blades)
 - deviations from manufacturing
- at the test rig (blade #1)
 - very high sensor density
 - larger deformations

} ideal database for FE model update



Context of test campaign

Process of finishing

Finish of rotor blades

- Removal of remains from previous manufacturing steps
- installing blade root connection
- additional layers of lay-up laminate
- colouring the blade
- approximated mass increase: 103kg

unfinished blade



Mass of individual rotor blades

	mass in kg
blade #1 w/o finish	1793
blade #2	1971
blade #3	1892
blade #4	1917

Overview of test campaign

	blade #1	blade #2	blade #3	blade #4
free (DLR)	x	x	x	
free w/ finish (NREL)		x	x	x
test rig (IWES)	x			



Experimental modal analysis of aeroelastic tailored rotor blades in different boundary conditions

Content

- 1 Context of modal test campaign
- 2 Test setups and realisation
 - Comparison of test scenarios
 - Sensor distribution
 - Modal testing procedure
- 3 Assorted results
- 4 Summary and future work



Test setups and realisation

Comparison of test scenarios



	feasibility	aspects of validation
free-free	<ul style="list-style-type: none"> • instrumentation and excitation on ground • suspension system • replaces hub connection • low test site requirements <p>➤ less than two days of testing</p>	<ul style="list-style-type: none"> • fewest mass loading • "blade only"
test rig	<ul style="list-style-type: none"> • instrumentation and excitation in heights • effort of blade attachment <p>➤ testing of non-linear behaviour</p>	<ul style="list-style-type: none"> • resemblance to hub connection • compliance of test rig • higher force input possible

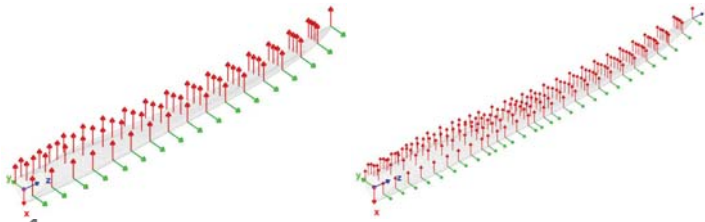


Test setups and realisation

Sensor distribution

- | | |
|---|--|
| <p>free-free</p> <ul style="list-style-type: none"> • equidistant spacing along length and chord axis • edgewise motion captured by sensors on leading edge • 3-4 instrumented cross-sections on suction side | <p>clamped to test rig</p> <ul style="list-style-type: none"> • equidistant spacing along length on girder, equidistantly to leading and trailing edge • 15 instrumented cross-sections on suction side in total 288 acceleration signals |
|---|--|

➤ high sensor density for validation purpose



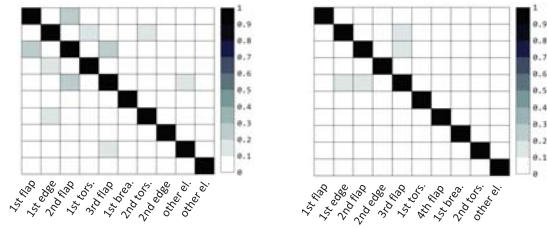
Test setups and realisation

Sensor distribution

- | | |
|---|--|
| <p>free-free</p> <ul style="list-style-type: none"> • equidistant spacing along length and chord axis • edgewise motion captured by sensors on leading edge • 3-4 instrumented cross-sections on suction side | <p>clamped to test rig</p> <ul style="list-style-type: none"> • equidistant spacing along length on girder, equidistantly to leading and trailing edge • 15 instrumented cross-sections on suction side in total 288 acceleration signals |
|---|--|

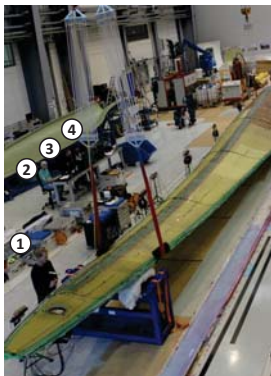
➤ high sensor density for validation purpose

AutoMAC from FE model



Test setups and realisation

Modal testing procedure



Sequence of operations

- ① hammer/shaker excitation
- ② data acquisition and signal generation
- ③ signal processing
- ④ modal analysis and correlation

impact hammer (free-free)

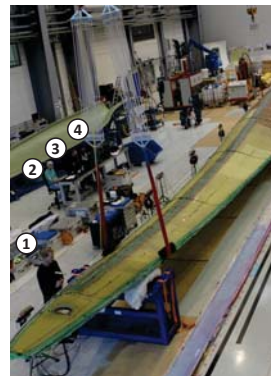
- soft tip, 10 averages
- 8 excitation points on leading edge, trailing edge, girder, blade shell
- huge windows (rigid body modes)

electrodynamical shaker (test rig)

- slow-paced logarithmic sine upsweeps (0.5 oct/min)
- different amplitude levels up to 800N
- multi-point excitation flapwise
- attachment built from mixed adhesive

Test setups and realisation

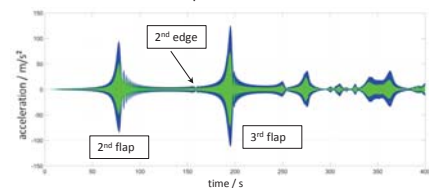
Modal testing procedure



Sequence of operations

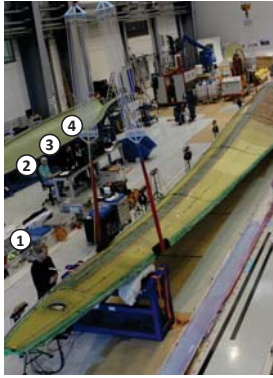
- ① hammer/shaker excitation
- ② data acquisition and signal generation
- ③ signal processing
- ④ modal analysis and correlation

time data of sine sweep



Test setups and realisation

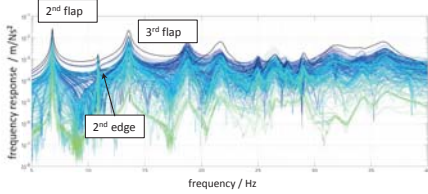
Modal testing procedure



Sequence of operations

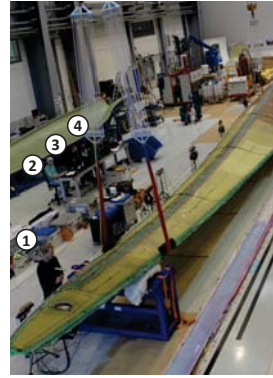
- ① hammer/shaker excitation
- ② data acquisition and signal generation
- ③ signal processing
- ④ modal analysis and correlation

frequency response functions



Test setups and realisation

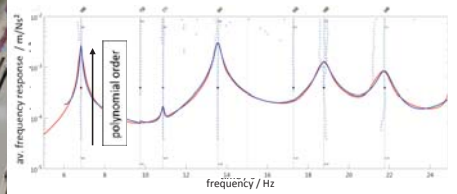
Modal testing procedure



Sequence of operations

- ① hammer/shaker excitation
- ② data acquisition and signal generation
- ③ signal processing
- ④ modal analysis and correlation

stabilisation diagram from identification algorithm



Experimental modal analysis of aeroelastic tailored rotor blades in different boundary conditions

Content

- 1 Context of modal test campaign
- 2 Test setups and realisation
- 3 Assorted results
 - Overview of mode shapes
 - Correlation with FE model
 - Impact of finishing process
 - Non-linearity study
- 4 Summary and future work



Assorted results

Overview of mode shapes from free-free test (blade #1)

no.	mode shape	f in Hz	D in %
1	rigid body heave	0.74	3.62
2	rigid body roll	0.86	2.42
3	rigid body pitch	0.99	4.03
4	1. bending flapwise	4.80	0.23
5	1. breathing mode	7.74	0.61
6	1. bending edgewise	10.13	0.43
7	2. bending flapwise	11.99	0.43
8	2. breathing mode	14.48	0.56
9	1. torsion	16.85	1.25
10	3. bending flapwise	20.90	0.66
11	3. breathing mode	22.20	0.50
12	2. bending edgewise	27.15	0.57
13	2. torsion	27.98	0.97



Assorted results

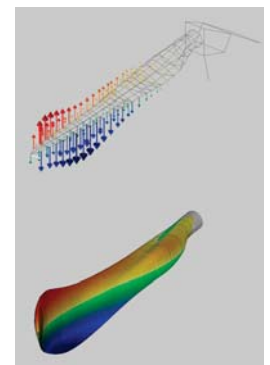
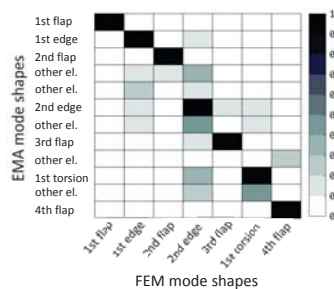
Overview of mode shapes from blade #1 being clamped

no.	mode shape	f in Hz	D in %
1	1. bending flapwise	2.20	0.35
2	1. bending edgewise	3.07	0.31
3	2. bending flapwise	6.85	0.28
4	lateral test rig mode	7.26	0.58
5	2. bending edgewise + 1. breathing	9.74	0.40
6	2. bending edgewise	10.88	0.31
7	2. bending edgewise + 2. breathing	11.95	0.63
8	3. bending flapwise	13.58	0.34
9	1. breathing mode	17.27	0.44
10	1. torsion	18.73	0.46



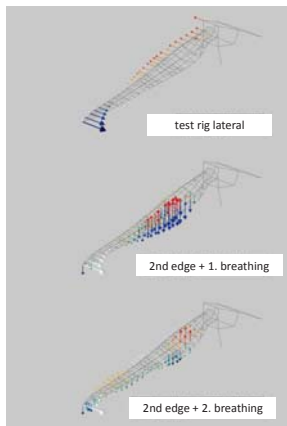
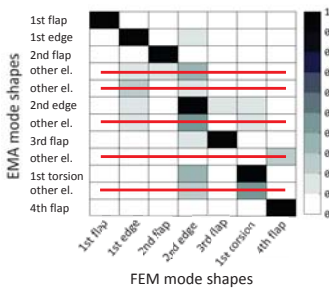
Assorted results

Correlation with FE model (test rig)



Assorted results

Correlation with FE model (test rig)



Assorted results

Impact of finishing process

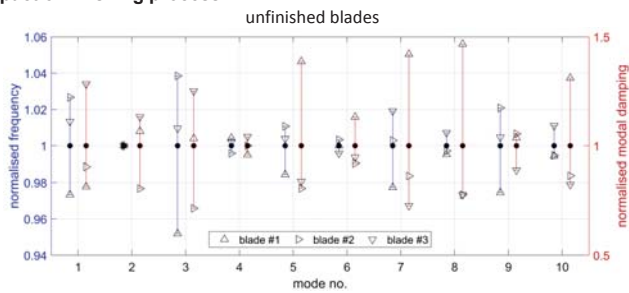
averaged eigenfrequencies and damping

mode no.	mode description	eigenfrequency in Hz		diff. in %	modal damping in %		diff. in %
		w/o finish	w/ finish		w/o finish	w/ finish	
1	rigid body heave	0.75	0.70	-6.7	2.86	2.53	-11.5
2	rigid body roll	0.86	0.84	-1.7	2.27	2.51	10.6
3	rigid body pitch	1.04	0.98	-5.8	3.90	3.19	-18.2
4	1 st bend. flapwise	4.78	4.72	-1.3	0.24	0.26	8.3
5	1 st bend. edgewise	10.29	9.81	-4.7	0.31	0.38	22.6
6	2 nd bend. flapwise	11.99	11.87	-1.0	0.38	0.23	-39.5
7	1 st torsion	17.24	17.14	-0.6	0.88	0.56	-36.4
8	3 rd bend. flapwise	21.00	20.58	-2.0	0.45	0.36	-20.0
9	2 nd bend. edgewise	27.86	26.67	-4.3	0.55	0.45	-18.2
10	2 nd torsion	28.14	28.69	2.0	0.74	0.47	-36.5



Assorted results

Impact of finishing process

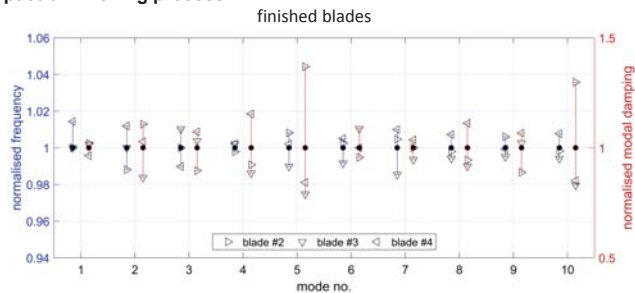


- blade #1: high damping and low frequencies
- flap modes (no. 4,6,8) insensitive to frequency variations



Assorted results

Impact of finishing process



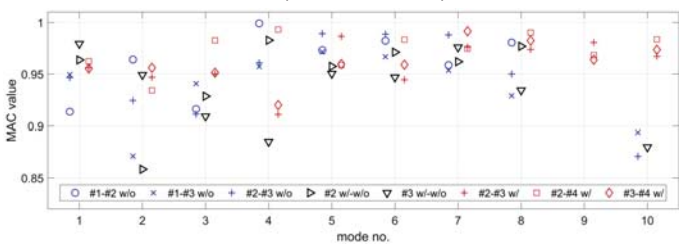
- smaller deviations in both frequency and damping
- some major changes in damping for blade #2 (no. 5,10)



Assorted results

Impact of finishing process

comparison of mode shapes

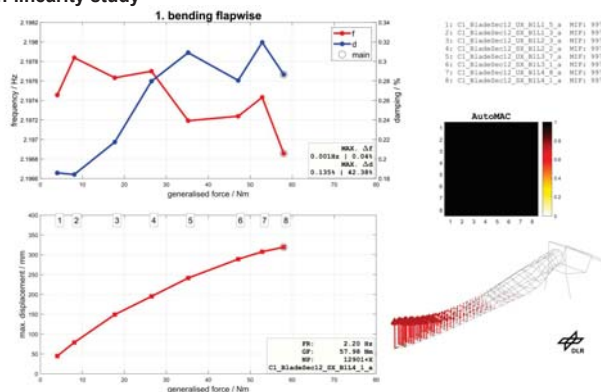


- correlation in higher modes only for finished data set
- mode shapes are affected significantly



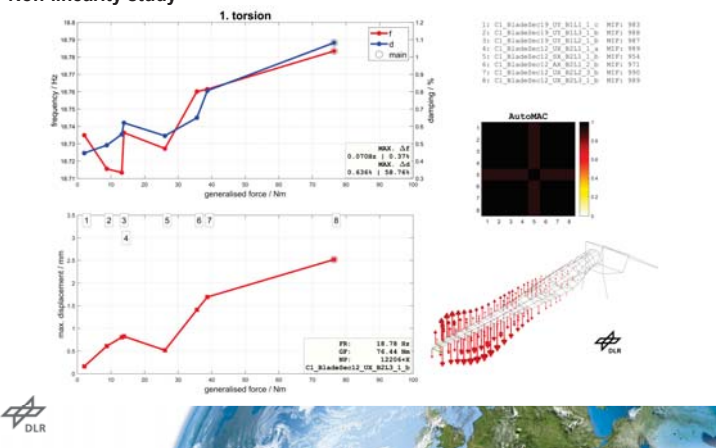
Assorted results

Non-linearity study



Assorted results

Non-linearity study



Experimental modal analysis of aeroelastic tailored rotor blades in different boundary conditions

Content

- 1 Context of modal test campaign
- 2 Test setups and realisation
- 3 Assorted results
- 4 Summary and future work

Summary and future work

Design and realisation of high-resolution modal tests in different boundary conditions

- free-free
 - time-efficient test option
 - finished vs. unfinished blades
 - reduction of eigenfrequencies
 - notable impact on mode shapes
- clamped to test rig
 - costly test option with resemblance to operation
 - realisation of larger flapwise deformations
 - insensitive eigenfrequencies but increase of damping
 - beneficial for critical load cases and aeroelastic stability

Summary and future work

- methodology for computational model updating of rotor blades
- modal identification incorporating load frames
- modal identification by using strain data

Thank you for your attention!

Janto Gundlach
janto.gundlach@dlr.de
Tel.: +49 551 709-2172

Yves Govers
yves.govers@dlr.de
Tel.: +49 551 709-2288

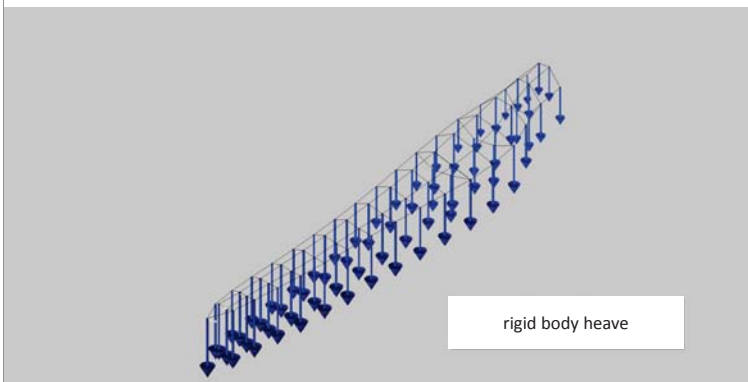


Supported by:

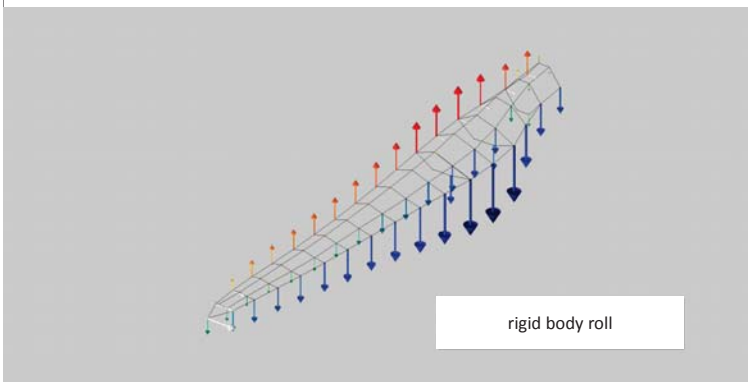


on the basis of a decision by the German Bundestag

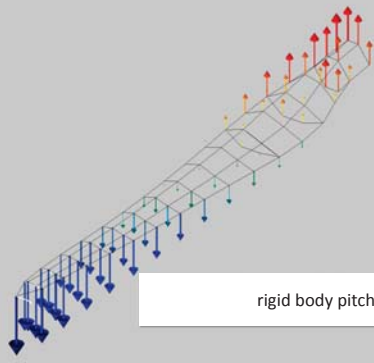
[back](#)



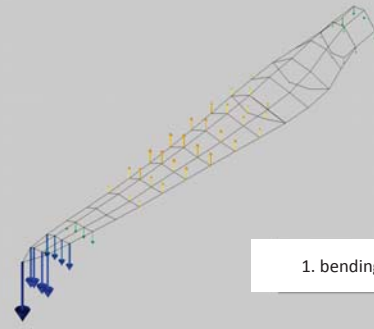
[back](#)



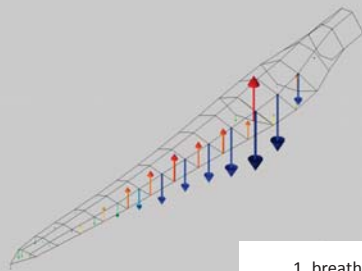
[back](#)



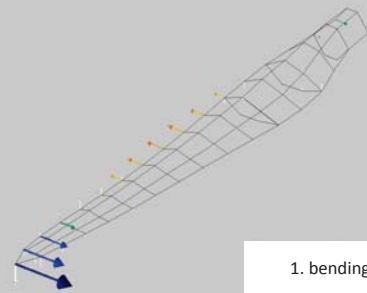
[back](#)



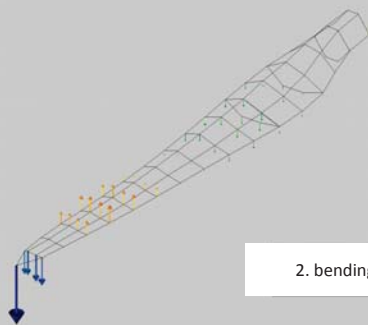
[back](#)



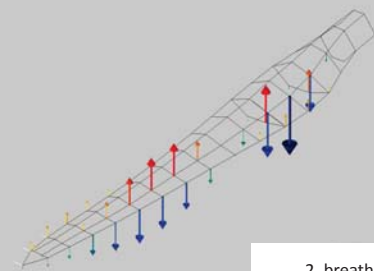
[back](#)



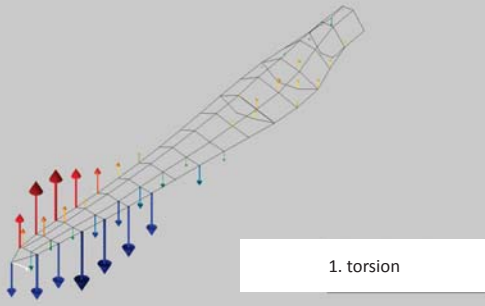
[back](#)



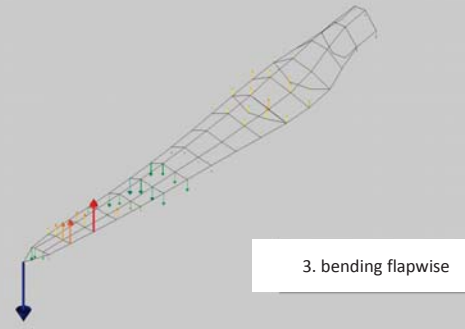
[back](#)



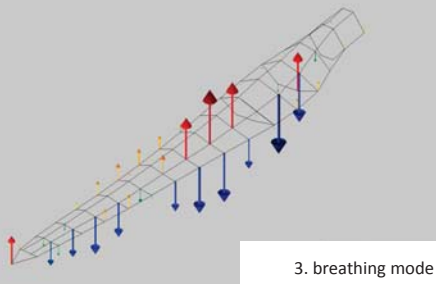
[back](#)



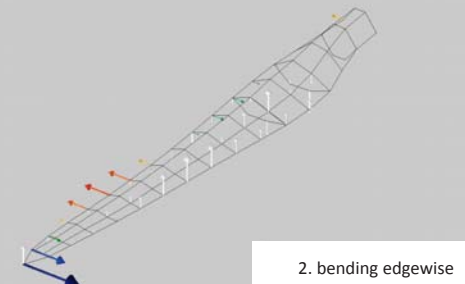
[back](#)



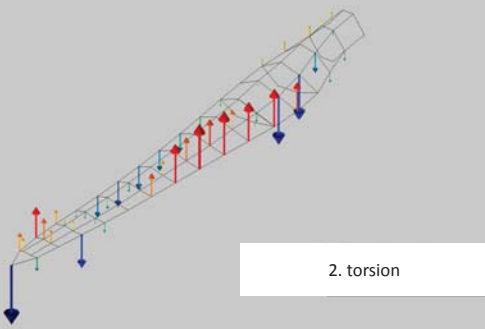
[back](#)



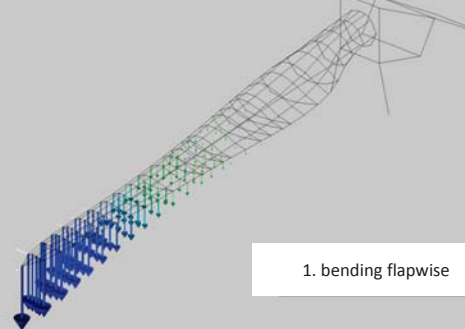
[back](#)



[back](#)

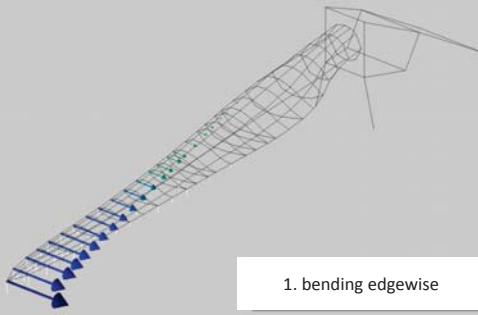


[back](#)



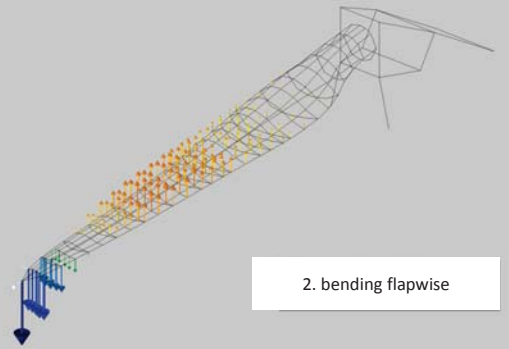
DLR.de • Chart 43 > Janto Gundlach • EERA Deepwind'19 > 17/01/2019

[back](#)



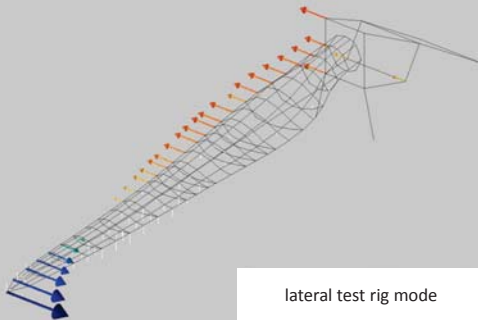
DLR.de • Chart 44 > Janto Gundlach • EERA Deepwind'19 > 17/01/2019

[back](#)



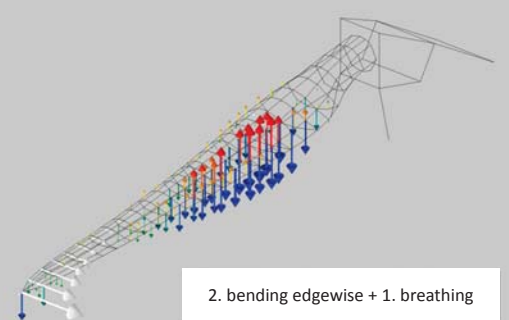
DLR.de • Chart 45 > Janto Gundlach • EERA Deepwind'19 > 17/01/2019

[back](#)



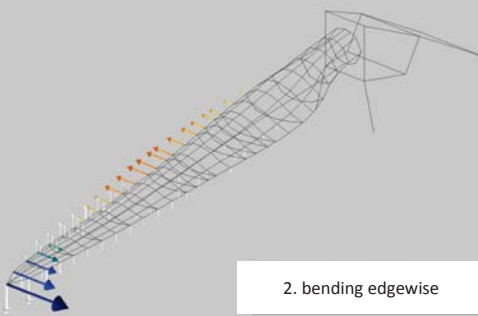
DLR.de • Chart 46 > Janto Gundlach • EERA Deepwind'19 > 17/01/2019

[back](#)



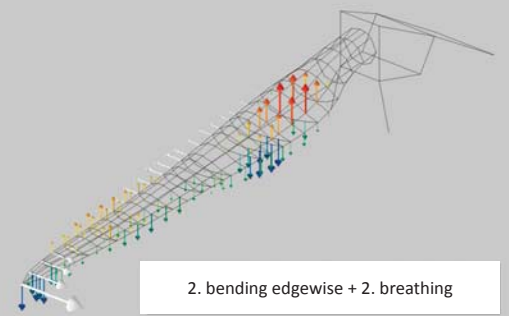
DLR.de • Chart 47 > Janto Gundlach • EERA Deepwind'19 > 17/01/2019

[back](#)

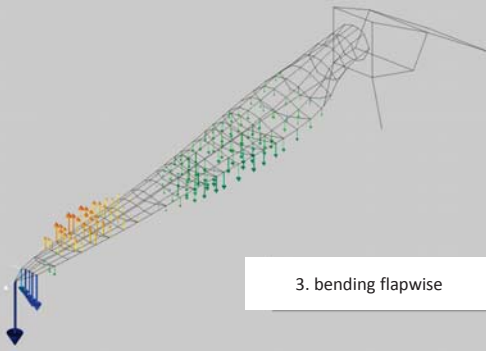


DLR.de • Chart 48 > Janto Gundlach • EERA Deepwind'19 > 17/01/2019

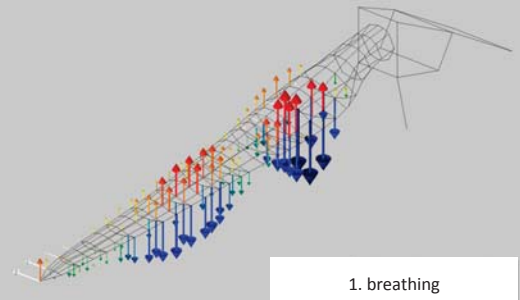
[back](#)



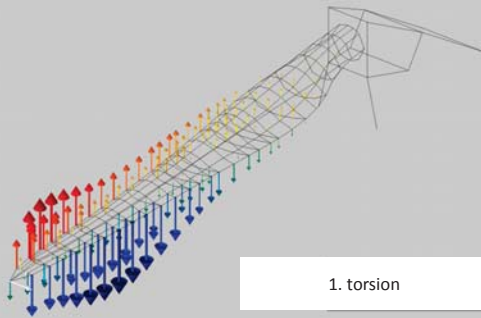
[back](#)



[back](#)



[back](#)



Low-frequency second-order **drift-forces** experimental validation for a **Twin Hull Shape Offshore Wind Platform - SATH**

saitec offshore technologies

Layout

saitec offshore technologies

- The Company
- Introduction to SATH concept
- Model testing motivation
- Experiments
- Numerical validation
- Main conclusions

EERA DeepWind'2019 | Araceli Martinez · Saitec Offshore Technologies | January 2019, Trondheim, Norway

The Company

saitec offshore technologies

Spin-off from International Infrastructure engineering company

SATH™ INNOVATIVE FLOATING WIND SOLUTION MAKING OFFSHORE WIND GLOBAL

Patented technology

COMPANY PURPOSE

EERA DeepWind'2019 | Araceli Martinez · Saitec Offshore Technologies | January 2019, Trondheim, Norway

Introduction to SATH concept

saitec offshore technologies

Swinging Around Twin Hull

- Transition piece** - Interface tower-floater
- Floaters** - Buoyancy
- Heave plates** - Motion dampers
- Internal bulkheads** - Load transmission
- SPM - External turret** - Self-alignment with the Wind Direction - Stresses reduction

CONCRETE

Reduced construction and maintenance costs

LOW DRAFT

2 MW – 6.5m
10 MW – 9.5m

SELF-STABLE

Easily transportation

EERA DeepWind'2019 | Araceli Martinez · Saitec Offshore Technologies | January 2019, Trondheim, Norway

Model testing motivation

saitec offshore technologies

- OBJECTIVE**: Mooring System optimization
- LIMITATIONS**: Potential theory assumptions
- METHODOLOGY**: EXPERIMENTS at IFREMER (July 2018)
 - Mean Drift Coefficients extraction
 - Full-QTF Coefficients extraction
- NUMERICAL CALIBRATION**: WADAM, FAST, Sima, SESAM

Collaboration Project **SINTEF**

EERA DeepWind'2019 | Araceli Martinez · Saitec Offshore Technologies | January 2019, Trondheim, Norway

Experiments

SINTEF IFREMER **saitec** offshore technologies

Scale model

	Scale model 1/36	Full prototype - 2MW
Length (m)	1.72	61.92
Width (m)	0.85	30.6
Total height (m)	2.05	73.8
Draft (m)	0.2	7.35
Total Mass (kg)	82.8	3863116.8

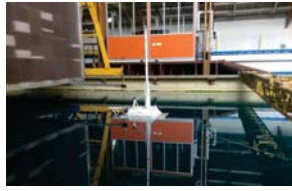
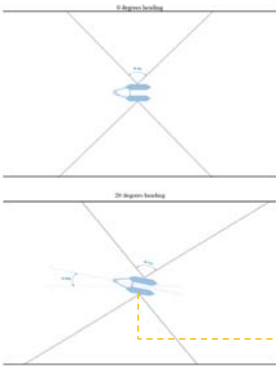
- Wind turbine**: Computer-controlled
- Analys**: Track motion
- Load cells mooring system**

EERA DeepWind'2019 | Araceli Martinez · Saitec Offshore Technologies | January 2019, Trondheim, Norway

Experiments



Experiments set-up



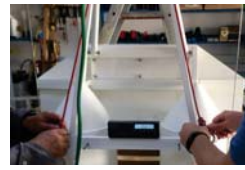
Soft Mooring
Simple an linear setup for identification of hydrodynamic coefficients.

VCG to decouple the pitch motion from the mooring system forces.

Experiments



Test campaign planning



Identification of mass properties



Calibration of waves



Characterization tests: decay; tilt; pull out

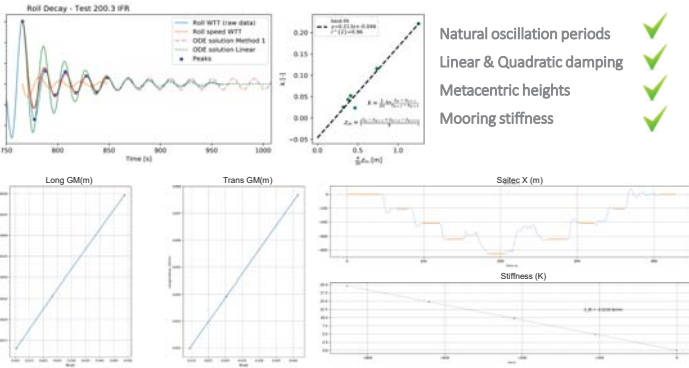


Tests in waves: periodic; irregular; pink noise

Experiments



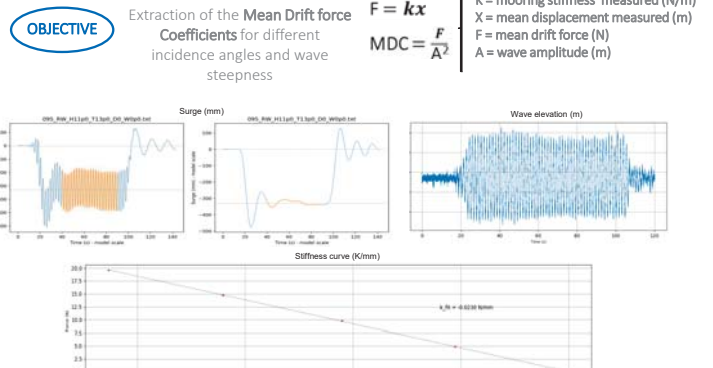
Characterization tests – Global verification of the structure behaviour



Experiments



Tests in waves– Periodic waves



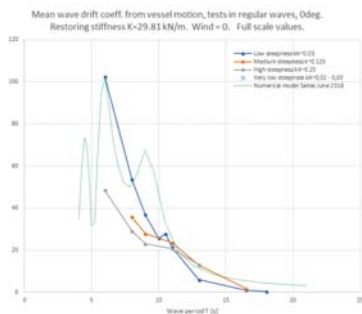
Experiments



Tests in waves– Periodic waves

Test Matrix:
Set 1: head waves; no wind; different steepness
Set 2: head waves; wind influence;
Set 3: 20° waves; no wind;

Real model		
Period	Height	Steepness
6.000	1.116	0.020
6.000	4.680	0.083
7.980	1.692	0.017
7.980	4.320	0.043
7.980	8.640	0.086
9.000	2.088	0.016
9.000	5.256	0.042
9.000	10.512	0.083
10.000	2.900	0.019
10.980	7.992	0.043
10.980	15.984	0.086
13.020	4.392	0.017
13.020	11.016	0.043
13.020	19.800	0.078
16.500	7.488	0.020
16.500	15.480	0.042

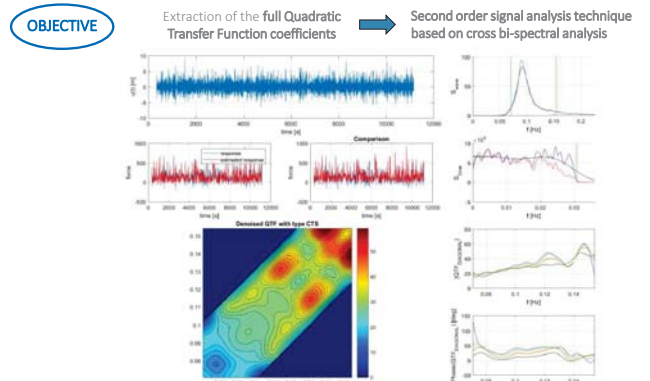


Potential theory over-estimates the coefficients
Favourable steepness dependency

Experiments



Tests in waves– Irregular waves



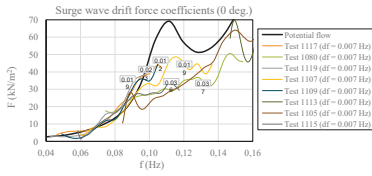
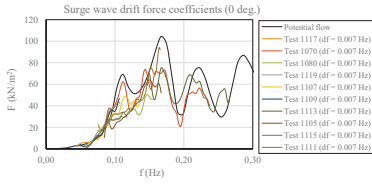
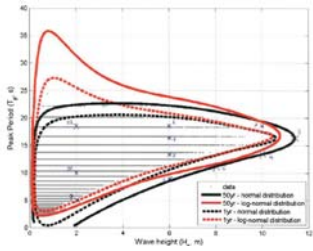
Experiments



Tests in waves– Irregular waves

Test Matrix:

- Set 1: pink noise (0° & 20° incidence)
- Set 2: sea-states along the 50 years environmental contour (0° & 20° incidence)
- Set 3: sea-states representative of operational conditions (0° & 20° incidence)



Favourable steepness dependency

Numerical validation



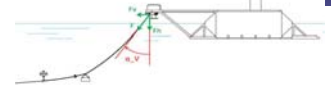
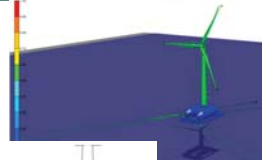
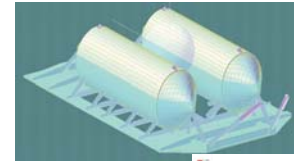
Frequency Domain Simulations (Based on potential theory)

Extraction of the Mean Drift Force Coefficients from tests

Correction of potential flow Mean Drift Coefficients f(steeptness)

Time Domain Simulations using Newman's Approximation

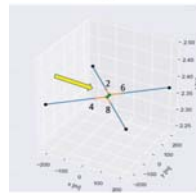
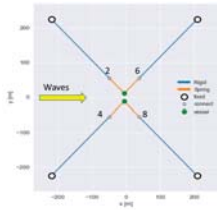
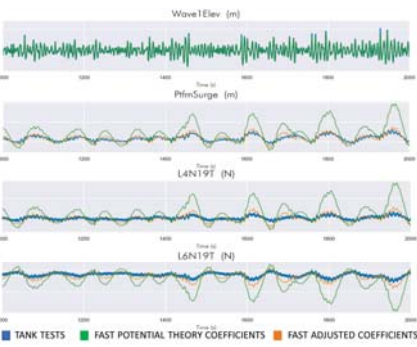
Optimization of the mooring system design



Numerical validation



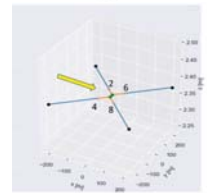
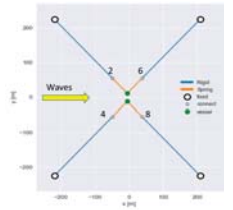
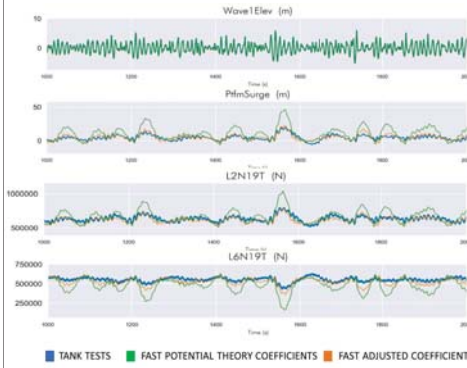
Hs = 5m Tp = 8.8s



Numerical validation



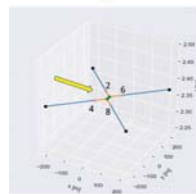
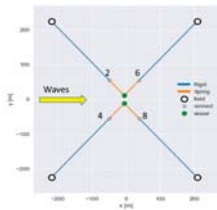
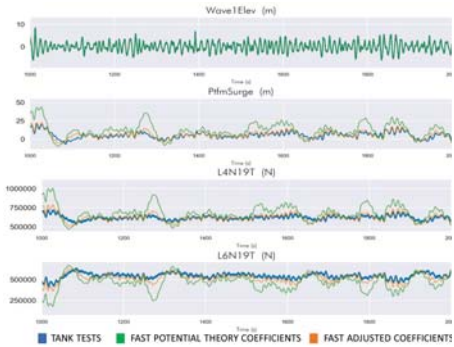
Hs = 7m Tp = 11s



Numerical validation



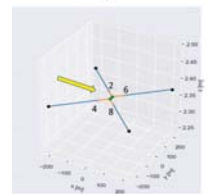
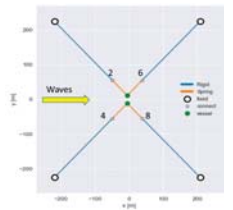
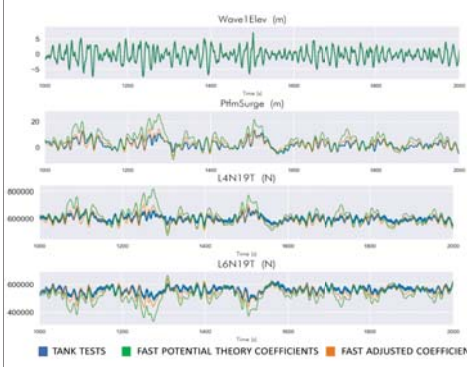
Hs = 9.4m Tp = 13s



Numerical validation



Hs = 9.7m Tp = 18s



Numerical validation



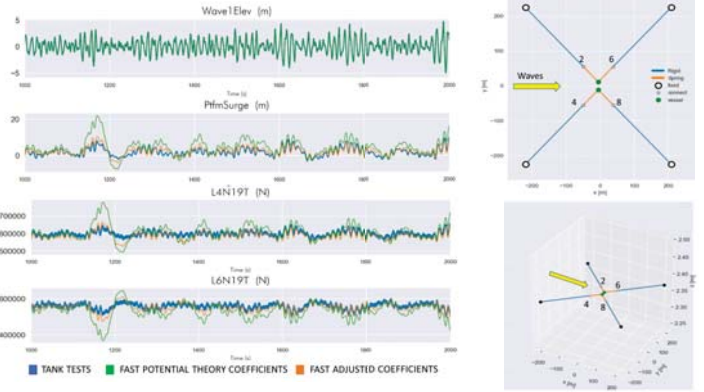
Hs = 9.7m Tp = 16s



Numerical validation



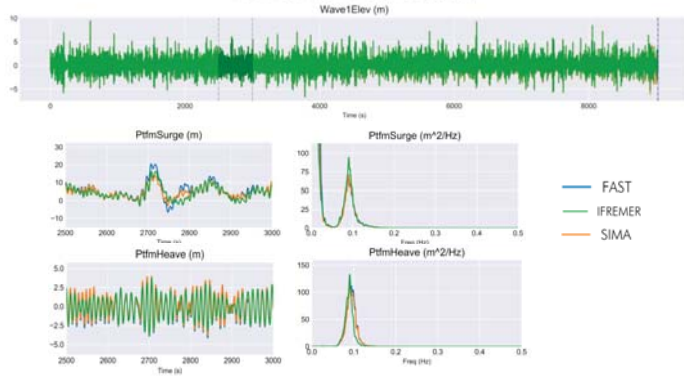
Hs = 5m Tp = 13s



Numerical validation



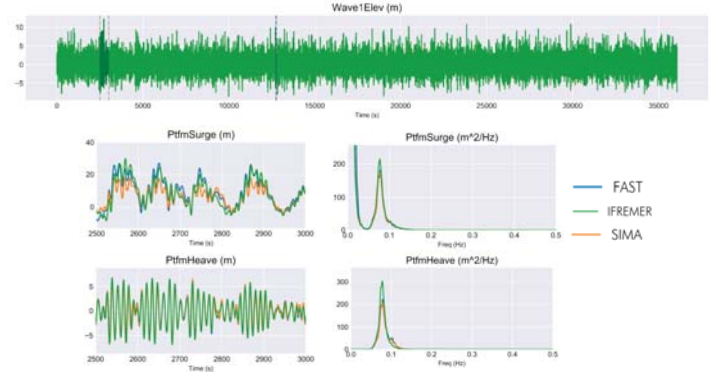
IFR_IR_H7p0_T11p0_D0_W0p0 (High steepness)



Numerical validation



IFR_IR_H9p4_T13p0_D0_W0p0 (High steepness)



Main conclusions

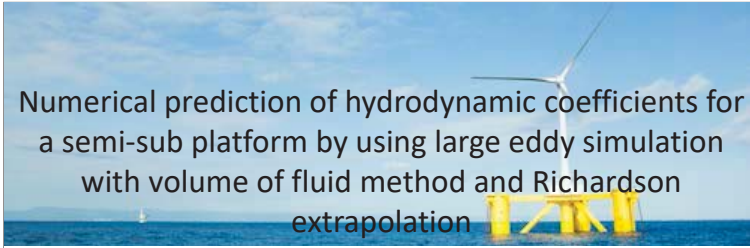


- Soft mooring set-up – Simplifications of results
- Only wave tests – No extra phenomena (wind or current)
- Duration of the tests – 3 hour sea-states
- Wave tank basin characteristics – No reflection
- Potential theory – Over-estimation of the results
- SATH Technology – Non-linear response for different wave steepness
- Newman's Approximation – Verified for SATH concept
- Optimization of the mooring system – Adjustment of numerical models



Thank you for your attention
 Araceli Martínez Rubio
 aracelimartinez@saitec.es





Numerical prediction of hydrodynamic coefficients for a semi-sub platform by using large eddy simulation with volume of fluid method and Richardson extrapolation

Jia, PAN
Takeshi, ISHIHARA

Bridge and Structure Lab, The University of Tokyo
2019/01/17

Hydrodynamic coefficients (Ca & Cd)

Target structures 1. Heave Plate 2. Floater	L.Tao,2004; Lpoez-Pavon, 2015 (CFD) (Shear Stress Transport (SST) model)	Chia-Rong Chen, 2016(CFD) (No free water surface)
Accuracy		

C_{ca} : Added mass coefficient; C_{cd} : Viscous drag coefficient
Keulegan-Carpenter (KC) number: $KC = \frac{2\pi A}{D} f$ (A: amplitude of motion; D: diameter of typical component)

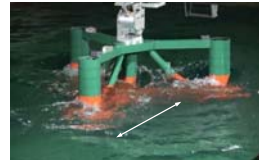
- The effects of **free water surface** and of **KC number** on hydrodynamic coefficients of a semi-sub model predicted should be systematically investigated by **LES with VOF**.
- Accuracy** of predicted hydrodynamic coefficients by CFD should be improved.

Objectives

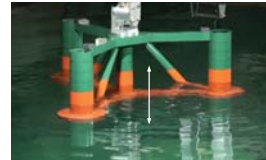
- To improve accuracy of the predicted hydrodynamic coefficients by Richardson extrapolation method.
- To study the effect of KC number and frequency on the hydrodynamic coefficients.
- To investigate the importance of the free water surface on evaluation of hydrodynamic coefficients by LES with VOF.

Water tank tests

- Forced vibration tests in the horizontal and vertical directions



Horizontally forced oscillation



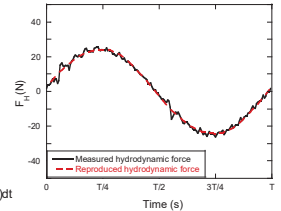
Vertically forced oscillation

- KC number $KC = \frac{V_{max}}{D_i f} = \frac{\omega a}{D_i f} = \frac{2\pi a}{D_i}$
- Definition of hydrodynamic coefficients Ca and Cd

$$F_x(t) = F(t) - F_0 - F_1(t) - F_2(t) \quad F_x(t) = -C_a M \dot{x}(t) - 0.5 C_d \rho_w A | \dot{x}(t) | \dot{x}(t)$$

$$C_a = \frac{\int_0^T F_x(t) \sin(\omega t) dt}{\rho_w \nabla a \omega^2 \int_0^T \sin^2(\omega t) dt} = \frac{1}{\pi \omega a \rho_w \nabla} \int_0^T F_x(t) \sin(\omega t) dt$$

$$C_d = \frac{\int_0^T F_x(t) \cos(\omega t) dt}{\frac{1}{2} \rho_w A (\omega a)^2 \int_0^T |\cos(\omega t)| |\cos(\omega t)| \cos^2(\omega t) dt} = \frac{3}{4 \rho_w A \omega a^2} \int_0^T F_x(t) \cos(\omega t) dt$$



Large eddy simulation (LES) with volume of fluid (VOF)

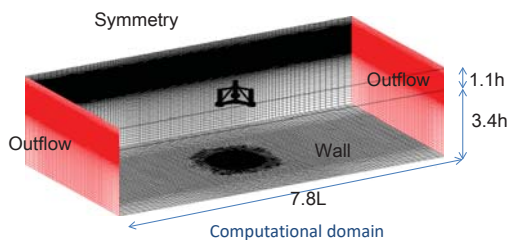
- Governing equation

$$\frac{\partial \tilde{u}_i}{\partial x_i} = 0$$

$$\rho \frac{\partial \tilde{u}_i}{\partial t} + \rho \frac{\partial \tilde{u}_i \tilde{u}_j}{\partial x_j} = -\frac{\partial \tilde{p}}{\partial x_i} + \frac{\partial}{\partial x_j} \left[\mu \left(\frac{\partial \tilde{u}_i}{\partial x_j} + \frac{\partial \tilde{u}_j}{\partial x_i} \right) \right] - \frac{\partial \tau_{ij}}{\partial x_j}$$

- Continuity equation for the volume fraction of water

$$\frac{1}{\rho_w} \left[\frac{\partial}{\partial t} (\alpha_w \rho_w) + \nabla \cdot (\alpha_w \rho_w \vec{v}_w) \right] = 0$$



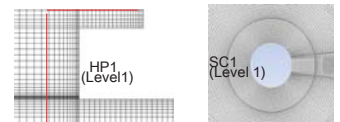
S.N.Zhang, T.Ishihara : Numerical study of hydrodynamic coefficients of multiple heave plates by large eddy simulations with volume of fluid method, Ocean Engineering, Vol.163, pp.583-598, 2018.

Numerical simulation by grid refinement

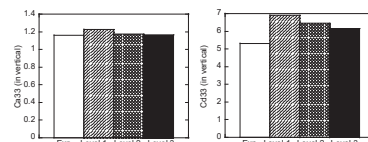
- Grid refinement

In the vertical : Refined area in a region of 5cm near Hp, Hp-C, Pntn
In the horizontal : Refined area in a region of 5cm near SC, CC

Grid level	1	2	3
Grid size	$h_1 = 8mm$	$h_2 = 4mm$	$h_3 = 2mm$
Grid number	13.7 million	18.8 million	63.8 million



- Predicted Ca & Cd by refined grids



- The accuracy of predicted Cd by using grid refinement is not enough.

Richardson Extrapolation Method

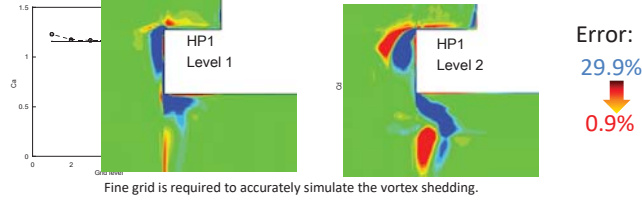
7

Richardson Extrapolation Method

The exact solution $\Phi = \phi_h + \epsilon_h = \phi_h + \alpha h_1^p + H$

where $p = \frac{\log((\phi_{h_2} - \phi_{h_1}) / (\phi_{h_1} - \phi_{h_2}))}{\log \lambda}$, $\alpha = \frac{\phi_{h_2} - \phi_{h_1}}{h_2^p (\lambda^p - 1)} = \frac{\phi_{h_1} - \phi_{h_2}}{h_1^p (\lambda^p - 1)}$, $\lambda = h_1 / h_2 = h_2 / h_3$

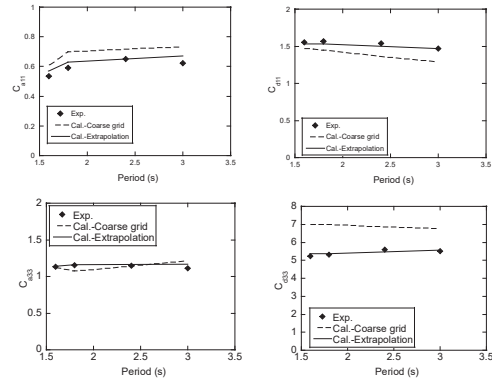
$p = 0.47 \Rightarrow \Phi = \phi_h + \epsilon_h = \phi_{h_2} + \frac{\phi_{h_1} - \phi_{h_2}}{(\lambda^p - 1)}$



- Richardson Extrapolation Method on the finest grid is applied and validated.

Effect of grid refinement

8

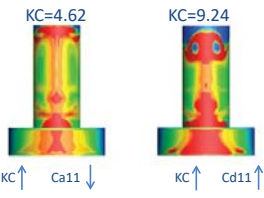
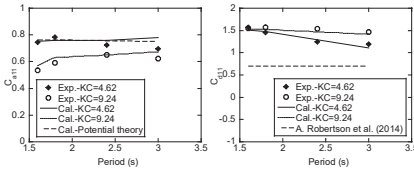


- The predicted hydrodynamic coefficients by using LES with VOF method agree well with the experimental data when Richardson extrapolation is performed.

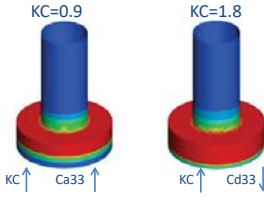
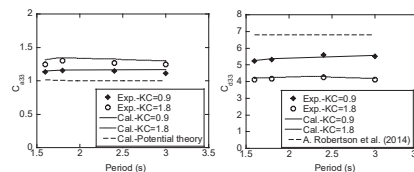
Effect of KC number and wave frequency

9

In the horizontal direction



In the vertical direction



- Potential theory and database have limited accuracy for Ca and Cd, while LES model with VOF can accurately predict the Ca and Cd for different KC numbers and wave frequencies.

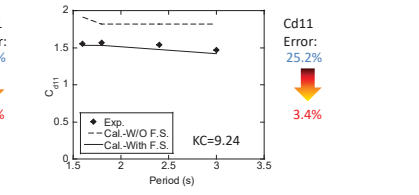
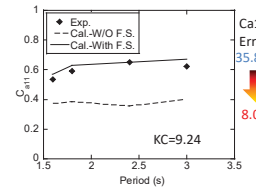
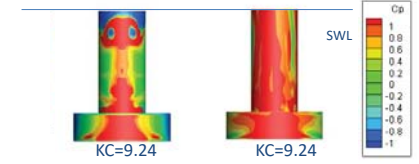
Effect of free water surface

10

In the horizontal direction



With free water surface W/O free water surface



- The free water surface should be included to accurately predict hydrodynamic coefficients in the horizontal direction and can be captured by using LES with VOF.

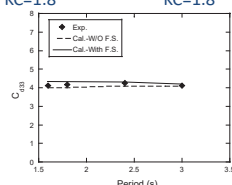
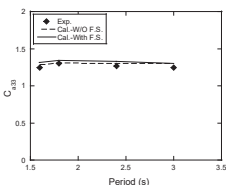
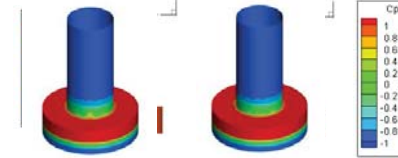
Effect of free water surface

11

In the vertical direction



With free water surface W/O free water surface



- The predicted Ca and Cd with and without free surface in the vertical direction coincide well with those from the water tank test, because the free surface has a limited effect on Ca and Cd in the vertical direction for the deep draft model.

Prediction of dynamic response

12

See the poster No.37

The predicted dynamic responses in different wave heights by proposed model show good agreement with those from the water tank tests.

Conclusions

13

1. The grid refinement can improve accuracy by capturing the vortex shedding near the model and the predicted drag coefficients by Richardson extrapolation method show good agreement with those from the water tank test.
2. LES model with VOF can accurately predict the KC number effect on the hydrodynamic coefficients in the horizontal and vertical directions, while potential theory and database have limited accuracy.
3. The hydrodynamic coefficients in the horizontal direction by LES with VOF show good agreement with the experimental data, while those predicted by LES without the free surface show significant differences.

Thank you for your attention!

This research is carried out as a part of the Fukushima floating offshore wind farm demonstration project funded by Ministry of Economy, Trade and Industry.



Total Experimental Uncertainty in Hydrodynamic Testing of a Semisubmersible Wind Turbine, Considering Numerical Propagation of Systematic Uncertainty

Amy Robertson
National Renewable Energy Laboratory
January 17, 2019

1

Acknowledgements

- Work being submitted for external journal publication, co-authors:
 - Erin E. Bachynski (NTNU)
 - Sebastien Gueydon (MARIN)
 - Fabian Wendt (NREL)
 - Paul Schünemann (Universität Rostock)
- MARINET2 project** (European Union's Horizon 2020 grant agreement 731084) supplied the tank test time and some travel support to accomplish the experimental testing campaign.
- Work was partially supported by the **U.S. Department of Energy** under Contract No. DE-AC36-08GO28308 with the National Renewable Energy Laboratory

2

Background

- Floating wind fast becoming a new industry
- To push the TRL of new designs, validation campaigns in wave tanks common

QUESTION: How do you define a successful validation – how close do simulations need to match measurements?

EXAMPLE: In OCS, validation of a floating wind semisubmersible was performed

- Tower-base force compared – simulations/measurements
- Modeling tools under-predicted the loads by about 20%
- Low-frequency response at its pitch and surge natural frequencies (nonlinear hydrodynamics) – biggest cause

ANSWER: Uncertainty assessment

- Define a bound on measurements
- Understand level of certainty in response characteristics

Instrumented OCS-DeepCwind model in basin (Heider, et al. 2013)

Ultimate Loads - All Cases

3

Overview

Objective: Assess uncertainty in motion response of OCS-DeepCwind semisubmersible, with special focus on low-frequency behavior

Approach:

- OCS-DeepCwind semisubmersible re-tested by sub-group.
 - Simple moored
 - No turbine
- Uncertainty assessment of motion response of floating configuration
 - ASME uncertainty approach
 - Random uncertainty calculated through repeat tests
 - Systematic uncertainty assessed on all components of test, and propagated to response metrics
 - Response metrics used for direct comparison between simulations/measurements – and uncertainty bounds for these metrics were calculated

Simplified configuration of OCS-DeepCwind Semi (Robertson)

Thus, successful validation can be identified if simulated values fall within uncertainty bounds

4

Tests and Metrics

Test Name	Waves	Number Repeats
Regular wave 1	H=7.1 m, T=12.1 s	5
Regular wave 2	H=4 m, T=9 s	2
White noise	Hs=7.1 m, T=6-26 s	2
Irregular wave	Hs=7.1 m, Tp=12.1 s	5

- RAO:** the response amplitude operator (RAO) in surge, heave, and pitch at 6 discrete frequency points within the wave energy range;
- PSD Sum, Low Frequencies:** the integral of the power spectral density (PSD) of surge and pitch motions over the low-frequency range (pink);
- PSD Sum, Wave Frequencies:** the integral of the PSD of surge and pitch motions over the wave-frequency range (blue)
- Mean Surge Offset**

Power spectral density (log scale abscissa) of platform response in surge for irregular wave excitation

** Note: Simulation models not fully tuned, and therefore do not represent the best results that could be obtained by the modeling tool

5

Systematic Uncertainty Sources

Parameter	Baseline Value	Uncertainty Level
1. Platform mass [kg]	1.4196E+7	8.75E-4
2. CM, x direction [m]	0	0.23
3. CM, y direction [m]	0	0.22
4. CM, vertical [m]	-7.53	0.21
5. Platform inertia, xx abt CM [kg-m²]	1.2898E+10	1.2898E-8
6. Platform inertia, yy abt CM [kg-m²]	1.2851E+10	1.2851E-8
7. Platform inertia, zz abt CM [kg-m²]	1.4189E+10	1.4189E-8
8. Draft [m]	20	0.25
9. Column angle, [deg]	0	0.5
10. Column diameter, [m]	12 or 24	0.1
11. Mooring stiffness [kN/m]	48.9	5.2
12. Mooring pretension [kN]	1122.5	62
13. Anchor position x [m]	Radially outward	0.25
14. Anchor position y [m]	Radially outward	0.25
15. Anchor position z [m]	Up/down	0.25
16. Mooring fairlead position [m]	Radially outward	0.05
17. Initial position [m]	0	0.12
18. Initial orientation [deg]	0	0.062
19. Water depth [m]	180	2
20. Water density [kg/m³]	1025	10.25
21. Wave elevation – due to sensor drift [m]	measured	0.03
22. Wave elevation – due to probe location and tilt [m]	measured	negligible
23. Translation measurement [m]	0	0.03
24. Rotation measurement [deg]	0	0.3

6

Down-selected Systematic Sources

- Parameters down-selected based on their influence on the response metrics according to simulations.
- Thresholded by examining the total combined systematic uncertainty of the response metrics.
 - Parameters causing less than 10% change in total combined systematic uncertainty on any metric were removed.
- Original set of 24 parameters down-selected to 8
- Parameters were adjusted to try to make them independent of each other

Parameter	Abbreviation
1 Center of mass, x direction	CMx
2 Center of mass, vertical	CMz
3 Mooring stiffness	Stiff
4 Draft	Draft
5 Column diameter	ColDia
6 Wave elevation – due to sensor drift	WaveElev
7 Platform inertia, Iyy abt CM	Iyy
8 Platform mass + Displaced Volume	Mass+Buoy

7

Systematic Uncertainty Propagation

- Systematic uncertainty of the response metrics due to a given uncertainty source:
 - Simulate model using the baseline properties and calculate associated response metrics.
 - Simulate model using a new value for given uncertain parameter, and calculate response metrics.
 - Difference between response metrics calculated using baseline properties and when changing one of the uncertain parameters is the systematic uncertainty for that parameter.
 - Variations performed in positive and negative directions -> asymmetric uncertainty bounds
- Sum all propagated uncertainty sources

8

Modeling Approaches

Propagation affected by the fact we are using a model. Addressed by:

- Using multiple models
- Using multiple modeling approaches
- Taking largest variation across all approaches

Model ID	Global linear and quadratic drag	Morison drag on vertical columns	Morison drag on heave plates	Wave loads above still water level
FAST		x	x	Morison-type drag up to 1 st order free surface based on constant potential
FAST_PQ	x			
SIMA		x	x	Morison-type drag up to 1 st order free surface based on constant potential
aNySIM			x	Morison loads applied on heave plate only, Therefore, no wave loads act above still water level.
aNySIM_PQ	x			

9

Total Uncertainty Calculation

- Combined random and propagated systematic uncertainty

$$u_c = \sqrt{(b_k)^2 + (s_x)^2}$$
- Expanded uncertainty: multiply standard uncertainty by a coverage factor
 - $k = 2$, level of confidence of approximately 95 %

$$U = k u_c \quad X = \bar{X} \pm U \quad \text{Response metric uncertainty band}$$

– For asymmetric uncertainty:

$$q_i = \frac{(\bar{X} + b_i^+) + (\bar{X} - b_i^-) - \bar{X}}{2}$$

$$X = \left(\bar{X} + \sum_{i=1}^N q_i \right) \pm U$$

b_j = systematic uncertainty of output metrics
 b_g = total combined systematic uncertainty
 p_i = parameter values
 d_j = systematic uncertainty sources
 X = output response metric
 θ = sensitivity coefficients

10

Metric: Mean Surge

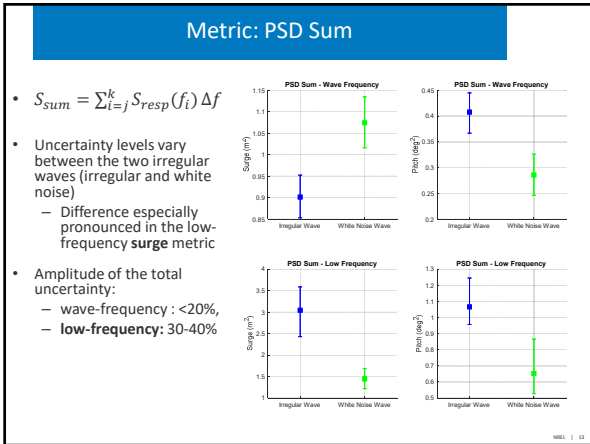
- Uncertainty in mean surge in regular wave case 1 is probably overstated
 - large variation was only seen for one of the simulation tools
 - much of the difference is likely related to static effects (which would have been zeroed out in the experimental measurements)

11

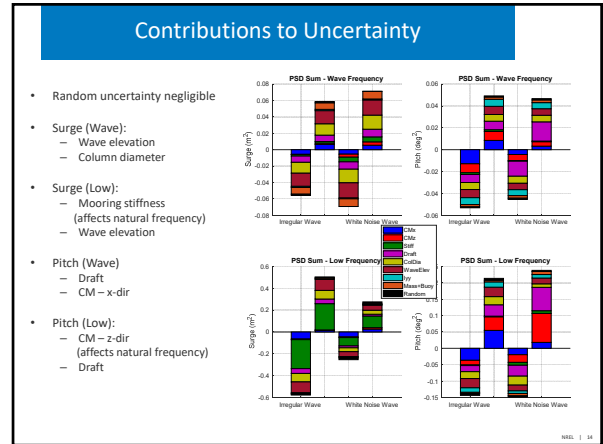
Metric: RAOs

- RAO calculations shown based on all waves
 - 6 points chosen for uncertainty assessment
- Frequencies on low end showed most uncertainty
 - Closeness to natural frequencies
 - Cancellation effects in the excitation
- Pitch response shows larger uncertainty than other DOFs

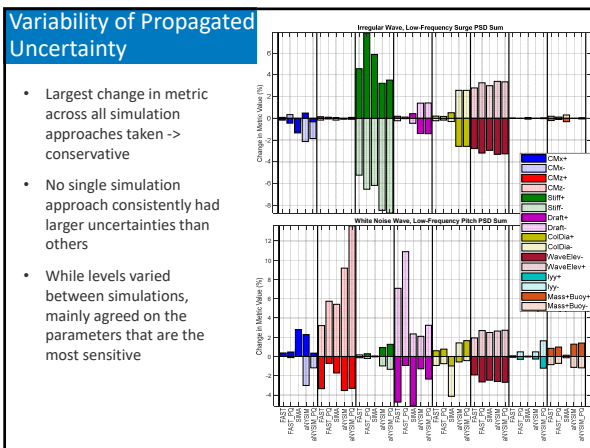
12



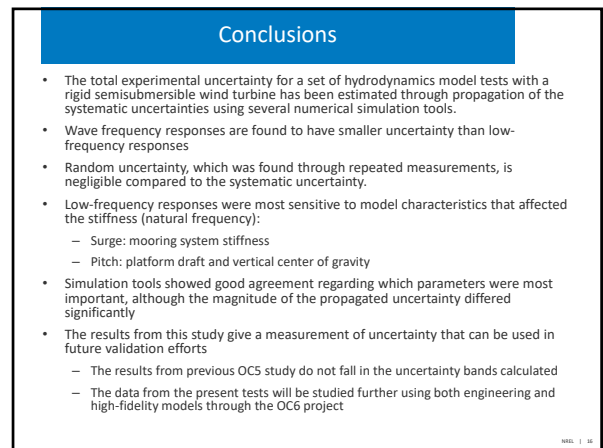
13



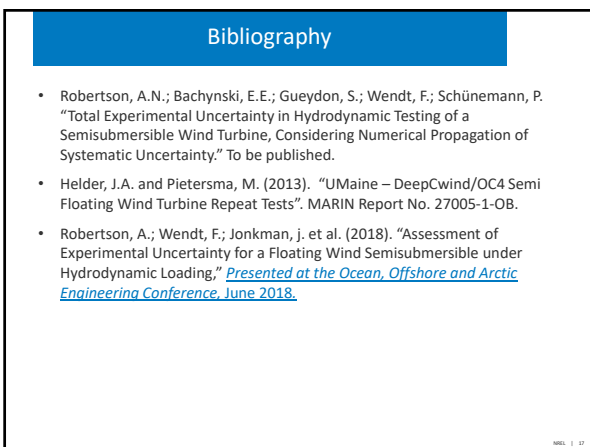
14



15



16



17



18

Systematic Uncertainty Propagation

- Systematic uncertainty of the response metrics due to a given uncertainty source:
 - Simulate model using the baseline properties and calculate associated response metrics.
 - Simulate model using a new value for given uncertain parameter, and calculate response metrics.
 - Difference between response metrics calculated using baseline properties and when changing one of the uncertain parameters is the systematic uncertainty for that parameter.
 - Variations performed in positive and negative directions -> asymmetric uncertainty bounds
- Sum all propagated uncertainty sources
- Propagation affected by the fact we are using a model. Addressed by:
 - Using multiple models
 - Using multiple modeling approaches
 - Taking largest variation across all approaches

$$\theta_i = \partial X / \partial p_i$$

$$b_i = \theta_i d_i$$

$$b_R^2 = \sum_{i=1}^N b_i^2$$

b_i = systematic uncertainty of output metrics
 b_R = total combined systematic uncertainty
 p_i = parameter values
 d_i = systematic uncertainty sources
 X = output response metric
 θ = sensitivity coefficients

19/21

G2) Experimental Testing and Validation

A review of heave plate hydrodynamics for use in floating offshore wind sub-structures,
K. Thiagarajan, University of Massachusetts

Variable-speed Variable-pitch control for a wind turbine scale model,
F.Taruffi, Politecnico di Milan

Experimental Investigation of a Downwind Coned Wind Turbine Rotor under Yawed
Conditions, C.W.Schulz, Hamburg University



Heave plate hydrodynamics for offshore wind turbine applications

Krish Thiagarajan Sharman, University of Massachusetts Amherst
 Amy Robertson, NREL
 Jared Lewis, University of Massachusetts Amherst



EERA DeepWind, Trondheim, 17 January 2019

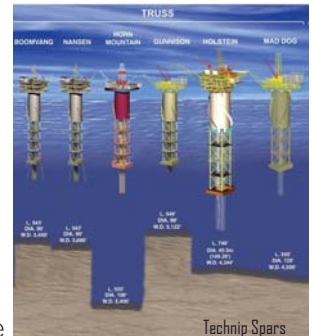
Outline

- Introduction
- Geometric configurations
 - Isolated heave plates
 - Heave plates attached to a column
- Issues common to both configurations
- Future Work

INTRODUCTION

Heave plate application in offshore oil and gas production – spar platforms

- To limit vertical plane motion of platforms for supporting rigid risers
- To protect risers and mooring equipment (Tao & Cai, 2003)
- Heave plates work by:
 - increasing added mass and detuning the system.
 - Increasing damping due to vortex formation and shedding.
- Heave plates allow for a shallower draft (more economic) by decoupling the hull from wave excitation (Molin, 2001).



Other recent heave plate applications

- Wave Energy Converters
- Floating bridge stabilization



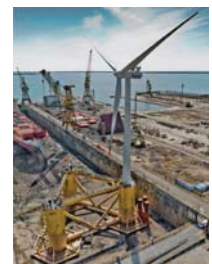
Side view of miniWEC (Brown et al. 2017)



Bridge section with pontoon and heave plate (Kleppa, 2017)

Heave plate applications in offshore wind energy industry

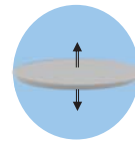
- Offshore wind turbines require stable floating structures
- Stability can be augmented through the use of heave plates



Close-up of a heave plate used on Principle Power's WindFloat platform; and platform assembly near Lisbon, Portugal; (Antonutti, et al. 2014)

Heave Plates and FOWT

- Hull is much lighter than oil and gas counterparts
- Shallower drafts of FOWTs can result in free surface effects and wave interaction with the heave plates
- Dynamic aerodynamic loading can affect hull pitch motion and effectiveness of heave plates
- Multiple plates located adjacent to each other.
- Numerical programs need hydrodynamic coefficients to represent heave plates in motion analysis of FOWT.

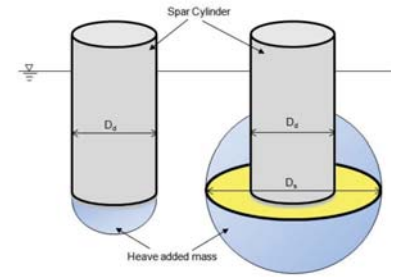


$$m_{a3} = \frac{1}{3} \rho D_{hp}^3$$

Classical solution (Lamb, 1932)

Added mass force

Increased inertial effect due to the acceleration of an additional volume of water along with the structure

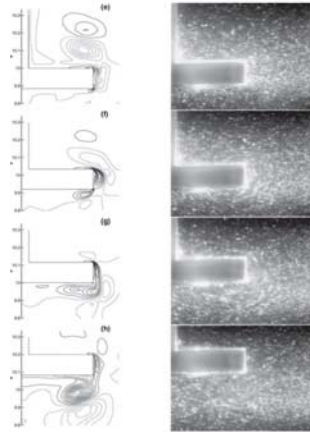


Added mass of a cylinder and cylinder with heave plate; (Sudhakar & Nallayarasu, 2011)

Damping force

Damping forces created by:

- Friction along the walls (small)
- Vortex shedding off the edges
- Wave radiation (small)



Vortex shedding and PIV (Tao & Thiagarajan, 2003)

Data Collection

Reviewed 66 papers from 1958 to present

Papers included 24 Experimental, 26 Numerical and 15 combined

Experiments and numerical analysis included

- free decay tests
- forced oscillations
- regular and irregular waves
- complex wind and wave loading

ISOLATED HEAVE PLATE

Key variables

Heave amplitude and frequency of motion are represented by

- Keulegan Carpenter number

$$KC = \frac{2\pi A}{D_{hp}}$$

- Frequency parameter

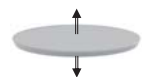
$$\beta = \frac{D_{hp}^2 f}{\nu}$$

A - amplitude

D - diameter

f - frequency

ν - kinematic viscosity



Dimensionless hydrodynamic coefficients

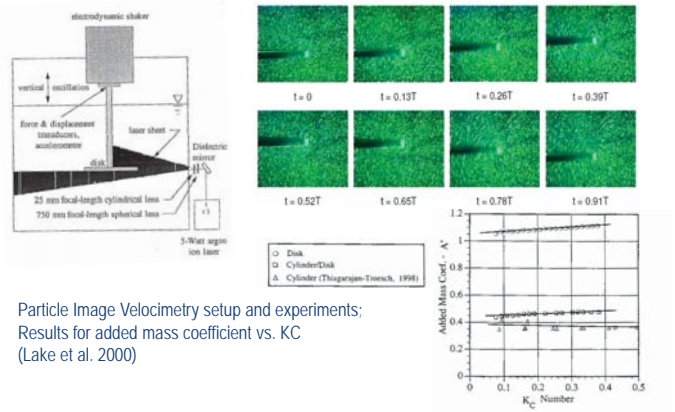
- Added mass coefficient

$$C_a \text{ or } A' = \frac{A_{33}}{\frac{1}{3}\rho D_{hp}^3}$$

- Damping coefficient

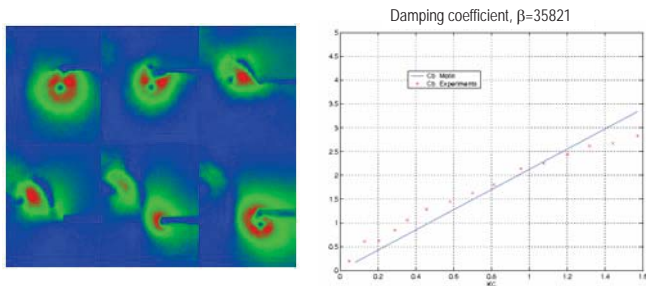
$$C_b \text{ or } B' = \frac{B_{33}}{\frac{1}{3}\rho\omega D_{hp}^3}$$

Flow features around an isolated disk



Particle Image Velocimetry setup and experiments; Results for added mass coefficient vs. KC (Lake et al. 2000)

Damping coefficients of isolated plates



Particle Image Velocimetry experiments; Results for damping coefficient vs. KC (Sireta et al. 2008) (Molin, 2001)

HEAVE PLATES ATTACHED TO A COLUMN

Added mass coefficient definition

C_a = ratio of added mass to displaced mass of the structure

$$C_a = \frac{A_{33}}{\rho \left(\frac{\pi}{4} D_{hp}^2 t_{hp} + \frac{\pi}{4} D_c^2 T_c \right)}$$

D_c – Column diameter
 T_c – column draft
 t_{hp} – heave plate thickness

Damping ratio vs. drag coefficient

- Linear vs. quadratic damping representation

$$F_{3d}(t) = B_{33}v_{rel}(t) \quad F_{3d} = C_d \frac{1}{8} \rho \pi D^2 v_{rel} |v_{rel}|$$

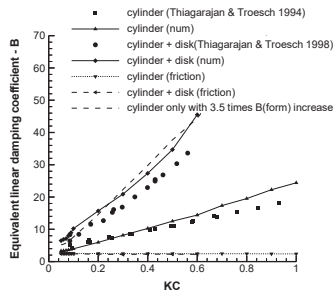
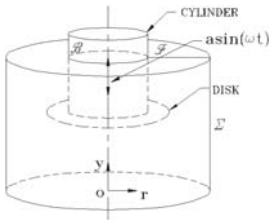
- By equivalent linearization

$$B_{33} = \frac{1}{3} \mu \beta D KC C_d$$

- Damping Ratio:

$$Z = \frac{\text{system damping}}{\text{critical damping}} = \frac{1}{3\pi^2} \frac{C_d}{C_m} \frac{D_{hp}^2 D_c}{(D_c^2 T_c + D_{hp}^2 t_{hp})} KC$$

Damping coefficients of deeply submerged plates

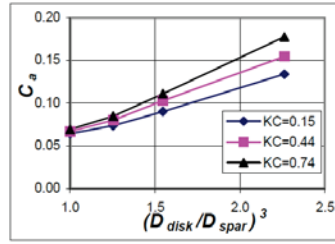


- Tao, L and Thiagarajan, K P, (2003) Low KC flow regimes of oscillating sharp edges Pt. 1: Vortex shedding observation. *Appl. Ocean Res.* 25, 1, 21-25.
- Thiagarajan, K P and Troesch, A W, (1998) Effect of Appendages and Small Currents on the Hydrodynamic Heave Damping of TLP Columns. *J. Offshore Mechanics and Arctic Eng.* 120, 1, 37-42.

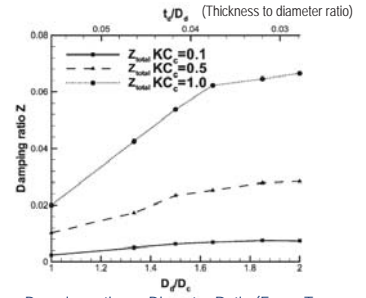
Data Trends: Size (Diameter Ratio)

Added mass increases with Diameter ratio

Damping increases with diameter ratio to an optimum 1.2-1.3 (Sudhaker and Nallayarasu 2011) or 1.2-1.4 (Subbulakshmi, Sundaravadivelu 2016)



Added mass coefficient vs. Diameter Ratio (Thiagarajan, Datta, Ran, Tao & Halkyard, 2002)



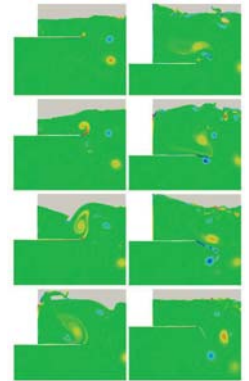
Damping ratio vs. Diameter Ratio (From: Tao & Cai, 2003)

ISSUES COMMON TO BOTH CONFIGURATIONS

Proximity to the free surface

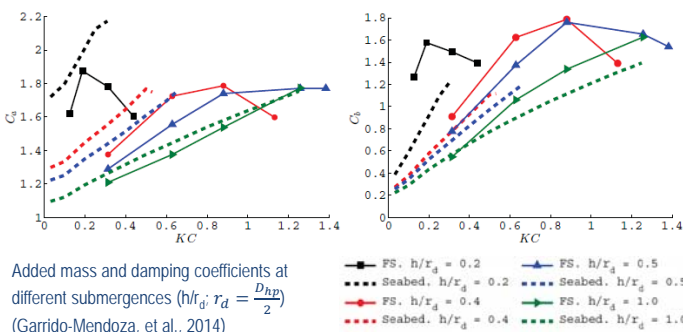
- At a constant frequency (fixed β), the added mass and damping coefficients increase with KC and with decreasing distance to free surface.
- Good agreement between numerics and experiments.

Vortex generation around disk at $KC = 0.65$ and submergence of 0.5 radius. Blue is negative and red is positive vorticity magnitude. (Mendoza et al. 2014)



Data Trends: Proximity To Free Surface

Drag Coefficient greatly effected by the free surface (An & Faltinsen, 2013)
Larger vortices observed when heave plate oscillates closer to the free surface (Garrido-Mendoza et al., 2014)



Added mass and damping coefficients at different submergences ($h/r_d = \frac{D_{HP}}{2}$) (Garrido-Mendoza, et al., 2014)

ONGOING WORK

Added mass coefficient definition

- Offshore oil and gas platforms
 - C_a = ratio of added mass to displaced mass of the structure

$$C_a = \frac{A_{33}}{\rho \left(\frac{\pi}{4} D_{hp}^2 t_{hp} + \frac{\pi}{4} D_c^2 T_c \right)}$$

- Floating offshore wind turbines (e.g. FAST)
 - C_a defined for top and bottom part of the plate:

$$C_{at} = \frac{A_{33t}}{\frac{1}{12} \rho \pi (D_{hp}^3 - D_c^3)} \quad C_{ab} = \frac{A_{33b}}{\frac{1}{12} \rho \pi D_c^3}$$

We assume:

$$\frac{A_{33t}}{A_{33}} = ? \quad \frac{A_{33b}}{A_{33}} = ? \quad C_{at} = C_{ab} = C_a$$

Drag coefficient definition

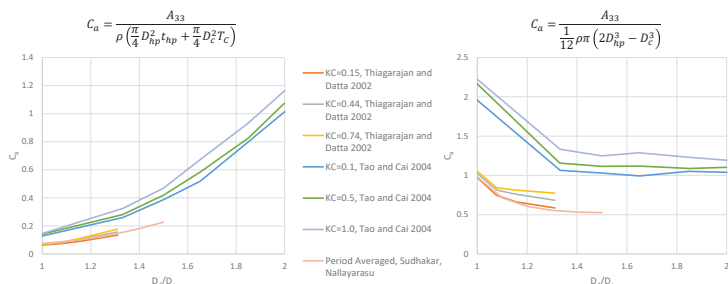
Assuming the drag force is equally split between top and bottom surfaces:

$$C_{db} = \frac{B_{33}}{\frac{2}{3} \rho D_{hp}^2 \omega A}$$

$$C_{dt} = \frac{B_{33}}{\frac{1}{3} \rho D_{hp}^2 \omega A (2 - R^2)} \quad R = \frac{D_c}{D_{hp}}$$

Coefficients in FAST format

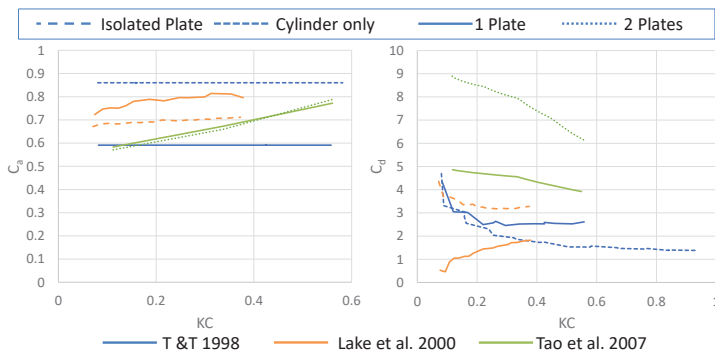
Splitting into top and bottom surfaces produces counter-intuitive results:



The new added mass coefficient decreases as the heave plate becomes relatively larger ($R = \frac{D_c}{D_{hp}}$ decreases) despite the actual added mass increasing.

Comparison of Heave Plate Quantity

Analysis of a Cylinder with 0, 1, and 2 heave plates (separated on cylinder by $0.375D_{hp}$) as well as an isolated heave plate with no cylinder:



Additional Heave plates increase the drag coefficient, but have less impact on added mass

Ongoing Work

- Use data trend lines to develop coefficients for top and bottom parts of a plate
- UMass small scale and PIV experiments to support NREL testing campaign as part of OC6.

References

An, S., & Fallinsen O. M., An Experimental and Numerical Study of Heave Added Mass and Damping of Horizontally Submerged and Perforated Rectangular Plates. *Journal of Fluids and Structures*, 39, 87-101.

Antonutti, R., Peyraud, C., Johanning, L., Incecik, A., & Ingram, D. (2014). An Investigation of the Effects of Wind-Induced Inclination on Floating Wind Turbine Dynamics: Heave Plate Excursions. *Ocean Engineering*, 91, 208-217.

Brown, A., Thomson, J., & Rusch, C. (2017). Hydrodynamic Coefficients of Heave Plates with Application to Wave Energy Conversion. *IEEE Journal of Oceanic Engineering*, 43(4), 983-996.

Garrido-Mendoza, C. A., Thiagarajan, K. P., Souto-Iglesias, A., Bouscasse, B., & Colagrossi, A. (2014). Proceedings from ASME 2014 OMAE: Numerical Investigation of the Flow Features Around Heave Plates Oscillating Close to a Free Surface or Seabed. San Francisco, California.

Keulegan, G. H., & Carpenter, L. H. (1958). Forces on Cylinders and Plates in an Oscillating Fluid. *Journal of Research of the National Bureau of Standards*, 60(5), 423-440.

Kleppa, E. (2017). Numerical Analysis of Wave-Induced Responses of Floating Bridge Pontons with Bilge Boxes (Masters Thesis). Retrieved from Nordic Master in Maritime Engineering. [Online] <http://www.nor-mar-eng.org/>.

Lake, M., Troesch, A. W., Perlin, M., and Thiagarajan, K. P. (2000). Scaling effects in hydrodynamic coefficient estimation of TLP and spar structures. *J. Offshore Mech and Arctic Eng.* 122 118-124.

Li, J., Liu, S., Zhao, M., Teng, B. (2013). Experimental Investigation of the Hydrodynamic Characteristics of Heave Plates Using Forced Oscillation. *Ocean Engineering*, 66, 82-91.

Molin, B. (2001). On the Added Mass and Damping of Periodic Arrays of Fully or Partially Porous Disks. *Journal of Fluids and Structures*, 15, 275-290.

Sirela, F.-X., Thiagarajan K. P., Molin, B., and Pislani, F. (2008). "Hydrodynamic coefficients of porous plates and application to subsea deployment", Proceedings Marine Operations Specialty Symposium (MOSS-2008), Paper 44, Singapore.

Subbalakshmi, A., & Sundaravadivelu, R. (2016). Heave Damping of Spar Platform for Offshore Wind Turbine With Heave Plate. *Ocean Engineering*, 121, 24-36.

Sudhakar, S., Nallayarasu, S. (2011). Proceedings from ASME 2011 OMAE: Influence of Heave Plate on Hydrodynamic Response of Spar. Rotterdam, The Netherlands.

Tao, L., & Cai, S. (2003). Heave Motion Suppression of a Spar With a Heave Plate. *Ocean Engineering*, 31, 669-692.

Tao, L., & Dray, D. (2008). Hydrodynamic Performance of a Spar and Porous Heave Plates. *Ocean Engineering*, 35, 1006-1014.

Tao, L., Molin, B., Scola, Y.-M., & Thiagarajan, K. (2007). Spacing Effects on Hydrodynamics of Heave Plates on Offshore Structures. *Journal of Fluids and Structures*, 23, 1119-1136.

Tao, L., & Thiagarajan, K. (2003). Low KC Flow Regimes of Oscillating Sharp Edges I. Vortex Shedding Observation. *Applied Ocean Research*, 25, 21-35.

Tao, L., Thiagarajan, K. (2003). Low KC Flow Regimes of Oscillating Sharp Edges II. Hydrodynamic Forces. *Applied Ocean Research*, 25, 53-62.

Thiagarajan, K. P., Datta, I., Ran, A. Z., Tao, L., & Halkyard, J. E. (2002). Proceedings from ASME 2002 OMAE: Influence of Heave Plate Geometry on the Heave Response of Classic Spars. Oslo, Norway.

Wadhwa, H., & Thiagarajan, K. P. (2009). Proceedings from ASME 2009 OMAE: Experimental Assessment of Hydrodynamic Coefficients of Disks Oscillating Near a Free Surface. Honolulu, Hawaii.

Zhang, S., Ishihara, T. (2018). Numerical Study of Hydrodynamic Coefficients of Multiple Heave Plates by Large Eddy Simulations with Volume of Fluid Method. *Ocean Engineering*, 163, 583-596.

EERA DeepWind'19

Trondheim - Norway

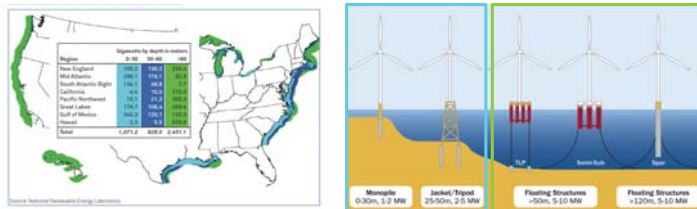


VARIABLE-SPEED VARIABLE-PITCH CONTROL FOR A WIND TURBINE SCALE MODEL

A. FONTANELLA, F. TARUFFI, I. BAYATI, M. BELLOLI

Politecnico di Milano
Department of Mechanical Engineering

FLOATING OFFSHORE



- Offshore wind energy LCOE is still high
- Floating offshore wind energy is a potential game changer for LCOE reduction
 - Greater energy production
 - Increased range of possible installation sites
 - Lower installation costs
- Deep seas represent a significant fraction of exploitable wind energy in Europe and worldwide

A. FONTANELLA / F. TARUFFI

POLITECNICO MILANO 1863

HIL FOWT TESTING

FOWTs WIND TUNNEL TESTING

- Experimental data required to calibrate/validate numerical simulation tools
- Scale model testing:
 - Lower costs than full-scale experiments
 - Control of environmental conditions
 - Lower uncertainties
- Hybrid/HIL testing
 - Rotor loads (including control) reproduced by a wind turbine scale model
 - Hydrodynamic loads and platform motion from numerical computations
 - 6-DOFs robot moves the wind turbine model in real-time



A. FONTANELLA / F. TARUFFI

POLITECNICO MILANO 1863

CONTROL SCALING

SCALE MODEL CONTROL

- Required to improve experiment fidelity
- Reproduction of rotor dynamics and control induced loads
- Direct investigation of FOWT control problem



- Non-ideal model scaling
- Low Reynolds flow
- Not possible to achieve target response with a scaled controller



A. FONTANELLA / F. TARUFFI

POLITECNICO MILANO 1863

WIND TURBINE SCALE MODEL

Scale	Expression	Value
Length	λ_L	75
Velocity	λ_v	3

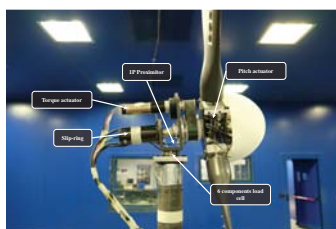
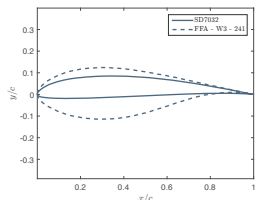
ROTOR

Performance scaling: low-Re blades

- Match thrust coefficient
- Match scaled weight
- Match first flapwise frequency

MECHATRONIC CONFIGURATION

- Similar to the full-scale turbine with torque and pitch actuators
- Onboard sensors acquired in real-time
- Embedded Control and Monitoring system



A. FONTANELLA / F. TARUFFI

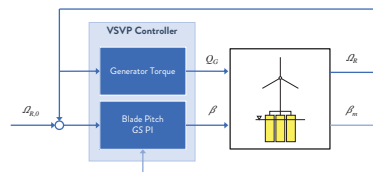
POLITECNICO MILANO 1863

WTM CONTROLLER

PARTIAL LOAD

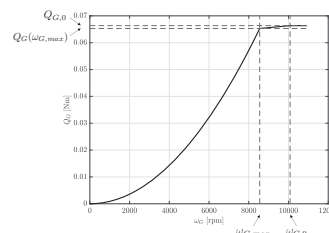
- Constant pitch angle $\beta = 5^\circ$
- Variable generator torque

$$Q_G = K_G \omega_G^2$$
- K_G chosen to maximize power coefficient



TRANSITIONS

- No region 1.5
- Linear transition to reach rated torque (no-PI torque controller)



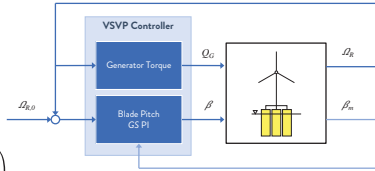
A. FONTANELLA / F. TARUFFI

POLITECNICO MILANO 1863

WTM CONTROLLER

FULL LOAD

- Constant torque
- Variable collective pitch angle
- Generator speed and generator power feedback



$$\beta = \left(k_p^{\omega} e_{\omega} + k_i^{\omega} \int e_{\omega} dt \right) + \left(k_p^{\beta} e_{\beta} + k_i^{\beta} \int e_{\beta} dt \right)$$

GAIN SCHEDULING

- Quadratic aerodynamic gains scheduling
- Additional non-linear gain scheduling for large speed excursions

$$\eta_A = \frac{1}{1 + \frac{\beta}{KK_1} + \frac{\beta^2}{KK_2}}$$

$$\eta_{NL} = 1 + \frac{e_{\omega}^2}{(\omega_2 - \omega_0)^2}$$

WTM DRIVETRAIN

DRIVETRAIN NON-IDEALITIES

Largely due to commercially available components and mechatronic design

- Not possible to have scaled generator/transmission
- Technological limits for blades realization

DRIVETRAIN PROPERTIES		
	DTU	WTM
Transmission ratio	50	42
LSS inertia	0.066	0.279
HSS inertia	6.323e-7	6.438e-6
Mechanical efficiency	1	0.735
Electrical efficiency	0.94	0.894

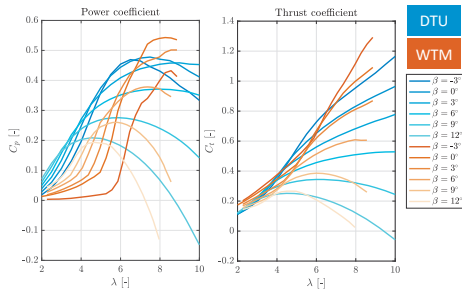
EFFECTS

- WT controller works on HSS feedback
- Drivetrain inertia directly affects rotor dynamics and pitch controller response

STEADY AERODYNAMICS

POWER COEFFICIENT

- Lower than target for small β and low values of λ
- Max C_p of 0.54 at $\beta = 0^\circ$ and $\lambda = 8.26$
- Influence on the WT start-up
- Above-rated: lower β to keep power at rated



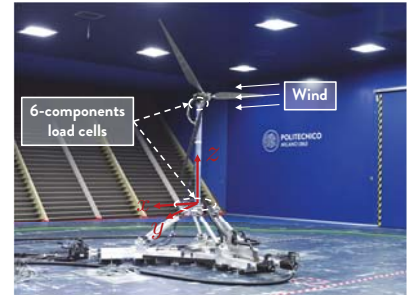
THRUST COEFFICIENT

- Closer to target
- Some differences for small β and low values of λ

WIND TUNNEL TESTS

SCALE MODEL TESTING

- Laminar wind conditions
- Load measurements from two load cells
- **Steady-state tests**
 - Full-scale wind speed from 9 to 25 m/s
 - Average loads and control inputs at regime
- **Dynamic tests**
 - Sinusoidal surge motion at different frequencies and amplitudes
 - Below and above rated mean wind speeds



WIND TUNNEL TESTS

CONTROLLER SETTINGS

- Based on the public definition of the LIFES50+ OO-Star Wind Floater Semi 10MW

1. Original parameters were scaled
2. Parameters referred to HSS were corrected for different efficiency/transmission ratio
3. Increased below-rated pitch angle
4. Modified generator torque constant (max C_p for $\beta = 5^\circ$)

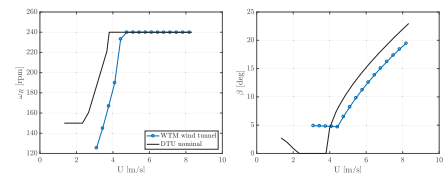


Parameter	Symbol	Unit	Value
Rated generator speed	$\omega_{G,D}$	rpm	10080
Region 2 transition speed	$\omega_{G,max}$	rpm	8550
Rated generator power	$P_{G,D}$	W	70.044
Generator torque constant	K_G	Nm/(rad/s) ²	8.143·10 ⁻⁸
Minimum pitch angle	β_{min}	deg	5
Proportional speed gain	k_p^{ω}	s	1.831·10 ⁻⁴
Integral speed gain	k_i^{ω}	-	2.095·10 ⁻⁴
Proportional power gain	k_p^P	rad/W	8.265·10 ⁻⁴
Integral power gain	k_i^P	rad/(Ws)	2.070·10 ⁻²
Linear gain scheduling factor	KK_1	deg	198.329
Quadratic gain scheduling factor	KK_2	deg ²	693.222
Speed for doubled gains	ω_2	rpm	13104

STEADY-STATE TESTS

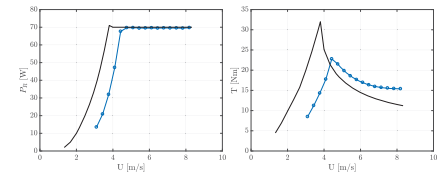
PARTIAL LOAD

- Rated reached at 14 m/s
- Steady-state angular speed lower than target
- Low λ and increased β lead to decreased power and low thrust force



FULL LOAD

- Pitch angle always lower than target
- Increased thrust force: WTM rotor designed to have target thrust at DTU 10MW nominal pitch angles



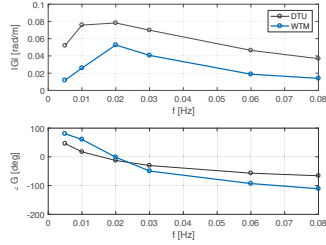
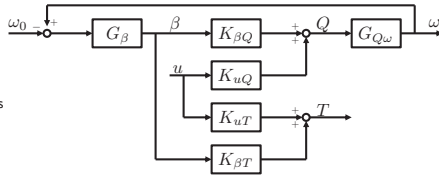
DYNAMIC TESTS

IDEAL CLOSED-LOOP

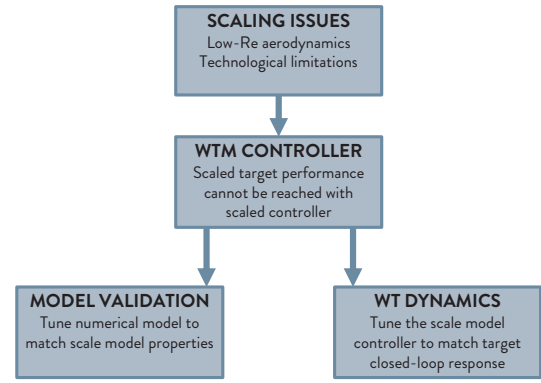
- Pitch controller disturbance rejection function
- Above-rated mean wind speed: 18 m/s

$$G(f) = \frac{\omega_R(f)}{u(f)} = \frac{G_{u\omega}}{1 - G_\beta G_{\beta\omega}}$$

- $G_{u\omega}$ depends both on the drivetrain mechanical properties and on rotor aerodynamics
- G_β is the PI-pitch controller transfer function
- $G_{\beta\omega}$ depends both on the drivetrain mechanical properties and on rotor aerodynamics



CONCLUSIONS



Experimental Investigation of a Downwind Coned Wind Turbine Rotor under Yawed Conditions

Christian Schulz

Supported by
Stefan Netzband
Klaus Wiczorek
Moustafa Abdel-Maksoud

christian.schulz@tuhh.de
Institute for Fluid Dynamics and Ship Theory
Hamburg University of Technology



MOTIVATION

Particular needs for new experimental investigations

- Only few investigations at higher yaw angles
- Focus on power and thrust

Support of new wind turbine concepts

- Free-yawing wind turbines
- Self-aligning floating offshore wind turbines (SFOWT)
 - Higher yaw angle
 - Self-aligning dependent on yaw moment

→ Detailed investigation of yaw moment and power up to 55° yaw angle



OVERVIEW: EXPERIMENTAL INVESTIGATION OF A DOWNWIND CONED ROTOR

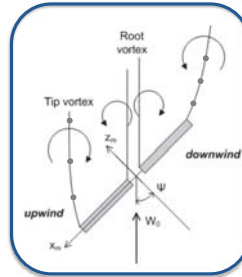


Experimental Investigation of a Downwind Coned Rotor

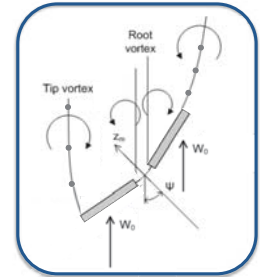
- 1 Motivation
- 2 Background
- 3 Wind tunnel model and technology
- 4 Results
- 5 Conclusion
- 6 Invitation to simulate



BACKGROUND: ORIGIN OF THE YAW MOMENT



1. Lower induction at the upwind side



2. Higher inflow angle on the upwind side

[W. HAANS, WIND TURBINE AERODYNAMICS IN YAW – UNRAVELLING THE MEASURED ROTOR WAKE (SLIGHTLY MODIFIED)]



BACKGROUND: PREVIOUS EXPERIMENTS

Previous experiments of under yawed conditions

- MEXICO
- NREL UAE Phase VI
- Sant and Haans, TU Delft
- ...

Only very few measured the yaw moment
Downwind coned rotor was only considered by NREL

- Extremely high cone angle or teeter dampers used, strong tower effects

aerodyn SCD 6MW
9° downwind cone



[AERODYN ENGINEERING]

[M. HAND, D. SIMMS, S. LARWOOD: Unsteady Aerodynamics Experiment Phase VI: Wind Tunnel Test Configurations and Available Data Campaigns]



OVERVIEW: EXPERIMENTAL INVESTIGATION OF A DOWNWIND CONED ROTOR



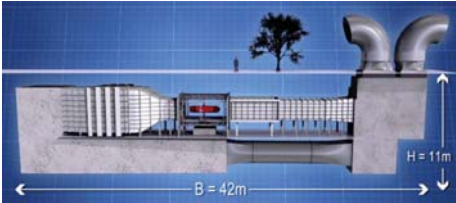
Experimental Investigation of a Downwind Coned Rotor

- 1 Motivation
- 2 Background
- 3 Wind tunnel model and technology
- 4 Results
- 5 Conclusion
- 6 Invitation to simulate



Experimental Investigation of a Downwind Coned Wind Turbine Rotor under Yawed Conditions 16.01.2019

WIND TUNNEL AT TUHH




TUHH Wind Tunnel		Operational Modes:	
Max. wind speed:	40 m/s	closed circuit (Göttingen – mode)	
Turbulence degree:	< 0.2%	open circuit (Eiffel – mode)	
Measuring section (L X B X T)	5 x 3 x 2 m	integrated 6-component balance	

TUHH Technische Universität Hamburg-Harburg

Experimental Investigation of a Downwind Coned Wind Turbine Rotor under Yawed Conditions 16.01.2019

WIND TUNNEL MODEL: OVERVIEW

TUHH Experimental Wind Turbine	
Rated power	130 W
Rotor diameter	0.925 m
Number of blades	2
Downwind cone angle	5°
Rated wind speed	9.3 m/s
Rated rotational speed	1200 RPM
Wind tunnel size	2 x 3 m
Blockage ratio	11.2 %
Sensor	6C - balance



TUHH Technische Universität Hamburg-Harburg

Experimental Investigation of a Downwind Coned Wind Turbine Rotor under Yawed Conditions 16.01.2019

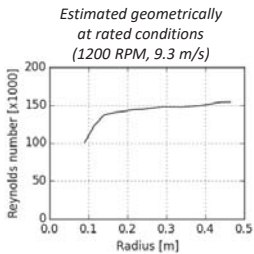
WIND TUNNEL MODEL: BLADE DESIGN

Design goals

- Validation case for simulations
 - Low Reynolds number dependency
 - No Stall
 - Availability of measurement data for airfoil
 - High power coefficient
 - Low blade deformation

Properties

- SD7062, 14% thickness (Experimental data available for Re 100,000 and 200,000)
- Nearly constant Reynolds number of 150,000 at 1200 RPM



Estimated geometrically at rated conditions (1200 RPM, 9.3 m/s)

TUHH Technische Universität Hamburg-Harburg

Experimental Investigation of a Downwind Coned Wind Turbine Rotor under Yawed Conditions 16.01.2019

WIND TUNNEL MODEL: BLADE MANUFACTURING AND QUALITY

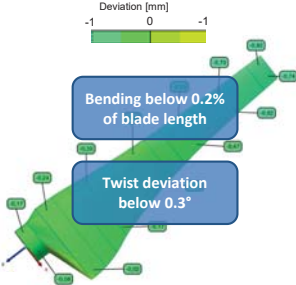
Choice of material driven by

- Manufacturing accuracy
- High inertia forces
 - Acceleration: 400 g at 50 % of radius
 - Induce bending moments due to cone angle

Rigid and lightweight structure needed

- Prepreg carbon fiber
- Shear web
- Hard resistance foam core
- High risk of undesired twisting

3D scan performed



Deviation [mm] scale: -1, 0, -1

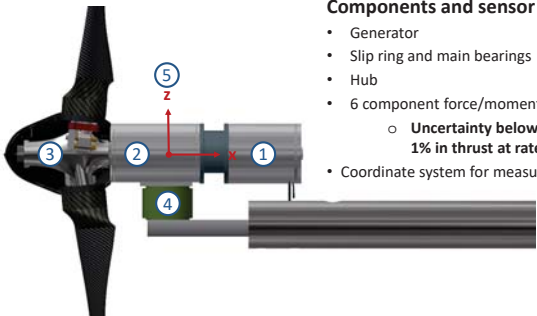
Bending below 0.2% of blade length

Twist deviation below 0.3°

TUHH Technische Universität Hamburg-Harburg

Experimental Investigation of a Downwind Coned Wind Turbine Rotor under Yawed Conditions 16.01.2019

WIND TUNNEL MODEL: NACELLE, SENSOR AND COORDINATE SYSTEM




Components and sensor

- Generator
- Slip ring and main bearings
- Hub
- 6 component force/moment sensor
 - Uncertainty below 2% in torque and 1% in thrust at rated conditions
- Coordinate system for measurements

TUHH Technische Universität Hamburg-Harburg

Experimental Investigation of a Downwind Coned Wind Turbine Rotor under Yawed Conditions 16.01.2019

OVERVIEW: EXPERIMENTAL INVESTIGATION OF A DOWNWIND CONED ROTOR

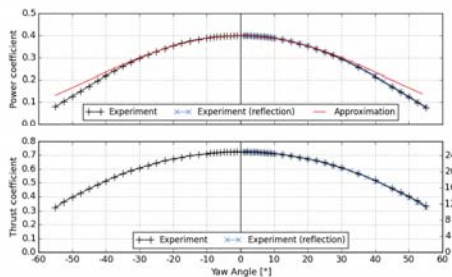


Experimental Investigation of a Downwind Coned Rotor

- Motivation
- Background
- Wind tunnel model and technology
- Results
- Conclusion
- Invitation to simulate

TUHH Technische Universität Hamburg-Harburg

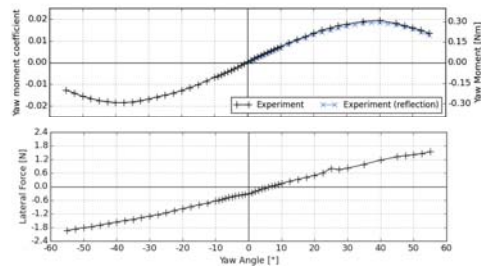
RESULTS: POWER AND THRUST COEFFICIENTS (MEAN VALUES)



- Results**
- Power coefficient of 0.4
 - Very smooth curves for power coefficient and thrust
 - Nearly symmetric behaviour
 - $\cos^2\gamma$ fits well up to 30°
 - Strong deviation at higher yaw angles

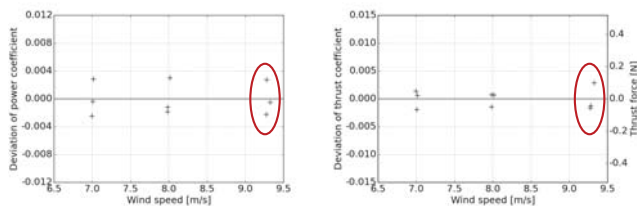
RESULTS: YAW MOMENT AND LATERAL FORCE (MEAN VALUES)

$$C_{m,yaw} = \frac{M_{yaw}}{\frac{1}{2} \rho v^2 A_{rotor} R_{rotor}}$$



- Results**
- **Yaw moment**
 - Maximum yaw moment at 40°
 - Smooth curve
 - Slight deviation to symmetric copy
 - Zero crossing nearly exactly at 0°
 - Low uncertainty in yaw angle
 - **Lateral force**
 - Slight offset in Lateral force (ca. 1% of thrust)
 - Mainly caused by nacelle drag force

RESULTS: REPEATABILITY OF TORQUE AND THRUST



- Repeatability checked on three different days
- Cables were moved
- Deviation between repetitions below 1% in C_p and 0.5% in C_t at rated conditions

RESULTS: CRITICAL ISSUES

Aspects that need to be considered

- Small offset in lateral force
- Yaw moment deviated by nacelle drag force and unknown lever arm
- Vibration induced periodic forces up to 2% of thrust
- Deviations in rotational speed up to 1% (considered in C_p calculation)
- Low pass filter was applied (40 Hz corner frequency)
- Small deviations due to cables' stiffness

➡ No serious issues were observed



OVERVIEW: EXPERIMENTAL INVESTIGATION OF A DOWNWIND CONED ROTOR



Experimental Investigation of a Downwind Coned Rotor

- 1 Motivation
- 2 Background
- 3 Wind tunnel model and technology
- 4 Results
- 5 Conclusion
- 6 Invitation to simulate

CONCLUSION



Conclusion

- High repeatability and low measurement uncertainty were achieved
- $\cos^x\gamma$ approach is not suitable for higher yaw angles
- Yaw moment increases up to 40°
- **Rare data for the yaw moment is now available for validation**
 - Validity of Blade Element Momentum Method for Self-aligning Floating Wind Turbines can be investigated

INVITATION TO SIMULATE

Every researcher is invited to validate his tool with the presented experiment!

- A detailed description will be published in the **conference proceedings** (if paper will be accepted)
- **Data sets or CAD models** may be handed out on request
- Publications welcome



Acknowledgement

The research project is financially supported by the *BMW*



THANK YOU FOR YOUR ATTENTION



Christian W. Schulz

H) Wind farm control systems

A survey on wind farm control and the OPWIND way forward, Leif Erik Andersson, NTNU

Hierarchy and complexity in Control of large Offshore Wind Power Plant Clusters,
A. Kavimandan, DTU

Verification of Floating Offshore Wind Linearization Functionality in OpenFAST,
J. Jonkman, NREL

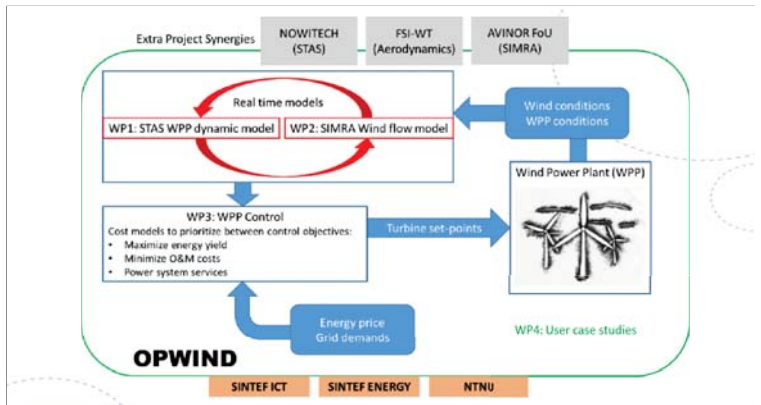
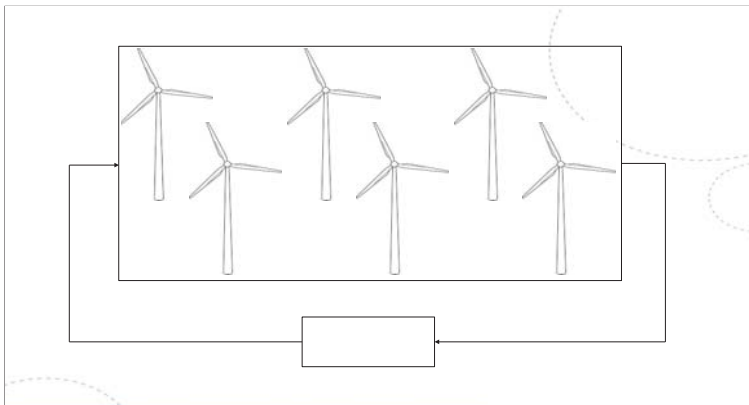
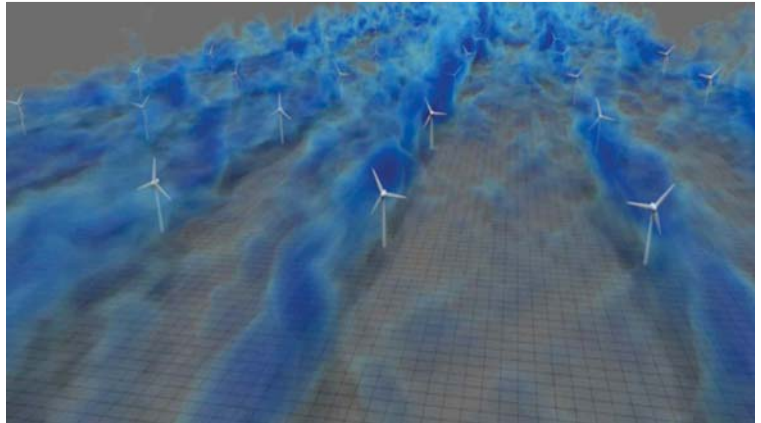
A survey on wind farm control and the OPWIND way forward

DeepWind 2019 – Leif Erik Andersson



18.01.2019



NTNU AMOS
Centre for Autonomous Marine Operations and Systems

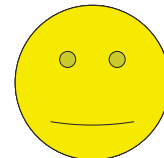


High fidelity models

- Task:
 - Solve numerically the 3D unsteady Navier-Stokes equations
- Direct Numerical Simulation (DNS) 
- Large Eddy Simulations (LES) 
 - e.g.:
 - Ellipsys3D (1995)
 - PALM (2001)
 - SP-Wind (2010)
 - SOWFA (2012)

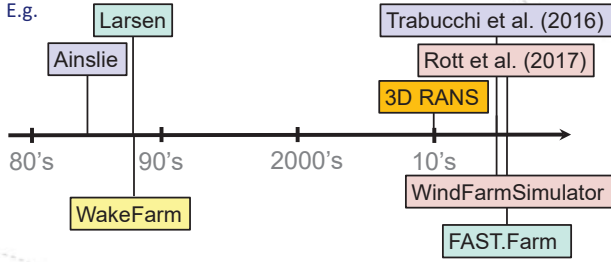
Medium fidelity models

- Compromise between accuracy and computational costs
- E.g.



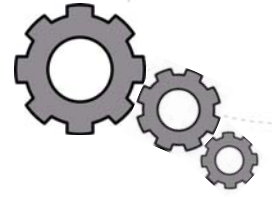
Medium fidelity models

- Compromise between accuracy and computational costs
- E.g.



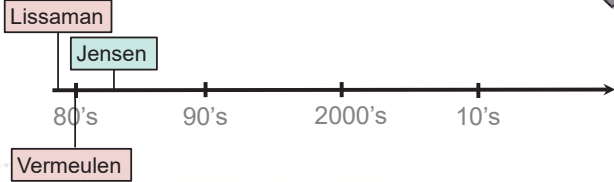
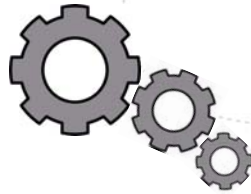
Engineering models

- Focus on simplicity
- Small number of parameters
- Steady-state vs dynamic



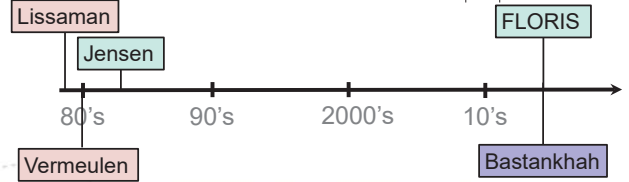
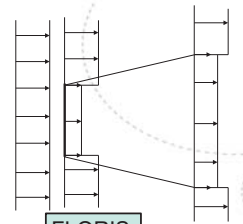
Engineering models

- Focus on simplicity
- Small number of parameters
- Steady-state vs dynamic
- E.g.



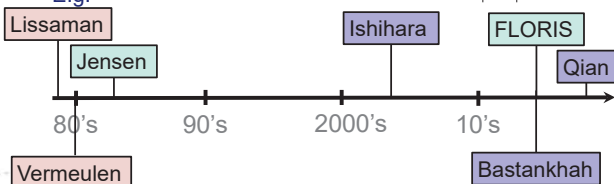
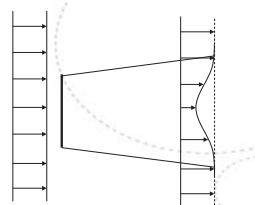
Engineering models

- Focus on simplicity
- Small number of parameters
- Steady-state vs dynamic
- E.g.

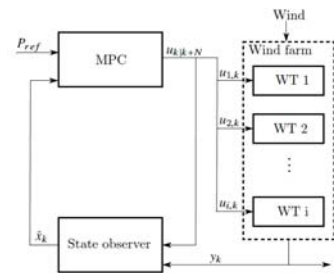


Engineering models

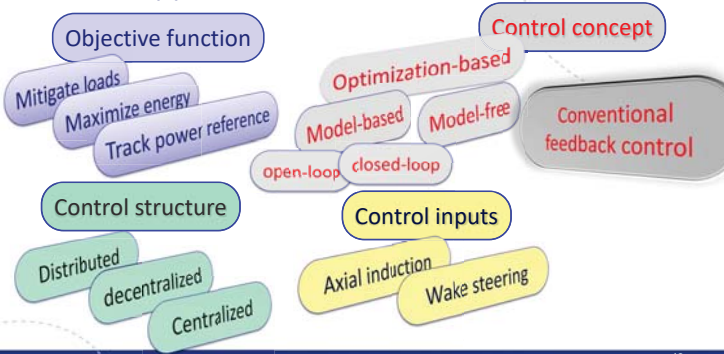
- Focus on simplicity
- Small number of parameters
- Steady-state vs dynamic
- E.g.



Example – centralized model-predictive control (MPC)



Control approaches

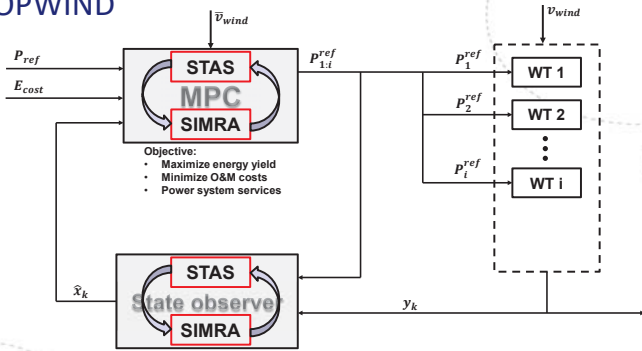


OPWIND

- Operational control for WIND power plants



OPWIND



Thank you!

Questions?



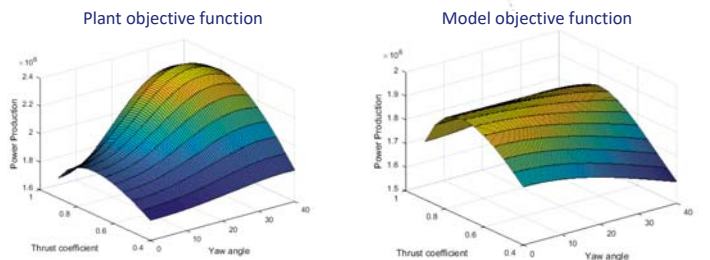
Modifier Adaptation with Gaussian process regression

- Optimize model does not necessarily optimize plant
- Idea: Correct the model with plant measurements

$$\begin{aligned}
 \mathbf{u}_{k+1}^* &= \arg \min_{\mathbf{u}} \phi(\mathbf{u}) + (\mathcal{G}\mathcal{P})_k^{\Phi_p - \Phi}(\mathbf{u}, \mathbf{U}_k) \\
 \text{s.t. } G_i(\mathbf{u}) + (\mathcal{G}\mathcal{P})_k^{(G_{p,i} - G_i)}(\mathbf{u}, \mathbf{U}_k) &\leq 0, \quad i = 1, \dots, n_g, \\
 \mathbf{u} &\in \mathcal{U},
 \end{aligned}$$

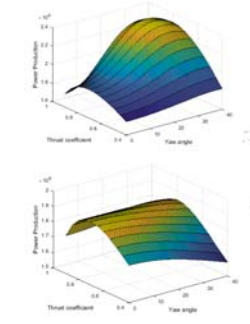
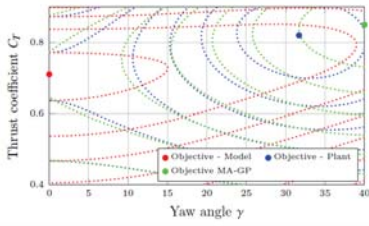


Example – 2 turbines & 2 control inputs



Example – 2 turbines & 2 control inputs

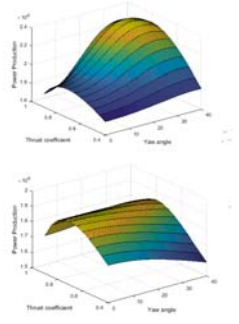
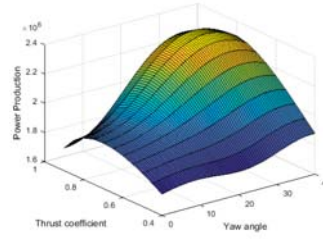
Corrected objective function – after training



NTNU AMOS
Centre for Autonomous Marine
Operations and Systems

Example – 2 turbines & 2 control inputs

Corrected objective function – 10 iteration

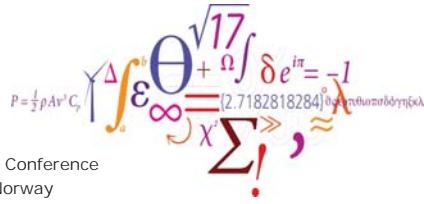


NTNU AMOS
Centre for Autonomous Marine
Operations and Systems



Hierarchy and complexity in control of large offshore wind power plant clusters

Anup Kavimandan, Kaushik Das, Anca D. Hansen, Nicolaos A. Cutululis
DTU Wind Energy, Risø, Denmark



EERA Deepwind'2019
16th Deep Sea Offshore Wind R&D Conference
15-17 January 2019, Trondheim, Norway

DTU Wind Energy
Department of Wind Energy



Outline

- Control Objectives
- What is a Cluster ?
 - Aim of a Cluster
- Control Hierarchies in an offshore Wind Power Plant (OWPP) cluster
- State-of-the-art literature in control of large OWPPs
- Control Architectures for large OWPP clusters
 - Centralized
 - Distributed
 - Decentralized
- Control complexities
- Case Study: Dogger Bank
- Summary

Control Objectives in WPPs

Wind Farm Active Power Control

- Maximize wind power extraction
- Gradient control, balance reserve, frequency control
- Minimize fatigue loads due to wakes

Frequency Control

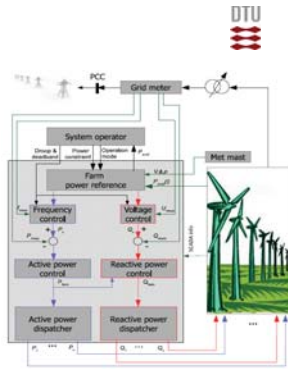
- Provides primary frequency control by adding a P-demand component to the reference farm power, based on measured frequency
- It is in cascade with active power control

Wind Farm Reactive Power Control

- Voltage regulation in the collection and transmission grid
- Improve power factor at the PCC
- Minimize losses and optimize transmission capacity

Voltage Control

- Voltage support to the operator by adding a Q-demand component to the reference farm power
- HVDC converter and tap changers also assist in voltage control



What is a Cluster ?

- Multiple WPPs existing in close proximity aggregated to form a 'Cluster'
- Individual WPPs could be owned by same or separate owners

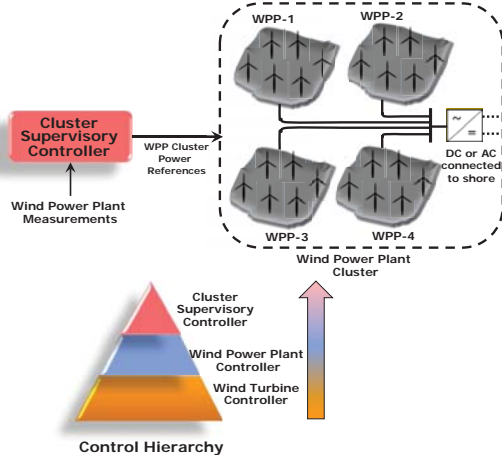


Aim of a Cluster ?

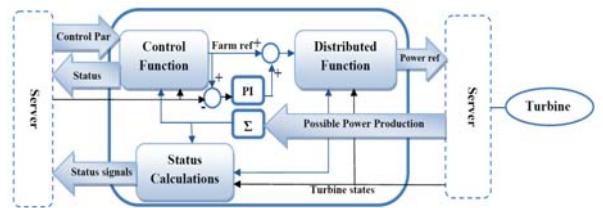
- Increased controllability to better fulfil the TSO requirements
- Sharing of electrical infrastructure (e.g., HVDC converter, export cable etc.)
- Increase the accuracy of wind power feed-in forecast
- Support the coordination between TSOs, dispatch centers, wind power producers and energy markets

https://www.siemens.com/press/pool/de/pressebilder/2013/photonews/300dpi/PN201312/PN201312-10a_300dpi.jpg

Control Hierarchies in a WPP cluster



State-of-the-art literature in control of large OWPPs Horns Rev Wind Farm Controller



- Advanced Control functions providing power (both active and reactive) reference for the wind farm
- Distribution functions converting the farm level power reference to set points for the individual turbines
- PI controller to ensure correct power production

State-of-the-art literature in control of large OWPPs

Wind Farm Hierarchical Control System

- A central WF controller to generate reference signals (active and reactive power) for each local WT controller
- Fault ride through capability is existing at the WT controller level rather than the WPP.
- The local WT controller is built-up with a hierarchical structure
- The WF control level consists of two control loops

7 DTU Wind Energy, Technical University of Denmark 18 January 2019

State-of-the-art literature in control of large OWPPs

Wind Farm Cluster Management System

- WPPs are grouped in 'clusters' physically
- Controlled from an 'upper' level in the hierarchy
- WCMS makes use of WF control strategies and wind energy forecast technologies
- The architecture, consists of two layers, namely the 'TSO layer' and the 'dispatch layer'

8 DTU Wind Energy, Technical University of Denmark 18 January 2019

Control Architectures for large OWPP clusters

Centralized Control

- All the information available about the system is centralized at one location.
- The controllers monitor and coordinate the operation of each turbine
- Challenge
 - Heavy computational burden to process the information
 - Vulnerable to loss or corruption and interruption of information

9 DTU Wind Energy, Technical University of Denmark 18 January 2019

Control Architectures for large OWPP clusters

Distributed Control

- The turbines talk to each other in order to agree on a global outcome
- Consists of a number of local controllers with capability of communication between them
- Data may be processed locally or remote-controlled by a central controller
- Improves cybersecurity and resilience of the network with respect to failure
- Challenges
 - Proper design of a distributed algorithm
 - Reliability of the communication network
 - Coordination of the agents to achieve the desired power regulation

10 DTU Wind Energy, Technical University of Denmark 18 January 2019

Control Architectures for large OWPP clusters

Decentralized Control

- Overall plant is controlled by several independent controllers
- Local regulators are designed to operate in an independent fashion
- Information could be shared between the local decentralized control centres
- Challenge
 - Strong interactions between regulators can even prevent one from achieving stability

11 DTU Wind Energy, Technical University of Denmark 18 January 2019

Control complexities in large offshore WPP clusters

- Control Coordination
- Communication Requirements
- Control during transients
- Assets owned by different operators

12 DTU Wind Energy, Technical University of Denmark 18 January 2019

Case Study: Dogger Bank Communication Requirements



Mode of Communication							
Case 1		Case 2		Case 3		Case 4	
Serial - 120 WTs Parallel - 4 WPPs		Serial - 480 WTs Parallel - 0		Parallel - 120 WTs Serial - 4 WPPs		Parallel - 480 WTs Serial - 0	
Action	Delay (ms)	Action	Delay (ms)	Action	Delay (ms)	Action	Delay (ms)
Send to WT1 Read Inverter1	500	Send to WT1 Read Inverter1	500	Send to WPP1 Read WPP1	500	Send to WT1 Read Inverter1	500
Send to WT2 Read Inverter2	1000	Send to WT2 Read Inverter2	1000	Send to WPP2 Read WPP2	1000	Send to WT2 Read Inverter2	500
.....
Send to WT120 Read Inverter120	6*10 ⁴	Send to WT480 Read Inverter480	24*10 ⁴	Send to WPP4 Read WPP4	2000	Send to WT480 Read Inverter480	500

- For big OWPP clusters with large number of assets, the cumulative delays can be high
- The delays will increase if more signals are required to be transmitted for every WT
- Delays like measurement filter delay, scada computation delay etc., can further make the response of the system slower

Summary



- Sharing of responsibility can make the system more resilient and reduce the high computational demand
- Distributed control approaches offer the capability to distribute the computational burden
- With the existing industrial practises and communication standards the delays can reach very high values for large OWPP clusters with hundreds of assets
- Appropriate techniques must be implemented in the controller to solve the communication delay related issues.



Thank you Questions & Discussions

This project has received funding from the European Union's Horizon 2020 research and innovation programme under the Marie Skłodowska-Curie grant agreement no. 765585
This presentation reflects only the author's view. The Research Executive Agency and European Commission are not responsible for any use that may be made of the information it contains.



NATIONAL RENEWABLE ENERGY LABORATORY



Verification of Floating Offshore Wind Linearization Functionality in OpenFAST

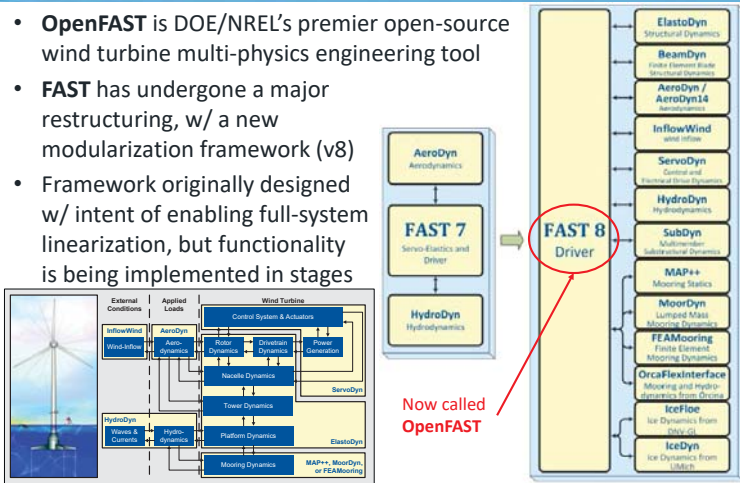
Nicholas Johnson
Jason Jonkman, Ph.D.
 Alan Wright, Ph.D.
 Greg Hayman
 Amy Robertson, Ph.D.

EERA DeepWind'2019
 16-18 January, 2019
 Trondheim, Norway

NREL is a national laboratory of the U.S. Department of Energy, Office of Energy Efficiency and Renewable Energy, operated by the Alliance for Sustainable Energy, LLC.

Introduction: The OpenFAST Multi-Physics Engineering Tool

- **OpenFAST** is DOE/NREL's premier open-source wind turbine multi-physics engineering tool
- **FAST** has undergone a major restructuring, w/ a new modularization framework (v8)
- Framework originally designed w/ intent of enabling full-system linearization, but functionality is being implemented in stages

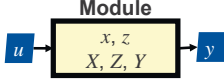


Now called **OpenFAST**

NATIONAL RENEWABLE ENERGY LABORATORY

Background: Why Linearize?

- **OpenFAST** primary used for nonlinear time-domain standards-based load analysis (ultimate & fatigue)
- Linearization is about understanding:
 - o Useful for eigenanalysis, controls design, stability analysis, gradients for optimization, & development of reduced-order models
- Prior focus:
 - o Structuring source code to enable linearization
 - o Developing general approach to linearizing mesh-mapping w/n module-to-module coupling relationships, inc. rotations
 - o Linearizing core (but not all) features of **InflowWind**, **ServoDyn**, **ElastoDyn**, **BeamDyn**, & **AeroDyn** modules & their coupling
 - o Verifying implementation
- Recent work (presented @ IOWTC 2018):
 - o Linearizing **HydroDyn**, & **MAP++**, & coupling
 - o State-space implementation of wave-excitation & wave-radiation loads
- This work – Verifying implementation for FOWT



$$\dot{x} = X(x, z, u, t)$$

$$0 = Z(x, z, u, t) \quad \text{with} \quad \left| \frac{\partial Z}{\partial z} \right| \neq 0$$

$$y = Y(x, z, u, t)$$


$$u = u|_{op} + \Delta u \quad \text{etc.}$$

$$\Delta \dot{x} = A \Delta x + B \Delta u$$

$$\Delta y = C \Delta x + D \Delta u$$

with

$$A = \left[\frac{\partial X}{\partial x} \quad \frac{\partial X}{\partial z} \quad \frac{\partial X}{\partial u} \right]^{-1} \frac{\partial Z}{\partial x} \quad \text{etc.}$$



NATIONAL RENEWABLE ENERGY LABORATORY

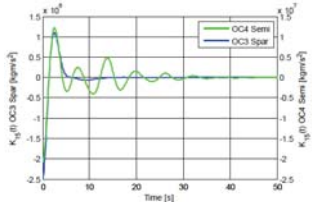
Background: State-Space-Based Wave Radiation

- Wave-radiation “memory effect” accounted for in **HydroDyn** by direct time-domain (numerical) convolution
- Linear state-space (SS) approximation:
 - o SS matrices derived from **SS_Fitting** pre-processor using 4 system-ID approaches

$$F_{Rdn} = - \int_0^t K_{Rdn}(t-\tau) \dot{q}_{Pffm}(\tau) d\tau \rightarrow F_{Rdn}$$

$$\dot{x}_{Rdn} = A_{Rdn} x_{Rdn} + B_{Rdn} \dot{q}_{Pffm}$$

$$F_{Rdn} \equiv C_{Rdn} x_{Rdn}$$



NATIONAL RENEWABLE ENERGY LABORATORY

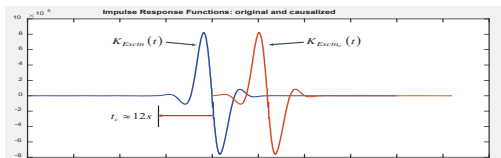
Background: State-Space-Based Wave Excitation

- First-order wave-excitation loads accounted for in **HydroDyn** by inverse Fourier transform
- Linear SS approximation:
 - o SS matrices derived from extension to **SS_Fitting** pre-processor using system-ID approach
 - o Requires prediction of wave elevation time t_c into future to address noncausality i.e. $\zeta_c(t) = \zeta(t + t_c)$

$$\zeta \rightarrow F_{Extm} = \frac{1}{2\pi} \int_{-\infty}^{\infty} X(\omega, \beta) \zeta(\omega) e^{i\omega t} d\omega \rightarrow F_{Extm}$$

$$\zeta \rightarrow F_{Extm} = \int_{-\infty}^t K_{Extm}(t-\tau) \zeta(\tau) d\tau \rightarrow F_{Extm}$$

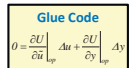
$$\zeta_c \rightarrow \begin{cases} \dot{x}_{Extm} = A_{Extm} x_{Extm} + B_{Extm} \zeta_c \\ F_{Extm} \equiv C_{Extm} x_{Extm} \end{cases} \rightarrow F_{Extm}$$



NATIONAL RENEWABLE ENERGY LABORATORY

Background: Final Matrix Assembly

InflowWind (IFW) $Ax^{(IFW)} = D^{(IFW)} Au^{(IFW)}$ $Ay^{(IFW)} = D^{(IFW)} Au^{(IFW)}$	ElastoDyn (ED) $Ax^{(ED)} = A^{(ED)} Ax^{(ED)} + B^{(ED)} Au^{(ED)}$ $Ay^{(ED)} = C^{(ED)} Ax^{(ED)} + D^{(ED)} Au^{(ED)}$
ServoDyn (Srvd) $Ax^{(Srvd)} = D^{(Srvd)} Au^{(Srvd)}$	BeamDyn (BD) $Ax^{(BD)} = A^{(BD)} Ax^{(BD)} + B^{(BD)} Au^{(BD)}$ $Ay^{(BD)} = C^{(BD)} Ax^{(BD)} + D^{(BD)} Au^{(BD)}$
AeroDyn (AD) $Ax^{(AD)} = D^{(AD)} Au^{(AD)}$	HydroDyn (HD) $Ax^{(HD)} = A^{(HD)} Ax^{(HD)} + B^{(HD)} Au^{(HD)}$ $Ay^{(HD)} = C^{(HD)} Ax^{(HD)} + D^{(HD)} Au^{(HD)}$
MAP++ (MAP) $Ax^{(MAP)} = D^{(MAP)} Au^{(MAP)}$	



Full System

$$\Delta \dot{x} = A \Delta x + B \Delta u^*$$

$$\Delta y = C \Delta x + D \Delta u^*$$

with

$$A = \begin{bmatrix} A^{(ED)} & 0 & 0 \\ 0 & A^{(BD)} & 0 \\ 0 & 0 & A^{(HD)} \end{bmatrix}$$

$$B = \begin{bmatrix} B^{(ED)} & 0 & 0 & 0 & 0 & 0 \\ 0 & 0 & 0 & 0 & 0 & 0 \\ 0 & 0 & 0 & 0 & 0 & 0 \end{bmatrix}$$

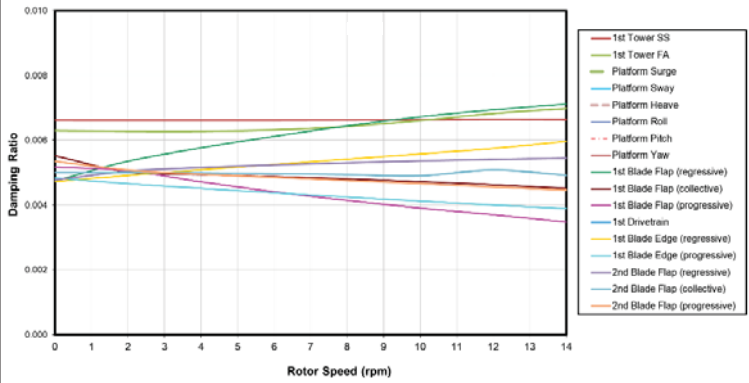
$$C = \begin{bmatrix} C^{(ED)} & 0 & 0 & 0 & 0 & 0 \\ 0 & C^{(BD)} & 0 & 0 & 0 & 0 \\ 0 & 0 & C^{(HD)} & 0 & 0 & 0 \\ 0 & 0 & 0 & 0 & 0 & 0 \end{bmatrix}$$

etc.

- D -matrices (included in G) impact all matrices of coupled system, highlighting important role of direct feedthrough
- While $A^{(ED)}$ contains mass, stiffness, & damping of **ElastoDyn** structural model only, full-system A contains mass, stiffness, & damping associated w/ full-system coupled aero-hydro-servo-elastics, including FOWT hydrostatics, radiation damping, drag, added mass, & mooring restoring

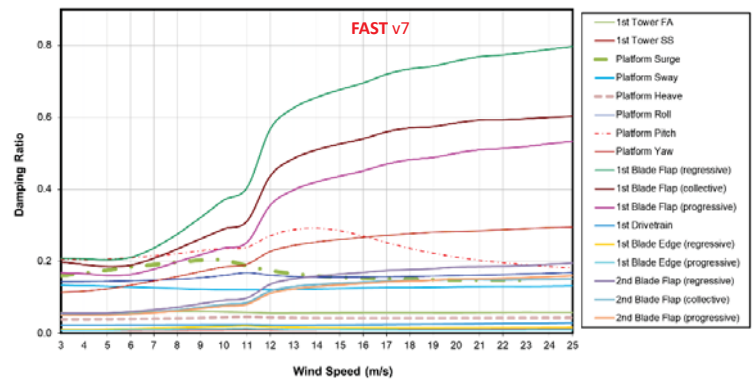
NATIONAL RENEWABLE ENERGY LABORATORY

Results: Campbell Diagram of NREL 5-MW Turbine Atop OC3-Hywind Spar



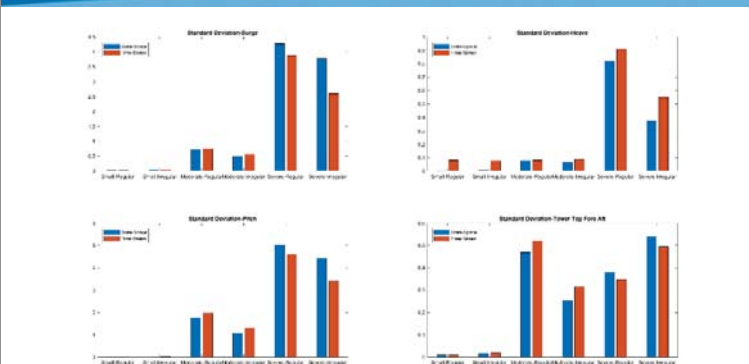
- Modules enabled: **ElastoDyn, ServoDyn, HydroDyn, & MAP++**
- Approach (for each rotor speed): Find periodic steady-state OP → Linearize to find A matrix → MBC → Azimuth-average → Eigenanalysis → Extract freq.s & damping

Results: Campbell Diagram of NREL 5-MW Turbine Atop OC3-Hywind Spar – w/ Aero



- Modules enabled: **ElastoDyn, ServoDyn, HydroDyn, MAP++, AeroDyn, & InflowWind**
- Approach (for each wind speed): Define torque & blade pitch → Find periodic steady-state OP → Linearize to find A matrix → MBC → Azimuth-average → Eigenanalysis → Extract freq.s & damping

Results: Time Series Comparison of Nonlinear & Linear Models



- Modules enabled: **ElastoDyn, ServoDyn, HydroDyn, & MAP++**
- Nonlinear approach (for each sea state): Time-domain simulation w/ waves
- Linear approach (for each sea state): Find steady-state OP → Linearize to find A, B, C, D matrices → Integrate in time w/ wave-elevation input derived from nonlinear solution

Conclusions & Future Work

- **Conclusions:**
 - Linearization of underlying nonlinear wind-system equations advantageous to:
 - Understand system response
 - Exploit well-established methods/tools for analyzing linear systems
 - Linearization functionality has been expanded to FOWT w/n **OpenFAST**
 - Verification results:
 - Good agreement in natural frequencies between **OpenFAST & FAST v7**
 - Damping differences impacted by trim solution, frozen wake, perturbation size on viscous damping, wave-radiation damping
 - Nonlinear versus linear response shows impact of structural nonlinearities for more severe sea states
- **Future work:**
 - Improved OP through static-equilibrium, steady-state, or periodic steady-state determination, including trim
 - Eigenmode automation & visualization
 - Linearization functionality for:
 - Other important features (e.g. unsteady aerodynamics of **AeroDyn**)
 - Other offshore functionality (**SubDyn**, etc.)
 - New features as they are developed

Carpe Ventum!

Jason Jonkman, Ph.D.
+1 (303) 384 – 7026
jason.jonkman@nrel.gov

www.nrel.gov

NATIONAL RENEWABLE ENERGY LABORATORY

NREL is a national laboratory of the U.S. Department of Energy, Office of Energy Efficiency and Renewable Energy, operated by the Alliance for Sustainable Energy, LLC.

Approach & Methods: Operating-Point Determination

- A linear model of a nonlinear system is only valid in local vicinity of an operating point (OP)
- Current implementation allows OP to be set by given initial conditions (time zero) or a given times in nonlinear time-solution
- Note about rotations in 3D:
 - Rotations don't reside in a linear space
 - **FAST** framework stores module inputs/outputs for 3D rotations using 3x3 DCMs (Δ)
 - Linearized rotational parameters taken to be 3 small-angle rotations about global X, Y, & Z ($\Delta\vec{\theta}$)

$u = u|_{op} + \Delta u$ for most variables

$\Delta = \Delta|_{op} \Delta \Delta$ for rotations

with

$$\begin{Bmatrix} x \\ y \\ z \end{Bmatrix} = \Delta \begin{Bmatrix} X \\ Y \\ Z \end{Bmatrix}$$

$$\Delta \approx \begin{bmatrix} 1 & \Delta\theta_z & -\Delta\theta_y \\ -\Delta\theta_z & 1 & \Delta\theta_x \\ \Delta\theta_y & -\Delta\theta_x & 1 \end{bmatrix} \quad \Delta\vec{\theta} = \begin{Bmatrix} \Delta\theta_x \\ \Delta\theta_y \\ \Delta\theta_z \end{Bmatrix}$$

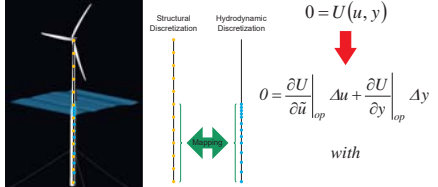
Approach & Methods: Module Linearization

Module	Linear Features	States (x, z)	Inputs (u)	Outputs (y)	Jacobian Calc.
ElastoDyn (ED)	<ul style="list-style-type: none"> • Structural dynamics of: <ul style="list-style-type: none"> ◦ Blades ◦ Drivetrain ◦ Nacelle ◦ Tower ◦ Platform 	<ul style="list-style-type: none"> • Structural degrees-of-freedom (DOFs) & their 1st time derivatives (continuous states) 	<ul style="list-style-type: none"> • Applied loads along blades & tower • Applied loads on hub, nacelle, & platform • Blade-pitch-angle command • Nacelle-yaw moment • Generator torque 	<ul style="list-style-type: none"> • Motions along blades & tower • Motions of hub, nacelle, & platform • Nacelle-yaw angle & rate • Generator speed • User-selected structural outputs (motions &/or loads) 	<ul style="list-style-type: none"> • Numerical central-difference perturbation technique*
HydroDyn (HD)	<ul style="list-style-type: none"> • Wave excitation • Wave-radiation added mass • Wave-radiation damping • Hydrostatic restoring • Viscous drag 	<ul style="list-style-type: none"> • State-space-based wave-excitation (continuous states) • State-space-based radiation (continuous states) 	<ul style="list-style-type: none"> • Motions of platform • Wave-elevation disturbance 	<ul style="list-style-type: none"> • Hydrodynamic applied loads along platform • User-selected hydrodynamic outputs 	<ul style="list-style-type: none"> • Analytical for state equations • Numerical central-difference perturbation technique* for output equations
MAP+ (MAP)	<ul style="list-style-type: none"> • Mooring restoring 	<ul style="list-style-type: none"> • Mooring line tensions (constraint states) • Positions of connect nodes (constraint states) 	<ul style="list-style-type: none"> • Displacements of fairleads 	<ul style="list-style-type: none"> • Tensions at fairleads • User-selected mooring outputs 	<ul style="list-style-type: none"> • Numerical central-difference perturbation technique*

*Numerical central-difference perturbation technique (see paper for treatment of 3D rotations) $\frac{\partial X}{\partial x} \Big|_{op} = \frac{X(x|_{op} + \Delta x, u|_{op}, t|_{op}) - X(x|_{op} - \Delta x, u|_{op}, t|_{op})}{2\Delta x}$ etc.

Approach & Methods: Glue-Code Linearization

- Module inputs & outputs residing on spatial boundaries use a mesh, consisting of:
 - Nodes & elements (nodal connectivity)
 - Nodal reference locations (position & orientation)
 - One or more nodal fields, including motion, load, &/or scalar quantities



- Mesh-to-mesh mappings involve:
 - Mapping search – Nearest neighbors are found
 - Mapping transfer – Nodal fields are transferred
- Mapping transfers & other module-to-module input-output coupling relationships have been linearized analytically etc.

$$0 = \frac{\partial U}{\partial \bar{u}} \Big|_{op} \Delta \bar{u} + \frac{\partial U}{\partial y} \Big|_{op} \Delta y$$

with

$$\frac{\partial U}{\partial \bar{u}} \Big|_{op} = \begin{bmatrix} I & 0 & 0 & 0 & \frac{\partial U^{(PW)}}{\partial \bar{u}^{(AD)}} & 0 & 0 \\ 0 & I & 0 & 0 & 0 & 0 & 0 \\ 0 & 0 & I & \frac{\partial U^{(ED)}}{\partial \bar{u}^{(BD)}} & \frac{\partial U^{(ED)}}{\partial \bar{u}^{(AD)}} & \frac{\partial U^{(ED)}}{\partial \bar{u}^{(MD)}} & \frac{\partial U^{(ED)}}{\partial \bar{u}^{(MAP)}} \\ 0 & 0 & 0 & \frac{\partial U^{(BD)}}{\partial \bar{u}^{(BD)}} & \frac{\partial U^{(BD)}}{\partial \bar{u}^{(AD)}} & 0 & 0 \\ 0 & 0 & 0 & 0 & \frac{\partial U^{(AD)}}{\partial \bar{u}^{(AD)}} & 0 & 0 \\ 0 & 0 & 0 & 0 & 0 & \frac{\partial U^{(MD)}}{\partial \bar{u}^{(MD)}} & 0 \\ 0 & 0 & 0 & 0 & 0 & 0 & I \end{bmatrix}_{op}$$

Closing session – Strategic Outlook

The way forward for offshore wind, Aidan Cronin, chair ETIPwind

Real time structural analyses of wind turbines enabled by sensor measurements and Digital Twin models, M. Graczyk, SAP Norway Engineering Center of Excellence

EERA DeepWind'2019 – Closing, J.O.Tande, SINTEF Energi

The way forward for offshore wind possible scenarios

Aidan Cronin, Chair, ETIPWind
EERA DeepWind 2019

Correction to answer on floaters.

Question:

How much of the installations shown would be floating by 2030?

Correct answer:

If there are sufficient breakthroughs, 10% of installations could be floating by 2030

Agenda

- ETIP
- Offshore market scenarios going forward.
- The technical challenges & the future.

Please note that this presentation contains copyrighted material from IHS Markit and Bloomberg New Energy Finance as licensed to SGRE. Permission is to be sought from these entities before further use of this material is attempted.

What are ETIPs?

European Technology and Innovation Platforms are industry-led stakeholder fora recognised by the European Commission

Goals

- Drive innovation, knowledge transfer and European competitiveness and support wind skill excellence.
- Develop research and innovation agendas and roadmaps for action at EU and national levels

Turbine Manufacturers



Universities, research institutes and consultants



Utilities and developers



Others



2018 Strategic Research & Innovation Agenda

Driving market development with targeted R&I



ETIP

- Would like to thank EERA, SINTEF and NTNU for allowing us to plan our ETIP workshop in conjunction with EERA Deepwind and Equinor for hosting us .
- Applaud the NOWRIC initiative that will clearly create a needed technology powerhouse for offshore wind in the Nordics
- Will support the SETWIND offshore initiative in every way we can to ease its success.
- Will continue to promote EERA DeepWind as an event of excellence that is, international, open and also helps redress the gender imbalance in our industry.



etipwind.eu

Blatent promotion



etipwind.eu

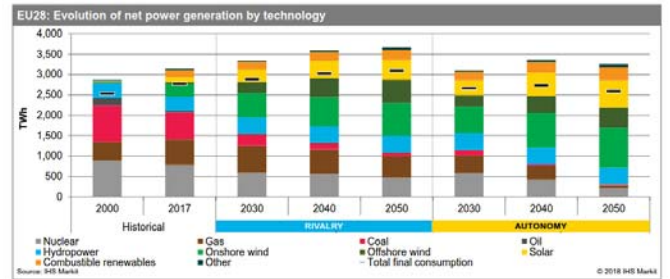


The economists view of offshore IHSMarkt and BNEF

etipwind.eu

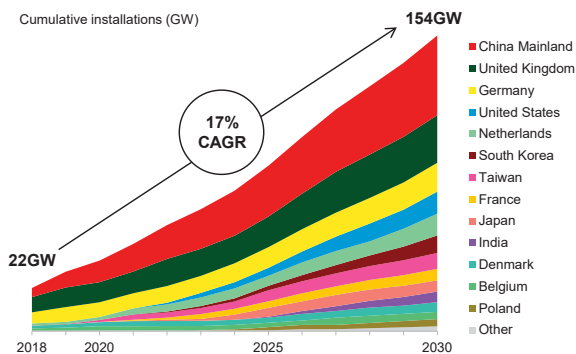
View from a major fossil analyst house

Renewables will dominate the power mix in the Rivalry and Autonomy IHS Markit long-term power scenarios



etipwind.eu

Global cumulative Offshore installation forecast

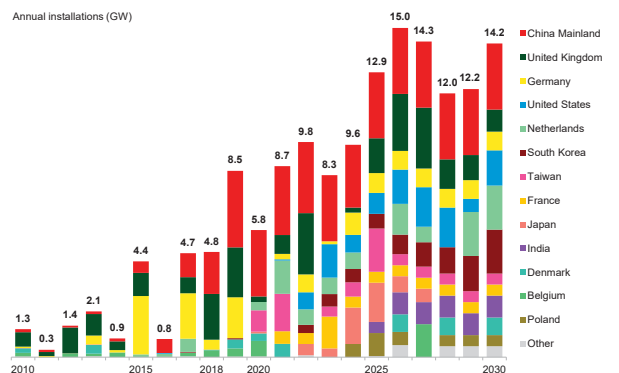


Source: BloombergNEF "Global Offshore" – Sweden, Ireland, Norway, Finland, Portugal, Spain, Italy.



etipwind.eu

Global offshore wind installations, by country

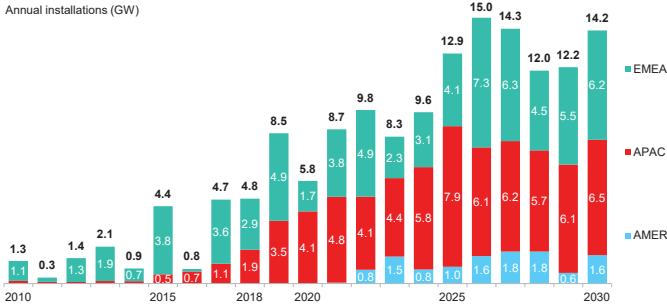


Source: BloombergNEF "Global Offshore" – Sweden, Ireland, Norway, Finland, Portugal, Spain, Italy.

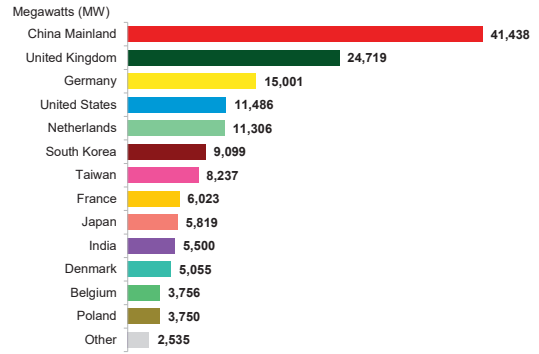


etipwind.eu

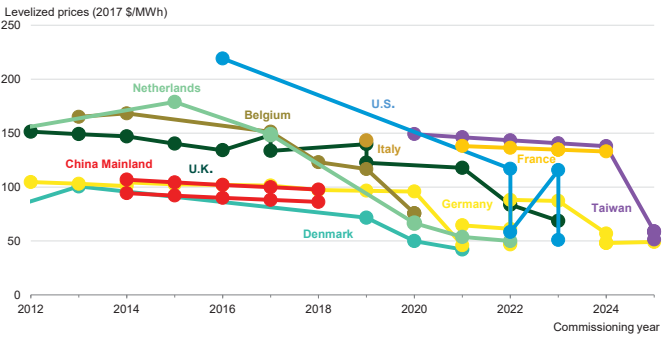
Global offshore wind installations, by region



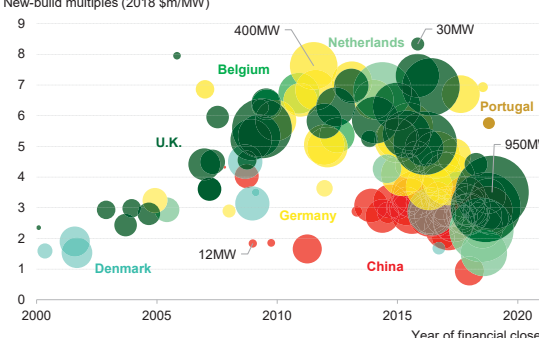
Offshore wind country ranking in 2030



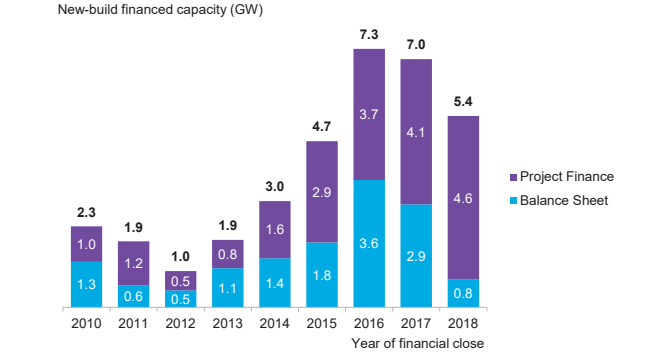
Levelized offshore wind prices



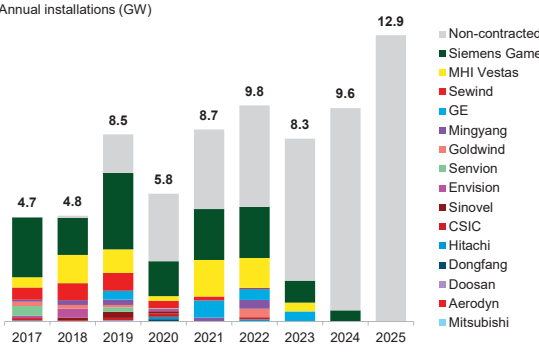
Offshore wind capex



Global offshore wind new-build capacity

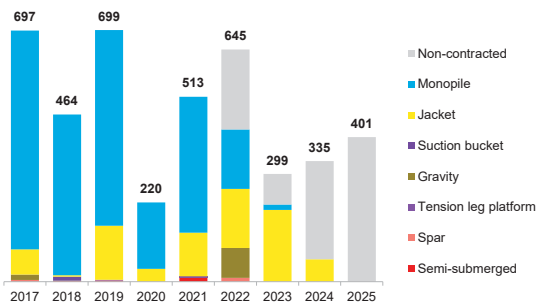


Global offshore turbine manufacturer market share



European unit installations by foundation type

Annual installations (units)



Source: BloombergNEF. Tension leg platform, Spar and Semi-submerged are floating solutions.

What are we facing?

Current offshore challenges

- Converters- the good & bad
- Cables – mistakes are expensive
- Leading edge erosion – God hates us
- MW arms race - will bigger continue to be better
 - Final size will probably be set by people in this room
- Need for industrialized floaters
 - Will drive huge installation numbers
- Penetration ceiling – Offshore wind is big too expensive to curtail so what is the solution (Ammonia as a maritime fuel??)
- Need applied robotics today
 - Extra set of eyes & ears
 - Increase redundancy & safety

Challenges we face going forward

- Wish - 2 floater designs that are easy to industrialise
- How we break the historic inertia of the legacy grid to enable high impact penetration of wind.
- As machines get bigger and time to market and maturity times decrease- we will need super engineering and scientific skills to prevent "Big bangs"
 - Customers expect next generation to be cheaper = Help for R&I funding vital
- Can the supply chain deliver quality and technology at the required level of lower prices.

Possible future in 15 years

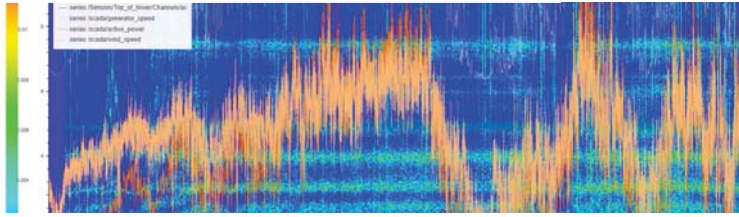
- Offshore still drives the state of the art in wind
- Machines of 15MW on average
- Standard average parks of 1GW+
- Offshore in 15 years costs same as onshore today
- Parks become fish recovery sanctuaries
- Hi-Tech Blade shells easily replaced every 5 years
- Foundation technology allows repowering so offshore sites will produce for 70 years

In Summary

- Offshore can deliver the bulk power needed for the energy transition.
- When offshore hits power parity it will be the biggest disrupter in the power industry - in newer times,
- China will become a leading driver of scale going forward – continued 2 way mutual cooperation is essential for local and global benefit.
- Delivering the promise of offshore will be an enormous effort driven by the research innovation community and investors seeing the opportunity.

"A humbled pilgrim now leaves as in the past, having visited this place of knowledge. Thank you all for sharing your work and helping to maintain the stubborn passion needed to drive the continued success of this sector."

Batteries now at 100% for the year ahead! 😊



Real time structural analyses of wind turbines enabled by sensor measurements and digital twin models

Mateusz Graczyk, Senior Project Manager
SAP Norway, Engineering Center of Excellence

EERA DeepWind '2019 Trondheim, January 16-18, 2019



© 2019 SAP SE or its SAP affiliate company. All rights reserved.

413,000+ Customers in more than 100 countries
46 yrs. Of history with innovation

95,000 Employees from 120+ countries

€23.46bn Total Revenue (FY2018)

170 mil. Total Assets in our most recent year

100+ Innovation and development centers

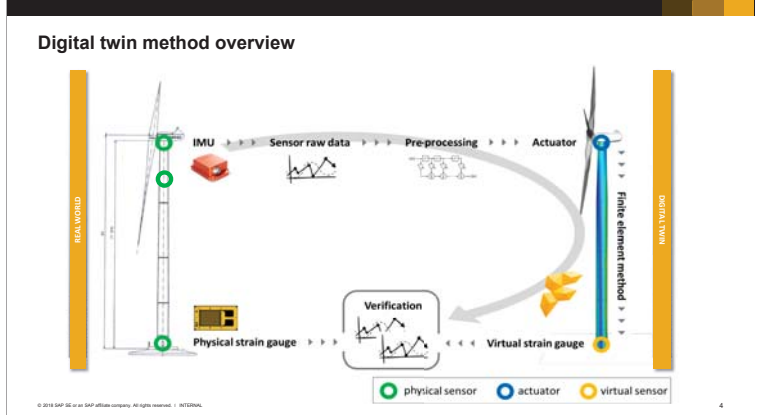
18,000+ SAP partner companies globally

92% SAP partner revenue from SAP customers

Engineering Center of Excellence

Do we need predictive maintenance?

© 2019 SAP SE or its SAP affiliate company. All rights reserved. | NCTD/NO



Tower structure monitoring

© 2019 SAP SE or its SAP affiliate company. All rights reserved. | NCTD/NO

Prototype at Havøygavlen

SAP Predictive Engineering Insights (PEI)

© 2019 SAP SE or its SAP affiliate company. All rights reserved. | NCTD/NO

SAP Predictive Engineering Insights application areas

1 Structural diagnostics

2 Fatigue and durability

3 Vibrations diagnostics

© 2018 SAP SE or its SAP affiliate company. All rights reserved. | PUBLIC 7

Why response of the tower structure

- Structural issues
 - Fatigue of the flanges
 - Top section of the tower
 - + for offshore WT:
 - Fundament and grouting
 - Taller towers

Insight of system state...

history → today → future

- Structural and wind loads for control decisions
- Fatigue analysis for remaining life
- Condition- and trend-based maintenance

...used for both **hindsight** and **foresight**

© 2018 SAP SE or its SAP affiliate company. All rights reserved. 8

Why response of the tower structure

- Structural issues
 - Fatigue of the flanges
 - Top section of the tower
 - + for offshore WT:
 - Fundament and grouting
 - Taller towers
- Wind response "gauge" for the system:
 - Emergency brake
 - Start/stop and yaw algorithms
 - Yaw misalignment
 - Mechanical issues

© 2018 SAP SE or its SAP affiliate company. All rights reserved. 9

Emergency stop due to sudden voltage drop from converter fault

© 2018 SAP SE or its SAP affiliate company. All rights reserved. 10

Extreme loads from rapid changes in state, production > stop > production

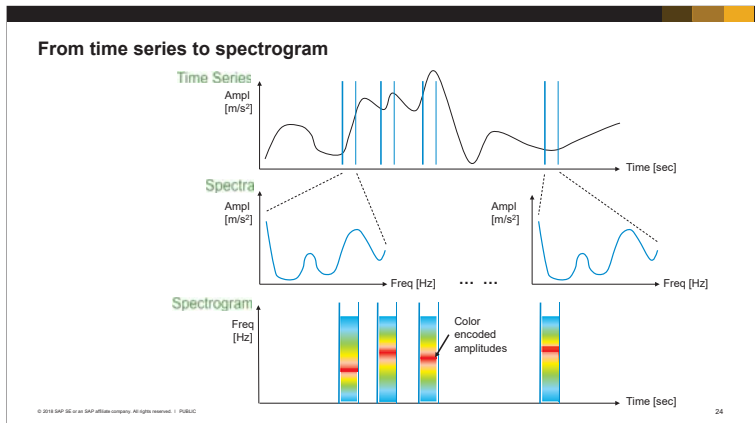
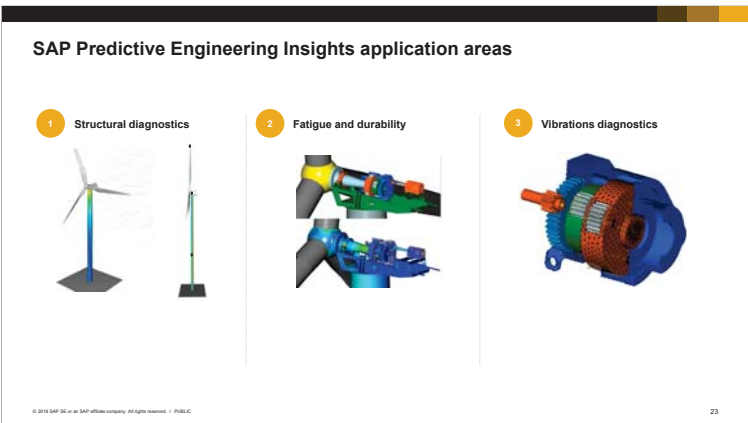
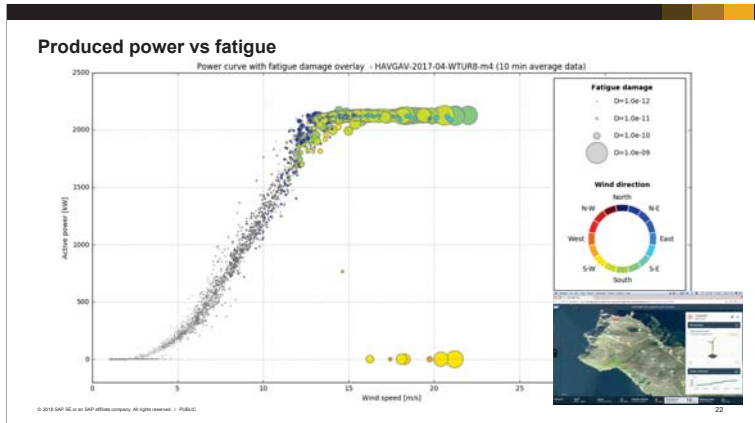
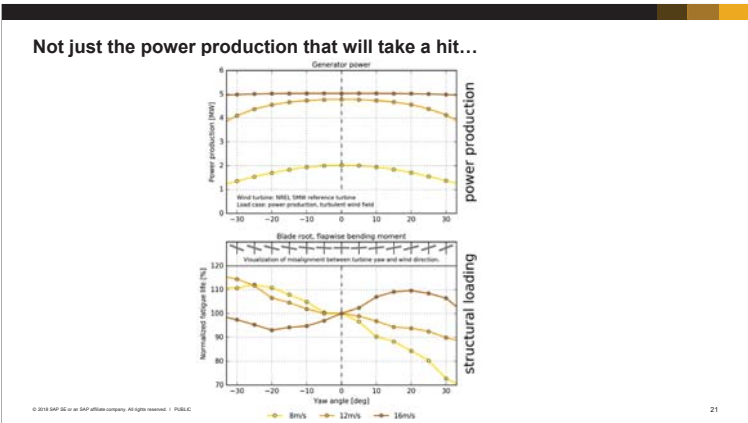
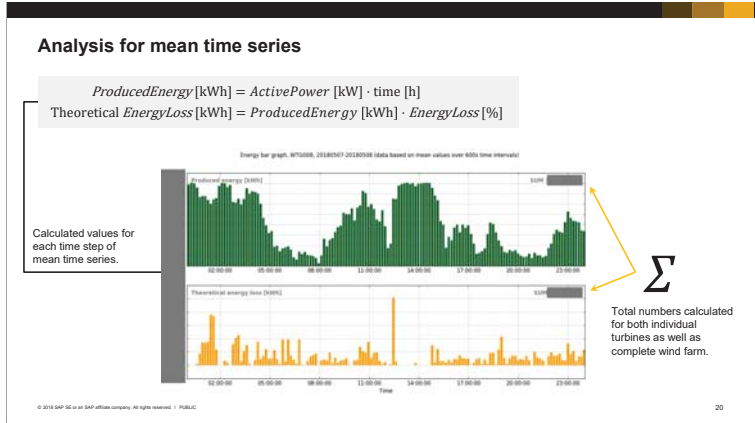
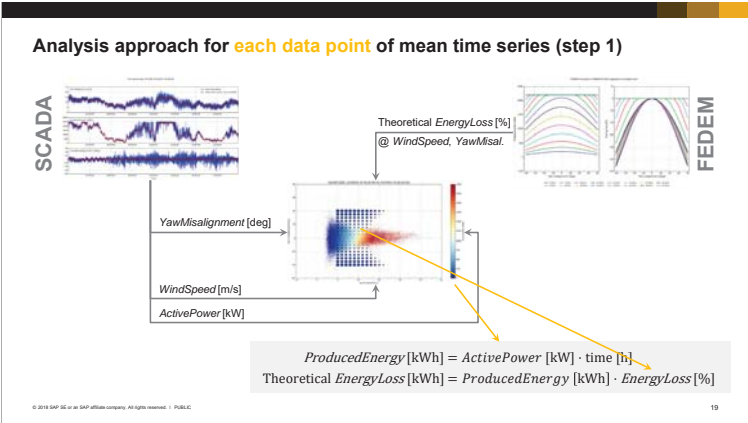
Local time: 04.06.2018, 21:25-21:45

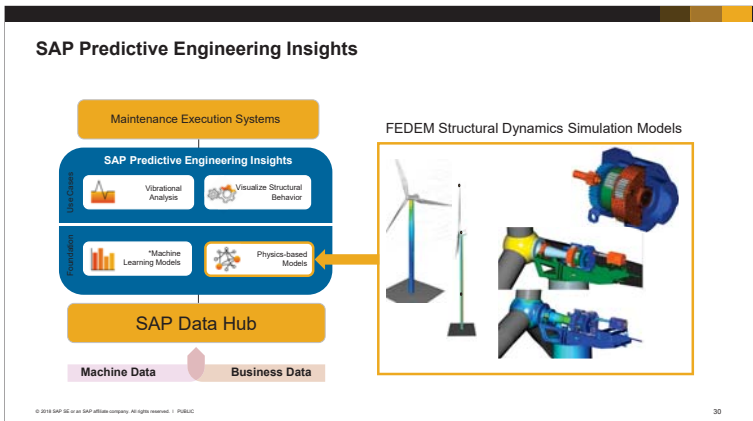
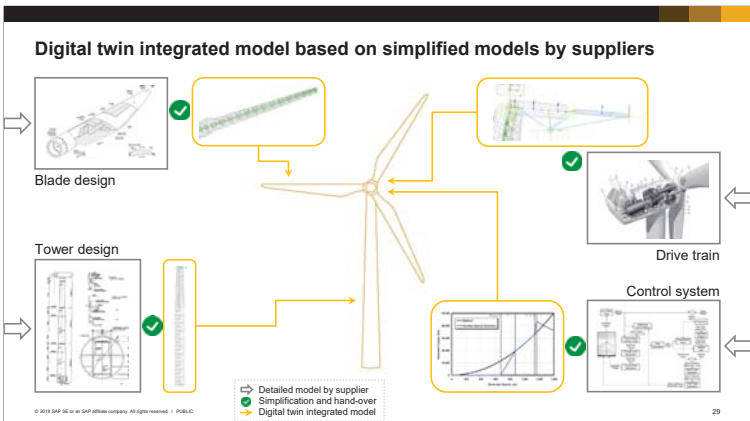
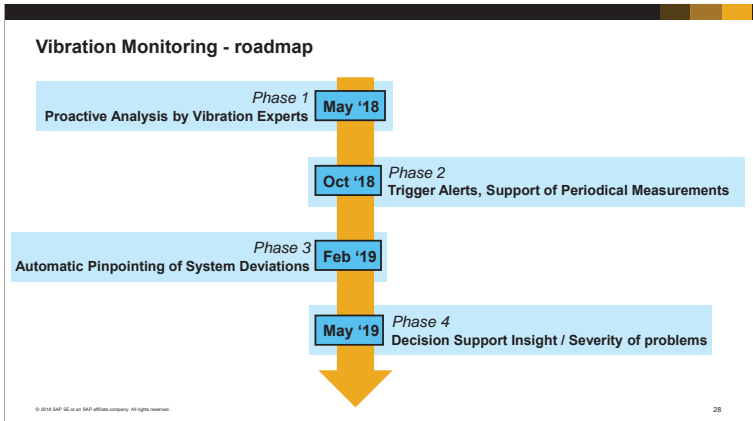
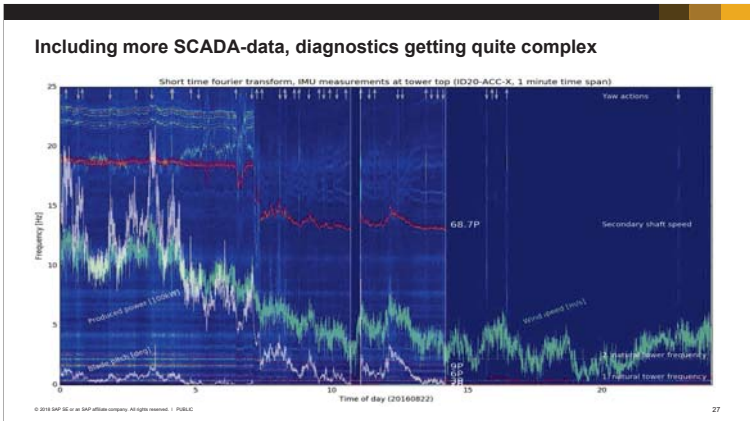
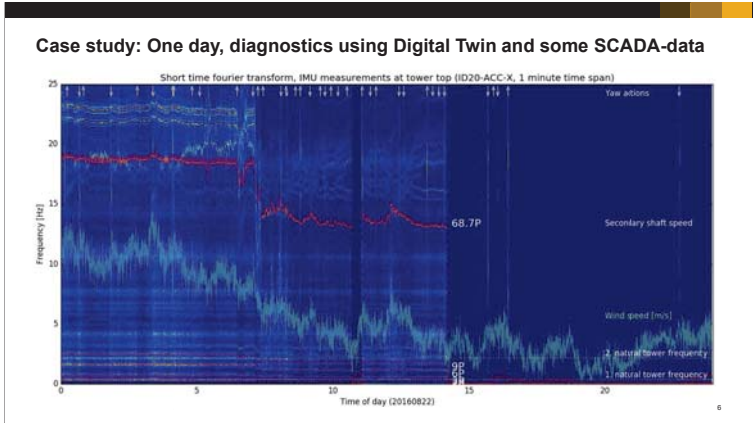
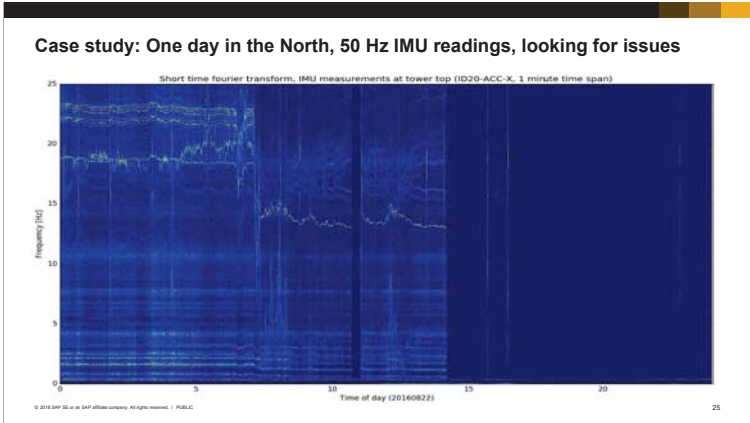
© 2018 SAP SE or its SAP affiliate company. All rights reserved. 11

One radical happening (orange and blue) ≈ 4 days normal life (green)

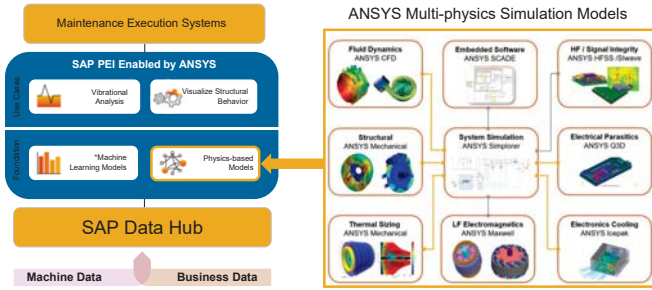
Virtual strain gauge 1 (tower bottom), 2018-06-04, UTC

© 2018 SAP SE or its SAP affiliate company. All rights reserved. 12





SAP Predictive Engineering Insights Enabled by ANSYS



© 2018 SAP SE or an SAP affiliate company. All rights reserved. | PUBLIC

31

Thank you!

Contact information:

Mateusz Graczyk
 Senior Project Manager
 Mateusz.Graczyk@sap.com



Follow all of SAP



www.sap.com/contactsap

© 2018 SAP SE or an SAP affiliate company. All rights reserved.

No part of this publication may be reproduced or transmitted in any form or for any purpose without the express permission of SAP SE or an SAP affiliate company.

The information contained herein may be changed without prior notice. Some software products marketed by SAP SE and its distributors contain proprietary software components of other software vendors. National product specifications may vary. These materials are provided by SAP SE or an SAP affiliate company for informational purposes only, without representation or warranty of any kind, and SAP or its affiliate companies shall not be liable for errors or omissions with respect to the materials. The only warranties for SAP or SAP affiliate company products and services are those that are set forth in the express warranty statements accompanying such products and services, if any. Nothing herein should be construed as constituting an additional warranty.

In particular, SAP SE or its affiliate companies have no obligation to pursue any course of business outlined in this document or any related presentation, or to develop or release any functionality mentioned therein. This document, or any related presentation, and SAP SE or its affiliate companies' strategy and possible future developments, products, and/or platforms, directions, and functionality are all subject to change and may be changed by SAP SE or its affiliate companies at any time for any reason without notice. The information in this document is not a commitment, promise, or legal obligation to deliver any material, code, or functionality. All forward-looking statements are subject to various risks and uncertainties that could cause actual results to differ materially from expectations. Readers are cautioned not to place undue reliance on these forward-looking statements, and they should not be relied upon in making purchasing decisions.

SAP and other SAP products and services mentioned herein as well as their respective logos are trademarks or registered trademarks of SAP SE (or an SAP affiliate company) in Germany and other countries. All other product and service names mentioned are the trademarks of their respective companies.

See www.sap.com/press-ansys for additional trademark information and notices.





Closing EERA DeepWind'2019

John Olav Giæver Tande
Conference chair, Chief scientist, SINTEF Energy Research

Michael Muskulus
Conference co-chair, Professor NTNU

EERA
EUROPEAN ENERGY RESEARCH ALLIANCE
JP WIND

SINTEF

NTNU

Thank you!

- Excellent presentations
- Vibrant positive atmosphere
- Global participation with delegates from all over Europe, USA, Japan, Korea, China and more!
- Good mix of academia and industry
- Gender balance is improving!
- Thank you to hotel staff, conference assisting staff from NTNU and SINTEF, session chairs, speakers and audience
- See you at EERA Deepwind 2020!



Technology for a better society

Poster session

Session A

1. Electrical Collector Topologies for Multi-Rotor WindTurbine Systems, I.H. Sunde, NTNU

Session B

2. Virtual Synchronous Machine Control for Wind Turbines: A Review, L. Lu, DTU
3. Use of energy storage for power quality enhancement in wind-powered oil and gas applications, E.F. Alves, NTNU-IEL

Session C

4. The OBLO infrastructure project – measurement capabilities for offshore wind energy research in Norway, M. Flügge, NORCE Technology
5. Abnormal Vertical Wind Profiles at a Mid-Norway Coastal Site, M.Møller, NTNU
6. Wind power potential and benefits of interconnected wind farms on the Norwegian Continental Shelf, I.M. Solbrekke, UiB
7. Wind conditions within a Norwegian fjord, Z. Midjyawa, NTNU

Session D

8. Experimental study of structural resonance in wind turbine's bearing fault detection, M.A. Rasmussen, NTNU
9. New coatings for leading edge erosion of turbine blades, A.von Bonin, NTNU

Session E

10. Mooring System Design for the 10MW Triple Spar Floating Wind Turbine at a 180 m Sea Depth Location J.Azcona, CENER
11. Consideration of the aerodynamic negative damping in the design of FWT platforms C.E. Silva de Souza, NTNU
12. Wind-Wave Directional Effects on Fatigue of Bottom-Fixed Offshore Wind Turbine S.H.Sørum, NTNU
13. Numerical Study of Load Effects On Floating Wind Turbine Support Structures S.Okpokparoro, University of Aberdeen
14. Conceptual Design of a 12 MW Floating Offshore Wind Turbine in the Ulsan Offshore Area, Korea P.T.Dam, University of Ulsan
15. Motion Performances of 5-MW Floating Offshore Wind Turbines under Combined Environmental Conditions in the East Sea, Korea Y.Yu, University of Ulsan
16. Influence of ballast material on the buoyancy dynamics of cylindrical floaters of FOWT C.Molins, UPC-BarcelonaTech
17. Hydrodynamic analysis of a novel floating offshore wind turbine W.Shi, Dalian University of Technology
18. A tool to simulate decommissioning Offshore Wind Farms C. Desmond, University College Cork
19. Can cloud computing help bend the cost curve for FOWTs? P.E.Thomassen, Simis AS
20. Performance study for a simplified floating wind turbine model across various load cases F.J.Madsen, DTU
21. Simulation Methods for Floating Offshore Wind Turbine Farms with Shared Moorings P.Connolly, University of Prince Edward Island
22. Spatial met-ocean data analysis for the North Sea using copulas: application in lumping of offshore wind turbine fatigue load cases A. Koochekali, NTNU
23. Numerical design concept for axially loaded grouted connections under submerged ambient conditions P.Schaumann, Leibniz University Hannover, ForWind

Session F

24. Collection Grid Optimization of a Floating Offshore Wind Farm Using Particle Swarm Theory M.Lerch, IREC
25. Investigating the influence of tip vortices on deflection phenomena in the near wake of a wind turbine model L.Kuhn, Technical University Berlin

Session G

26. Implementation of potential flow hydrodynamics to time-domain analysis of flexible platform of floating offshore wind turbines S. OH, ClassNK
27. Validating numerical predictions of floating offshore wind turbine structural frequencies in Bladed using measured data from Fukushima Hamakaze H.Yoshimoto, Japan Marine United Corporation
28. Prediction of dynamic response of a semi-submersible floating offshore wind turbine in combined wave and current condition by a new hydrodynamic coefficient model Y.Liu, University of Tokyo
29. The experimental investigation of the TELWIND second loop platform T.Battistella, IH Cantabria
30. Model validation through scaled tests comparisons of a semi-submersible 10MW floating wind turbine with active ballast R.F.Guzmán, University of Stuttgart

Electrical Collector Topologies for Multi-Rotor Wind Turbine Systems Power Loss Calculations

Ingvar Hinderaker Sunde¹, Raymundo E. Torres-Olguin², Olimpo Anaya-Lara³

¹Department of Electric Power Engineering, Norwegian University of Science and Technology (NTNU), Trondheim, Norway. E-mail: ingvath@stud.ntnu.no

²Department of Energy Systems, SINTEF Energy Research, Trondheim, Norway

³University of Strathclyde, Strathclyde, United Kingdom

Introduction

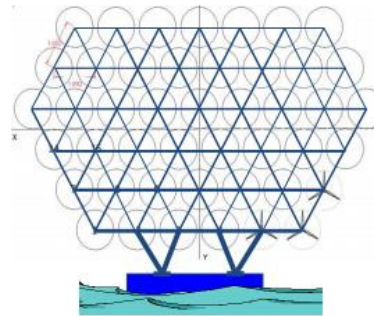
- Increasing demand for new innovations in the wind power industry
- P. Jamieson proposed the Multi-Rotor Wind Turbine System (MRWTS) [1]
- Vestas has already installed a 4-rotor system in Denmark [2]

Objectives:

- Propose different electrical collector topologies for a MRWTS
- Develop appropriate control systems
- Develop a way of calculating power electronic losses



Vestas 4-rotor demonstrator turbine. Source: Vestas (www.vestas.com)



Proposed MRWTS in the FP7 INNWIND.EU project. Source: Innwind (www.innwind.eu)

Methodology

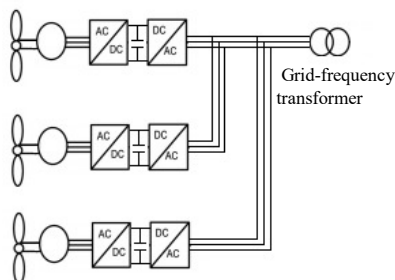
- Perform a literature search in order to propose three different collector topologies
- Implement the topologies in Matlab/Simulink
- Implement controllers for the power converters used in the topologies
- Perform a literature search on power losses in power converters and implement a way of calculating power losses in Simulink
- Perform simulations and make comparisons of the topologies

Proposed topologies

Design considerations:

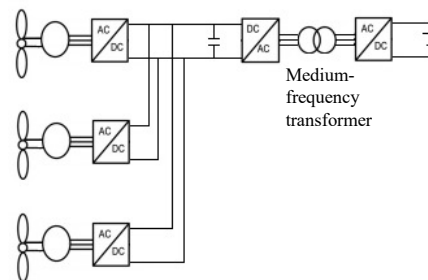
- Limit number of heavy transformers/power electronics
- Remain stable operation in case of fault in one rotor
- Compromise between controllability, efficiency and costs
- Be scalable, in terms of reaching 20 MW or more

AC Cluster



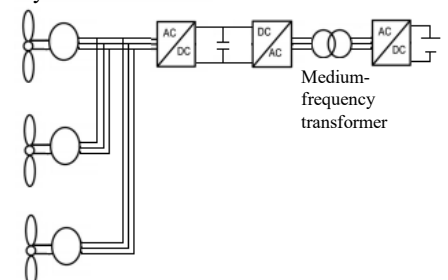
- One back-to-back converter for each turbine
- Allows individual optimised operating point
- High number of power electronics and large AC transformers

DC Cluster



- Individual optimised operating point through individual converters
- DC-to-DC converter using medium frequency power converters may save space and weight
- High power DC-to-DC converters still not commercially available

Hybrid Cluster



- Drastically reduces the number of power converters needed
- Issues regarding the controllability, one converter must control several turbines
- High power DC-to-DC converters needed

Control

Machine side controller:

- Control active and reactive power
- Compares measured power to reference values
- PI controller in inner and outer loop

Grid side controller:

- Control DC link voltage
- Compare measured DC voltage to reference values
- PI controller in inner and outer loop

DC-DC converter controller:

- DC-to-AC converter equal control as the grid side controller in the AC cluster
- Can operate in non-grid frequency by customised PLL – island mode
- PI controllers used in the inner and outer loop to control the AC voltage

Loss calculation

Power electronic losses found by [3]

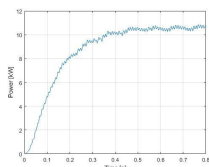
- IGBT losses $P_{IGBT} = N \left((V_{sw0}(T_j) \cdot I_{C,av} + R_C(T_j) I_{C,rms}^2) + (E_{sw,on} + E_{sw,off}) f_{sw} \right)$
- Diode losses $P_D = N \left((V_{D,0}(T_j) \cdot I_{D,av} + R_D(T_j) I_{D,rms}^2) + E_{sw,on} f_{sw} \right)$

Simulink loss calculation method [4]:

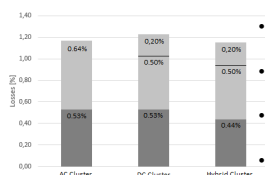
- Define IGBT/Diode module specifications in Matlab from datasheet
- Obtain current and voltage measurement from the Simulink module
- Divide signals in to IGBT and diode power loss calculation blocks
- Compute desired energy or voltage Based on current and voltages, and the temperature in the device
- Convert energy to power
- Input power to the thermal model to obtain the temperature in the device

Simulation results

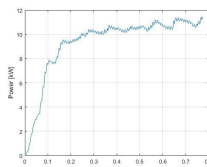
AC Cluster



Power converter losses of 1.17 %

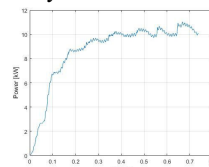


DC Cluster



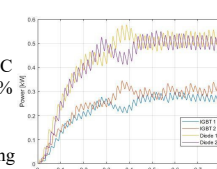
Power converter losses of 1.23 %

Hybrid Cluster



Power converter losses of 1.14 %

- Hybrid cluster experiences lowest losses
- High voltage side of DC-DC converter losses of just 20 %
- IGBT losses higher than diode losses
- Reasonable results according to theory



Conclusion and future work

Conclusion

- Similar results at a reasonable level
- Controllers work
- Power loss calculation method works
- Higher complexity needed to favour a topology

Future work

- Increase complexity in terms of number of turbines
- Develop controllers for dynamic conditions
- Investigate the use of medium frequency transformers

References

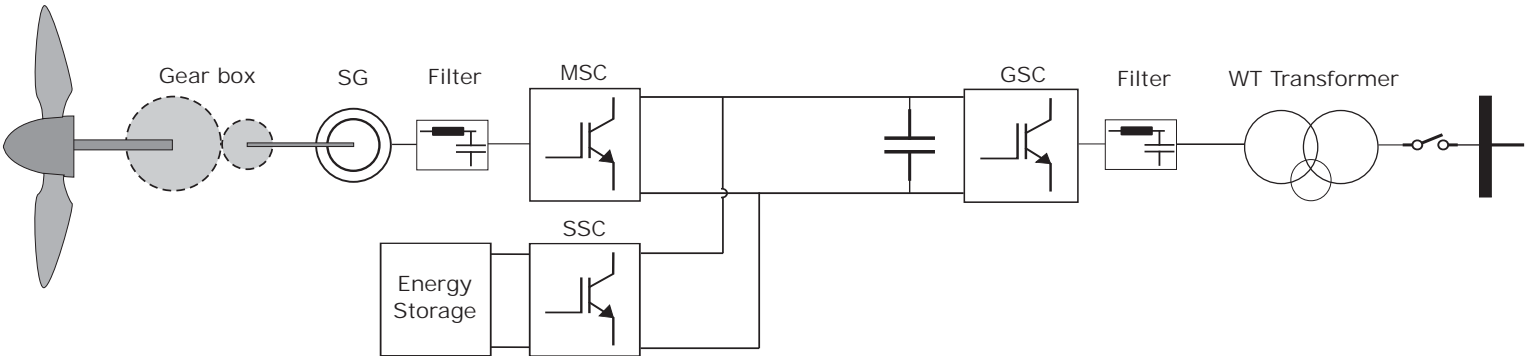
- P. Jamieson, et al., (2015), INNWIND.EU, Innovative Turbine Concepts – Multi-Rotor System
- Vestas Wind Systems A/S, (2016), News release, Vestas challenges scaling rules with multi-rotor concept demonstration turbine
- R.A. Barrera-Cardenas, (2015), Doctoral thesis, Meta-parametrised meta-modelling approach for optimal design of power electronics conversion systems: Application to offshore wind energy
- Mathworks, Loss Calculation in a 3-Phase 3-Level Inverter Using SimPowerSystems and Simscape, <https://www.mathworks.com/help/physmod/sps/examples/loss-calculation-in-a-three-phase-3-level-inverter.html>

Virtual Synchronous Machine Control for Wind Turbines: A Review



Liang Lu* and Nicolaos A. Cutululis
*Email: lilu@dtu.dk

1 VSM Control Schemes for WTs



Swing equations

$$\frac{d\Delta\bar{\omega}_r}{dt} = \frac{1}{2H} (\bar{T}_m - \bar{T}_e - K_D \Delta\bar{\omega}_r)$$

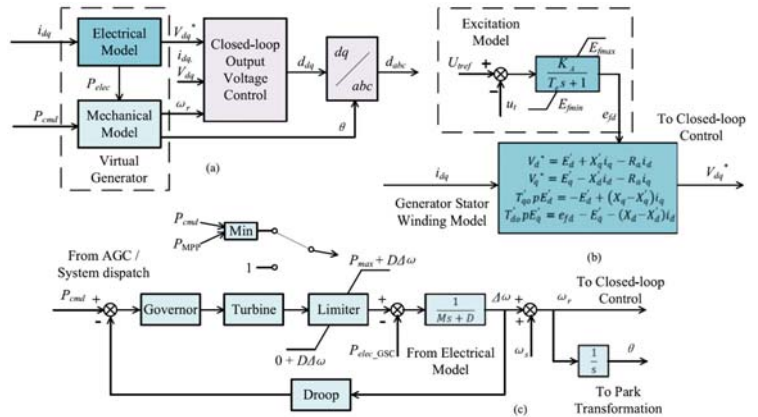
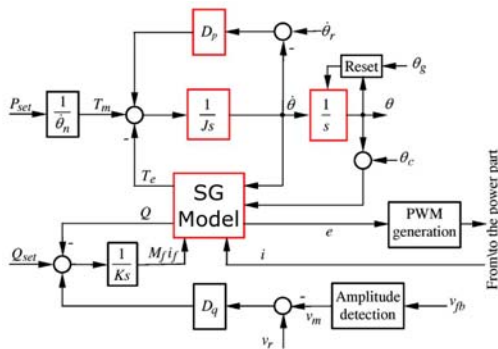
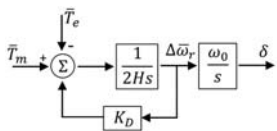
$$\frac{d\delta}{dt} = \omega_0 \Delta\bar{\omega}_r$$

Electrical equations

$$T_e = M_f i_f \langle i, \widehat{\sin\theta} \rangle$$

$$e = \dot{\theta} M_f i_f \widehat{\sin\theta}$$

$$Q = -\dot{\theta} M_f i_f \langle i, \widehat{\cos\theta} \rangle$$



Electrical equations

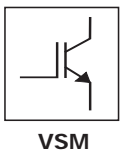
$$U_d = -x'_q I_q + E'_d$$

$$U_q = x'_d I_d + E'_q$$

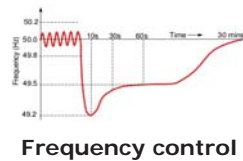
$$T'_{q0} \dot{E}'_d = -E'_d - (x_q - x'_q) I_q$$

$$T'_{d0} \dot{E}'_q = E_f - E'_q + (x_d - x'_d) I_d$$

2 Further Research Work



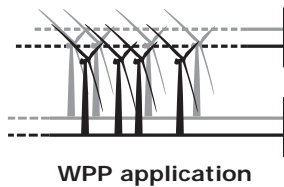
Field tests of availability
Performance and stability comparison of different schemes
Special requirements like parameter design and tuning
Standardisation of control parameters, interface etc.
Influence on WTs in mechanical load and stress



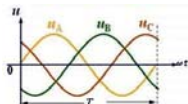
Frequency second drop
Performance indexes to be defined quantitatively
Assessment methods to be developed
Optimized control from a WPP



Techno-economic analysis
Advantage of MPPT+frequency control
Suitability of different types
Locations, especially in WPPs
Control strategy of SoC
Optimization of capacity

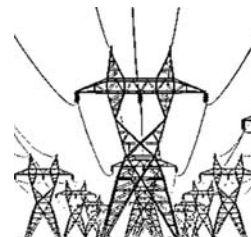


Coordinated control & stable operation of multiple VSM-controlled WTs
Optimization of ES configuration and layout



Voltage control

Well-founded verifications
Availability in different grid conditions
Fault ride-through capability



Grid conditions

Voltage sags
Unbalanced voltages
Grid faults
Weak grids
Islanded systems with black start



RESEARCH QUESTIONS

In offshore platforms with high penetration of wind power:



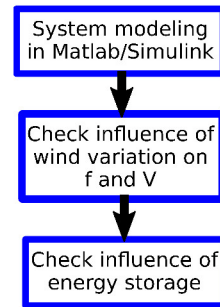
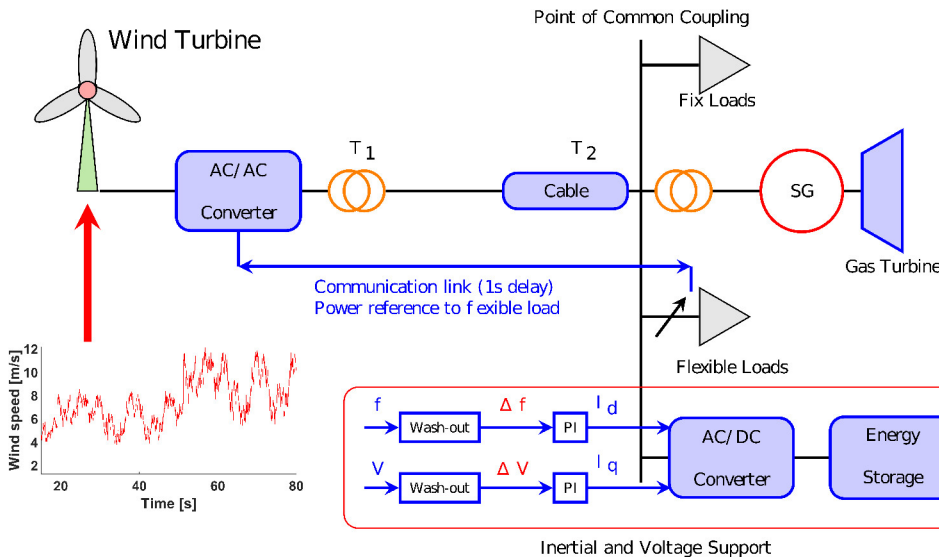
1. Which **power quality** problems in the **time-scale of seconds** appear with **no power from shore**?
2. How **energy storage** can improve **power quality**?
3. What influences the **sizing of the energy storage**?

CONTACT INFORMATION

R^G <https://tinyurl.com/HES-OFF>

erick.f.alves@ntnu.no
santiago.sanchez@ntnu.no
elisabetta.tedeschi@ntnu.no

METHOD



RESULTS

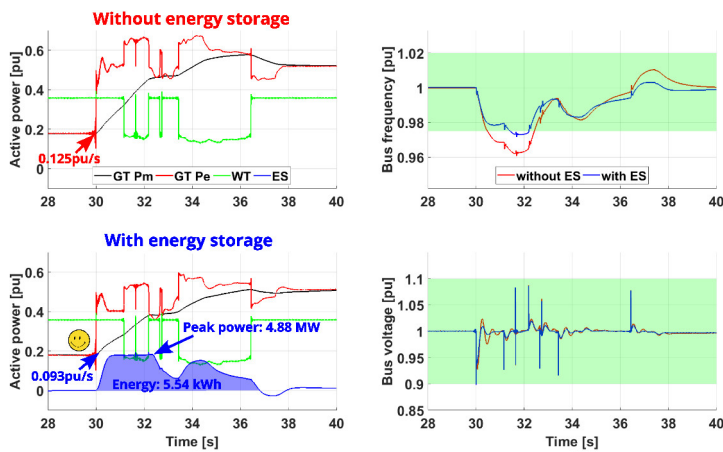


Figure 1: 10 MW load is switched on (1 pu = 25 MVA)

Electrical power quality problems:

- $\uparrow \Delta f$ \Rightarrow \uparrow governor actuation \Rightarrow \uparrow wear and tear ☹️
- $\uparrow \Delta V$ \Rightarrow \uparrow ($P_m - P_e$) \Rightarrow \uparrow mechanical stresses

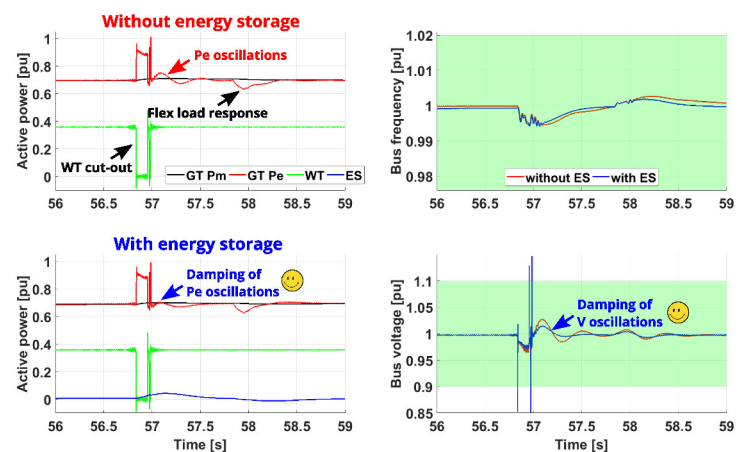


Figure 2: Wind power stops due to cut-out (1 pu = 25 MVA)

Energy storage as inertial and voltage support:

- $\downarrow \Delta f$ oscillations \Rightarrow \downarrow wear and tear ☺️
- Shorten $\Delta V / \Delta P_e$ oscillations \Rightarrow \downarrow mechanical stresses

CONCLUSIONS

- 1 \uparrow wind penetration \Rightarrow \downarrow power quality \Rightarrow \uparrow maintenance + \downarrow reliability
- 2 Energy storage \Rightarrow f and V support \Rightarrow \uparrow power quality
- 3 Energy storage MW \propto max(wind penetration) + max(load on/off)
- 4 Energy storage kWh \propto control parameters \Rightarrow frequency droop

The OBLO infrastructure project

Measurement capabilities for offshore wind energy research in Norway

Martin Flügge^{1,4}, Joachim Reuder^{2,4}, Jeremy Cook^{1,4}, Mostafa Bakhoday-Paskyabi³, Annette F. Stephansen^{1,4}

¹ NORCE Technology, Bergen, Norway
² Geophysical Institute and Bergen Offshore Wind Centre, University of Bergen, Bergen, Norway
³ Nansen Environmental and Remote sensing Centre, Bergen, Norway
⁴ Norwegian Research Cluster for Offshore Wind Energy (NORCOWE)



Extensive measurement campaigns are carried out in order to assess the wind potential at offshore wind farm sites, both before and after the erection of the wind turbines. The use of state-of-the-art Lidar technology enables researchers and wind farm operators to gain valuable information on the wind field and wake effects. To gain a complete understanding of the wind conditions at an offshore wind farm site, Lidar measurements should also be supplemented by measurements of other meteorological and oceanographic parameters, such as air and water temperature, humidity, wave and current speed, and wave height.

The OBLO infrastructure project offers access to state-of-the-art remote measurement capabilities for wind energy applications, as well as supplemental scientific oceanographic instrumentation. The instrumentation is available for public and private research institutions dealing with wind energy in Norway. OBLO also offers services for planning and execution of field deployments and post-processing and quality control of collected data as well as the scientific analysis of the data set. A complete list of available OBLO instrumentation and information regarding infrastructure access can be found at <http://oblo.uib.no>.



Data visualization

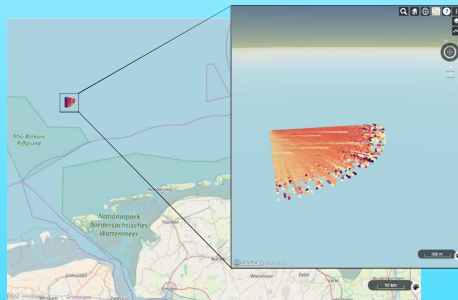
The collection of both Lidar data and additional met-ocean measurements generates large and complex data sets, resulting in time consuming and resource demanding data analysis efforts.

To simplify the planning and execution of measurement campaigns and the subsequent data analysis, NORCE Technology is investigating the potential of:

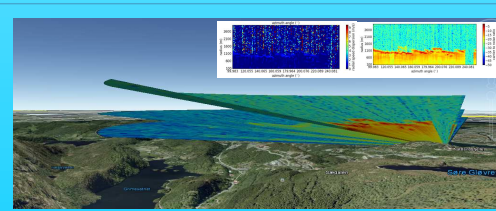
- Standardized methods and user friendly tools for pre- and post-evaluation of uncertainty and validity of Lidar measurements
- Interactive, multivariate data visualization for analysis of complex measurement datasets

A multivariate visualization tools with interactive parameter filtering is highly valuable for e.g.:

- Rapid assessment of early results for quality control of measurement setup
- Simplified evaluation of multi-instrument campaign results
- Evaluating parameter settings versus performance (e.g. CNR thresholds)
- Search for correlation factors



Example of the NORCE Technology in-house developed Enlighten-web computation and visualization tool for analysis of multidimensional data, which can easily visualize large and complex Lidar data sets.



3D visualization of measurements is of high value for analysis of scanning Lidar data, e.g. for wakes and complex terrain

Example Google Earth integration of wind measurement data.

OBLO wind Lidar field deployments

Lidar motion platform test, NORWAY

Investigation of measurement errors when performing Lidar wind measurements from a moving platform.

August 2011



LIMECS at Stavanger airport, NORWAY

Investigating coastal boundary layer flows.

Additionally, validation of Lidar measurements against radio soundings.



March – August 2013

WINTWEX at Wieringermeer, Netherlands

Combining 4 Lidar systems for investigation of wind turbine wakes at the ECN test site.



November 2013 – May 2014

Some of the available instrumentation within OBLO



- 2 x WindCube V1 (vertical wind profiles) [A]
- 1 x ZephIR 300 (vertical or horizontal wind profiles) [B]
- 2 x Passive microwave radiometer (vertical temperature and humidity profiles) [C]
- 1 x WindCube V2 offshore [D]
- 3 x WindCube100s [E]
- 1 x Furgo Wavescan buoy [F]
- 2 x oceanographic bottom frame [G]
- 2 x submerged buoys [H]

A complete list of all available OBLO instrumentation can be found at <https://oblo.uib.no/>

OBLEX-F1 at FINO1, GERMAN North Sea sector

Improving our knowledge of the marine atmospheric boundary-layer stability, turbulence generation processes and wind turbine wake propagation effects close to the Alpha Ventus wind farm.



June 2015 – October 2016

COTUR at Obrestad Lighthouse, Norway



Improving our knowledge regarding offshore wind turbulence and horizontal coherence, with respect to offshore wind energy.

Starting from January 2019

Mathias Møller¹, Piotr Domagalski² and Lars Roar Sætran¹

¹ Department of Energy and Process Engineering, Norwegian University of Science and Technology, Trondheim, Norway

² Institute of Turbomachinery, Lodz University of Technology, Lodz, Poland

Abstract

Phenomena such as internal boundary layers and low-level jets can cause short-term fluctuations resulting in the vertical wind profile deviating from its expected logarithmic shape. Analysis of the vertical wind profile at an on-land coastal site reveals that deviations in the form of 1 or 2 local maxima, or a completely reversed and monotonically decreasing profile is present in close to half of the analyzed profiles. Inflections are generally found to be progressively more common at higher elevations regardless of the direction of incoming wind. Local maxima have been found to occur at lower wind speeds, and in unstable atmospheric conditions.

Site description

The studied Skipheia site is at an on-land coastal location in Mid-Norway. The incoming wind is divided into 3 directional sectors; onshore incoming, offshore incoming, or a mixed-fetch direction.



Fig 1. Skipheia location

Profile identification

The vertical wind profile is categorized as abnormal if it exhibits local maxima. With 6 wind measurement heights (10m, 16m, 25m, 40m, 70m, 100m) this results in the 4 possibilities shown below.

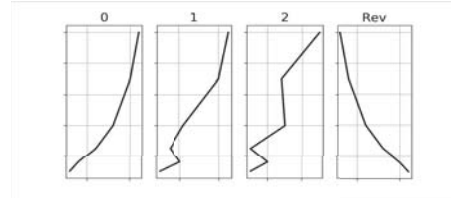


Fig 2. Profile categorization

Results

Wind speed and stability analysis

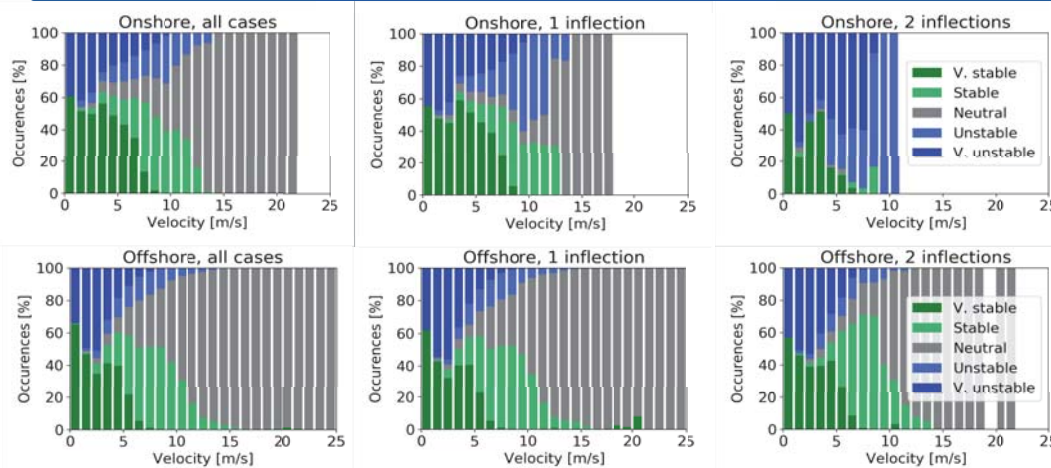


Fig 3. Stability analysis results

Abnormal profiles occurrences

Inflections	0	1	2	Rev
All directions	55.33%	38.71%	5.18%	0.78%
Onshore sector	64.19%	31.61%	2.88%	1.32%
Offshore sector	54.10%	39.74%	5.83%	0.33%

Tab 1. Inflected wind profiles

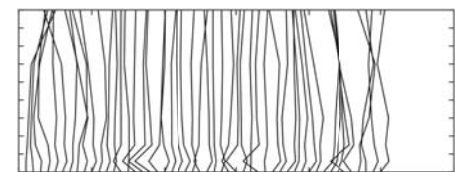


Fig 4. Abnormal profiles found in dataset

Inflection height

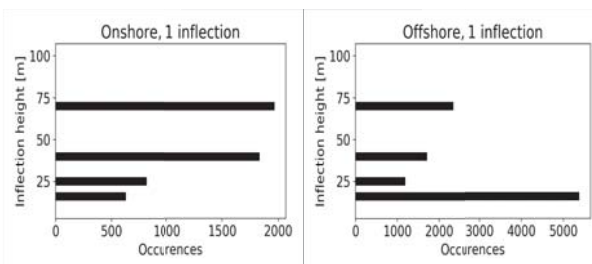


Fig 5. Height distribution of 1-inflection case

Results summary

- Offshore incoming profiles more likely to exhibit local maxima
- Inflections occur more often in unstable atmospheric conditions, offshore also in stable conditions
- Inflections occur at lower mean wind speeds compared to site average
- Duration decreases with number of inflections
- IBL-formation in offshore sector, inflection height matches fetch
- If disregarding this IBL, inflections are progressively more common at higher elevations
- Cause could be low-level jet or departure from surface layer both onshore & offshore

Conclusion

- Significant portion of both offshore and onshore profiles have one or more local maxima
- The local maxima could prove a challenge for future wind power estimation and fatigue calculations
- Likely a result of several phenomena such as internal boundary layers, low level jets and sea-land breezes.
- Coherence with very unstable atmospheric conditions could aid in predicting these abnormal profiles

References (selected)

- [1] Kettle A J 2014, *Journal of Wind Engineering and Industrial Aerodynamics* **134** 149-162
- [2] Nunalee C G and Basu S 2014 *Wind Energy* **17** 1199-1216

Acknowledgement

The authors would like to acknowledge the support of the European Commission in form of the MaRINET project (project ID: 262552) funded under FP7-INFRASTRUCTURES program

Experimental study: Structural resonances in wind turbine’s mechanical drive-train

Morten Rasmussen, Amir Nejad
 Department of Marine Technology
 Norwegian University of Science and Technology, Norway



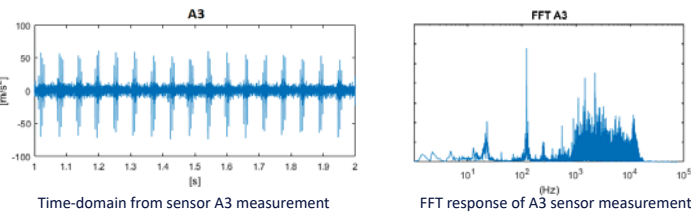
Abstract: What is this about?

This poster gives a review of a real data-set from an offshore wind turbine showing shock impulses. These shock pulses comes from structural resonances, which comes from spalls and cracks in the mechanical drive-train, propagating through the structure and are picked up by inertial acceleration sensors. Low-pass filtering the signal reveals that high-frequency response between 1-10 kHz is what is causing the shock impulses and vibration amplitudes.

Introduction

The left figure show time-domain sensor measurements of a 2,5 MW, three bladed wind turbine. The mechanical drive-train consist of a two-stage planetary gearbox with a one-stage spur gear. The right figure show the corresponding FFT response.

The given measurement is from an inertial acceleration sensor located at the spur gear of the gearbox.



Theory

Structural resonances comes from shock impulses when mechanical parts impact each other. This occurs when a spall, crack or other defect develops in any of the mechanical parts.

The phenomenon can be visual detectable as it often appears as signal modulation of the high resonance frequency of the structure and the lower characteristic frequency of the mechanical component.

Structural resonances are often not as obvious as shown here. Then advanced methods (spectral kurtosis and envelope analysis) are utilized.



Method

Characteristic bearing fault frequencies are determined by:

$$BPF1 = f \frac{N}{2} \left(1 + \frac{B}{P} \cos(\theta) \right) \quad BPF0 = f \left(1 - \frac{B}{P} \cos(\theta) \right)$$

$$FTF = \frac{f}{2} \left(1 - \frac{B}{P} \cos(\theta) \right) \quad BSF = f \frac{P}{2B} \left(1 - \left(\frac{B}{P} \cos(\theta) \right)^2 \right)$$

The concept of low-pass filtering is given as:

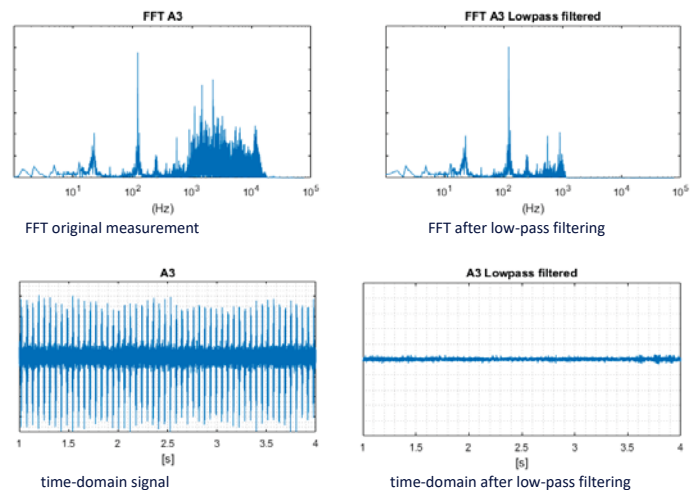
$$b(s) = \frac{\omega_c^2}{s^2 + \sqrt{2}\omega_c s + \omega_c^2} \quad \text{frequency domain}$$

$$\ddot{x}_f + \sqrt{2}\omega_c \dot{x}_f + \omega_c^2 x_f = \omega_c x \quad \text{time domain}$$

Results and discussion

Applying filtering techniques as discussed in the Method-section, shows how removal of frequencies above 1000 Hz removes the characteristic amplitude peaks.

The FFT shows clear amplitude peaks at the characteristic frequency of the HSS pinion (approx. 16 Hz) and the associated BPFI (approx. 180 Hz) of the bearing. In addition, there is a large response in a range of frequencies from 1 – 10 kHz.



The results imply that the original measurement’s large amplitudes are not caused by the amplitude peaks at the characteristic frequencies from the HSS pinion and BPFI bearing, but rather from the frequency response a much higher range than any of the characteristic frequencies.



Conclusion and further work

Structural resonances has been investigated from a case study of a wind turbine drive-train. Low-pass filtering has been performed on the raw measurement, revealing how the time-domain measurement amplitude shock impulses are created by frequency response between 1-10 kHz.

Further work should look into how these frequency ranges are decided, and if these resonances are affected by the transferring path of the structure. It should also be looked into if these structural resonances actually creates mechanical damage, or are only structure propagations that are picked up by inertial vibration measurement.

New coatings for leading edge erosion of turbine blades

Author: Aidan von Bonin¹, Astrid Bjørgum², Sergio Armada², Nuria Espallargas¹

*1) Norwegian University of Science and Technology, Trondheim, Norway

*2) Sintef Industry, Trondheim, Norway

Benefits of offshore wind turbines are:

- stronger, more stable winds,
- larger turbines with higher tip speed,
- reduced noise regulations,
- no near housing etc.

➤ Thus the power output increases

However, stronger winds result in severe erosion on the leading edge of the turbine blade.



Image 1: Leading edge erosion (<http://www.hogrehojder.se/vindkraft.html>)

Leading edge erosion is the mechanical degradation of the turbine blade due to the impact of particles and raindrops at high velocities.

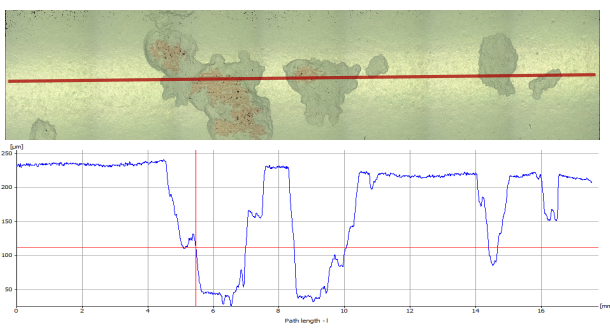


Image 2: Surface scan and profile of tested rain erosion sample.



Image 3: Offshore wind park (<https://de.wikipedia.org/>)

In this project:

- we evaluate and characterize coatings systems,
 - develop a multi parameter test machine.
- Combined with results from partners and data from a wind park operator we research the reasons and develop solutions for leading edge erosion.

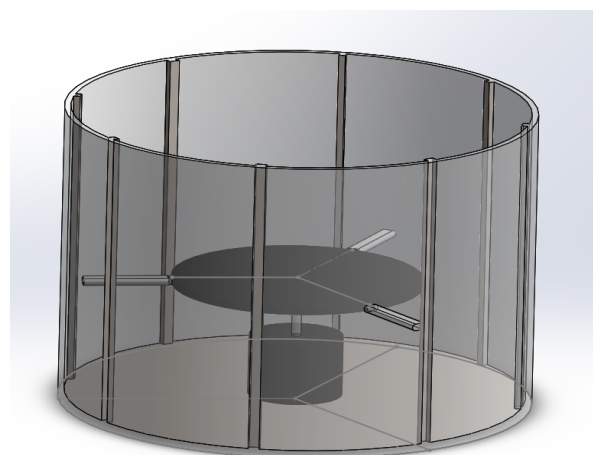


Image 4: Schematic design of a rain erosion test machine.

A test machine is being designed and build to simulate leading edge erosion. Parameters such as velocity, temperature and rain density, among others, will be variable.

The goal is to get deep understanding of the phenomenon and design, and develop stronger, more reliable and longer lasting protective coatings.

Mooring system design for the 10MW Triple Spar wind turbine at a 180 m Sea Depth Location



José Azcona, and Felipe Vittori
Wind Energy Department
Renewable Energy National Center, CENER, Spain



Introduction

This work presents the design of a mooring system for the Triple Spar floating wind turbine that supports the INN WIND 10MW wind turbine. A semi-taut mooring system configuration, combining steel chain and polyester is chosen to reduce the cost. The basic configuration is defined using static equations. A dynamic analysis for the environmental conditions of the Gulf of Maine, at a 180 m depth location, is performed to verify the performance of the design.

Floating wind turbine model

The Triple Spar platform, shown in Figure 1, is a hybrid design with characteristics of the semisubmersible and the spar concepts. It is composed of three concrete cylinders with a draft of 54.464 m. A steel transition piece connects the platform with the 10MW INN WIND wind turbine. Table 1 collects the main parameters of the floating wind turbine.



Floating wind turbine parameters	
Nominal power	10 MW
Rotor diameter	178,3 m
Hub height	119 m
Rotor rated thrust force	1500 kN
Platform draft	54,464 m
Columns diameter	15,0 m
Columns distance to platform center	26,0 m
Total mass	29574,3 Tons
Platform mass	28268,2 Tons

Figure 1. Triple Spar geometry

Table 1. Parameters of the floating wind turbine

Design methodology

The static catenary equations were used to iteratively reach the adequate mooring configuration. A smooth relationship between the platform displacement and the restoring force is obtained to prevent snap loads during the operation. The curve (Figure 2) also shows that the semi-taut system is able to counteract the rotor thrust force of 1500 kN at rated wind speed and the design extreme wind load of 2050 kN.

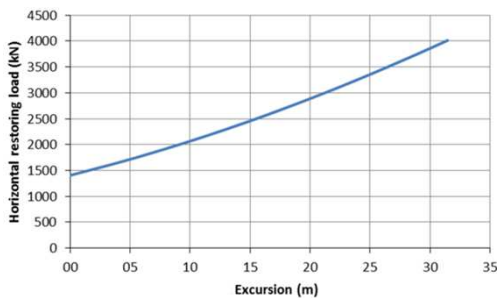


Figure 2. Horizontal restoring load vs. platform displacement

Figure 3 shows that the chain segment lays on the seabed connected to the anchor, meanwhile the polyester segment, at the upper part, connects the platform fairlead to the chain.

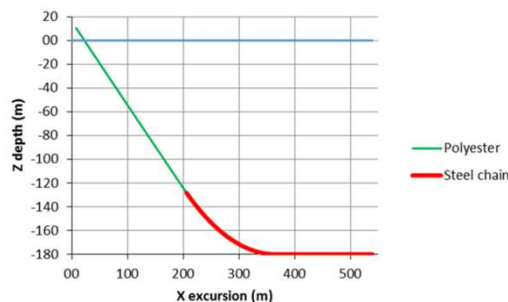


Figure 2. Mooring shape for the undisplaced position

Dynamic verification of the design

The final design of the mooring system is shown in Table 2.

Mooring system final design			
Number of lines	3	Chain weight/length	6350 N/m
Pretension at fairlead	1700 kN	Chain equivalent diameter	0,324 m
Fairlead position above MSL	10,5 m	Polyester length	239,0 m
Fairlead radial position	33,5 m	Polyester weight/length	240 N/m
Anchor radial position	572,9 m	Polyester equivalent diameter	0,151 m
Chain length	344 m	Polyester axial stiffness	4,32 E4 kN

Table 2. Parameters of the mooring system

A dynamic verification of the design was performed based on a reduced set of load cases, including DLC 1.6, 2.2, 6.1 and 7.1 from IEC61400-3 Ed.1. The extreme tensions and the maximum depth of the connection point between the polyester and the chain are shown in Table 3 and Table 4.

	DLC	Tension L1 (kN)	Tension L2 (kN)	Tension L3 (kN)
Max	6,1	4139	1038	2649
Min	6,1	564	1048	2062
Max	1,6	1953	1808	1938
Min	7,1	3484	61	3181
Max	6,1	2757	1078	4033
Min	6,1	1885	1050	446

Table 3. Extreme line tensions

DLC	Connection depth L1 (m)	Connection depth L2 (m)	Connection depth L3 (m)
6,1	142,2	141,3	115,2
7,1	110,2	165,6	112,3
6,1	117,0	135,7	142,9

Table 4. Maximum depth of the connection between polyester and chain

In addition, natural periods were calculated resulting 166.0 s for surge and sway and 25.5 s for pitch and roll.

Conclusions

The dynamic analysis confirmed the adequacy of the design through the verification of these aspects:

- Maximum tensions are below maximum breaking load of polyester (13172 kN) and steel chain (30689 kN).
- The resulting natural frequencies of the platform are located out of the dominant frequencies of the wave spectrum (4 s - 25 s).
- Maximum angle between water plane and mooring lines is always below 86,7 deg, avoiding the contact between the platform and the lines.
- The polyester segments do not contact the seabed, that could potentially damage them.
- The anchors do not experience vertical loads that could displace them.

A complete load case analysis must be performed to fully validate the proposed design.

Acknowledgements

This project has received funding from the European Union's Seventh Framework Programme for research, technological development and demonstration under grant agreement No.308974 (INN WIND.EU). We also want to thank Carlos López Pavón and Frank Lemmer for their help and advice.

Consideration of negative aerodynamic damping in the design of floating wind turbines

Carlos E. S. Souza (carlos.souza@ntnu.no), Erin E. Bachynski

Abstract

The success of floating wind turbines as feasible solutions for harvesting offshore wind energy still depends on significant cost reductions. An efficient structural design is fundamental, but the strongly coupled dynamics make accurate prediction of the global responses and lifetime estimates challenging. A phenomenon of particular interest is the so-called *aerodynamic damping*, an effect resulting from the interaction between rotor thrust and nacelle motion. This work introduces a method to estimate the magnitude of the aerodynamic damping effect, as a function of the incident wind velocity and the nacelle period of motion. Special focus is given to the conditions where the thrust induces negative damping to the FWT – an effect known to amplify its surge and pitch motions, with dramatic consequences for the integrity of mooring lines and FWT substructure and tower.

Thrust as a function of f_0 and ϕ and nacelle velocity/acceleration

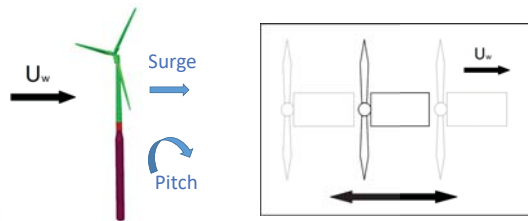
$$\dot{x} = \omega x_0 \cos(\omega t)$$

$$T(t) = T_0 + T_{var}(t)$$

$$T_{var} = f_0 \omega x_0 \cos(\omega t + \phi) = f_0 \left[\dot{x} \cos(\phi) + \frac{\ddot{x}}{\omega} \sin(\phi) \right]$$

Objectives

- Develop a method to analyze the interaction between nacelle horizontal motions and rotor thrust.
- Apply the above-mentioned method to a 5 MW wind turbine, with different control strategies.
- Estimate the aerodynamic damping coefficients for different operational conditions.
- Provide insight for the preliminary design of floating wind turbines



Nacelle equations of motion

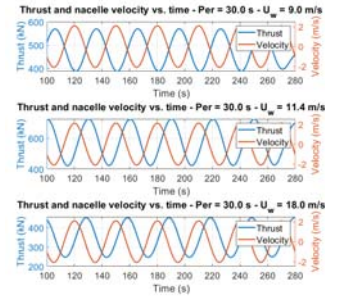
$$m\ddot{x} + c\dot{x} + kx = T(t) \rightarrow$$

$$\left[m - \frac{f_0}{\omega} \sin(\phi) \right] \ddot{x} + [c - f_0 \cos(\phi)] \dot{x} + kx = T_0$$

Aer. Damping: $b_{aer} = -f_0 \cos(\phi)$

Methodology

- Forced oscillation of rigid NREL 5 MW rotor, modelled in AeroDyn and coupled to controller.
- U_w covering the entire above-rated operational range; oscillation periods from 20.0 s to 160.0 s, with increments of 1.0 s.
- Control strategies: land-based control gains, detuned gains, variable reference.
- Prediction of damping values based on the phase between time-series of nacelle velocity and rotor thrust.

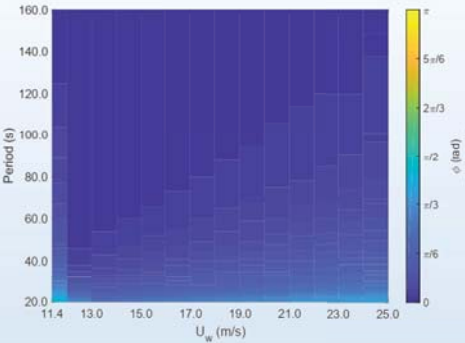


Blade-pitch control system

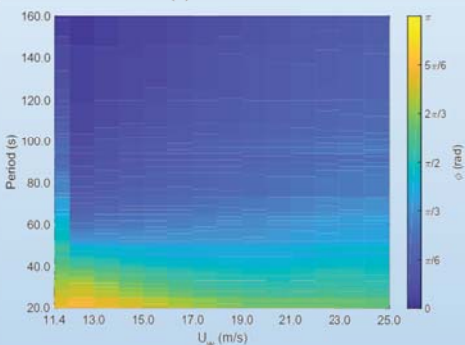
PI controller: $\Delta\theta = K_p \Delta\omega + K_i \int_0^t \Delta\omega dt$

Variable reference: $\omega_r = \omega_0 (1 + k\theta)$

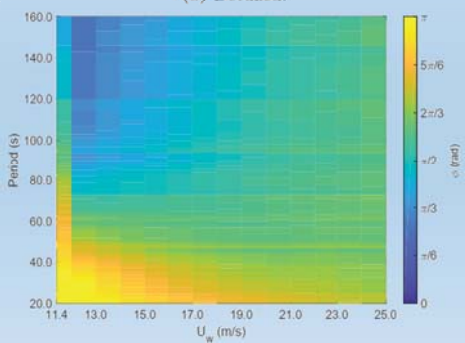
Phase ϕ between nacelle velocity and rotor thrust



(a) Land-based.



(b) Detuned.



(c) Detuned with var. reference.

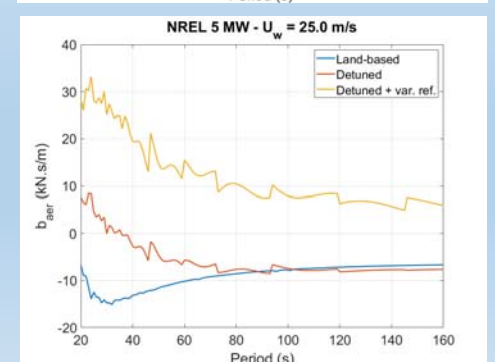
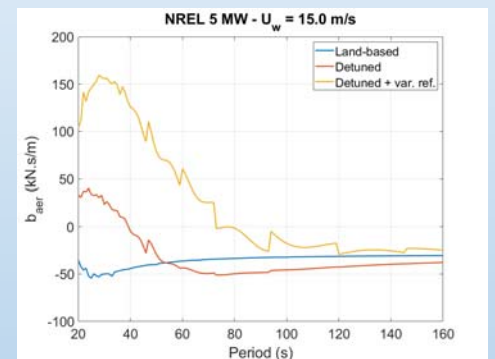
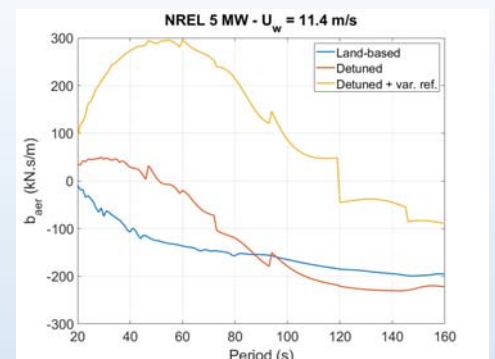
Results

- When land-based control gains are adopted, the relative phase between nacelle velocity and thrust is always lower than $\pi/2$, leading to negative aerodynamic damping for all combinations of period and phase.
- When the controller is detuned (i.e., the gains are reduced), the phase may be greater than $\pi/2$, for lower wind velocities. The aerodynamic damping then tends to be positive, helping to damp the nacelle motions. As U_w increases, the phase is reduced and the damping eventually gets negative again.
- The combination of detuned gains and variable reference significantly increases the region $\phi > \pi/2$, meaning higher aerodynamic damping for all operational conditions.
- In general, the aerodynamic damping coefficient is higher in magnitude for wind velocities closed to rated.

Conclusions

The aerodynamic damping effect arises from the relative phase between nacelle motion and rotor thrust, and is dependent on nacelle period of motion and incident wind velocity. Damping may be negative in surge and positive in pitch, depending on controller gains, wind velocity and platform natural periods. Blade-pitch controller detuning is more efficient in increasing the damping near rated wind velocity, but its performance is reduced when the velocity increases. Variable reference results in more damping for the entire range of periods and wind velocities.

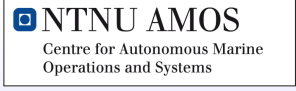
Aerodynamic damping coefficient (b_{aer})



Wind-Wave Directional Effects on Fatigue of Bottom-Fixed Offshore Wind Turbine

Stian Høegh Sørum^(a,b), Jørgen Amdahl^(a,b), Jørgen Krokstad^(b)
^(a)Centre for Autonomous Marine Operations and Systems (NTNU AMOS),
^(b)Department of Marine Technology, NTNU, Trondheim, Norway.

Email: stian.h.sorum@ntnu.no



Motivation

- Importance of wind-wave misalignment on fatigue damage is well known
- Effect of wave spreading is less known
- Assuming long-crested waves is shown conservative for a few isolated cases [1, 2]
- Deeper water and increased monopile diameter increases importance of wave loads and relevance of wave spreading
- Assuming long-crested waves may become non-conservative as wave loads become dominating

Method

- The DTU 10 MW reference turbine is placed on a monopile foundation
- Different wave sensitivity is modelled by altering the mode shapes
- Three soil stiffnesses analysed
- Natural period tuned to same value by varying wall thickness in tower
- All other design parameters kept unchanged

Models

- Variation in 1st and 2nd fore-aft mode shapes are shown in Fig. 1
- Equal natural frequencies achieved for first global modes
- 2nd modes are outside wave-frequency range

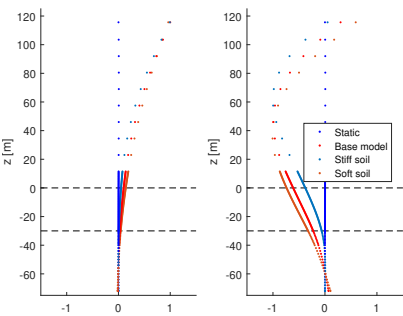


Figure 1: 1st (left) and 2nd (right) global fore-aft modes

Mode	Base model	Stiff soil	Soft soil
1st fore-aft	0.21 [Hz]	0.21 [Hz]	0.21 [Hz]
2nd fore-aft	1.05 [Hz]	1.30 [Hz]	0.97 [Hz]
1st side-side	0.21 [Hz]	0.21 [Hz]	0.21 [Hz]
2nd side-side	1.01 [Hz]	1.37 [Hz]	1.00 [Hz]

Lifetime fatigue analyses

- Lifetime fatigue damage calculated at most critical positions in monopile and tower
- Environmental data from Dogger Bank area
- Damage calculated for aligned wind and waves, as well as misaligned wind and waves with long-crested and short-crested waves
- DLC 1.2 and DLC 6.4 considered

Sensitivity to wind and wave loads

- Variations in the mode shapes will influence the importance of wind and wave loads for fatigue
- Sensitivity is illustrated by calculating fatigue damage assuming aligned wind and waves
- Contribution to lifetime fatigue damage per wind speed is shown for most critical position on monopile (Fig. 2) and tower (Fig. 3)

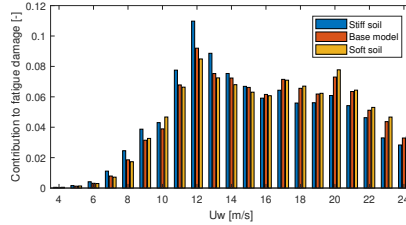


Figure 2: Monopile

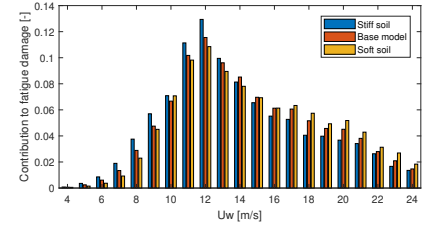


Figure 3: Tower

- Model with soft soil has a larger contribution to lifetime fatigue damage from wave loads. This corresponds to high wind speeds in Fig. 2 and 3
- Model with stiff soil has a larger contribution to lifetime fatigue damage from wind loads. This corresponds to wind speeds close to rated in Fig. 2 and 3

Effect of short-crested waves

- The lifetime fatigue damage is calculated assuming both long-crested and short-crested waves
- Wind-wave misalignment now taken into account

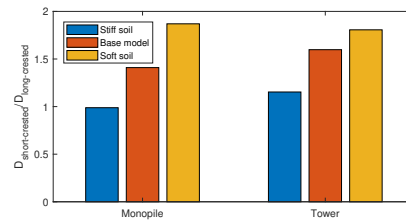


Figure 4: Ratio of maximum fatigue damage when assuming short-crested or long-crested waves

- Fig. 4 shows the effect of assuming short-crested or long-crested waves
- For all models, assuming short-crested waves increases the fatigue damage in the tower
- For the monopile, assuming long-crested waves is conservative only with the stiffest soil
- This is consistent with the reduced sensitivity to wave loads as the soil stiffness increases

Conclusion

- It may be both conservative and non-conservative to assume long-crested waves when designing offshore wind turbines
- As the sensitivity to wave loads increases, assuming long-crested waves becomes increasingly non-conservative

References

[1] Jan-Tore Horn, Jørgen R Krokstad, and Jørgen Amdahl. Long-term fatigue damage sensitivity to wave directionality in extra-large monopile foundations. *Proceedings of the Institution of Mechanical Engineers, Part M: Journal of Engineering for the Maritime Environment*, 232(1):37–49, 2018.

[2] Jenny M. V. Trumars, Johan O. Jonsson, and Lars Bergdahl. The effect of wind and wave misalignment on the response of a wind turbine at Bockstigen. In *ASME 2006 25th International Conference on Offshore Mechanics and Arctic Engineering*, volume 1. ASME, June 2006.

Acknowledgements

This work has been carried out at the Centre for Autonomous Marine Operations and Systems (NTNU AMOS). The Norwegian Research Council is acknowledged as the main sponsor of NTNU AMOS. This work was supported by the Research Council of Norway through the Centres of Excellence funding scheme, Project number 223254 - NTNU AMOS.

INTRODUCTION

Designing floating wind turbine (FWT) systems to withstand imposed loads (especially from random excitations which introduce uncertainties) at minimal cost requires robust engineering tools that ensure neither overdesign nor under-design but rather optimal design. Accounting for these uncertainties as presented in this work, would lead to more accurate estimation of failure rates that are close to reality hence FWTs can be designed just strong enough. The maximum von Mises stress in the tower is the load effect considered in this study.

METHODOLOGY

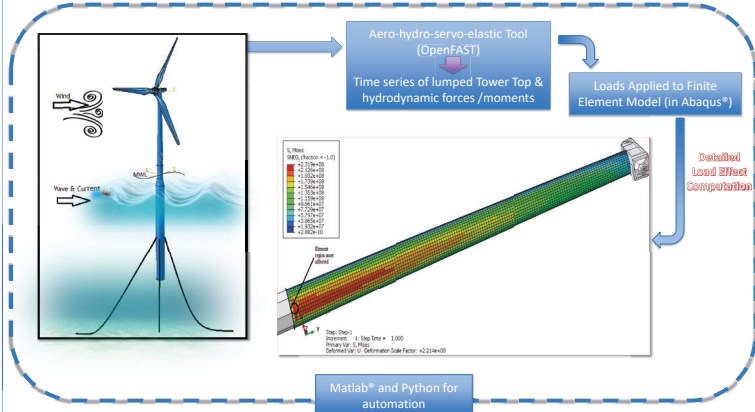


Figure 1. Scheme for fully coupled load effect computation

EFFECT OF START-UP TRANSIENTS (mainly due to improper ICs)

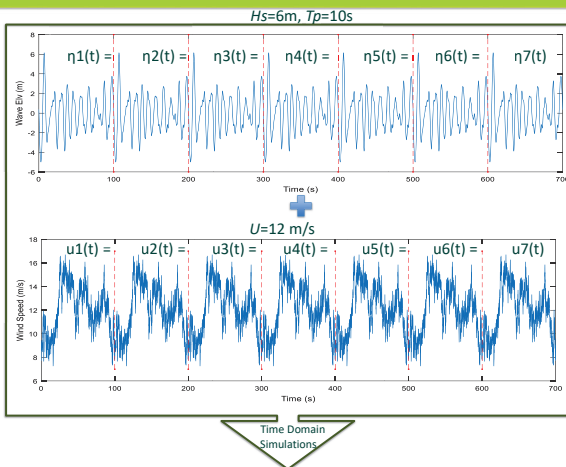


Figure 2. Repeated 100s Wave (Top) and wind (Bottom) realizations making up 7 windows used as inputs

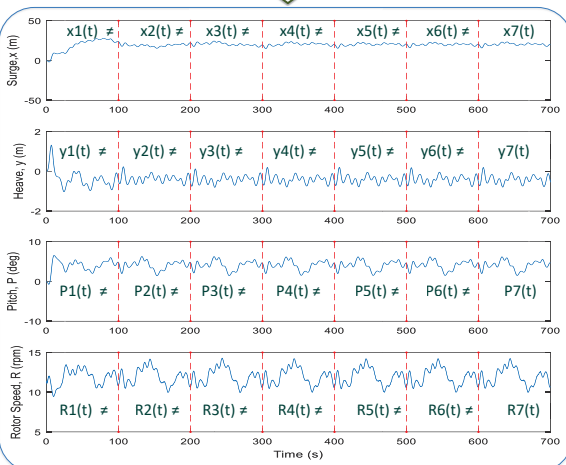


Figure 3. Resulting outputs in the 7 windows

Using the averages of out-of-plane and in-plane blade-tip displacements, blade pitch angles, rotor speed, platform surge, heave and pitch of the 7th window as Initial conditions, a convergence study is presented where paired comparison between values in each step of each window is matched with corresponding values of the 7th window

CONVERGENCE STUDY

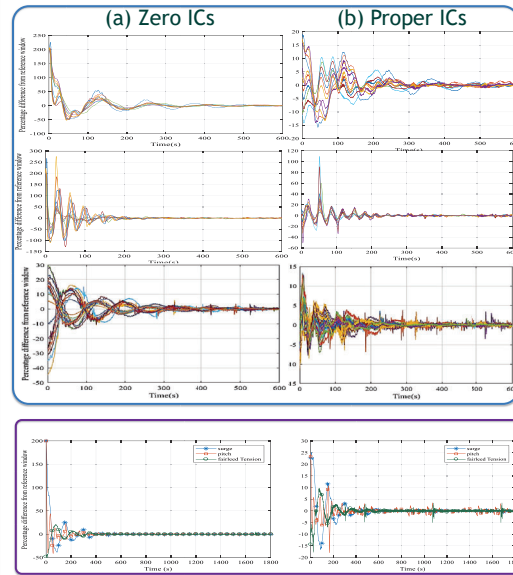
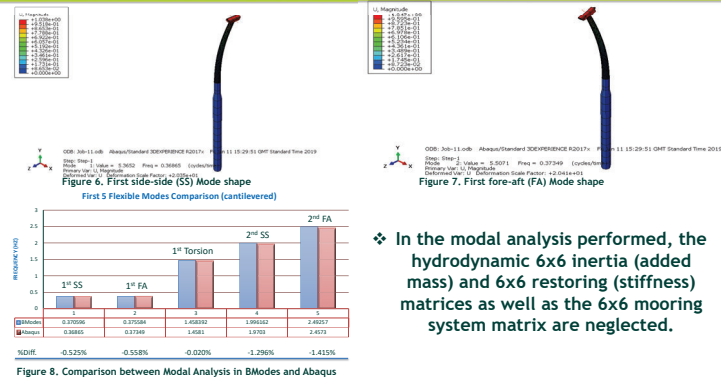


Figure 4. Convergence results (7x100s windows) based on IEC 61400-3 DLC 1.2 (Wind bins $U=4\text{m/s}:2\text{m/s}:24\text{m/s}$). Top to bottom: Surge, Pitch and tensions at fairleads

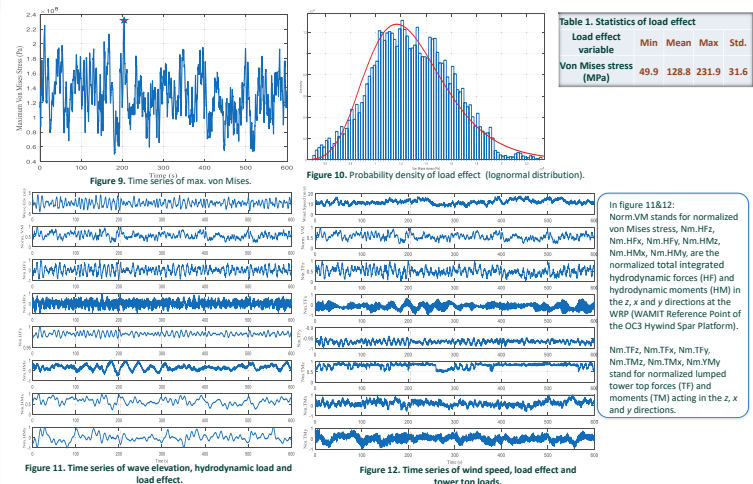
Figure 5. 1800s of convergence results for 4800s simulation using 600s windows, $U=12\text{m/s}$, $H_s=6\text{m/s}$ and $T_p=10\text{s}$

FE MODEL VALIDATION



In the modal analysis performed, the hydrodynamic 6x6 inertia (added mass) and 6x6 restoring (stiffness) matrices as well as the 6x6 mooring system matrix are neglected.

LOAD EFFECT RESULTS AND CHARACTERIZATION



CONCLUSIONS

- With $\pm 20\%$ as convergence criterion in the paired comparison, it is concluded that 50-60 s would suffice as the run-in-time to be excluded from response statistics if proper ICs are set as described in this work.
- The influence of the applied loads on the load effect was examined. The tower top thrust force and hydrodynamic force acting in the direction of wave/wind visibly showed coupling with the load effect studied. So also did the platform pitching moment.
- From a reliability standpoint, this study presents an approach that treats load effects as stochastic variables and could be used in establishing uncertainty models for robust reliability assessment leading to calibration of currently used partial safety factors and thus translate to cost reductions.

ACKNOWLEDGEMENT

Salem Okpokparoro thankfully acknowledges the financial support granted by Petroleum Technology Development Fund (PTDF), Nigeria.

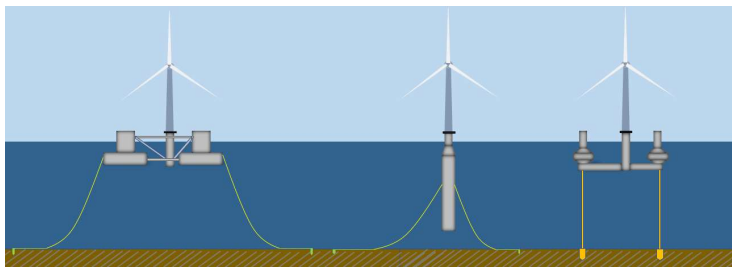


Conceptual Design of a 12 MW Floating Offshore Wind Turbine in the Ulsan Offshore Area, Korea

Pham Thanh Dam*, Hyunyoung Shint
School of Naval Architecture and Ocean Engineering, University of Ulsan, Korea

Introduction

- Korean Government announce a plan "Renewable Energy 3020" to rise 48.7 GW new renewable energy by 2030. The target includes 13 GW offshore wind. Ulsan City plans to develop a 200 MW demonstration wind farm project (phase 1) and 1 GW wind farm (phase 2) in Ulsan offshore area, Korea.
- University of Ulsan introduced a 12 MW wind turbine concept, this is a gearless wind turbine and uses super-conducting generator to reduce the wind turbine top mass.
- To investigate a feasible concept for supporting the 12 MW wind turbine in 150 m water depth in the Ulsan Offshore area, three concepts of platform are designed and analyzed. These are semi-submersible, spar and TLP.



Three concepts of 12 MW floating offshore wind turbine

12 MW Wind Turbine and Floater Concepts

- Semisubmersible concept is stabilized by the water plane area of column separation which provide large roll and pitch stiffness.
- Spar concept length is limited by water depth. Concrete is used to distribute the center of mass lower than center of buoyancy.
- TLP is stabilized by high tension of the tendon system.
- Semi-submersible and spar are moored by catenary mooring systems

12 MW wind turbine specifications	Value
Rated power of wind turbine	12-MW
Rotor orientation	Upwind, 3 blades
Control	Variable Speed, Collective Pitch
Rotor diameter [m]	195.2
Hub height [m]	120.25
Rated wind speed [m/s]	11.2
Rated rotor speed [rpm]	8.25 (gearless)
Hub mass [kg]	169,440
Hub inertia about shaft [kg·m ²]	829,590
Nacelle mass (target) [kg]	400,000

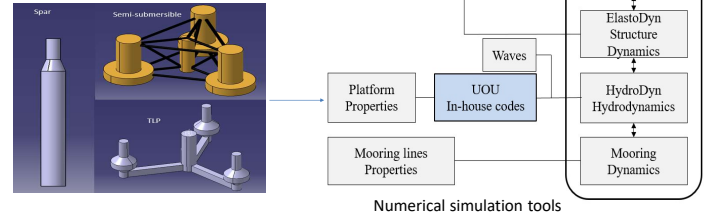
Platform properties	Unit	Semi-sub.	Spar	TLP
Depth to platform base below	m	27	120	36
Elevation to platform top	m	10	10	10
Platform mass, including ballast	ton	28,975	23,028	10,265
Platform center of mass	m	-20.15	-96.14	-28.00
Platform roll inertia	ton·m ²	1.96E+07	1.00E+07	1.08E+07
Platform pitch inertia	ton·m ²	1.96E+07	1.00E+07	1.08E+07
Platform yaw inertia	ton·m ²	3.55E+07	8.50E+05	3.52E+07

Mooring line properties	Unit	Semi	Spar	TLP
Number of mooring lines	-	3	3	3
Mooring type	-	Studless chain	Studless chain	Tendon
Mooring nominal diameter	m	0.142	0.142	1.04
Mooring line weight in water	N/m	3708.8	3708.8	0
Axial stiffness (EA)	MN	1815	1815	22290
Unstretched mooring length	m	950	750	113.95

Numerical Simulation

Numerical simulations were performed the fully coupled aero-hydro-servo-elastic wind turbine by NREL FAST V8

UOU in-house codes calculated hydrodynamics coefficients



Environmental Condition in the Ulsan Offshore Area



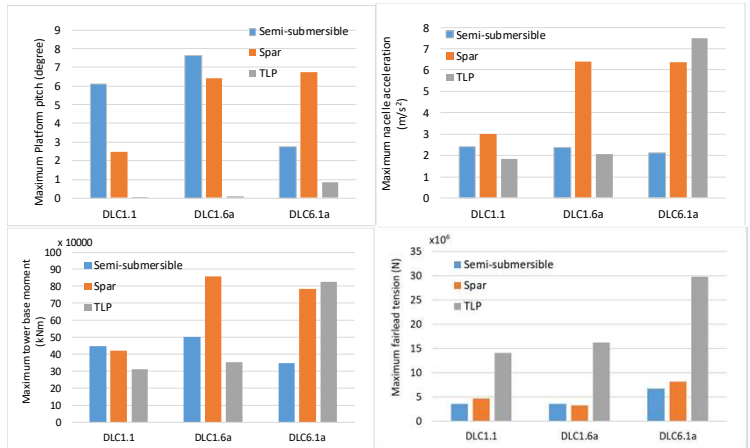
Three design load cases were selected to analyze the ultimate loads and fatigue loads based on the environmental condition of Ulsan offshore area

Design load cases

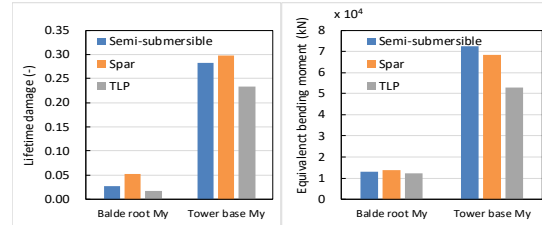
Item	Wind	Waves	Current	WT status
DLC 1.1	NTM 4 - 24 m/s	NSS	NCM	Operation
DLC 1.6a	NTM 10-24 m/s	SSS Hs 10 m, Tp 13 s	NCM	Operation
DLC 6.1a	EWM 41.3 m/s	ESS Hs 12.49 m, Tp 15.46 s	ECM 0.93 m/s	Parked

Reference location of Ulsan offshore area

Numerical Simulation Results



Maximum responses and loads



Fatigue damage of 20 years operation

Conclusions

- TLP concept is preferable in operation condition, however in extreme condition at high speed of current, the nacelle acceleration and tower bending moment are higher than other concepts
- In general, semi-submersible concept is suitable design
- Further investigation about installation, transportation is needed

ACKNOWLEDGEMENT
This research was supported by the Korea Institute of Energy Technology Evaluation and Planning (KETEP) grant funded by the Korea Government (MOTIE) (No. 20184030202280 & No. R18XA03).

Motion Performances of 5-MW Floating Offshore Wind Turbine under Combined Environmental Conditions in the East Sea, Korea

Young Jae. Yu*, Hyun Kyoung. Shin**

*Naval Architecture and Ocean Engineering, University of Ulsan, South Korea

Introduction

The world is interested in renewable energy more than ever, and Korea plans to increase the proportion of renewable energy to 20% by 2030 under the 3020 renewable energy policy. Among them, 16.5GW (34%) is planned to be covered from wind energy, and the capacity of offshore wind energy is about 13GW. Considering domestic technological wind resource potential (33.2GW), it seems to be a sufficient target amount. Offshore wind power is fixed type that is installed in shallow water depth, and there is floating type which is installed in deep sea. In order to achieve the renewable energy 3020 target, floating offshore wind turbine must be considered which can utilize abundant wind resources and extensive sea area. Therefore, in this paper, the motion analysis of a floating offshore wind turbine system using a semi-submersible and a spar platform based on the domestic marine environment conditions was performed. The domestic marine environment was designated the area near the East Sea gas field 50km away from the coast of Ulsan. Numerical analysis was performed using FAST v8 developed by NREL

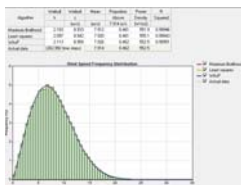
Environmental Conditions



- For the domestic environmental conditions, we used the area within 50km from the East Sea gas field.
- MERRA-2 is the reanalysis data carried out by NASA, and its coordinates are located about 38.5km from the East Sea gas field.
- Wave data based on the observation at the Meteorological Department of Ulsan buoy(22189), located about 17.3km away from the East Sea gas field.
- Current based on the observed data in Ulsan port, the observation station located about 51.73km away from the East Sea gas field.

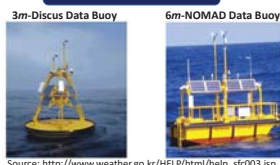


Wind Data



Description	Value
Data name	MERRA-2
Measurement location	N35.30, E130.00
Measurement period	1998-01-01 00:00 ~ 2018-01-01 00:00
Measurement height	50 [m]
Measurement interval	1 [hr]
Mean wind speed	7.914 [m/s]
Weibull k	2.103
Power law exponent (α)	0.14
Description	Value
V _{ref} (50yr) wind speed	40.424 [m/s]
Main wind direction	45°, 225°, 315°

Wave Data



Description	Value
Data name	Ulsan (22189)
Measurement period	1998-01-01 00:00 ~ 2018-01-01 00:00
Measurement interval	1 [hr]
Significant Wave height (50yr)	11.459 [m]
Significant Wave period1 (50yr)	11.996 [s]
Significant Wave period2 (50yr)	13.726 [s]
Significant Wave period3 (50yr)	15.455 [s]

Current Data

Description	Value
Summer	Surface layer 0.7716 ~ 0.9259 [m/s]
	Bottom layer 0.2572 ~ 0.5144 [m/s]
Winter	Surface layer 0.2572 ~ 0.3086 [m/s]
	Bottom layer 0.0360 ~ 0.1698 [m/s]

Description	Value
Water depth	150 [m]
Design wave height	10 [m]
Design wave period	13 [s]
Current speed of bed	0.5144 [m/s]
Strength of bed	Middle

Design Load Cases

- Design load cases were selected by referring to IEC 61400-3.

- DLC1.2 and DLC1.6a was selected for considering the power production condition and DLC6.1a was selected for considering the parked condition.
- In DLC1.2, fatigue analysis was performed.
- In DLC1.6a, severe sea state of the East Sea gas field was applied under normal operating condition.
- In DLC6.1a, extreme environmental conditions were applied in order to consider stability in situations such as typhoons.

Description	IEC 61400-3 INTERNATIONAL STANDARD		
	DLC 1.2	DLC 1.6a	DLC 6.1a
Wind	NTM	NTM	EWM
Waves	NSS	SSS	ESS
Wind and wave directionality	0°, COD	0°, COD	MUL, COD
Current	NCM	NCM	ECM
Water level	150 [m]	150 [m]	150 [m]
Safety factor	No factor	1.35	1.35

5-MW wind turbine systems



- The NREL 5-MW wind turbine was selected for the upper structure used in the numerical analysis.
- OC3-spar and OC4 semi-submersible type platforms are used for the comparison.
- Mooring system is redesigned for 150m water depth. Pretension of the redesigned mooring line was maintained, and the diameter was adjusted to maintain the angle at the fairlead. Touchdown length was redesigned, that was longer than before to prevent lift up at the anchor.

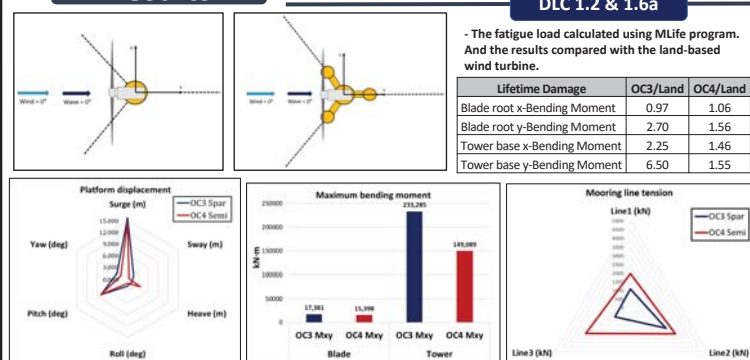
Source: Definition Floating system for phase II of OC4



Source: Definition Floating system for phase IV of OC3

Parameters	unit	OC3-Spar	OC4-Semi
Number of Mooring Lines	-	3	3
Angle Between Adjacent Lines	°	120	120
Depth to Anchors Below SWL (Water Depth)	m	150	150
Depth to Fairleads Below SWL	m	70	14
Radius to Anchors from Platform Centerline	m	485.4	812
Radius to Fairleads from Platform Centerline	m	5.2	40.868
Unstretched Mooring Line Length	m	500	800
Mooring Line Diameter	m	0.117	0.09
Equivalent Mooring Line Mass Density	kg/m	300	178
Equivalent Mooring Line Weight in Water	N/m	2567	1519
Equivalent Mooring Line Extensional Stiffness	MN	1.30E+03	729

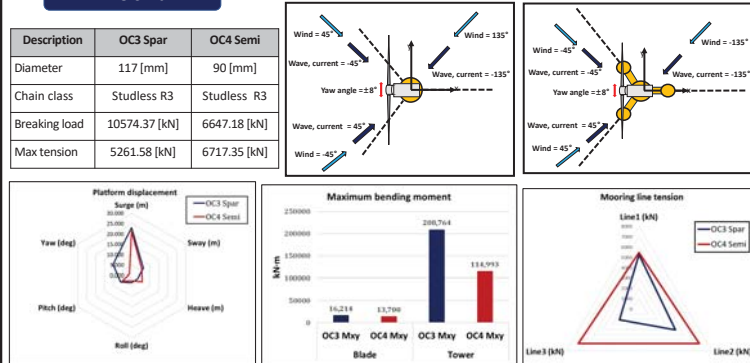
Results



- The fatigue load calculated using MLife program. And the results compared with the land-based wind turbine.

Lifetime Damage	OC3/Land	OC4/Land
Blade root x-Bending Moment	0.97	1.06
Blade root y-Bending Moment	2.70	1.56
Tower base x-Bending Moment	2.25	1.46
Tower base y-Bending Moment	6.50	1.55

DLC 6.1a



Conclusions

- In DLC1.6a and DLC 6.1a, the Heave motion of Semi type is about 2m larger than spar type. And, the Yaw motion of Spar type is about 5° larger. From this result, in order to use Spar type platform, additional yaw spring stiffness should be estimated appropriately when designing mooring line.
- Under extreme environmental conditions, the spar type receives a larger bending moment than semi type at blade root and the tower base part. Also, the fatigue load of spar type at tower base part is 6.5 times of the land-based wind turbine and more than 4 times of semi type. From these results, it becomes necessary to design sufficient stiffness for stress concentration part in order to use spar type platform.
- Under the extreme environment conditions, the maximum mooring line tension acting on the semi type exceeded the fracture limit. Therefore, mooring system should be redesigned after selecting the appropriate platform for allowing the floating offshore wind turbine that could operate within the mooring line fracture limit.

Acknowledgement : This research was supported by the Korea Institute of Energy Technology Evaluation and Planning(KETEP) grant funded by the Korea government(MOTIE) (No. 20184030202280 & 20183010025270).

Influence of ballast material on the buoyancy dynamics of cylindrical floaters of FOWT

Daniel Alarcón; Climent Molins; Pau Trubat
Universitat Politècnica de Catalunya. Escola de Camins



UPC BARCELONATECH

Structural Model

The FlowDyn structural FEM model is based on a non-element depending Corotational internal loads approach, based on a formulation derived for dynamic analysis [1]. Corotational local axes for shell elements are based on a drift correction angle [2], known as Linear Triangle Best Fit.

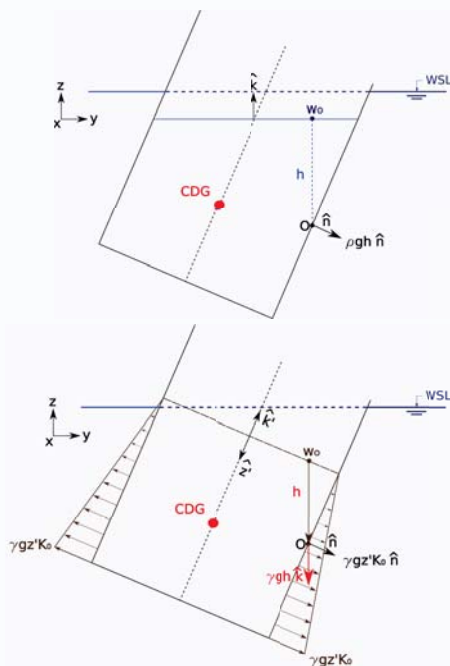
The dynamic analysis is performed in the time domain by solving the equations of motion of the system, based on the Newton's 2nd law. For the time integration a alpha-Generalized Method [3] scheme is adopted in combination of an iterative Newton-Raphson method to deal with the nonlinearity.

The model presented allows to compute the displacements field at mesh nodes and internal loads over all the geometry by a nodal interpolation computation.

Ballast Model

Offshore structures are usually ballasted with granular materials or water. The different behavior of these materials modifies the structure motion depending mainly on its geometry. The granular ballast model is defined by a constant radial At-Rest pressure and a weight component, which depends on the material column over each shell element. For liquid ballasting, an hydrostatic internal fluid pressure law is applied, computing at each step the new position of the free surface.

Both models deal with inertial loads by distributing the ballast mass and inertia over the most close nodes.

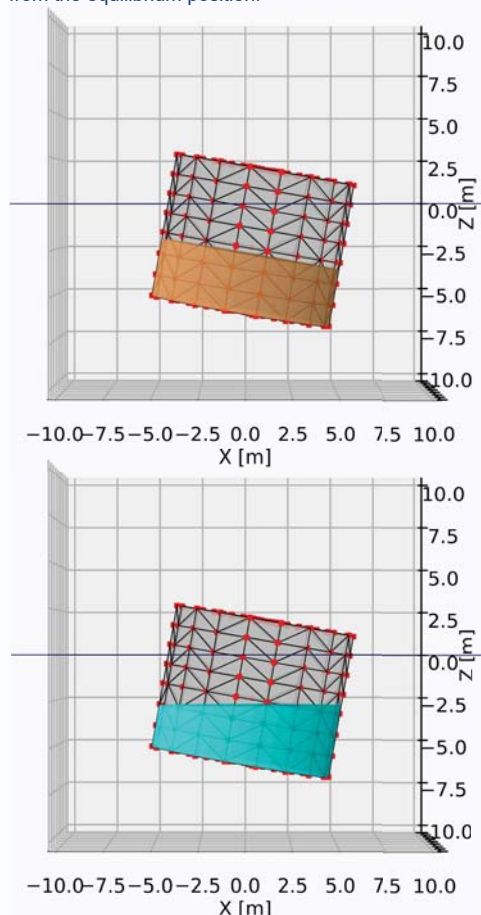


Granular ballast model is reduced to rotations smaller than the internal friction angle, to ensure that free surface remains parallel to the base. For liquid ballast, only a vertical hydrostatic distribution is applied, thus the structure needs quasi-static movements with low inertial accelerations and also with a frequency movements far enough from sloshing phenomena, which is no modeled in this approach.

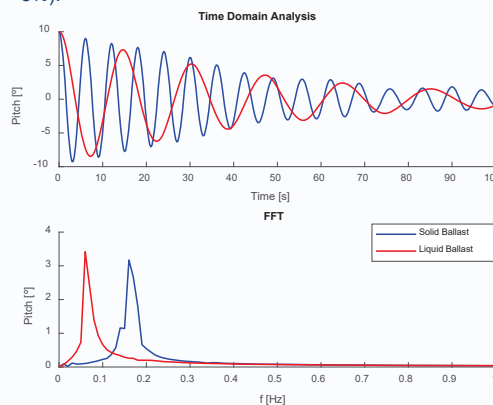
Simulation Models

In order to compare the model behavior over different geometries, two pitch free decay analysis have been performed. For comparison reasons, same mass and density of the ballast materials are considered.

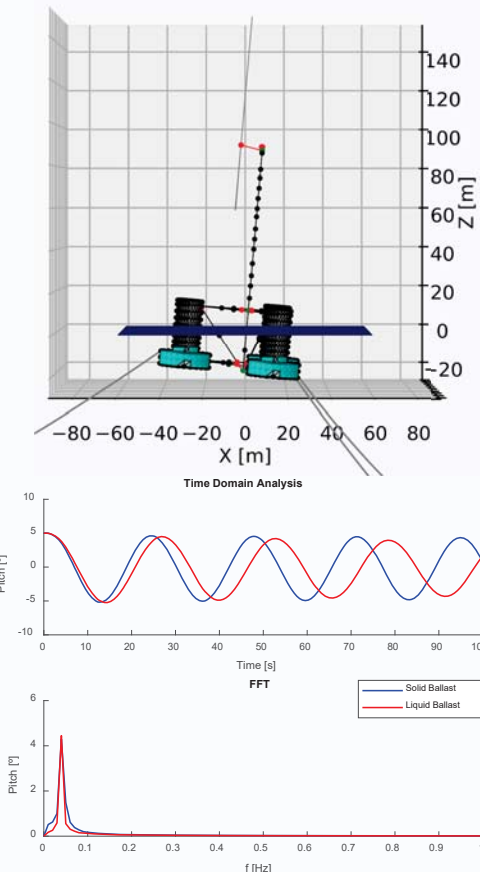
The first analysis is based on a cylinder of 8m height and a radius of 5m, with an initial rotation of 10 degrees from the equilibrium position.



Due to the cylinder geometry, the effect of the liquid ballasting produces a considerable increasing of the pitch period of the structure. Also an amplitude increment of the related frequency is noted considering liquid ballasting instead of granular ballasting (about 8%).



Second simulation is based on a FEM model of the DeepCwind semisubmersible platform, composed of 48 beam and 2592 shell elements. The initial pitch rotation is fixed in 5 degrees from the equilibrium position.



In this case, the influence of the ballast model is less accused than in the cylinder due to the geometry of the platform, but as shown in time domain analysis, the period of the platform is slightly shifted and also the amplitude associated increases about 4% with liquid ballasting.

Conclusions

The results obtained show that the platform dynamic behavior is affected by the nature of the ballast. The geometry of the platform and also its dynamics are related with the differences noticed.

Then, further studies are expected to better assess the range of these effects.

References

- [1] A.Campos, C.Molins, P.Trubat, D.Alarcon, "A 3D FEM model for floating wind turbines support structures", Volume 137, 2017, Pages 177-185 14th Deep Sea Offshore Wind R and D Conference, EERA DeepWind 2017; Trondheim; Norway; Code 133177
- [2] C.A.Felippa, B.Haugen, "Unified Formulation of Small-Strain Corotational Finite Elements: I. Theory". Department of Aerospace Engineering Sciences and Center for Aerospace Structures. University of Colorado, 2005.
- [3] C.M.Shearer, C.E.S.Cesnik, "Modified Generalized- α Method for Integrating Governing Equations of Very Flexible Aircraft", Structural Dynamics and Materials Conference. 3. 22. 10.2514/6.2006-1747.

EERA DeepWind'2019
16th Deep Sea Offshore Wind R&D Conference,
Trondheim, 16 - 18 January 2019

Hydrodynamic Characteristics of the Modified V-shaped Semi Floating Offshore Wind Turbine with a Heave Plate

Wei Shi^{1,*}, Lixian Zhang¹, Jikun You², Madjid Karimirad³ and Constantine Michailides⁴

¹Dalian University of Technology, Dalian, Liaoning, China,

²Connect Lng AS, Oslo, Norway

³Queen's University Belfast, Belfast, UK

⁴Cyprus University of Technology, Limassol, Cyprus

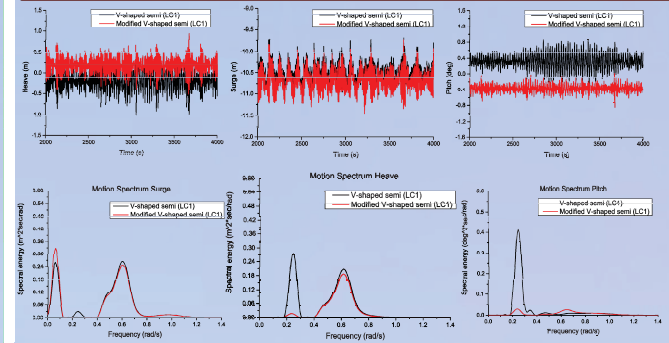
Abstract

In recent years, there is a great ambition to develop offshore wind energy globally due to greenhouse effect and energy crisis. Great efforts have been devoted to develop a reliable floating offshore wind energy technology in order to take advantage of the large amount of wind energy resources that exist in deep water. In this paper, a novel concept of a floating offshore wind turbine (FOWT), namely the modified V-shaped Semi with a heave plate is proposed and its hydrodynamic characteristics are studied. A numerical model based on ANSYS/AQWA is used to investigate the dynamic motion, response characteristics and mooring performance of the new concept. Moreover, the response amplitude operators (RAOs) of different response quantities are also elaborated. A comparative study of the dynamic response of different response quantities of the modified V-shape and original V-shaped Semi is carried out for operational environmental conditions. It is found that the modified V-shape Semi shows relatively better performance in platform motion and mooring line response.

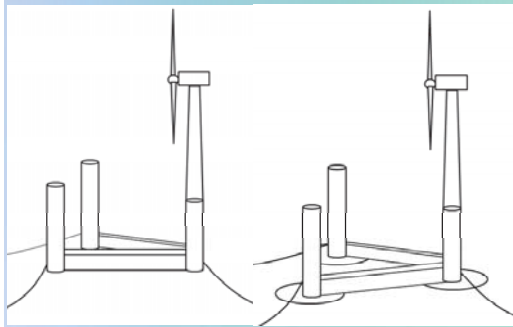
Keyword

Offshore wind; Floating foundation; Heave plate; wave-wind induced

Motion Responses



Concept of Two Platforms



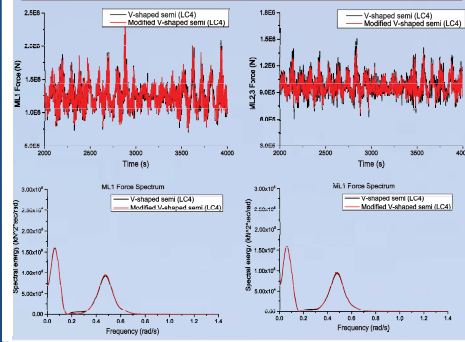
Theory

Hydrodynamic loads are calculated by Linear potential theory method;
 Mooring line forces are calculated by lumped mass method;
 Aerodynamic loads are calculated by force-speed curve;
 Heave plate is modeled as panel element, a viscous damping equal to 8% of the critical damping in heave motion is added to simulate the damping effect of heave plate.

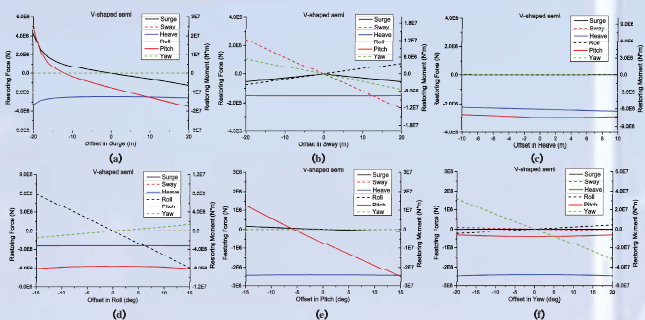
Examined Load Cases

Load cases	U_w (m/s)	H_w (m)	T_p (s)	Notes
LC1 (wave only)		3	10	Irregular wave
LC2 (wind+wave)	11.4	5	12	Constant wind, Irregular wave
LC3 (wind+wave)	17	5	12	Constant wind, Irregular wave
LC4 (wind+wave)	49	14.1	13.3	Constant wind, Irregular wave

Mooring Responses



Restoring Force vs Displacement



When the platform have a surge displacement, the mooring restoring load exerting on the platform increases quickly in V-shaped semi as shown above. Due to the asymmetry characteristic in pitch direction, the pitch-pitch stiffness of the V-shaped semi is not symmetry with respect to positive and negative pitch displacements. In addition, due to the asymmetry of the V-shaped semi, its platform displacement in heave and roll lead to pitch restoring as well. This shows the motion coupling between those modes.

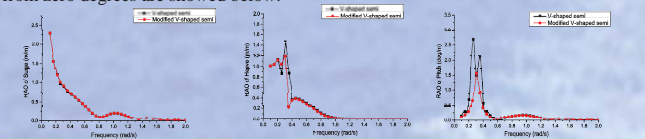
Conclusions

In this paper, the dynamic responses of motion and mooring line loads for modified V-shaped semi and V-shaped semi FOWT under wave-wind induced loads are simulated. Based on the numerical results, we obtain the following conclusions:

1. Modified V-shaped semi shows better motion performance than V-shaped semi. It is found that the two platforms perform quite well during several wind and wave load cases. The motion statistics are quite acceptable with consideration of the chosen significant wave height. Modified V-shaped semi shows better performance than V-shaped semi. For instance, compared with V-shaped semi, the Heave motion ranges of Modified V-shaped semi are reduced by 20%, while the pitch motion ranges are reduced by 46% under extreme wind-wave induced condition.
2. The mooring performance of modified V-shaped semi is slightly better than V-shaped semi. The standard deviation value of ML 2 and ML 3 force are reduced by 18% under LC 4, which means less fatigue load to reduce the chance of break in mooring line. And it also can be concluded that the spectra of mooring line force is not only affected by surge motion but also pitch motion.
3. Due to the asymmetry of the V-shaped semi, its platform displacement in heave and roll lead to pitch restoring as well. This shows the motion coupling between heave, roll and pitch motion. That is the main reason why the pitch motion can be minimized when the heave plate are attached to semisubmersible platform's column base.
4. In the future, the short-term fatigue life of mooring lines should be considered for that it is directly related to costs. And the fully coupled analysis should also be conducted to consider the effect of turbulence wind and aerodynamic load.

RAO of two Platforms

For a linear system, when a periodical excitation of a certain frequency is given, for instance, under a regular condition, the response would also be periodical with the same frequency. Normally, this is how the response amplitude operators (RAOs) are defined and calculated, which generally represent the system's natural attributes versus the wave frequency. The calculation is made by AQWA-line with a series of regular waves ranging from 0.1 rad/s to 2rad/s, which is set as 0.05 rad/s, 0.1 rad/s, 0.15 rad/s...2 rad/s. The calculation is carried out in free floating state by frequency domain analysis. The RAO of motions in Surge, Heave and Pitch motions for the waves from zero degrees are showed below:



Reference

- [1] Zhang L, Shi W, Karimirad M, Ning D. *Proc. of the 17th (2018) ISOPE Pacific/Asia Offshore Mechanics Symposium*(Jeju)
- [2] Shi W, Tan X, Gao Z and Moan, T 2016 *J. Cold Regions Science & Technology* **123** 121-139
- [3] Karimirad M and Michailides C 2016 *J. of Renewable and Sustainable Energy* **8** 89-144
- [4] Jiang Z and Karimirad M and Moan T 2013 *J. of Offshore and Polar Engineering (IJOPE)* **23** 120-128



Cyprus University of Technology



A tool to simulate decommissioning offshore wind farms

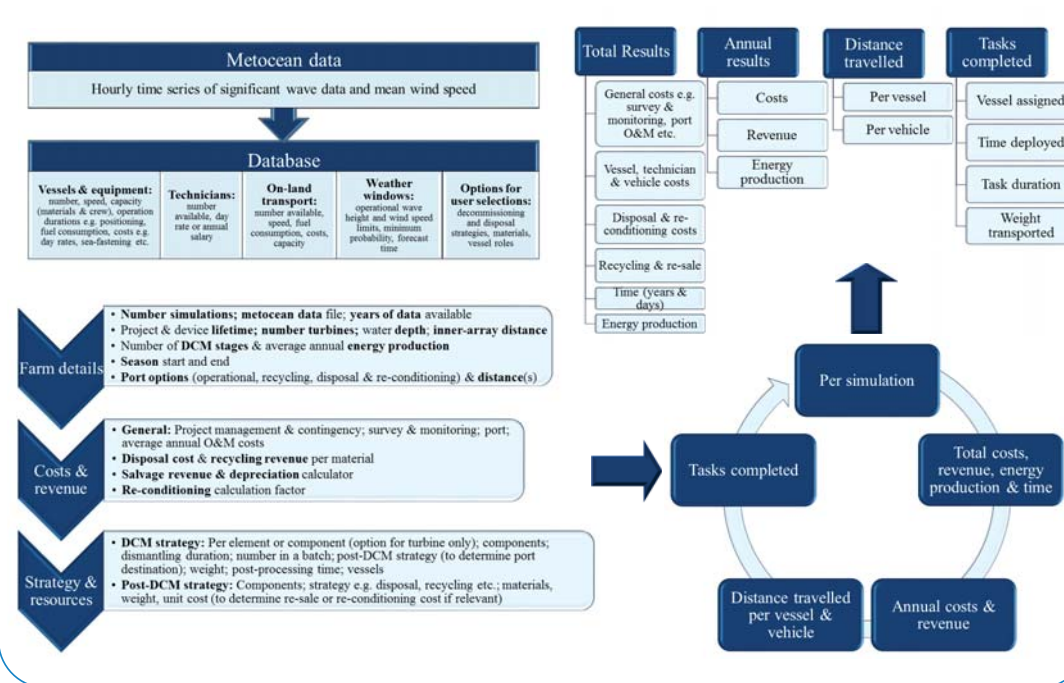
Fiona Devoy McAuliffe^{1*}, C Desmond¹, R Chester¹, B Flannery¹, F Judge¹, K Lynch¹, J Murphy¹
¹MaREI Centre, ERI, University College Cork, Ireland *f.devoy@ucc.ie

Background & Objectives

Decommissioning is an emerging practice for the offshore wind industry. Due to the lack of reliable data or experience, existing decommissioning plans are high-level estimates of the expected strategy, time required and costs. However, if underestimated, decommissioning may result in significant and unexpected outgoings at the end of a farm lifecycle. Simulation is an effective way to test a plan is both executable and cost-effective, as well as optimising activities for an individual site. Therefore, a stochastic tool was developed to simulate a wide range of decommissioning methods, using the Monte Carlo method to consider the impact of uncertain factors such as weather and costs on time and expenditure. The LEANWIND DCM model is the first detailed simulation model developed for this crucial project phase. This paper

- Describes the scope of the model (Figure 1);
- Documents a case-study to validate outputs (Figure 2);
- Demonstrates the model's capabilities through extensive sensitivity analysis (Figures 3-5).

Scope & methodology — Figure 1 Decommissioning model



Case-study

- North Sea (UK) site
- 100 × 8MW turbines & monopile foundations
- 40km from shore
- 2 jack-up vessels and 2 barge & tugs
- 72 technicians
- 10 on-land vehicles
- 1000 simulations

Table 1 — Recoverable materials: [1-7]

Component	Materials	Weight	Disposal strategy
Total rotor mass		195t	
Hub casing	nodular cast iron	90t	Recycling
Blades (3)	carbon fibre	105t	Disposal
Total nacelle mass		285t	
Gearbox		114t	Re-sale
Generator	65% steel 35% copper	114t	Recycling
Main shaft & bearings	Steel components	11.4t	Recycling
Transformer & power converter		2.28t	Re-sale
Housing	fiberglass	43.32t	Disposal
Tower		558t	
Tubular steel		558t	Recycling
Monopile		900t	
Hollow steel		900t	Recycling
Transition piece		300t	
Tubular steel		300t	Recycling

Key Findings

- The model was validated against existing cost (Figure 2) and time estimates. Sensitivity analysis confirmed the tool is working as expected.
- Analysis also demonstrates how the model can identify general trends, potential time/cost savings and areas for further optimisation.
- To summarise a selection of key findings:
 - DCM took less time with more resources (vessels and technicians) and vice versa, but more in-depth analysis could examine the optimal number of vessels and technicians considering the trade-off between time and cost-effectiveness. (Figure 3)
 - Increasing operational weather limits = increased accessibility, reducing time and costs. However, this did not consider the added cost of vessels with improved capabilities. Further research could find the ideal balance within fleet in terms of vessel capabilities and cost. (Figure 4)
 - The greater the distance from shore, the fewer Weather Windows available for feeder vessels to transit to and from site, highlighting whether this strategy is effective. Further study indicates that while they saved time, the additional cost of feeder vessels could negate the benefit. (Figure 5)
 - A number of studies indicate the importance of ensuring strategies are optimised for a given farm scenario and site conditions e.g. a strategy may suit OWFs close to shore with benign weather conditions, but the optimal scenario may change further offshore in more extreme conditions.

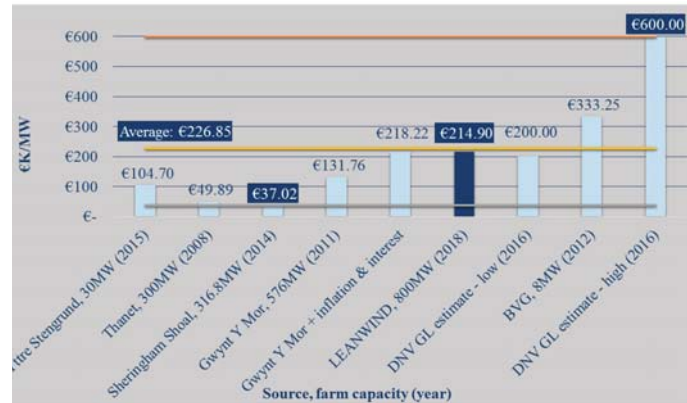


Figure 2 DCM cost comparison [3, 8-12]

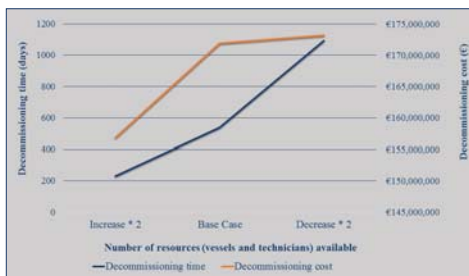


Figure 3 Number of vessels & technicians

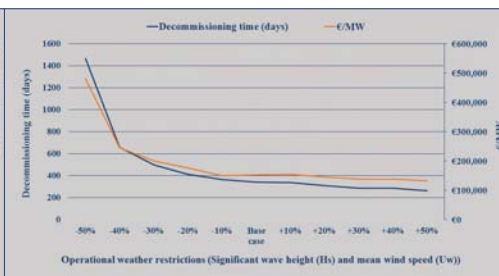


Figure 4 Weather restrictions (Hs & Uw)

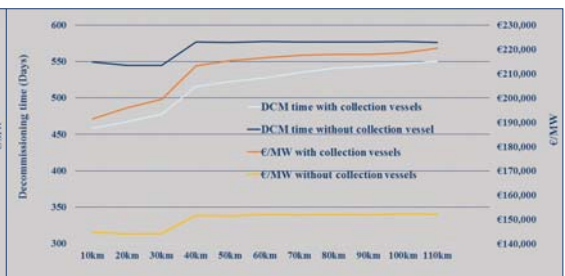


Figure 5 Distance from shore - with and without feeder vessels

[1] Larsen K 2018 *Recycling wind - Materials Today* (<https://www.materialstoday.com/composite-applications/features/recycling/>)
 [2] Desmond C, Murphy J, Blonk L, and Haans W 2016 Description of an 8 MW reference wind turbine *J. Phys. Conf. Ser.* 753 p. [8]
 [3] Drew J 2011 *Decommissioning strategy: Gwynn Mór Offshore Wind Farm LTD*
 [4] Greater Gabbard Offshore Winds Ltd. 2007 *Decommissioning Programme - Greater Gabbard Offshore Wind Farm Project*
 [5] Bak C, Zahle F, Bitsche R, and Kim T 2013 *The DTU 10-MW reference wind turbine* (Technical University of Denmark).
 [6] Ancona D and McVeigh J 2001 *Wind turbine-materials and manufacturing fact sheet* (<http://citeseerx.ist.psu.edu/viewdoc/download?doi=10.1.1.464.5842&rep=rep1&type=pdf>).
 [7] Energinet.dk 2015 *Technical Project Description for Offshore Wind Farms (200 MW)* (https://naturstyrelsen.dk/media/162607/offshore-technical-project-description_generic_april-2015.pdf)
 [8] Topham E and McMillan D 2017 Sustainable decommissioning of an offshore wind farm, *Renewable Energy* 102 pp 470-480
 [9] Lincs Wind Farm Limited 2010 *LINCS Offshore Wind Farm Decommissioning Plan*
 [10] BVG Associates May and June 2012 *Offshore wind cost reduction pathways - Technology work stream*
 [11] News from Vattenfall 2015 *Without a trace* (<http://news.vattenfall.com/en/article/without-trace>)
 [12] Chamberlain K 2016 *Offshore Operators Act on Early Decommissioning* <http://newenergyupdate.com/wind-energy-update/offshore-operators-act-early-decommissioning-data-limit-costs>; New Energy Update



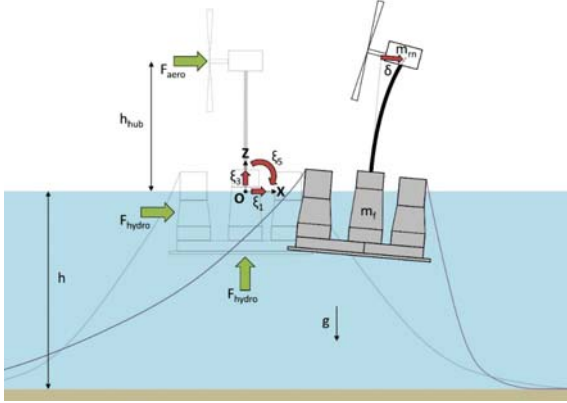
This project has received funding from the European Union's Seventh Programme for research, technological development and demonstration under grant agreement No. 614020



Performance study of the QuLAF model

Freddy J. Madsen (fjma@dtu.dk), Antonio Pegalajar-Jurado and Henrik Bredmose
 DTU Wind Energy, Nils Koppels Allé, Building 403, DK-2800 Kgs. Lyngby, Denmark

Integrated analysis at ~2000 x real time



QuLAF [1] is a floater pre-design tool based on linearized equations of planar motion, precomputed rotor loads, parameterized aerodynamic damping and WAMIT output for the floater motion.

Present study:

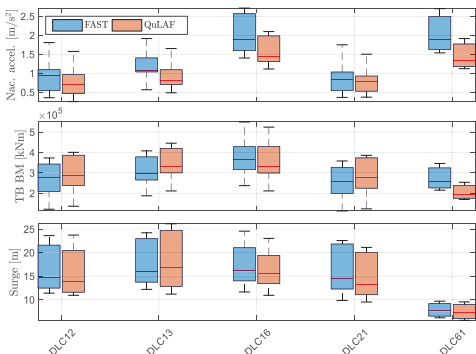
- DTU 10MW Reference Wind Turbine on the LIFES50+ OO-Star Wind Floater Semi 10MW platform [2].
- 2 x 480 load cases (DLC 1.2, 1.3, 1.6, 2.1, 6.1): The state-of-the-art FAST model [3] and the simplified model QuLAF.

Two questions addressed:

- How accurate results can be obtained from simplified models for different load cases?
- In what load cases is it sufficient to apply the simplified models?

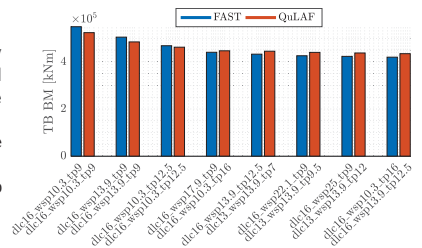
Main results in Ultimate Limit State

- The ultimate nacelle accelerations are governed by the extreme sea states (DLC1.6 and DLC6.1), with an under-prediction of the values in QuLAF.
- The ultimate tower base bending moments are obtained in DLC1.6 and both models agree very well.
- The largest surge motions are obtained in DLC1.3 with a slight over-prediction in QuLAF.

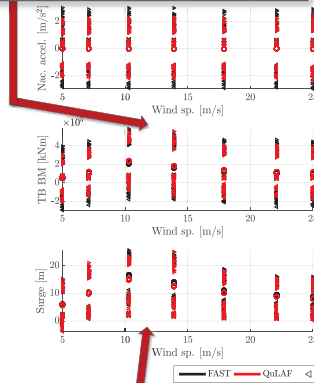


Detailed results of DLC 1.6

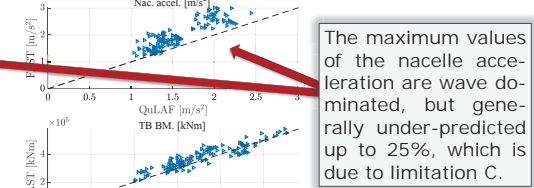
- QuLAF has been found to be a fairly accurate load and response prediction tool for aligned wind-wave load cases, despite the model limitations.
- Comparing the maximum values of the tower-base bending moment across all design load cases, QuLAF has also found to generally predict the same ranking of cases.



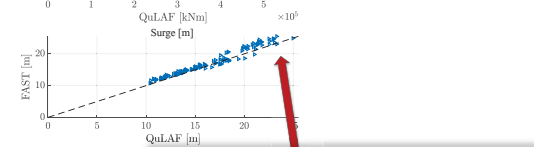
The largest tower-base bending moments are obtained around rated conditions and are matched very well by QuLAF.



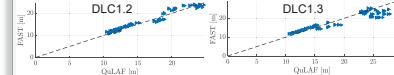
The largest surge response is obtained around rated conditions and a slight under-prediction in QuLAF, due to a combination of limitation A and B



The maximum values of the nacelle acceleration are wave dominated, but generally under-predicted up to 25%, which is due to limitation C.



Surge motion: Larger waves (DLC1.6) lead to an under-prediction in QuLAF. Extreme wind (DLC1.3) lower, leads to an over-prediction due to limitation B.



Limitations

Approximations have been made to allow for the linearization and fast solution in the frequency domain. Three limitations have been identified from the results and from [1]:

- Under-prediction of hydrodynamic loads in severe sea states due to the omission of viscous drag forcing
- Difficulty to capture the complexity of aerodynamic loads around rated wind speed, where the controller switches between the partial- and full-load regions
- Errors in the estimation of the tower response due to under-prediction of the coupled tower natural frequency and over-prediction of the aerodynamic damping.

Perspectives

QuLAF can be used as a fairly accurate load and response prediction tool for aligned wind-wave load cases. After the necessary pre-computations, it runs about 1300-2700 times faster than real time.

QuLAF can thus be used to speed up pre-design of floaters where many designs are evaluated and where early decisions on feasibility and cost are taken.

Further details on the simulation setup, the results and the model availability can be found in [4].

Literature cited

- [1] Pegalajar Jurado, A., Borg, M., & Bredmose, H. (2018). "An efficient frequency-domain model for quick load analysis of floating offshore wind turbines", *Wind Energy Science*, 3(2), 693-712. DOI: 10.5194/wes-3-693-2018
- [2] W. Yu, K. Müller and F. Lemmer, "LIFES50+ D4.2: Public definition of the two LIFES50+ 10MW floater concepts," University of Stuttgart, 2018
- [3] Pegalajar-Jurado et al., 2018. "State-of-the-art model for the LIFES50+ OO-Star Wind Floater Semi 10MW floating wind turbine", *Journal of Physics: Conference Series*. **1104** 012024.
- [4] Madsen et al., 2019. "Performance study for a simplified model of a floating wind turbine across various load cases", *Journal of Physics: Conference Series*. Unpublished.

Acknowledgments

This work is part of the project LIFES50+. The research leading to these results has received funding from the European Union Horizon2020 programme under the agreement H2020-LCE-2014-1-640741.



Simulation Methods for Floating Offshore Wind Turbine Farms with Shared Moorings

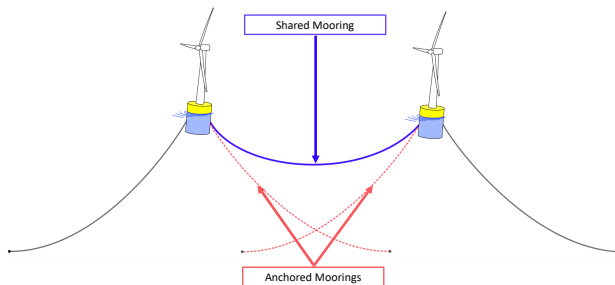
Patrick Connolly*, Matthew Hall
Faculty of Sustainable Design Engineering
University of Prince Edward Island, Charlottetown, PEI, Canada
*paconnolly@upepei.ca

January 16-19 2019
Trondheim, Norway

Shared Moorings

One of the largest challenges to the development floating offshore wind turbines (FOWTs) is their capital cost [1]. For this reason, cost reduction is a research area which deserves particular interest. The concept of shared moorings (pictured right) seeks to reduce cost of a FOWT farm by reducing the total material cost of mooring lines and anchors used. It has been shown that cost savings are possible in pilot-scale farms that incorporate shared moorings [2].

Despite representing cost benefits, using shared mooring lines also complicates the dynamics of the FOWT farm. Each shared mooring line in a farm serves as a coupling link between two FOWTs and the effect of using many shared moorings is to couple many degrees of freedom (DOFs) of the complete FOWT farm.



Research Objectives

To better understand how the use of shared moorings may impact FOWT farms, the following research objectives have been identified:

- Develop methods of analyzing the dynamics of FOWT farms with shared moorings
- Verify the results of these methods in the limiting case of a single FOWT
- Incorporate these methods in an optimization scheme with the main objective of minimizing total farm cost

The end goal of this research is to create a tool to determine cost optimal FOWT farm designs that use shared moorings, for a given set of inputs defining the site characteristics. The optimization routine will make use of the analysis methods described here.

Methodology

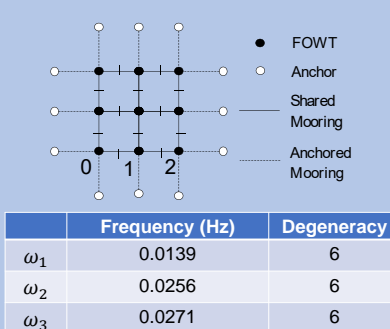
Eigenvalue Analysis:

For preliminary estimates of the natural frequencies of FOWT farms with shared moorings, an eigen-analysis method was developed. This method calculates natural frequencies from a linearized equation of motion for the farm:

$$[M + m_a(\omega_n)]\{\ddot{x}\} + [K]\{x\} = 0$$

Here the matrix $[M + M_a(\omega_n)]$ represents the combined mass and added mass matrix and $[K]$ represents the linearized stiffness matrix. By determining the eigenvalues of the above system of equations the natural frequencies (ω_n) are also determined. This method is limited to degrees of freedom in surge and sway, but includes the degrees of freedom for many FOWTs. This method also makes the assumption of linear mooring lines and zero damping.

Results: Farm Scale



Verification: Single Turbine

All 3 methods are compared in the case of a single-turbine. Specifications were used for the DeepCWind semi-submersible, and results of the methods were compared against results of the OC4 Phase II meta-analysis [3].

The natural frequency in surge calculated by the eigen-analysis method used here was:

$$\omega = 0.00902 \text{ Hz}$$

Which falls in the range of natural frequencies calculated by other independently developed method for the OC4:

$$\omega_1 = [0.00858, 0.0114] \text{ Hz}$$

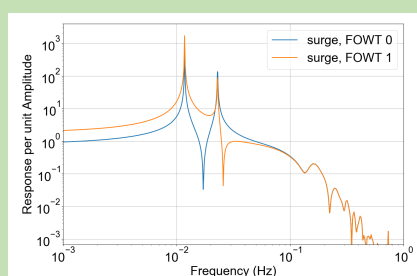
Frequency Domain:

A frequency-domain method was developed to determine response amplitude operators (RAOs) for FOWT farms with shared moorings. The RAO is determined using frequency-dependent added-mass (m_a) and damping coefficients (B) as well as linear mooring stiffnesses (K):

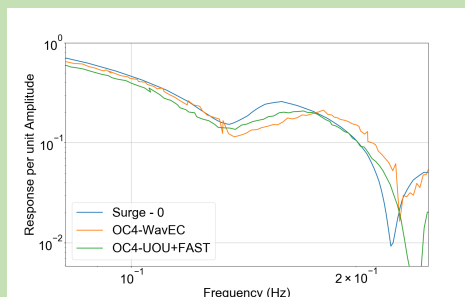
$$F_{ex}(\omega) = [-\omega^2(M + m_a(\omega)) + i\omega B(\omega) + K]q(\omega)$$

This method assumes that the platform response (q) in any degree of freedom is harmonic, and therefore would ignore any transient behavior. Determining the RAO is useful since it allows for comparison of platform response independent of environmental factors such as the sea state.

RAO for a 3-by-3 square grid farm layout



Surge RAO verification against OC4 Phase II Results [3]



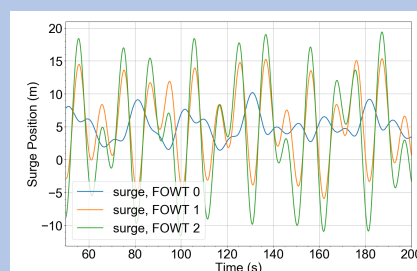
Time Domain:

A time-domain method is useful because it is higher fidelity and can generate time-series results for platform motions and line tensions. This leads to results which are. In general, a time-domain method uses an equation of motion which integrates all forces acting on each FOWT in a farm through time:

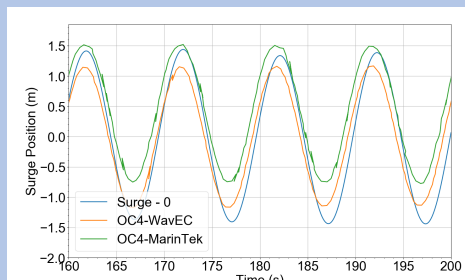
$$F_{Platform} = F_{Wind} + F_{Lines} + F_{Hydro}$$

The method used here uses an actuator disc method to determine wind thrust force, a quasi-static model for mooring forces, and a time-domain representation of linear hydrodynamics to determine hydrodynamic forces. From integrating the forces, a time-series for the position of each platform can be determined. Also of importance for shared mooring concepts is the time-series of the tension in the mooring lines.

Surge position time-series for a 3-by-3 square grid farm layout



Regular wave surge time-series verification against OC4 Phase II Results [3]



Method Improvements

The results from the developed methods do not yet adequately match published results for the DeepCWind semi-submersible. More tweaking and debugging will be done with the methods to achieve better agreement. As well, there may be significant second-order wave forcing near the natural frequencies of the FOWT farm system [4]. These frequencies are very low (<0.1 Hz) and so difference-frequency terms may be important to add to one or more of the analyses.

Optimization

Once fully developed and verified, these methods will be used in an optimization scheme. The parameter space of the optimization will include parameters defining the layout and properties of the mooring system. The main objective function will be a cost function, and constraints will be made on the dynamics of each farm. The analysis methods developed will ensure that all trial configurations are dynamically feasible.

References

- [1] T. Stehly, D. Heimiller, and G. Scott, "2016 Cost of Wind Energy Review," National Renewable Energy Laboratory, Technical Report TP-6A20-70363, Dec. 2017.
- [2] P. Connolly and M. Hall, "Comparison of pilot-scale floating offshore wind farms with shared moorings," *Ocean Engineering*, vol. 171, pp. 172–180, Jan. 2019.
- [3] A. Robertson *et al.*, "Offshore Code Comparison Collaboration Continuation Within IEA Wind Task 30: Phase II Results Regarding a Floating Semisubmersible Wind System," in *Proceedings of the 33rd International Conference on Ocean, Offshore and Arctic Engineering*, San Francisco, California, USA, 2014, p. V09BT09A012.
- [4] S. Gueydon, T. Duarte, and J. Jonkman, "Comparison of Second-Order Loads on a Semisubmersible Floating Wind Turbine," p. V09AT09A024, Jun. 2014.



North Sea met-ocean data analysis using copula for lumping of offshore wind turbine fatigue load cases

Alahyar Koochekali, Michael Muskulus

Norwegian University of Science and Technology, Trondheim, Norway

Introduction

This research was done because

- Joint measurements of wind and wave data are not available everywhere at the North Sea
- Cost-efficient design of offshore wind turbines for fatigue damage needs joint met-ocean data
- Planning of marine installation and maintenance-operation needs joint met-ocean data

This research used:

- Copula that isolates the marginal properties from the dependence structure of random variables
- Copula + Marginal = Generating joint distribution
- Lumping to reduce a full-sea-state to some load cases by weighting wind and wave data

This research was done by:

- Collecting long-term joint wind and wave data at four different locations at the North Sea
- Calculating empirical copula and empirical marginal at all location
- Combining copula at one location with wave height marginal at another location
- Using the generated joint distribution to lump wind speed
- Comparing the generated lumped wind speed with real data lumped wind speed
- Comparing the fatigue damage caused by lumped wind speed and real lumped wind speed

Applied theory

(H_s, W_s)	Wave height and wind speed	Pairs of two stochastic random variable measured jointly between 16 to 24 years 4 station at North Sea
$U =$	(1) $F_{H_s}(h_s) = P(H_s \leq h_s)$	Empirical Cumulative Distribution function of H_s (marginal)
$V =$	(2) $F_{W_s}(w_s) = P(W_s < w_s)$	Empirical Cumulative Distribution function of W_s (marginal)
$F_{H,W} =$	(3) $C(F_{H_s}(h_s), F_{W_s}(w_s)) = P[F_{W_s}(w_s) \leq u \cap F_{H_s}(h_s) \leq v]$	Joint cumulative distribution C is copula which is a function of only marginal
$C_n(u, v) =$	(4) $\frac{1}{n} \sum_{i=1}^n 1(\frac{R_i}{n+1} \leq u, \frac{S_i}{n+1} \leq v)$	Empirical copula; R is the Rank of Wave height; S is the rank of Wind speed; n is the number of measurements

Lumping method: Preservation of wave height distribution and lumping wind speed

$W_{s,i} =$	(5) $\frac{\sum_{j=1}^n P_{i,j} W_{s,j}}{\sum_{j=1}^n P_{i,j}}$	Lumped wind speed; P is the probability of occurrence; i, j are scatter diagram cell number
-------------	---	---

Fatigue damage can be simply estimated using the relation based on quasi static response

D	(6) $D \propto \Delta \sigma \propto H_s^\mu$ (7) $D \propto \Delta \sigma^\mu \propto W_s^\mu$	D is fatigue damage; $\Delta \sigma$ is the stress range, T_z is the wave period; μ is the S-N curve slope
---	--	--

Data gathering and analysis



Figure 1. Data set locations

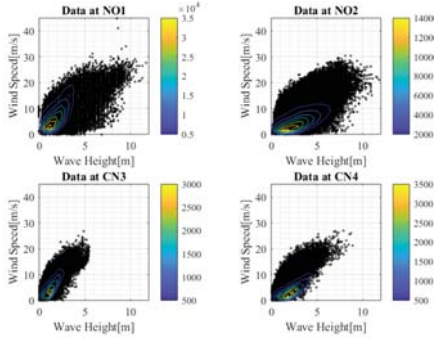


Figure 2. Scatter plot of long-term measurements at different stations

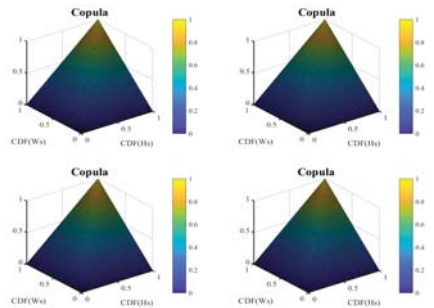


Figure 3. Copula at different stations

Method

- Copula domain, $[0,1]^2$ is a 100×100 mesh grid

$$c_{i,j}(U, V) = \frac{dC}{dUdV} = \frac{C_{i+1,j+1} - C_{i+1,j} - C_{i,j+1} + C_{i,j}}{dU \cdot dV} = f(X, Y)$$

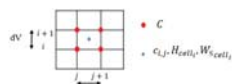


Figure 4. Numerical Stencil of copula mesh grid, $dU=dV=0.01$

- While Copula is calculated at the nodes copula density and wave height and wind speed are calculated in the centre of each cell.

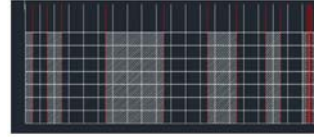


Figure 5. Import marginal to copula domain

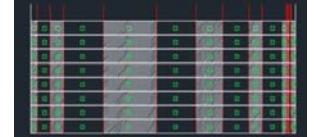


Figure 6. Average bins based on copula density

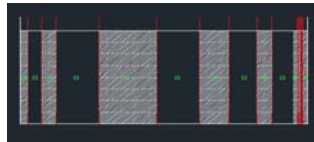


Figure 7. Lumping bin data

- White lines represent copula mesh grid
- Red lines are imported wave height bins transformed to $[0,1]$ domain using $CDF(H_s)$.
- Copula density of bin is summation of copula density of cells inside each bin.
- Wind speed is lumped using formula in applied theory where $P_{i,j}$ equals to $c_{i,j}$ in each row of copula mesh grid.

Results

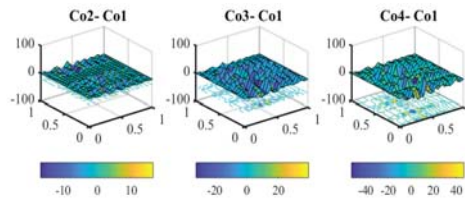


Figure 8. Copula difference

- Copula that is calculated at No1 is subtracted from the copula at other locations.
- the average copula difference is less than 15%.

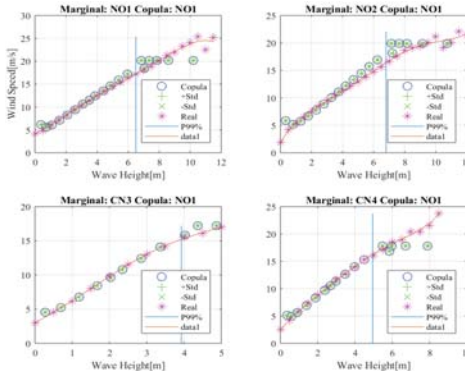


Figure 9. Copula generated lumped data versus real lumped data

- Generating lumped met-ocean data at different sites using copula calculated at NO1.
- Comparing lumped real data with lumped generated data.
- The difference between stars and circles show how well copula at NO1 can predict the joint behaviour in other locations in the North Sea.

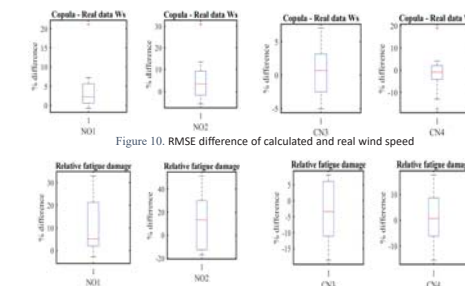


Figure 10. RMSE difference of calculated and real wind speed

- The blue line represents the upper tale of copula density domain and calculation of extreme values with $P > 99\%$ is not accurate

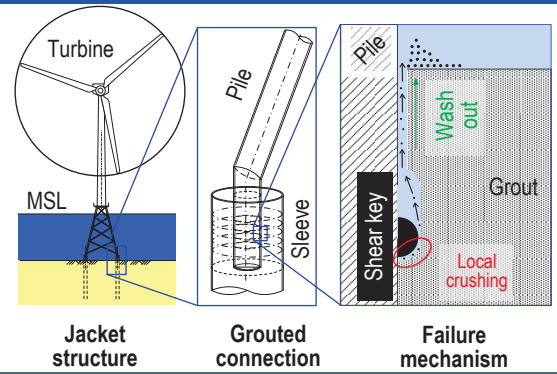
Conclusion and further research

- This research examines effectiveness of combining bivariate Copula of W_s and H_s at one location in the North Sea with wave height at other location to generate lumped wind speed
- Copula difference at stations close to each other shows an average difference of less than 10%. An increase in the distance of measurement locations show that the average copula difference is increased up to 15%.
- The average difference of real lumped data from copula generated lumped data is less than 5% which suggests lumped data are predictable using Copula.
- The average difference of fatigue damage by real lumped W_s from copula generated lumped W_s is less than 12%.
- The similarity of copula at different locations around the North Sea suggests that joint behaviour of wind speed and wave height in the North Sea is predictable using a same copula. Therefore, it is recommended to find a family of analytical copula that fits the joint behaviour of wind speed and wave height at the North Sea.



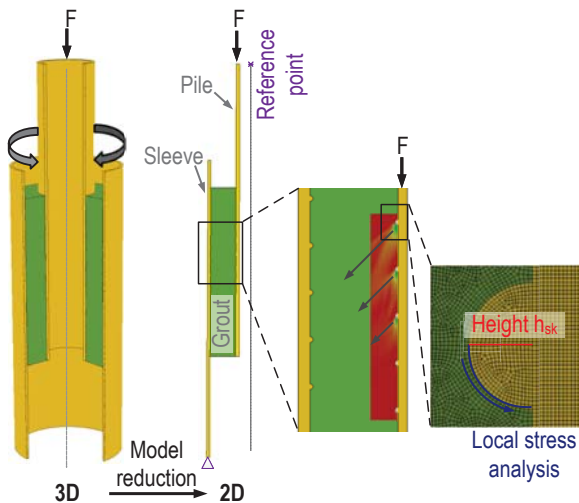
Motivation

Jacket support structures are fixed by grouted connections, a tube-in-tube hybrid connection, to the foundation piles. Current guidelines (e.g. DNV-GL and ISO 19902) base on experimental data of grouted connections tested in dry ambient conditions. However grouted connections of jacket support structures are completely covered with water. Raba investigated the influence of axially loaded grouted connections under submerged ambient conditions [1]. These connections show significantly less fatigue resistance compared to grouted connections tested in dry ambient conditions. As ingressing water washes out locally crushed grout material, which lead to a continuous vertical displacement and failure over time. With a change in failure mechanism of grouted connections in submerged ambient conditions current design concepts should be adjusted or changed.



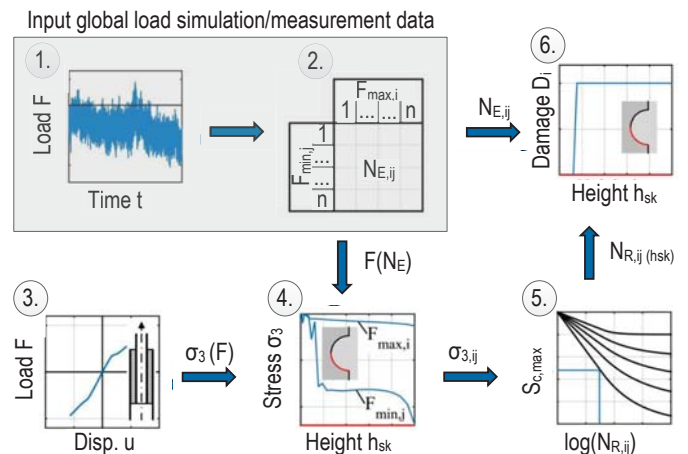
Numerical model

- Discrete depiction of shear keys
- Rotational symmetric elements (reduction from 3D to 2D)
- Fine mesh (mesh independent local stress analysis)
- Displacement controlled loading by reference point
- Contact interaction (hard contact and penalty method in tangential direction $\mu=0.4$)



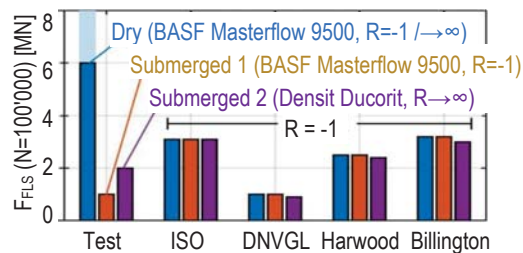
Design concept

1. Global load simulation or measurement data (loading of grouted connection)
2. Markov matrix
3. FEM simulation of grouted connection
4. Extraction of principle stresses σ_3 in grout material close to shear keys
5. S-N-curve according ModelCode 2010
6. Accumulated fatigue damage according Palmgren Miner

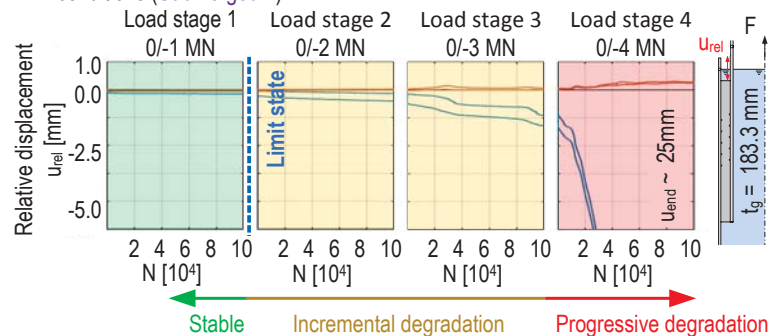


Experimental results and comparison of design concepts

- Fatigue resistance of tested grouted connections significantly reduced (Dry and Submerged 1)
- Current design concepts (excluding DNVGL) over estimate tested grouted connections' fatigue resistance for axial loading under submerged ambient conditions
- Further tests needed for statistical coverage of results



- **Limit state:** local crushing of grout material [2]
- Experimental test with cyclic axial compression loading under submerged ambient conditions (Submerged 2)



Acknowledgment

Research work has been carried out within the project "Überwiegend axial wechselbeanspruchte Grout-Verbindungen in Tragstrukturen von Offshore-Windenergieanlagen (GROWup)", financially supported by the Federal Ministry for Economic Affairs and Energy, Germany.

References

- [1] Raba A.: Fatigue behaviour of submerged axially loaded grouted connections. Dissertation. Leibniz Universität Hannover. 2018
- [2] Schaumann, P. et al.: Axially loaded grouted connections in offshore conditions using ordinary portland cement, 12th International Conference on Advances in Steel-Concrete Composite Structures (ASCCS), Valencia, 2018

Markus Lerch¹, Mikel De-Prada-Gil¹, Climent Molins²
¹ Catalonia Institute for Energy Research (IREC), ² Universitat Politècnica de Catalunya (UPC)

Introduction

Floating substructures for offshore wind turbines are a promising solution that enable to harness the abundant wind resources of deep water sites [1]. Floating offshore wind (FOW) is now reaching a pre-commercial phase where first multi-unit FOW farms are being constructed in European waters [2]. Recently, WindEurope has announced the large potential of FOW and the ability to reach a LCOE of about 40€/MWh to 60€/MWh by 2030 [3]. However, this is only achievable by significant cost reductions along the whole supply chain. The cost of the electrical system of offshore wind farms can take up to 15% to 30% of the total investment [4]. For FOW farms the costs might be even higher since new technologies and installations procedures are applied. Besides that, commercial scale FOW farms will likely include wind turbines with power ratings up to 10MW or more, which require dynamic power cables with higher voltage levels. Hence, it is desirable to optimize the cable connection layout to obtain the most cost-effective solution.

Objectives

- Develop a model to solve the problem of optimizing the electrical collection grid of a floating offshore wind farm
- Base the model on particle swarm theory (PSO) and adapt appropriately
- Increase complexity of the problem by including:
 - All wind turbine connection possibilities
 - Stochasticity of wind speed and wind direction
 - Acquisition and installation costs of dynamic power cables
 - A number of different power cable cross sections
 - Power losses in the cables
 - A comprehensive wake effect model
- Apply the model to a large floating offshore wind farm
- Study the effect of a quantity discount

Methodology

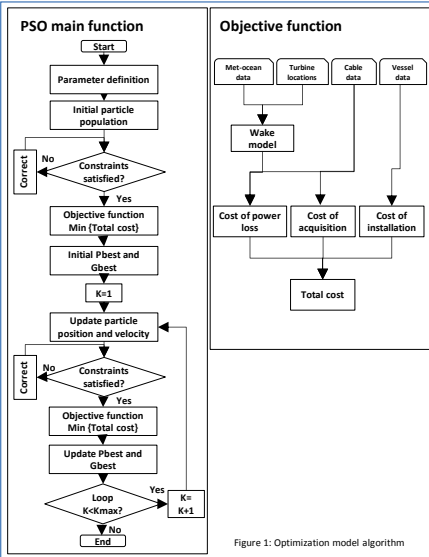


Figure 1: Optimization model algorithm

Objective function

The objective function for a single particle solution:
$$\text{Min} (C_{\text{acquisition}} + C_{\text{installation}} + C_{\text{loss}})$$

The acquisition cost takes into account:

$$C_{\text{acquisition}} = \left(\sum_1^{N_{\text{iac}}} C_{\text{iac}} * L_{\text{iac}} + \sum_1^{N_{\text{exc}}} C_{\text{exc}} * L_{\text{exc}} \right) * \left(T \frac{i(1+i)^T}{(1+i)^T - 1} \right)$$

The installation cost is obtained by:

$$C_{\text{installation}} = \left(\sum_1^{N_{\text{iac}}} L_{\text{iac}} + \sum_1^{N_{\text{exc}}} L_{\text{exc}} \right) * C_{\text{vessel}} * r_{\text{install}} \left(T \frac{i(1+i)^T}{(1+i)^T - 1} \right)$$

The cost of energy loss is calculated by:

$$C_{\text{loss}} = \sum_{v_{\text{min}}}^{v_{\text{max}}} \sum_{0^\circ}^{360^\circ} \left[\left(\sum_1^{N_{\text{iac}}} P_{\text{loss}_{\text{iac}}} + \sum_1^{N_{\text{exc}}} P_{\text{loss}_{\text{exc}}} \right) H_{\text{ws}} * H_{\text{wd}} * T \right] * C_{\text{energy}}$$

The power loss is computed as following:

$$P_{\text{loss}} = 3 \left(\frac{P_{\text{gen}} + P_{\text{trans}}}{\sqrt{3} * U} \right)^2 * R_{\text{cable}} * L_{\text{cable}}$$

with

$$P_{\text{gen}} = \frac{1}{2} * p_a * A_{\text{rotor}} * C_p(\lambda, \beta) * v_{\text{ws}}^3$$

Constraints

- The energy leaving a turbine must be supported by a single cable.
- A maximum of one cable can be placed between two turbines.
- The crossing of power cables is not allowed.
- The building of a ring connection is not permitted.
- The power transmitted by a cable cannot exceed the capacity of the installed cable.

Wake model

A comprehensive wake effect model has been included considering [5]:

- Single wake
- Partial wakes
- Multiple wakes

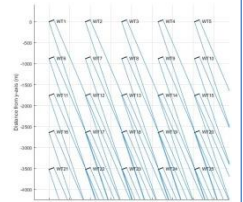


Figure 2: Wake model illustration

Application

Study case

- 500MW floating offshore wind farm
- DTU 10-MW reference wind turbine
- Golfe de Fos offshore location in France
- Reference water depth is 70m
- Collection grid operated at 66kV
- Transmission voltage is 220kV

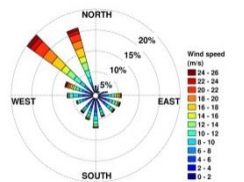


Figure 3: Wind rose

	Inter-array cables	Export cables	Total
Acquisition cost (M€)	91.92	69.09	161.01
Installation cost (M€)	19.71	8.12	27.83
Cost of energy loss (M€)	27.38	3.34	30.72
Total cost (M€)	139.01	80.55	219.56
Annual energy loss (GWh)	17.11	2086.85	19199.1
Length of cables (km)	155.73	64.20	219.93

Table 1: Cost and power losses of actual layout

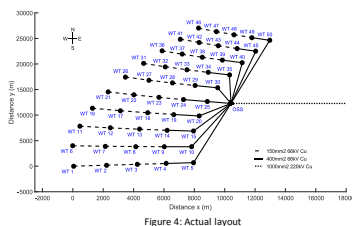


Figure 4: Actual layout

Optimized layout results

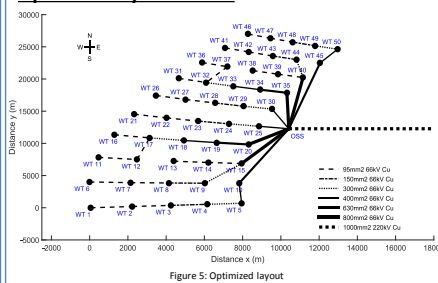


Figure 5: Optimized layout

	Acquisition cost (M€)	Installation cost (M€)	Cost of energy loss (M€)	Total cost (M€)	Annual energy loss (GWh)	Length of cables (km)
Optimized layout	86.34	18.06	25.15	129.55	15.72	142.73
Difference (%)	-6.07	-9.56	-8.15	-6.81	-8.12	-8.35

Table 2: Inter-array cable costs and losses of optimized layout

Quantity discount effect

- Discount of 15% on C_{iac}
- Use of the 2 largest cross sections only

	Cross section (mm ²)	Resistance (Ω/km)	Unit cost (€/m)	Power capacity (MW)
66kV IAC	95	0.25	220	26
	150	0.158	300	31
	300	0.078	423	44
	400	0.059	475	51
220kV EXC	630	0.037	554	62
	800	0.029	683	71

Table 3: Power cable data (without discount)

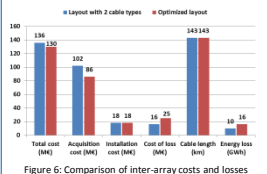


Figure 6: Comparison of inter-array costs and losses



The research leading to these results has received funding from the European Union Horizon2020 program under the agreement H2020-LCE-2014-1-640741.

For more information:
<https://lifes50plus.eu>
Contact: mlerch@irec.cat

References:

[1] Rhodi, J., & Costa Ros, M. (2015). Floating offshore wind: Market and technology review. Carbon Trust.
[2] WindEurope (2017). Floating Offshore Wind: Vision Statement.
[3] WindEurope (2018). Floating offshore wind energy. A policy blueprint for Europe.
[4] Ling-Ling, H. et al. (2012). Optimization of large-scale offshore wind farm electrical collection systems based on improved PSO.
[5] De-Prada-Gil, M. et al. (2015). Maximum wind power plant generation by reducing the wake effect. Energy Conversion and Management, 101, 73-84.

Investigating the influence of tip vortices on deflection phenomena in the near wake of a wind turbine model



Ludwig Kuhn¹, Jan Bartl², Franz Mühle³, Lars Sætran⁴



¹ Institute of Fluid Dynamics and Technical Acoustics, Technical University of Berlin, Germany
² Department of Mechanical and Marine Engineering, Western Norway University of Applied Sciences, Bergen, Norway
³ Faculty of Environmental Sciences and Natural Resource Management, Norwegian University of Life Science, Ås, Norway
⁴ Department of Energy and Process Engineering, Norwegian University of Science and Technology, Trondheim, Norway

Introduction

- Wake of wind energy turbines operating in steady yaw deflected
- Downstream turbines in wind farm may experience partial/full aerodynamic influence by wake of upstream turbines → power losses, wake induced loads (Kim et al., 2015)
- Bartl et al. (2018) investigate active yawing to increase total power output of multiple turbines
- Burton et al. (2011) describes induced velocity (normal to rotor plane) as main reason for wake deflection
- Eriksen and Krogstad (2017) implement non-yaw phase-locked measurements → equal distribution of tip vortices in the wake
- Purpose of study: investigating tip vortex interaction, determine influence on wake deflection

Measurement methods

- Measurements in closed-loop wind tunnel at NTNU (test section 11.15x2.71x1.80m)
- Inflow conditions: $u_{\infty}=10\text{ms}^{-1}$, $TI=0.23\%$
- Wind turbine model: 3-bladed rotor ($d=0.89\text{m}$, 0.94m hub height), NREL S826 airfoil, long nacelle due to optical RPM sensor and torque meter, 12.9% blockage
- Optimal TSR $\lambda=6$, $\text{RPM}=1280\text{min}^{-1}$
- Wake measured with TFI Cobra probe (4-hole Pitot tube), traversed at hub height (-0.8D to 0.8D), 13 lines (1D to 4D downstream)
- Phase-locking by coupling sampling frequency (10240Hz, oversampling ratio 4) to rotational speed
- Points measured for $t=40\text{s}$ (~850 rotor revolutions)

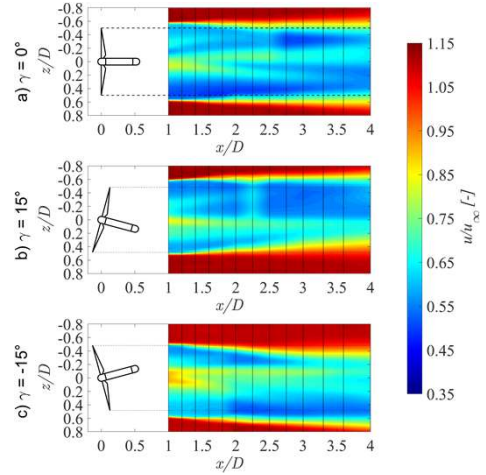


Figure 2: Interpolated normalized streamwise velocity. a) non-yaw reference case, b) positive yaw angle, c) negative yaw angle

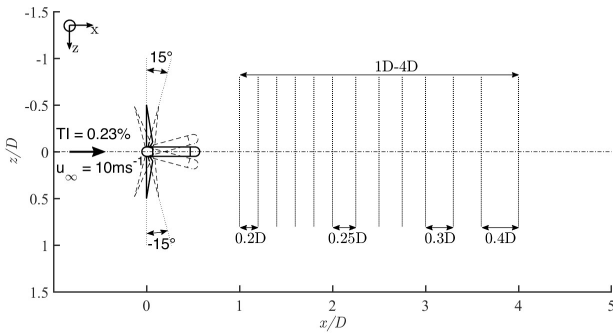


Figure 1: Measurement setup in the wind tunnel test section. Dotted lines indicate Cobra probe traversing.

Results

- Experiments successful: non-yaw reference case confirmed earlier results by Eriksen and Krogstad (2017), wake deflection is detected (Figure 2), phase-locked averaged data gives overview over position and behavior of tip vortices
- Total kinetic energy leads to conclusions about vortex core size and behavior (Figure 4)
- Patterns of vortex interaction are observed to be asymmetric with respect to yaw angle
- Earlier interaction observed for negative yaw
- Sizes of vortex cores tend to be the same for reference case, vortices shed upstream -4 times bigger than downstream ones
- Differences in size and interaction starting position directly related: outer turbulent region of big vortices connect with each other, forcing vortices to wrap around each other
- Early vortex interaction leads to earlier dissolving into less energetic turbulent structures

Conclusions

- Vortices shed on upstream side are bigger, interact earlier, dissolve faster
- Dissolving can be used to prevent heavy loads on downstream turbines
- Wake spreading on upstream side more distinct
- Actual influence on wake deflection not determined
- Further studies to investigate vortex strength, spin, wrapping process needed

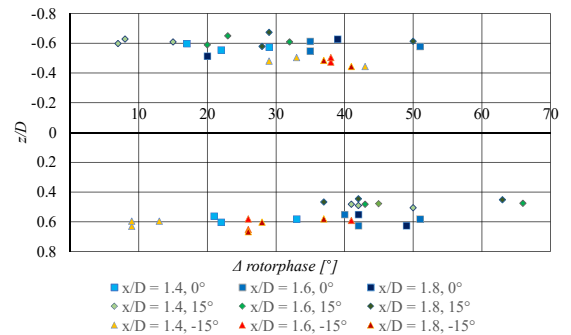


Figure 3: Vortex core sizes in degrees for three downstream positions, left and right side of the wake.

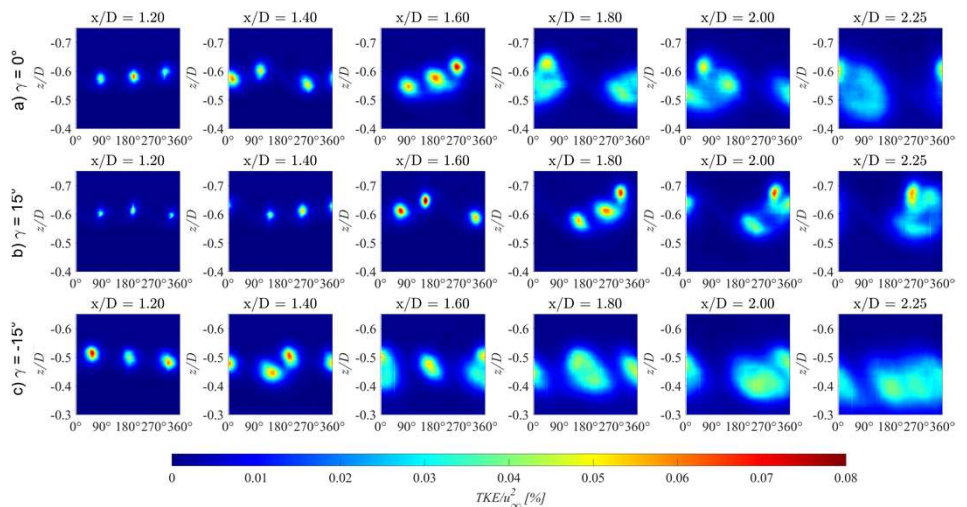


Figure 4: Normalized total kinetic energy at selected downstream positions, left side of the wake. a) non-yaw reference case, b) positive yaw angle, c) negative yaw angle

References

Bartl, J., Mühle, F., Schottler, J., Sætran, L., Peinke, J., Adaramola, M., and Hölling, M.: Wind tunnel experiments on wind turbine wakes in yaw: Effects of inflow turbulence and shear, *Wind Energy Science*, 3, 329–343, doi:10.5194/wes-3-329-2018, 2018.
 Burton, T., Jenkins, N., Sharpe, D., and Bossanyi, E.: *Wind Energy Handbook*, Second Edition, 177–203, doi:10.1002/9781119992714, 2011.
 Eriksen, P.-E. and Krogstad, P.-Å.: Development of coherent motion in the wake of a model wind turbine, *Renewable Energy*, 108, 449–460, doi:10.1016/j.renene.2017.02.031, 2017.
 Kim, S.-H., Shin, H.-K., Joo, Y.-C., and Kim, K.-H.: A study of the wake effects on the wind characteristics and fatigue loads for the wind turbines in a wind farm, *Renewable Energy*, 74, 536–543, doi:10.1016/j.renene.2014.08.054, 2015.

Implementation of potential flow hydrodynamics to time-domain analysis of flexible platforms of floating offshore wind turbines

Sho Oh¹⁾, Kimiko Ishii¹⁾, Kazuhiro Iijima²⁾, Hideyuki Suzuki³⁾

1) ClassNK, 2) Osaka University, 3) University of Tokyo

1. Introduction

In the design of supporting platforms of floating offshore wind turbines, global response analysis is essential to predict the response under various loads from wave, wind, moorings and the wind turbines. However, the literature of the global analysis of floating offshore wind turbines combining flexible modelling of the supporting platform and the potential flow theory for hydrodynamic evaluation is limited. In this study, first the framework implementing the potential flow hydrodynamics to the time-domain analysis of the three-dimensional frame model for offshore wind turbines is developed using modal decomposition for the hydrodynamic evaluations. The number of modes can be limited to those with larger contributions, which can lead to the reduction of the calculation cost. Next, a spar-type floating offshore wind turbine is modelled to verify the developed code when only the rigid mode motions are considered for hydrodynamic loadings.

2. Theoretical Backgrounds

The floating offshore wind turbine is discretized into structural beam elements with N number of nodes.

$$\{M\}_{6N,6N}\{\ddot{x}\}_{6N,1} + \{C\}_{6N,6N}\{\dot{x}\}_{6N,1} + \{K\}_{6N,6N}\{x\}_{6N,1} = \{F^{hydro} + F^{lines} + F^{buoyancy} + F^{aero}\}_{6N,1}$$

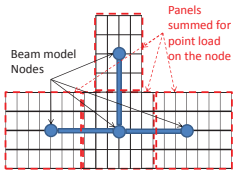
To reduced the calculation cost, it is assumed that only limited modes of the floater response contribute to hydrodynamic forces

$$\{F^{radiation}\}_{6N,1} = - \begin{bmatrix} A_{1,1}(\infty) & \dots & A_{1,M}(\infty) \\ \vdots & \ddots & \vdots \\ A_{6N,1}(\infty) & \dots & A_{6N,M}(\infty) \end{bmatrix} \begin{Bmatrix} \ddot{u}_1 \\ \vdots \\ \ddot{u}_M \end{Bmatrix} - \int_{-\infty}^t \begin{bmatrix} L_{1,1}(t-\tau) & \dots & L_{1,M}(t-\tau) \\ \vdots & \ddots & \vdots \\ L_{6N,1}(t-\tau) & \dots & L_{6N,M}(t-\tau) \end{bmatrix} \begin{Bmatrix} \dot{u}_1(\tau) \\ \vdots \\ \dot{u}_M(\tau) \end{Bmatrix} d\tau$$

$$\{u\}_{m,1} = [\phi]_{m,6N}\{x\}_{6N,1}$$

$$\{F^{radiation}\}_{6N,1} = - \begin{bmatrix} A_{1,1}(\infty) & \dots & A_{1,m}(\infty) \\ \vdots & \ddots & \vdots \\ A_{6N,1}(\infty) & \dots & A_{6N,m}(\infty) \end{bmatrix} [\phi]_{m,6N}\{\ddot{x}\}_{6N,1} - \int_{-\infty}^t \begin{bmatrix} L_{1,1}(t-\tau) & \dots & L_{1,m}(t-\tau) \\ \vdots & \ddots & \vdots \\ L_{6N,1}(t-\tau) & \dots & L_{6N,m}(t-\tau) \end{bmatrix} \begin{Bmatrix} \dot{u}_1(\tau) \\ \vdots \\ \dot{u}_m(\tau) \end{Bmatrix} d\tau$$

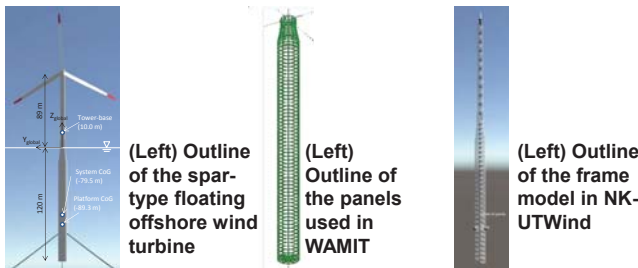
Hydrodynamic coefficients assigned to each node by summing the coefficients of the related panels



$$\omega^2 A_{i,j} = \begin{cases} \sum_{s_i} \text{Re}(p_s^r) (\phi_j \cdot n_s) ds & (n = 1,2,3) \\ \sum_{s_i} \text{Re}(p_s^r) (\phi_j \cdot n_s) \cdot r_s ds & (n = 4,5,6) \end{cases} \quad \omega^2 B_{i,j} = \begin{cases} \sum_{s_i} \text{Im}(p_s^r) (\phi_j \cdot n_s) ds & (n = 1,2,3) \\ \sum_{s_i} \text{Im}(p_s^r) (\phi_j \cdot n_s) \cdot r_s ds & (n = 4,5,6) \end{cases} \quad p_j^d = \begin{cases} \sum_{s_i} p_s^d (\phi_j \cdot n_s) ds & (n = 1,2,3) \\ \sum_{s_i} p_s^d (\phi_j \cdot n_s) \cdot r_s ds & (n = 4,5,6) \end{cases}$$

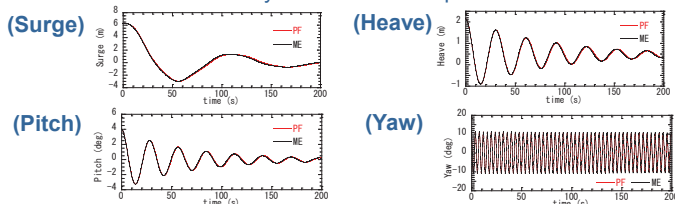
3. Numerical model for verification

The spar-type floater with the 5MW reference wind turbine used in OC3 project is used for the verification of the developed code.



Platform mass	7466.3 ton	Depth of platform base	-120 m
Platform CoG height	-89.9 m	Platform diameter below taper	9.5 m
System CoG height	-75.5 m	Platform diameter above taper	6.5 m
Platform bending stiffness	3290GNm ²	Platform roll / pitch inertia about CoG	4.23Mtonm
Platform axial stiffness	301GN		

Calculated free-decay process showed similar results for potential flow theory and Morison's equation

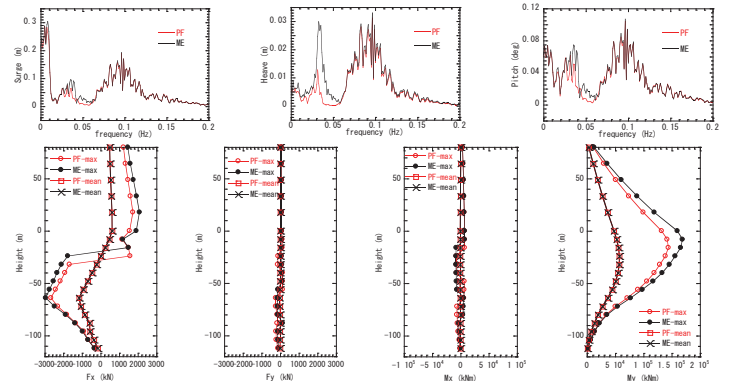


4. Results

Developed calculation framework is verified by comparing the calculated results with those calculated with Morison's equation.

	Wind	Wave	Wind Turbine
LC.3	U = 11.3 m/s, I _w = 7 % Mann model	Irregular airy JONSWAP, H _s =3.25, T _s =10 sec	Operating

Calculated results were similar for the two hydrodynamic models. The difference in the low frequency region may be attributed to the steady and low frequency external forces introduced in the Morison's equation by considering the instantaneous position of the floater.



	Potential Flow Theory (Rigid mode only)	Morison's Equation
Irregular wave without wind	179.4 min	43.95 min
Irregular wave with operational wind turbine	875.4 min	739.5 min

Validating Numerical Predictions of Floating Offshore Wind Turbine Structural Frequencies in Bladed using Measured Data from Fukushima Hamakaze

Haruki Yoshimoto, Takumi Natsume (Japan Marine United Corporation)

Junichi Sugino, Hiromu Kakuya (Hitachi, Ltd.)

Robert Harries, Armando Alexandre, Douglas McCowen (DNV GL)

1. Fukushima FORWARD

The government of Japan has started the experimental research project of **the world's first floating offshore wind farm**, which is conducted by the consortium made up of industry-academic-government organization. This project is sponsored by Ministry of Economy, Trade and Industry and named as "Fukushima FORWARD (Fukushima Floating Offshore Wind Farm Demonstration Project)".

The wind farm consists of **three floating offshore wind turbines (FOWTs)** and a **substation** floater. The wind farm's total amount of rating capacity is 14 MW.



Fig. 1. Overview of Fukushima FORWARD <http://www.fukushima-forward.jp/>

2. Fukushima Hamakaze (5MW FOWT)



Item	Value
Length	58.9 m
Breadth	51.0 m
Hub height	86.4 m
Draft	33.0 m

Fukushima Hamakaze is floating offshore wind turbine with a 5 MW horizontal axis wind turbine, has been installed at about 20 km off the coast of Fukushima Prefecture of Japan since July 2016 and is now operating.

The structure of the floating offshore wind turbine is "**Advanced Spar Type**". Advanced spar is the newly developed structure for FOWT and enables to suppress the motion of the float.

This floater was designed using commercial wind turbine modelling software "Bladed". The purpose of this paper is to **validate the structural frequencies using measured data**.

Fig. 2. Isometric view and principal particulars

4. Modelling Structural Flexibility

The submerged structure was divided into **rigid and flexible sections** and the added mass was distributed to each part. To break down **the added mass into several parts**, the boundary element method hydrodynamics was post processed using outputs of the individual panel potentials.

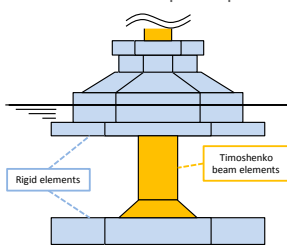


Fig. 4. Flexible structure model

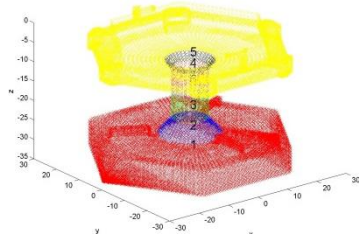


Fig. 5. Hydrodynamic model & sections

3. Method of Validation

To validate the first tower natural frequency estimation model, we investigated **several approaches to the modelling** of the floater.

Tab. 1. Investigated models

Model	Structural Flexibility	Dynamic Mooring Lines
#1 Baseline	✗	✗
#2 Flex	✓	✗
#3 Flex + DynML	✓	✓

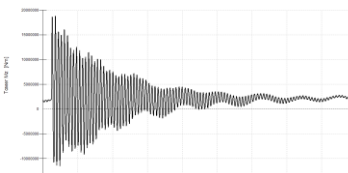


Fig. 3. Hammer test example result

The natural frequencies are extracted through counting the tower base overturning moment peaks after an external impulsive load is applied to the tower top. (like "Hammer test")

6. Result and Recommendation

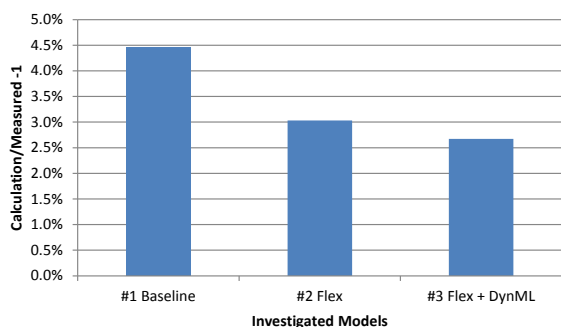


Fig. 7 Comparison result of tower natural frequencies

Each model in Tab.1 has been simulated in Bladed and the results are shown in Fig.7, the percentage difference between the calculation and measured values.

Effect of Structural Flexibility (#1 - #2)

About **1.5% improvement** in the tower frequency prediction can be seen.

Effect of Dynamic Mooring Lines (#2 - #3)

Reducing the tower natural frequency, however the differences are **very small** (0.4%).

- It is recommended to identify where significant flexibilities exist within the floater and model it appropriately for the estimation of the tower natural frequencies. (This will be platform dependent.)
- For this model, dynamic mooring lines could be safely ignored.

5. Modelling Dynamic Mooring Lines

To consider the inertia of the chain and hydrodynamic added mass, dynamic mooring lines were included in the model.

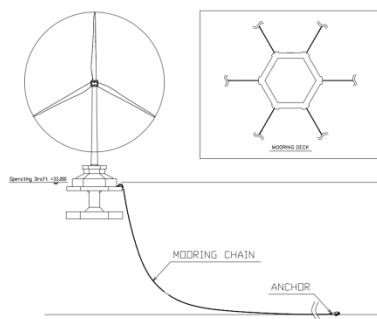


Fig. 6. Mooring arrangement

The FOWT is moored by **six chain catenary**. Nominal diameter of the chain is 132mm. The water depth at which the anchor is installed is 110 to 120 m. The upper end of the chain is connected to the submerged deck.

The lines hydrodynamic loadings are modelled as Morison model.

Prediction of dynamic response of a semi-submersible floating offshore wind turbine by using KC dependent hydrodynamic coefficients

Yuliang Liu, Takeishi Ishihara

E-mail: yuliang.liu@bridge.t.u-tokyo.ac.jp

Department of Civil Engineering, School of Engineering, The University of Tokyo



東京大学
THE UNIVERSITY OF TOKYO

Introduction

The added mass and drag coefficients are two critical parameters for accurate prediction of hydrodynamic forces on the floaters. For the dynamic response analysis of floating offshore wind turbine (FOWT), the added mass coefficient is usually calculated by using the boundary element method (BEM) and the drag coefficient is used as a constant value as mentioned in the references [1] and [2]. It implies that the effect of KC number on the hydrodynamic coefficients is neglected in the previous studies.

In this study, a model is developed to estimate global hydrodynamic coefficients for a semisubmersible FOWT from the added mass and drag coefficients for each element, considering effects of interaction of elements, KC number and wave frequency in the hydrodynamic coefficients. The proposed model is validated by the global hydrodynamic coefficients and dynamic responses obtained from the water tank tests.

Water tank tests

The motions and mooring tensions for a 2MW semisubmersible FOWT located at Fukushima offshore site are investigated by the water tank tests. The Froude scaling law is used and the scale factor is 1:50. The model is positioned by 4 catenary mooring lines of 10.3 m anchored on the bottom of water tank at a depth of 2.5 m as shown in Fig.1. The origin of coordinate locates at the centerline of center column of floater on the water surface and the reference point for the floater motions is defined at the gravity center. The global hydrodynamic coefficients are measured by the forced oscillation test using the same model

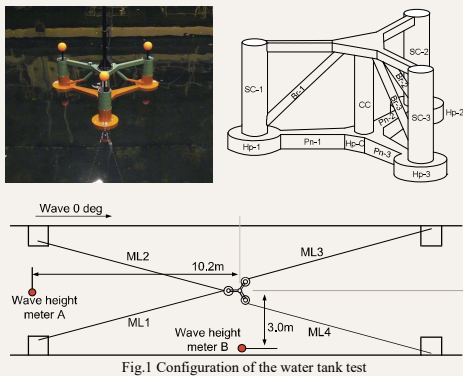


Fig.1 Configuration of the water tank test

Hydrodynamic coefficients

The hydrodynamic coefficients are different for each floater because they are affected by interaction of elements, KC number and frequency of wave. A model is proposed to calculate hydrodynamic coefficients for a semisubmersible FOWT from those for each element considering these factors.

Hydrodynamic coefficients of each element

The hydrodynamic coefficients of each element can be expressed as a function of interaction of elements (β), KC number (KC) and normalized frequency of wave (η)

$$iC_a^k(\beta, KC, \eta) = iC_a^k(KC_0, \eta_0) \times i\gamma_a^k(\beta) \times i\gamma_a^k(KC) \times i\gamma_a^k(\eta|KC)$$

$$iC_d^k(\beta, KC, \eta) = iC_d^k(KC_0, \eta_0) \times i\gamma_d^k(\beta) \times i\gamma_d^k(KC) \times i\gamma_d^k(\eta|KC)$$

where i denotes the number of element for a floater; k indicates the normal and tangential directions for an element, γ presents correction factors. $iC_a^k(KC_0, \eta_0)$ and $iC_d^k(KC_0, \eta_0)$ are the added mass and drag coefficients at a specified KC_0 and η_0 . The normalized frequency η is defined as a ratio of wave frequency to a typical wave frequency $\omega_{typical}$, which is 0.628 Hz for a typical wave period of 10s in full scale.

$$\eta = \frac{\omega_w}{\omega_{typical}}$$

The hydrodynamic coefficients of the floater shown in Fig.1 are investigated by using the horizontal and vertical forced oscillations with CFD [1] for various KC number and frequency of wave. C_a and C_d for each element at a specified KC_0 and η_0 shown in Ref. [1] are used to model C_a and C_d for different KC and η in this study.

Interaction correction factor

The interaction correction factor for each element is defined in [1] as a ratio of hydrodynamic coefficient between each element and the referenced one at KC_0 and η_0 :

$$i\gamma_a^k(\beta) = \frac{iC_a^k(KC, \eta_0)}{iC_a^k(KC_0, \eta_0)}, \quad i\gamma_d^k(\beta) = \frac{iC_d^k(KC, \eta_0)}{iC_d^k(KC_0, \eta_0)}$$

KC number correction factor

C_a and C_d for each element vary with KC number related to the amplitude of floater motion. The KC number correction factor, $i\gamma^k(KC)$, is defined as a ratio of the hydrodynamic coefficients of element to those at a specified KC_0 and η_0 . The predicted and measured C_a and C_d for a square, cylinders with different aspect ratios and a heave plate are compared as shown in Fig.2 and are used for calculation of C_a and C_d of a whole floater.

$$i\gamma_a^k(KC) = \frac{iC_a^k(KC, \eta_0)}{iC_a^k(KC_0, \eta_0)}, \quad i\gamma_d^k(KC) = \frac{iC_d^k(KC, \eta_0)}{iC_d^k(KC_0, \eta_0)}$$

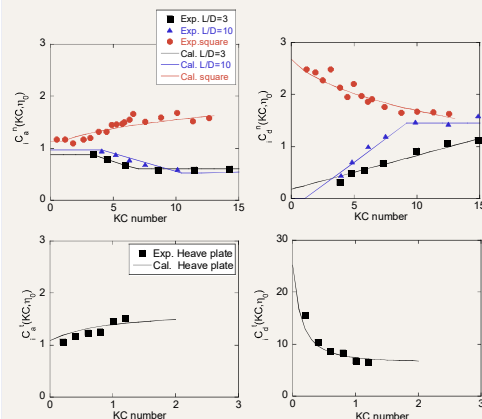


Figure.2 Variation of hydrodynamic coefficients with KC number

In Fig.2, the experimental data is fitted as function of KC number shown as solid line. Upper two figures present variation of hydrodynamic coefficients for isolated circular cylinder with different aspect ratio and square cylinder. Other two figures shows C_a and C_d of heave plates in varied KC number.

Frequency correction factor

The frequency of wave is an important factor which affects hydrodynamic coefficients and dynamic responses of floater as shown in [2]. The frequency correction factor, $i\gamma(\eta|KC)$, is introduced to account the effect of wave frequency on the hydrodynamic coefficients for each element at a KC number.

$$i\gamma_a^k(\eta|KC) = \frac{C_a^k(KC, \eta)}{C_a^k(KC, \eta_0)}, \quad i\gamma_d^k(\eta|KC) = \frac{C_d^k(KC, \eta)}{C_d^k(KC, \eta_0)}$$

It is noticed that the frequency correction factors for each component is the same as that for the whole floater as shown in [2]. This factor can also be assumed as a constant value except for the drag coefficient in the surge direction, which is expressed as a function of KC number:

$$i\gamma_a^s(\eta|KC) = 1$$

$$i\gamma_d^s(\eta|KC) = \begin{cases} 1.19 - \frac{0.6}{\pi} \tan^{-1} \left(\frac{2.7}{\eta} - 3.8 \right) & KC \leq 4.62 \\ \text{Linear Interpolation} & 4.62 < KC < 9.26 \\ 1 & KC \geq 9.26 \end{cases}$$

$$i\gamma_a^t(\eta|KC) = 1$$

$$i\gamma_d^t(\eta|KC) = 1$$

Validation

Global hydrodynamic coefficients

The formulas shown in Ref. [2] are used to calculate the global hydrodynamic coefficients from the proposed hydrodynamic coefficients for each element. Predicted global hydrodynamic coefficients by the proposed model are compared with those obtained from the forced oscillation tests. The effect of wave frequency on C_d in the surge direction is significant as shown in Fig.3.

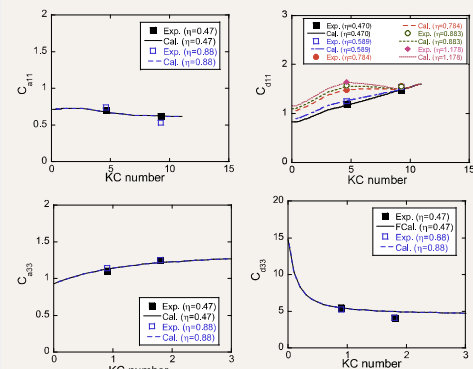


Figure.3 Variation of global hydrodynamic coefficients with KC number

Dynamic responses

The added mass and drag coefficients calculated by the proposed model as well as the diffraction force and radiation damping obtained by BEM are used to predict the dynamic responses of the floater. C_d of cylinders without consideration of KC number dependency as shown in OCA4 project is also used to investigate the effect of KC number on the dynamic responses of FOWT. From Fig. 4, the effect of KC number dependency of C_d appears at the periods near the natural period of motion in the heave direction. The predicted RAOs by the proposed model show good agreement with those from the water tank tests.

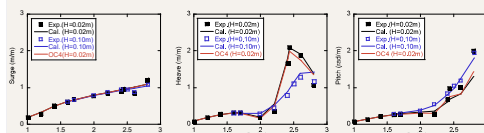


Figure 4 Dynamic responses in the surge, heave and pitch directions

Conclusion

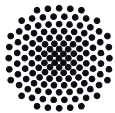
In this study, a model is proposed to estimate global hydrodynamic coefficients for a semisubmersible FOWT, considering interaction between elements, KC number and frequent dependencies.

1. The predicted global coefficients from added mass and drag coefficients of each element by proposed model show good agreement with those obtained from the water tank tests.
2. The predicted dynamic responses in different wave heights by proposed global hydrodynamic coefficients agree well with those from the experiments.

This research is carried out as a part of the Fukushima floating offshore wind farm demonstration project funded by the Ministry of Economy, Trade and Industry.

Reference

- [1] Pan, J. and Ishihara, T., "Numerical prediction of hydrodynamic coefficients for a semi-sub platform by using large eddy simulation with volume of fluid method and Richardson extrapolation method" EERA DeepWind'2019 conference
- [2] Ishihara, T. and Zhang, S.N., "Prediction of dynamic response of semi-submersible floating offshore wind turbine using augmented Morison's equation with frequency dependent hydrodynamic coefficients." Renewable Energy 131 (2019): 1186-1207.



University of Stuttgart

Model validation through scaled tests comparisons of a semi-submersible 10MW floating wind turbine with active ballast

Ricardo Faerron Guzmán, Frank Lemmer, Viola Yu, Po Wen Cheng
faerron@ifb.uni-stuttgart.de
Stuttgart Wind Energy (SWE), University of Stuttgart, Germany

DeepWind 2019
Trondheim

Semi-submersible model test campaign

In the EU H2020 project LIFES50+, a 1:36 scaled model test campaign was carried out for the NAUTILUS-DTU10, a semi-submersible 10MW floating offshore wind turbine (FOWT) with active ballast in 130m water depth [1]. The platform has 4 columns connected underwater by a square shaped ring pontoon (pon). They system has a design draft of 14.95 with empty water ballast [2]. The test included the use of a Real-Time Hybrid (ReaTHM) robot to simulate the aerodynamic loads in a wave basin. The turbine modeled was the DTU 10MW reference wind turbine, while the mooring system is based on 4 steel chain catenary lines. The wave basin testing was done by performing a variety of decay, pull out, regular wave, pink wave spectrum and extreme irregular wave spectrum tests, with and without simulated wind loads.



Fig 1: considered system

Modelling of Hydrodynamics

The research presented concentrates on the hydrodynamic modelling of state of the art simulation software FAST8 for FOWT. Its purpose is to compare the scaled model to the simulations, specifically looking at modelling the drift forces through second-order difference-frequency wave forces either through Newman's approximation or with the full quadratic transfer functions (QTFs).

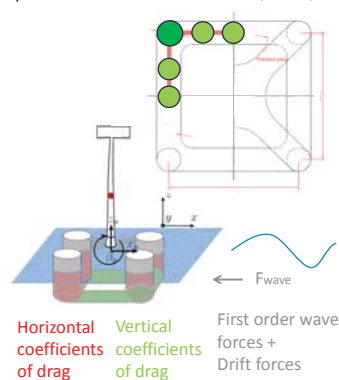


Fig 2: hydrodynamic drag and wave forcing on model

horizontal direction and a set of 12 circles in the vertical direction (light green area). The columns have a coefficient of drag (Cd) in the horizontal and vertical direction (red and dark green areas respectively).

The hydrodynamic forces used on the platform model can be summarized as follows:

$$F_{hydrodynamics} = F_{wave} + F_{hydrostatic} + F_{linear\ radiation} + F_{drag}$$

Decay test tuning of model

The Morison element model is first calibrated to the free decay tests in the wave basin. Tuning of the drag coefficients to the experimental data can lead to an approximation of the free decay tests. When the moored decay tests were compared, tuning of the mooring model was needed to be able to better match the Eigen-frequencies of the yaw and surge DOFs. The following decay frequencies were obtained:

	Surge	Heave	Pitch	Yaw
Moored Tests (Hz)	0.0082	0.0511	0.0322	0.010
Model (Hz)	0.0079	0.0527	0.0314	0.011

Acknowledgements and References

The research leading to these results has received partial funding from the European Union's Horizon 2020 research and innovation programme under grant agreement No. 640741 (LIFES50+). We also extend our thanks to the project partners from DTU, Nautilus, Technalia and Sintef for their support.
[1] J. Galvan, M. Sanchez-Lara, I. Mendikoa, V. Nava, F. Boscolo-Papo, C. Garrido-Mendoza, J. Berque, G. Perez Moran, and R. Rodriguez Arias, "Definition and analysis of Nautilus-DTU10 MW floating offshore wind turbine at Gulf of Maine," tech. rep., Technalia, 2017.
[2] M. Thys, V. Chabaud, T. Sauder, L. Eliassen, L. O. Saether, Ø. B. Magnussen, "Real-time hybrid model testing of a semi-submersible 10MW floating wind turbine and advances in the test method", Proceedings of the IOWTC 2018 1st International Offshore Wind Technical Conference, November 4-7, 2018, San Francisco, CA

Validation of wave tests

The results are presented in terms of power spectral density of the 3 hour simulation results with an additional 1000s run in time not taken into consideration. Comparison with a pink wave test with significant wave height of 2m and wave period range from 4.5-18.2s were performed.

The decay tuned models for Newman's approximation and Full QTFs shows a good agreement in the wave frequency range. Below these frequencies the models yields a good match in the slow-drift response in surge and sway, and tuning of the vertical coefficients of drag was necessary to obtain good agreement for the roll, pitch and heave. The low frequency yaw response was not reproduced properly.

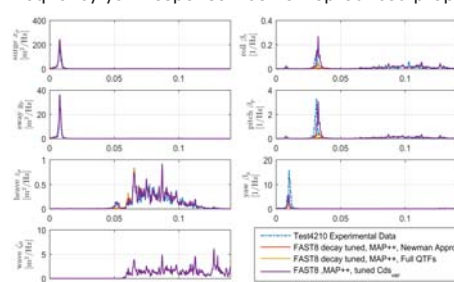


Fig 3: Pink noise spectrum test comparison

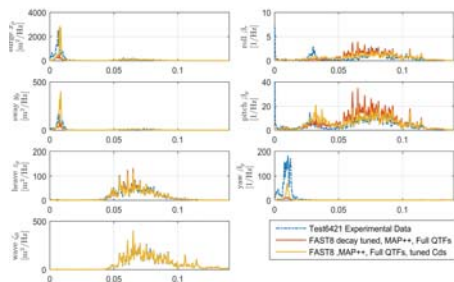


Fig 4: PM Extreme irregular wave spectrum test comparison

Model	Cd _{ver col}	Cd _{ver pon}	Cd _{hor col}	Cd _{hor pon}
Decay tuned	78.05	12.95	0.715	2.05
Pink noise tuned Cds.	23.415	3.885	Unchanged	Unchanged
PM extreme tuned Cds	31.22	5.18	0.5125	0.1787

Conclusions and Outlook

Regarding the use of second order wave forces (with Morison elements for viscous effects) for modelling the motions of the NAUTILUS-DTU10 FOWT when compared to wave tank tests:

- For the Morison element model with decay tuned coefficients of drag, the use of difference frequency full QTF increased the response of the platform for the low frequency region (below the wave excitation region), mostly for pitch and roll, when compared to Newman's approximation. However, the decay tuned model was not able to reproduce all 6 degrees of freedom for the pink wave and JONSWAP irregular extreme wave spectrum tests.
- Sea state dependant coefficients of drag were necessary for the model. The pink noise tests with the full QTF model showed that through changes in the drag coefficients, the numerical model could approximate the test response well for all degrees of freedom except the yaw. The reason why the model cannot capture this is not clear. The extreme irregular wave showed larger discrepancies.

Further analysis on the modelling approach could include:

- Load case dependant coefficients of drag were necessary for the tests yet changing the coefficients for different sea states as well as dependency of the coefficients of drag on the Reynolds number, possible marine growth, and incoming wave direction necessitate more comprehensive studies.
- Scaling effects of the platform response and loads will also be of interest for the future development of the platform concept.



Technology for a better society

www.sintef.no